

This electronic thesis or dissertation has been downloaded from the King's Research Portal at <https://kclpure.kcl.ac.uk/portal/>



## **New Routes to Carbon-11 Based Molecular Imaging Agents for In Vivo PET Imaging**

Downey, Joseph

*Awarding institution:*  
King's College London

The copyright of this thesis rests with the author and no quotation from it or information derived from it may be published without proper acknowledgement.

### **END USER LICENCE AGREEMENT**



**Unless another licence is stated on the immediately following page** this work is licensed

under a Creative Commons Attribution-NonCommercial-NoDerivatives 4.0 International

licence. <https://creativecommons.org/licenses/by-nc-nd/4.0/>

You are free to copy, distribute and transmit the work

Under the following conditions:

- Attribution: You must attribute the work in the manner specified by the author (but not in any way that suggests that they endorse you or your use of the work).
- Non Commercial: You may not use this work for commercial purposes.
- No Derivative Works - You may not alter, transform, or build upon this work.

Any of these conditions can be waived if you receive permission from the author. Your fair dealings and other rights are in no way affected by the above.

### **Take down policy**

If you believe that this document breaches copyright please contact [librarypure@kcl.ac.uk](mailto:librarypure@kcl.ac.uk) providing details, and we will remove access to the work immediately and investigate your claim.

# **New Routes to Carbon-11 Based Molecular Imaging Agents for In Vivo PET Imaging**

Joseph Downey

Submitted in partial fulfilment of the requirements for  
the degree of Doctor of Philosophy in Radiochemistry

King's College London  
School of Biomedical Engineering and Imaging Sciences,  
Department of Imaging Chemistry and Biology  
Rayne Institute, 4<sup>th</sup> Floor Lambeth Wing  
St Thomas' Hospital  
London, SE1 7EH

*October 2021*



## ACKNOWLEDGEMENTS

Firstly, I want to thank my supervisor Professor Tony Gee. I am so privileged to have had the opportunity to complete this work under your supervision. Thank you for the confidence you've shown in my abilities and ideas, and for the support you've given to help realise these. It's not been an easy process, but your wealth of experience and guidance has been invaluable. I would also like to thank Dr Salvatore Bongarzone for the huge amount of day-to-day support and advice that you've given me throughout this entire project. It was a real joy learning from and working alongside you, and so much of your advice has stuck with me throughout this writeup. Special thanks also go to Dr Michelle Ma, in addition to your fantastic and valuable advice as part of my TPC, you looked out for me when I was really struggling, going far above and beyond what was necessary. In addition, your eagerness in discussing chemistry is infectious and has helped inspire me to think more deeply about my work. You're a fantastic asset to the department and I feel lucky to have crossed paths with you in my time here.

Thanks to my TPC Chair, Professor Stephen Keevil, for your considered advice and advocacy, I really do appreciate all of the support. Thanks also to the other members of my TPC, Dr Philip Miller and Dr Ran Yan, for the valuable feedback, advice, and encouragement throughout. Thank you also to the many other academics within the department for your valuable advice and input during group meetings: Phil Blower, Rick Southworth, Sam Terry, Rafa Torres, Tom Eykyn. To the PET centre team, thanks for your advice and assistance: Mitja Kovac, Stefan Hader, Sheba Adu-Kwaako. Possibly the most vital support of all came from the cyclotron engineers Phil Halsted and Gary Dyer, keeping that old cyclotron chugging along. David Thakor and Matt Hutchinson, thanks for always being there when you're most needed and for running a tight ship with limited space. Steve Catchpole, thanks for the lab management but also for looking out for me when I needed it most. Your positive attitude has stuck with me, and I hope one day to be able to look out for others like you looked out for me.

Thank you to the members of the Gee group, past and present, for your support and collaboration: Francesca Goudou (your help and input into the PSMA work was invaluable), Federico Luzi, Igor Fontana, Abdul Karim Haji Dheere, Carlotta Taddei. Thanks also to my other colleagues within the department for your help in the lab as well as checking in during tough patches: Peter Gawne, Alex Rigby, George Firth, Filipa Da Mota Quinteiro, Truc Pham, Charlotte Rivas, Ed Waters, Mauricio Da Silva Morais, and Jen Young, along with many others! To my friends outside the department, thanks for keeping me going through the rough patches: Tim Westwood (I knew we'd make it!), Tom Arrow, Jack Wicks, Mike Wraw and Chris Lloyd.

I am extremely grateful to PMB Alcen for part-funding the project, as well as for the support and expertise provided by your team members: Laurent Tanguy, Virginie Hourtané, Florian Pineda, and Yahya Cisse. I am also grateful to the King's College London and Imperial College London EPSRC Centre for Doctoral Training in Medical Imaging for part-funding the project, as well as for the valuable training/development program that was provided.

To my Mum and Dad, my eternal cheerleaders, thank you both for having confidence in me when I don't always have it in myself. You've both helped me in so many ways to get through this, and I'm so grateful. Mum, thank you for your relentless and proactive help; whenever I've needed a boost you've always been one step ahead of the game. Dad, you've always told me "you'll be alright" and it's never been wrong yet! Oh and thanks both of you for dissuading me from trying to follow in your footsteps, I'm much better at this anyway. To my sister Molly and her fiancé Tom, thanks for always being there for me guys, your confidence and encouragement has meant so much!

Most important of all, to my wife Kate. I mean it when I say this could never have happened without Team Katie and Joe. This has been the hardest thing I've ever done, and you've just stuck at it alongside me. I can't imagine how hard it has been for you at times but your patience, kindness, and love has shone through it all. Let's move onto the next step, shall we?



## Table of Abbreviations

<b>2-PMPA</b>	2-Phosphonomethyl pentanedioic acid
<b>AA</b>	Amino acid
<b>A<sub>m</sub></b>	Molar activity
<b>APCI</b>	Atmospheric-pressure chemical ionization
<b>BEMP</b>	2-tert-Butylimino-2-diethylamino-1,3-dimethylperhydro-1,3,2-diazaphosphorine
<b>Bq</b>	Bequerels
<b>C18</b>	Octadecyl
<b>CDI</b>	1,1'-Carbonyldiimidazole
<b>cLogP</b>	Calculated partition coefficient (octanol/water)
<b>COSY</b>	Correlation spectroscopy
<b>CT</b>	Computerised tomography
<b>d.c.</b>	Decay corrected
<b>DBAD</b>	Di-tert-butyl azodicarboxylate
<b>DBU</b>	1,8-Diazabicyclo[5.4.0]undec-7-ene
<b>DEAD</b>	Diethyl azodicarboxylate
<b>DEPT</b>	Distortionless enhancement by polarisation transfer
<b>DIPEA</b>	N,N-Diisopropylethylamine
<b>DMF</b>	Dimethylformamide
<b>DMS</b>	Dimethylsulfate
<b>DMSO</b>	Dimethylsulfoxide
<b>EoB</b>	End of cyclotron bombardment
<b>ESI</b>	Electrospray ionisation
<b>ETFE</b>	Ethylene tetrafluoroethylene
<b>eV</b>	Electronvolt
<b>FDG</b>	fluorodeoxyglucose
<b>FTIR</b>	Fourier-transform infrared spectroscopy
<b>GCPII</b>	Glutamate carboxypeptidase II
<b>GMP</b>	Good manufacturing practice
<b>HILIC</b>	Hydrophilic interaction liquid chromatography
<b>HPLC</b>	High performance liquid chromatography
<b>HRRT</b>	High-resolution research tomograph

<b>HSQC</b>	Heteronuclear single quantum coherence
<b>I.D.</b>	Internal diameter
<b>IC<sub>50</sub></b>	Half-maximal inhibitory concentration
<b>K<sub>i</sub></b>	Inhibitory constant
<b>LC-MS</b>	Liquid chromatography-mass spectrometry
<b>LogP</b>	Partition coefficient (octanol/water)
<b>MRI</b>	Magnetic resonance imaging
<b>MS</b>	Mass spectrometry
<b>NAAG</b>	N-acetylaspartylglutamate
<b>NHP</b>	Non-human primate
<b>NMR</b>	Nuclear magnetic resonance
<b>O.D.</b>	Outer diameter
<b>PCa</b>	Prostate cancer
<b>PEEK</b>	Polyether ether ketone
<b>PET</b>	Positron emission tomography
<b>PG</b>	Protecting group
<b>pKa</b>	Dissociation constant
<b>pKa<sub>H+</sub></b>	Dissociation constant (of conjugate acid)
<b>ppm</b>	Parts per million
<b>PSMA</b>	Prostate specific membrane antigen
<b>PTFE</b>	Polytetrafluoroethylene
<b><sup>Pyr</sup>Glu</b>	Pyroglutamic acid
<b>QC</b>	Quality control
<b>R</b>	Organyl group
<b>RCC</b>	Radiochemical conversion
<b>RCP</b>	Radiochemical purity
<b>RCY</b>	Radiochemical yield
<b>RP</b>	Reversed phase
<b>RY</b>	Radioactivity yield
<b>S.D.</b>	Standard deviation
<b>S<sub>A</sub></b>	Asymmetric Selectivity
<b>SAR</b>	Structure-activity relationship
<b>SAX</b>	Strong anion exchanger
<b>SN<sub>2</sub></b>	Nucleophilic substitution (bimolecular)

<b>SPE</b>	Solid phase extraction
<b>SPECT</b>	Single-photon emission computed tomography
<b>SS</b>	Stainless steel
<b>t<sub>1/2</sub></b>	Half life
<b>TBD</b>	Triazabicyclodecene
<b>TFA</b>	Trifluoroacetic acid
<b>THF</b>	Tetrahydrofuran
<b>TLC</b>	Thin-layer chromatography
<b>t<sub>r</sub></b>	Retention time
<b>UV</b>	Ultraviolet
<b>v/v</b>	Volume/volume
<b>W<sub>ave</sub></b>	Average baseline-width

## ABSTRACT

Carbon-11 is a short half-life (20.4 min) positron emitting radionuclide which is commonly incorporated into small organic molecules to produce radiotracers for PET imaging. Carbon-11 is generally produced in a cyclotron as carbon dioxide ( $[^{11}\text{C}]\text{CO}_2$ ), but this is fairly unreactive and so is generally converted to secondary, more-reactive “synthons” such as methyl iodide ( $[^{11}\text{C}]\text{CH}_3\text{I}$ ). Whilst highly useful for incorporating carbon-11 into methyl positions on many molecules, this limits the chemical space that can be radiolabeled with carbon-11 and there is a need for the development of novel  $^{11}\text{C}$ -radiochemistry to allow radiolabeling of more diverse molecular structures. Some recently developed methods allow for the direct fixation of  $[^{11}\text{C}]\text{CO}_2$  into organic molecules, to produce *carbonyl*- $^{11}\text{C}$ -radiolabeled compounds. This thesis covers two key implementations of this new chemistry.

The first of these involved the development of a thin-film in-loop setup for  $[^{11}\text{C}]\text{CO}_2$ -fixation and  $^{11}\text{C}$ -urea synthesis.  $[^{11}\text{C}]\text{CO}_2$ -fixation methods involve bubbling  $[^{11}\text{C}]\text{CO}_2$  through fixation solutions, but this step can be difficult to incorporate into a routine automated synthesis due to inefficiencies in  $[^{11}\text{C}]\text{CO}_2$  trapping, as well as losses incurred during transfer of the solution from the vial to an HPLC injector-loop for purification.

To address these issues, an “in-loop” setup was developed in which  $[^{11}\text{C}]\text{CO}_2$  was efficiently trapped (~ 99%) in a thin-film of amine/DBU solution supported on the inner surface of a short section of polymer tubing. Passing Mitsunobu reagents through this tubing resulted in the rapid and efficient production of symmetric  $^{11}\text{C}$ -ureas in-flow. The use of cheap and widely-available components should make the developed methodology straightforward to implement in other labs; while its use of disposable plastic components could make it well suited to GMP production. *N,N'*- $[^{11}\text{C}]$ dibenzylurea (82% RCY), *N,N'*- $[^{11}\text{C}]$ diphenylurea (24% RCY), and *N,N'*- $[^{11}\text{C}]$ dicyclohexylurea (21% RCY) were all produced with this setup, in < 3 min from the EoB.

The second of these implementations involved the development of a generally-applicable method for  $^{11}\text{C}$ -radiolabeling PSMA-targeted radioligands *via*  $[^{11}\text{C}]\text{CO}_2$ -fixation. PSMA is a well-validated molecular target for PET imaging (and increasingly, targeted radioligand therapy) of prostate cancer. There is an ongoing effort worldwide into the

development of newer generation PSMA-targeted ligands, to modify their target binding affinities, off-target uptake, and clearance pathways. This effort is hampered by the difficulties in developing custom radiolabeling methods for each new candidate compound. The aim was therefore to develop a method to  $^{11}\text{C}$ -radiolabel all of these PSMA ligands within the ubiquitously-present PSMA-targeting glutamate-urea pharmacophore.

Initially, two different  $[^{11}\text{C}]\text{CO}_2$ -fixation and  $^{11}\text{C}$ -urea synthesis approaches were explored: DBU/Mitsunobu-mediated, and BEMP/ $\text{POCl}_3$ -mediated. It was found that the (harsher) BEMP/ $\text{POCl}_3$  method was still compatible with these substrates, whilst being somewhat more efficient and reproducible. Furthermore, during the optimisation of this method, several key factors were considered to ensure the method is useful and widely-applicable: the  $[^{11}\text{C}]\text{CO}_2$ -fixation must be efficient, the  $^{11}\text{C}$ -urea synthesis must be selective for the asymmetric urea product, and the stereochemistry must be retained. Ultimately, a small diverse library of PSMA-targeted  $^{11}\text{C}$ -radioligands were synthesised (13-35% RCYs) in < 14 minutes from the EoB using a single well-optimised and generally-applicable “one-pot” radiosynthetic method.

# TABLE OF CONTENTS

1	INTRODUCTION .....	1
1.1	Positron Emission Tomography .....	1
1.1.1	Overview .....	1
1.1.2	Operating principles .....	2
1.1.3	Applications .....	12
1.2	PET Radionuclides .....	16
1.2.1	Production .....	16
1.2.2	Radioactive decay .....	19
1.3	Radiochemistry – Carbon-11 .....	24
1.3.1	Why Carbon-11? .....	24
1.3.2	Cyclotron <sup>11</sup> C-production.....	28
1.3.3	Standard synthons .....	28
1.3.4	<sup>11</sup> C-Methylation .....	31
1.3.5	<sup>11</sup> C-Carbonylation .....	36
1.4	Radiochemistry – [ <sup>11</sup> C]CO <sub>2</sub> -Fixation .....	52
1.4.1	Why direct reaction with [ <sup>11</sup> C]CO <sub>2</sub> ? .....	52
1.4.2	Practicalities of [ <sup>11</sup> C]CO <sub>2</sub> as a synthon .....	53
1.4.3	<sup>11</sup> C-Carboxylic acids from Grignard reagents .....	56
1.4.4	Fixation on amines .....	57
1.4.5	Superbase-mediated [ <sup>11</sup> C]CO <sub>2</sub> fixation.....	63
1.5	PSMA .....	90
1.5.1	General biology and role/relevance in prostate cancer .....	91
1.5.2	Antibody-based molecular imaging .....	93
1.5.3	Small-molecule inhibitors .....	94
1.5.4	First generation small-molecule radiotracers .....	97
1.5.5	Second generation small-molecule radioligands.....	100
1.5.6	Outlook.....	103
2	IN-LOOP [ <sup>11</sup> C]CO <sub>2</sub> FIXATION .....	104
2.1	Introduction.....	104
2.1.1	Overview .....	104
2.1.2	Development of thin-film captive solvent techniques .....	105
2.2	Results & Discussion – Three Component In-Loop Fixation .....	134
2.2.1	Apparatus design and development .....	134
2.2.2	Exploration of [ <sup>11</sup> C]CO <sub>2</sub> fixation chemistry .....	141

2.2.4	Solution viscosity and its relation to in-loop retention .....	158
2.3	Results & Discussion – In-Loop Synthesis of <sup>11</sup> C-Ureas .....	161
2.3.1	Apparatus design and development .....	162
2.3.2	Quenching .....	167
2.3.3	Improved in-loop [ <sup>11</sup> C]CO <sub>2</sub> fixation .....	171
2.3.4	In-loop synthesis of <i>N,N'</i> -[ <sup>11</sup> C]dibenzylurea .....	174
2.3.5	Expanded substrate scope .....	186
2.4	Discussion – Recent Developments.....	191
2.4.1	Comparison with contemporaneous Dahl method.....	191
2.4.2	Recent applications .....	193
2.4.3	Other recent in-loop radiochemistry .....	199
2.5	Summary and Conclusion.....	203
2.6	Materials & Methods .....	206
2.6.1	General .....	206
2.6.2	Radiolabeling solution preparation .....	208
2.6.3	Radiochemistry apparatus setups .....	209
2.6.4	Generic radiosynthetic procedures .....	210
2.6.5	Synthesis of <i>N,N'</i> -dibenzylurea .....	210
3	PSMA SECTION 1 – NON-RADIOACTIVE SYNTHESIS .....	212
3.1	Introduction.....	212
3.2	PSMA Ligands .....	212
3.2.1	Synthetic strategy .....	216
3.2.2	Section overview .....	221
3.3	Results & Discussion – Urea Synthesis.....	222
3.3.1	Mitsunobu-mediated CO <sub>2</sub> fixation.....	222
3.3.2	Urea synthesis – CDI-method .....	222
3.3.3	Final library of compounds synthesised.....	226
3.4	Results & Discussion – Deprotection .....	228
3.4.1	Initial attempt at TFA deprotection.....	228
3.4.2	Glutamate cyclisation: pyroglutamate impurity.....	230
3.4.3	Final method .....	239
3.5	Materials & Methods .....	241
3.5.1	General .....	241
3.5.2	General protocol for CDI-mediated urea synthesis: Leu-Glu-(OtBu) <sub>3</sub> .....	241
3.5.3	General protocol for deprotection: Leu-Glu ( <i>aka ZJ43</i> ).....	242
3.5.4	Characterisation of protected ureas.....	242
3.5.5	Characterisation of deprotected ureas .....	244

4	PSMA SECTION 2 – MITSUNOBU-BASED <sup>11</sup> C-RADIOLABELING.....	247
4.1	Introduction.....	247
4.1.1	Choice of target.....	247
4.1.2	Mitsunobu-mediated symmetric <sup>11</sup> C-urea radiolabeling.....	250
4.2	Results & Discussion – Mitsunobu-Mediated <sup>11</sup> C-Urea Synthesis .....	253
4.2.1	Ammonium-salt precursor: aqueous extraction <i>versus</i> deprotonation <i>in-situ</i> .....	254
4.2.2	Representative HPLC trace – common peaks identified .....	256
4.2.3	General optimisation .....	262
4.3	Results & Discussion – HILIC: an alternative to RP-HPLC? .....	277
4.3.1	Why HILIC? .....	277
4.3.2	Role of buffers in HILIC.....	280
4.3.3	Ammonium formate (pH 3.2) .....	283
4.3.4	Microspecies distribution.....	286
4.3.5	Ammonium acetate (pH 5.8).....	292
4.3.6	Equilibration.....	300
4.3.7	Summary and alternative HPLC options .....	300
4.4	Discontinuation and future direction .....	303
4.5	Conclusions .....	304
4.5.1	Step 1 – <sup>11</sup> C-urea synthesis .....	304
4.5.2	Step 2 – acidic deprotection .....	306
4.6	Materials & Methods .....	309
4.6.1	General.....	309
4.6.2	HILIC buffers and mobile phase preparation .....	310
4.6.3	HPLC details .....	310
4.6.4	Radiolabeling solution preparations.....	311
4.6.5	Radiochemistry: synthesis of [ <i>ureido</i> - <sup>11</sup> C]Glu-Glu-(O <sup>t</sup> Bu) <sub>4</sub> .....	312
5	PSMA SECTION 3 – GENERALLY-APPLICABLE ASYMMETRIC <sup>11</sup> C- RADIOLABELING METHOD .....	315
5.1	Introduction.....	315
5.1.1	Context & motivations .....	315
5.1.2	Synthetic approach.....	320
5.2	Results & Discussion – Asymmetric <sup>11</sup> C-Urea Synthesis .....	322
5.2.1	Approach and general considerations .....	322
5.2.2	Proof-of-concept symmetric <sup>11</sup> C-urea synthesis: [ <i>ureido</i> - <sup>11</sup> C]Glu-Glu-(O <sup>t</sup> Bu) <sub>4</sub> .....	326
5.2.3	Fixation optimisation .....	331



5.2.4	Dehydration and asymmetric urea formation.....	345
5.3	Results & Discussion – Deprotection .....	359
5.3.1	Approach and general considerations .....	359
5.3.2	HPLC method development.....	361
5.3.3	Deprotection: first successful radiosynthesis of [ <sup>11</sup> C]Leu-Glu ([ <sup>11</sup> C]ZJ43) ..	363
5.4	Results & Discussion - General Method and Substrate Scope .....	369
5.4.1	General radiosynthetic methodology .....	369
5.4.2	Substrate scope.....	371
5.5	Conclusion .....	374
5.6	Materials & Methods .....	376
5.6.1	General .....	376
5.6.2	Radiolabeling solution preparation: .....	377
5.6.3	General radiolabeling procedures .....	378
5.6.4	Radio-HPLC methods .....	379
6	CONCLUSIONS & FUTURE WORK .....	380
6.1	Summary.....	380
6.2	In-Loop [ <sup>11</sup> C]CO <sub>2</sub> Fixation .....	380
6.2.1	Conclusions.....	380
6.2.2	Future work.....	382
6.2.3	Outlook.....	383
6.3	Generally Applicable Method for <sup>11</sup> C-Radiolabeling PSMA ligands .....	385
6.3.1	Conclusions.....	385
6.3.2	Future work.....	386
6.3.3	Outlook.....	388
7	BIBLIOGRAPHY .....	390

# 1 INTRODUCTION

## 1.1 Positron Emission Tomography

### 1.1.1 Overview

Positron emission tomography (PET) is a molecular imaging technique that enables the acquisition of functional images from within a living organism in a non-invasive manner.<sup>1</sup> This is achieved with the administration (usually *via* injection) of radiotracers: molecules that have been labeled with positron-emitting radionuclides. These radiotracers can be detected from outside of the organism with the use of a PET scanner, and the location data obtained can be used to construct a three-dimensional image of its distribution. Depending on the specific structure and characteristics of the molecule that is radiolabeled, its resultant distribution *in vivo* can give clinicians and researchers a vast array of insights into biological functions and biochemical features that are otherwise difficult to achieve, especially non-invasively in a living organism. To give a few examples, this can range from the monitoring of fundamental physiological processes (metabolism, excretion, etc.), to tissue-specific characteristics (tissue hypoxia, inflammation, etc.), up to imaging and quantifying specific molecular targets (regional neuroreceptor density and distribution, receptor expression levels in cancerous tissue, etc.).

PET differs from X-ray/CT and MRI in that it is a true *molecular* imaging modality which can be used to generate highly informative images of biological function, however by itself it gives very little anatomical context for the images. CT and MRI can provide highly-detailed anatomical imaging (with MRI better suited to soft-tissue anatomical imaging), but can give limited insights into *in vivo* molecular processes. These functionalities are therefore highly complementary, and PET images are usually co-registered with a CT scan (or increasingly an MRI scan) to provide anatomical context and other complementary data for the construction of the PET image.

In this first section, the basic principles underlying PET scanning will be explained and a few illustrative example applications will be presented.

## 1.1.2 Operating principles

### 1.1.2.1 Radioactivity and positron emission

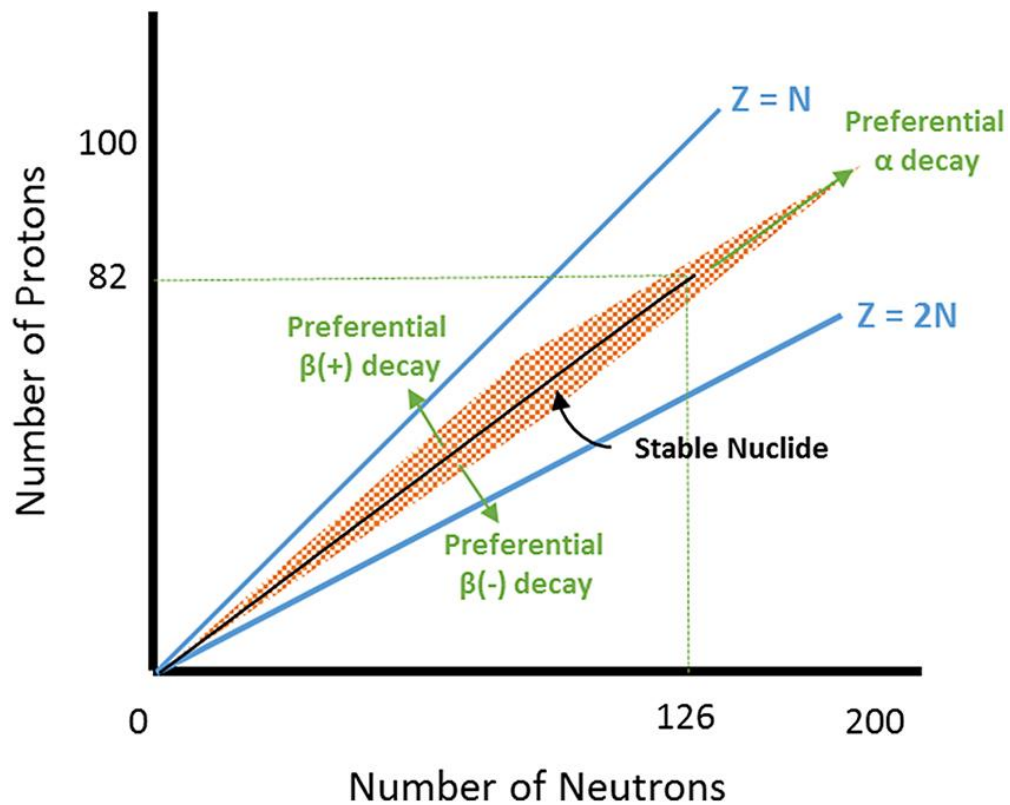


**Figure 1.1 Chart of nuclides, indicating regions of stable and unstable nuclides**

Typical radioactive decay modes depend on proton-neutron ratios in unstable nuclides:  $\beta^+$ -decay (positron emission) tends to occur with relatively more proton-rich nuclides, whereas  $\beta^-$ -decay (electron emission) occurs with relatively more neutron-rich nuclides;  $\alpha$ -decay is typically only seen with heavier nuclides ( $[Z+N] \geq 104$ ). Figure reproduced from work by Bryant<sup>2</sup>

The term “radionuclide” can refer to any atomic nuclei rendered unstable by their excess nuclear energy. The process of shedding this excess energy is termed “radioactive decay”, and this can occur *via* several pathways, termed  $\gamma$ -,  $\alpha$ -, and  $\beta$ -decay (which can in turn be separated into  $\beta^+$  and  $\beta^-$  decay).<sup>3</sup>

$\gamma$ -emission is the process whereby a radionuclide sheds energy by the emission of a gamma photon. This can occur via “prompt” gamma emission (where the excited state nucleus is very short-lived, typically  $\sim 10^{-12}$ - $10^{-9}$  seconds), but this is not easily applied in

medical imaging. SPECT imaging relies on the detection of gamma rays emitted during either electron capture, or as a result of a metastable isomeric transition. This latter process involves an excited state nuclear isomer (usually a product of  $\alpha$  or  $\beta$  decay itself) relaxing to its ground-state isomer by emitting a gamma photon of equivalent energy.<sup>3</sup> In this case, the atomic number does not change as it is merely a decay from a high energy to a low energy isomeric state. An example of this is the decay of technetium-99m to technetium-99, which is accompanied by the emission of a  $\gamma$ -ray of 141 keV.<sup>4</sup>

$\alpha$ -decay is the process whereby an atomic nucleus decays to a different atomic nucleus by emission of an  $\alpha$ -particle (2 protons and 2 neutrons), and tends to be the primary decay path of heavier nuclides (since it is highly efficient at shedding both nucleons and energy). An example of an  $\alpha$ -decay process is the decay of radium-223 to radon-219, accompanied by the emission of a 5.78 MeV  $\alpha$ -particle.<sup>5</sup>

$\beta$ -decay is the process whereby energy is emitted from an atomic nucleus in the form of an electron ( $\beta^-$ ) or a positron ( $\beta^+$ ) and in the process, a proton or neutron is converted into the other, hence the nucleus keeps the same mass-number but the atomic number is changed. An example of a  $\beta^-$  decay process is the decay of carbon-14 to nitrogen-14 accompanied by the emission of a 156 keV electron (and an electron antineutrino).

Figure 1.1 above shows a nuclide chart, where different nuclides are plotted on a chart with proton number and neutron number as the two axes. It can be seen that certain regions of the chart tend to favour decay by certain pathways to return towards the central line of stable nuclides. For example, heavy nuclides tend to decay by  $\alpha$ -emission, whereas nuclides above the central line of stability (those with a higher proton:neutron ratio) tend to decay by positron emission.<sup>2</sup>

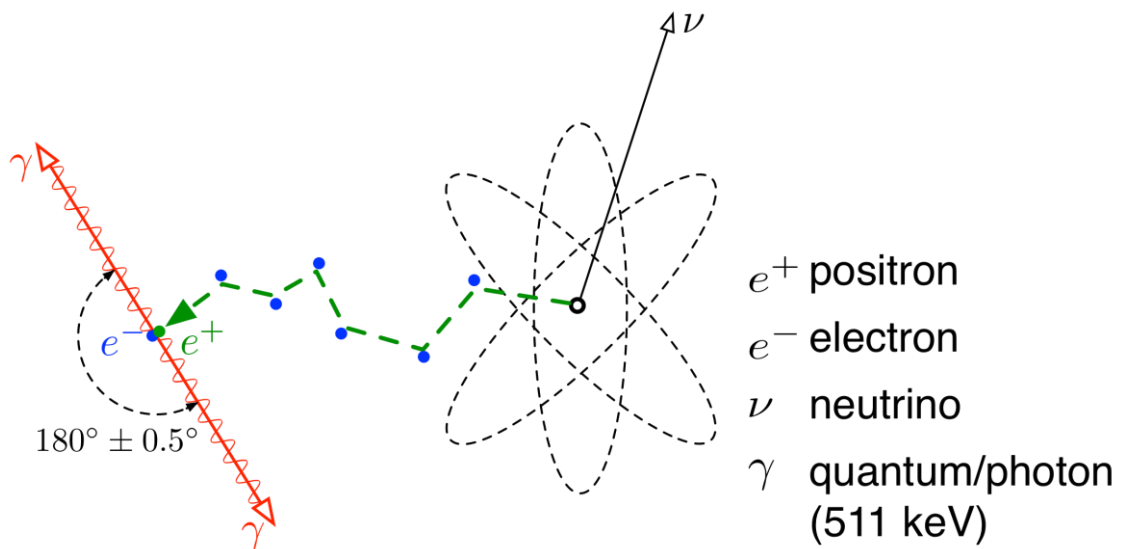
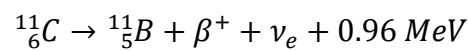


**Figure 1.2 Positron emission and annihilation producing two 511 keV photons**

Figure reproduced from public domain work by Maus<sup>6</sup>

This thesis is primarily concerned with positron ( $\beta^+$ ) emitting radionuclides, and so this process will be further discussed here. Many radionuclides decay by positron emission, so as an example we will discuss carbon-11, the decay equation of which is shown below.



A positron is an anti-particle of an electron, so when a positron meets an electron (of the correct energy) the two particles can undergo a matter-antimatter reaction known as annihilation. Due to conservation of momentum and energy, while the two particles annihilate one another, two gamma photons are emitted at  $\sim 180^\circ$  from one another (referred to as antiparallel emission). These emitted gamma photons are of a characteristic 511 keV energy, corresponding to the rest mass of a positron/electron.<sup>3,7</sup> A schematic diagram demonstrating the process of positron emission, followed by positron-electron annihilation with the resultant gamma emission, is shown in Figure 1.2 above.<sup>6</sup> Crucially, these photons can be detected from outside of the body, and the fact that they are emitted in an antiparallel manner at this characteristic energy is the fundamental principle upon which a PET scan functions.

While the resultant nuclides produced in these radioactive decay processes (commonly referred to as “daughter isotopes”) are usually stable (at least for most PET radionuclides), on occasion these “daughter isotopes” can themselves be radioactively unstable which can pose a problem for the interpretation of any resultant images. For example, iron is an essential bioelement which plays an active redox role in many enzymatic processes, and therefore an iron PET-radionuclide would be of great interest to enable the investigation of its uptake, transport and distribution. The most promising candidate for this is  $^{52}\text{Fe}$  with its half-life of 8.3 hours, which is well suited for such PET metallomics studies.<sup>8,9</sup> However, the “daughter” nuclide from  $^{52}\text{Fe}$  decay is the unstable radionuclide  $^{52\text{m}}\text{Mn}$ , which itself decays by positron emission with a half-life of 21.1 min (to the stable  $^{52}\text{Cr}$ ).<sup>10</sup> Since both the “parent” and “daughter” radionuclides decay by positron emission, any 511 keV annihilation photons actually detected by a PET scanner are therefore indistinguishable from one-another and as such, it is impossible to accurately determine whether a detected photon originated from an iron or manganese atom. While some interesting kinetic models have been developed in an attempt to deconvolve these signals and remove the interference from the  $^{52\text{m}}\text{Mn}$  decay,<sup>11</sup> such techniques are highly application specific and cannot be broadly applied to all  $^{52}\text{Fe}$ -based investigations, severely limiting the wider appeal of this PET radionuclide.

### 1.1.2.2 Detection – PET scanner

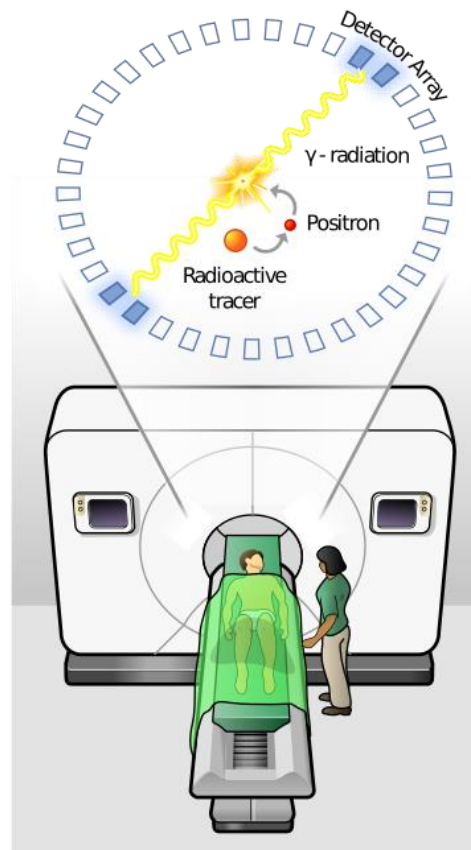


**Figure 1.3 PET scanner schematic showing coincidence detection of  $\gamma$ -photons**

Figure reproduced from open source work by Long<sup>12</sup>

A PET scanner consists of a circular array of scintillation detectors which absorb the energy of incident gamma photons and re-emit the energy by scintillation (light emission). This scintillation is converted to an electrical signal by a coupled photomultiplier, and this electrical signal allows the PET scanner to register a photon detection.<sup>7</sup> If the detected gamma photon originated from a positron annihilation event, then its counterpart antiparallel photon should be near-simultaneously detected by another of the detectors in the array. Therefore, a line can be drawn between the two detectors, and it can be assumed with a reasonable probability that the positron annihilation occurred somewhere along this line, termed the line of response (LoR); this is the principle commonly referred-to as coincidence detection. It is important to note that this coincidence detection mechanism necessitates that both photons are intercepted by the ring of detectors, but due to the small

axial FOV of traditional PET scanners (~ 20cm), only a small percentage of the annihilation events result in emissions within the solid angle of the scanner, which limits the overall sensitivity of the technique.

Over the course of a PET scan, this process will occur many thousands of times, and by algorithmically superimposing these LoRs, a three-dimensional map of these likely annihilation sites can be constructed in a process referred to as filtered backprojection; a basic method of image reconstruction. There are a number of different approaches to image reconstruction which attempt to mathematically solve this problem: if the process of photon emission (from positron annihilation) and simultaneous detection is referred to as “projection” and gives us a huge data set of detection times and locations, how can this data be best mathematically treated to “backproject” and reproduce the original spatial distribution of the radiotracer as faithfully as possible? This process is approached in a number of different ways and often involves a tradeoff between image noise and resolution.<sup>13</sup> Furthermore, due to the short range a positron can travel through tissue before annihilation (~1-5 mm),<sup>14</sup> these annihilation sites are taken as analogous to the location of the positron-emitting radiotracer but must be modelled as a point-spread function, further limiting the inherent resolution of a PET image.

A major advantage of this coincidence detection mechanism compared to the single-photon detection approach used for SPECT scans is that it enables the detection of photons that are not perpendicularly incident to the plane of the non detector scintillator crystals, since a LoR can be drawn between the two detection sites, regardless of angle of incidence. In a SPECT scanner by comparison, due to the absence of a second photon detection, collimation is required to ensure a 90° angle of incidence to enable a LoR to be drawn. The elimination of collimation in PET scanners when compared with SPECT leads to significant improvements in scanning sensitivity and quantification.<sup>15</sup>

### ***1.1.2.3 Fundamental limitations and improving technologies***

PET has an inherently low spatial resolution (~ 3-5 mm), when compared with CT and MR (typically ~ 0.1 mm),<sup>16</sup> and this resolution is fundamentally limited by three factors: the non-collinearity of the emitted  $\gamma$ -photons during the annihilation process, the distance



travelled between positron emission and annihilation (positron range), and the physical size of the scintillation detectors.

There is some small inherent uncertainty to the LoR due to the fact that (due to conservation of momentum) the two photons are not always emitted at precisely 180° from one another.<sup>7,17</sup> This inherent uncertainty is relatively small and must be accounted for by drawing a broader LoR, resulting in a lower resolution PET image than could be obtained if all  $\gamma$ -emissions were strictly co-linear.<sup>17</sup>

Another factor which contributes to the inherently lower resolution of PET (*versus* CT/MRI) is the fact that the detected gamma photons actually originate from the site of the positron/electron annihilation, and are not emitted directly from the radiotracer itself. As was alluded to previously, an emitted positron can travel a short distance through tissue before annihilation. To annihilate with an electron (at rest) the positron must be of approximately the same energy. However, the positrons are initially emitted with substantially more energy than their rest mass, and before annihilation this excess energy is lost in a process referred to as thermalisation, whereby the higher energy positron travels randomly through the tissue, shedding thermal energy by collision with atomic electrons. This process continues until sufficient energy is dissipated, at which time the positron can undergo annihilation with an electron.<sup>7</sup> This process of random-walk thermalisation is shown in Figure 1.2 above.

The higher the initial positron energy at the point of emission, the further it will travel through tissue on average (referred to as the mean free path length), and therefore the more uncertain the real location of the positron-emitting radiotracer becomes, lowering the theoretical spatial resolution further. In essence, this serves to “blur” the PET image due to the uncertainty in the positron origin requiring the calculated location of annihilation to be treated as a point spread function, rather than a specific point. The energy with-which a positron is emitted is characteristic to the specific radionuclide, and thus some positron emitting radionuclides can have a theoretically superior resolution to others, by virtue of their lower energy positron emission.<sup>17</sup> To take two extreme examples, a low energy, <sup>18</sup>F-emitted positron ( $E_{\max} = 0.634$  MeV,  $E_{\text{mean}} = 0.250$  MeV) has a maximum range in tissue of 2.4 mm, and mean range of 0.6 mm. By comparison, a higher

energy,  $^{15}\text{O}$ -emitted positron ( $E_{\text{max}} = 1.732 \text{ MeV}$ ,  $E_{\text{mean}} = 0.735 \text{ MeV}$ ) has a maximum range in tissue of 8.4 mm, and a mean range in tissue of 3 mm.<sup>14</sup> Although it should be noted that it is still a matter of debate as to whether this has any real impact at-present on practically-achieved resolution, since most current PET scanners remain fundamentally limited in their resolution by the physical size of their detection scintillators.<sup>17,18</sup> However with the development of newer silicon photomultiplier-based PET (SiPM-PET) systems enabling the further miniaturisation of scintillators,<sup>19</sup> the effect of positron energy on resolution may soon become a more relevant concern.

The main factor restricting the further reduction in size of these scintillators is the huge cost required to construct a scanner with a greater number of smaller scintillators, since this increased resolution is not necessarily of the utmost importance in the day-to-day clinical usage of the scanner, or at-least not to the extent that it could justify the cost increase. For research purposes however, such scanners have been constructed: the high resolution research tomograph (HRRT) has scintillators with 2.3 x 2.3 mm dimensions (compared to the standard size of 5 x 5 mm or larger in standard PET scanners), but the system is much more expensive than a standard scanner. To compensate for this somewhat, the internal bore diameter is significantly smaller, meaning it can only be used for brain PET imaging; an application which is most likely to benefit from maximal resolution.<sup>20</sup>

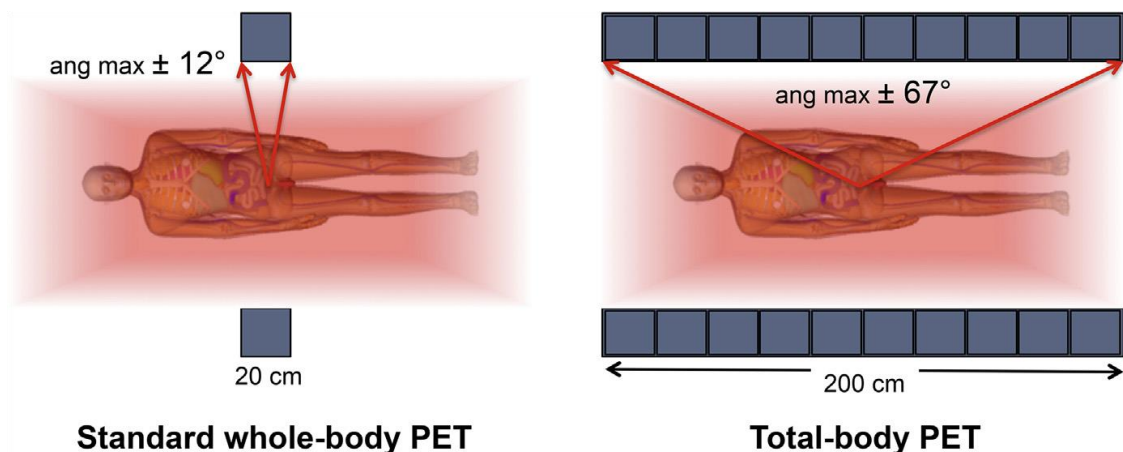


**Figure 1.4 Schematic comparing a standard and total-body PET scanner**

Significantly increased axial field-of-view is demonstrated. Figure reproduced with permission from work by Schmall *et al.*<sup>21</sup>

One final area of improvement in PET scanner technology is in the development of a total-body PET scanner.<sup>22</sup> In a traditional system, the axial coverage of the detectors is ~20 cm, and thus only a small fraction of the total annihilation events are detected, since the vast majority are emitted in a plane which is not covered by the detectors. This results in a poor sensitivity of traditional PET, and to overcome this, significant quantities of radiotracers must be injected. As a result, scanning times are much longer (to ensure adequate signal acquisition), and only one region of the body can be imaged at a time – different bed positions are required to move the patient through the scanner and enable the capturing of whole-body images. By extending the detector length to ~ 100-200 cm, the scanner's sensitivity increases as much as 40-fold (the United Imaging uExplorer system has a 194 cm axial FOV, whereas the Siemens Biograph Vision Quadra system has a 106 cm axial FOV). As such, injected doses and scanning times can be significantly reduced, as well as enabling the simultaneous acquisition of whole body images. It has been reported that a traditional multiple-bed-position scan taking 12 minutes could be replaced with a single 30 second single bed position scan using the 194cm UI uExplorer system.<sup>22</sup> These scanners are still new with both United Imaging and Siemens only recently bringing their systems to market, and of course the construction costs are orders of magnitude higher, but initial results from these scanners are highly impressive and have already enabled the acquisition of whole-body dynamic PET images.<sup>23</sup>

#### ***1.1.2.4 Imaging and therapy: differing requirements***

As was discussed in section 1.1.2.1 above, there are a number of different radioactive decay modes inherent to different radionuclides. As a result of these differing decay modes, some radionuclides are better suited to certain applications in imaging or therapy. Gamma emission processes – whether they be single gamma photon emission *via* electron capture (e.g. <sup>123</sup>I, <sup>111</sup>In, etc.) or isomeric transition (e.g. <sup>99m</sup>Tc), or two photon emission as a result of positron emission and annihilation (e.g. <sup>11</sup>C, <sup>18</sup>F, etc.) – are typically used for imaging applications. Single gamma photon emitting radionuclides are used in both SPECT scanning and planar scintigraphy, whereas positron emitting radionuclides (ultimately resulting in the emission of two gamma photons) are applied in PET scanning.<sup>7</sup> Alternatively, radionuclides which predominantly decay by alpha (e.g. <sup>223</sup>Ra)

or beta (e.g.  $^{177}\text{Lu}$ ) emission are much more commonly employed in targeted radionuclide therapeutic applications.<sup>24</sup>

This difference in applications arises as a result of the fundamental properties of these emitted particles: the degree to which they interact with surrounding tissue as well as the nature of these interactions dictates the most suitable applications of these different radioactive decay modes. In imaging, the intention is to externally detect the emitted radiation and use this to non-invasively determine the in-vivo location and distribution of the radionuclide, therefore minimal tissue attenuation of the radiation is required. In therapeutic applications, by contrast, since external detection/localisation of the radionuclide is not the priority, the aim is instead for the emitted particle to deposit as much of its energy as possible into the surrounding tissue. Typically, this is used to selectively damage/destroy malignant tissue by virtue of attaching the radionuclide to a targeted pharmacophore leading to specific uptake and accumulation in diseased sites.

Gamma photons are well suited for imaging due to their limited interaction with surrounding tissue: as uncharged particles, they experience only limited attenuation by soft tissue as a result of scattering and absorption processes and the majority of emitted gamma photons will escape the tissue and so can be efficiently detected by the external scanning equipment. As charged particles however, alpha and beta emissions, can undergo coulombic interactions with surrounding tissue, leading to a much greater deposition of energy (and thus destructive interactions) in addition to reducing their tissue penetrance ( $\alpha \sim 40\text{-}100 \mu\text{m}$ ,  $\beta \sim 0.05\text{-}12 \text{ mm}$ ) and therefore limiting collateral damage to non-target tissues.<sup>24,25</sup>

### 1.1.3 Applications

Depending on the molecule that is radiolabeled, PET can image a wide variety of physiological processes, molecular targets, or biological pathways, and can therefore be useful in a wide range of clinical and research-based investigations.

These can be categorised under three broad classes of applications: disease diagnosis and monitoring of treatment, fundamental biological research, and drug development. A representative example of each of these three applications are presented here.

Regardless of the application, the operating principle which enables any PET study and gives it such a powerful ability to probe complex biochemical systems, is that it operates according to the “tracer principle”. By virtue of PET’s extremely high sensitivity, radiotracers can be detected easily even when administered in trace quantities (typically sub-nanomolar) and as such, can be used without perturbing a normally sensitive system (e.g. receptor binding).<sup>26</sup>

#### *1.1.3.1 Disease diagnosis and treatment monitoring*

The obvious and most prevalent example of such an application is the use of [<sup>18</sup>F]fluorodeoxyglucose, a radiofluorinated analogue of glucose which accumulates in sites with high metabolic activity. While this is an incredibly versatile radiotracer, as a result of its broadly-applicable mechanism of uptake,<sup>27</sup> its primary usage in clinical settings is as an oncological diagnostic tool for the location and staging of tumours in a variety of cancers.<sup>28</sup> The mechanism exploited by [<sup>18</sup>F]FDG is the Warburg effect, whereby a relative increase in aerobic glycolysis is seen for cancer cells compared to the non-malignant surrounding tissue.<sup>29</sup> As a glucose analogue, [<sup>18</sup>F]FDG will be disproportionately taken-up in malignancies, however unlike glucose which can be fully metabolised in these cells, [<sup>18</sup>F]FDG cannot be further metabolised beyond the hexokinase phosphorylation step, resulting in enhanced accumulation of radioactivity in metabolically active tumours over time, as can be seen in Figure 1.5 below.<sup>30</sup>

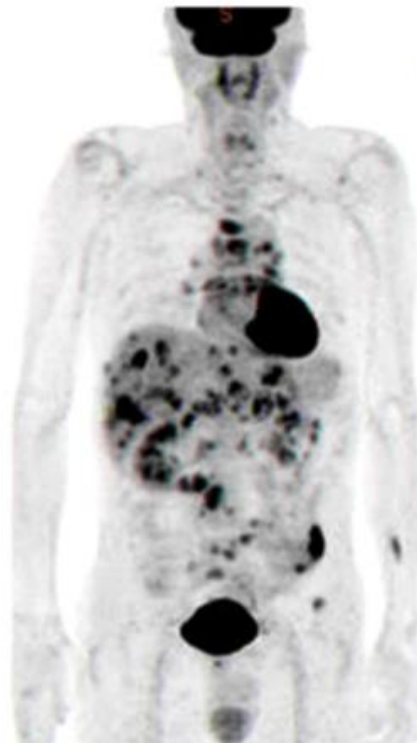


**Figure 1.5** [ $^{18}\text{F}$ ]FDG PET scan of a patient with metastatic gastric adenocarcinoma

Multiple hypermetabolic metastatic lesions are visible throughout the patient's body. Additionally, incidental non-malignant accumulation can be observed primarily in the brain, heart, and bladder  
Figure reproduced from Kim et al<sup>31</sup> (CC BY-NC 3.0)

This can be used in the diagnosis of cancer, but can also be a valuable tool in monitoring therapeutic response. Traditionally, tumour response to therapy is assessed by monitoring changes in tumour size by anatomical imaging modalities (x-ray/CT/MR).<sup>32,33</sup> However with the use of a functional imaging modality such as [ $^{18}\text{F}$ ]FDG PET, the metabolic activity of these tumours can be monitored, and in many cases, changes in tumour metabolic activity (as a result of successful therapy) can pre-empt anatomical changes by weeks or even months.<sup>34,35</sup> So moving from anatomical to functional monitoring of such treatments can allow for significantly quicker management/modification of treatment protocols.<sup>34-36</sup>

### 1.1.3.2 Fundamental biological research

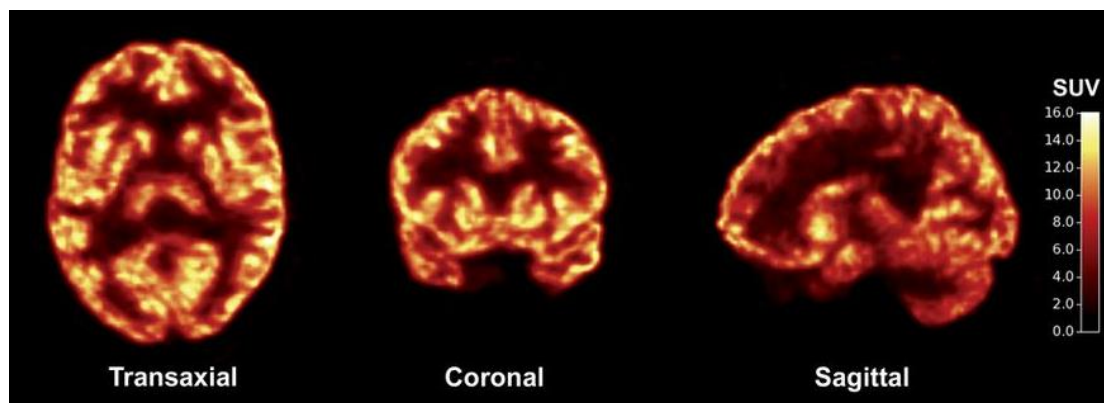


**Figure 1.6** Synaptic density imaging in a healthy human subject, using [ $^{11}\text{C}$ ]UCB-J  
Figure reproduced from publication by Finnema *et al.*<sup>37</sup>

One example of a recently-developed novel PET-radiotracer that can be highly useful in biological research, is the case of synaptic density imaging using [ $^{11}\text{C}$ ]UCB-J, a PET-radioligand for synaptic vesicle glycoprotein 2A (SV2A).<sup>37</sup> Previously, assessing synaptic density required the ex-vivo examination of brain tissue obtained through surgery or autopsy. This made it impossible to perform longitudinal PET studies of synaptic density in normal human development as well as the role of synaptic dysfunction in multiple different neuropsychiatric disorders such as Parkinsons disease, Alzheimers disease, autism spectrum disorders, and epilepsy, to name a few examples.<sup>38</sup> With the development of [ $^{11}\text{C}$ ]UCB-J and the subsequent development of a number of second generation SV2A radiotracers,<sup>38</sup> a new avenue of research into the biological implications of synaptic density and dysfunction has been opened.

### 1.1.3.3 Drug development

There are many possible applications of PET imaging in drug-development and pharmacology,<sup>39,40</sup> but in this example we will briefly discuss the concept of PET microdosing. This concept was first fully-articulated and advocated by Bergström, Grahnén, and Långström in a 2003 review,<sup>41</sup> and essentially involves the isotopologous PET-radiolabeling of drug candidate molecules which can theoretically be safely administered to subjects in the sub-pharmacological doses inherent to PET imaging. This

can in theory enable the assessment of a drug's *in vivo* pharmacokinetics, tissue penetrance, and target interaction, since *in vivo* measurements of these are much more clinically-relevant than *in vitro* data.<sup>42</sup> Additionally, providing this information at a much earlier stage in the drug-development timeline, due to the reduced concerns regarding toxicity, PET microdosing approaches are theoretically able to streamline drug-development pipelines, and allow unsuitable drug candidates to fail during the earlier, cheaper stages of drug development.<sup>41,43,44</sup>



## 1.2 PET Radionuclides

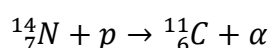
### 1.2.1 Production

#### 1.2.1.1 Cyclotron

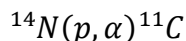
The majority of commonly-used PET radionuclides are produced with a type of small particle accelerator, called a cyclotron.<sup>45</sup> In general, these operate by circularly accelerating charged particles by applying a rapidly alternating voltage between two electrodes (termed “dees”), before directing the beam of high energy particles at a target. Upon bombardment of the material contained within this target (the target material can be solid, liquid, or gas), nuclear reactions occur to produce the desired radionuclide.

The charged particles move under the initial applied voltage and as they reach the edge of an electrode, the polarity is flipped and the particles are accelerated across the gap between the electrodes, gaining energy and velocity in the process. This higher velocity leads to the particle orbiting inside the cyclotron with a larger radius. As this process continues and the particle continues to gain energy, it spirals from the centre towards the outside edge of the cyclotron. At this point the beam of particles is “extracted”, either by deflection (for positive ions) or by stripping electrons (from negative ions) by passing the beam through an “extraction foil”, this switches a particle’s charge from negative to positive, and thus causes it to behave in an opposite manner in the magnetic field, deflecting it away from the circular path it was previously following.

In medical cyclotrons, the particles usually accelerated are hydride ions ( $H^-$ ), which are converted to protons ( $H^+$ , or  $p$  in nuclear reactions) or deuterons ( $[^2H]H^+$ , or  $d$  in nuclear reactions) once passed through the stripper foil to remove the electrons and extract the particle beam. These particles bombard the material held in the target, initiating nuclear reactions and producing the intended radionuclide. As an example, the production of carbon-11 by proton bombardment of nitrogen-14 will be presented:



In this reaction, the bombardment of nitrogen-14 with a high energy proton beam has resulted in its conversion to carbon-11 by the expulsion of an alpha particle. This radionuclide production route is more commonly depicted as such:



In the following table, a few of the most commonly encountered cyclotron-produced radionuclides are shown along with their common production routes.<sup>46</sup>

**Table 1.1 Common PET radionuclides and their cyclotron production routes**

Radionuclide	Half-life	Production route
<sup>11</sup> C	20.4 min	<sup>14</sup> N(p,α) <sup>11</sup> C
<sup>13</sup> N	10 min	<sup>16</sup> O(p,α) <sup>13</sup> N
<sup>15</sup> O	122 sec	<sup>15</sup> N(p,n) <sup>15</sup> O
<sup>18</sup> F	109.7 min	<sup>18</sup> O(p,n) <sup>18</sup> F

While cyclotrons can be extremely powerful tools, giving on-demand access to a wide variety of useful radionuclides, they are extremely expensive to install, run, and maintain, often necessitating a significant amount of dedicated supporting infrastructure. This is possible for major research facilities/hospitals, but is not possible for smaller sites. Some of the longer half-life PET radionuclides (like fluorine-18) can be produced at a central site and distributed to nearby hospitals etc.. However this model is essentially incompatible with shorter-lived radionuclides such as carbon-11, meaning that these are generally only used in facilities with an on-site cyclotron.

### 1.2.1.2 Generator

An alternative approach to cyclotron production, for some limited radionuclides, involves the use of “generators”. These are essentially self-contained resin columns containing an immobilised, long-lived “parent” radionuclide which decays over time producing the “daughter” radionuclide which can be selectively eluted from the column for use in

radiolabeling reactions. The prototypical radionuclide generator is the  $^{99}\text{Mo}/^{99\text{m}}\text{Tc}$  system, whereby molybdenum-99 decays to technetium-99m (a SPECT radionuclide).<sup>47</sup> This can be selectively eluted from the column (while leaving the molybdenum-99 in place) as pertechnetate ( $[^{99\text{m}}\text{Tc}]\text{TcO}_4^-$ ) and used for further radiolabeling reactions.

A more recently developed generator system is the  $^{68}\text{Ge}/^{68}\text{Ga}$  generator that is used for the production of gallium-68, a positron emitting radionuclide with a 68 min half life.<sup>48</sup> These are typically eluted with aqueous HCl to yield solutions of  $[^{68}\text{Ga}]\text{GaCl}_3$ , which can be used to radiolabel molecules of interest, usually by incorporation into a chelator.<sup>48,49</sup>

Whilst the radiolabeling options are theoretically somewhat more limited with gallium-68 (it typically must be incorporated into a chelator), this ease of access afforded by virtue of avoiding cyclotron production, has led to the development of many  $^{68}\text{Ga}$ -based radiotracers in recent years.<sup>49</sup>

## 1.2.2 Radioactive decay

### 1.2.2.1 Decay equations

While the radioactive decay of a single radioactive atom is a probabilistic but ultimately random process, the decay rate of a sufficiently large bulk sample is highly predictable. Each radionuclide has an associated half-life ( $t_{1/2}$ ), that remains constant: that is the time taken for half of a sample to decay. As a result of the constant nature of a radionuclide's  $t_{1/2}$ , the amount of radioactivity that will remain after a given amount of time has elapsed can be calculated using the decay equation:

$$A = A_0 e^{-\lambda t}$$

where,

$A$  = radioactivity at time  $t$

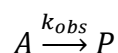
$A_0$  = radioactivity at time 0

$$\lambda = \frac{\ln 2}{t_{1/2}}$$

### 1.2.2.2 Implications for radiochemistry

A key difference between standard non-radioactive synthetic chemistry and synthetic chemistry performed with radionuclides is that the decay rate of a given radionuclide must always be taken into consideration. In synthetic chemistry, generally the goal for any reaction optimisation is to increase the chemical yield, whereas in radiochemistry, generally the aim is to increase the radioactivity yield. Generally, while the chemical yield of a process increases over time, the amount of radioactivity in a reaction decreases, so these two factors must be balanced out. The practicalities of this were recently discussed in an excellent concepts paper from Holland,<sup>50</sup> but a simple theoretical example will be presented here.

Consider a reaction of reagents  $A$  and  $B$  to yield product  $P$ . For the sake of this example,  $B$  is used in a multifold molar excess, so its concentration can be assumed to be roughly constant, and therefore the simplified reaction can be depicted as follows:



Where  $k_{obs}$  is the observed rate constant of the reaction; as  $B$  is in excess, the reaction can be said to obey pseudo-first-order kinetics with respect to  $[A]$  (the concentration of  $A$ ). If  $k_{obs}$  is known,  $[A]$  and  $[P]$  can be calculated/plotted as a function of reaction time. However, if we now consider that that  $A$  and  $P$  are radioactive species, while these theoretical concentrations of  $[A]$  and  $[P]$  are informative with regards to the chemical reaction progress, one must also account for the radioactive decay (according to the decay equation presented above) and calculate/plot the real-world radioactivity yield of  $P$ ,  $RY_P$ . This accounts for both the rate of conversion from  $A$  to  $P$ , but also for the continuous radioactive decay of the sample over time.

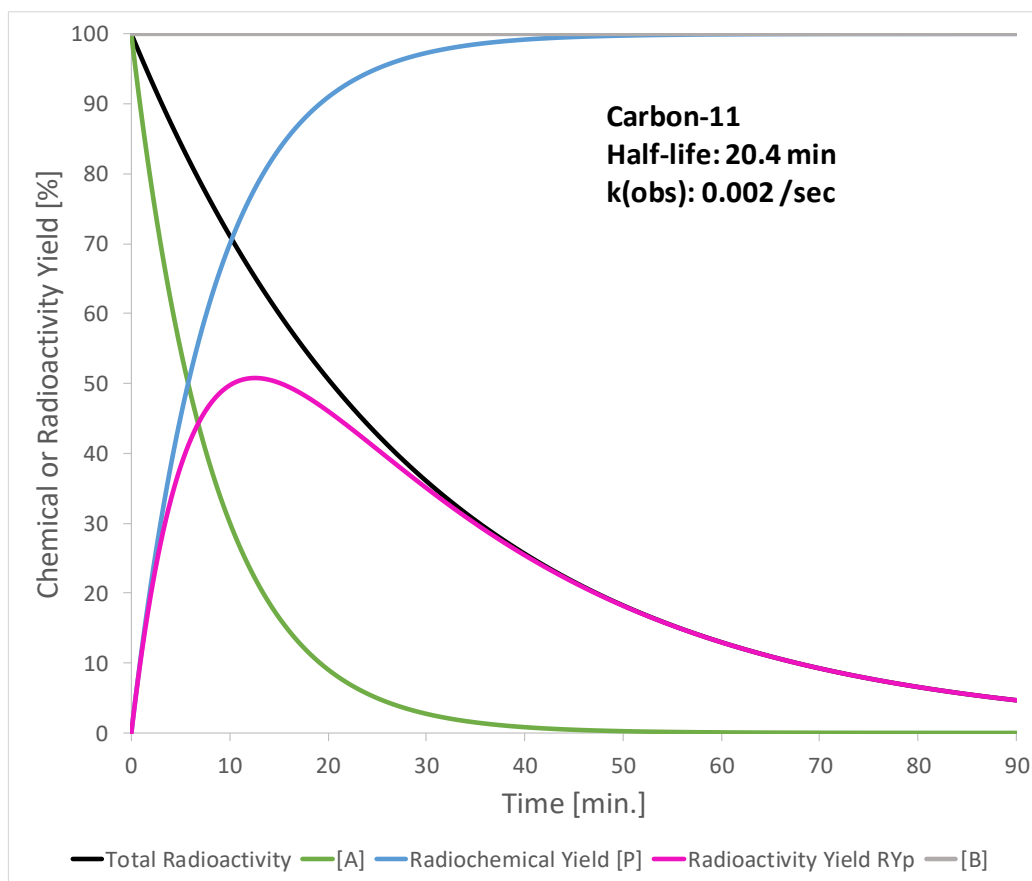


**Figure 1.7 “Radiochemical yield” versus “radioactivity yield” in  $^{11}\text{C}$ -radiochemistry**

Kinetic plot indicates that while radiochemical yield  $[P]$  exceeds 99% at around 35 mins, the radioactivity yield peaks at ~50% between 12 and 13 mins. Inspired by similar kinetic plots presented by Holland<sup>50</sup>

In the plot, shown in Figure 1.7 above, while the theoretical yield of *P* approaches 100% as the reaction time exceeds 35-40 mins, because of the radioactive decay of the carbon-11, the real radioactivity yield of *P* ( $RY_P$ ) reaches a maximum at ~12.5 mins. At this point, the losses due to radioactive decay start to outweigh the chemical yield increase achieved by allowing the reaction to proceed further.

Generally, when radiosyntheses are reported, one figure always reported is the radiochemical yield (decay corrected); in Figure 1.7, this is represented by the blue line [*P*]. It is clear by inspecting this chart, that while this can be an important measure to make, particularly early in the optimisation of a new radiolabeling methodology, it can be meaningless without considering also the reaction time and the consequential radioactivity yield (the amount of radioactivity actually obtained at the end of the radiolabeling process); in this plot this is represented by the pink line,  $RY_P$ . For example, if this example reaction was left to run for 80 mins, the RCY (decay corrected) would be an impressive 100%. However accounting for the real decay of the sample, the radioactivity yield would be a significantly worse 7%. By contrast, allowing the reaction to only run for 12.5 mins would give a less impressive RCY of 78%, but a significantly improved radioactivity yield of 50%. As such, a quoted RCY can be misleading without also accounting for the reaction time and the particular radionuclide used.

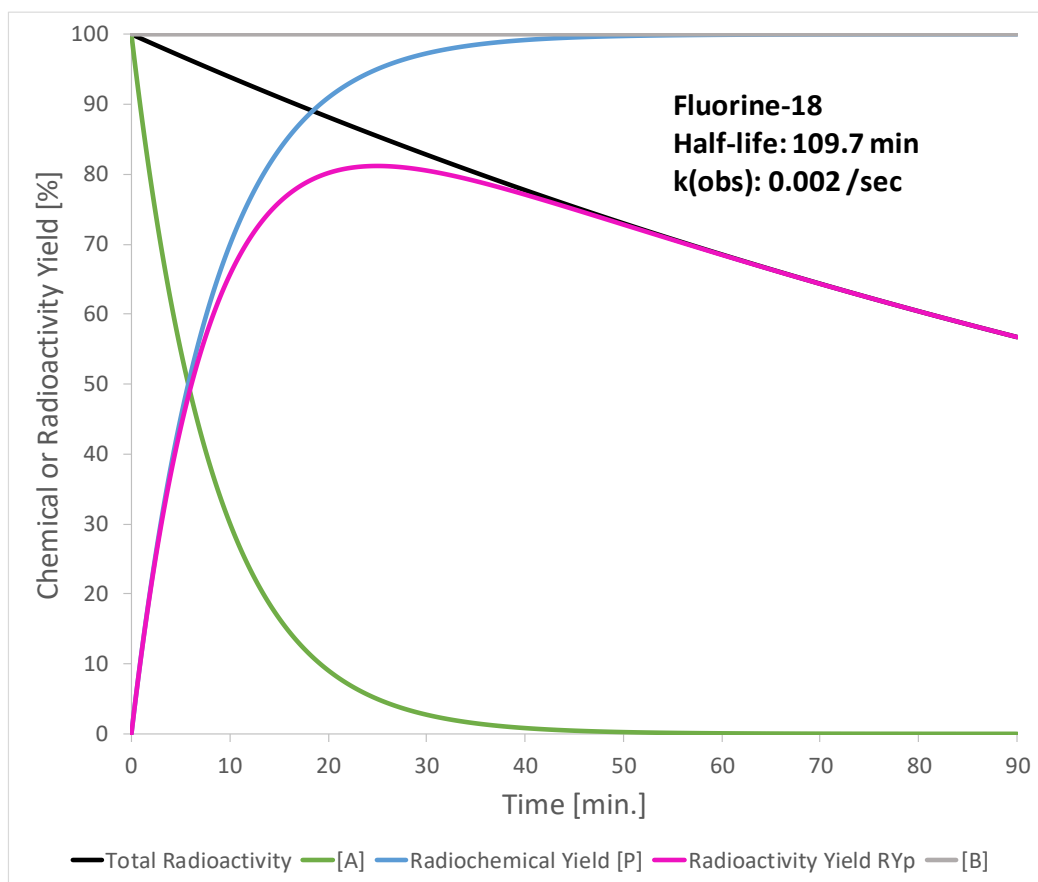


**Figure 1.8 “Radiochemical yield” versus “radioactivity yield” in  $^{18}\text{F}$ -radiochemistry**

Radiolabeling kinetic plot with same  $k_{\text{obs}}$  as the plot shown in Figure 1.7 above. While radiochemical yield [P] exceeds 99% at around 35 mins, the radioactivity yield peaks at ~80% at 25 mins. Due to the longer  $t_{1/2}$  of fluorine-18, the difference between maximum theoretical RCY and RY is smaller than it is for the similar  $^{11}\text{C}$ -radiolabeling process. Inspired by similar kinetic plots presented by Holland<sup>50</sup>

The disparity between radiochemical yield and radioactivity yield is heightened for radionuclides with shorter half-lives. As a comparison, the same reaction plot (with the same  $k_{\text{obs}}$ ) is presented in Figure 1.8 above, but this time for a fluorine-18 radiolabeling reaction. In this case, while the radiochemical yield as a function of time remains the same as in the carbon-11 example (Figure 1.7) (compare the blue lines in both figures), the radioactivity yield is substantially different. In this case, by virtue of its significantly slower radioactive decay rate, the fluorine-18 reaction achieves a maximal radioactivity yield of 80% after 25 mins.

This is presented to underscore the importance of paying attention to radioactive decay in developing novel radiolabeling methodologies. Whilst it can be informative to state the (decay-corrected) RCY of a particular radiosynthesis, this must be put into context by also considering reaction times and radioactive decay. This is all-the-more important for radiochemists working with radionuclides with particularly short half-lives (carbon-11, nitrogen-13, etc.). Ultimately the goal must be to produce sufficient quantities of a given radioactive product, not simply to achieve the highest possible RCY.



### 1.3 Radiochemistry – Carbon-11

#### 1.3.1 Why Carbon-11?

##### 1.3.1.1 *Isotopologous radiolabeling*

The biggest advantage of the use of carbon-11 over any other PET radionuclide is the near-total ubiquity of carbon in both drugs and biomolecules. If a molecule of interest contains a carbon-12 atom, then this can (theoretically) be radiolabeled by substitution with a carbon-11 atom. This is what is termed “isotopologous radiolabeling”, the exchange of a carbon-12 for a carbon-11 enables the radiolabeling of a molecule without affecting its biological function/behaviour in any way. This can sometimes be possible for other radionuclides, where the molecule of interest contains a non-radioactive isotope of the same atom, such as the  $^{18}\text{F}$ -radiolabeling of fluorine containing drugs. However due to the presence of carbon in almost every drug or biologically relevant molecule, there are many potential molecules of interest for which isotopologous radiolabeling is only possible with the use of carbon-11.

The short half-life (20.4 min) of carbon-11 is a major caveat to its usage. It is better suited to imaging relatively fast processes: and as such it is commonly applied in the radiolabeling and tracking of small-molecules, as generally the *in vivo* circulatory half-lives of these are comparatively short, with imaging often occurring no more than an hour after injection. Therefore,  $^{11}\text{C}$ -radiolabeling of these molecules allows for the molecule’s biodistribution and uptake to be monitored without significant radiation exposure to the patient, as a result of using an unnecessarily long-lived radionuclide. This does however, mean that  $^{11}\text{C}$ -radiolabeling of larger biomolecules (antibodies, proteins, cell labeling) is rarely of any practical use: these typically circulate for days before imaging is possible, hence the typical usage of radionuclides such as technetium-99m ( $t_{1/2} = 6$  hours, SPECT), indium-111 ( $t_{1/2} = 67$  hours, SPECT), and zirconium-89 ( $t_{1/2} = 78$  hours, PET), for the radiolabeling of larger biomolecules.

This shorter half-life does also have a drawback with regards to routine clinical applications. Whereas the possible radiolabeling chemistry with carbon-11 is extremely versatile, the short half-life has thus far practically confined the use of  $^{11}\text{C}$ -radiotracers to

facilities with on-site cyclotrons, typically larger, better-funded hospitals. As a comparison, by virtue of its 109.7 min half-life, fluorine-18 is amenable to central production and distribution models, allowing PET scans to be performed at sites without on-site cyclotrons or radiochemistry facilities. The possibility of such production/distribution models has arguably been a major contributor to the near-ubiquity of [ $^{18}\text{F}$ ]FDG PET compared with any  $^{11}\text{C}$ -diagnostic agent.

### ***1.3.1.2 Where does $^{11}\text{C}$ “fit in”?***

As a result of this isotopologous radiolabeling made possible with carbon-11, it is often the first radionuclide used in proof-of-concept studies. In the early stages of developing a method to image a particular target distribution or physiological pathway, often the first study will involve taking a previously published molecule (e.g. a high-affinity ligand for the target in question) and attempting to radiolabel that. While occasionally this may already contain a fluorine atom, an isotopologously radiolabeled version much more likely to be radiochemically accessible with carbon-11 (this is typically only constrained by the availability of radiosynthetic methodologies, there is almost always a carbon-12 atom that could *theoretically* be exchanged for a carbon-11). If the proof-of-concept imaging studies are promising using this  $^{11}\text{C}$ -radiolabeled compound, this can justify the development of more-versatile second generation  $^{18}\text{F}$ -radiolabeled radiotracers.

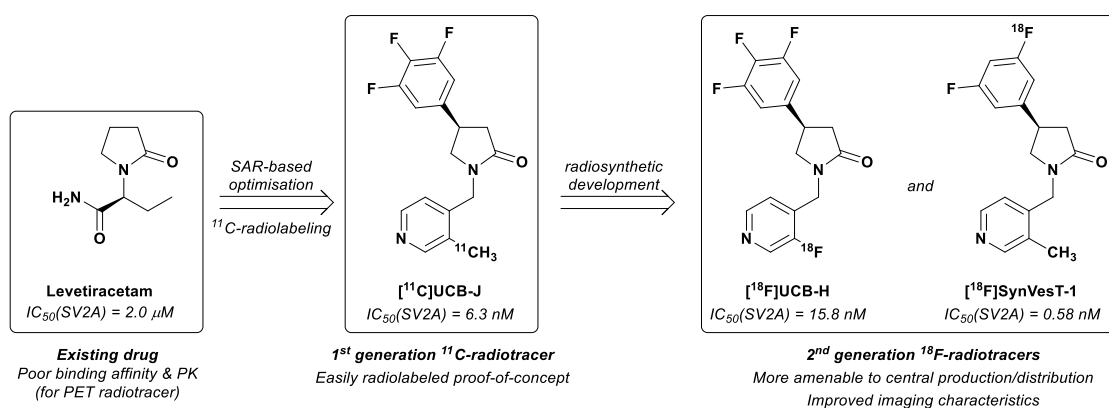


**Figure 1.9 Development of SV2A  $^{18}F$ -radiotracers via a 1<sup>st</sup> generation  $^{11}C$ -radiotracer**

$[^{11}C]$ UCB-J was the first-developed  $^{11}C$ -radiotracer for SV2A,<sup>51</sup> which proved the utility of imaging this target.<sup>52</sup> This was then built upon to develop the second generation radiotracers  $[^{18}F]$ UCB-H and  $[^{18}F]$ SynVesT-1.<sup>53,54</sup>

An example of such a radiotracer development process is in the development of synaptic density imaging, by targeting SV2A. The anti-epileptic drug levetiracetam was known to act (in part) by inhibition of SV2A,<sup>55</sup> but its poor binding affinity was insufficient for application as a radiotracer. However it was used as a starting point for structure activity relationship (SAR) optimisation, with the result being the generation of a series of single-digit nanomolar SV2A ligands, of which UCB-J was one.<sup>56</sup> The  $^{11}C$ -radiolabeling and PET imaging of  $[^{11}C]$ UCB-J demonstrated the utility of SV2A imaging, serving as a promising proof-of-concept.<sup>51,52</sup> This led to the development of newer second generation  $^{18}F$ -radiotracers, such as  $[^{18}F]$ SynVesT-1,<sup>53,54</sup> which should be theoretically more amenable to centralised production/distribution. A similar story can be seen in the development of radiotracers for TSPO: the first prototypical radiotracer for this was  $[^{11}C]$ PK11195, but this has since inspired the development of a number of different  $^{18}F$ -radiolabeled second generation radiotracers.<sup>57</sup>

### 1.3.1.3 Library $^{11}C$ -radiosynthesis

Another general application for which  $^{11}C$ -radiochemistry arguably shows a great deal of promise, is in “library  $^{11}C$ -radiosynthesis” for the higher-throughput screening of candidate molecules for  $^{18}F$ -based radiotracers. This is an idea put forth persuasively by Liang and Vasdev in their discussion of “total radiosynthesis”:<sup>58</sup> wherein they addressed possible strategies to improve the efficiency and productivity of the early stages of the

radiotracer development and assessment “pipeline”. Additionally, this strategy was described and advocated in the report from a consultants meeting convened by the IAEA for the discussion of the future directions of radionuclide imaging in neuroscience.<sup>59</sup>

Essentially, in approaching a new target for PET imaging, only a limited number of candidate <sup>18</sup>F-radiotracers for a particular target can be practically produced and screened, due to the laborious unique radiolabeling processes each candidate typically requires. This is due to the fact that fluorine-18 is typically incorporated at the periphery of any molecule. As such, across even a small library of candidate molecules, the <sup>18</sup>F-label will likely be in chemically inequivalent positions and require relatively divergent radiosynthetic methods for any late-stage <sup>18</sup>F-radiolabeling. By comparison, with the use of <sup>11</sup>C-carbonylation methods (covered in greater detail shortly),<sup>60</sup> <sup>11</sup>C-radiosynthesis allows for the installation of a radiolabel within the core of a molecule, in a position that likely remains relatively unchanged across a library of candidate radiotracers (<sup>11</sup>C-carbamate, <sup>11</sup>C-urea, or <sup>11</sup>C amide linkages are some examples of these). As such, a single <sup>11</sup>C-radiolabeling methodology can more easily be applied in the radiolabeling of an entire library of candidate compounds. This theoretically enables the higher-throughput preclinical screening of a larger library of candidate radiotracers. From this higher-throughput screening, the most promising candidate can be selected and a customised <sup>18</sup>F-radiosynthesis must only be developed for this one molecule.

As an example, such an approach was used to great effect by Wilson and Vasdev in their efforts to develop an <sup>18</sup>F-analogue to [<sup>11</sup>C]CURB, for the PET imaging of fatty acid amide hydrolase (FAAH).<sup>61</sup> The prototypical radiotracer for FAAH, [<sup>11</sup>C]CURB, is constructed around an *N*-cyclohexyl, *O*-biphenyl substituted <sup>11</sup>C-carbamate scaffold. The authors hoped to explore this scaffold, and simple amine and alcohol-based building blocks were used to generate a small library of candidate carbamates. 8 candidate radiotracers, each exhibiting high *in vitro* affinity for FAAH, were radiolabeled with a single <sup>11</sup>C-carbamate radiolabeling methodology, without any individual reaction optimisation. The radiotracers were assessed for their uptake and biodistribution behaviors, and the results indicated that the dihydrooxazole substituted ligands exhibited superior imaging characteristics. This led to the subsequent development of an analogous dihydrooxazole-containing <sup>18</sup>F-radiolabeled FAAH radiotracer, [<sup>18</sup>F]DOPP, that has shown promising performance in rodent and NHP imaging studies.<sup>62,63</sup>

### 1.3.2 Cyclotron $^{11}\text{C}$ -production

As was discussed briefly in a previous section, carbon-11 is produced in most medical cyclotrons by proton bombardment of a nitrogen-14 containing gas target, producing carbon-11 *via* the  $^{14}\text{N}(p,\alpha)^{11}\text{C}$  reaction. In addition to the  $^{14}\text{N}_2$ , the target gas is enriched with additional  $\text{O}_2$  or  $\text{H}_2$ , which will form the most-stable fully-oxidised or fully-reduced carbon containing compounds in-target:  $[^{11}\text{C}]\text{CO}_2$  or  $[^{11}\text{C}]\text{CH}_4$ . Due to the atmospheric abundance of  $\text{O}_2$  providing competition, a higher concentration of  $\text{H}_2$  (typically 10%) must be added to ensure selective production of  $[^{11}\text{C}]\text{CH}_4$ , whereas selective production of  $[^{11}\text{C}]\text{CO}_2$  can be achieved with just trace addition of  $\text{O}_2$  (typically 0.5-1%).<sup>45,64</sup> Due to the difficulties that can be encountered in the production of  $[^{11}\text{C}]\text{CH}_4$  in-target,<sup>65</sup> a majority of routine  $^{11}\text{C}$ -radiochemistry begins with  $[^{11}\text{C}]\text{CO}_2$  production in-target, even if it is immediately reduced to  $[^{11}\text{C}]\text{CH}_4$  as part of the subsequent radiosynthesis.<sup>66</sup>

### 1.3.3 Standard synthons

While some molecules can be radiolabeled in a single step, using  $[^{11}\text{C}]\text{CO}_2$  directly from the cyclotron, the compounds accessible with these methods have been (until recently) typically limited to  $^{11}\text{C}$ -carboxylic acids via reaction with Grignard reagents, since these are some of the only reagents powerful enough to overcome the inherent unreactivity of  $[^{11}\text{C}]\text{CO}_2$  (due to the strength of the  $\text{C}=\text{O}$  bonds). More commonly therefore, these less-reactive precursors are converted into secondary  $^{11}\text{C}$ -synthons which are more reactive, as well as enabling the isotopologous  $^{11}\text{C}$ -radiolabeling of different and less-oxidised functionalities, that would be otherwise inaccessible with carbon-11. This varied toolbox available to the carbon-11 radiochemist enables fairly complex organic synthesis even on timescales compatible with the half-life of carbon-11, with many different functionalities now radiochemically accessible via these synthons (a diagram showing some of the more prominent  $^{11}\text{C}$ -synthons is shown in Figure 1.10 below), and a selection of these will be discussed in more detail in this introduction.

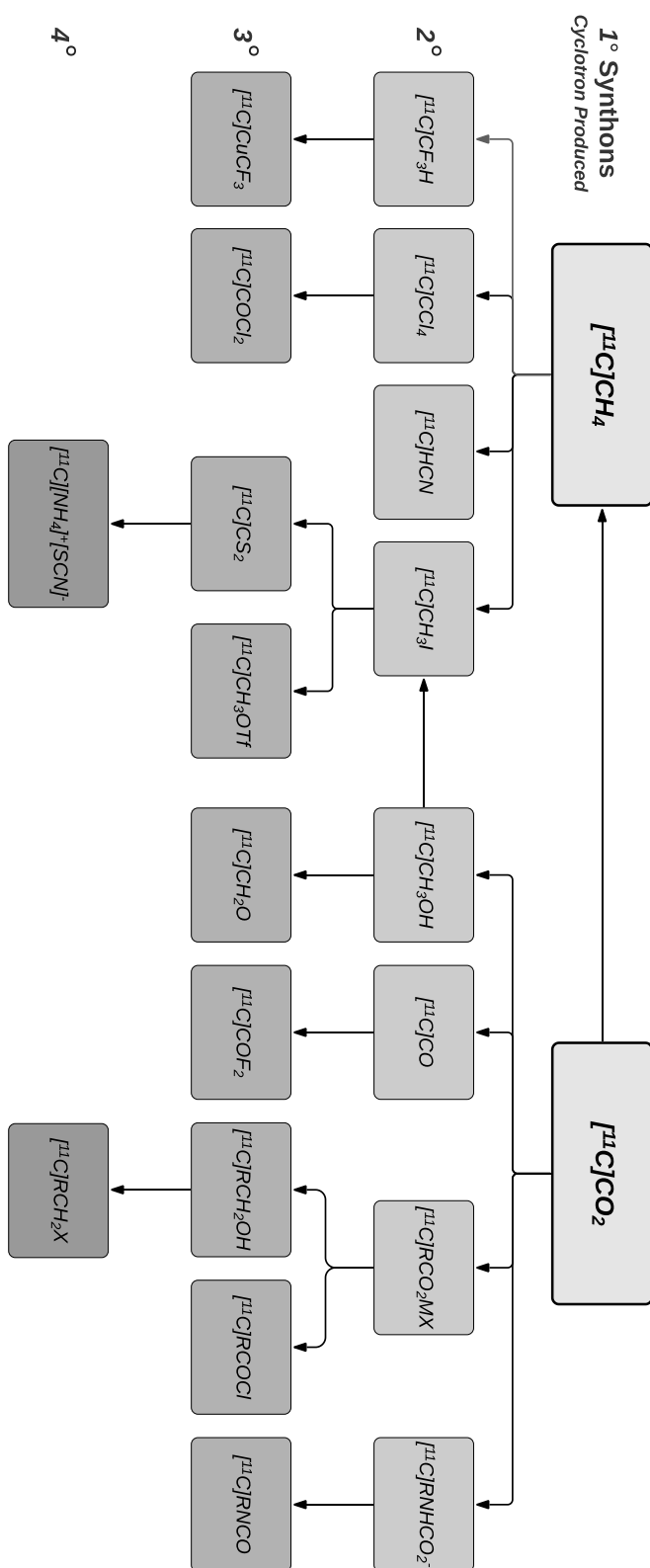


**Figure 1.10** Scheme of various  $^{11}\text{C}$ -synthons used for  $^{11}\text{C}$ -radiochemistry  
 Figure based upon similar schemes from Miller *et al.*,<sup>67</sup> and Yang *et al.*<sup>66</sup>

A major barrier to the more widespread use of many of the synthons in this “toolbox” is that it can require significant in-house radiochemical expertise to implement these in a lab (limiting the ease of implementation in facilities without the same level of experience), and additionally, the production of many of these  $^{11}\text{C}$ -synthons can require costly and/or custom-constructed production instrumentation. This can be acceptable if there are enough important applications of these methods to justify the purchase/construction and maintenance of this instrumentation, but for those  $^{11}\text{C}$ -synthons with fewer or more-niche applications, their widespread usage has remained fairly limited.

Take, for example, the case of [ $^{11}\text{C}$ ]phosgene ( $[^{11}\text{C}]\text{COCl}_2$ )<sup>68</sup> as a  $^{11}\text{C}$ -synthon for the radiolabeling of  $^{11}\text{C}$ -ureas and  $^{11}\text{C}$ -carbamates. While there are some interesting PET applications of  $^{11}\text{C}$ -radiolabeled urea and carbamate compounds (some of which are a major focus of this thesis),<sup>60,68,69</sup> the production of [ $^{11}\text{C}$ ]COCl<sub>2</sub> is challenging, requiring the use of elemental Cl<sub>2</sub> gas for the production of the intermediate [ $^{11}\text{C}$ ]CCl<sub>4</sub> followed by high temperature oxidation (at up to 750°C).<sup>70,71</sup> It therefore requires costly custom-built synthesis units, which serves as a prohibitive barrier to the wider implementation of this chemistry, due to its fairly niche radiolabeling applications.

As a counter-example, [ $^{11}\text{C}$ ]methyl iodide ( $[^{11}\text{C}]\text{CH}_3\text{I}$ ) is a  $^{11}\text{C}$ -synthon that also requires high temperature, multi-step preparation (generally using automated synthesis units). However, the chemical versatility, and practical ease of routine implementation of [ $^{11}\text{C}$ ]CH<sub>3</sub>I for the  $^{11}\text{C}$ -radiolabeling of *N*-, *O*-, and *S*-methyl functionalities,<sup>72</sup> in addition to the methods employing [ $^{11}\text{C}$ ]CH<sub>3</sub>I in Pd-mediated cross-coupling reactions,<sup>73</sup> evidently justify both the initial efforts in developing, and cost of purchasing automated synthesis units for the production of [ $^{11}\text{C}$ ]CH<sub>3</sub>I. This combination of factors has helped to make it easily the most widely and routinely used  $^{11}\text{C}$ -radiolabeling synthon.

### 1.3.4 $^{11}\text{C}$ -Methylation

The vast majority of  $^{11}\text{C}$ -radiolabeled compounds have been produced with the “workhorse” *N*-, *O*-, and *S*-methylation reactions using  $[^{11}\text{C}]\text{CH}_3\text{I}$ . The combination of the prevalence of these methylated-heteratomic motifs in a diverse range of biologically active compounds (endogenous biomolecules as well as pharmaceuticals), in addition to the simple, fast, and high-yielding nature of these radiolabeling reactions explains the relative dominance of this one radiolabeling approach within the carbon-11 literature.

#### 1.3.4.1 $[^{11}\text{C}]\text{CH}_3\text{I}$ production: the “wet method” vs the “gas-phase” method.

There are two major pathways by-which  $[^{11}\text{C}]\text{CH}_3\text{I}$  is produced. The first of these that was developed is what has come to be referred to as the “wet method”:<sup>74,75</sup> in this approach  $[^{11}\text{C}]\text{CO}_2$  is trapped in a solution containing  $\text{LiAlH}_4$  (generally in THF) where it is reduced to  $[^{11}\text{C}]\text{CH}_3\text{OH}$  *in situ*. The solvent is removed by evaporation and  $\text{HI}$  is added to complete the process by converting the  $[^{11}\text{C}]\text{CH}_3\text{OH}$  to  $[^{11}\text{C}]\text{CH}_3\text{I}$ . This is then distilled from the solution in a stream of inert carrier gas (*via* a  $\text{P}_2\text{O}_5$  drying trap) into the reaction vial containing the radiolabeling precursors and reagents in order to effect the  $^{11}\text{C}$ -methylation. It should be noted that subsequent developments of this method have used alternative iodinating reagents ( $\text{P}_2\text{I}_4$ , and polymer-supported  $\text{PPh}_3\text{I}_2$ ),<sup>76,77</sup> but the fundamental process remains largely the same.

By comparison, the more recently-developed “gas phase” method<sup>78,79</sup> begins with  $[^{11}\text{C}]\text{CH}_4$ , although due to the fact that many facilities only have access to  $[^{11}\text{C}]\text{CO}_2$  from the cyclotron, many of the instruments designed for the automation of this “gas phase”  $[^{11}\text{C}]\text{CH}_3\text{I}$  production method will also incorporate the necessary components to first achieve the  $[^{11}\text{C}]\text{CO}_2$  to  $[^{11}\text{C}]\text{CH}_4$  conversion (a high temperature Sabatier reduction over a nickel catalyst).<sup>78–80</sup> Following production of  $[^{11}\text{C}]\text{CH}_4$  (in target or *via*  $[^{11}\text{C}]\text{CO}_2$  reduction), it is heated in the presence of  $\text{I}_2$  vapour and a free-radical iodination reaction results in the formation of  $[^{11}\text{C}]\text{CH}_3\text{I}$ . This can be selectively trapped on a porapak column, removing the  $[^{11}\text{C}]\text{CH}_3\text{I}$  from the gas stream, while the remaining  $[^{11}\text{C}]\text{CH}_4$  is recirculated through the system to ensure high yielding conversions. The porapak column can then be heated to release the gaseous  $[^{11}\text{C}]\text{CH}_3\text{I}$  for delivery to a radiolabeling reaction vial.



$[^{11}\text{C}]\text{CH}_3\text{I}$  produced by either of these two methods can also be further converted to the more-reactive  $[^{11}\text{C}]\text{methyl triflate}$  ( $[^{11}\text{C}]\text{CH}_3\text{OTf}$ ) for reactions on more challenging substrates in-which its superior reactivity and volatility are required to achieve the best  $^{11}\text{C}$ -methylation performance.<sup>72,81</sup> This conversion is achieved by passing the  $[^{11}\text{C}]\text{CH}_3\text{I}$  through a silver triflate column at  $200^\circ\text{C}$ <sup>82</sup> and has become another “workhorse” reagent for  $^{11}\text{C}$ -methylation, with many automated synthesis units having triflate ovens incorporated as standard.<sup>83,84</sup>

#### ***1.3.4.2 Typical heteroatom methylations***

Most heteroatom methylations proceed in a similar fairly substrate-independent manner, without much requirement for operator intervention or reaction optimisation, indeed, this is one reason for the widespread adoption of  $^{11}\text{C}$ -methylation as a standard  $^{11}\text{C}$ -radiolabeling reaction. The  $[^{11}\text{C}]\text{CH}_3\text{I}$  is distilled into a vial containing a solution (in DMF, DMSO, or other aprotic solvents) of the desmethyl labeling precursor (typically an amine, aryl alcohol, or thiol) with an additional quantity of base ( $\text{K}_2\text{CO}_3$ ,  $\text{NaOH}$ ,  $\text{TBAOH}$ ) sometimes required for removal of the proton liberated during the nucleophilic substitution. The  $[^{11}\text{C}]\text{CH}_3\text{I}$  typically traps well in solution and is heated to  $80\text{-}130^\circ\text{C}$  for 2-10 mins to achieve near quantitative  $^{11}\text{C}$ -methylation yields.<sup>67,72,81</sup> Several representative examples of compounds radiolabeled with this approach are presented in Figure 1.11 below.

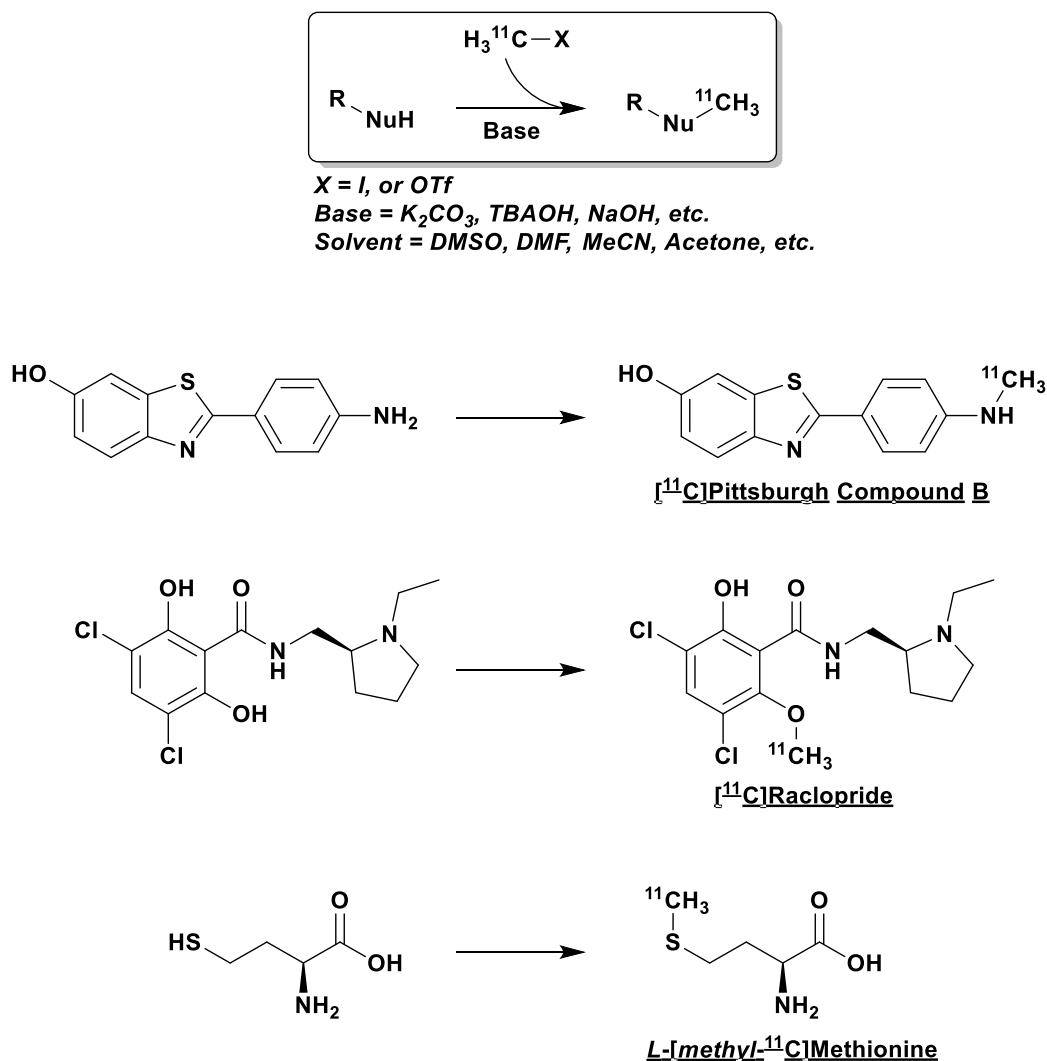


**Figure 1.11 Heteroatom <sup>11</sup>C-methylation – general procedure and examples**

*N*-, *O*-, and *S*-<sup>11</sup>C-methylations possible with [<sup>11</sup>C]CH<sub>3</sub>I and [<sup>11</sup>C]CH<sub>3</sub>OTf.

If the trapping efficiency of the gaseous [<sup>11</sup>C]CH<sub>3</sub>I is insufficient, [<sup>11</sup>C]CH<sub>3</sub>OTf can be used instead due to its reduced volatility making quantitative trapping in small solvent volumes easier. It should also be noted that due to the large excess (multiple orders of magnitude) of the desmethyl precursors relative to the total CH<sub>3</sub>I present in solution, no polyalkylation is observed in <sup>11</sup>C-methylation reactions compared with the analogous but stoichiometric non-radioactive methylation reactions.

### 1.3.4.3 Pd-mediated cross-coupling with $[^{11}\text{C}]\text{CH}_3\text{I}$

While these heteroatom  $^{11}\text{C}$ -methylation reactions are fantastic for incorporating carbon-11 into a variety of molecules, if there is no suitably nucleophilic heteroatom available for labeling, (or if this is a particularly metabolically labile position within the molecule) then these radiolabeling approaches are unavailable. However, it is highly likely that any PET centre with access to carbon-11 production facilities will also have an automated  $[^{11}\text{C}]\text{CH}_3\text{I}$  production system available, so any novel chemistry beginning from  $[^{11}\text{C}]\text{CH}_3\text{I}$  is of interest due to the lowered barrier-to-entry compared with other chemistry employing more novel intermediate synthons.

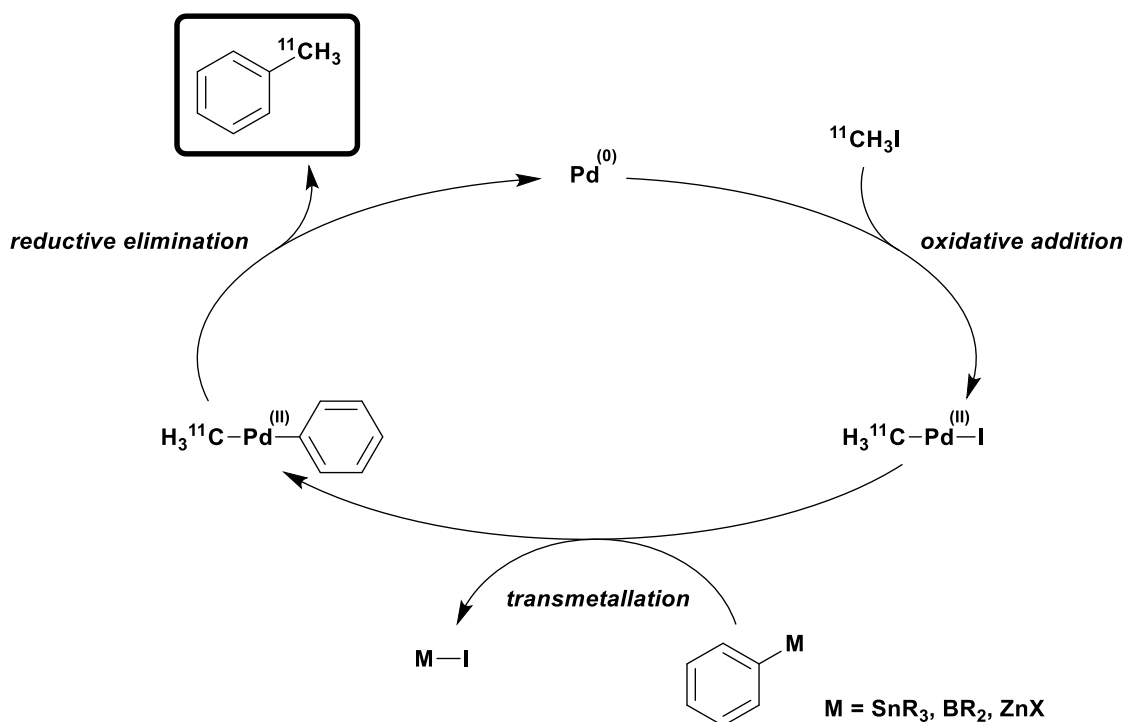


**Figure 1.12** Generic catalytic cycle of Pd-mediated cross couplings with  $[^{11}\text{C}]\text{CH}_3\text{I}$

Figure adapted from publication by Doi<sup>73</sup>

Beginning in the 1990s, several researchers (starting with the Långström group at Uppsala<sup>85</sup>) began developing methods for C- $^{11}\text{C}$  bond-formation using  $[^{11}\text{C}]\text{CH}_3\text{I}$  in Pd-mediated cross-coupling reactions. Typically, in a standard TM-catalysed cross-coupling reaction, an organometallic compound and an organohalide are coupled to produce the C-C bonded organic product (and the metal-halide byproduct). In these  $^{11}\text{C}$ -cross coupling reactions,  $[^{11}\text{C}]\text{CH}_3\text{I}$  is used as the organohalide component, and cross coupled

with aryl organometallic substrates to yield the Ar- $^{11}\text{C}$  product, see Figure 1.12 above for a generic catalytic cycle of these reactions. The development of these reactions opened a wide new area of chemical space to carbon-11 radiochemists, and is a highly valuable development.<sup>73</sup> The vast majority of these methods use organotin (Stille couplings)<sup>86–89</sup> and organoboron reagents (Suzuki-Miyaura couplings),<sup>85,90–93</sup> but there have been some examples of Negishi<sup>94</sup> and Sonogashira<sup>95</sup> type cross-couplings as well. In 2015, an excellent review summarising the development of this chemistry was published by Hisashi Doi,<sup>73</sup> which discussed not only the applications of these methods, but also their mechanistic underpinnings.

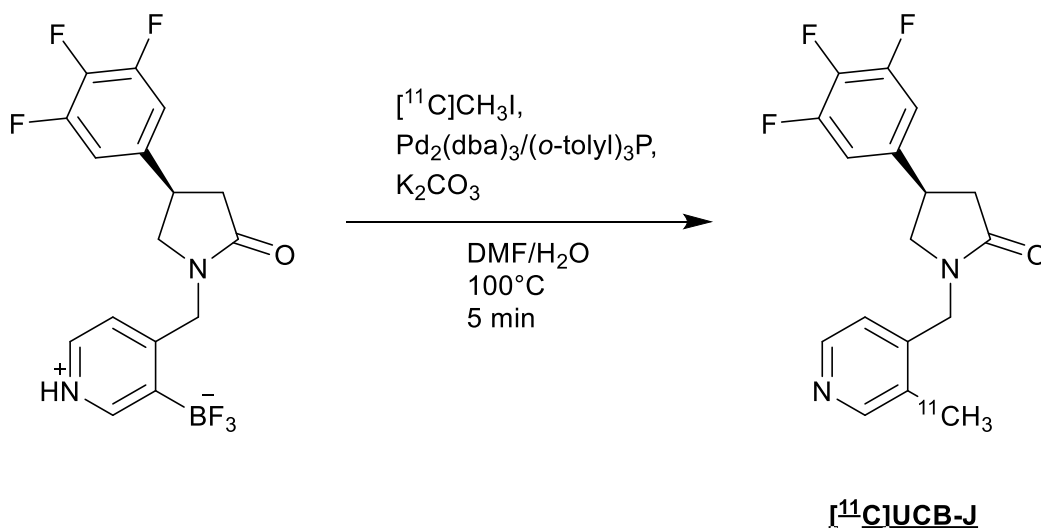


**Figure 1.13** Synthesis of  $[^{11}\text{C}]$ UCB-J via Pd-mediated cross-coupling with  $[^{11}\text{C}]\text{CH}_3\text{I}$

Figure adapted from work by Nabulsi *et al.*<sup>51</sup>

One example of a recent application of this methodology is the synthesis of  $[^{11}\text{C}]$ UCB-J in a Suzuki-Miyaura style cross-coupling with  $[^{11}\text{C}]\text{CH}_3\text{I}$ .<sup>51</sup> In this example, the boronic acid was first converted to the trifluoroborate salt (a substrate which is more resistant to protodeboronation) before performing a Pd-mediated cross coupling with  $[^{11}\text{C}]\text{CH}_3\text{I}$  (representing the first  $^{11}\text{C}$ -cross coupling using a trifluoroborate precursor).

### 1.3.5 $^{11}\text{C}$ -Carbonylation

#### 1.3.5.1 *Motivations*

The previous section has demonstrated the fantastic versatility of  $[^{11}\text{C}]\text{CH}_3\text{I}$  for the synthesis of  $^{11}\text{C}$ -methylated compounds, but even with the more recently developed cross-coupling chemistry, this chemistry is somewhat limiting with regards to the accessible chemical space as many target molecules of interest do not contain heteroatom-methyl positions to be radiolabeled. On this basis alone, there is a clear need for alternative  $^{11}\text{C}$ -radiolabeling methodologies; to enable the installation of a carbon-11 radiolabel in other more-diverse positions. While this is the primary motivation for the development of alternative  $^{11}\text{C}$ -radiolabeling strategies, there are several other instances in-which  $^{11}\text{C}$ -methylation may not be the best possible method for radiolabeling a target molecule, even in cases where a theoretically-radiolabellable heteroatom-methyl moiety is present.

Firstly, by only forming a single bond to the  $^{11}\text{C}$ -atom these methodologies inherently radiolabel at the periphery of molecules, these “tagging” approaches do not lend themselves readily to library  $^{11}\text{C}$ -radiosynthesis; since the peripheral functionalities of a molecule (of-which methylated heteratomic motifs are a prime example) are likely to be varied/modified across a compound screening library, one cannot easily radiolabel all candidates across the library (at-least without significant methodological modification/optimisation). As such, there is also the need for  $^{11}\text{C}$ -radiolabeling methodologies to enable access to more central positions within target compounds, as well as labeling more diverse functionalities than  $^{11}\text{C}$ -methyl groups. Such methods are theoretically able to be used in a more combinatorial manner;<sup>58,96</sup> that is to say that the  $^{11}\text{C}$ -atom can be incorporated within the covalent linking-unit joining two building-block reagents. This allows higher-throughput radiolabeling of target compound-libraries under more generalised conditions.

The class of methodologies discussed in this section meet these requirements, as they enable  $^{11}\text{C}$ -carbonylation: that is the  $^{11}\text{C}$ -radiolabeling of the core *carbonyl*-carbon within  $^{11}\text{C}$ -amides,  $^{11}\text{C}$ -ureas,  $^{11}\text{C}$ -carbamates,  $^{11}\text{C}$ -carbonates,  $^{11}\text{C}$ -aldehydes, and  $^{11}\text{C}$ -ketones. With the exception of the more-recently developed direct  $[^{11}\text{C}]\text{CO}_2$ -fixation

methodologies, which will be discussed separately in the section following this, the majority of these  $^{11}\text{C}$ -carbonyl products have generally been accessed *via* the reactive secondary synthons  $[^{11}\text{C}]\text{CO}$  ( $[^{11}\text{C}]$ carbon monoxide) and  $[^{11}\text{C}]\text{COCl}_2$  ( $[^{11}\text{C}]$ phosgene). More recently the usage of a promising novel  $^{11}\text{C}$ -carbonylation reagent has been reported,  $[^{11}\text{C}]\text{COF}_2$  ( $[^{11}\text{C}]$ carbonyl difluoride), with roughly comparable reactivity to  $[^{11}\text{C}]\text{COCl}_2$  but with a much more straightforward production route. This section will provide a brief overview of the production and usage of these  $^{11}\text{C}$ -carbonylation synthons.

### 1.3.5.2 $[^{11}\text{C}]$ Carbon monoxide

#### 1.3.5.2.1 Production

The development of transition-metal-mediated carbonylation chemistry has led – in recent years – to the more widespread usage of  $[^{11}\text{C}]\text{CO}$  as a versatile radiolabeling synthon.<sup>97–99</sup> Similarly to  $[^{11}\text{C}]\text{CH}_3\text{I}$ , the production methods of  $[^{11}\text{C}]\text{CO}$  *via* the reduction of  $[^{11}\text{C}]\text{CO}_2$  can be broadly classified as either “gas-phase”, or “wet” methods.

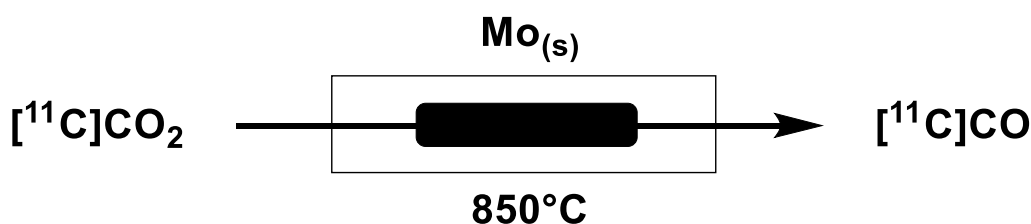


**Figure 1.14 “Gas-phase”  $[^{11}\text{C}]\text{CO}$  production method**

$[^{11}\text{C}]\text{CO}$  is produced by the reduction of gaseous  $[^{11}\text{C}]\text{CO}_2$  across a molybdenum-packed column at  $850^\circ\text{C}$

The “gas-phase” methods generally involve the passage of the cyclotron-produced  $[^{11}\text{C}]\text{CO}_2$  through heated columns packed with metal reductants, resulting in the on-line conversion of  $[^{11}\text{C}]\text{CO}_2$  to  $[^{11}\text{C}]\text{CO}$ . This has been achieved over zinc at  $400^\circ\text{C}$ ,<sup>100,101</sup> and more recently over zinc supported on fused silica at  $485^\circ\text{C}$ .<sup>102</sup> While these methods effectively convert the  $[^{11}\text{C}]\text{CO}_2$  to  $[^{11}\text{C}]\text{CO}$  under ideal conditions, the temperatures used (close to the  $420^\circ\text{C}$  melting point of zinc) as well as the effects of catalyst poisoning (by surface oxide formation) can lead to less reliable and more variable real-world performance. The most commonly used alternative method employs a molybdenum column heated at  $850^\circ\text{C}$ ,<sup>103</sup> which – while it requires a higher temperature than the zinc

methods – actually leads to a more robust performance across multiple sequential runs. The use of these molybdenum ovens has therefore seen a reasonably wide uptake in recent years, producing 70-80% conversion yields of  $[^{11}\text{C}]\text{CO}$ .<sup>97,98</sup>

While the “gas-phase” production methods are straightforward in their application, the fact that they require dedicated and expensive apparatus has limited the wider uptake of  $[^{11}\text{C}]\text{CO}$ -based carbonylation methods. Setting aside the immediate cost considerations that accompany specialised production apparatus, for many space-constrained radiochemistry facilities it can be difficult to justify the semi-permanent installation of a dedicated  $[^{11}\text{C}]\text{CO}$  production oven within the limited hot-cell space available, particularly when the existing applications of this synthon (although growing) are still relatively niche.

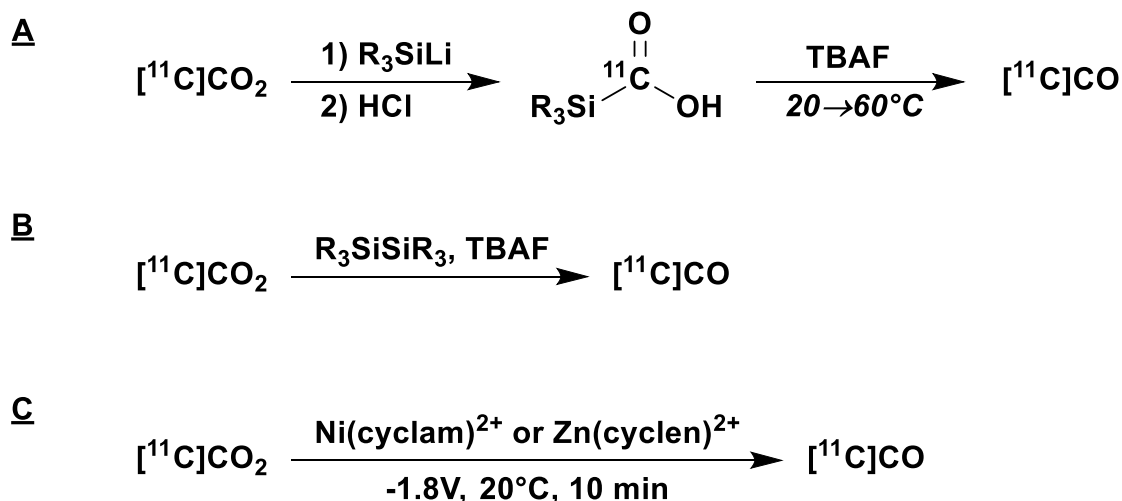


**Figure 1.15** “Wet”  $[^{11}\text{C}]\text{CO}$  production methods

Prominent examples of solution-based trap-reduce-and-release methods for  $[^{11}\text{C}]\text{CO}_2$  reduction. **A** is the 2 stage method in which the  $[^{11}\text{C}]\text{CO}_2$  first traps as an intermediate  $[^{11}\text{C}]\text{silicarboxylic acid}$ , before TBAF addition with gentle warming leads to decomposition and release of  $[^{11}\text{C}]\text{CO}$ ; **B** is the single step reaction of  $[^{11}\text{C}]\text{CO}_2$  with fluoride-activated disilanes to produce  $[^{11}\text{C}]\text{CO}$ ; **C** is the electroreduction of  $[^{11}\text{C}]\text{CO}_2$  to  $[^{11}\text{C}]\text{CO}$ , catalysed by metal electrocatalysts.

As an alternative to these “gas-phase” production methods, several groups have investigated alternative  $[^{11}\text{C}]\text{CO}$ -production methods employing solution-based chemical reduction approaches: the “wet” methods. Since these can be performed in-vial, the methods are theoretically more amenable to temporary implementation using pre-existing radiosynthesis units. The first example of this involved the trapping and reduction of

$[^{11}\text{C}]\text{CO}_2$  in a solution of lithium triethylborohydride (a strong reducing agent) to produce  $^{11}\text{C}$ -formate. This is followed by secondary conversion to  $^{11}\text{C}$ -formyl chloride, which subsequently decomposes to release  $[^{11}\text{C}]\text{CO}$ .<sup>104</sup> While this is an interesting method, and the first reported of its kind, it has yet to be replicated or employed by other groups. This could possibly be due to the highly reactive nature of the key lithio-organoboron reagent, with the consequential handling difficulties that this incurs.

Two alternative “wet” methods involve the reduction of  $[^{11}\text{C}]\text{CO}_2$  with organosilanes. The first of these reported was the trapping of  $[^{11}\text{C}]\text{CO}_2$  on freshly-prepared lithiosilanes, forming  $^{11}\text{C}$ -silacarboxylic acids *in situ*. The intermediate solution is then treated with TBAF (as a fluoride source) to initiate decomposition of this intermediate and release of  $[^{11}\text{C}]\text{CO}$  in an overall one-vial, two-step procedure.<sup>105,106</sup> The second method involves pre-activation of alkyl-substituted disilanes by treatment with TBAF to form an activated species. Upon bubbling of  $[^{11}\text{C}]\text{CO}_2$  through this solution, it reacts in a single step to release  $[^{11}\text{C}]\text{CO}$  and a disiloxane byproduct.<sup>107</sup> This procedure improved on the previous lithiosilane method by combining the organosilane and TBAF in solution prior to  $[^{11}\text{C}]\text{CO}_2$  bubbling, thus condensing the method to a single-step  $[^{11}\text{C}]\text{CO}$ -production.

One final method that has been reported is the electrochemical reduction of  $[^{11}\text{C}]\text{CO}_2$  to  $[^{11}\text{C}]\text{CO}$  in the presence of nickel or zinc electrocatalysts.<sup>108</sup> This method presents another promising alternative to the gas-phase production methods, but its relatively low-yielding nature ( $[^{11}\text{C}]\text{CO}_2$  conversion < 10%) means that further methodological development would be required before this method were practically applicable by other researchers.

The gas-phase production methods present several barriers to wider implementation of  $[^{11}\text{C}]\text{CO}$  as a synthon for  $^{11}\text{C}$ -carbonylation, as a result of the requirement for expensive dedicated apparatus. It is this major drawback which the “wet” methods aim to address, by enabling the chemical-reduction of  $[^{11}\text{C}]\text{CO}_2$  to  $[^{11}\text{C}]\text{CO}$  in-vial, using pre-existing radiosynthetic apparatus. However, one key area where the gas-phase methods excel is in their simplicity of operation: maintenance of the zinc or molybdenum columns is only required periodically, compared to the fresh preparation of solutions and reagents as required by the alternative “wet” methods. Another is related to the theoretically achievable molar activities: the solutions used for “wet”  $[^{11}\text{C}]\text{CO}_2$  reductions are theoretically capable of reacting with any adventitious  $[^{12}\text{C}]\text{CO}_2$  as a result of atmospheric



contamination, leading to isotopic dilution and resulting in a significantly reduced molar activity. As such, solutions must be prepared under strictly-controlled inert atmospheres, and care must be taken when transferring these solutions into the radiosynthetic apparatus so as to avoid any atmospheric exposure. By comparison, the inert gas purging of gas-phase production columns before heating (it is only upon heating that they are able to convert CO<sub>2</sub> to CO) allows for greater control over atmospheric contamination, and therefore enables theoretically superior molar activities. While both production methods have use cases in-which they are more appropriate, in any case, these imperfect [<sup>11</sup>C]CO production methods present significant barriers to the wider uptake of <sup>11</sup>C-carbonylation chemistry.

#### ***1.3.5.2.2 Overcoming poor solubility of [<sup>11</sup>C]CO***

While [<sup>11</sup>C]CO is a more reactive synthon than [<sup>11</sup>C]CO<sub>2</sub>, it is sparingly soluble in most organic solvents.<sup>109–112</sup> Therefore, unlike [<sup>11</sup>C]CH<sub>3</sub>I which can be added to a reaction simply by bubbling the gaseous reagent through a vial containing the other reagents in solution, bubbling [<sup>11</sup>C]CO at atmospheric pressure through a reaction solution will only lead to a poor trapping efficiency, with the majority of the [<sup>11</sup>C]CO passing through the solution without dissolution or reaction (typically, less than 10% trapping efficiency is achieved with a single passthrough).<sup>101</sup> As such, one of the major avenues of [<sup>11</sup>C]CO research has focused on innovative approaches to overcome this inherently poor solubility: if the [<sup>11</sup>C]CO cannot be effectively brought into solution, then no further reactions can be performed upon it, regardless of how promising or versatile the reactivity is in theory. A representative selection of these approaches are summarised in Figure 1.16 below.

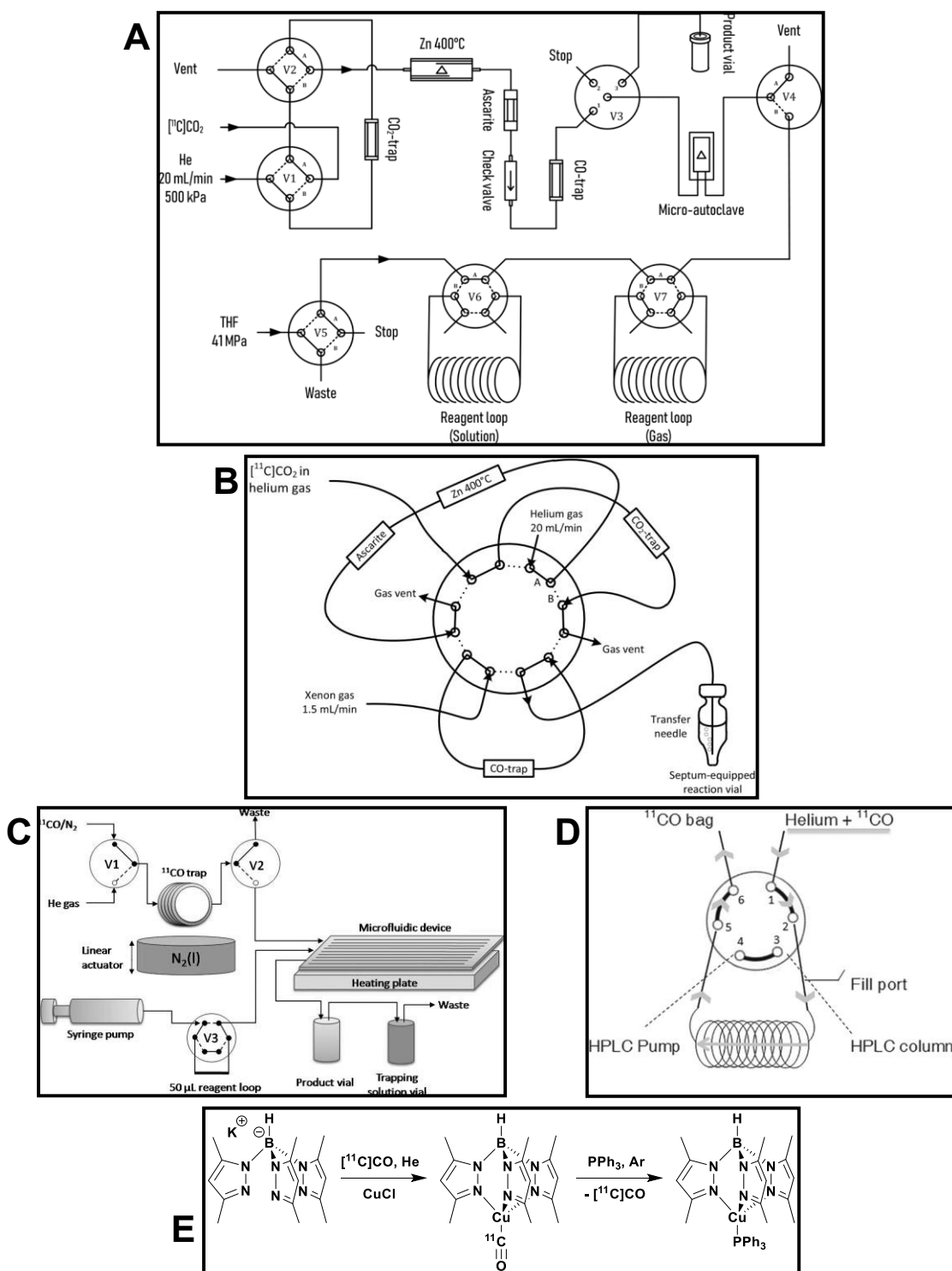


**Figure 1.16** Methods used to overcome poor solubility of  $[^{11}\text{C}]\text{CO}$

**A)** High-pressure autoclave<sup>98,113</sup> (reproduced under CC-BY); **B)** Xenon carrier-gas in sealed vial<sup>98,114</sup> (reproduced under CC-BY); **C)** Microfluidic reactor<sup>115</sup> (reproduced with permission); **D)** In-loop reaction<sup>116</sup> (reproduced under CC-BY-NC); **E)** Chemical trapping with copper (I) scorpionate.<sup>117</sup>

An early approach to this poor [ $^{11}\text{C}$ ]CO solubility, while theoretically simple, was fairly effective: gas recirculation. While a single passthrough at atmospheric pressure tends to result in a <10% trapping efficiency,<sup>101</sup> Långstrom and coworkers developed a system for recirculation of the [ $^{11}\text{C}$ ]CO gas through the reaction solution, achieving 80% trapping efficiencies after 5 min recirculation.<sup>118</sup> An alternative approach involved the use of a high-pressure autoclave to confine the [ $^{11}\text{C}$ ]CO gas under high pressure (400-500 kPa) in contact with the reaction solution, enhancing its dissolution, resulting in essentially quantitative trapping efficiency.<sup>113,119,120</sup> A significant caveat is that unlike most synthesis units based on either disposable cassettes or glass reaction vessels, the central autoclave reactor cannot easily be removed for cleaning or replacement.<sup>98,121</sup> This raises concerns regarding the practical prospect of using such an approach for GMP-grade manufacture of multiple different radiotracers due to the risk of contamination, the so called “carry-over effect”.<sup>121</sup>

To avoid the installation and maintenance of any such instrumentation required to achieve and maintain these high-pressure setups, several alternative low-pressure approaches have been taken to enhance the solubility, and by extension the reactivity, of [ $^{11}\text{C}$ ]CO. One promising approach has seen the use of xenon as a carrier gas for [ $^{11}\text{C}$ ]CO delivery into sealed reaction vials.<sup>114,122</sup> [ $^{11}\text{C}$ ]CO delivery with more-routinely used carrier gases (nitrogen, helium, argon) into unvented reactor vials would result in a build-up of backpressure within the system. By comparison, xenon is highly soluble in THF, and therefore delivery of [ $^{11}\text{C}$ ]CO in a stream of xenon does not result in a significant backpressure buildup, even in fully-sealed and unvented reaction vials. This ultimately leads to near quantitative trapping of the [ $^{11}\text{C}$ ]CO within the THF solution and has been used successfully for a great number of different  $^{11}\text{C}$ -carbonylations.<sup>97,98</sup> Another interesting low-pressure option that has been explored, involves the use of microfluidics for  $^{11}\text{C}$ -carbonylation.<sup>115,123</sup> In this approach, [ $^{11}\text{C}$ ]CO carrier gas and the reaction solution are mixed at the inlet of a long-channel glass-fabricated microreactor, imposing an annular or gas-liquid segmented flow-regime through the microchannel which results in a very high gas-liquid interfacial contact area; ultimately resulting in 80-90% trapping efficiencies.

Finally, the most recent example of process innovation in this space is in the development by Ferrat *et al.*, of an “in-loop” [ $^{11}\text{C}$ ]CO trapping setup, an analogous approach to that

popularised by Wilson *et al.*, in their seminal-method for “in-loop”  $^{11}\text{C}$ -methylation (a full discussion of the development of these methods will follow in chapter 2). In this approach, the reaction solution is loaded into an HPLC sample loop, the  $[^{11}\text{C}]\text{CO}$  is passed through this loop and traps in the liquid on the inside surface of the loop. Similarly to the microfluidic approach, this results in a high gas-liquid interfacial contact area, enhancing the trapping efficiency in a single pass. This method has also been successfully adapted and expanded upon by Donnelly *et al.* in their  $^{11}\text{C}$ -radiolabeling of a number of Bruton’s Tyrosine Kinase inhibitors.<sup>124</sup> These “macrofluidic” approaches give many of the benefits of microfluidic setups without the requirement for highly specialised and expensive equipment.

In addition to these physical process innovations, there have been chemical trapping approaches employed to bring the  $[^{11}\text{C}]\text{CO}$  into solution efficiently. The most prominent of these is the method, developed by Kealey *et al.*, using copper scorpionate (copper(I) tris(pyrazolyl)borate). These scorpionate species efficiently (>99%) trap  $[^{11}\text{C}]\text{CO}$  in a single pass at ambient temperatures and pressures. The addition of phosphines to scorpionate complexes displaces carbonyl ligands,<sup>125</sup> and so the addition of a solution containing a palladium pre-catalyst (with excess phosphine ligand) results in the re-release of the trapped  $[^{11}\text{C}]\text{CO}$ , followed immediately by a  $^{11}\text{C}$ -carbonylation reaction in solution.

While the methods presented above represent several effective approaches to facilitate the dissolution and reaction of  $[^{11}\text{C}]\text{CO}$ , the highly complex nature of the dedicated equipment makes their wider implementation less feasible in other laboratories.

#### **1.3.5.2.3 Transition metal-mediated $^{11}\text{C}$ -carbonylations**

$[^{11}\text{C}]\text{CO}$  incorporation into organic molecules is most commonly achieved with transition metal mediated carbonylative cross couplings (most commonly Palladium catalysed).<sup>97,98</sup> These methodologies generally operate under mild conditions and are tolerant of a range of substrate functionalities.<sup>99,126</sup> The development of this chemistry was very recently summarised in an excellent and comprehensive review by Eriksson *et al.*,<sup>98</sup> but its application in the synthesis of  $^{11}\text{C}$ -ureas will be discussed here.

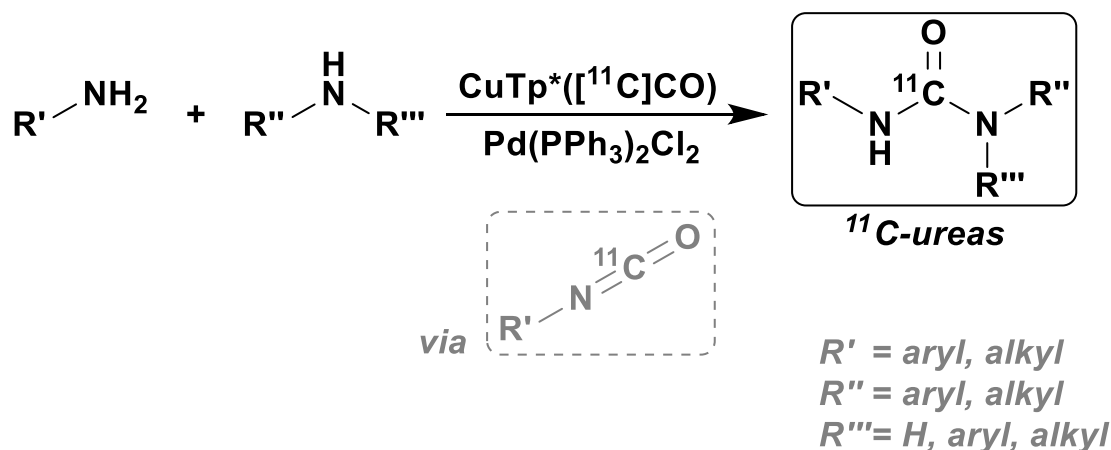


**Figure 1.17 Synthesis of  $^{11}\text{C}$ -ureas *via* carbonylative Pd-coupling<sup>127</sup>**

For symmetric ureas, coupling performed with primary aromatic or aliphatic amines. For asymmetric ureas, coupling performed with aromatic or aliphatic primary amine and an aliphatic secondary amine, to produce trisubstituted  $^{11}\text{C}$ -ureas. As the reaction proceeds *via* formation of an  $^{11}\text{C}$ -isocyanate, tetrasubstituted  $^{11}\text{C}$ -ureas are inaccessible.  $\text{CuTp}^*([^{11}\text{C}]\text{CO})$  indicates the prior trapping and activation of  $[^{11}\text{C}]\text{CO}$  in solution on a scorpionate complex.<sup>117</sup>

Whilst Pd-mediated  $^{11}\text{C}$ -carbonylation has been more-widely applied to the synthesis of  $^{11}\text{C}$ -ketones<sup>101,128</sup> and  $^{11}\text{C}$ -amides,<sup>129,130</sup> for the purposes of this thesis it is most important to consider the synthesis of  $^{11}\text{C}$ -ureas by oxidative carbonylative cross coupling. Initially reported by Kealey *et al.*<sup>117</sup> and expanded by Roslin *et al.*,<sup>131</sup> it was shown that this methodology proceeds *via* the formation of an  $^{11}\text{C}$ -isocyanate intermediate which reacts with a second (primary or secondary) amine molecule to form the  $^{11}\text{C}$ -urea product, precluding the synthesis of tetrasubstituted  $^{11}\text{C}$ -ureas.

This methodology was also limited with regards to its product selectivity: whilst symmetric  $^{11}\text{C}$ -ureas were relatively straightforward to produce with this approach, the only asymmetric  $^{11}\text{C}$ -ureas reported by either Kealey or Roslin were tri-substituted. For these, asymmetric selectivity is achieved as a result of the fact that the reaction proceeds *via* the formation of an  $^{11}\text{C}$ -isocyanate intermediate. As such, if only one of the two amines (the primary amine) is capable of forming this  $^{11}\text{C}$ -isocyanate intermediate, the reagent stoichiometry can be altered to use an excess of the corresponding secondary amine, selectively favouring the formation of the asymmetric  $^{11}\text{C}$ -urea product. Such an approach is not applicable to the synthesis of asymmetric  $N,N'$ -disubstituted  $^{11}\text{C}$ -ureas, however, due to the fact that both amine substrates are theoretically able to form  $^{11}\text{C}$ -

isocyanates. Transition metal-mediated  $^{11}\text{C}$ -carbonylations are arguably better-suited to the synthesis of  $^{11}\text{C}$ -amides and ketones, with the synthesis of  $^{11}\text{C}$ -ureas from  $[^{11}\text{C}]\text{CO}$  being somewhat limited in scope.

### 1.3.5.3 $[^{11}\text{C}]\text{Phosgene}$

Prior to the advent of direct  $[^{11}\text{C}]\text{CO}_2$  fixation approaches<sup>132</sup> (to be discussed in section 1.4),  $[^{11}\text{C}]\text{phosgene}$  ( $[^{11}\text{C}]\text{COCl}_2$ ) has been the most reliable route to the production of  $^{11}\text{C}$ -ureas and  $^{11}\text{C}$ -carbamates, by enabling the insertion of a  $^{11}\text{C}$ -carbonyl moiety between two heteroatoms.<sup>68</sup> However its wider availability has remained limited as a result of its troublesome production routes requiring specialized apparatus with constant upkeep and maintenance required.<sup>60,67,68</sup>

#### 1.3.5.3.1 Production

There have been a number of different methods developed for the production of  $[^{11}\text{C}]\text{COCl}_2$ ; originally it was produced from  $[^{11}\text{C}]\text{CO}$ , either with UV-initiated free-radical chlorination with  $\text{Cl}_2$  gas,<sup>133</sup> or by reaction with  $\text{PtCl}_4$  at elevated temperatures ( $430^\circ\text{C}$ ).<sup>134</sup> However these methods were relatively complex and inconsistent, so it is now generally produced by one of several methods involving the intermediate production of  $[^{11}\text{C}]\text{CCl}_4$ .

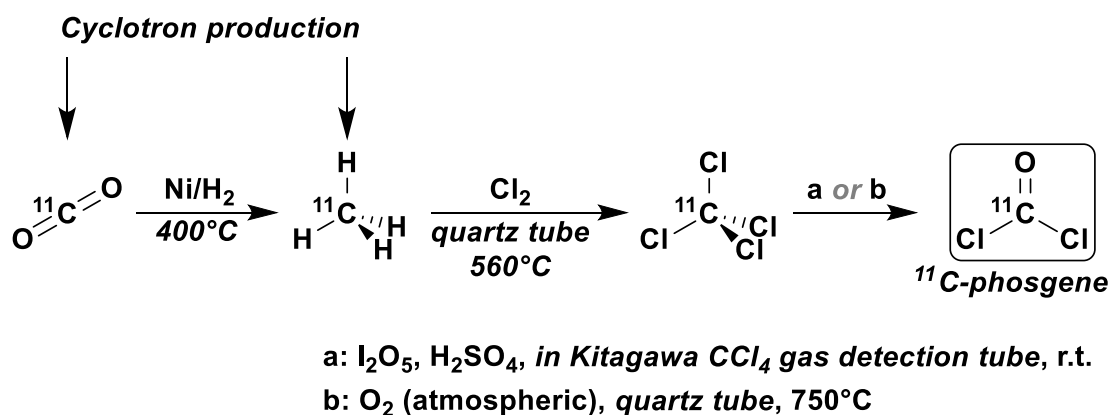


**Figure 1.18** Production of  $[^{11}\text{C}]\text{COCl}_2$  from  $[^{11}\text{C}]\text{CH}_4$  or  $[^{11}\text{C}]\text{CO}_2$  via  $[^{11}\text{C}]\text{CCl}_4$ <sup>70,71</sup>

Method **a** uses a commercially available Kitagawa gas detection tube.<sup>70</sup>  
 Method **b** uses a heated empty quartz tube without added  $\text{O}_2$ .<sup>71</sup>

These alternative methods first involve the conversion of  $[^{11}\text{C}]\text{CH}_4$  (commonly derived from  $[^{11}\text{C}]\text{CO}_2$ ) to  $[^{11}\text{C}]\text{CCl}_4$ , and while many approaches for this chlorination have been developed,<sup>60,68</sup> the most commonly used has involved the heating of  $[^{11}\text{C}]\text{CH}_4$  and elemental chlorine gas ( $\text{Cl}_2$ ) in an empty quartz tube at 530-560°C.<sup>135</sup> Following the chlorination step, the  $[^{11}\text{C}]\text{CCl}_4$  must be oxidised to  $[^{11}\text{C}]\text{COCl}_2$ . Again, while several methods have been proposed for this, often involving oxidation over iron or iron oxide,<sup>135</sup> the two most-simple and reliable are arguably the methods from Ogawa *et al.*,<sup>70</sup> and Bramoullé *et al.*<sup>71</sup> The method from Ogawa *et al.* (route **a** in Figure 1.18 above) involves passing the  $[^{11}\text{C}]\text{CCl}_4$  at room temperature through a commercially obtained Kitagawa  $\text{CCl}_4$  gas detection tube. These tubes contain immobilised sources of  $\text{I}_2\text{O}_5$  and  $\text{H}_2\text{SO}_4$ , which serve to efficiently oxidise the  $[^{11}\text{C}]\text{CCl}_4$  to  $[^{11}\text{C}]\text{COCl}_2$ , with an 80-90% conversion efficiency at 50 mL/min. In the alternative method from Bramoullé *et al.* (route **b**),  $[^{11}\text{C}]\text{CCl}_4$  is oxidised through an empty quartz tube heated to 750°C. In this method, no additional  $\text{O}_2$  is required, with either contamination in the carrier gas or on the surface of the quartz being sufficient to effect reasonably efficient (~ 40%) oxidation.

The major issues with any of these routes is the unavoidable usage of elemental  $\text{Cl}_2$  gas, a highly corrosive and hazardous gas. This necessitates careful handling protocols and tedious regular maintenance of synthesis systems and seals etc. In addition to these specific drawbacks of chlorine usage, all methods, even those employing the Kitagawa detection tube, require multiple high-temperature gas-phase reactions. This therefore requires the construction or adaptation of specialized production apparatus. As a result of these highly operationally-inconvenient production routes, there is today very-little widespread usage of  $[^{11}\text{C}]\text{COCl}_2$ , regardless of any potential appeal or interesting radiochemistry it could enable.

### 1.3.5.3.2 $^{11}\text{C}$ -Urea synthesis: symmetric and cyclic products

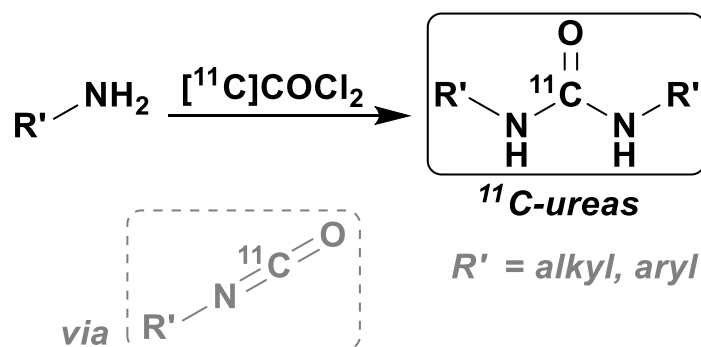


**Figure 1.19 Production of symmetric  $^{11}\text{C}$ -ureas from  $[^{11}\text{C}]\text{COCl}_2$**

$[^{11}\text{C}]\text{COCl}_2$  initially reacts with one molecule of amine to form  $^{11}\text{C}$ -isocyanate intermediate, this reacts rapidly with a second amine molecule

The central carbon within phosgene is highly electrophilic, and as such, it will react readily with nucleophiles, the reaction of a primary amine with  $[^{11}\text{C}]\text{COCl}_2$  produces an  $^{11}\text{C}$ -isocyanate. These  $^{11}\text{C}$ -isocyanates are also highly reactive with nucleophiles and will therefore tend to react immediately with a second amine molecule (always present in excess, relative to the sub nanomolar quantities of  $^{11}\text{C}$ -radiolabeled species present) to form the corresponding symmetric  $^{11}\text{C}$ -urea. As a result, symmetric disubstituted  $^{11}\text{C}$ -ureas can be formed by distilling  $[^{11}\text{C}]\text{COCl}_2$  into a solution of primary amine, and at room temperature the reaction is essentially instantaneous and quantitative.<sup>133</sup> By itself however, a method for the synthesis of symmetric  $^{11}\text{C}$ -ureas is of limited utility due to the general scarcity of biologically active symmetric ureas, although there are some promising symmetric inhibitors of soluble epoxide hydrolase.<sup>136</sup>



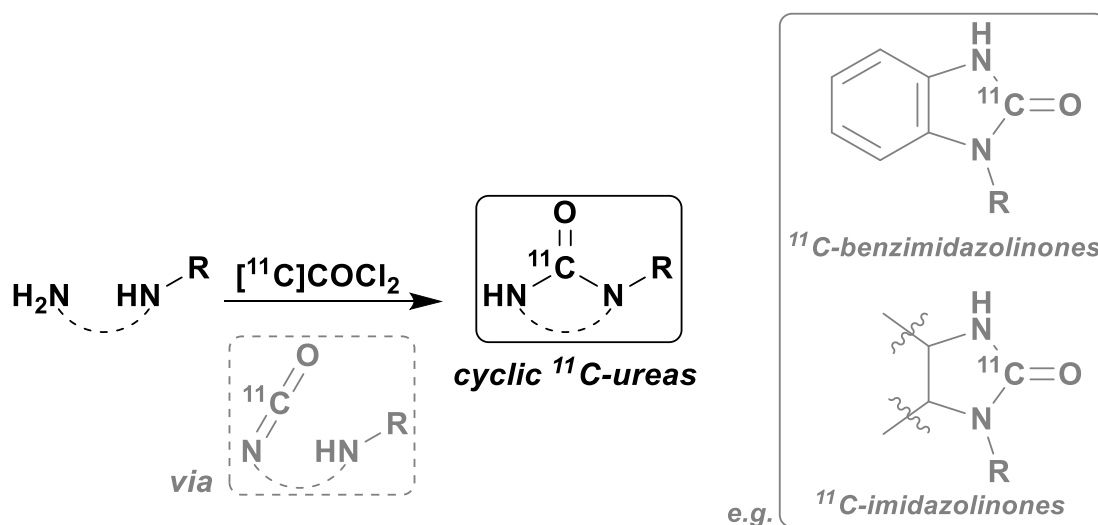


**Figure 1.20 Production of cyclic intramolecular  $^{11}\text{C}$ -ureas from  $[^{11}\text{C}]\text{COCl}_2$**

$[^{11}\text{C}]\text{COCl}_2$  initially reacts with one amine to form an  $^{11}\text{C}$ -isocyanate which rapidly reacts with the nearby second amine moiety to form a cyclic  $^{11}\text{C}$ -urea (commonly  $^{11}\text{C}$ -benzimidazolinones or  $^{11}\text{C}$ -imidazolinones).

Notably however, a similarly simple synthetic method can be applied extremely effectively in the radiosynthesis of cyclic  $^{11}\text{C}$ -ureas ( $^{11}\text{C}$ -benzimidazolinones and  $^{11}\text{C}$ -imidazolinones), a much more commonly encountered motif in biologically relevant molecules. These methods proceed again by the initial reaction of the  $[^{11}\text{C}]\text{COCl}_2$  with a primary amine moiety on the substrate to form an  $^{11}\text{C}$ -isocyanate intermediate. Whilst this could theoretically react with another molecule of the amine precursor to form a symmetrical  $^{11}\text{C}$ -urea, it is much more likely to react intramolecularly with the nearby amine that is well positioned to immediately capture this  $^{11}\text{C}$ -isocyanate, leading to a strong preference for the formation of the cyclic  $^{11}\text{C}$ -urea derivative. Such methods have been employed with great success to label a great number of molecules of interest (recently reviewed comprehensively by Fukumura *et al.*).<sup>68</sup> One example of this is in the radiosynthesis of  $[^{11}\text{C}]\text{CGP12177}$ , a benzimidazolinone derivative used for imaging of the  $\beta$ -adrenergic system.<sup>137,138</sup>

### 1.3.5.3.3 $^{11}\text{C}$ -Urea synthesis: asymmetric products

The most challenging target molecules for  $[^{11}\text{C}]\text{COCl}_2$ -mediated carbonylations are the asymmetric disubstituted  $^{11}\text{C}$ -ureas. As a result of the highly reactive nature of the intermediate  $^{11}\text{C}$ -isocyanate, it is difficult to isolate this *in situ*, as it tends to immediately

react with any nucleophiles available in solution. Generally this occurs with another molecule of the initial amine, producing the undesired symmetric  $^{11}\text{C}$ -urea byproduct.

One approach to this problem has relied on the direct reaction of  $[^{11}\text{C}]\text{COCl}_2$  with amines in their less-nucleophilic hydrochloride salt forms at low temperatures ( $< -15^\circ\text{C}$ ).<sup>139</sup> Under these conditions, the extremely highly-reactive  $[^{11}\text{C}]\text{COCl}_2$  is still able to produce the intermediate  $^{11}\text{C}$ -isocyanate as previously. However, while isocyanates are generally considered to be highly reactive, they are generally less reactive than phosgene itself; as a result of the lowered temperatures, as well as the presence of amines in their less-nucleophilic hydrochloride salts, the  $^{11}\text{C}$ -isocyanate to symmetric  $^{11}\text{C}$ -urea conversion does not occur under these conditions. This allows the addition of a stoichiometric excess of the second amine component (as the more reactive free-base), which preferentially reacts to give the desired asymmetric  $^{11}\text{C}$ -urea upon warming. While it has been used successfully in the radiosynthesis of [*carbonyl*- $^{11}\text{C}$ ]sorafenib,<sup>140</sup> this approach is somewhat limited and tends to work better with less nucleophilic aniline based substrates.

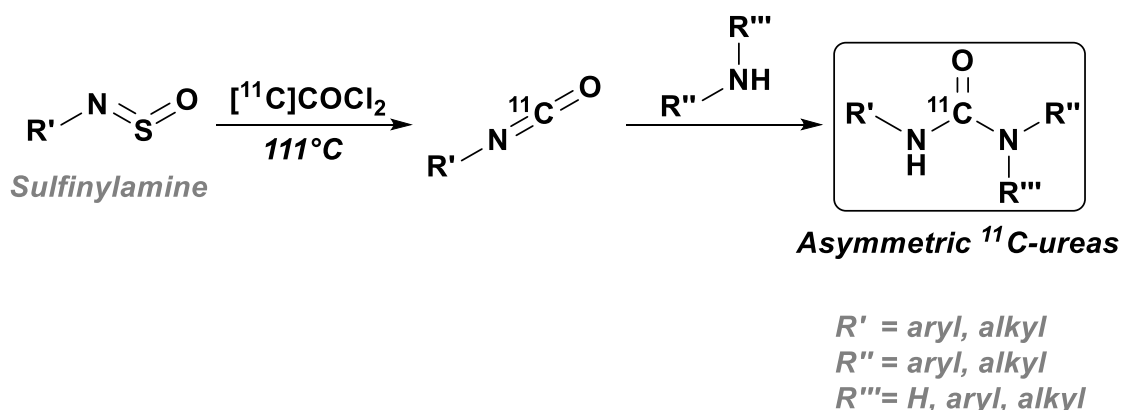


**Figure 1.21 Asymmetric  $^{11}\text{C}$ -ureas from  $[^{11}\text{C}]\text{COCl}_2$  via “masked amines”<sup>141</sup>**

$[^{11}\text{C}]\text{COCl}_2$  initially reacts with a sulfinylamine at high temperatures to produce the  $^{11}\text{C}$ -isocyanate which cannot react further to produce a symmetric  $^{11}\text{C}$ -urea byproduct. A second amine substrate is then added, effecting the clean conversion of this isolated  $^{11}\text{C}$ -isocyanate to the asymmetric  $^{11}\text{C}$ -urea product.

Another innovative approach to this problem was to first convert the initial amine substrate to a less-reactive sulfinylamine species: a so-called “masked” amine.<sup>141</sup> At elevated temperatures these sulfinylamine derivatives are still capable of reacting with  $[^{11}\text{C}]\text{COCl}_2$  to produce an  $^{11}\text{C}$ -isocyanate intermediate. However this  $^{11}\text{C}$ -isocyanate is not able to form the symmetric urea as there is no amine present in solution and it is

insufficiently reactive to directly interact with the sulfinylamine. Following the synthesis of this isolated  $^{11}\text{C}$ -isocyanate, a non-masked amine can be added to the reaction leading to the selective formation of the asymmetric  $^{11}\text{C}$ -ureas.

#### 1.3.5.4 [ $^{11}\text{C}$ ]Carbonyl difluoride

During the preparation of this thesis, Jakobsson *et al.* published their synthesis and application of a novel and highly promising C-1 synthon for  $^{11}\text{C}$ -radiolabeling, [ $^{11}\text{C}$ ]carbonyl difluoride ([ $^{11}\text{C}$ ]COF<sub>2</sub>).<sup>142,143</sup> In many ways – from the limited data available thus far – it appears that the reactivity of [ $^{11}\text{C}$ ]COF<sub>2</sub> is roughly comparable to that of the previously-described [ $^{11}\text{C}$ ]COCl<sub>2</sub>. However, the major difference between these two is in the vastly simplified production route for [ $^{11}\text{C}$ ]COF<sub>2</sub>. Whereas [ $^{11}\text{C}$ ]COCl<sub>2</sub> production requires the high temperature conversion of [ $^{11}\text{C}$ ]CO<sub>2</sub> to [ $^{11}\text{C}$ ]CH<sub>4</sub>, before the problematic chlorination (usually using the highly corrosive and hazardous Cl<sub>2</sub> gas) to produce [ $^{11}\text{C}$ ]CCl<sub>4</sub>, followed by a final oxidation (at elevated temperatures, or in a commercially obtained Kitagawa gas detection tube) to produce [ $^{11}\text{C}$ ]COCl<sub>2</sub>. By comparison with this troublesome and exceedingly difficult to set-up and maintain synthon production, [ $^{11}\text{C}$ ]COF<sub>2</sub> is vastly simpler and more accessible.

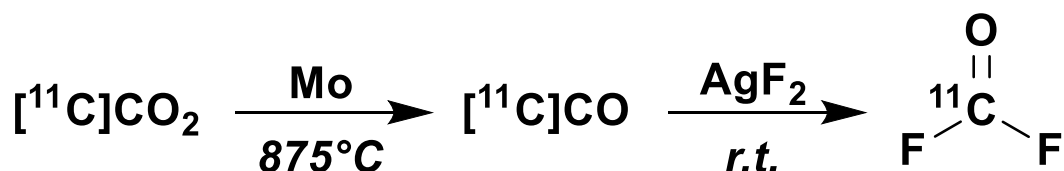


**Figure 1.22** Production of [ $^{11}\text{C}$ ]COF<sub>2</sub> from [ $^{11}\text{C}$ ]CO<sub>2</sub> via [ $^{11}\text{C}$ ]CO<sup>142</sup>

Produced by single-pass conversion of [ $^{11}\text{C}$ ]CO through a silver(II) fluoride cartridge at r.t.

The production of [ $^{11}\text{C}$ ]COF<sub>2</sub> begins with a now-relatively-routine and previously described high temperature catalytic reduction of [ $^{11}\text{C}$ ]CO<sub>2</sub> to [ $^{11}\text{C}$ ]CO. After [ $^{11}\text{C}$ ]CO production, this is passed through a cartridge containing silver(II) fluoride (AgF<sub>2</sub>), a fairly cheap and widely available solid reagent that is typically used for small-scale hydrocarbon fluorination. Upon passage through the AgF<sub>2</sub> cartridge (containing as little as 0.4g) at room temperature, [ $^{11}\text{C}$ ]CO is cleanly and quantitatively converted to [ $^{11}\text{C}$ ]COF<sub>2</sub>. The authors report that a single cartridge was used reproducibly for 10

sequential syntheses, although it has yet to be determined whether these cartridges can be stored for longer periods of time between productions.

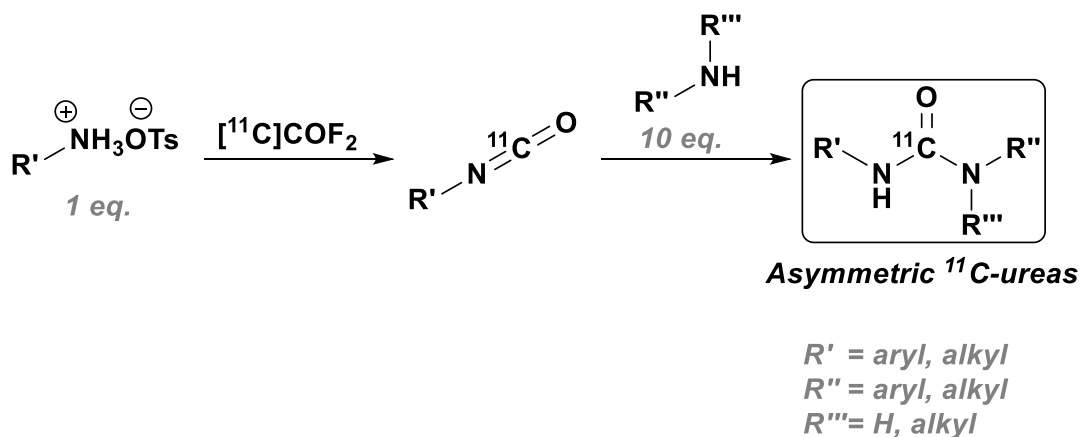


**Figure 1.23 Asymmetric  $^{11}\text{C}$ -ureas from  $[^{11}\text{C}]\text{COF}_2$  via alkylammonium salts<sup>143</sup>**

Reaction with less nucleophilic ammonium tosylate salts allows for the isolation of  $^{11}\text{C}$ -isocyanates. Subsequent addition of excess quantities of amines results in the selective production of asymmetric  $^{11}\text{C}$ -ureas

As mentioned,  $[^{11}\text{C}]\text{COF}_2$  seems to exhibit broadly comparable reactivity to  $[^{11}\text{C}]\text{COCl}_2$ , in that it has been used extremely successfully for the rapid production of cyclic  $^{11}\text{C}$ -urea derivatives ( $^{11}\text{C}$ -benzimidazolidones and  $^{11}\text{C}$ -imidazolidones).<sup>142</sup> Furthermore they have successfully applied it in the synthesis of asymmetric disubstituted  $^{11}\text{C}$ -ureas via initial reaction of  $[^{11}\text{C}]\text{COF}_2$  with a less-nucleophilic alkylammonium tosylate salt derivative of the intended amine to produce an isolated  $^{11}\text{C}$ -isocyanate.<sup>143</sup> Treatment with an excess of a second amine building block led to the preferential formation of the asymmetric product; again this is broadly comparable to previous work developed with  $[^{11}\text{C}]\text{COCl}_2$ .<sup>139,140</sup>

As yet, the production and usage of  $[^{11}\text{C}]\text{COF}_2$  has not been replicated by other groups, as it has only recently been published, but it appears extremely promising as a C-1 synthon for  $^{11}\text{C}$ -carbonylations. It will certainly be interesting to see whether it can possibly serve as a like-for-like replacement for the more practically-inaccessible  $[^{11}\text{C}]\text{COCl}_2$ . Admittedly its production is still limited to facilities with the capability to produce  $[^{11}\text{C}]\text{CO}$ , and  $\text{AgF}_2$  itself is still hardly an innocuous reagent (strongly hygroscopic, corrosive, and light sensitive). Nevertheless, it represents a promising and hopefully valuable new addition to the  $^{11}\text{C}$ -radiolabeling toolkit.

## 1.4 Radiochemistry – [ $^{11}\text{C}$ ]CO<sub>2</sub>-Fixation

### 1.4.1 Why direct reaction with [ $^{11}\text{C}$ ]CO<sub>2</sub>?

Upon considering the methods for  $^{11}\text{C}$ -carbonylation covered in the previous section, it becomes clear that regardless of the technical and chemical ingenuity involved in the production and usage of these secondary synthons, there remain significant barriers to their easy and more widespread implementation. Most of the synthons require dedicated production equipment (high-temperature catalytic ovens etc.), and face major practical hurdles in the subsequent chemistry (issues with [ $^{11}\text{C}$ ]CO solubility, etc.). The major barrier to usage of the [ $^{11}\text{C}$ ]CO<sub>2</sub> directly from the cyclotron is generally attributed to the inherently poor reactivity of CO<sub>2</sub>. However in practice these alternative secondary synthons – while overcoming this poor reactivity – present their own inherent and substantial drawbacks. Therefore, if sufficiently-powerful methods can be developed to directly incorporate this [ $^{11}\text{C}$ ]CO<sub>2</sub> into complex organic molecules, it presents an opportunity to bypass this complex and time-consuming production of secondary synthons necessary to produce  $^{11}\text{C}$ -carbonylated products.

Additionally, whilst many cyclotrons are technically capable of producing [ $^{11}\text{C}$ ]CO<sub>2</sub>, the requirement for a dedicated [ $^{11}\text{C}$ ]CH<sub>3</sub>I production system (or any alternative [ $^{11}\text{C}$ ]CO/COCl<sub>2</sub> production systems) has tended to confine the usage of  $^{11}\text{C}$  to more specialised research facilities; those which expect to perform  $^{11}\text{C}$ -methylations regularly enough to dedicate sufficient space and resources to this instrumentation. By contrast, it is possible to envisage that the development of robust and easy to implement chemical methods for direct [ $^{11}\text{C}$ ]CO<sub>2</sub> fixation could lead to widened access to  $^{11}\text{C}$ -radiolabeled compounds, by allowing  $^{11}\text{C}$ -radiolabeling using existing radiosynthesis units.

### 1.4.2 Practicalities of [ $^{11}\text{C}$ ]CO<sub>2</sub> as a synthon

As has been alluded-to thus far, there are two major impediments to the trapping and reactivity of [ $^{11}\text{C}$ ]CO<sub>2</sub>:

1. CO<sub>2</sub> is fairly insoluble in the most routinely-used organic solvents. Therefore, by contrast to [ $^{11}\text{C}$ ]CH<sub>3</sub>I, [ $^{11}\text{C}$ ]CO<sub>2</sub> cannot effectively be passively trapped in solution by bubbling.
2. CO<sub>2</sub> itself is a relatively inert molecule. The strong C=O bonds are fairly resistant to chemical attack, and this is exemplified by the harsh reducing conditions traditionally required for its conversion to [ $^{11}\text{C}$ ]CH<sub>4</sub> or [ $^{11}\text{C}$ ]CO (T > 350°C).

The solubility issue is difficult to overcome simply, but some practical methods for enhancing gas-solvent transfer efficiency have involved the usage of thin-film in-loop methods which effectively increase the interfacial contact area. The use of these approaches for [ $^{11}\text{C}$ ]CO<sub>2</sub> chemistry is discussed more thoroughly in chapter 2, and the development of such a method was one focus of this thesis. More commonly, the focus has been on developing sufficiently strongly reactive radiolabeling solutions that are capable of immediately reacting with [ $^{11}\text{C}$ ]CO<sub>2</sub> as it is bubbled through the solution. However, this runs into the second impediment listed above: the inherent unreactivity of CO<sub>2</sub> generally means that highly reactive reagents are required to effect sufficiently rapid and efficient CO<sub>2</sub> fixation.

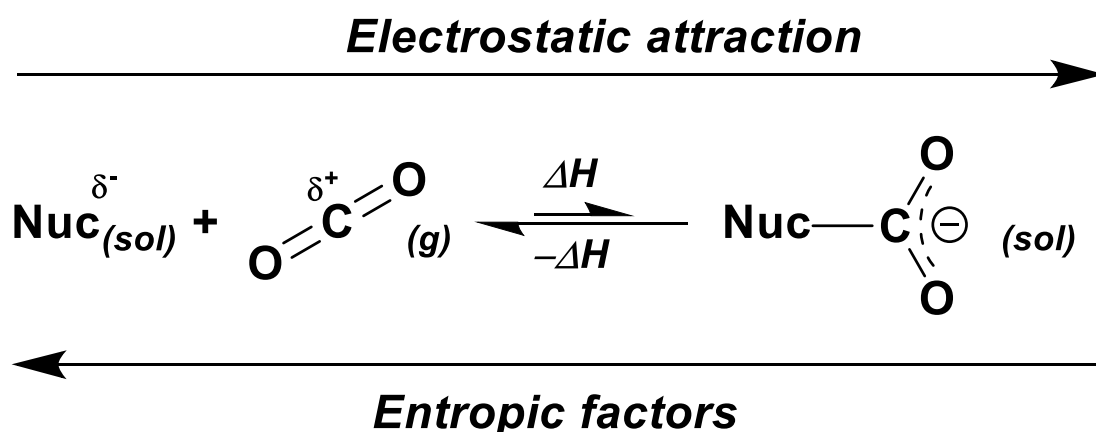


**Figure 1.24 Generic nucleophilic CO<sub>2</sub> fixation schematic**

*Nuc* represents a generic nucleophile, whether it has a formal negative charge or a partial negative charge due to bond polarisation.

The majority of these chemical [<sup>13</sup>C]CO<sub>2</sub> fixation methods exploit the electropositive character of the central carbon atom that is afforded to it as a consequence of its two double-bonds to electronegative oxygen atoms. As a result, this electropositive character leaves the carbon theoretically vulnerable to nucleophilic attack, and it is through such an approach that most of the direct [<sup>13</sup>C]CO<sub>2</sub> fixation methods have operated. This is exemplified in Figure 1.24 above.

The “forward” reaction is driven by electrostatic attraction between the  $\delta^-$  charge of the nucleophile and the  $\delta^+$  charge on the carbon atom in CO<sub>2</sub>. The “reverse” reaction is strongly favoured by the entropic driving force provided by the re-release of gaseous CO<sub>2</sub>. The equilibrium position is therefore determined by the magnitude and sign of the enthalpic change ( $\Delta H$ ), hence the use of highly energetic nucleophilic reagents or sufficiently energetically stabilising the fixation products both lead to more effectively favouring the “forward” CO<sub>2</sub> fixation reaction

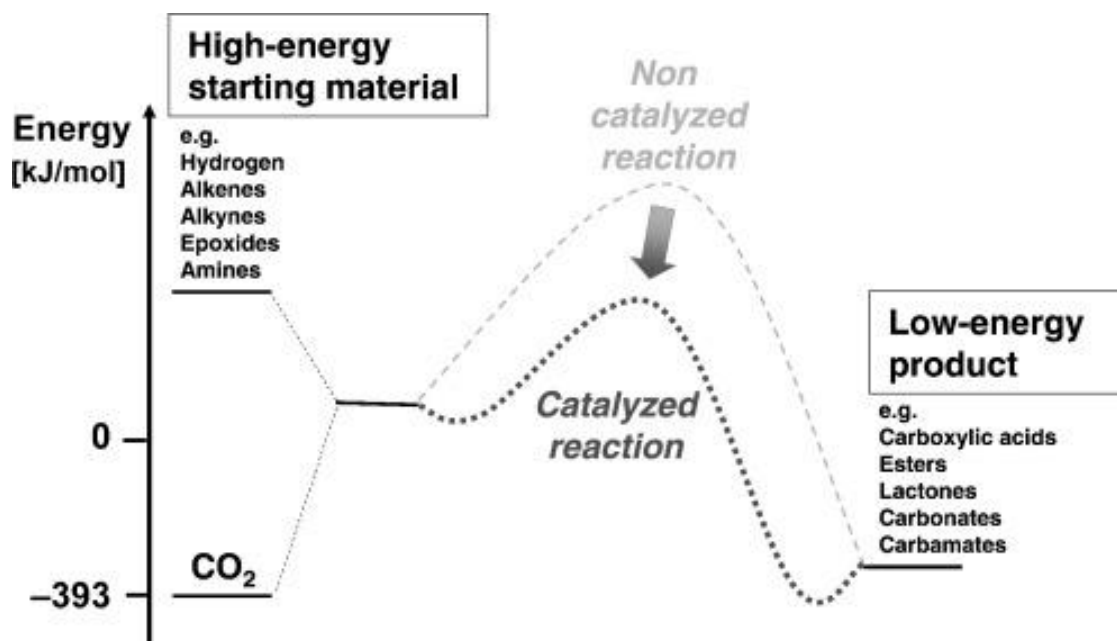


**Figure 1.25 Potential energy profile of CO<sub>2</sub> fixation processes**

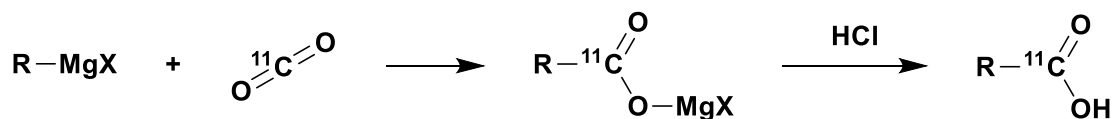
Highlights the importance of using sufficiently energetic starting materials, or sufficiently stabilising the product to drive CO<sub>2</sub> fixation. Figure reproduced with permission from Peters *et al.*<sup>144</sup>

Any nucleophilic attack at the carbon will lead to the breaking of one or more of the C-O bonds, and therefore requires a sufficiently energetic reagent or a strongly energetically-stabilised fixation product to make this an enthalpically favourable process. Without such energetic driving forces, many of these intermediate fixation products are liable to undergo the reverse decarboxylative processes, re-releasing [<sup>11</sup>C]CO<sub>2</sub>. This enthalpic driving force for the reverse reaction is further accompanied by the entropic factor: the release of a gas from a molecule in solution, and the splitting of a single component into two components both tend to increase the entropy of the system.



### 1.4.3 $^{11}\text{C}$ -Carboxylic acids from Grignard reagents

As has been set out thus far, nucleophilic  $[^{11}\text{C}]\text{CO}_2$  fixation often relies on the usage of highly energetic starting materials. In the course of  $[^{11}\text{C}]\text{CO}_2$  fixation method development, one key example of this approach involves the usage of Grignard reagents: compounds with the generic formula  $R\text{-MgX}$ . The carbon-magnesium bond in such compounds is highly polarised, resulting in the carbon exhibiting a strongly anionic character which can attack the electrophilic carbon centre in  $\text{CO}_2$ , producing an  $^{11}\text{C}$ -carboxylate product. Acidic workup of this intermediate results in the production of  $^{11}\text{C}$ -carboxylic acids.<sup>145–149</sup>



$X = \text{Br, Cl, I}$

**Figure 1.26**  $^{11}\text{C}$ -Carboxylic acid synthesis with Grignard reagents

$[^{11}\text{C}]\text{CO}_2$  reacts with strongly nucleophilic Grignard reagents to form intermediate  $^{11}\text{C}$ -carboxylates. Upon workup with  $\text{HCl}$ , these yield the desired  $^{11}\text{C}$ -carboxylic acid products.

There are however some consequent drawbacks that come with the use of such highly reactive starting materials. Primary among these is the limited substrate compatibility: Grignard reagents are highly reactive with many commonly occurring functionalities (electrophilic carbonyl carbons, and acidic protons on hydroxyl and amine substituents, to name a few examples). As such, these approaches are typically limited to the radiolabeling of simple aliphatic or aromatic carboxylates; of which  $[^{11}\text{C}]\text{acetate}^{147}$  and  $[^{11}\text{C}]\text{palmitate}^{150,151}$  are two notable examples. Furthermore, due to the highly reactive nature of these reagents, they are prone to reaction with atmospheric  $[^{12}\text{C}]\text{CO}_2$ , resulting in isotopic dilution of the radiolabeling product and the subsequent lowering of the practically-achieved molar activities for these syntheses. Finally, (due to their ability to abstract even moderately acidic protons) such reagents are extremely moisture sensitive, so all glassware, solvents, and reagents must be strictly controlled to limit adventitious moisture contamination resulting in unpredictable reaction failures.

### 1.4.4 Fixation on amines

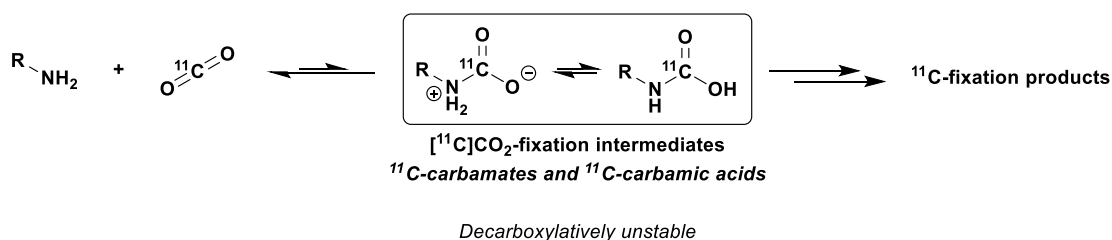


**Figure 1.27 [<sup>11</sup>C]CO<sub>2</sub> fixation on amine substrates**

Intermediate <sup>11</sup>C-carbamates and <sup>11</sup>C-carbamic acids are susceptible to decarboxylative degradation.

Amines are another class of moderately energetic nucleophiles used for [<sup>11</sup>C]CO<sub>2</sub> fixation, although they are significantly less-reactive than the previously-discussed Grignard reagents. Amines are capable of directly reacting with CO<sub>2</sub> to form intermediate zwitterionic carbamate betaines, and in the case of primary or secondary amine substrates, it is suggested that these rapidly undergo a tautomeric rearrangement to form the corresponding carbamic acid.<sup>152–154</sup> There is however some debate regarding the exact mechanisms of this fixation process, with some DFT calculations suggesting that the zwitterionic betaine intermediate is merely a transition state as part of a concerted, single-step mechanism producing the carbamic acid.<sup>155,156</sup> While other DFT calculations suggest that for more strongly basic amines this zwitterionic species is still a true intermediate, albeit a relatively short-lived one.<sup>152,157</sup>

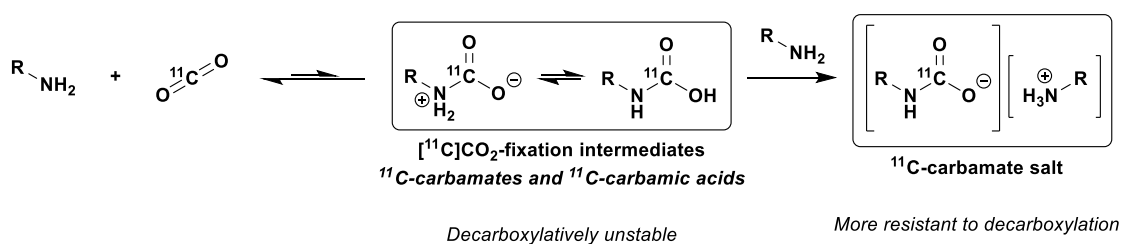


**Figure 1.28 [<sup>11</sup>C]CO<sub>2</sub> fixation and deprotonation to form <sup>11</sup>C-carbamate salts**

Unstable <sup>11</sup>C-carbamic acids are deprotonated by a second molecule of the amine, to form the <sup>11</sup>C-carbamate salt, which is more strongly-resistant to decarboxylation.

In any case, because of the less energetic nature of these reagents, the intermediate carbamates/carbamic acids are highly vulnerable to the reverse decarboxylative decomposition process, as previously described. As such, these fixation intermediates are

typically rapidly reacted with a second reagent to further convert them to more stable secondary products, further suppressing the decarboxylative decomposition. In radiochemistry, due to the inherent multifold excesses of non-radioactive reagents relative to the total  $[^{11/12}\text{C}]\text{CO}_2$  added, this first stabilisation almost always occurs as deprotonation of the carbamic acid by a second molecule of the mildly-basic original amine precursor to form the corresponding ammonium  $^{11}\text{C}$ -carbamate salt: a somewhat more stable species than the  $^{11}\text{C}$ -carbamic acid.<sup>152,154,155,158-161</sup> However, due to the limited basicity of most commonly used amine substrates, this deprotonation does not confer significant stability against decarboxylative degradation.<sup>162-165</sup> In our own experience (as will be presented later), in addition to reports in the literature,<sup>166</sup> while amines are indeed capable of trapping  $[^{11}\text{C}]\text{CO}_2$  in the absence of any additional reagents, the resultant carbamate salts are relatively unstable, and significant re-release of  $[^{11}\text{C}]\text{CO}_2$  is observed.

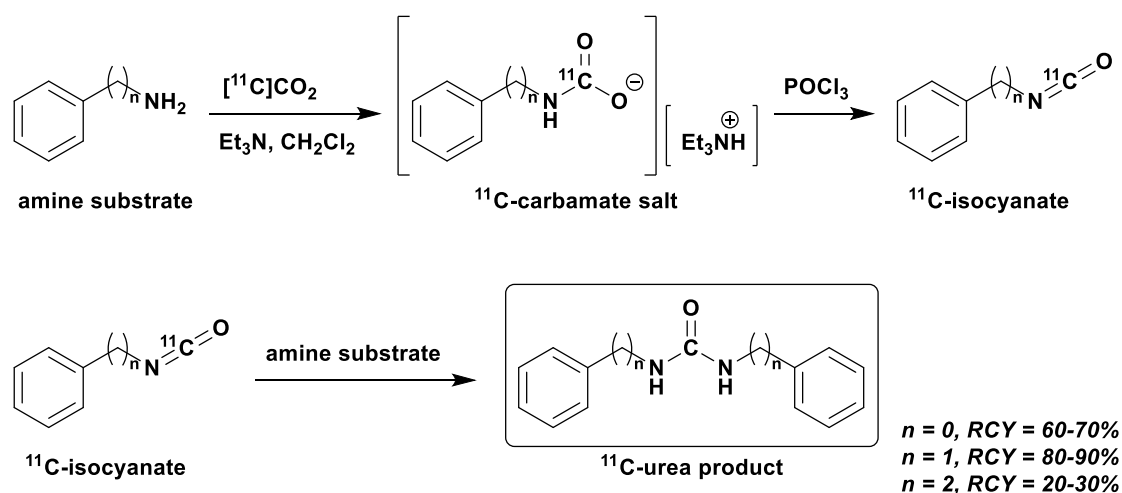


**Figure 1.29**  $[^{11}\text{C}]\text{CO}_2$  fixation and  $^{11}\text{C}$ -urea formation (Schirbel *et al.*)<sup>166</sup>

Production of  $^{11}\text{C}$ -ureas via  $[^{11}\text{C}]\text{CO}_2$  fixation, followed by  $\text{POCl}_3$  mediated dehydration to form the  $^{11}\text{C}$ -isocyanate which reacts with another amine substrate molecule to form  $^{11}\text{C}$ -urea products. It is not clear from the paper whether the reported RCYs are simply derived from the crude radio-HPLC analyses, or whether they also account for any inefficiencies in the initial trapping stage.

An early use of such an approach with  $[^{11}\text{C}]\text{CO}_2$  was in the work reported by Schirbel *et al.*,<sup>166</sup> whereby  $[^{11}\text{C}]\text{CO}_2$  was fixed on simple aliphatic and aromatic amines in the presence of triethylamine. The  $[^{11}\text{C}]\text{CO}_2$  trapped initially on the amine substrate as the intermediate carbamic acid, immediately followed by subsequent deprotonation with

triethylamine to form the moderately stabilised triethylammonium  $^{11}\text{C}$ -carbamate salt. This  $^{11}\text{C}$ -carbamate salt was then treated with phosphorous oxychloride ( $\text{POCl}_3$ , a strong dehydrating reagent)<sup>167</sup> to produce the corresponding  $^{11}\text{C}$ -isocyanate *in situ*, which promptly reacts with the remaining excess quantity of unreacted amine substrate to form the desired symmetric  $^{11}\text{C}$ -urea product.

This was an interesting novel approach to the synthesis of  $^{11}\text{C}$ -ureas, avoiding the previously-discussed issues encountered with the use of  $[^{11}\text{C}]$ phosgene. However the method is somewhat limited by the  $[^{11}\text{C}]\text{CO}_2$  fixation stage's strong temperature dependency. The  $[^{11}\text{C}]\text{CO}_2$  fixation (measured by the final RCY of the  $^{11}\text{C}$ -urea, as a proxy) performs best at  $-20^\circ\text{C}$ , but just a  $10^\circ\text{C}$  change in either direction causes the yield to drop by more than 50%. This is indicative of a poorly stabilised  $[^{11}\text{C}]\text{CO}_2$  fixation product, the triethylammonium  $^{11}\text{C}$ -carbamate in this case. Where the temperature is too low, the reaction is too sluggish to effect efficient fixation, but at elevated temperatures, the fixation product is decarboxylatively unstable, and the  $[^{11}\text{C}]\text{CO}_2$  is re-released from the solution before the  $\text{POCl}_3$  can be added. In hindsight, this seems to be attributable to their use of  $\text{Et}_3\text{N}$  as the fixation base: its basicity ( $\text{pK}_a\text{H}^+_{\text{MeCN}} = 18.8$ ) is only slightly stronger than that of benzylamine itself (16.9),<sup>168</sup> used as a model amine substrate in this work. Therefore, one would not expect a triethylammonium cation to confer a great deal more stability to the benzyl- $[^{11}\text{C}]$ carbamate salt than it would achieve were the  $^{11}\text{C}$ -carbamic acid intermediate to be deprotonated by a second molecule of the benzylamine.

Presumably the triethylamine was chosen as a fixation base due to its usage in other reported  $\text{CO}_2$  fixation processes.<sup>167,169</sup> But in these non-radioactive examples  $\text{CO}_2$  was used stoichiometrically with the amine substrate, and as such, no excess unreacted amine would be present to serve as the counterion. In these cases, the use of triethylamine as a fixation base is more logical as its low nucleophilicity precludes it from reacting with the isocyanate intermediate to form undesired urea byproducts. However, in this case where a similarly basic compound is already present in solution, it is not entirely clear whether much improvement in fixation efficiency was achieved with the addition of  $\text{Et}_3\text{N}$ . Likely based on previous literature precedent,<sup>165,169</sup> the authors themselves speculate that the use of stronger penta-alkylguanidine bases could see improvements in trapping efficiencies, and indeed this seems reasonable. To date no  $[^{11}\text{C}]\text{CO}_2$  fixation methods have employed

such bases, although as will be discussed shortly, comparable or even stronger amidine and phosphazene bases have been used to great effect.

Another major drawback of this method was that it was only applied to the synthesis of symmetric  $^{11}\text{C}$ -ureas, and while no asymmetric  $^{11}\text{C}$ -urea syntheses were attempted, the fact that they struggled to isolate the intermediate  $^{11}\text{C}$ -isocyanate suggests that this would be difficult to achieve in any case. Isocyanates are so strongly reactive that in the presence of any remaining amine in solution, they will likely rapidly react to form the symmetric  $^{11}\text{C}$ -urea product, and this was what happened in this case. Furthermore, RCYs were further limited by the formation of significant quantities of the corresponding  $^{11}\text{C}$ -carbodiimide byproduct, a decomposition product resulting from the over-reaction of the  $^{11}\text{C}$ -urea with  $\text{POCl}_3$ . This further highlighted that whilst this method was the first of its kind using  $[^{11}\text{C}]\text{CO}_2$ , it was still relatively poorly optimised and required further improvement in several key areas:  $\text{Et}_3\text{N}$  was insufficient for achieving robust thermal stability of the  $^{11}\text{C}$ -fixation products, the method was unsuitable for producing asymmetric  $^{11}\text{C}$ -ureas, and the reagent stoichiometry resulted in undesired product decomposition.

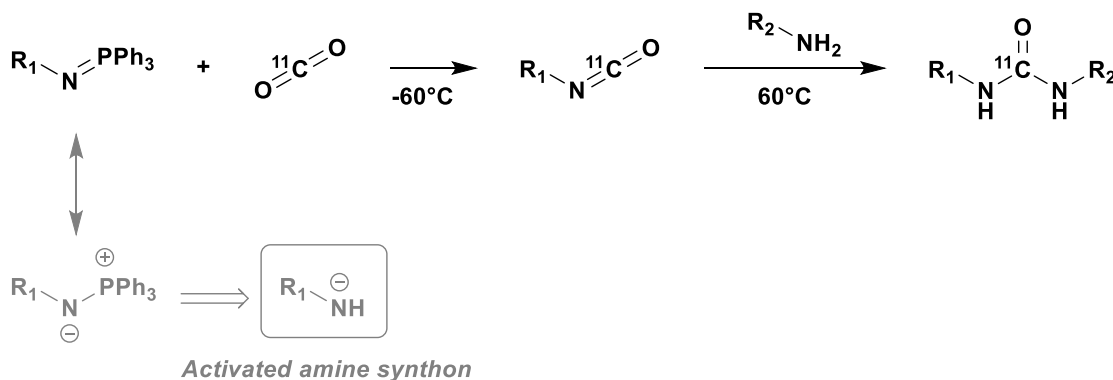


**Figure 1.30**  $^{11}\text{C}$ -urea synthesis via  $[^{11}\text{C}]\text{CO}_2$  fixation on iminophosphoranes<sup>170</sup>

$[^{11}\text{C}]\text{CO}_2$  traps directly on the nucleophilic nitrogen of iminophosphoranes. Note the negatively charged nitrogen on the iminophosphorane resonance form, this is the basis for these species' ability to trap  $[^{11}\text{C}]\text{CO}_2$  directly at even  $-60^\circ\text{C}$ .

The method from Schirbel *et al.* attempted to enhance the  $[^{11}\text{C}]\text{CO}_2$  fixation on amines by stabilisation of the intermediate  $^{11}\text{C}$ -carbamate salt with the use of a moderately more basic fixation base ( $\text{Et}_3\text{N}$ ). With reference to the potential energy diagram in Figure 1.25 above, this method serves drive the  $[^{11}\text{C}]\text{CO}_2$  fixation process by lowering the energy of

the fixation products. An alternative approach (comparable to the aforementioned Grignard approach) to solving this fixation problem is to use comparatively more energetic starting materials. One such early approach to  $[^{11}\text{C}]\text{CO}_2$  fixation on amine substrates was presented by van Tilburg *et al.* in their use of iminophosphoranes (sometimes referred to as phosphinimines) as activated amine surrogates.<sup>170</sup> These species act to trap  $[^{11}\text{C}]\text{CO}_2$  directly, before undergoing an intermolecular rearrangement, likely *via* an aza-Wittig-type mechanism, resulting in the production of the corresponding  $^{11}\text{C}$ -isocyanates. These can then be reacted with an amine substrate to form  $^{11}\text{C}$ -ureas. The trapping ability of these species can likely be attributed to the strongly-nucleophilic character of the nitrogen atom within iminophosphoranes, as is illustrated by the plausibly drawn resonance form which shows a negative charge on the resonance form in Figure 1.30 above. In the previously discussed method from Schirbel *et al.*, the  $[^{11}\text{C}]\text{CO}_2$  fixation on amines was optimal at  $-20^\circ\text{C}$ ,<sup>166</sup> but was far too slow and inefficient at any temperatures lower than this; by comparison, these iminophosphoranes achieved highly efficient  $[^{11}\text{C}]\text{CO}_2$  trapping at  $-60^\circ\text{C}$ , serving as testament to the enhanced  $[^{11}\text{C}]\text{CO}_2$  fixation ability of these iminophosphoranes as activated amine surrogates.

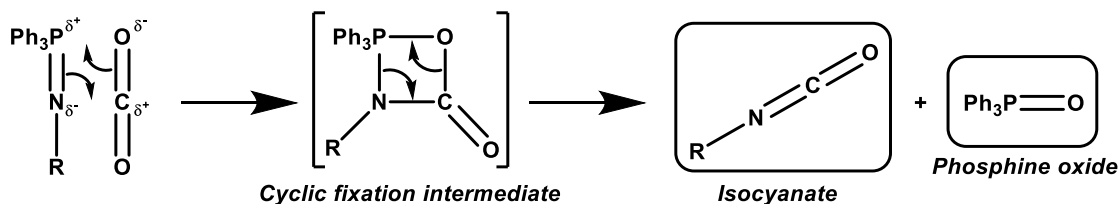


**Figure 1.31 Mechanism of aza-Wittig reaction, a [2+2] cycloaddition-cycloreversion**

As for the better known Wittig reaction, this reaction is driven by the formation of the stable and low-energy phosphine oxide

As mentioned, this reaction likely proceeds *via* the aza-Wittig cyclic reaction mechanism: a [2+2] cycloaddition-cycloreversion which proceeds *via* the oxazaphosphazetidine cyclic intermediate,<sup>171,172</sup> the driving force of which is the stable and low-energy P=O bond in the phosphine oxide byproduct. Since this produces the  $^{11}\text{C}$ -isocyanate *in situ* almost immediately, care must be taken with this highly reactive product, since the iminophosphorane starting material is also highly reactive. Whilst the intention is for this  $^{11}\text{C}$ -isocyanate to react with an amine substrate to produce an asymmetric  $^{11}\text{C}$ -urea, in the absence of this amine substrate, isocyanates are equally able to react with iminophosphoranes in another [2+2] cycloaddition-cycloreversion process to form

carbodiimides.<sup>173,174</sup> Likely for this reason, the reaction proceeded best with the initial [<sup>11</sup>C]CO<sub>2</sub> delivery done at -60°C, into a solution containing both the iminophosphorane and the second amine substrate (in a 3-4 fold excess). The highly reactive iminophosphorane is still able to react efficiently with the [<sup>11</sup>C]CO<sub>2</sub>, whereas one would not expect an unactivated amine to exhibit any major competition for the [<sup>11</sup>C]CO<sub>2</sub> at such a low temperature. The solution is then warmed to 60°C at which point the <sup>11</sup>C-isocyanate is released, and preferentially reacts with the comparative excess quantity of amine, to form the <sup>11</sup>C-urea, instead of the undesired side-reaction with the remaining iminophosphorane to produce the <sup>11</sup>C-carbodiimide.

Only a single iminophosphorane (*N*-(triphenylphosphoranylidene)aniline) was used in this initial work, and this was commercially obtained; so as reported, it is difficult to easily apply this method to more diverse substrates. Nevertheless, this work demonstrated that iminophosphoranes are clearly a highly powerful reagent for [<sup>11</sup>C]CO<sub>2</sub> fixation chemistry: not only do they essentially act as activated amines for the purposes of [<sup>11</sup>C]CO<sub>2</sub> trapping, but they also result in the formation of <sup>11</sup>C-isocyanates without any further reagent addition being required. It should be noted that they later attempted to implement this in the synthesis of [*ureido*-<sup>11</sup>C]sorafenib, but the method was unsuccessful.<sup>175</sup> They attribute this to the poor reactivity of one of the amine building blocks (4-chloro-3-trifluoromethyl aniline), and this seems reasonable considering the already low reactivity of aniline in conjunction with the strongly electron-withdrawing substituents on the phenyl ring.

Much more recently, methods for the synthesis of <sup>11</sup>C-urea and <sup>11</sup>C-carbamate products have been reported based around similar aza-Wittig<sup>176</sup> and Staudinger-aza-Wittig<sup>177,178</sup> chemistry, but these will be discussed in more detail in a later section.

### 1.4.5 Superbase-mediated [ $^{11}\text{C}$ ]CO $_2$ fixation

In the previously discussed synthesis of  $^{11}\text{C}$ -ureas reported by Schirbel *et al.*,<sup>166</sup> the [ $^{11}\text{C}$ ]CO $_2$  was first fixed on an amine substrate as a  $^{11}\text{C}$ -carbamic acid intermediate, which was rapidly deprotonated by Et $_3$ N to form the moderately stable triethylammonium- $^{11}\text{C}$ -carbamate salt. As was noted (and briefly discussed by the original authors), this compound was not particularly thermally stable (with optimal yields obtained at  $-20^\circ\text{C}$ ) and thus it seemed possible that this approach could benefit from the use of more strongly basic reagents (the authors suggest penta-alkyl guanidine reagents). This section covers the paradigmatic use of so-called “superbases” for mediating [ $^{11}\text{C}$ ]CO $_2$  fixation chemistry, as an introduction to the radiochemistry which makes up the bulk of this thesis.

#### 1.4.5.1 What is a “superbase”?

Generally, the term “superbase” is used to refer to a neutrally-charged organic compound with a Brønsted-Lowry basicity (proton abstraction ability) greater than that of Proton-sponge<sup>®</sup> (1,8-bis(dimethylamino)naphthalene;  $\text{pK}_{\text{a}}\text{H}^+_{\text{MeCN}} = 18.6$ ).<sup>179,180</sup> In that sense it is a somewhat arbitrary definition, but suffice to say that any organic compounds meeting these criteria are very strongly basic (approaching the range of many organolithium bases), whilst simultaneously being poorly nucleophilic and compatible with most non-polar organic solvents. As a result of this high basicity, low nucleophilicity, and organic solubility, organic superbases have seen a great deal of use in modern organic chemistry to catalyse otherwise stubborn reactions by either their ability to abstract less acidic protons from unreactive substrates, or in their ability to provide a soft and highly polarisable cationic counterion to a key anionic intermediate.<sup>179–181</sup>



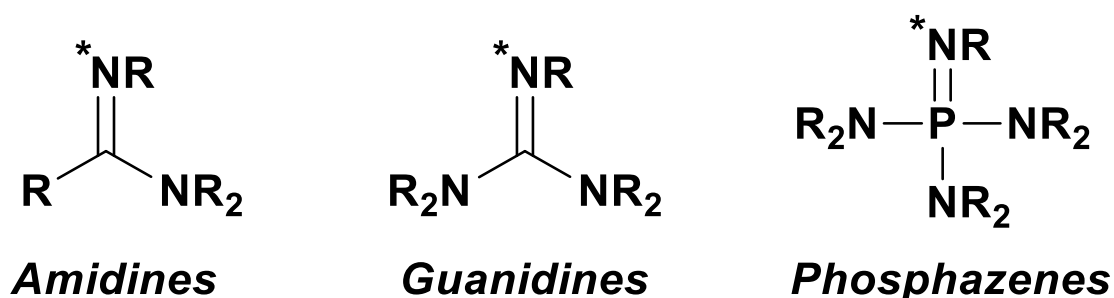


**Figure 1.32 Generic structures of the three major superbases**

\*Indicates the basic site of these species (the atom which will accept an abstracted proton)

The vast majority of compounds meeting this definition fall under one of three structural categories: amidines, guanidines, and phosphazenes.<sup>179</sup> In the case of amidines and guanidines, the basic site (the atom which initially accepts the proton) in these compounds is the nitrogen of an imine moiety ( $R_2C=NR$ ); whereas in phosphazenes the basic site is the nitrogen in the analogous iminophosphorane moiety ( $R_3P=NR$ ).

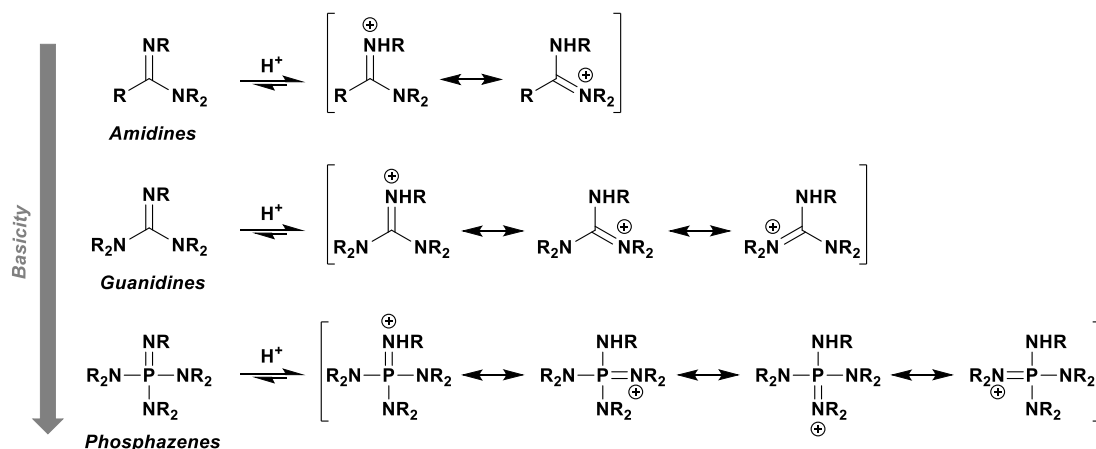


**Figure 1.33 Protonated superbases charge delocalisation resonance structures**

Accounts for the superbasicity of these species, the more the charge can be delocalised across the structure, the stronger the base. Hence the general basicity trend: amidines < guanidines < phosphazenes.<sup>168,179</sup>

The origin of the superbasicity of compounds containing these structures is their ability to delocalise a positive charge acquired during proton abstraction.<sup>179,180,182</sup> In Figure 1.33 above, this charge delocalisation is illustrated with the use of resonance structures. Such charge delocalisation results in the overall energetic stabilisation of the protonated cationic species, and conversely the deprotonated conjugate base (the neutral superbases)

itself) is therefore said to be stronger base. Accordingly, species which are better able to delocalise any such charge over a wider area are correspondingly more strongly basic, hence the phosphazenes (with delocalisation over a larger structure) being generally more basic than the analogously substituted amidines.<sup>182,183</sup>

#### 1.4.5.2 Application in radiochemistry – DBU and BEMP

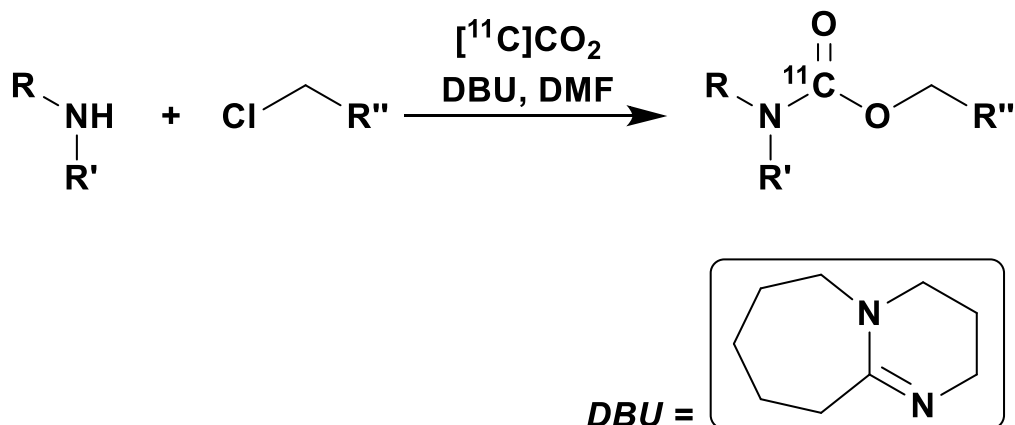


**Figure 1.34 DBU-mediated synthesis of <sup>11</sup>C-carbamates<sup>184</sup>**

[<sup>11</sup>C]CO<sub>2</sub> trapping performed at r.t. before heating at 75°C for 10 mins to complete the <sup>11</sup>C-carbamate formation

Despite the suggestion by Schirbel *et al.* in 1999 that the use of guanidine bases could lead to more efficient [<sup>11</sup>C]CO<sub>2</sub> fixation,<sup>166</sup> superbases of any kind were not used in [<sup>11</sup>C]CO<sub>2</sub> fixation until Hooker *et al.*'s landmark 2009 report of the synthesis of <sup>11</sup>C-carbamates mediated by 1,8-diazabicyclo[5.4.0]undec-7-ene (DBU), an amidine superbase.<sup>184</sup> In this method, [<sup>11</sup>C]CO<sub>2</sub> was bubbled through a solution of DMF containing an amine, an organochloride, and DBU. After [<sup>11</sup>C]CO<sub>2</sub> trapping was complete (as measured by radioactivity detectors) the vial was sealed and heated at 75°C for 10 mins. This method was successfully used to label a small library of model *N*-alkyl- and *N*-aryl-benzyl-<sup>11</sup>C-carbamates as well as the serotonin receptor antagonist [<sup>11</sup>C]metergoline, in substrate-variable but moderately satisfactory RCYs (4-60%).

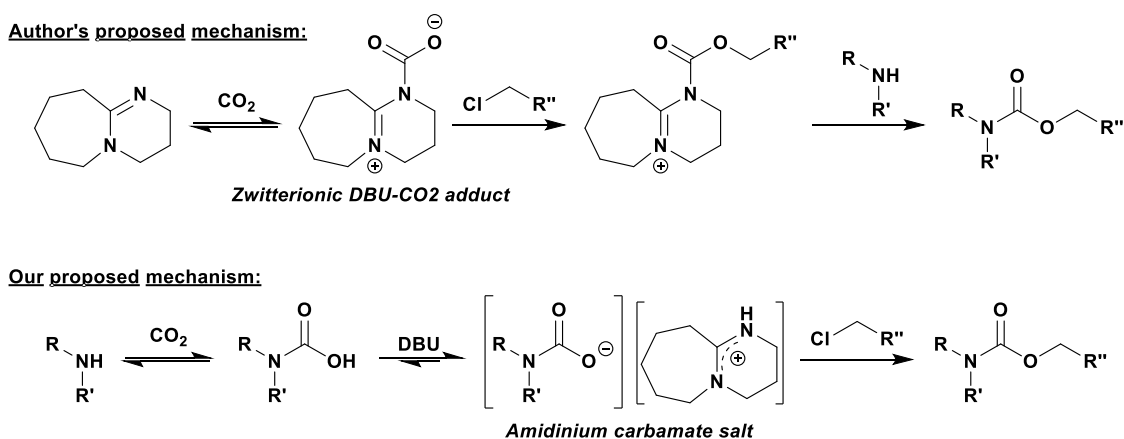


**Figure 1.35 Comparison of proposed DBU-mediated [<sup>11</sup>C]CO<sub>2</sub> mechanisms**

The upper mechanism is that proposed in the original report from Hooker *et al.*, invoking a zwitterionic DBU-CO<sub>2</sub> adduct.<sup>184</sup> By comparison, our proposed mechanism avoids this trapping/CO<sub>2</sub> activation role of DBU altogether, proposing that its predominant mechanistic role is the deprotonation of the <sup>11</sup>C-carbamic acid to form an energetically stabilised amidinium carbamate salt.

In their discussion the authors proposed that in this reaction DBU plays a catalytic transcarboxylative role (illustrated in Figure 1.35 above), in which it first acts to trap and activate the [<sup>11</sup>C]CO<sub>2</sub> as the zwitterionic DBU-CO<sub>2</sub> adduct. They then propose that this activated zwitterion reacts with the organochloride, displacing the chloride to produce a carbamate intermediate, followed by nucleophilic attack of the amine at the electrophilic <sup>11</sup>C-carbonyl position to yield the desired <sup>11</sup>C-carbamate product. This proposal that DBU acts to catalyse transcarboxylation by trapping and activating [<sup>11</sup>C]CO<sub>2</sub>, was probably informed in part by the observation that a solution of DBU in DMF can efficiently trap [<sup>11</sup>C]CO<sub>2</sub> even in the absence of any other reagents. In fact, several other alternative superbases were screened for their ability to trap [<sup>11</sup>C]CO<sub>2</sub> in solution, and DBU was found to be the optimal reagent in this regard.

As will be discussed in the following section however, on the balance of available evidence this well-documented superbase-[<sup>11</sup>C]CO<sub>2</sub> adduct formation,<sup>185,186</sup> (whether it is truly a covalently-bonded zwitterionic form, or simply an amidinium bicarbonate salt formed in the presence of adventitious water) is ultimately at-best incidental to DBU's ability to mediate [<sup>11</sup>C]CO<sub>2</sub> fixation in the presence of an amine.<sup>152,159,160,187</sup> This transcarboxylative role of DBU in forming an activated zwitterionic intermediate with

CO<sub>2</sub> is repeatedly invoked in explanations of superbase-mediated CO<sub>2</sub> fixation and, as such, will be addressed in greater depth in the following section.

With hindsight, it seems that the major mechanistic role of DBU in this chemistry can be attributed more simply to its strongly basic character. [<sup>11</sup>C]CO<sub>2</sub>, bubbled through a solution containing even a moderately nucleophilic amine will initially react to produce the <sup>11</sup>C-carbamic acid intermediate. As was discussed previously, this is a highly energetically unstable species, and is rapidly deprotonated by another basic molecule to form a <sup>11</sup>C-carbamate salt.<sup>152,154,155</sup> In the absence of any other reagents in solution, this deprotonation will be effected by a second molecule of the amine substrate, but if a stronger amine base is also present (such as Et<sub>3</sub>N in the work from Schirbel *et al.*)<sup>166</sup> this will preferentially serve as the ammonium counter cation (Et<sub>3</sub>NH<sup>+</sup>). By comparison to Et<sub>3</sub>N (pK<sub>a</sub>H<sup>+</sup><sub>MeCN</sub> = 18.8), DBU is a much stronger base, by a factor of nearly 10<sup>6</sup> (pK<sub>a</sub>H<sup>+</sup><sub>MeCN</sub> = 24.3). As was explained previously, this enhanced basicity arises as a result of the charge delocalisation that is possible in amidine bases, and which allows them to better support and stabilise a positive charge acquired by protonation.<sup>179</sup> So in our proposed mechanism, as presented in Figure 1.35 above, DBU acts simply to deprotonate the unstable <sup>11</sup>C-carbamic acid intermediate, forming the stabilised amidinium <sup>11</sup>C-carbamate salt. This stability leads to a more efficient [<sup>11</sup>C]CO<sub>2</sub> trapping in solution, and then allows the carbamate oxygen to attack at the comparatively electrophilic carbon of the organochloride reagent, forming the desired <sup>11</sup>C-carbamate product.

Setting aside this mechanistic discussion however, this method demonstrated the power of superbase-mediated [<sup>11</sup>C]CO<sub>2</sub> fixation, allowing efficient trapping of [<sup>11</sup>C]CO<sub>2</sub> on amine substrates under mild conditions. The method was rapid and efficient, and gave access to carbonyl-<sup>11</sup>C-radiolabeled molecules without the use of more-reactive yet tedious-to-produce secondary synthons ([<sup>11</sup>C]CO, [<sup>11</sup>C]COCl<sub>2</sub>).<sup>68</sup>

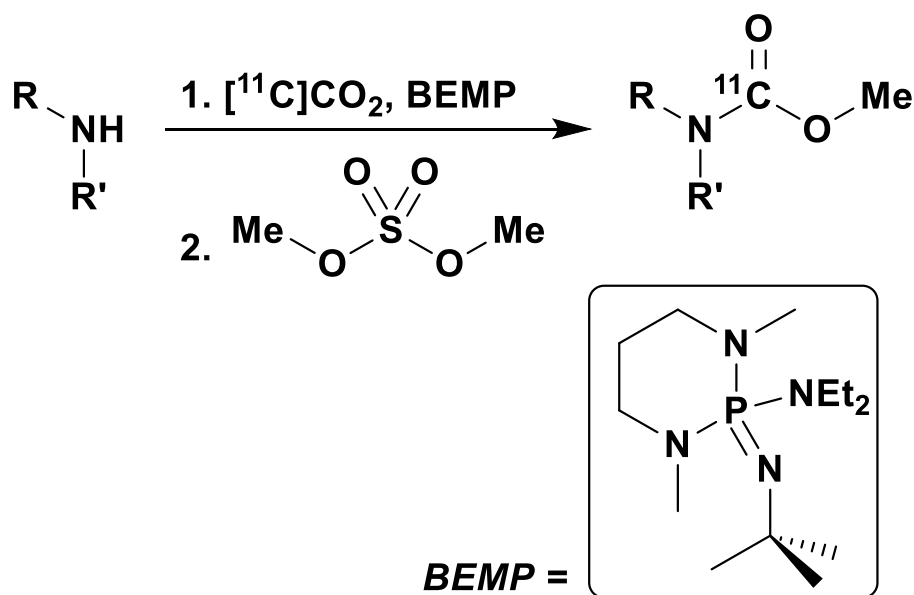


**Figure 1.36 BEMP-mediated synthesis of  $^{11}\text{C}$ -methylcarbamates<sup>188</sup>**

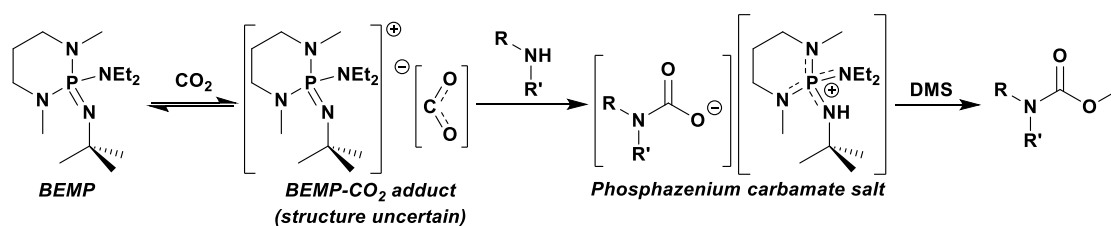
$^{11}\text{C}$ CO<sub>2</sub> trapping performed at r.t. for 1 min before adding DMS (a methylating reagent) and reacting for a further 10 sec at rt to complete the  $^{11}\text{C}$ -methylcarbamate formation

Shortly following this method from Hooker *et al.*, Wilson *et al.* reported a similar method for the synthesis of  $^{11}\text{C}$ -methylcarbamates *via* direct superbases-mediated  $^{11}\text{C}$ CO<sub>2</sub>-fixation. Where the previous method used DBU as the fixation base, this approach instead employed the phosphazene superbases BEMP (2-tert-butylimino-2-diethylamino-1,3-dimethylperhydro-1,3,2-diazaphosphorine). In this method,  $^{11}\text{C}$ CO<sub>2</sub> was trapped by bubbling through a solution of the amine and BEMP in DMF for 1 min. Following the trapping, a solution of dimethylsulfate (DMS), a strong methylating agent, was added to the reaction. After just a 10 second reaction (at r.t.), the reaction was quenched with an aqueous ammonia solution. This approach yielded model  $^{11}\text{C}$ -methylcarbamate compounds in high RCYs (>75%), and was used to successfully radiolabel the kappa opioid receptor agonist [*carbonyl*- $^{11}\text{C}$ ]GR103545 in 20-30% RCYs (d.c.) in 23 min, with molar activities of 108-162 GBq/ $\mu\text{mol}$  (from an initial 24 GBq production of  $^{11}\text{C}$ CO<sub>2</sub>). This was a highly impressive molar activity for a direct  $^{11}\text{C}$ CO<sub>2</sub> fixation approach, considering the highly sensitive nature of these reagents to any atmospheric  $^{12}\text{C}$ CO<sub>2</sub>.

BEMP ( $\text{pK}_a\text{H}^+_{\text{MeCN}} = 27.6$ )<sup>189</sup> is  $\sim 10^3$  times more basic than even DBU ( $\text{pK}_a\text{H}^+_{\text{MeCN}} = 24.3$ ) and accordingly one would expect it to perform at least as well as DBU in mediating

$[^{11}\text{C}]\text{CO}_2$  fixation on the amine substrate. Indeed, exactly this phenomenon was observed; under otherwise identical conditions, RCYs increased by  $\sim 20\%$  upon switching the fixation base from DBU to BEMP. By comparison with the previous method from Hooker *et al.* in which the  $[^{11}\text{C}]\text{CO}_2$  was trapped in a solution containing all reagents in a single-step procedure; this method followed a different order of reagent addition, with the DMS added only after the  $[^{11}\text{C}]\text{CO}_2$  fixation had taken place on the amine/DBU solution. Accordingly this could not proceed *via* an entirely analogous manner to that proposed by Hooker *et al.* (as illustrated in Figure 1.35 above), but the authors did invoke a similar transcarboxylative BEMP- $\text{CO}_2$  intermediate in their proposed mechanism (but without speculating regarding its exact structure), illustrated in Figure 1.37 below. Again this was likely informed in part by the observation that BEMP is able to trap  $[^{11}\text{C}]\text{CO}_2$  in the absence of any other reagents, but in an analogous manner to the previously discussed role of DBU, it seems more likely that this direct BEMP- $\text{CO}_2$  interaction is somewhat incidental. With its true mechanistic role as a strong base capable of deprotonating and stabilising a phosphazanium  $^{11}\text{C}$ -carbamate intermediate.

**Author's proposed mechanism:**



**Our proposed mechanism:**

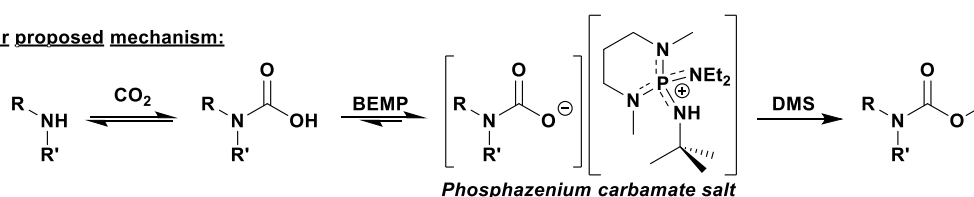


**Figure 1.37 Comparison of proposed BEMP-mediated  $[^{11}\text{C}]\text{CO}_2$  mechanisms**

The upper mechanism is that proposed in the original report from Wilson *et al.*, invoking a transcarboxylative BEMP- $\text{CO}_2$  adduct.<sup>188</sup> By comparison, our proposed mechanism avoids this transcarboxylative role of BEMP altogether, proposing that its predominant mechanistic role is the deprotonation of the  $^{11}\text{C}$ -carbamate to form an energetically stabilised phosphazanium carbamate salt (in an analogous manner to DBU).

Whilst these mechanistic discussions may seem a relatively meaningless distinction in these cases, if BEMP or DBU are assumed to play an active trap-activate-transcarboxylate

role in these  $[^{11}\text{C}]\text{CO}_2$  fixation reactions, this could have potential detrimental implications in any future applications and adaptations of these methodologies. These implications, and some recent examples of this will be discussed in the following section.

### 1.4.5.3 Mechanistic role of superbases

As was seen in the previous section, there is a common perception that superbases such as DBU and BEMP can play an active transcarboxylative role in  $\text{CO}_2$ -fixation on amines; this mechanistic role was suggested by both Hooker<sup>184</sup> and Wilson<sup>188</sup> in their methods for  $^{11}\text{C}$ -carbamate synthesis. In addition to these examples in radiochemistry, there are plenty of examples in the wider organic literature which invoke some form of transcarboxylative mechanism to explain the extraordinary fixation ability of superbases.<sup>186,190–197</sup> In this section, these claims will be examined, alternative explanations will be offered, and the relevance and importance of this distinction will be justified.

#### 1.4.5.3.1 Superbase- $\text{CO}_2$ adduct formation

As was seen in both the reports from Hooker and Wilson, these bases are able to efficiently trap  $[^{11}\text{C}]\text{CO}_2$  in solution even in the absence of any other reagents. Accordingly, it is not unreasonable to suspect that these superbase- $\text{CO}_2$  adducts could play a role in activating  $\text{CO}_2$  and transferring it to amine substrates.

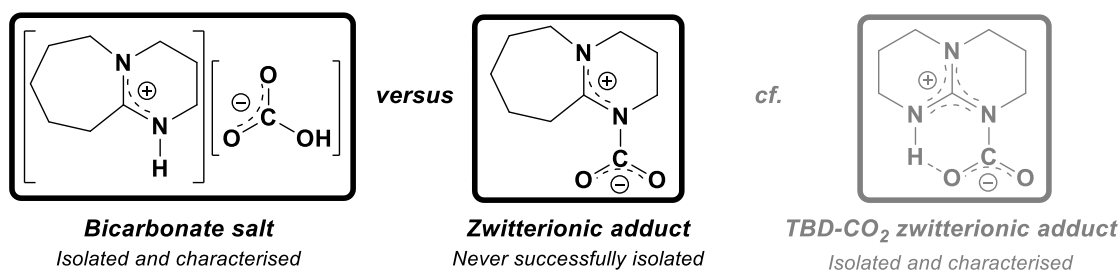


**Figure 1.38 Possible forms of the DBU- $\text{CO}_2$  adduct**

The TBD- $\text{CO}_2$  zwitterionic adduct is also shown to illustrate a successfully isolated analogous zwitterionic- $\text{CO}_2$  adduct

DBU's ability to trap  $\text{CO}_2$  has been widely recognised, although there remains some ambiguity regarding the exact nature of this interaction. While often proposed,<sup>186,190,191,193–195,198</sup> a DBU- $\text{CO}_2$  zwitterionic adduct has never been successfully isolated; any compound that has been isolated has been shown to be the  $[\text{DBU-H}^+][^-]$

HCO<sub>3</sub>] bicarbonate salt, which forms in the presence of even trace amounts of adventitious water.<sup>185,186</sup> The persistent invocation of this hypothetical zwitterionic adduct in mechanistic discussions, even in the absence of any isolation or even observation in solution, can possibly be explained in part by the verified isolation of a similar TBD-CO<sub>2</sub> zwitterionic adduct.<sup>199–201</sup> The key difference between these two compounds however, is that TBD is a guanidine base whereas DBU is an amidine base. As guanidine bases are better able to stabilise a positive charge, this possibly compensates for the energetic cost of maintaining the charge separation in a zwitterionic species. Furthermore, the disubstituted secondary amine in TBD has been shown to provide a stabilising H-bond to the carbamate oxygen in the zwitterionic structure,<sup>199,200</sup> whereas DBU is unable to provide an equivalent stabilisation.

BEMP on the other hand, has seen comparatively little use in the wider organic literature for CO<sub>2</sub> fixation, although it is arguably the most widely used superbase for [<sup>11</sup>C]CO<sub>2</sub> fixation processes. It is generally recognised, as discussed in the aforementioned Wilson method,<sup>188</sup> as providing slightly superior [<sup>11</sup>C]CO<sub>2</sub> fixation performance to DBU. However this discrepancy between bases used for radiochemical and stable isotope CO<sub>2</sub> fixation may be explained in part by considering reagent costs. At the time of writing, consulting the website of Sigma-Aldrich shows DBU available for £49.60/50mL, whereas BEMP is available for £91.10/1g. This approx. 100-fold price discrepancy is clearly a barrier to the use of BEMP in gram-scale organic chemistry, whereas in <sup>11</sup>C-radiochemistry where these reagents are typically used on or below the microlitre scale, this cost difference does not cause much concern in absolute terms.



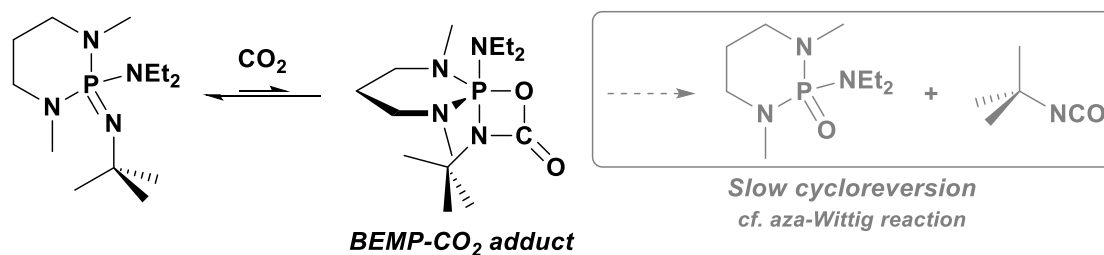


**Figure 1.39 BEMP-CO<sub>2</sub> adduct, an intermediate in [2+2] cycloaddition/reversion**

This adduct was a hypothesised intermediate in the work by Courtemanche *et al.*,<sup>172</sup> and seems a reasonable assumption given the similarities to the aza-Wittig mechanism<sup>171</sup> already discussed in the iminophosphorane [<sup>11</sup>C]CO<sub>2</sub> fixation chemistry from van Tilburg *et al.*<sup>170</sup> Note the ultimate production of the *tert*-butyl isocyanate (although this was only observed after approx. 8 hours).

As a result of this comparative lack of interest in the use of BEMP as a fixation base, there has been much less discussion regarding any BEMP-CO<sub>2</sub> adduct formation, despite the fact that it is clearly able to efficiently trap [<sup>11</sup>C]CO<sub>2</sub> in solution. In 2015 however, Courtemanche *et al.* reported a method for carbon dioxide hydrosilylation, catalysed by phosphazene bases.<sup>172</sup> In this, they observed that BEMP (in the absence of any other reagents) would react with CO<sub>2</sub>, ultimately yielding the corresponding phosphine oxide as well as *tert*-butyl isocyanate. They hypothesised that this could have proceeded via a [2+2] cycloaddition, forming the cyclic BEMP-CO<sub>2</sub> adduct, an oxazaphosphazetidine (as shown in Figure 1.39 above), and over a sufficiently long time frame (8 hours), this slowly underwent the subsequent [2+2] cycloreversion process which produced the phosphine oxide and the *tert*-butyl isocyanate. This proposed mechanism seems realistic, since it is the same mechanism by-which the previously-discussed aza-Wittig reaction proceeds, driven again by the strong P=O bond in the phosphine oxide product. In fact, BEMP (along with other phosphazene bases) is highly structurally similar (RN=P(NR<sub>2</sub>)<sub>3</sub>) to the iminophosphoranes used in most aza-Wittig chemistry (RN=PR<sub>3</sub>). It was also noted that the rate of phosphine oxide/isocyanate production was inversely proportional to the steric bulk around the phosphorous centre: a much less hindered phosphazene reacted fully in 15 min, whereas the much more bulkily-substituted BEMP reached completion in approx. 8 hours, suggesting that this cyclic intermediate is sufficiently long-lived in solution, and it therefore seems possible that this cyclic adduct is the species which forms during BEMP-[<sup>11</sup>C]CO<sub>2</sub> trapping experiments (in the absence of other reagents), and which is responsible for the highly efficient [<sup>11</sup>C]CO<sub>2</sub> trapping activity it exhibits.

This discovery prompts two considerations. The first is whether this BEMP-CO<sub>2</sub> adduct plays an active transcarboxylative role in CO<sub>2</sub> fixation on amines, or whether in the presence of an amine substrate, it simply serves as a strong base (as we initially suspected). Secondly, it raises some concern as to whether this slow production of the *tert*-butyl isocyanate is observed in BEMP-catalysed [<sup>11</sup>C]CO<sub>2</sub>-fixation reactions. If it were, the resultant [<sup>11</sup>C]*tert*-butyl isocyanate could lead to the formation of undesired *tert*-butyl-substituted <sup>11</sup>C-urea byproducts.

#### **1.4.5.3.2 Do these adducts really mediate transcarboxylation?**

As has been alluded-to thus far, there exists no evidence for either DBU-CO<sub>2</sub> or BEMP-CO<sub>2</sub> adducts playing a transcarboxylative role in CO<sub>2</sub> fixation. One interesting investigation into such a possibility was reported in 2012 by Mizuno *et al.*; in this work they investigated the DBU-catalysed CO<sub>2</sub> fixation on 2-aminobenzonitrile, forming 1*H*-quinazoline-2,4-dione.<sup>202</sup> The baseline experiment involves bubbling CO<sub>2</sub> through a solution of the amine precursor and DBU in DMF at 20°C. After 24 hours, the expected product is obtained in an 88% yield. They hypothesised that if the DBU-CO<sub>2</sub> adduct played an active transcarboxylative role in this reaction, one should be able to pre-form this DBU-CO<sub>2</sub> adduct and add it to a solution of the amine to achieve the same results. However this approach yielded no CO<sub>2</sub> fixation product whatsoever. However, when the same reaction is performed at 80°C, the expected product is yielded. From earlier data it is known that this DBU bicarbonate salt decomposes at 58°C, re-releasing CO<sub>2</sub> and DBU.<sup>186</sup> Accordingly, in this reaction at 80°C, one can deduce that the reaction only occurs because this DBU-CO<sub>2</sub> adduct had decomposed to release the CO<sub>2</sub> and DBU back into solution where they were now able to react as intended, with the DBU only acting as a strong base for the stabilisation of the intermediate carbamate salt.

Additionally, in work from Nicholls *et al.*, a series of guanidine bases known to catalyse CO<sub>2</sub> fixation on amines were investigated, and their abilities to form zwitterionic-adducts with CO<sub>2</sub> (in the same manner as TBD)<sup>201</sup> were assessed.<sup>200</sup> In this work, they found that while some bases were able to form zwitterionic adducts with CO<sub>2</sub>, this was not necessarily predictive of their efficacy in promoting CO<sub>2</sub> fixation on amines. Conversely, some bases were unable to form adducts with CO<sub>2</sub>, but were still able to efficiently promote CO<sub>2</sub> fixation. Ultimately, it seemed that across this series of bases, the strongest

determinant of CO<sub>2</sub> fixation efficacy was simply the compound's basicity. To quote from their conclusion, "the catalytic activity of these nitrogen bases in reactions between propargylamines and CO<sub>2</sub> did not support activation of CO<sub>2</sub> via this mode of [zwitterionic] complexation. Instead, the basicity of the catalyst has been shown to be important to the catalytic activity."

Finally, several studies have investigated the process of superbase-mediated CO<sub>2</sub> fixation on amines with *in situ* dynamic NMR studies<sup>203–205</sup> and DFT simulations,<sup>155</sup> and none have found evidence of such a superbase-CO<sub>2</sub> adduct. Instead, they have all observed the same mechanistic scheme as that already described thus far; the initial formation of carbamic acid between the unhindered amine substrate and CO<sub>2</sub>, followed by deprotonation and stabilisation by the superbase to form an amidinium carbamate salt. Kortunov *et al.* summarised the broad principles underlying this reactivity best by describing the "interplay between Lewis and Brønsted basicities".<sup>203</sup> In these superbase-mediated CO<sub>2</sub> fixation processes, a "mixed-base" system works best: the amine substrate (an unhindered Lewis base) reacts rapidly with the CO<sub>2</sub>, forming the unstable carbamic acid as the kinetic product; this is followed immediately by deprotonation and thermodynamic stabilisation by the Brønsted base, the more-strongly-basic but significantly less-nucleophilic superbase.

Ultimately, considering this evidence in its totality, there is scant evidence to suggest any special transcarboxylative role of superbases in CO<sub>2</sub> fixation, even for the limited cases where a superbase (usually a guanidine) has been shown unequivocally to form zwitterionic adducts in the absence of other amines. The overall conclusion of this discussion was best summarised recently by Hulla and Dyson in their excellent review of the field:<sup>160</sup> "activation of CO<sub>2</sub> by the formation of base-CO<sub>2</sub> adducts has also been hypothesized, but in the presence of an amine, direct carbamate formation appears energetically favourable".

#### **1.4.5.3.3 Why is this mechanism important?**

This could seem a relatively trivial distinction, but as was briefly alluded-to earlier, the persistence of this mechanistic misapprehension could potentially lead to poorly designed radiosynthetic methods that are at-best inefficient, and at-worst actively detrimental to the intended reaction. To give a first example, in both of the previously discussed methods

for  $^{11}\text{C}$ -carbamate synthesis,<sup>184,188</sup> the “optimal” superbases for fixation were selected by screening several candidate bases for their ability to trap  $[^{11}\text{C}]\text{CO}_2$  in solution, but crucially this was done in the absence of any Lewis-basic amine substrate. Theoretically, this was a logical decision based upon their understanding that these bases act to trap and transfer  $[^{11}\text{C}]\text{CO}_2$  to amine substrates. In such a case, the base that traps  $[^{11}\text{C}]\text{CO}_2$  most efficiently in isolation would therefore be expected to be the most efficient base for mediating  $[^{11}\text{C}]\text{CO}_2$  fixation on amines. However, as was shown by Nicholls *et al.*, the ability of a base’s ability to form adducts with  $\text{CO}_2$  does not necessarily correlate with its catalytic activity in mediating  $\text{CO}_2$  fixation on an amine substrate.<sup>200</sup> This base screening method could theoretically lead to the erroneous rejection of a promising fixation superbase simply because it is insufficiently nucleophilic (due to steric hindrance) to achieve efficient direct reaction with  $[^{11}\text{C}]\text{CO}_2$ .

Hypothetically, it is possible to envisage occasions in which this mechanistic misapprehension could lead to someone designing a process whereby they attempt to decouple these two stages: first the  $[^{11}\text{C}]\text{CO}_2$  is trapped in a superbase solution, only for the amine substrate to be added at a later point. For the case of DBU, this could lead to a situation akin to that encountered by Mizuno *et al.*,<sup>202</sup> where the DBU-bicarbonate salt is pre-formed, and therefore no reaction can occur. In this case, the reaction would require sufficient heating in order to decompose the salt to re-release free  $[^{11}\text{C}]\text{CO}_2$  with which the amine substrate can react.

In a recent collaborative publication from the labs of Ming-Rong Zhang and Steven Liang, Yu *et al.* attempted to employ a BEMP-mediated  $[^{11}\text{C}]\text{CO}_2$  fixation for the radiolabeling of a TARP radioligand,<sup>206</sup> however they were unsuccessful in this endeavour, with less than 1% RCY achieved for a theoretically straightforward benzothiazolone substrate. As such, they altered their strategy, developing a  $^{11}\text{C}$ -methylation approach to radiolabel the target molecule. However, in their detailed methods section, it is made clear that they attempted to first trap  $[^{11}\text{C}]\text{CO}_2$  in a solution of BEMP to form a BEMP- $[^{11}\text{C}]\text{CO}_2$  complex, before adding this to the amine substrate. This is an example of the situation envisaged above: the misapprehension that superbases form active transcarboxylative complexes with  $[^{11}\text{C}]\text{CO}_2$  has led to a potentially poorly designed reaction protocol. Had the order of reagent addition been adjusted to ensure

[<sup>11</sup>C]CO<sub>2</sub> fixation was done in the simultaneous presence of the amine substrate and the BEMP, this could theoretically have led to a superior reaction performance.

In the case of BEMP-mediated reactions a similar decoupling of the fixation step into: 1) trapping on BEMP; and 2) transcarboxylation onto the amine substrate; could also lead to additional issues. As was demonstrated by Courtemanche *et al.*, BEMP reacts with CO<sub>2</sub> to form a cyclic adduct, which in turn slowly undergoes a cycloreversion producing *tert*-butyl isocyanate.<sup>172</sup> If [<sup>11</sup>C]CO<sub>2</sub> were trapped on BEMP in the absence of an amine, it seems possible that some of this [<sup>11</sup>C]CO<sub>2</sub> could be unintentionally converted to [<sup>11</sup>C]*tert*-butyl isocyanate, leading to unexpected <sup>11</sup>C-urea byproducts.

Finally, it is important to understand that [<sup>11</sup>C]CO<sub>2</sub> directly reacting with a superbases is at-best unproductive. If instead it is understood as simply activating [<sup>11</sup>C]CO<sub>2</sub>, it could lead to the addition of superbases into [<sup>11</sup>C]CO<sub>2</sub> radiosynthetic methods that don't require fixation on nucleophilic substrates, in which case they would really only serve to compete with the desired reaction pathway, unproductively consuming some of the limited [<sup>11</sup>C]CO<sub>2</sub> starting material.

#### **1.4.5.3.4 Do superbases play any other activating roles?**

While the previous discussions focused on the uncertainty regarding the predominant mechanistic role of superbases in mediating CO<sub>2</sub> fixation, there have been some suggestions that DBU and BEMP could play a further “activating” role as the counterion to the carbamate anion, in the key carbamate salt intermediate. Two synergistic mechanisms have been proposed in the cases of DBU and BEMP. The first of these is the suggestion that, by virtue of their ability to delocalise a charge across a relatively bulky molecule, protonated superbases represent large and easily polarisable cations which gives rise to increased ionic separation in the carbamate salt.<sup>164,165</sup> This in turn renders the carbamate oxygens more nucleophilic, activating them towards further reaction. In addition to this, their highly organic nature would be expected to render the salts more soluble in organic solvents. This putative role draws comparison to the routine usage of cryptands as phase transfer catalysts in <sup>18</sup>F-fluorination chemistry:<sup>207</sup> Kryptofix® 222 encapsulates the potassium cation in potassium fluoride, which serves to “activate” the fluoride by increasing the charge separation, rendering it a comparatively more “naked” anion, in addition to helping solubilise the salt in organic solvents by presenting a more

lipophilic cation.<sup>208</sup> In fact, protonated phosphazene bases (phosphazanium ions) have been shown to serve as excellent “activating” counterions for nucleophilic anions, on account of exactly this mechanism.<sup>209,210</sup>

Where this first suggested “activation” mechanism involves enhancing the nucleophilicity of the carbamate oxygen, the second suggested mechanism pertains to the activation of the carbonyl bond, rendering the carbamate carbon more electrophilic. Protonated superbases are good hydrogen-bond donors,<sup>211</sup> and it has been shown, based upon FTIR, crystallography, and NMR, that the H-bonding between the protonated superbase cation and the carbonyl-oxygen of the carbamate weakens the carbonyl bond, rendering the central carbon more electrophilic.<sup>212,213</sup> As such, this is another mechanism by which it is possible to envisage these superbases assisting in the activation of these carbamate salts towards further reaction, although the data on this is still limited currently and certainly requires further investigation.

#### 1.4.5.4 <sup>11</sup>C-Urea synthesis: POCl<sub>3</sub> and Mitsunobu methods

Whilst serving as excellent proofs-of-concept for superbase-mediated [<sup>11</sup>C]CO<sub>2</sub> fixation, these previous [<sup>11</sup>C]CO<sub>2</sub> fixation methods were thus far limited to the production of <sup>11</sup>C-carbamates. It was recognised that the <sup>11</sup>C-carbamate salt intermediate formed by these [<sup>11</sup>C]CO<sub>2</sub> fixation methods was a potentially versatile reaction intermediate, with the potential to be further converted to a wider range of <sup>11</sup>C-radiolabeled functionalities. As this thesis is predominantly focused on the use of [<sup>11</sup>C]CO<sub>2</sub> fixation for <sup>11</sup>C-urea synthesis, the various methods for <sup>11</sup>C-urea synthesis will form the main focus of this section.

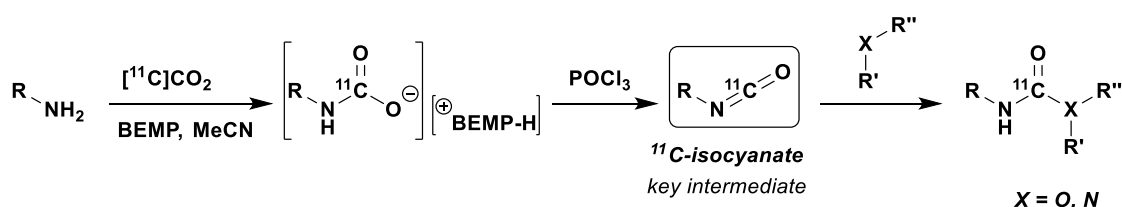
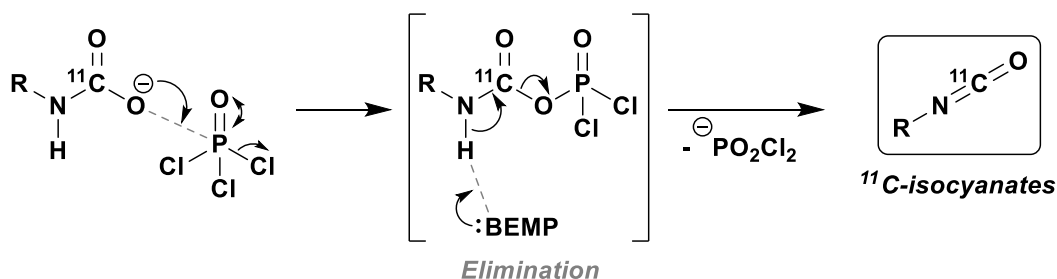


**Figure 1.40** General scheme for <sup>11</sup>C-isocyanate synthesis and application<sup>214</sup>

Operates via POCl<sub>3</sub>-mediated dehydration of phosphazanium <sup>11</sup>C-carbamate salts, to form the <sup>11</sup>C-isocyanate as the key reactive intermediate

In 2011, Wilson *et al.* reported their synthesis (and subsequent application) of  $^{11}\text{C}$ -isocyanates, this built upon their previous method for BEMP-mediated  $[^{11}\text{C}]\text{CO}_2$  fixation which allowed the efficient production of phosphazanium  $^{11}\text{C}$ -carbamate salts. Where previously these were reacted with organochlorides to produce  $^{11}\text{C}$ -carbamates, in this instance, the carbamates were further dehydrated with phosphoryl trichloride ( $\text{POCl}_3$ ) to produce  $^{11}\text{C}$ -isocyanates. This methodology represented a development of the earlier method for  $\text{POCl}_3$ -mediated  $^{11}\text{C}$ -urea synthesis from Schirbel *et al.*,<sup>166</sup> as was discussed earlier. However in addition to the increased  $[^{11}\text{C}]\text{CO}_2$  trapping efficiency afforded by the use of BEMP, the reaction was much better explored and optimised to allow the isolation of the  $^{11}\text{C}$ -isocyanate. Additionally, in this previous iteration the reaction was insufficiently controlled, with the  $^{11}\text{C}$ -isocyanate reacting immediately with the excess quantity of the original amine substrate, forming the symmetrical  $^{11}\text{C}$ -urea almost exclusively.

#### With 1° amines



#### With 2° amines

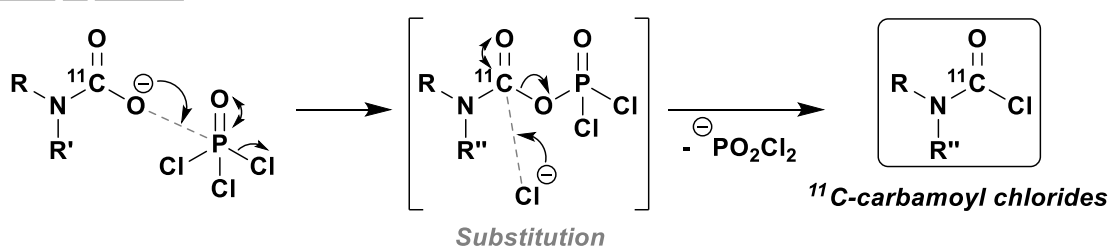


**Figure 1.41 Possible mechanisms for  $\text{POCl}_3$  reaction with  $^{11}\text{C}$ -carbamates**

Reaction between  $\text{POCl}_3$  and carbamate oxygen produces dichlorophosphate intermediate (a good leaving group). With primary amines, amine proton abstraction leads to elimination, and the production of a  $^{11}\text{C}$ -isocyanate. With secondary amines, a chloride anion attacks at the electrophilic carbon centre, displacing the dichlorophosphate and producing a  $^{11}\text{C}$ -carbamoyl chloride.

$\text{POCl}_3$  is a highly energetic but versatile reagent used in many synthetic processes, predominantly on account of its strongly electrophilic nature.<sup>215</sup> One of the most common applications it sees is as a strong dehydration reagent, used for the conversion of amides to nitriles,<sup>216</sup> and alcohols to alkenes.<sup>217</sup> This generally proceeds *via* the conversion of a hydroxyl group to a dichlorophosphate intermediate, a superior leaving group, before an E2-elimination occurs with the loss of the dichlorophosphate.<sup>218</sup> Prior to these  $^{11}\text{C}$ -radiochemical applications, it had been demonstrated that  $\text{POCl}_3$  was capable of dehydrating carbamates to form isocyanates or carbamoyl chlorides; with the product depending upon whether the corresponding amine starting material was a primary or secondary amine, with secondary amines being incapable of forming isocyanates.<sup>167,169</sup>

The mechanism for  $\text{POCl}_3$ -mediated isocyanate formation has generally been presumed to proceed *via* a comparable mechanism to the other more-commonly implemented dehydration processes (depicted in Figure 1.41 above).<sup>167,214</sup> Initially, the nucleophilic carbamate oxygen attacks at the electrophilic phosphorous in  $\text{POCl}_3$  to form the dichlorophosphate intermediate (the aforementioned superior leaving group), while displacing a chloride from the phosphorous. Following this, the amine proton is abstracted (by BEMP in this case), causing the elimination of the dichlorophosphate with the resultant production of the isocyanate. It is presumed that for secondary amines, the initial dichlorophosphate formation step remains the same. However in the absence of an amine proton available for elimination, the chloride lost during the initial step is able to react with this intermediate, undergoing a nucleophilic substitution at the *carbonyl*-carbon to form the corresponding carbamyl chloride.

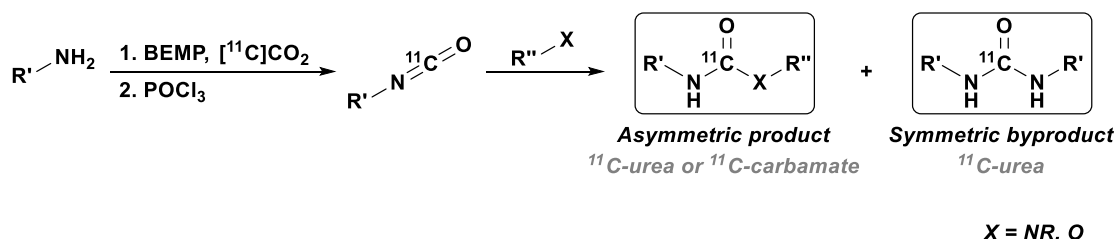


**Figure 1.42 The problem of incidental symmetric  $^{11}\text{C}$ -urea byproduct formation**

The  $^{11}\text{C}$ -isocyanate intermediate is intended to react with  $\text{R}''\text{-X}$ , the second nucleophile, but is also able to react with any of the original amine substrate remaining in solution, forming the symmetric  $^{11}\text{C}$ -urea byproduct. Figure adapted from similar figure by Wilson *et al.*<sup>214</sup>



As was discussed earlier, aside from the issues regarding inefficient [ $^{11}\text{C}$ ]CO<sub>2</sub> fixation (addressed here by the addition of BEMP), a major drawback to the method reported by Schirbel *et al.* pertained to the reactivity of the  $^{11}\text{C}$ -isocyanates. Isocyanates are highly energetic reagents,<sup>219</sup> effectively “spring loaded” towards clean and high-yielding reactions with nucleophiles, on account of their highly electrophilic carbon centres.<sup>220,221</sup> When such isocyanate-nucleophile reactions are performed stoichiometrically in non-radioactive chemistry, these reactions are relatively easy to control and give reliably-high yields of the desired product: reaction with an amine gives a urea product, alcohols lead to carbamates, and thiols to thiocarbamates.

However, when implemented in  $^{11}\text{C}$ -radiochemistry, the stoichiometry is vastly different. Sub nanomolar quantities of [ $^{11/12}\text{C}$ ]CO<sub>2</sub> (accounting for both the desired [ $^{11}\text{C}$ ]CO<sub>2</sub> as well as the adventitious [ $^{12}\text{C}$ ]CO<sub>2</sub>) are introduced into the system, meaning that the resultant  $^{11/12}\text{C}$ -carbamate and  $^{11/12}\text{C}$ -isocyanate intermediates are also produced in sub nanomolar quantities. As was covered comprehensively by Holland in his excellent 2018 discussion of radiolabeling reaction kinetics,<sup>50</sup> in most organic  $^{11}\text{C}$ -radiolabeling reactions the non-radioactive reagents must be used in sufficiently high concentrations to drive these reactions towards completion in a timeframe that is compatible with a 20.4 min half-life radionuclide. As a result, unless these reactions can be performed in microvolume reactors,<sup>222</sup> these necessarily high concentrations of non-radioactive reagents result in consequently high stoichiometric excesses relative to the limiting quantities of  $^{11/12}\text{C}$ -labeled reactive intermediates. As a result, the  $^{11}\text{C}$ -isocyanate is produced in the presence of significant quantities of the unreacted initial amine substrate. If this is not controlled for in some way, the  $^{11}\text{C}$ -isocyanate cannot be isolated as it proceeds immediately to reaction with this amine, producing the typically-undesired symmetric  $^{11}\text{C}$ -urea product, as was seen in the method from Schirbel *et al.*

To address this issue and selectively promote the formation of asymmetrically substituted  $^{11}\text{C}$ -urea products, Wilson *et al.* exploited the natural electrophilic reactivity of POCl<sub>3</sub> with this otherwise unreacted amine substrate (to form phosphoramidate products).<sup>223,224</sup> Upon increasing the quantity of POCl<sub>3</sub> added (relative to the amine), whilst the  $^{11}\text{C}$ -carbamate was dehydrated to produce the key  $^{11}\text{C}$ -isocyanate intermediate, the remaining unreacted amine was simultaneously consumed, effectively isolating the  $^{11}\text{C}$ -isocyanate *in situ*. At this point, the second nucleophilic substrate can be added to the solution,

leading to selective formation of the desired product ( $^{11}\text{C}$ -ureas from reaction with amines, or  $^{11}\text{C}$ -carbamates from reaction with alcohols).

It should be noted that the RCYs of *N*-aryl substituted  $^{11}\text{C}$ -ureas were significantly lower than those of alkyl-substituted equivalents, likely due to the decreased nucleophilicity of aromatic amines. Furthermore secondary amine substrates formed  $^{11}\text{C}$ -urea/carbamate products in comparatively low RCYs, and required elevated reagent concentrations to even achieve this. This is possibly due to the comparative difficulty of the  $^{11}\text{C}$ -carbamoyl chloride formation, in addition to the potentially hampered nucleophilicity of comparatively more sterically hindered secondary amines. In any case however, this careful balancing of reagent stoichiometries and concentrations led to a well optimised methodology that was applied successfully to a variety of model  $^{11}\text{C}$ -ureas and  $^{11}\text{C}$ -carbamates, as well as the FAAH inhibitor [*carbamyl*- $^{11}\text{C}$ ]CURB.

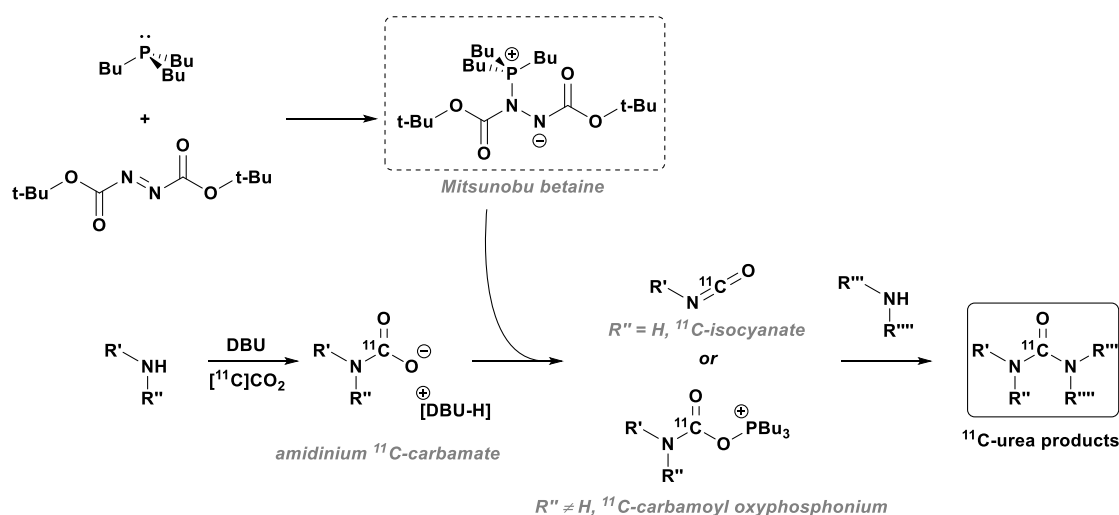


**Figure 1.43** General scheme of Mitsunobu-mediated  $^{11}\text{C}$ -urea synthesis<sup>225,226</sup>

$^{11}\text{C}\text{CO}_2$  fixation mediated by DBU produces amidinium  $^{11}\text{C}$ -carbamate intermediate (as expected), this reacts with pre-reacted Mitsunobu reagents to produce  $^{11}\text{C}$ -isocyanates or  $^{11}\text{C}$ -carbamoyl oxyphosphonium intermediates. These react with a second amine substrate to produce  $^{11}\text{C}$ -ureas.

In 2013 (with a followup in 2015) an alternative method for  $^{11}\text{C}$ -urea synthesis was published by Haji-Dheere and co-workers from our laboratory.<sup>225,226</sup> a DBU-mediated [ $^{11}\text{C}$ ]CO<sub>2</sub> fixation on amines is followed by Mitsunobu dehydration of the  $^{11}\text{C}$ -carbamate salt to produce  $^{11}\text{C}$ -isocyanates (or  $^{11}\text{C}$ -carbamoyl oxyphosphonium intermediates for secondary amines), which can in-turn react with amines to produce  $^{11}\text{C}$ -urea products. On

its face, this methodology is similar to the BEMP/ $\text{POCl}_3$ -mediated method from Wilson *et al.*, however it exhibited a different substrate tolerance, being better suited to the synthesis of *N*-aryl-substituted  $^{11}\text{C}$ -ureas. Additionally, it has more recently become clear that this method, while slightly more operationally complex, is more tolerant of acid sensitive substrates.

This radiosynthetic method was based on previous non-radioactive work where amines were reacted with  $\text{CO}_2$  and Mitsunobu reagents, with<sup>227,228</sup> or without<sup>229–232</sup> a fixation superbase, and used for the synthesis of 2-oxazolidones (intramolecular cyclic carbamates),<sup>227,229</sup> isocyanates,<sup>230,231</sup> and ureas.<sup>228,232</sup>

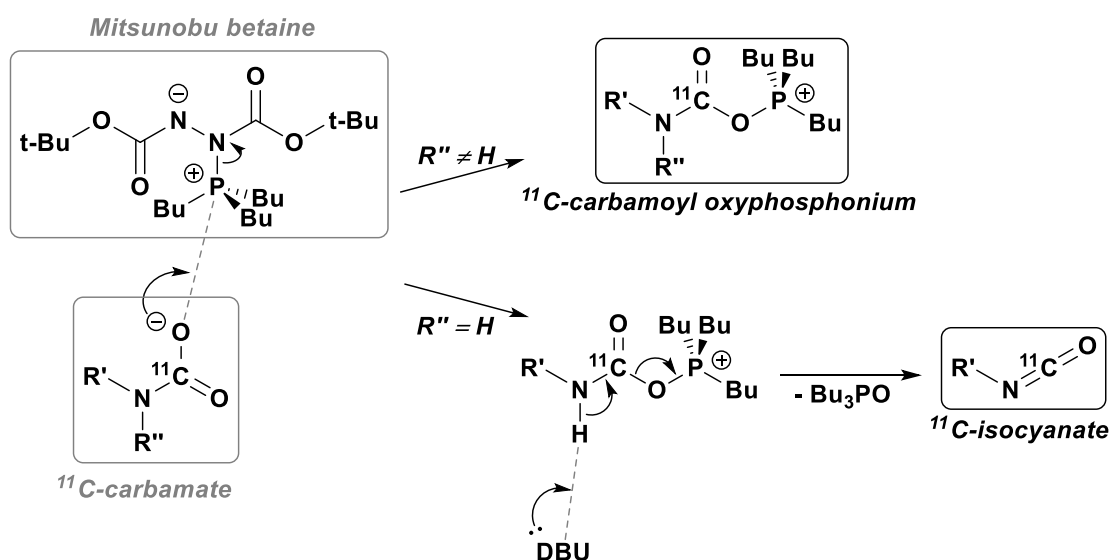


**Figure 1.44 Possible mechanisms for Mitsunobu reactions with  $^{11}\text{C}$ -carbamates**

Both primary and secondary amine substrates initially react to produce the  $^{11}\text{C}$ -carbamoyl oxyphosphonium species, however only the primary amine-derived products can undergo a subsequent E2 elimination to yield the respective  $^{11}\text{C}$ -isocyanate

As with Hooker's original method for  $^{11}\text{C}$ -carbamate synthesis,  $[^{11}\text{C}]\text{CO}_2$  is first trapped on the amine substrate as the  $^{11}\text{C}$ -carbamic acid, before deprotonation and stabilisation by DBU, forming the amidinium  $^{11}\text{C}$ -carbamate salt. This carbamate salt is then reacted with a pre-formed Mitsunobu betaine to yield the active  $^{11}\text{C}$ -isocyanate or  $^{11}\text{C}$ -carbamoyl oxyphosphonium intermediates.

The Mitsunobu reaction is a common and widely-used organic reaction for the conversion of alcohols into a broad range of functional groups *via* substitution with a variety of

nucleophiles (alcohols, carboxylic acids, amines, amides, thiols, etc.).<sup>233–235</sup> Essential to this reactivity is the use of (what are now generally referred to as) Mitsunobu reagents: a phosphine (typically triphenylphosphine) and an azodicarboxylate (typically diethyl azodicarboxylate, DEAD, or diisopropyl azodicarboxylate, DIAD). These components react to form the active species, sometimes referred to as the Morrison-Brunn-Huisgen betaine (a betaine is an aprotic zwitterionic species that is therefore unable to isomerize by proton transfer).<sup>234–237</sup> This forms as a result of the nucleophilic attack of the strongly Lewis acidic phosphine at an azo nitrogen of the azodicarboxylate, leaving the active species bearing a negatively charged nitrogen atom and positively charged phosphorous.

These active betaine species are susceptible to nucleophilic attack at the electrophilic positively charged phosphorous centre, transferring a phosphonium moiety to the nucleophile. Attack from a hydroxyl-based nucleophile, for example, converts this hydroxyl functionality into the superior oxyphosphonium leaving group, that is then in-turn more susceptible to nucleophilic substitution. In this Mitsunobu-mediated [<sup>11</sup>C]CO<sub>2</sub> fixation chemistry, the betaine (formed from di-*tert*-butyl azodicarboxylate, DBAD, and tri-*n*-butyl phosphine, PBU<sub>3</sub>) reacts with the oxygen of an <sup>11</sup>C-carbamate to form a <sup>11</sup>C-carbamoyl oxyphosphonium species (as can be seen in Figure 1.44 above). If the substrate used for <sup>11</sup>C-carbamate formation is a secondary amine, the reaction cannot proceed further. However, if the substrate is a primary amine, the proton can be abstracted (by either DBU or the negatively charged nitrogen on the betaine) leading to an E2 elimination, expelling the tri-*n*-butyl phosphonium oxide (Bu<sub>3</sub>PO) and producing the desired <sup>11</sup>C-isocyanate. Both this <sup>11</sup>C-carbamoyl oxyphosphonium species and the <sup>11</sup>C-isocyanate present a highly electrophilic carbon centre, and react with nucleophiles to yield <sup>11</sup>C-ureas.

This method was applied very successfully to the synthesis of symmetric <sup>11</sup>C-ureas,<sup>226</sup> but as was previously discussed, these tend to be more straightforward to produce in <sup>11</sup>C-radiochemistry. In the published methods, the only asymmetric <sup>11</sup>C-ureas produced were trisubstituted compounds formed as a result of trapping [<sup>11</sup>C]CO<sub>2</sub> in solutions containing both a primary and secondary amine substrate as well as DBU, followed by the addition of Mitsunobu reagents.<sup>225</sup> Interestingly these seemed to favour the formation of asymmetric <sup>11</sup>C-ureas, with these products generally being formed in RCYs in excess of

75%, when statistically (all other factors being equal), one would expect a 50:50 distribution of symmetric to asymmetric  $^{11}\text{C}$ -urea products.

No disubstituted asymmetric  $^{11}\text{C}$ -ureas were attempted using an equivalent method (two primary amines trapping  $[^{11}\text{C}]\text{CO}_2$  simultaneously), so it is difficult to comment further regarding the mechanisms underlying this asymmetric  $^{11}\text{C}$ -urea preference. Due to the documented reactivity of these Mitsunobu betaines with nucleophiles (including amines),<sup>238–240</sup> it seems plausible that asymmetric  $^{11}\text{C}$ -urea formation could be promoted with a similar approach to that employed in the BEMP/ $\text{POCl}_3$  method. This would involve trapping  $[^{11}\text{C}]\text{CO}_2$  on a single amine substrate, reacting with a stoichiometric excess of  $\text{PBU}_3/\text{DBAD}$  to produce the  $^{11}\text{C}$ -isocyanate while consuming any remaining first amine to isolate the  $^{11}\text{C}$ -isocyanate *in situ*, before reacting with a second amine to selectively form the asymmetric  $^{11}\text{C}$ -urea. In fact, as a proof of such a concept, Mair *et al.* recently published their method for the synthesis of  $^{11}\text{C}$ -amides via the Rhodium catalysed addition of organozinc iodides to  $^{11}\text{C}$ -isocyanates.<sup>241</sup> In this work, they generated  $^{11}\text{C}$ -isocyanates using this DBU/Mitsunobu-based methodology, seemingly achieving reasonable isolation of the  $^{11}\text{C}$ -isocyanate (avoiding symmetric  $^{11}\text{C}$ -urea formation) with just a 2:1 stoichiometric excess of the Mitsunobu reagents relative to the amine. Whilst they employed these  $^{11}\text{C}$ -isocyanates in a different reaction, it seems reasonable to assume that these could be reacted with a second amine to selectively produce disubstituted asymmetric  $^{11}\text{C}$ -ureas.

As was mentioned, the other notable feature of this DBU/Mitsunobu chemistry was its demonstrated ability to react equally well with aromatic and aliphatic amine substrates, whereas Wilson *et al.* could only achieve significantly reduced yields of aromatic isocyanates with their BEMP/ $\text{POCl}_3$  approach. No obvious explanation exists for the difference in substrate tolerance between these two relatively similar methods. It is of note that in the original non-radioactive report of isocyanate preparation from primary amines and  $\text{CO}_2$  using Mitsunobu chemistry, Saylik *et al.* justified their use of  $\text{PBU}_3$  in place of the more commonly used  $\text{PPh}_3$  on account of its superior ability to mediate carbamate to isocyanate dehydration on aromatic amine substrates.<sup>230</sup> The reaction between the aniline derived phenylcarbamate and a Mitsunobu betaine was followed with dynamic  $^{31}\text{P}$  NMR: the reaction was almost instantaneous when using  $\text{PBU}_3$ , as was observed by the solitary signal corresponding to the  $\text{Bu}_3\text{PO}$  byproduct immediately after

mixing; whereas with  $\text{PPh}_3$  even 3 minutes after mixing, only 26% of the signal corresponded to  $\text{Ph}_3\text{PO}$ . Clearly then, these Mitsunobu reagents are well-tuned for the production of both aliphatic and aromatic isocyanates, but this still does not attest as to the difference between Mitsunobu and  $\text{POCl}_3$  methods. To further add to this confusing picture, no such issues with aromatic amines were encountered in the previously published non-superbase-mediated  $\text{POCl}_3$  methods. This includes the method from Schirbel *et al.*, for  $^{11}\text{C}$ -urea synthesis (with  $\text{Et}_3\text{N}$  as fixation base), as well as the even earlier method from Dean *et al.*, for  $^{14}\text{C}$ -isocyanate synthesis (with  $\text{Et}_3\text{N}$  or CyTMG as fixation bases). There arguably still exists therefore, some scope for further investigations to determine what difference, if any, there really is between these two similar methodologies.

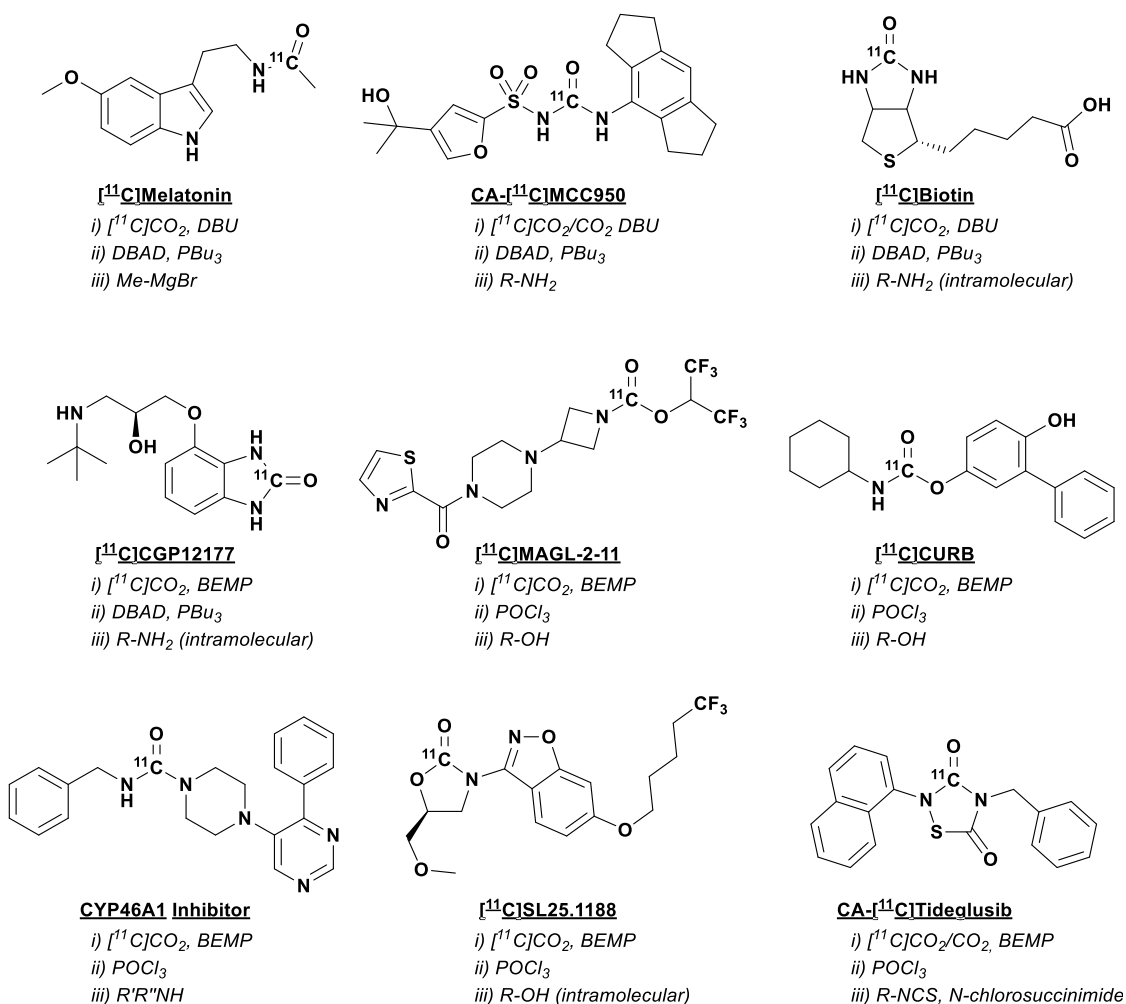


**Figure 1.45 Radiotracers labeled using  $\text{POCl}_3$ /Mitsunobu  $^{11}\text{C}$ -isocyanate methods**

Non exhaustive list demonstrating the broad range of new *carbonyl*- $^{11}\text{C}$ -radiolabeled compounds now accessible using these techniques. **i)** fixation base used; **ii)** dehydration reagents used to generate  $^{11}\text{C}$ -isocyanate; **iii)** second nucleophile reacted with  $^{11}\text{C}$ -isocyanate. **CA** denotes carrier-added syntheses, where carrier  $\text{CO}_2$  was required to achieve successful radiolabeling.

Over the past 7-10 years, these two methodologies have enabled much easier access to  $^{11}\text{C}$ -isocyanates, a key reactive intermediate used for the synthesis of *carbonyl*- $^{11}\text{C}$ -radiolabeled compounds. These methods have been implemented in the synthesis of  $^{11}\text{C}$ -ureas<sup>242–247</sup> and  $^{11}\text{C}$ -carbamates<sup>214,248–250</sup> *via* reaction with amine and alcohol-based nucleophiles, and a representative selection of these have been highlighted in Figure 1.45 above. Additionally, these  $^{11}\text{C}$ -isocyanates have also been employed in more chemically complex radiolabeling strategies. For example,  $^{11}\text{C}$ -amides have been produced by reaction with these  $^{11}\text{C}$ -isocyanates. For simple aliphatic amides, Bongarzone *et al.*

achieved this by reaction with Grignard reagents, although the substrate scope of this method is somewhat limited by the highly-reactive nature of these reagents.<sup>251</sup> A recent method from Mair *et al.* coupled <sup>11</sup>C-isocyanates with organozinc iodides using a rhodium catalyst;<sup>241</sup> this method appears to be more tolerant of diverse functionality and so appears to be an appealing alternative to <sup>11</sup>C-amide synthesis with [<sup>11</sup>C]CO. One final example of the more-novel radiochemistry enabled by this ready access to <sup>11</sup>C-isocyanates is exemplified by the collaboration between Peter Scott's lab at the University of Michigan and the PET radiochemistry team at Bristol-Myers Squibb, in their synthesis of [<sup>11</sup>C]tideglusib.<sup>243</sup> The 1,2,4-thiadiazolidine-3,5-dione heterocyclic core was radiolabeled by an intermolecular cycloaddition between an <sup>11</sup>C-isocyanate and an isothiocyanate in the presence of a chlorinating reagent (N-chlorosuccinimide).<sup>252</sup> This served to further demonstrate the synthetic utility of <sup>11</sup>C-isocyanates beyond straightforward nucleophilic attack at the central carbon. It should be noted that this was only made possible with the addition of carrier [<sup>12</sup>C]CO<sub>2</sub>, in addition to the [<sup>11</sup>C]CO<sub>2</sub>, a problem they also encountered in their later synthesis of [<sup>11</sup>C]MCC950.<sup>242</sup> Whilst this is not ideal by any means, carrier-added syntheses of radiotracers can still answer some vital questions, particularly with regards to the question of brain penetrance. It is not exactly clear why these were only successful with the addition of carrier CO<sub>2</sub> and this warrants further exploration.

Some of these compounds had previously been *carbonyl*-<sup>11</sup>C-radiolabeled previously with [<sup>11</sup>C]COCl<sub>2</sub> or by transition-metal-mediated carbonylative cross coupling reactions using [<sup>11</sup>C]CO. However as was already discussed, these processes can be time consuming, unreliable, and often require highly specialised and expensive dedicated production apparatus. These [<sup>11</sup>C]CO<sub>2</sub> fixation methodologies arguably give some of these radiotracers a renewed appeal; in the case of [<sup>11</sup>C]CGP12177 for example, the compound is a highly-promising ligand for β-adrenoreceptor imaging.<sup>137,253–255</sup> However the troublesome synthesis *via* [<sup>11</sup>C]COCl<sub>2</sub> has arguably limited its usage; with few facilities prepared to set-up, validate, and maintain such a problematic production setup.<sup>68,256,257</sup> If instead it can be radiolabeled reliably *via* [<sup>11</sup>C]CO<sub>2</sub> fixation<sup>177,258</sup> under mild conditions within existing radiosynthetic apparatus, it is certainly possible to envisage wider usage.<sup>256</sup> Furthermore, it is to be hoped that the newfound ease of access to *carbonyl*-<sup>11</sup>C-radiolabeled compounds will actively drive the development of novel radiotracers based around structures and pharmacophores that were heretofore considered



radiochemically inaccessible (at least in practical terms). Just consulting the example compounds shown in Figure 1.45, only two of the nine examples could theoretically be labeled with a more “routine” heteroatomic  $^{11}\text{C}$ -methylation.

**Table 1.2 Comparison of  $\text{POCl}_3$  and Mitsunobu-based  $^{11}\text{C}$ -isocyanate synthesis**

	<u><i>POCl<sub>3</sub></i></u>	<u><i>DBAD/PBu<sub>3</sub></i></u>
<u><i>Solution prep</i></u>	<ul style="list-style-type: none"> <li>- Straightforward</li> <li>- Single component in solution</li> </ul>	<ul style="list-style-type: none"> <li>- More complex</li> <li>- Two components in solution</li> <li>- More chance of failure</li> </ul>
<u><i>Substrate scope</i></u>	<ul style="list-style-type: none"> <li>- Difficulties with arylamines</li> <li>- HCl byproduct can affect some sensitive substrates</li> </ul>	<ul style="list-style-type: none"> <li>- Better yields with arylamines</li> <li>- No acidic byproduct, hence more tolerant of sensitive substrates</li> </ul>
<u><i>Purification</i></u>	<ul style="list-style-type: none"> <li>- Straightforward</li> <li>- Dichlorophosphinic acid (<math>\text{Cl}_2\text{HO}_2\text{P}</math>)</li> <li>- Highly polar, should elute early on RP-HPLC</li> </ul>	<ul style="list-style-type: none"> <li>- More complex</li> <li>- Phosphine oxide (<math>\text{Bu}_3\text{PO}</math>)</li> <li>- Hydrazine (<math>\text{DBAD-H}_2</math>)</li> <li>- Lipophilic, more difficult to remove with RP-HPLC</li> </ul>

In the years since these methods were published, a picture has arisen in which these are relatively complementary methods, and a comparative summary of these methods is presented in Table 1.2 above. Using  $\text{POCl}_3$  tends to be more operationally simple: the fact that it is a single component makes preparation of radiolabeling solutions more straightforward, and troubleshooting in the case of failure or contamination is somewhat simpler. Additionally, its major byproduct, the dichlorophosphinic acid is highly polar and it is therefore comparatively easy to remove chemical impurities during purification by reversed-phase HPLC. By comparison, the Mitsunobu solution preparation is somewhat more time consuming and susceptible to error, as a consequence of the need to pre-form the betaine from two components. Furthermore, the byproducts from the Mitsunobu reagents - particularly the tributylphosphine oxide – are much more lipophilic in nature, and are correspondingly more troublesome with regards to reversed-phase HPLC purification.

However, while POCl<sub>3</sub> is somewhat more operationally straightforward to implement, its major drawback is in its other major byproduct: HCl. While only small quantities of hydrogen chloride are actually produced during the reaction, if a substrate is particularly acid sensitive, this can result in unintended decomposition of reagents or products. If this is the case, then the milder Mitsunobu approach is more appropriate. This was encountered in Hill *et al.*'s synthesis of the sulfonylurea-based [<sup>11</sup>C]MCC950, these products are more sensitive to acidic hydrolysis of the urea linkage<sup>259</sup> and therefore they opted to use the gentler Mitsunobu approach. Additionally, Mair *et al.* opted to produce <sup>11</sup>C-isocyanates with the Mitsunobu method due to the acid sensitivity of the rhodium catalyst used for subsequent <sup>11</sup>C-amide production.<sup>241</sup>

Ultimately, it is clear that the use of superbases for mediating direct [<sup>11</sup>C]CO<sub>2</sub> fixation, in combination with the powerful dehydration protocols using POCl<sub>3</sub> or Mitsunobu reagents, has led to much more simple and easier to implement <sup>11</sup>C-carboxylation processes that bypass the time consuming and often unreliable production of secondary synthons such as [<sup>11</sup>C]CO or [<sup>11</sup>C]COCl<sub>2</sub>. These methods have been a fantastic addition to the <sup>11</sup>C-radiochemist's toolbox, and it is hoped that it will ultimately lead to the more widespread development and usage of <sup>11</sup>C-labeled radiotracers, beyond the more-routine heteroatom-<sup>11</sup>C-methylated compounds.

## 1.5 PSMA

As a result of reductions in the rates of stroke and coronary heart disease, cancer is increasingly becoming the leading cause of premature mortality, particularly in the world's most economically advanced countries. It represents the primary cause of premature mortality in 57 countries, and is the second most prominent cause in 55 more; with these rates only expected to increase in the coming years.<sup>260</sup> Of the global cancer burden in 2020,<sup>261</sup> prostate cancer (PCa) was the fourth most common type, accounting for 7.3% of new cases; and furthermore, it was responsible for 3.8% of the total global cancer mortality. As such, it represents a significant and growing burden on global healthcare systems, and accordingly warrants continuing efforts into the development and improvement of PCa diagnosis, detection, and treatment.

From a PET imaging standpoint, the detection and diagnosis of cancers often begins with the use of [<sup>18</sup>F]FDG, due to its broad mechanism-of-action allowing it to detect the characteristic metabolic changes that are often indicative of malignancy.<sup>262</sup> However [<sup>18</sup>F]FDG is of more-limited utility for the diagnosis and management of PCa, on account of its lowered tumour glucose utilization compared with other cancers, as well as its difficulties in distinguishing PCa from benign prostatic hyperplasia.<sup>263–265</sup> Accordingly there is a strong need for a more specific biomarker for PCa to enable improvements in its diagnosis and treatment management. The previous 15 years have seen the advent of prostate specific membrane antigen (PSMA) as a molecular target for the imaging and therapy of PCa, and it could be argued that it is leading to a paradigm shift in these areas. The development of targeted radioligands for PSMA has been extensively and comprehensively reviewed elsewhere,<sup>266–273</sup> but this section will briefly introduce the subject with appropriate highlights, with a view to better contextualising the work within this thesis.

### 1.5.1 General biology and role/relevance in prostate cancer

PSMA is a 750 amino-acid type-II transmembrane protein that is highly expressed on the epithelial cells of PCa tumours,<sup>274</sup> but is also expressed at lower levels in several other sites including the brain, the small intestine and the salivary glands.<sup>275</sup> Importantly for its use as a biomarker for PCa, expression is weak or absent in healthy prostatic tissue as well as in benign prostatic hyperplasia.<sup>276</sup> Additionally, the degree of overexpression in PCa tumours is correlated with their pathologic stage and is predictive of biochemical recurrence.<sup>277</sup> The general absence of significant levels of confounding expression in the majority of healthy tissues, in combination with this predictive correlation between overexpression levels and tumour stage and aggression, have resulted in a significant interest in the use of PSMA as a molecular target for both PET imaging and targeted therapies (radionuclide and antibody/small-molecule drug conjugates) of metastatic PCa.

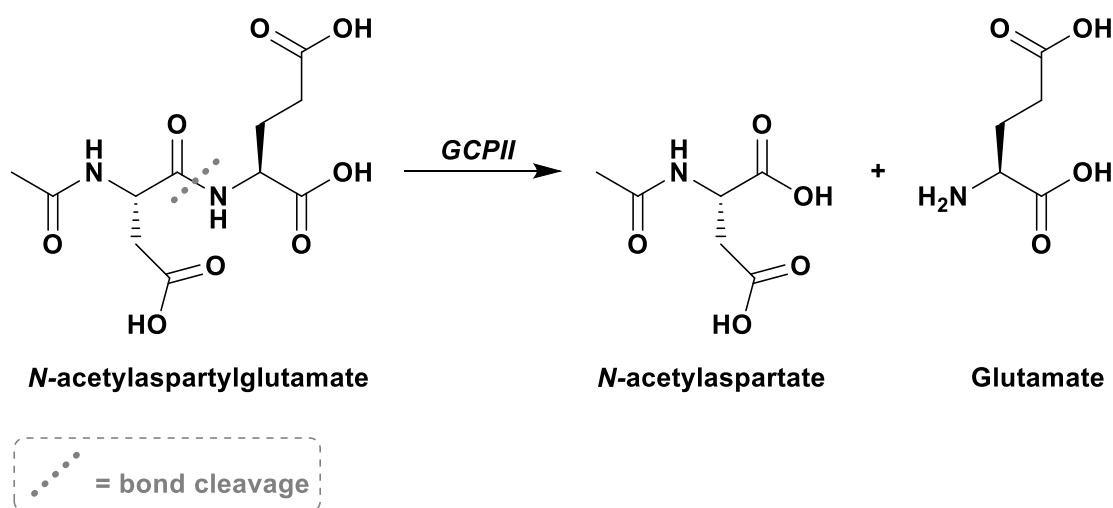


**Figure 1.46 GCPII enzymatic activity: cleavage of NAAG to release glutamate**

GCPII and PSMA are simply different names for the same protein. Customarily GCPII is used to refer to the protein in the brain, whereas PSMA is typically used when referring to expression in prostatic tissue.

As a zinc-carboxypeptidase, the biological role of PSMA in PCa is still a matter of some debate;<sup>275,278</sup> however in the other non-prostatic tissues in which it is expressed, its function is somewhat more clear. In the small intestine its role is likely related to its ability to catalyse the cleavage of the glutamate-moiety of folic acid (hence one alternative name for PSMA: folate hydrolase), and there is some suggestion that its role in cancer could be related to folate regulation or metabolism.<sup>279</sup> Furthermore, the identical protein expressed

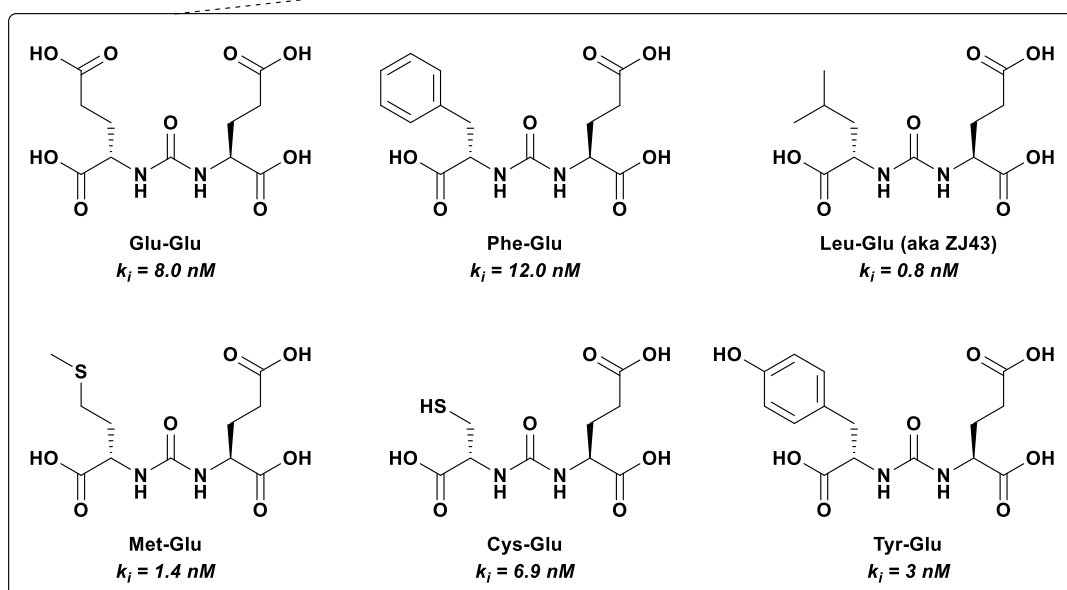
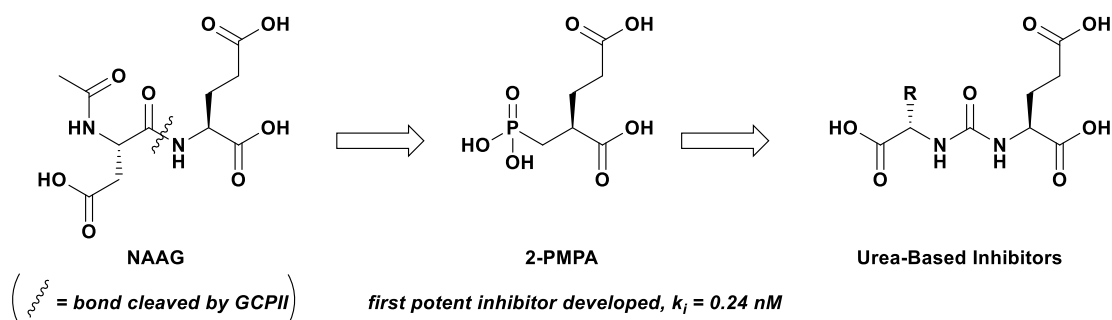
in the brain (predominantly on astrocytes) is commonly referred to as glutamate-carboxypeptidase II (GCPII).<sup>280,281</sup> As GCPII its role is somewhat better characterised: it modulates synaptic glutamate concentrations by cleaving the neurotransmitter *N*-acetyl aspartyl glutamate (NAAG) to produce glutamate (in the same active enzymatic site as its folate hydrolytic activity).<sup>267,282–286</sup> Prior to much of the interest in using PSMA as a PCa biomarker, there were significant medicinal chemistry efforts in developing inhibitors for the modulation of GCPII activity in brain,<sup>266,287,288</sup> and it is from these efforts that the structures of the majority of the current PSMA-targeted ligands are ultimately derived.<sup>289</sup>

### 1.5.2 Antibody-based molecular imaging

Prior to the advent of small-molecule-based PSMA imaging agents, there were several antibody-based agents developed. These were initially based on the original murine monoclonal antibody used in the immunohistochemical investigations of PSMA.<sup>276,290–293</sup> 7E11-C5.3, with the most prominent example of these being the SPECT imaging agent [<sup>111</sup>In]capromab-pendetide ([<sup>111</sup>In]Prostascint®).<sup>291,294,295</sup> However the applications of this were somewhat limited by the fact that the epitope recognised by this antibody is on an intracellular domain of PSMA; and as such, is only able to detect PSMA in dying or necrotic cells, limiting its sensitivity.<sup>291</sup>

To address this major shortcoming, there have been several second generation antibody-based agents developed utilising the J591 antibodies, which recognise an extracellular epitope of PSMA.<sup>296,297</sup> These have shown better sensitivity, but are still hampered by the inherent issues associated with antibody-based imaging: the slow bloodpool clearance results in long intervals between administration and imaging (3-5 days), and the slow excretion leads to increased radiation dose to the patient. As a result, the vast majority of the PSMA research to date has focused on the use of small-molecule inhibitors.

### 1.5.3 Small-molecule inhibitors



Example high-affinity amino acid-glutamate-urea-based GCPII Inhibitors

**Figure 1.47 Development of small-molecule inhibitors of GCPII**

NAAG (natural substrate) inspired the design of the first high-affinity ligand 2-PMPA.<sup>298</sup> This was further built-upon to produce ligands with a common glutamate-urea pharmacophore.<sup>288,299,300</sup>

As was discussed previously, prior to the current interest in using PSMA as a PCa biomarker, there was a significant effort in the development of compounds intended to modulate GCPII activity in the brain. The first high-affinity synthetic PSMA inhibitor developed was the phosphonate-derived 2-phosphonomethyl pentanedioic acid (2-PMPA).<sup>298</sup> The rationale behind the design of which was to mimic the glutamate moiety found in the natural substrates for this protein, NAAG and folate. This compound is still to-date one of the highest affinity ligands to have been developed for GCPII/PSMA, and

as such is still regularly used as a blocking agent for cell-binding assays and displacement studies, etc.

In an effort to build upon these initially developed phosphonate-derivatives, Kozikowski *et al.* hypothesised that a urea moiety could serve as a substitute for the phosphonate linkage, while simultaneously enabling the easier synthesis of analogue libraries for SAR exploration.<sup>299</sup> This would be more straightforward to achieve with a urea backbone, as these can be formed through the condensation of two building-block amines (or amino acids in this case) with the use of phosgene/triphosgene. Following this methodology, they developed a series of high affinity ( $k_i < 10$  nM) ligands, all of which featured the core glutamate-ureido pharmacophore (an example of some of the more-promising compounds are highlighted in Figure 1.47 above).<sup>288,299,300</sup> Notably, even the symmetric diglutamate urea (Glu-Glu) showed excellent PSMA binding ( $k_i = 8$  nM), with the asymmetric leucine-glutamate urea (Lys-Glu,  $k_i = 0.8$  nM) being the highest affinity of these simple amino-acid-substituted glutamate ureas. In fact, by virtue of this high affinity and relatively simple synthesis, Leu-Glu (commonly referred to as ZJ43) is often used as an alternative blocking agent to 2-PMPA in cell-binding assays and receptor occupancy measurements. It is important to note that this binding affinity is entirely compromised if the stereochemistry at either amino-acid  $\alpha$ -carbon is inverted, thus unless-stated, all future ligands discussed should be implicitly assumed to be the (*S*)-(*S*)-diastereomer.



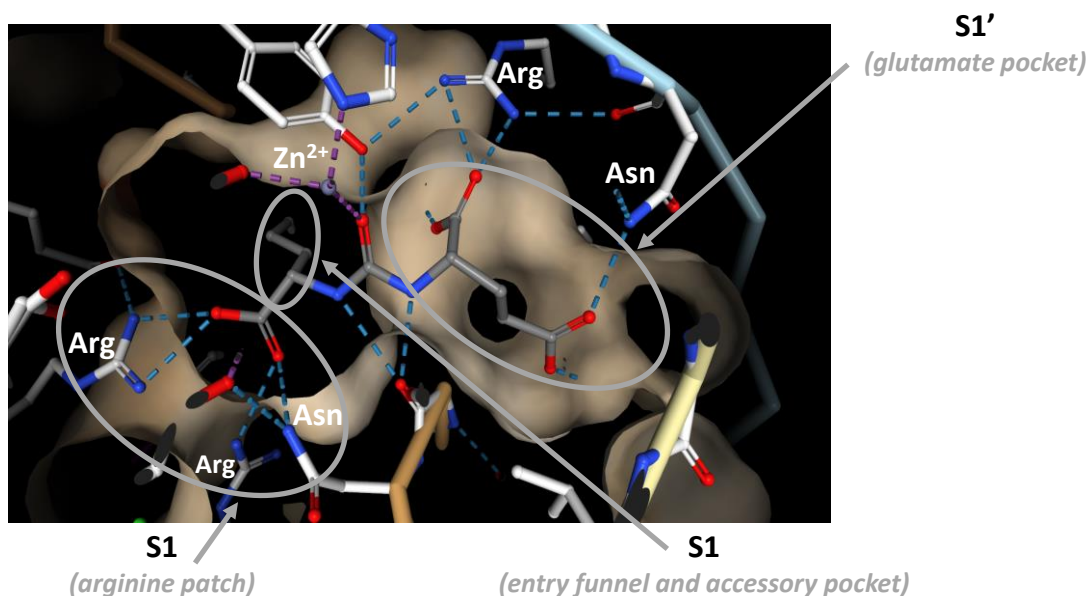


**Figure 1.48 Glutamate-urea inhibitor within GCPII/PSMA binding site**

Major binding regions annotated, image generated from published crystal structure of GCPII complex with bound DCIBzL, an ultra-high affinity inhibitor (PDB: 3D7H).<sup>301</sup> Blue dashed lines show hydrogen-bonds between DCIBzL and surrounding peptide residues, purple dashed lines show co-ordination of carbonyl-oxygen to  $Zn^{2+}$  ion.

The general nature of the interaction between these simple glutamate ureas and PSMA was characterised by virtue of the co-crystallisation of PSMA/GCPII with bound ligands, both 2-PMPA<sup>302</sup> and a series of high-affinity halogenated glutamate-ureas.<sup>301</sup> In general, the glutamate moiety fits within the polar S1' binding pocket, the urea carbonyl-oxygen co-ordinates to the  $Zn^{2+}$  ion, and the  $\alpha$ -carboxylate moiety strongly binds to the positively-charged “arginine patch” in the S1 pocket. Furthermore, the sidechain of these compounds resides within the entrance funnel of the binding site itself, which is larger and therefore allows for a greater degree of flexibility. Finally, there is also the so-called “S1 accessory pocket”, a lipophilic patch leading off the entrance funnel, which for many high-affinity ligands is often occupied by a lipophilic aryl moiety.

## 1.5.4 First generation small-molecule radiotracers

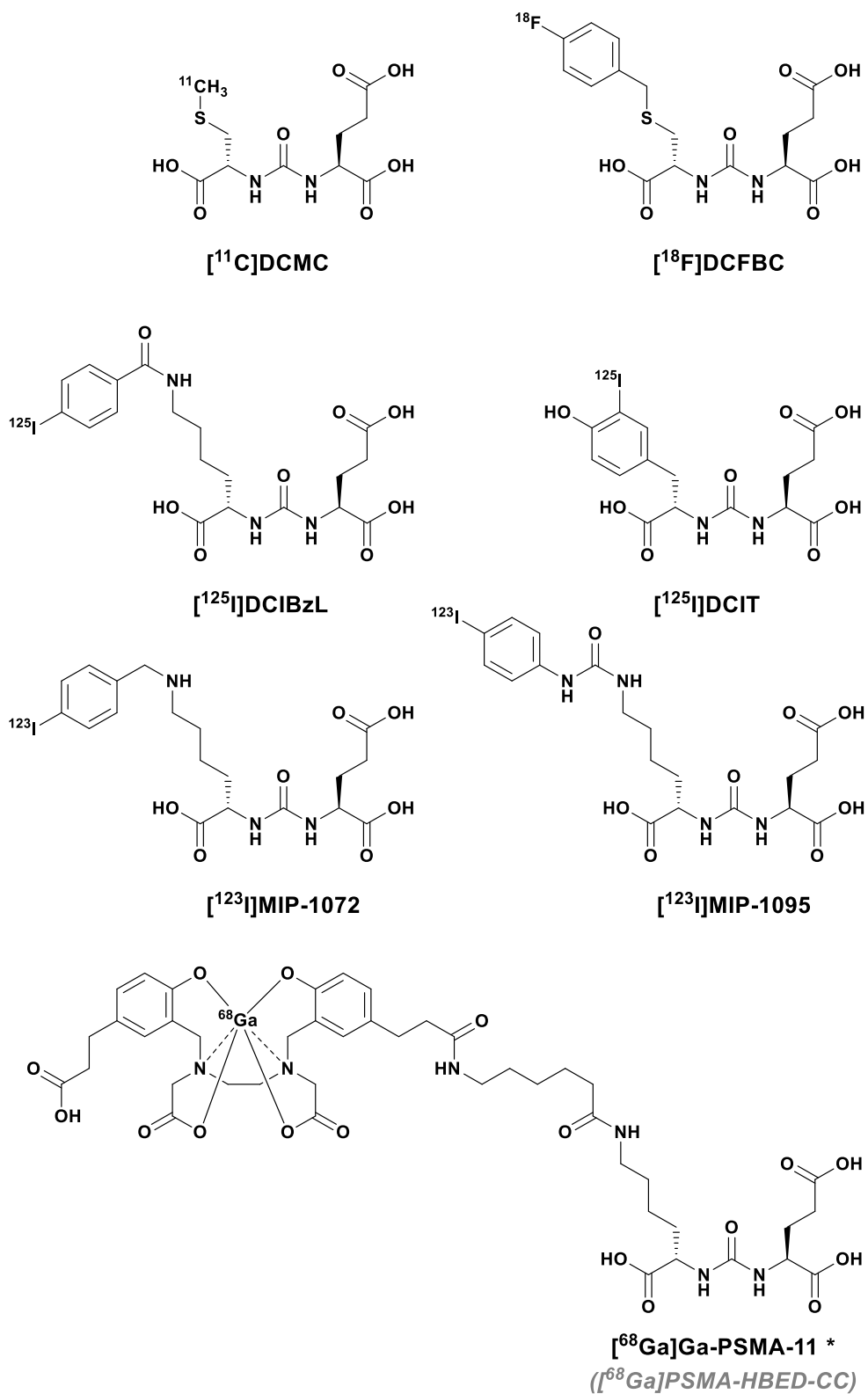


Figure 1.49 Example first generation PSMA-targeted radiotracers

\* Indicates FDA approval

Building upon this drug-development effort, in 2002 Pomper *et al.* produced the first small-molecule radiotracer for PSMA: [ $^{11}\text{C}$ ]DCMC (aka [ $^{11}\text{C}$ ]MCG), produced *via*  $^{11}\text{C}$ -methylation at the thiol sidechain of the Cys-Glu urea (the structure of this, and several other first generation radiotracers are depicted in Figure 1.49 above).<sup>303</sup> This was initially investigated in NHPs, showing specific displaceable uptake in organs known to express PSMA/GCPII in healthy tissue. Encouraged by these results indicating that such a compound could be useful for imaging this target in the periphery, they went on to develop [ $^{125}\text{I}$ ]DCIT (an iodotyrosine-glutamate urea), as a radioiodinated analogue for SPECT imaging.<sup>304</sup> [ $^{11}\text{C}$ ]DCMC and [ $^{125}\text{I}$ ]DCIT were investigated in mice using PSMA+ tumour xenograft models, with imaging encouragingly showing specific uptake in these tumours, with relatively low background non-specific binding (although [ $^{11}\text{C}$ ]DCMC was superior in this regard as a result of its decreased lipophilicity).<sup>304</sup> These were followed up with the development of several more promising radioiodinated ligands, ([ $^{123}\text{I}$ ]MIP-1072, [ $^{123}\text{I}$ ]MIP-1095, and [ $^{125}\text{I}$ ]DCIBzL).<sup>305–307</sup> However despite their excellent target affinities and promising imaging potential, there was more demand and interest in the development of PET radiotracers, rather than those incorporating these iodine radioisotopes typically used for SPECT imaging.

These successful proof-of-concept PSMA radiotracers led the same group to investigate the possibility of developing a  $^{18}\text{F}$ -radiolabeled analogue that would theoretically be more amenable to use as a routine clinical diagnostic agent as a result of its longer half-life, with the result being the production of [ $^{18}\text{F}$ ]DCFBC.<sup>308</sup> This compound, like [ $^{11}\text{C}$ ]DCMC, was constructed around a Cys-Glu scaffold *via* modification of the thiol sidechain by reaction with [ $^{18}\text{F}$ ]fluorobenzylbromide, to produce the corresponding  $^{18}\text{F}$ -fluorobenzylthioether. [ $^{18}\text{F}$ ]DCFBC has been investigated extensively in patients with metastatic prostate cancer, exhibiting excellent lesion detection, including those which were not identified by conventional anatomic imaging.<sup>309,310</sup> Despite its significant persistent blood-pool radioactivity,<sup>309</sup> this was arguably one of the first prototypical PSMA radiotracers with clinical potential.

As an alternative approach to  $^{18}\text{F}$ -radiolabeling, other groups investigated the  $^{68}\text{Ga}$ -radiolabeling of these glutamate-urea targeting moieties, with the use of a bifunctional chelator approach. The most successful early example of this was the work from Eder *et al.*, in their development of [ $^{68}\text{Ga}$ ]PSMA-HBED-CC (commonly also referred to as

[<sup>68</sup>Ga]Ga-PSMA-11), consisting of a <sup>68</sup>Ga chelator (HBED-CC) attached (*via* an aminohexanoic acid linker) to a PSMA-targeting Lys-Glu motif, through attachment at the lysine sidechain.<sup>311,312</sup> This long flexible linker allowed the glutamate-urea pharmacophore to enter the binding pocket while allowing the bulky HBED-CC chelator to remain at the exterior of the active site, so as to not interfere significantly with the target affinity.<sup>313</sup> After showing promising imaging performance in extensive patient studies,<sup>314</sup> with excellent sensitivity and specificity for the detection of primary and metastatic PCa lesions, in December 2020 [<sup>68</sup>Ga]PSMA-11 became the first PSMA-targeted small molecule radiotracer to receive FDA approval,<sup>315</sup> with Telex Pharmaceutical's kit for [<sup>68</sup>Ga]PSMA-11 preparation (Illucix®) receiving FDA approval in December 2021.<sup>316</sup>

## 1.5.5 Second generation small-molecule radioligands

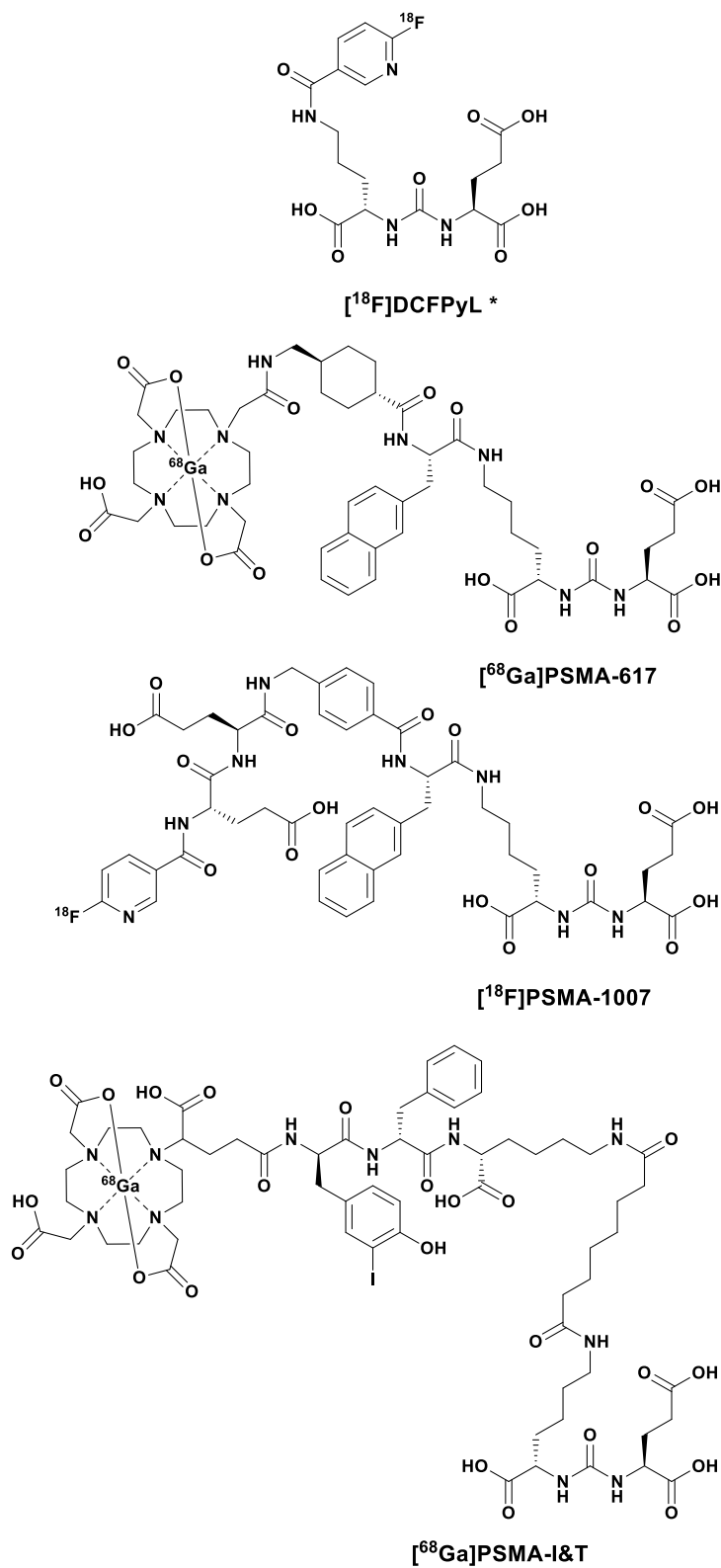


Figure 1.50 Example second generation PSMA-targeted radiotracers

\* Indicates FDA approval

The previously discussed radiotracers served excellently to prove the clinical utility of PSMA-targeted radiotracers for the imaging of metastatic PCa, however they were not without their flaws. A common issue with these initial compounds was their often significant background non-specific uptake and slow blood pool clearance. In the years since these were developed, a “second generation” of radiotracers have been developed, explicitly intended to address some of the shortcomings of the previous generation. One excellent example of this is [<sup>18</sup>F]DCFPyL,<sup>317–321</sup> a second-generation radiotracer developed to address the slow blood pool clearance of the previously-discussed [<sup>18</sup>F]DCFBC.<sup>309,319</sup> Not only did it achieve much improved clearance kinetics as was hoped, but it also demonstrated superior target binding leading to high accumulation in primary and metastatic lesions. Accordingly in May 2021, [<sup>18</sup>F]DCFPyL became the second PSMA-targeted PET radiotracer to receive FDA approval, for the same indications as [<sup>68</sup>Ga]PSMA-11.<sup>322</sup>

One other major issue facing many of the first generation PSMA-targeted radiotracers was their excretion pathways. The highly-polar and hydrophilic nature of the tricarboxylic glutamate-urea pharmacophore results in the excretion of most PSMA-targeted small-molecules through the kidneys/bladder which can be problematic for PCa imaging as a result of the proximity of the bladder and prostate. In an effort to address this, the team who initially developed [<sup>68</sup>Ga]PSMA-11 set out to develop a second generation <sup>68</sup>Ga-labeled PSMA radiotracer, in part to address this clearance pathway. Additionally, they hoped to develop a single compound that could be radiolabeled with <sup>68</sup>Ga for imaging, or with <sup>177</sup>Lu/<sup>90</sup>Y for targeted radionuclide therapy. The HBED-CC chelator used in [<sup>68</sup>Ga]PSMA-11 is well suited for gallium, but is unable to effectively chelate these therapeutic radionuclides. As such, to address both of these concerns a second generation compound was designed: [<sup>68</sup>Ga]PSMA-617.<sup>323</sup> In this, HBED-CC was replaced with the more-universal DOTA chelator to enable the chelation of various different radiometals, and the excretion pathways were modified with the addition of a lipophilic naphthyl moiety on the linker. The results from these modifications were promising, and the compound is currently in clinical trials in patients with metastatic PCa,<sup>324</sup> additionally, it is promising for use as a counterpart imaging agent as part of the theranostic pair [<sup>68</sup>Ga/<sup>177</sup>Lu]PSMA-617.<sup>325</sup>

Interestingly, the same team also developed a  $^{18}\text{F}$ -radiolabeled analogue of PSMA-617: [ $^{18}\text{F}$ ]PSMA-1007.<sup>326</sup> Even more than observed with [ $^{68}\text{Ga}$ ]PSMA-617, this new radiotracer exhibits reduced urinary clearance as a result of comparatively preferred hepatobiliary clearance.<sup>327,328</sup> As a result, [ $^{18}\text{F}$ ]PSMA-1007 potentially enables superior assessment of the prostate by reducing background radioactivity in the nearby bladder.

One final example of a second generation PSMA radiotracer is [ $^{68}\text{Ga}$ ]PSMA-I&T (Imaging & Therapy),<sup>329,330</sup> explicitly designed to be used as a theranostic ligand; labeled with  $^{68}\text{Ga}$  for imaging, and  $^{177}\text{Lu}$  for therapy. Similarly to most of these newer PSMA-radiotracers this is built upon the Lys-Glu scaffold, but incorporating a DOTAGA chelator instead of DOTA (increasing the hydrophilicity and therefore reducing non-specific binding). Additionally, the peptide linker moiety is constructed from unnatural *D*-amino acids to avoid premature proteolytic cleavage.<sup>329</sup>

Ultimately, while the first generation radiotracers proved the utility of PSMA-targeted PET imaging, these second generation radiotracers were explicitly designed with the intention of improving the real-world imaging performance of PSMA-targeted radioligands. Much of the focus was on the alteration and optimisation of clearance pathways *etc.*, to improve the *in vivo* imaging performance of these radioligands. These factors are particularly of interest for those developing PSMA-targeted therapeutics, since off-target binding and uptake is of particular importance for such therapeutic applications.

### 1.5.6 Outlook

In the previous 5-6 years, there has been a surge in the use of PSMA as a target for therapeutics. These range from targeted radionuclide therapies with  $\beta$ -emitters,<sup>330–334</sup>  $\alpha$ -emitters,<sup>335–338</sup> and Auger-emitters,<sup>339</sup> as well as boron neutron capture therapy (BNCT),<sup>340</sup> and small-molecule drug conjugates.<sup>341</sup> As a result of the correlation between PSMA overexpression and tumour stage/aggression, these approaches are highly promising, with [<sup>177</sup>Lu]PSMA-617 giving superior results compared with the standard of care in phase III trials.<sup>342</sup>

It should be noted that accurate calculation of dosimetry is essential for targeted radionuclide therapies, and this explains the particular interest in developing single ligands which can incorporate <sup>68</sup>Ga and <sup>177</sup>Lu (such as PSMA-617 and PSMA-I&T). Even still, the non-prostatic expression of PSMA in healthy tissue (salivary glands etc.) poses a significant concern for the usage of such PSMA-targeted therapeutics, and as such there is an ongoing effort to develop novel chemistries or techniques which can lead to greater specificity for malignancy and reduce uptake in healthy tissue.<sup>343,344</sup>

In addition to the development of these therapies, it could be argued that there is possibly a third generation of PSMA-targeted ligands in development: bispecific ligands which target more than just PSMA. These include bispecific GRPr/PSMA ligands which contain both the glutamate-urea pharmacophore as well as a bombesin derivative, to target the gastrin-releasing peptide receptor (GRPr) which is also overexpressed in prostate cancer.<sup>345,346</sup> Additionally, there is an interest in incorporating albumin-binding groups into PSMA-ligands, to increase persistent tumour uptake (particularly important for therapy).<sup>347,348</sup>

Ultimately, it is clear that while there are some excellent recently approved PSMA-targeted imaging agents, the issue of slow renal clearance still somewhat hampers the imaging of primary prostatic lesions and nearby metastases and as such, there is still an ongoing effort to develop further improved or even bispecific radiotracers. Additionally, with the potential benefits of PSMA-targeted therapeutics becoming clearer all the time, it is easy to anticipate significant future interest into the development of PSMA-targeted compounds, the vast majority of-which are constructed around the ubiquitous glutamate-urea pharmacophore.



## 2 IN-LOOP [ $^{11}\text{C}$ ]CO<sub>2</sub> FIXATION

### 2.1 Introduction

#### 2.1.1 Overview

Due to the short half-lives of the typical radionuclides it employs, PET radiochemistry is essentially synthetic medicinal chemistry performed on a several orders-of-magnitude shorter timescale. Where the production of some standard small-molecule drugs may take days-to-weeks to synthesise, purify, and formulate; a radiochemist has minutes-to-hours to achieve this same feat. The vast majority of these well-developed and understood synthetic processes occur in homogenous, solution-phase reactions, and it is generally these which we first attempt to adapt for use in radiochemical syntheses.

This translation of reactions from a standard synthetic-organic laboratory environment to a radiochemical “hot” laboratory already poses a difficult challenge when starting with solution phase starting materials (aqueous solutions of [ $^{18}\text{F}$ ]F<sup>-</sup> or [ $^{68}\text{Ga}$ ]GaCl<sub>3</sub>, for example). Compared with these other typical radionuclides used for PET radiochemistry, however, carbon-11 presents another, nearly-unique challenge to the radiochemist. The vast majority of carbon-11 radiotracers are produced by  $^{11}\text{C}$ -methylation of alcohols, amines, or thiols with [ $^{11}\text{C}$ ]CH<sub>3</sub>I, a gaseous reagent. Additionally the other major carbon-11 synthons commonly used in PET radiochemistry are [ $^{11}\text{C}$ ]CO<sub>2</sub> and [ $^{11}\text{C}$ ]CO, again both gaseous reagents. Therefore for the radiochemist, both these standard  $^{11}\text{C}$ -methylations as well as the direct incorporation of [ $^{11}\text{C}$ ]CO<sub>2</sub>/[ $^{11}\text{C}$ ]CO must begin with a heterogenous gas-liquid phase reaction. This necessitates the trapping of the gaseous radiolabeling synthon into solution either by passive solubilisation of the compound in many organic solvents (as for [ $^{11}\text{C}$ ]CH<sub>3</sub>I), or by active chemical trapping/fixation (as for [ $^{11}\text{C}$ ]CO<sub>2</sub>/[ $^{11}\text{C}$ ]CO). Once in solution the synthon reacts with the radiolabeling precursor to produce the desired  $^{11}\text{C}$ -labeled target molecule.

Initially this introduction will focus on the traditional  $^{11}\text{C}$ -methylation chemistry, and how radiochemists have historically approached performing and optimising these heterogenous gas-liquid phase reactions. The focus will then shift to more recent work in

which these now well-developed techniques are applied to the use of [<sup>11</sup>C]CO<sub>2</sub> and [<sup>11</sup>C]CO as radiolabeling synthons.

## 2.1.2 Development of thin-film captive solvent techniques

### 2.1.2.1 General introduction to gas-liquid <sup>11</sup>C-methylations

When [<sup>11</sup>C]methyl iodide ([<sup>11</sup>C]CH<sub>3</sub>I) is produced, it is generally carried in a stream of inert gas from the radiosynthesiser to the reaction vial. The reaction vial usually contains a solution of precursor (alcohol, amine, etc.) and a base, in an organic solvent. The [<sup>11</sup>C]CH<sub>3</sub>I is then bubbled through this reaction vial, usually via a needle situated at the base. As the bubbles pass through the solution, the [<sup>11</sup>C]CH<sub>3</sub>I (soluble in most organic solvents) will dissolve into the solution and react with the precursor, forming the desired <sup>11</sup>C-methylated radiotracer. This bubbling through the solution is highly effective and usually leads to near-quantitative trapping of the gaseous [<sup>11</sup>C]CH<sub>3</sub>I, however the process is not yet complete as the reaction still needs time to reach completion before purification and reformulation ready for injection.

Depending on the radiotracer, purification is generally achieved with either semi-preparative HPLC or solid-phase extraction (SPE) so the reaction mixture must be transferred from the reaction vial to the injection loop or cartridge respectively. It is in this transfer stage where product can be lost, either on the walls of the vials or the surfaces of the transfer tubing/channels. These are referred to as “transfer losses” and can lead to a reduction in radiochemical yields and as such, significant efforts have been spent to mitigate these.

In addition to these transfer losses, the other major drawbacks of these vial-based methods result from the complexity of this setup. Firstly, when dealing with carbon-11 radiochemistry, time is of paramount importance when determining the actual effective radioactivity yield. Unnecessary operational complexity of a reaction can result in an undesirable increase in reaction time, associated with transferring reagents from one vial to another. Both due to the physical time taken for these transfers, as well as the increased likelihood of breakdown associated with multiple operational components involved in a process. So any method which simplifies and reduces the complexity of a reaction setup

can present a significant increase in radioactivity yields by shortening the overall reaction time. In addition to this, another governing factor for clinical radiochemists is the standards imposed by GMP regulations. All equipment must be fully cleaned before each production, and a more complex setup will necessarily require a more laborious and time-consuming cleaning procedure, both reducing the operational capacity/productivity of a lab, as well as increasing the likelihood of failures due to cross-contamination etc.

It should also be noted that while the radioactive species produced in the sub-nanomole range (1 GBq of [<sup>13</sup>C]CO<sub>2</sub> = approx. 2.93 pmol), and even accounting for the essentially-unavoidable contamination of atmospheric [<sup>12</sup>C]CO<sub>2</sub> (typically in the range of 10<sup>0</sup>-10<sup>2</sup> nmol), the quantity of radiolabeling precursors used is usually in a large excess, being typically in the micromole range. This mismatch is largely due to the fact that these vial syntheses are performed on a 1-10 mL scale, and as such, using and handling lower than nanomolar quantities is often not practically feasible. While this stoichiometric excess of other reagents can sometimes help in affecting the reaction kinetics, as discussed in the introduction section, the absolute degree of this excess is often unnecessary. Using greater quantities of precursors can lead to higher than necessary raw materials costs, as well as making purification (by HPLC or SPE) more of a challenge. Therefore, miniaturisation of these reactions would help to keep costs low, as well as simplify any purification, while not necessarily affecting the chemical performance of the synthesis.

Taken altogether, these issues make a strong case for the need to develop alternative simplified methods for these standard one-step gas-liquid phase reactions. Any new methods should:

- i) Keep transfer losses to a minimum
- ii) Lower quantities of reagents required
- iii) Simplify cleaning required
- iv) Condense the setup to the minimum number of necessary components
- v) Be robust and widely applicable.

Of the attempts to address these criteria, the most widely implemented is the in-loop captive-solvent synthetic method. The development of this has been most widely attributed to Wilson *et. al.*, and the paper describing the setup,<sup>349</sup> as well as its follow-up describing process automation,<sup>350</sup> are arguably the most clearly and completely described publications on this novel technique. They are certainly the most directly implemented and referenced works in the field. However, to describe this method as a completely ground-breaking development by Wilson *et. al.* would not be entirely accurate. In the decade preceding the publication of this work, a number of other groups developed similar techniques to address these same issues. While none of them are as fully-developed, simplified, or described as well as the in-loop method, they certainly established the preliminary proof of the concept that Wilson's method built upon. To begin a review of the development and use of in-loop captive-solvent methods for <sup>11</sup>C-radiolabeling, it is first important to start by discussing these proof-of-concept methodological developments.

#### ***2.1.2.2 Initial application of the thin-film captive-solvent concept to <sup>11</sup>C-radiochemistry***

Arguably the first real step in the development of this methodology was described in a 1985 paper from Jewett *et al.* at the University of Michigan, as part of their work on automating and miniaturising the process for reacting [<sup>11</sup>C]CO<sub>2</sub> with a Grignard reagent to form [<sup>11</sup>C]palmitic acid.<sup>351</sup> Previously, this reaction had been performed in a similar fashion to the previously described <sup>11</sup>C-methylations in glass vials/vessels, the rough details of these standard synthetic setups follow.<sup>146,150,151,352</sup> The [<sup>11</sup>C]CO<sub>2</sub> from the cyclotron would be pre-concentrated in a cryogenic trap, before being bubbled directly through a vessel containing a solution of 1-pentadecyl-magnesium bromide in diethyl ether, where it would react to form [<sup>11</sup>C]palmitate. This reaction mixture is transferred to another vial to be quenched with aqueous sulfuric acid, before further transferring to a third vial for liquid-liquid extraction from aqueous sodium chloride. The ethereal phase is finally transferred to an alumina column for purification by solid phase extraction of the [<sup>11</sup>C]palmitic acid product. This existing process was i) complex (comprising 3 vessels plus an alumina cartridge), ii) time consuming, iii) difficult to automate, iv) required extensive cleaning before each synthesis, and v) made purification difficult due to the

quantities of reagents employed. To attempt to solve some of these problems, Jewett *et al.* developed a radically different approach to this synthesis: a “captive-solvent” approach.

The “captive-solvent” approach they describe<sup>351</sup> is based on a small plastic cartridge packed with a microporous polypropylene powder. This cartridge is filled with a small quantity of a solution of 1-pentadecyl-magnesium bromide in THF before subsequently flushing any free liquid from the cartridge, leaving just a thin film of this precursor solution coating the pores of this polypropylene powder. This provides a high surface area distribution of the precursor which allows for a better gas-liquid interface – an important feature to consider in these heterogenous gas-liquid trapping reactions.

The [<sup>11</sup>C]CO<sub>2</sub> from the cyclotron is cryogenically preconcentrated before being blown through the cartridge where it traps and reacts with the thin film of precursor solution retained on the surface of the microporous polypropylene powder. The quench, previously performed with a solution of sulfuric acid, is this time performed by passing gaseous hydrogen chloride through the cartridge. This achieves the same aim of deactivating the Grignard precursor as well as working-up the [<sup>11</sup>C]palmitate to form [<sup>11</sup>C]palmitic acid, still held in the thin film of THF on the surface of the polypropylene powder. This crude solution containing the desired product is then eluted from this cartridge with a mixture of diethyl ether and hexane, into a second cartridge containing alumina, where it is trapped on the cartridge, while impurities are washed off. The purified [<sup>11</sup>C]palmitic acid is then simply eluted from the column where it could be analysed.

This cartridge-based captive-solvent system presents a marked improvement over the pre-existing vial-based methods for the synthesis of <sup>11</sup>C-labeled fatty acids. To address the problems listed above with the vial-based method, this captive-solvent method is: i) simpler and easier to maintain (comprising just 2 disposable cartridges), ii) much quicker (12 min vs 30 min), iii) easier to automate (would require just a few remotely operated valves, and also avoids the liquid-liquid separation), iv) much simpler to clean (largely constructed from disposable plastic components), and v) easier to purify since much smaller amounts of starting material are used. As this demonstrates, this new captive-solvent cartridge-based setup improves in almost every way upon the previous vial-based method, while still producing comparable radiochemical yields (and higher radioactivity

yields, by virtue of the reduced synthesis times). This work was really the first demonstration of the power of miniaturising and simplifying carbon-11 radiochemistry, using thin-film captive-solvent techniques.

A few years later in 1988, the same Michigan group then applied the captive-solvent concept to an <sup>11</sup>C-methylation for the first time, to synthesise the benzodiazepine [<sup>11</sup>C]RO5-4864.<sup>353</sup> In this case, instead of using a small cartridge containing microporous polypropylene as the inert high-surface-area support, they used a small length (40mm) of acrylic yarn pulled through a PTFE liquid chromatograph injector loop. The yarn was impregnated with a small amount of NaOH (a base used in the alkylation) by passing a 3% methanolic solution of NaOH before passing N<sub>2</sub> through the loop to evaporate the MeOH, leaving a residual amount of NaOH adsorbed on the otherwise clean/dry yarn. Immediately before radiosynthesis, a solution of the amide precursor in acetone is pipetted into the loop containing the yarn, before cooling the entire loop to -50 °C using a novel heating/cooling device they developed for this work. The [<sup>11</sup>C]CH<sub>3</sub>I is then passed through the cooled loop where it trapped with a 95% efficiency. The loop was sealed and pressurised to 4 atm with N<sub>2</sub> (to avoid evaporation of the acetone and [<sup>11</sup>C]CH<sub>3</sub>I), and heated to 60 °C for 5 minutes to react, before cooling to room temperature. The loop was then eluted with a flow of pentane/EtOH to an on-line disposable alumina column for chromatographic separation/purification.

Compared with the previous solution-based synthesis, this reaction setup produced greatly improved (decay corrected) radiochemical yields (75% *versus* 27%), which combined with the significantly reduced synthesis times led to significantly higher radioactivity yields (45% *versus* 7%), and 10-fold higher molar activities.<sup>354</sup> This work, as the first application of a thin-film captive-solvent technique to an <sup>11</sup>C-methylation reaction, further demonstrated the power of this concept as applied to heterogenous gas-liquid phase reactions for carbon-11 radiochemistry. It allows the miniaturisation/simplification of a reaction setup while still achieving near quantitative trapping of the gaseous <sup>11</sup>C-synthons and providing otherwise similar or improved reaction performance to traditional solution-in-vial based methods. However, while this undoubtedly novel implementation works well for its primary aim, the synthesis of [<sup>11</sup>C]RO5-4864, it was possibly so over-specialised so as to preclude the wider application

of this setup to other  $^{11}\text{C}$ -methylations in other labs. Firstly, while most of the setup is easy to reproduce with standard equipment found in a typical radiochemistry lab, the cooling/heating device was entirely custom-built, which would almost certainly make this setup somewhat laborious and difficult to reproduce. More importantly though, this radiotracer in particular could be purified using low-pressure LC on an alumina column, so therefore it made sense to build this captive-solvent system into the PTFE injector loop of an LC system. However, there are many other  $^{11}\text{C}$ -methylated radiotracers which require HPLC purification, and for these radiotracers this low-pressure LC based system would not be suitable for easy integration into an HPLC system. This lack of general applicability likely explains why although this specific work was successful, this yarn-in-loop setup has not to-date been reproduced for the  $^{11}\text{C}$ -methylation of any other compounds.

This was partially addressed in 1991 with their captive-solvent synthesis of [ $^{11}\text{C}$ ]PK11195,<sup>355</sup> and their introduction succinctly summarises the issue at hand: to achieve direct integration of  $^{11}\text{C}$ -methylations in the injection circuit of a liquid chromatograph, “the solvent containing the precursor must be restrained during reaction with [ $^{11}\text{C}$ ]CH<sub>3</sub>I but later be readily displaced by the chromatographic solvent”. For this synthesis of [ $^{11}\text{C}$ ]PK11195, they chose to integrate a small HPLC-column (3.5 mm x 50 mm i.d.) into the injection circuit of an HPLC. The solid support packed into the column consisted of a mixture of equal weights of KOH powder (a base necessary for the alkylation reaction) and polyethylene powder (the inert high-surface area support). The idea was that this would meet the stated aims of restraining precursor solution during reaction with [ $^{11}\text{C}$ ]CH<sub>3</sub>I (due to the high-surface area supporting a thin-film of the captive-solvent), while allowing the crude reaction mixture to disperse/dissolve back into solution when washed through with the chromatographic solvent (inert polyethylene support has no significant affinity for the starting-materials/compounds produced) for injection onto an analytical reversed-phase HPLC column for purification. In their synthesis of [ $^{11}\text{C}$ ]PK11195, the authors noted a significant amount of unreacted [ $^{11}\text{C}$ ]CH<sub>3</sub>I left at the end of reaction, as well as a significant byproduct formed (they suggest [ $^{11}\text{C}$ ]MeOH, formed by non-specific reaction of the [ $^{11}\text{C}$ ]CH<sub>3</sub>I with the hydroxide base). These issues were much more pronounced in this captive-solvent method than the equivalent solution based method, although the captive-solvent method still produced

reasonable radiochemical yields on the order of approx. 55%. They suggest a reason for this discrepancy being the higher kinetic accessibility of the amide ion to the [<sup>11</sup>C]CH<sub>3</sub>I in a stirred solution as compared with the captive-solvent method, but they also note that the traditional stirred solution setup is more complex and time-consuming than the more streamlined captive-solvent method.

In the paper the authors raise a thought-provoking point regarding whether one can rationalise accepting a lower yielding process if its labour costs are reduced. To summarise their thoughts: one must consider the goals of a radiopharmaceutical production facility, and aim to maximise the use of available resources. In this case, the constant and non-negotiable requirement is for a set amount of [<sup>11</sup>C]PK11195 (specified in *x* MBq in *y* mL saline for injection) to be provided to clinicians for injection and scanning of a patient, but how this is achieved depends on the resources available. The limited resources of a radiopharmaceutical production facility are generally money, availability of radiochemical precursors ([<sup>11</sup>C]CO<sub>2</sub> or [<sup>11</sup>C]CH<sub>4</sub> as provided by the cyclotron), and staff availability. In their case, higher initial quantities of [<sup>11</sup>C]CH<sub>3</sub>I were readily available, whereas staff availability was limited. Therefore it was of greater benefit to implement a mechanically simpler but lower yielding procedure: a captive-solvent synthesis. The higher initial radioactivity would compensate for the lower radiochemical yields, but the savings in staff labour (due to the simplified setup, operation, and cleaning) would be of greater benefit to the facility. Compared with the marginal cost savings from producing less radioactivity, but significantly higher labour burden that would result from adopting the more chemically efficient mechanically-stirred solution-phase synthesis, the benefits of the captive-solvent methodology win-out.

While this sort of cost-benefit analysis is rarely discussed in the majority of radiochemical literature, it is arguable that more attention ought to be paid to this decision making process: it is essential for a radiochemist to remain aware of the context in which they are working. What is our ultimate goal in developing and optimising novel radiosynthetic procedures? It can be easy to focus on tweaking and fine-tuning a reaction to marginally improve our radiochemical yields, but ultimately the RCY is never on the list of specifications provided by a clinician. Generally, the final product must: be sterile, have an RCP of >99%, meet residual solvent limits, and be of the correct dosage. It is surely



the primary role of a production radiochemist to meet these criteria as efficiently and cost-effectively as possible, the exact RCY is essentially irrelevant as long as enough of the final radiolabelled compound is produced within these criteria.

It is this reasoning which often justifies the adoption of thin-film captive-solvent methodologies. Sometimes the raw chemical efficiency of the process may not match up to that of a standard solution-in-vial reaction, however this can often be outweighed by the major benefits in terms of cost/labour savings attributable to the overall streamlining and simplification of the process that these methodologies enable.

In 1992, two papers from the group of Iwata *et al.* described their novel method for on-line <sup>13</sup>C-methylation.<sup>356,357</sup> In the development of this methodology, the authors were trying to address what they saw as an inadequacy of the previously-discussed acrylic yarn-supported <sup>13</sup>C-methylation methodology as developed by Watkins *et al.*<sup>358</sup> Namely, the difficulty of applying this synthesis to any radiotracers which require HPLC purification, since the setup is not suited to withstand the requisite high pressures. In this work, the radiolabeling substrate is adsorbed onto an inert gas-chromatographic solid support, Flusin T, and this solid-supported precursor was mixed with either silica gel or porapak Q to facilitate trapping of the [<sup>13</sup>C]CH<sub>3</sub>I. This mixture was loaded into a small stainless steel pre-column and attached in place of the sample loop on a standard 6-port HPLC injector. This entire injector/reaction column setup was attached to a pneumatic arm which allowed the reaction column to be moved up and down as well as laterally. The column was initially lowered into an acetonitrile-dry ice bath at -42°C before passing the gaseous [<sup>13</sup>C]CH<sub>3</sub>I through the reaction column, where it is cryogenically condensed/trapped on the high-surface area silica gel/porapak. A reaction solvent, consisting of tetrabutylammonium hydroxide in DMF was loaded into the column, before pneumatic transfer of the reaction column to an adjacent oil bath at 80°C for 5 minutes. This reaction mixture was then injected directly onto a semi-prep HPLC column for purification.

While this method gave reasonable radiochemical yields for their model substrate, 3-*N*-[<sup>13</sup>C]methyl-spiperone, there was also a significant quantity of radioactive residue remaining on the reaction column, even after 50 seconds of continuous washing through to the HPLC column. This was likely due to interactions between the radiolabeled

products and the silica gel/porapak in the column. As such, this method has a largely unavoidable drawback in that while it enables a relatively straightforward on-line methylation reaction, the desired product is not easily displaced by the chromatographic solvent and radiochemical yields of this process are hindered. While, as discussed above, maximising the RCY of a process is not always necessary if it also leads to a much simplified/streamlined process, this process is also arguably not significantly simpler than a mechanically stirred  $^{13}\text{C}$ -methylation. Its specialised pneumatic setup, as well as the necessity of preparing the solid-supported precursor, means that it is difficult to foresee any significant savings in labour that adopting this methodology would entail. As such, the reduced RCYs as a result of unrecovered product on the column are a major disadvantage to this method, and certainly leave room for further improvement. Although it should be noted that this setup did broaden the scope of on-line methylation reactions by integrating it into a standard HPLC purification system.

The same group then applied this methodology to the preparation of L-[*methyl*- $^{13}\text{C}$ ]methionine from L-homocysteine thiolactone.<sup>359</sup> In this case however, instead of directly injecting the reaction mixture onto an HPLC column for purification, the reaction mixture was fully eluted into a rotary evaporator flask to remove the reaction solvent, before re-dissolution in saline ready for injection. While this entire process was still technically on-line and fully automated, incorporation of a rotary evaporator into the setup made this a more difficult and laborious process to replicate elsewhere, and the lack of any HPLC purification in this setup precluded it from being widely applied to the synthesis of many other radiotracers.

Over the next two years, the same group further expanded this methodology to the synthesis of several  $^{13}\text{C}$ -labeled fatty acids from the reaction of Grignard reagents with [ $^{13}\text{C}$ ]CO<sub>2</sub>: [ $^{13}\text{C}$ ]acetic and [ $^{13}\text{C}$ ]palmitic acid.<sup>360</sup> To achieve this, they moved away from the use of silica/porapak as the solid support for the captive solvents, and instead used Extrelut, a highly-porous polar stationary phase traditionally used to simplify liquid-liquid extractions as it will retain hydrophilic compounds when washed with hydrophobic solvents; and Extrelut was chosen for two reasons. Firstly, its highly-porous nature presented a high-surface area to support a thin film of the captive-solvent, enabling excellent gas-liquid interfacial contact, as seen in all methodologies previously discussed.

Secondly, they exploited the polarity of Extrelut to simplify purification of the final products: after trapping the  $^{11}\text{C}$ CO<sub>2</sub> with Grignard reagents, the free fatty acids must be released by a work-up with HCl, but purification of the  $^{11}\text{C}$ -fatty acids from the aqueous acid is somewhat difficult and traditionally requires liquid-liquid extraction. However, Extrelut retained the polar aqueous HCl solution, releasing the  $^{11}\text{C}$ -fatty acids when eluted with the hydrophobic diethyl ether or hexane, avoiding the need for further laborious purification. This work was the first example of the use of a dual-purpose solid-support for both its high surface area (to support a thin-film of captive-solvent), but also for its selective retention of certain reagents to simplify purification.

These dual-purpose Extrelut columns were also used by Iwata for the first application of a thin-film captive-solvent methodology to a radiosynthesis with  $^{11}\text{C}$ HCN, a less commonly used gaseous  $^{11}\text{C}$ -radiolabeling reagent. 1-Aminocyclopentane-1- $^{11}\text{C}$ carboxylic acid ( $^{11}\text{C}$ ACPC) was synthesised in an analogous manner to the  $^{11}\text{C}$ -fatty acids produced previously. The porous high-surface-area extrelut supported a thin-film of an aqueous solution of the aminosulfite precursor, which when flushed with  $^{11}\text{C}$ HCN trapped with efficiencies exceeding 99%, forming a nitrile intermediate. This intermediate could be quantitatively eluted with diethyl ether onto a second column of Extrelut, preloaded with an aqueous solution of HCl, where the nitrile intermediate then back-extracted into the aqueous solution retained by the Extrelut. Heating of this second column hydrolysed the intermediate, producing the desired  $^{11}\text{C}$ ACPC product which was simply eluted with water for HPLC purification. This work further demonstrated the adaptability/versatility of thin-film captive-solvent techniques, having now been applied for reactions with  $^{11}\text{C}$ CO<sub>2</sub>,  $^{11}\text{C}$ CH<sub>3</sub>I, and  $^{11}\text{C}$ HCN.

The next major development of a thin-film captive-solvent methodology was in the 1996 synthesis of [*carbonyl*- $^{11}\text{C}$ ]WAY-100635 by McCarron *et al.*<sup>361</sup> This methodology involved the immobilization of a Grignard reagent on the walls of a length of polypropylene tubing, a stream of  $^{11}\text{C}$ CO<sub>2</sub> was passed through the tubing and achieved near quantitative trapping as an intermediate adduct. A solution of thionyl chloride was then passed through the tubing, producing the [*carbonyl*- $^{11}\text{C}$ ]acid chloride radiolabeling reagent *in situ*, before releasing into a vial containing a solution of the secondary amine precursor and a necessary base. The reaction in the vial produced the desired amide

product, labeled at the central carbonyl within the molecule. Compared with the other examples discussed in this review thus far, this reaction is significantly more complex than a single step gas-liquid reaction to form an <sup>13</sup>C-methylated compound within the thin-film of captive solvent itself. In this work, they successfully performed a multi-stage reaction that involved heterogenous gas-liquid trapping of [<sup>13</sup>C]CO<sub>2</sub>, conversion to a reactive radiolabeling intermediate, and finally reaction with a second precursor compound to produce the desired product.

This reaction was previously developed using a more standard one-pot stirred-solution process, whereby the [<sup>13</sup>C]CO<sub>2</sub> was bubbled through a first vial containing a solution of Grignard reagent, before subsequent addition of thionyl chloride to form the acid chloride <sup>13</sup>C-radiolabeling reagent. This reagent was then transferred to a second vial containing the precursor/base solution. There were however some major drawbacks associated with this vial-based synthesis method. The crucial issue was the requirement that the precursor, WAY-100634, be used in at least equimolar amounts as the Grignard in the trapping solution. To achieve sufficient trapping of [<sup>13</sup>C]CO<sub>2</sub> in solution, significant concentrations of this Grignard are required, thus requiring significant quantities (60 mg) of the WAY-100634 precursor in the second vial. These large quantities of reagents are not compatible with HPLC purification, and even after pre-purification/sample-enrichment, significant quantities of the biologically active precursor were still present in the sample, which would potentially interfere with the binding of the radiotracer to its 5-HT<sub>1A</sub> target. Additionally, this two vial reaction was fairly time consuming, and thus led to only moderate yields and molar activities.

The immobilized Grignard method coated the inside walls of a length of polypropylene tubing with a residual thin film of Grignard solution (likely held in-place by hydrophobic interactions), which was still sufficient to trap >95% of [<sup>13</sup>C]CO<sub>2</sub> passed through the tubing. The following reaction with the thionyl chloride was near instantaneous, allowing the *in situ* generation of the reactive acid chloride intermediate within the tubing, allowing immediate reaction with the labelling precursor. In addition to the resultant time savings from this streamlining, the significantly reduced quantities of Grignard allowed a respective decrease in the quantities of WAY-100634 precursor used (3.5 mg vs 60 mg). This significant reduction in reagents vastly simplified HPLC purification while also

reducing the troublesome contamination of the final product by this biologically active precursor. This work demonstrated the real benefits to both purification and reaction time/setup that could be achieved by the effective miniaturisation of a reaction that this thin-film technique allows. All while retaining comparable or improved radiochemical yields and molar radioactivities, essential for saturable neuroreceptor-binding radiotracers. In addition, high-surface-area substrates (microporous polypropylene powder, acrylic yarn, etc.) were not necessary in this method: the internal walls of the polypropylene tubing provided sufficient surface area for the retention of the captive solvent, achieving near-quantitative trapping. The elimination of any additional inert substrates further enhanced the attractiveness of this technique as it further simplified the reaction setup, and increased the reproducibility of the method as no further column/tube packing was required by operators.

This methodology was adapted by Davenport *et al.*, of the same group, for three further publications detailing their syntheses of [*carboxyl*-<sup>11</sup>C]propionyl-L-carnitine ([<sup>11</sup>C]PLC),<sup>362</sup> [<sup>11</sup>C]acetate,<sup>363</sup> [<sup>11</sup>C]bunazosin,<sup>364</sup> as well as a series of <sup>11</sup>C-labeled acyl analogues of WAY-100635.<sup>364</sup> All of this work adapted the setup from their initial synthesis of [<sup>11</sup>C]WAY-100635, but with some minor modifications for the individual radiotracer. The majority of these reactions were instead performed in a PTFE loop, as opposed to polypropylene, and some involved a second vial-based reaction as for [<sup>11</sup>C]WAY-100635. But all syntheses were based around the same simple, efficient, and easy to implement/reproduce process. Trapping cyclotron-produced [<sup>11</sup>C]CO<sub>2</sub> on the walls of a short length of polymer tubing coated in a thin-film of Grignard reagent, before flushing the tubing through to either a second reaction vial, or directly into an HPLC injector loop. Flushing with an aqueous acidic solution produced the carboxylic acid species (as for [<sup>11</sup>C]acetate) directly, ready for purification. Flushing into a vial allowed a secondary reaction: either enzymatic in the example of [<sup>11</sup>C]PLC; or *via* the same in-line conversion to an acid chloride before reaction with an amine forming an <sup>11</sup>C-amide, as in the synthesis of [<sup>11</sup>C]bunazosin and [<sup>11</sup>C]WAY-100635 and its analogues. These further publications demonstrated the genuine wide applicability of this methodology, showing that it can be used for both the simple production of <sup>11</sup>C-carboxylic acids as well as simplifying the heterogenous gas-liquid trapping step in an otherwise complex multi-step reaction. The fact that the setup itself is composed of a cheap, disposable length of

polymer tubing just added to the attractiveness of this methodology. A statement that can be attested to by the fact that [<sup>11</sup>C]acetate is still produced in this way in many PET centres more than 20 years later.<sup>365–367</sup>

A different captive-solvent synthesis of [<sup>11</sup>C]WAY-100635 was reported concurrently by Wilson *et al.*, but this time radiolabeled at the more conventionally radiochemically-accessible *O*-methyl position, using [<sup>11</sup>C]CH<sub>3</sub>I.<sup>368</sup> Similarly to the concurrent work from McCarron *et al.*, this on-cartridge synthesis represented a step forward from the previously developed thin-film methodologies. Instead of a custom packed column or tubing as before, this method simply employed a standard commercially-available C18 SPE cartridge as the solid-support for retention of a thin-film of the captive solvent, allowing both a simple setup as well as a much streamlined cleaning process. In this case, a methanolic solution of the nor-methyl precursor and TBAH base were preloaded on the C18 cartridge, before the [<sup>11</sup>C]CH<sub>3</sub>I was swept through the cartridge where it trapped and reacted to form the radiotracer on-cartridge. The cartridge was flushed with HPLC buffer into an HPLC injector loop and purified by semi-preparative reverse-phase HPLC before reformulation for injection. The synthesis was complete within 25 minutes from EOB, with an average non-decay corrected RCY of 25%. These results represented a significant improvement from the regular stirred-solution reactions (10-12% in a 50 minute reaction time), demonstrating that a simple on-cartridge thin-film synthesis could be advantageous in terms of both simplicity of setup/automation as well as superior chemical performance. The authors also noted that they had applied the method to several related compounds with comparable success, and therefore expressed hope that this could be applied as a general method for <sup>11</sup>C-methylation.

This “on-cartridge” <sup>11</sup>C-methylation methodology was further applied by Pascali *et al.*, in the synthesis of [<sup>11</sup>C]methionine and [<sup>11</sup>C]choline.<sup>369,370</sup> In their earlier work on “on-column” <sup>11</sup>C-radiolabeling, they exploited Extrelut as a dual-purpose substrate: both as a high surface area support for the captive solvent; as well as a chromatographic substrate to selectively retain certain compounds to simplify purification. One of the major limitations of this earlier work was the requirement that the cartridge be cooled to -42°C for trapping before heating to 80°C for the reaction, however the authors noted that this was not necessary in the work by Wilson *et al.* They therefore combined both of these

methodologies initially in their synthesis of [<sup>11</sup>C]methionine. In it, they loaded the homocysteine thiolactone precursor (at room temperature) onto a commercially available C18 cartridge before distilling [<sup>11</sup>C]CH<sub>3</sub>I across the cartridge, forming the [<sup>11</sup>C]methionine *in situ*. They were then able to selectively elute the [<sup>11</sup>C]methionine from the cartridge, due to its selectively higher retention of [<sup>11</sup>C]CH<sub>3</sub>I. The eluate was passed through a second C18 sep-pak to ensure removal of any breakthrough [<sup>11</sup>C]CH<sub>3</sub>I, resulting in a final radiochemical purity of >99.5%, without any further purification. At this point, the compound could be fully formulated in saline ready for injection. In their synthesis of [<sup>11</sup>C]choline this SPE methodology had to be further expanded to enable the retention/purification of the choline chloride product, a quarternary ammonium salt. As such, while the 2-dimethylaminoethanol precursor can be loaded/retained on the C18 cartridge, the positively charged choline product is too polar for retention. They therefore added a second cartridge in series with the C18: a weak cation-exchange cartridge (Sep-Pak Accell Plus CM) which would trap the [<sup>11</sup>C]choline product, but allow any unreacted [<sup>11</sup>C]CH<sub>3</sub>I to wash through to waste. The product could then simply be eluted from the cartridge with saline as the final chloride salt of [<sup>11</sup>C]choline, without requiring further purification. This work again demonstrated that the use of thin-film captive-solvent techniques could lead to major benefits including: simplification of reaction setup, enabling automation, and ease of purification. In particular, this work reinforced the conclusion from Wilson *et al.* that complex custom-filled columns were not necessary to provide high surface-area substrate supports for thin-films of captive-solvents, instead a common commercially-available C18 SPE cartridge would suffice.

In approximately 15 years, the body of work discussed above introduced the radical concept of using thin-films of captive-solvents in <sup>11</sup>C-radiochemistry. Unlike for say, <sup>18</sup>F-radiochemistry, the majority of the fundamental <sup>11</sup>C-radiolabeling reagents are gaseous, and so the vast majority of <sup>11</sup>C-radiolabeling processes will involve a heterogenous gas-liquid phase reaction. While traditionally these reactions were performed by bubbling the gaseous <sup>11</sup>C-reagent through a mechanically stirred vial containing a solution of the precursor, this methodology could hinder the wider implementation of these <sup>11</sup>C-radiotracers. The processes can be difficult to automate, time consuming to both set-up as well as routinely produce, and the scale can require using reagent quantities that make SPE or semi-prep HPLC purification challenging. By effectively miniaturising this

heterogenous gas-liquid reaction, reactions could be more amenable to automation, faster to setup/clean, reaction times could be shortened, and purification could be simplified. However, while these new methodologies presented these vast improvements, broad adoption of a single technique was difficult as the syntheses of some radiotracers were better suited to one method or another. Although what does emerge upon surveying and synthesising the body of work to this point, is a set of broad criteria by which a thin-film captive-solvent methodology can be assessed.

Initially, just considering  $^{11}\text{C}$ -methylation, the method should:

1. Be broad in substrate scope
2. Use cheap, easy to clean commercially available components
3. Perform well at ambient temperatures
4. Be easy to automate both production and purification
5. Provide comparable radiochemical yields to conventional stirred-solution methods

### ***2.1.2.3 The landmark “remarkably simple captive solvent method” – the loop-method for $^{11}\text{C}$ -methylation***

It was in an effort to address these aforementioned criteria, that in 2000 Wilson and co-workers published the landmark paper describing their “remarkably simple captive solvent method” for  $^{11}\text{C}$ -methylation with [ $^{11}\text{C}$ ]CH<sub>3</sub>I inside a standard HPLC injector loop.<sup>349</sup> In essence, a solution of radiolabeling-precursor and base is loaded into a stainless-steel HPLC injector loop connected to a commercial 6-port HPLC injector valve set to LOAD. The loop is then connected to the [ $^{11}\text{C}$ ]CH<sub>3</sub>I transfer line where it is initially flushed with a flow of N<sub>2</sub> to disperse the captive-solvent as a thin-film along the inside surface of the loop. Following this, [ $^{11}\text{C}$ ]CH<sub>3</sub>I is delivered through the loop where it traps near quantitatively (>92%) forming the  $^{11}\text{C}$ -methylated product *in situ*. The injector valve simply has to be switched to INJECT, to quantitatively wash the contents of the loop through to a connected HPLC column for purification. The entire reaction was performed



at ambient temperature and was applied successfully to 9 diverse and clinically-relevant nor-methyl precursors in the first instance, consisting of both amino and alcoholic substrates, resulting in comparable or superior RCYs to traditional stirred-solution-in-vial syntheses. In addition to this simplification of the reaction process, cleaning was straightforward too. Since the HPLC solvent should have already cleaned the loop, it just required rinsing with water or ethanol (to remove any traces of buffer), then acetone, before blowing dry. A follow-up note described the full automation of this process including cleaning, meaning that the only requirement for human operator interaction was the injection of precursor solution shortly before [<sup>11</sup>C]CH<sub>3</sub>I delivery.<sup>350</sup>

This work vastly simplified all steps of the process and addressed the criteria set-out above; where other earlier thin-film captive-solvent methodologies fell short in at least one of these areas, this “loop method” was the first process which truly satisfied all requirements. The instrumentation setup was incredibly elementary and simple, being performed within an HPLC injector system, ubiquitous within radiochemistry laboratories. It is also notable that as in the earlier work by McCarron *et al.*<sup>361</sup> no additional high-surface area substrate was required: the inside walls of the loop were sufficient for retention of a thin-film. No heating or cooling was required as the reaction proceeded well at ambient temperatures. This was crucial so as to avoid the use of either pneumatic systems to move the loop from cooling baths to heated oil baths,<sup>356</sup> or complex proprietary heating/cooling jacket setups,<sup>358</sup> as were both seen in previous work. Since no moving parts (excepting switchable valves) were required and the entire setup was composed of a few simple components, automation and remote operation were straightforward. The remote switching valves required for this were commercially available, and so this obviated the need for an expensive, large-footprint, proprietary system to perform methylations (of course a system for [<sup>11</sup>C]CH<sub>3</sub>I production is still required).

Finally, as mentioned briefly above, the method produced comparable or superior radiochemical yields to the traditional solution-in-vial syntheses. While – as discussed by Jewett *et al.*<sup>355</sup> – the highest RCY possible is not necessarily the highest priority, improving the radiochemical performance while also simplifying and streamlining a

reaction process is a very impressive feat, and some potential explanations for this will be considered in the following section.

This “loop method” as described by Wilson and co-workers was an incredibly simple, versatile, ambient-temperature method for the synthesis of a wide variety of <sup>13</sup>C-methylated radiotracers. Its use of commercially available, standardised HPLC components enabled for the first-time a wide implementation of a thin-film captive-solvent methodology for <sup>13</sup>C-methylations (beyond the 4 groups implementing similar techniques until this point), bringing with it all of the associated advantages discussed herein. The paper has over 200 citations at time of writing, and for many PET centres has become their routine method for standard heteroatom <sup>13</sup>C-methylation. The further implementation of this method more recently will be reviewed shortly, however first, the mechanism of this “loop method” warrants additional discussion.

#### ***2.1.2.4 Study and discussion of the mechanism of the “loop method”***

In their original paper, Wilson and coworkers only briefly discussed the increased reaction rates/radiochemical yields seen in-loop compared with the same reaction performed in vial. This increased rate was particularly notable considering that their method proceeded well at ambient temperatures, whereas most methods in vial required heating to approx. 90°C. Their major line of reasoning was that the reaction rate increased as a result of the increased precursor concentration in their captive-solvent. While they significantly reduced the volume of solvent compared with a vial-synthesis, the quantities of precursor were kept in the same range, resulting in concentrations of at least 3 times those in vial. Radiochemical reactions already benefit from pseudo-first-order kinetics when compared to conventional non-radioactive reactions, as a result of the large excess of the precursor (micromolar quantities) compared to the nanomolar quantities of the <sup>13</sup>C-radiolabeling reagent.<sup>371</sup> Under these conditions, radiolabeling reactions proceed much faster than their respective non-radioactive counterparts. This further-increased concentration arising from the use of thin-films of the captive solvents would be expected to lead to increased reaction rates, although it's not easy to predict the magnitude of this expected increase. Their other suggestion was simply that due to the inherent reactivity

of [<sup>11</sup>C]CH<sub>3</sub>I, researchers in the field were perhaps already using longer reaction times/higher temperatures than was strictly necessary.

While it is not discussed in their paper, the use of a thin-film of reaction solvent could speculatively play a role in the superior rates/yields resulting from this method, when compared with the relatively large bulk of solution in a stirred-vial synthesis. Primarily, the rate of trapping must be a function of the gas-liquid contact at the interface which enables mass transfer of the [<sup>11</sup>C]CH<sub>3</sub>I into the liquid phase. So dispersing the captive-solvent across the inside surface of the loop as a thin-film gives a much higher interfacial surface-area for the mass-transfer, per given volume of solution, when compared with standard solution-in-vial chemistry. This is reflected in the fact that near-quantitative trapping was seen for the in-loop setup, even considering the faster trapping times and the use of smaller volumes of solution. It is also tempting to consider the benefits sometimes afforded to reactions by constraining the dimensions of their reaction vessels (in this case, in the 20 μm thick film of captive-solvent). Microfluidic reactions, for example, have been demonstrated to increase the rates of diffusion-controlled processes, by limiting the diffusional distances of the reaction.<sup>372,373</sup> In this case however, it is highly unlikely that these standard S<sub>N</sub>2 methylation reactions are fast enough to be limited by the rate of diffusion of reactants through the solution (a situation more commonly seen for much faster complexation or enzymatic reactions). So in this case, the major benefits associated with performing these reactions in the micro-scale of a thin-film are largely expected to be due to the increased gas-to-liquid mass-transfer rate resulting from the high interfacial contact afforded by this setup, and not due to any kinetic advantages associated with the reduced diffusion-lengths.

One further area that has not been discussed widely in the context of radiochemistry in-loop is the phenomenon of radiolysis.<sup>374,375</sup> Radiolysis is the process of molecular degradation by radiation-induced chemical bond cleavage, and can occur in radiotracer production as well as in fully formulated radiopharmaceuticals, reducing chemical and radiochemical purity/yields. Higher radioactivity concentrations lead to greater degrees of radiolysis, so it is more likely in batch productions, with high starting quantities of radioactivity. Before annihilation, high energy positrons undergo a thermalization process to lose kinetic energy by colliding with solvent molecules as well as starting materials

and final products, to gradually lose their kinetic energy. In this process, the positron moves away from its site of emission, depositing its kinetic energy in its surroundings along the way. It is this energy which can cause chemical degradation by a number of mechanisms including radical formation, and this is why final radiotracer product formulations often include an antioxidant as a radiolysis inhibitor, however antioxidants cannot be used to reduce radiolysis during radiotracer synthesis itself. It has been shown however in microfluidic devices, that decreasing the dimensions of the reaction vessel itself (i.e. microcapillaries), to dimensions smaller than the mean-free-path length of a positron will mean that the positron will leave the reaction media before it has had a chance to deposit all of its energy, reducing the degree of radiolysis within the reaction.<sup>374</sup> In one investigation by Rensch *et al.*, it was demonstrated that confinement of a <sup>18</sup>F-labeled product within a 250 μm capillary could limit radiolysis to just 14% of that which occurred in a vial.<sup>376</sup> It stands to reason therefore, that one could hope to see a reduction of radiolysis as a result of performing radiosynthesis in the 20 μm thin-films of reaction solvent as used in the loop-method, and could be one further explanation for the superior performance of this loop-methodology compared with standard vial methods.

In 2004 an in-depth study of the in-loop methodology was published by Studenov *et al.*, in which they creatively probed the exact mechanisms behind loop-methylations, the results of which are enlightening.<sup>377</sup> They explored the effects of different loop materials (stainless steel (SS), PEEK, and ETFE), the kinetics and spatial-distribution of [<sup>13</sup>C]CH<sub>3</sub>I trapping within a loop, as well as the effects of altering the amounts and composition of the reaction solutions. This investigation involved dynamic PET imaging of a loop during the trapping process, scanning a loop containing trapped [<sup>13</sup>C]CH<sub>3</sub>I with a linear radio-TLC plate-reader, separate elution of different sections of the loop, and finally, they investigated the dependence of trapping and <sup>13</sup>C-methylation on the amounts of precursor and solvent. These experiments were all relatively simple, but by using existing technologies available to most radiochemistry research facilities (PET scanners, TLC readers etc.) they revealed a lot about the mechanisms governing this process and probed the limits of solvent/precursor minimisation that an in-loop methodology was hypothesised to allow.

Firstly, in their dynamic PET imaging of the [<sup>11</sup>C]CH<sub>3</sub>I trapping process, they observed that the initial trapping is a reversible process, whereby the trapped activity peaked at approx. 1.5 mins, but was almost entirely flushed from the loop by 2 minutes. This is particularly important for [<sup>11</sup>C]CH<sub>3</sub>I since its primary trapping mechanism is a passive dissolution in the solvent, the methylation reaction occurs secondarily to this step. This suggested that it is essential to monitor the loop during the trapping process, and stop the flow of carrier gas as soon as trapping reaches its peak. Secondly, on comparing SS, PEEK, and ETFE loops (all 2 ml volumes), it was found that the steel and PEEK loops would retain all of the captive solvent added, while the ETFE loop would release some of the solvent after a short time of flushing, likely due to the poor wettability of fluorinated polymers such as ETFE. As such, this release of [<sup>11</sup>C]CH<sub>3</sub>I was more rapid in the ETFE loop, due to the combined factors of the reversible trapping dynamics as well as expulsion of solvent containing trapped radioactivity. In the SS and PEEK loops, it was found that the majority of the activity was trapped close to the inlet of the loop (and not evenly distributed down the length of the loop) as was expected, assuming that the process of [<sup>11</sup>C]CH<sub>3</sub>I diffusive mass-transfer into the solvent is not at equilibrium. In their experiments on the reduction of precursor/solvent amounts. They found that a 5-fold reduction in solvent volume and precursor amount led to halved trapping efficiencies but did not affect the conversion of the trapped [<sup>11</sup>C]CH<sub>3</sub>I to the <sup>11</sup>C-methylated products. When just the precursor quantity was reduced 5-fold while keeping the solvent volume the same, they found that the trapping efficiency was unaffected (unsurprising given that a loop filled with just solvent will trap [<sup>11</sup>C]CH<sub>3</sub>I quantitatively). However the <sup>11</sup>C-methylation was more variable: for the synthesis of [<sup>11</sup>C]carfentanil, the reaction proceeded unaffected; whereas in the synthesis of [<sup>11</sup>C]SCH23390, the yields halved. They therefore showed that while in-loop reactions can possibly allow reductions in the quantities of precursor used, this is variable depending on the reaction, and as such it must be explored on a case-by-case basis in situations where excess precursor can lead to difficulties in purification or troublesome side-products. Finally, they investigated the use of acetonitrile, a lower-boiling solvent, and found that it tended to give much more variability in product yields compared with DMF/DMSO. They theorised that evaporation of the acetonitrile could lead to regions within the loop with no-solvent, hindering the reaction in those areas. However the authors noted that for reactions which

did not proceed well in DMF/DMSO (e.g. [<sup>11</sup>C]DTBZ), they still adopted an in-loop process with acetonitrile for routine synthesis since the loop-method is so much more simple/convenient that the variability in yields was not a sufficient hindrance to adoption of this method. In summary, this work helped to expand the understanding of the mechanisms and limitations of this in-loop methodology, and must be kept in mind if looking to further adapt this sort of approach for other chemistries. In the following years, this loop-methodology was very widely implemented, and this study of the mechanism itself helped to refine the methodology and defined the limits under which reactions could be further miniaturised.

#### 2.1.2.5 Further applications of the “loop method”

In the original work by Wilson *et al.*, the loop-method was applied for the synthesis of: [<sup>11</sup>C]RTI-32, [<sup>11</sup>C]SCH 23390, [<sup>11</sup>C]FLB 457, [<sup>11</sup>C]NMS, [<sup>11</sup>C]raclopride, [<sup>11</sup>C]Ro 15-1788, [<sup>11</sup>C]rolipram, [<sup>11</sup>C]SKF 82957, and [<sup>11</sup>C]DASB; demonstrating the broad applicability of this method to the synthesis of a variety of *O*- and *N*-methylated <sup>11</sup>C-radiotracers. In the intervening years this methodology has been widely applied by many groups/PET centres for routine <sup>11</sup>C-methylations, an exhaustive account of all implementations of this in-loop approach would be difficult to assemble, but as a representative sample the loop-method has since been used for <sup>11</sup>C-methylation in the synthesis of: [<sup>11</sup>C]choline;<sup>378,379</sup> [<sup>11</sup>C]methionine<sup>380,381</sup> (demonstrating applicability to *S*-methylations); [<sup>11</sup>C]carfentanil;<sup>382,383</sup> [<sup>11</sup>C]doxepin;<sup>384,385</sup> [<sup>11</sup>C]Pittsburgh compound-B;<sup>386-388</sup> [<sup>11</sup>C]AR-A014418;<sup>389</sup> [<sup>11</sup>C]P943;<sup>390</sup> [<sup>11</sup>C]nicotine;<sup>391</sup> [<sup>11</sup>C]PABA;<sup>392</sup> and d-[<sup>11</sup>C]threo-methylphenidate.<sup>393</sup> This extensive list demonstrates the widespread implementation of in-loop <sup>11</sup>C-methylations, following the landmark work by Wilson, and in several cases it was further applied to reactions using [<sup>11</sup>C]CH<sub>3</sub>OTf.<sup>384,385,394-396</sup> The ultra-simplicity of the methodology, and the near-universal substrate-applicability allowed many PET centres to take advantage of the aforementioned benefits that a thin-film captive-solvent methodology can bring to otherwise routine <sup>11</sup>C-radiolabeling procedures.

The translation of vial-based syntheses to in-loop setups has not always been completely straightforward. In the synthesis of [<sup>11</sup>C]gefitinib from [<sup>11</sup>C]CH<sub>3</sub>OTf reported by Holt *et*

*al.*, the standard in-vial reaction was compared with an in-loop methodology.<sup>396</sup> In this example, their trapping efficiency in-loop was significantly lower than that seen in the equivalent vial-based procedure (25% vs 95%). This result deviates strongly from those seen for the majority of in-loop methylations, which is surprising considering that it has been shown that loop trapping efficiency (at least for [<sup>11</sup>C]CH<sub>3</sub>I) is near-quantitative for a loop containing pure solvent with no added precursor.<sup>349,377</sup> This implies that trapping rate is independent of the methylation reaction rate itself, and is instead simply a function of gas-solvent mass-transfer rates, which should largely be governed by solubility. Since [<sup>11</sup>C]CH<sub>3</sub>I and [<sup>11</sup>C]CH<sub>3</sub>OTf have comparable solubilities in DMSO, one would therefore expect similar near-quantitative trapping for the [<sup>11</sup>C]CH<sub>3</sub>OTf in this work. The fact that it was significantly lower in this case suggests that the flushing conditions to coat the loop were too harsh and expelled too much of the captive-solvent from the loop, or instead the authors did not monitor the loop activity to ensure that gas flow was stopped at the trapping peak (keeping in-mind the reversibility of trapping, as discussed by Studenov *et al.*<sup>377</sup>). However, the experimental details provided in this paper were minimal, and as such, it is difficult to speculate confidently why this particular work was unsuccessful. A similar comparison of a methylation performed in-vial as well as in-loop was presented in 2004 by Wilson *et al.*, in their synthesis of [<sup>11</sup>C]Pittsburgh Compound-B from [<sup>11</sup>C]CH<sub>3</sub>OTf.<sup>386</sup> In this case, however, no significant difference in RCYs or molar activities were found, and as such, the simpler in-loop methodology appears the more attractive prospect. One further comparison was the work in 2010, reported by Nabulsi *et al.* in their synthesis of [<sup>11</sup>C]P943.<sup>390</sup> In this, they found similar results for both in-vial and in-loop syntheses, however the in-loop method gave marginally lower RCYs as well as molar activities. It should be noted though, that in this case, the in-vial methylation was performed with [<sup>11</sup>C]CH<sub>3</sub>OTf, whereas the in-loop methylation used the less reactive [<sup>11</sup>C]CH<sub>3</sub>I. This could go some way to explaining the discrepancy observed here, but it is important to note that the authors state that either method produced sufficient quantities of radiotracer meeting all specifications, and as such, one could still benefit from the time/cost savings of the simpler to setup and clean in-loop methodology.

As well as <sup>11</sup>C-methylation, the in-loop methodology was also adapted for <sup>11</sup>C-carboxylations via the reaction of Grignard reagents with [<sup>11</sup>C]CO<sub>2</sub> in-loop, similarly to the earlier work by McCarron and Davenport.<sup>361,363,364</sup> The first major examples of this

were the concurrently published methods for in-loop synthesis of [<sup>11</sup>C]acetate from LeBars<sup>366</sup> and Soloviev<sup>365</sup>. In these methods, a polymer loop (either ETFE tubing or commercially available sterile polyethylene catheter, respectively) was coated with a thin-film of a solution of methylmagnesium bromide, which quantitatively traps the [<sup>11</sup>C]CO<sub>2</sub> passed through. The loop is then simply eluted with water onto a SAX cartridge where it is trapped and washed, before elution with saline as sodium [<sup>11</sup>C]acetate, ready for injection. This methodology deviates from the standard SS HPLC injector loop protocol, instead using a disposable polymer loop. In standard <sup>11</sup>C-methylation chemistry, the product is formed directly on the walls of the loop, and usually requires HPLC purification. Such a <sup>11</sup>C-methylation in the injector system makes sense, as has already been discussed at length. However, the products of <sup>11</sup>C-carboxylation reactions with [<sup>11</sup>C]CO<sub>2</sub> can often be purified with SPE, negating the need for HPLC. In these cases therefore, the loop used does not need to be compatible with high-pressures etc. and so the use of single-use disposable loops (even sterile, commercially available catheters<sup>365,367</sup>) can be advantageous. They can still interface with standard radiosynthesis automation units through Luer/Fingertight fittings, but single-use components negate the need for thorough cleaning and are therefore ideal from a GMP-standpoint. Similarly, Zhang and co-workers employed a polyethylene loop-method for the synthesis of [<sup>11</sup>C]2-iodopropane and [<sup>11</sup>C]iodoethane, whereby the respective alkylmagnesium bromide precursors were reacted with [<sup>11</sup>C]CO<sub>2</sub> in-loop forming the carboxylate intermediates.<sup>397</sup> The loop was washed through with LiAlH<sub>4</sub> into a reaction vial containing a concentrated solution of HI, forming the [<sup>11</sup>C]alkyliodide products. In this case since a secondary reaction was required, direct interfacing with an HPLC purification system was unnecessary, and again, a disposable sterile polymer loop was preferred. This work further demonstrated that loop-methodologies can also be used to streamline/simplify one stage of a multi-step radiosynthesis, in addition to simple one-step methylations/carboxylations. Similar in-loop <sup>11</sup>C-carboxylations from [<sup>11</sup>C]CO<sub>2</sub> have been implemented in the multi-step syntheses of a number of radiotracers/radiolabeling reagents including: [<sup>11</sup>C]acetyl chloride,<sup>398</sup> [*carbonyl*-<sup>11</sup>C]WAY-100635,<sup>399</sup> (+)-[<sup>11</sup>C]PHNO,<sup>399</sup> and [<sup>11</sup>C]PABA.<sup>392</sup>

While the in-loop methodology – as originally described – can theoretically be implemented within any remotely-operated HPLC injector system, a commercially



produced proprietary loop-methylation system was marketed in accordance with Wilson's original patent,<sup>400</sup> as the Bioscan AutoLoop.<sup>387,390,396</sup> This device was a proprietary synthesis unit that essentially contained an internal semi-preparative radio-HPLC system with integrated radiation detectors monitoring the loop, the HPLC eluent, and the charcoal trap for unreacted [<sup>11</sup>C]CH<sub>3</sub>I. The rationale behind the design of this system was that the loop-methylation process was fully automated – without the need for adapting existing radiosynthesis automation units, or constructing a “DIY” automation module from generic remotely-controllable components – which should allow simple technician operation without the need for input from research chemists. In addition, the system allowed automation of cleaning procedures and generated full reports for each batch/run, to ensure GMP-compliance. While these features are attractive, in a typical radiopharmaceutical production facility hot-cell space is at a premium. It is therefore debatable whether this self-contained loop-methylation unit is an efficient use of that space, particularly since it must necessarily be connected to a separate standalone methylation unit as well. As an alternative to the Bioscan AutoLoop, many groups have modified or adapted their existing radiosynthesis modules to allow them to perform <sup>11</sup>C-methylations in-loop: Wilson<sup>401</sup> and Shao<sup>383</sup> simultaneously reported the respective modifications of GE TRACERlab FX<sub>FN</sub> and TRACERlab FX C Pro modules. Both of these provided comparable results to vial based reactions, and since the modules both contained semi-preparative radio-HPLC units, adaptation for in-loop chemistry was relatively trivial. The comparable disadvantage of the method from Wilson and co-workers was that they adapted a module designed for <sup>18</sup>F-radiochemistry, and as such, it had to be connected with a separate [<sup>11</sup>C]CH<sub>3</sub>I synthesis unit. The work from Shao *et al.* adapted a GE TRACERlab FX C Pro, a single unit which can produce [<sup>11</sup>C]CH<sub>3</sub>I and [<sup>11</sup>C]CH<sub>3</sub>OTf, so their modifications produced a highly-impressive single radiosynthesis module which could take [<sup>11</sup>C]CO<sub>2</sub> through a multistep process to produce [<sup>11</sup>C]CH<sub>3</sub>I, apply this in a loop-methylation reaction, and purify/reformulate the final radiotracer products ([<sup>11</sup>C]carfentanil and [<sup>11</sup>C]raclopride): an ideal situation where hot-cell space is at a premium. Shao further applied this modified setup for the automated syntheses of [<sup>11</sup>C]DASB and [<sup>11</sup>C]Pittsburgh Compound-B,<sup>402</sup> and demonstrated the utility of ethanol in loop-methylations,<sup>403</sup> in an effort to reduce the usage of the undesirable and toxic aprotic solvents more commonly used for these setups. More recently, Synthra have

developed their line of MeIplus synthesisers,<sup>391</sup> some of which include a reaction-loop module. These modules incorporate a [<sup>11</sup>C]CH<sub>3</sub>I and [<sup>11</sup>C]CH<sub>3</sub>OTf production unit, vial and loop reactors, as well as semi-preparative radio-HPLC modules. These all-in-one synthesis units make loop-methylation more straightforward than either modification of existing synthesis units, or purchasing an additional loop module to use alongside a stand-alone methylation device. In any case, it has been shown that both home-made synthesis units and commercially developed modules allow facile adoption of in-loop <sup>11</sup>C-methylation, bringing with it all of the aforementioned benefits.

One final subject that must be discussed is the single report of superbase-mediated in-loop [<sup>11</sup>C]CO<sub>2</sub> fixation predating our work in this area. As part of their 2010 synthesis of [*carbonyl*-<sup>11</sup>C]methylcarbamates *via* BEMP-mediated [<sup>11</sup>C]CO<sub>2</sub> fixation, Wilson and Vasdev sought to apply the method in radiolabeling GR103545 (a potent κ-opioid receptor agonist).<sup>188</sup> Whilst they had thus far developed the method using a traditional vial-based approach, for this substrate they implemented the radiosynthesis in-loop. A solution of BEMP and the norcarbomethoxy-GR103545 precursor (in DMF) was added to a stainless-steel HPLC injector loop, [<sup>11</sup>C]CO<sub>2</sub> was passed through the loop where it trapped in the solution coating the walls of the loop. Following this, a solution of dimethylsulfate was flushed through the loop into a reaction vial before aqueous dilution and analysis by radio-HPLC confirming the formation of the [*carbonyl*-<sup>11</sup>C]methylcarbamate product.

Whilst this was an interesting demonstration, to our knowledge, this particular in-loop setup had not been further replicated or commented upon since its initial disclosure. Primarily, any wider application was likely hindered by the lack of any substantive discussion of the development/optimisation of the procedure, the absence of some key experimental details, and by the lack of any further investigations into the substrate scope. Frustratingly, no [<sup>11</sup>C]CO<sub>2</sub> trapping efficiencies are disclosed, with the only measurable values given being the radiochemical yield of the final product (20-30%, significantly lower than those obtained for other amines in-vial), as well as its molar activity. These omitted details are essential for assessing the success of any new process, and as such it is difficult to have confidence in implementing this method elsewhere. Furthermore, there was no further discussion of any alternative substrates labeled within the same setup;

crucially, the norcarbomethoxy-GR103545 precursor is a piperazinyl secondary amine, and as such would be expected to be significantly more reactive than most primary amines. As a result, even if the [<sup>11</sup>C]CO<sub>2</sub> trapping efficiency was sufficiently high with this particular amine precursor (although no efficiencies were quoted in this instance), it was not clear whether the same methodology could be applied to less reactive primary amine substrates.

Ultimately, whilst this was a promising sign for further in-loop [<sup>11</sup>C]CO<sub>2</sub> fixation methodology development, the method was incomplete at-best. As such, there remained a need for a more in-depth investigation into the applications and limitations of such a process.

#### **2.1.2.6 Recent developments**

Since starting this work, a number of groups including our own have begun translating some more recently-developed novel radiochemistry to thin-film captive-solvent loop methodologies. In 2018, we published our novel method for [<sup>11</sup>C]CO<sub>2</sub> fixation chemistry in-loop, for the <sup>11</sup>C-radiolabeling of ureas,<sup>404</sup> the development and optimisation of this methodology is the subject of this chapter. Simultaneously, but previously unbeknownst to us, Dahl and co-workers published a similar method for in-loop [<sup>11</sup>C]CO<sub>2</sub> fixation.<sup>405</sup> To ensure their work is presented in context, their method is further discussed alongside ours in section 2.4.1. It should be noted however, that these methods of in-loop [<sup>11</sup>C]CO<sub>2</sub> fixation chemistry have since been applied in the synthesis of several novel *ureido*-<sup>11</sup>C-labeled radiotracers<sup>206,245,248,406</sup> Additionally, there have been two other novel in-loop radiosynthesis methods developed for radiolabeling with [<sup>11</sup>C]CO and [<sup>18</sup>F]triflyl fluoride. Again, these are discussed later in section 2.4.3, in order to better contextualise them.

#### **2.1.2.7 Introduction to this research**

The relatively recent development of a number of methods for superbase-mediated [<sup>11</sup>C]CO<sub>2</sub> fixation has hugely expanded the chemical space accessible to carbon-11 PET radiochemists by helping to move further beyond the [<sup>11</sup>C]CH<sub>3</sub>I methylation paradigm.<sup>60,132</sup> It has enabled rapid and efficient radiolabeling at positions within

molecules that were previously either entirely inaccessible, or which were only possible with the use of difficult to produce synthons such as [<sup>11</sup>C]COCl<sub>2</sub>. There are several reasons that [<sup>11</sup>C]CO<sub>2</sub> has been traditionally more difficult to utilise as a direct radiolabeling synthon: the strength of the C=O bonds as well as its poor organic solubility have combined to make it difficult to first trap the gaseous reagent into solution and – once it has been trapped – to “activate” it towards further reactivity and incorporation into novel radiotracers. While these [<sup>11</sup>C]CO<sub>2</sub> fixation methods have helped address many of these barriers, there still remains some difficulties associated with the actual implementation of these heterogenous gas-liquid phase reactions. To ensure adequate fixation efficiency, large excesses of reagents can often be required, which can hinder purification as well as make the process more difficult to miniaturise. In addition, the apparatus setup and routine cleaning can be laborious and difficult to reproduce reliably, which can result in a less efficient radiopharmacy operation.

As was discussed in this introduction, many of these issues arising from multiphase gas-liquid radiochemical processes have already been encountered in more “traditional” [<sup>11</sup>C]CH<sub>3</sub>I methylation chemistry. For these better-established radiolabeling reactions, a number of robust and reliable processes have been developed to counter these issues. Instead of just bubbling the gaseous <sup>11</sup>C-synthon through a vial of precursor solution, it is instead passed through a channel (commonly an HPLC injector loop or polymer tubing) which has been pre-loaded with a thin-film of a captive solvent coating its inner surface. This serves to provide a large gas-liquid interfacial contact area, resulting in highly efficient <sup>11</sup>C-mass transfer into the liquid, while minimising the quantities of solution/reagents required. Once trapped in the solution, the <sup>11</sup>C-synthon reacts with the precursor, forming the desired radiolabeled product *in situ*. In addition to this effective miniaturisation these processes are remarkably simple to automate, direct integration with an HPLC system for purification is straightforward, and setup/cleaning of the apparatus is streamlined due to the reduction in the number of components and vessels required.

The aim in the preceding review was to present a reasonably comprehensive account of the development of thin-film, captive-solvent and in-loop <sup>11</sup>C-radiolabeling methods. Drawing on inspiration and taking account of the lessons learnt from the development of these methods, the aim in this section of work was to investigate the feasibility of

transferring these superbase-mediated [ $^{11}\text{C}$ ]CO<sub>2</sub> fixation methods into an in-loop thin-film fixation process. Once this was established, the aim was to integrate this in-loop [ $^{11}\text{C}$ ]CO<sub>2</sub> fixation into a simple proof-of-concept radiosynthesis of some model  $^{11}\text{C}$ -ureas.

For further context, this was done with a particular view towards further miniaturisation still, in alignment with our industrial partner's ongoing development of a microfluidic radiosynthesis unit (PMB iMiLAB).<sup>407</sup>. Unfortunately due to circumstances out of our control it was not possible for us to attempt any translation of this method onto the microfluidic device within the timescale of this project, but the general aim was to develop a streamlined in-loop [ $^{11}\text{C}$ ]CO<sub>2</sub> fixation process with a view towards implementing it as part of PMB's "cyclotron-to-syringe" iMiGiNE microfluidic production platform. As such, this governed some decisions made in this scheme of work, particularly regarding our decision to use polymer-based instead of stainless steel tubing, as well as our use of very small volume (150  $\mu\text{L}$ ) loops, compared with the well-established but significantly larger HPLC injector loop setups (typically on the order of 2-3 mL).

The particular model reaction that was adapted in this work was the DBU-mediated fixation of [ $^{11}\text{C}$ ]CO<sub>2</sub> on benzylamine to form the amidinium [*carbamyl*- $^{11}\text{C}$ ]benzylcarbamate salt. Once this fixation was successfully implemented in-loop it was integrated into the larger  $^{11}\text{C}$ -urea synthesis, adapting a previous synthetic method published by members of our group: the Mitsunobu-mediated synthesis of symmetrical  $^{11}\text{C}$ -ureas.<sup>225,226</sup> This was selected as our model reaction for this work due to our group's familiarity with this work, its generally robust nature, and its broad substrate scope. For more details regarding this specific reaction, please refer to the general introduction to this thesis.

Drawing on the lessons learnt in reviewing the development of other in-loop thin-film  $^{11}\text{C}$ -radiolabeling methods, there were several general criteria which were at the forefront of our minds when developing this method. It should:

- i) Be broad in substrate scope*
- ii) Use cheap, easy to clean, commercially-available components*

*iii) Perform well at ambient temperatures*

*iv) Be amenable to automation*

*v) Provide roughly comparable radiochemical yields to conventional stirred-solution methods*

## 2.2 Results & Discussion – Three Component In-Loop Fixation

### 2.2.1 Apparatus design and development

To begin this work, it was essential to test whether the initial [ $^{11}\text{C}$ ]CO<sub>2</sub> fixation on amine step was amenable to being performed in-loop. So a simple in-loop fixation testing setup had to be developed, in which amine based solutions could be screened for their [ $^{11}\text{C}$ ]CO<sub>2</sub> fixation ability, with a view to further implementing this in a more elaborate synthetic procedure.

#### 2.2.1.1 *Choice of loop material*

The initial decision to be made in the development of this method was whether to use a disposable polymer loop (as used in much of the Grignard-based in-loop radiochemistry), or whether to use a stainless steel HPLC injection loop as is commonly used in loop-methylation chemistry.

SS loops have their advantages in one-step  $^{11}\text{C}$ -methylation procedures, as they can be integrated directly into the injection system of an HPLC for streamlined purification. [ $^{11}\text{C}$ ]CO<sub>2</sub> fixation chemistry however, is a multi-step process, firstly the [ $^{11}\text{C}$ ]CO<sub>2</sub> is incorporated into a carbamate species, before further reaction on this to form the desired products. As such, this multi-step procedure cannot simply be incorporated into an HPLC injector setup as there must necessarily be additional fluidic pathways etc. for the introduction of secondary reagents, and so the advantages often afforded by the use of SS loops are not so easily realised.

Polymer loops by comparison afford much more versatility to the radiochemist: volumes and dimensions of the loops can be easily changed, and standard 1/16" O.D. tubing is compatible with universal fluidic fittings/connections allowing the integration of these loops into different setups, and the interfacing with a variety of different radiosynthetic modules. In addition to this versatility, as the vast majority of the tubing options available are relatively cheap polymer loops can be used in a disposable single-use manner, so no cleaning is therefore required between uses, bringing two major advantages. Firstly, multiple loops can be prepared in advance, to allow multiple experimental runs to be performed quickly without time consuming cleaning/drying between each run. Secondly

from a GMP perspective, single-use fluidic pathways are often preferred to more permanent glass/metal architecture since these components can be produced in a sterile environment and the lack of cleaning between productions avoids the possibility of operator errors compromising the product sterility from run-to-run. This preference for disposable polymer-based fluidic pathways is reflected in the increasing popularity of the disposable-cassette-based radiosynthesis units (e.g. GE FastLab, Trasis AllInOne, etc.).

With this in mind, a polymer loop seemed a more reasonable option, and initially ethylene tetrafluoroethylene (ETFE) tubing was selected. ETFE is widely used in our laboratory for fluidic connections/pathways on the E&Z Modular Lab. It is an optically transparent and chemically-inert partially-fluorinated polymer, with similar mechanical and chemical properties to PTFE, but with a much superior radiolytic resistance.<sup>408</sup> Optical transparency is helpful particularly in the early stages of process development as it allows visual inspection of the loop during filling/flushing, for identification of any droplet formation or any other observations. Of course chemical inertness is also an essential property for any tubing used in a radiosynthetic process, for the avoidance of any undesired leaching of impurities into solution. One final important consideration when selecting the tubing material was solvent wettability. As this fixation chemistry is performed in acetonitrile, it was important to choose a polymer with an intermediate acetonitrile contact angle ( $\theta$ ): to ensure sufficient retention of a thin-film of acetonitrile captive solvent; while also ensuring the loop can be adequately flushed after [<sup>13</sup>C]CO<sub>2</sub> fixation without incurring significant solvent retention and transfer losses. ETFE also meets this requirement, with a moderate acetonitrile wettability ( $\theta = 50^\circ$ ), it is more wettable than PTFE ( $\theta = 70^\circ$ ), while not being fully wetting, which could lead to undesirable solvent retention.<sup>409</sup>

#### ***2.2.1.2 Selection of loop dimensions***

1/16" O.D. tubing was a natural choice due to the wide variety of 1/16" fluidic fittings available to us, as the industry standard tubing diameter for low volume liquid handling purposes. The choice of an internal diameter of 0.75 mm was selected due to its compatibility with standard 22s gauge (0.718 mm) flat point 100 $\mu$ L HPLC needles. To enable us to precisely and reproducibly load sub-100  $\mu$ L quantities of solvents into the



loop, it was important to be able to directly inject the solution into the tubing, without requiring luer-type connections. While on a larger millilitre-scale luer fittings enable easy and leak-free fluidic connections, on a microlitre-scale they have a not-insignificant dead-volume, which could introduce significant variability in terms of loop-filling injection volumes. A 22s gauge needle can be inserted directly into 0.75mm I.D. tubing, allowing precise, reproducible loop-filling.

To decide on an initial loop volume, the future applications of this work had to be considered. It was hoped that this methodology could eventually be applied in a microfluidic setting, in accordance with the general advantages afforded by performing radiochemistry on a microlitre-scale<sup>374</sup>, including minimisation of reagent quantities, enhanced molar activities, and simplified purification. So initially a 150  $\mu$ L loop volume was selected, with a scope to increasing this if it was found to be insufficiently large to allow efficient [<sup>13</sup>C]CO<sub>2</sub> fixation.

### ***2.2.1.3 Three component concept***

As the aim of these initial experiments was both to explore [<sup>13</sup>C]CO<sub>2</sub> fixation chemistry, as well as the viability of performing it in-loop, it was important to capture as much information as possible in one experiment. The apparatus captures all [<sup>13</sup>C]CO<sub>2</sub> passed through it (for the calculation of trapping percentages), as well as allowing the determination of in-loop fixation, and the fixation ability of the solution as a whole. This is crucial since in this work, these two key properties must be considered, but can be difficult to decouple from one another. A good and efficient [<sup>13</sup>C]CO<sub>2</sub> fixation solution does not necessarily make a good captive solvent for in-loop fixation. A discrepancy between these two would likely be due to insufficient retention of a thin-film of the captive solvent in the loop. Even if a given solution composition can quantitatively trap [<sup>13</sup>C]CO<sub>2</sub> when bubbled through a vial containing the bulk solution, if it is not retained on the internal surface of a loop, it clearly cannot effectively be used in an in-loop fixation process. It is therefore important that the experimental apparatus used allows the independent measuring of both the in-loop fixation ability as well as the total fixation ability of a given solution, to determine whether the chemistry itself is giving rise to poor in-loop fixation, or whether it is just failing to retain in-loop.

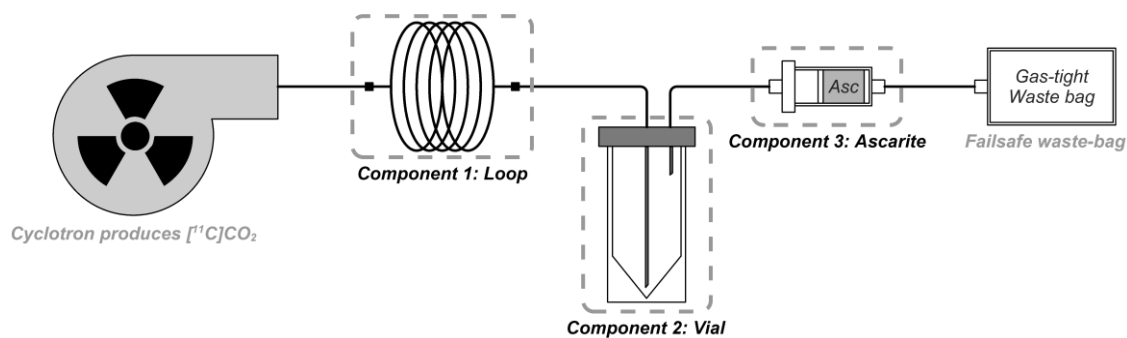


**Figure 2.1 Three component in-loop fixation apparatus schematic**

The **Loop** (*Component 1*) is constructed from a 35 cm length of ETFE tubing (1/16" O.D., 0.75 mm I.D., 150  $\mu$ L total volume), connected at one end via a finger-tight screw fitting to an E&Z modular lab switchable valve that is connected directly to the cyclotron output. The **Vial** (*Component 2*) is a glass vial, crimped with a rubber seal, through which the end of the loop and a vent needle are both inserted. The **Ascarite** (*Component 3*) is constructed from a refillable polypropylene SPE-ED cartridge filled with Ascarite II and held in place with polypropylene frits. This cartridge is connected between the vent needle and the gas waste bag with luer-slip fittings.

The three-component apparatus was designed to assess these criteria, and allow the untangling of these otherwise inextricable values. The components are

1. Loop
2. Vial
3. Ascarite

The inlet end of the 150  $\mu$ L loop is fitted with a fingertight screw fitting for connection with the E&Z Modular Lab switching valves, via a luer-slip attachment, to allow gas flushing and [<sup>13</sup>C]CO<sub>2</sub> delivery. The outlet end of the loop is cut at a 45° taper to allow it to pierce the rubber septum of the crimped vial and was pushed to the base of the vial. The crimped vial is vented with a short luer needle attached directly to the luer slip fitting of the Ascarite trap. The Ascarite trap is an empty 1 mL SPE cartridge containing Ascarite II, a form of granulated sodium hydroxide coated silica, widely used as a quantitative carbon dioxide adsorbent. This is finally connected to a gas-tight waste bag, this is in-place to ensure any [<sup>13</sup>C]CO<sub>2</sub> not trapped in this apparatus is not accidentally released to

the environment, although if connected properly, the Ascarite II should quantitatively scrub any untrapped [ $^{11}\text{C}$ ]CO<sub>2</sub>.

This setup is ideal for our purposes for a number of reasons

- Luer-slip fittings allow easy disconnection of the three components
- Quantitatively traps all [ $^{11}\text{C}$ ]CO<sub>2</sub> passed through
- Direct connection of loop to vial has no dead volume (c.f. needle)
- Cheap/disposable – several can be pre-prepared, allowing high-throughput

#### **2.2.1.4 Experimental procedure**

The standard in-loop fixation experimental procedure is relatively simple. In brief, the procedure is as follows:

1. Apparatus is connected to Modular Lab and flushed with helium
  - *Excludes [ $^{12}\text{C}$ ]CO<sub>2</sub> from diluting molar activity*
2. Loop is disconnected and filled with 75  $\mu\text{L}$  captive solvent
  - *Directly injected with flat-tipped 22s gauge HPLC syringe*
3. Loop is reconnected and flushed with helium (70 mL/min) for 3 minutes
  - *Flushes excess to vial leaving residual as a thin-film in-loop, while purging atmospheric [ $^{12}\text{C}$ ]CO<sub>2</sub> from the system*
4. [ $^{11}\text{C}$ ]CO<sub>2</sub> is flushed directly through the apparatus (in helium, 70 mL/min) directly from cyclotron (without cryogenic pre-concentration)
  - *[ $^{11}\text{C}$ ]CO<sub>2</sub> traps in-loop, in solution in the vial, or in the Ascarite*
5. Three components are separated and their radioactivity contents are measured in Capintec dose calibrator

- *Determines radioactivity distribution across the apparatus for a given solution composition*

6. Components can be disposed of and next experiment can begin

- *No cleaning is required*

This procedure is simple to perform, easy to reproduce, and rapid. It takes no more than 10-15 minutes per experiment, allowing high-throughput screening of many solution compositions in a short space of time. In addition, as the flushing step **3** pushes the vast majority of the solution through to the vial, when [<sup>13</sup>C]CO<sub>2</sub> is passed through the system, if it is not trapped in-loop, it is bubbled through the solution. This means that the results from this experiment give an insight into the solution's inherent propensity for [<sup>13</sup>C]CO<sub>2</sub> fixation, as well as its suitability for in-loop fixation, the importance of which was discussed in the previous section.

### 2.2.1.5 Interpretation of three-component fixation results

To allow full explanation and interpretation of the results, some terms must first be defined. The radioactivity levels in the loop, vial, and ascarite are termed **R<sub>loop</sub>**, **R<sub>vial</sub>**, and **R<sub>asc</sub>**, respectively. Using these measurements, two key values can be extracted. These are the loop-fixation percentage, **F<sub>loop</sub>**

$$F_{loop} = \frac{R_{loop}}{R_{loop} + R_{vial} + R_{asc}} \times 100$$

and the total solution-fixation percentage, **F<sub>tot</sub>**

$$F_{tot} = \frac{R_{loop} + R_{vial}}{R_{loop} + R_{vial} + R_{asc}} \times 100$$

These two values give us insight into the two key properties of a given fixation solution. **F<sub>tot</sub>** reflects the inherent [<sup>13</sup>C]CO<sub>2</sub> fixation ability of a solution, as it accounts for the activity trapped in the thin-film in-loop, as well as, crucially, the activity trapped by bubbling through the solution in the vial. **F<sub>loop</sub>** however, only accounts for the proportion of the total radioactivity that is trapped in any thin-film in-loop. It therefore follows that

a solution with high  $F_{\text{tot}}$  can have a high or low  $F_{\text{loop}}$ , depending on the degree to which the solution is retained as a thin-film in-loop. However a solution with low  $F_{\text{tot}}$ , due to poor [<sup>13</sup>C]CO<sub>2</sub> fixation ability cannot have a high  $F_{\text{loop}}$ , regardless of whether the solution itself is retained well in loop. Therefore one must first optimise  $F_{\text{tot}}$  before focusing on optimising the factors affecting  $F_{\text{loop}}$ .

Additionally, since the  $F_{\text{tot}}$  term is indicative of the [<sup>13</sup>C]CO<sub>2</sub> fixation ability of the solution, independent of any in-loop fixation considerations, this three-component fixation apparatus can also be used to rapidly screen a variety of different solutions for a more fundamental exploration of [<sup>13</sup>C]CO<sub>2</sub> fixation chemistry.

## 2.2.2 Exploration of [<sup>13</sup>C]CO<sub>2</sub> fixation chemistry

### 2.2.2.1 Motivations for initial testing

As discussed in the introduction to this thesis the exact chemical mechanisms behind CO<sub>2</sub> fixation processes are still of some debate, and as such, it was first thought that this 3-component apparatus should be used to assess the  $F_{\text{tot}}$  for a number of different solution compositions, as well as allowing a number of control experiments to separate the contributory effects of each component of a standard fixation solution, as well as allowing any operational issues to be addressed before further chemical optimisation. A standard [<sup>13</sup>C]CO<sub>2</sub> fixation solution contains 2 key components in solution: the amine, and the fixation base. As already discussed, the exact mechanistic roles of these two components are still up for some debate, with some putative mechanisms invoking a covalently bonded DBU-CO<sub>2</sub> adduct, acting to first trap the CO<sub>2</sub> on the DBU before “activating” it and enabling its transfer to the amine substrate. There is however, precious little evidence to confirm this mechanistic role of fixation bases, and upon further literature study and consideration there seems a simpler explanation for the utility and mechanistic role of superbases in [<sup>13</sup>C]CO<sub>2</sub> fixation that also is in accordance with the results obtained herein.

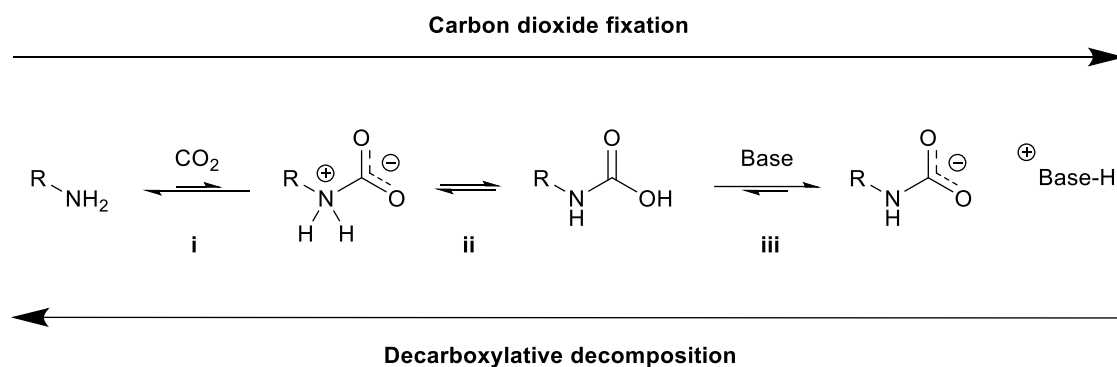


**Figure 2.2 Representative [<sup>13</sup>C]CO<sub>2</sub> fixation scheme**

Complex equilibrium composed of three steps: i) initial CO<sub>2</sub> fixation to form Zwitterionic carbamate species; ii) proton transfer from nitrogen to oxygen forming carbamic acid intermediate; iii) deprotonation of carbamic acid by base (in this case DBU) forming stabilised (and potentially “activated”) carbamate salt

The working hypothesis (the literature justifications/origins of this are further explained in the main introduction) for this work was that the fixation base plays a more

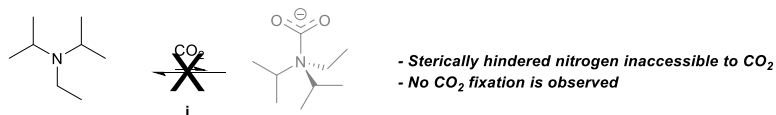
straightforward role, but it is not involved in the initial stage of [<sup>13</sup>C]CO<sub>2</sub> fixation upon contact with solution (in-loop or vial). The suggested mechanism, as illustrated in Figure 2.2 above, is a relatively complex equilibrium with three major equilibrating reaction steps that must be considered. Initially, in *i* the lone-pair of electrons on the substrate amine, (primary to allow subsequent dehydration to an <sup>13</sup>C-isocyanate intermediate) will react with the weakly-electrophilic carbon in CO<sub>2</sub> forming a zwitterionic [R-<sup>+</sup>NH<sub>2</sub>-CO<sub>2</sub><sup>-</sup>] species. Given the relatively strong C=O bonds in CO<sub>2</sub>, and the relatively weak basicity of most amines used in this chemistry, this equilibrium tends to favour the reverse reaction (re-release of CO<sub>2</sub>) and thus at this point the zwitterionic product is fairly unstable. The second step *ii* is a relatively straightforward tautomeric proton transfer yielding the carbamic acid species [R-NH-CO<sub>2</sub>H]. This equilibrium is fairly balanced and still does not confer much stability to the species. However in step *iii*, the base deprotonates this carbamic acid to yield a salt, consisting of the anionic carbamate [R-NH-CO<sub>2</sub><sup>-</sup>] with the protonated base [Base<sup>+</sup>-H] as a counter-cation. It is the nature of this base that determines the position of the equilibrium *iii*, and therefore also the stability of this final carbamate salt towards decarboxylative decomposition.

In the absence of a fixation base, and given the huge stoichiometric excess (relative to [<sup>13</sup>C]CO<sub>2</sub>) of the amine substrate, the “base” which deprotonates the carbamic acid in step *iii* can also be a second molecule of amine, yielding the [R-NH-CO<sub>2</sub><sup>-</sup>][H<sub>3</sub>N<sup>+</sup>-R] carbamate salt. The key difference between a pure amine solution and one containing amine and a superbase is the nature and stability of the protonated cationic counterion, which in turn affects the balance of the equilibrium in *iii*. A more powerful base (in terms of the pK<sub>a</sub> of its conjugate acid, pK<sub>aH</sub>) is better able to deprotonate the carbamic acid intermediate by better stabilising the positive charge it acquires in the process. In the case of DBU, as an amidine base, it forms a resonance stabilised cation whereby the positive charge is delocalised across two bonds. This resonance stabilisation makes DBU a significantly stronger base (pK<sub>aH</sub>(MeCN) = 24.3) than, for example, benzylamine (pK<sub>aH</sub>(MeCN) = 16.9). Since pK<sub>a</sub> is a logarithmic scale, this corresponds to a 25-million-fold difference in basicity between an amidine base such as DBU and a primary alkylamine such as benzylamine. It is the formation of this highly stabilised amidinium carbamate which strongly drives the [<sup>13</sup>C]CO<sub>2</sub> fixation reaction towards stable carbamate salt formation in mixed DBU/amine solutions when compared with fixation-base-free conditions. The

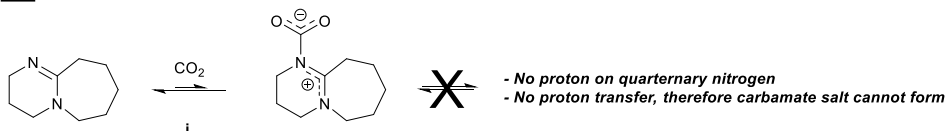
fundamental mechanistic steps *i*, *ii*, and *iii* are the same, but the equilibrium balance of these (particularly *iii*) are significantly different, due to the varying degrees of cationic charge stabilisation in the carbamate salt.

While this mechanistic hypothesis has a strong grounding from literature precedent,<sup>154,160,162,165,167,169,213,410-413</sup> it has still not been entirely embraced in the <sup>13</sup>C-radiochemistry literature. In light of this fact, the simple three component trapping apparatus was initially used to screen some simple fixation solutions in an effort to investigate this hypothesis.

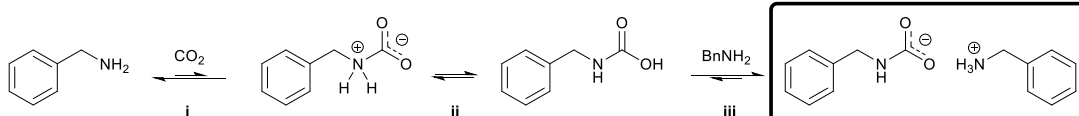
**A) DIPEA**



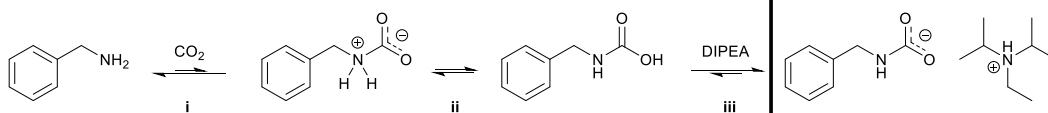
**B) DBU**



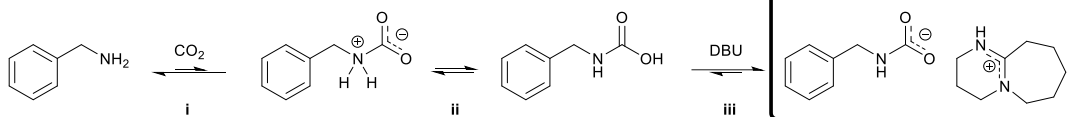
**C) 1° Amine**



**D) DIPEA/1° Amine**



**E) DBU/1° Amine**



Benzylcarbamate salts

**Figure 2.3** [<sup>13</sup>C]CO<sub>2</sub> fixation equilibria for several screened solutions

1° amine was benzylamine, carbamate species in entry B is just a suggestion – no direct evidence for Zwitterionic carbamate existence has been found.



### 2.2.2.2 Choice of fixation solutions

Firstly, as a simple control experiment it was clearly important to test a solution of pure **MeCN**: as it is the solvent used for all subsequent chemistry (MeCN was found to be the optimal solvent for the Mitsunobu-based <sup>13</sup>C-urea synthesis)<sup>225,226</sup>. No significant trapping was expected due to the low solubility of CO<sub>2</sub> in most organic solvents, and the absence of any nucleophilic additives which could act to chemically react with CO<sub>2</sub> itself. However it is of course essential to quantify the “background” [<sup>13</sup>C]CO<sub>2</sub> trapping levels as a result of passive dissolution etc., that would be common to all other solutions.

Five key solutions were selected to shed further light on the roles played by superbases in [<sup>13</sup>C]CO<sub>2</sub> fixation chemistry, in particular focusing on the hypothesised role of a highly-stabilised amidinium counterion being the driving force for efficient and stable [<sup>13</sup>C]CO<sub>2</sub> fixation for solutions containing DBU. Hence, three solutions were selected containing (each component 10% v/v in MeCN): **DBU**; **1° amine** (benzylamine); and **DBU/1° amine**. Further to these three solutions, two more were screened as well: **DIPEA** (di-isopropylethylamine); and **DIPEA/1° amine**. The motivation for exploring these was primarily since there is still uncertainty regarding the direct interaction between DBU (a highly basic but supposedly sterically hindered nucleophile) and CO<sub>2</sub>. There is disagreement as to whether a truly covalent DBU-CO<sub>2</sub> adduct can form, or whether it is simply forming a bicarbonate salt due to the presence of adventitious water? DIPEA was selected for these experiments since it has a marginally stronger basicity than benzylamine (certainly strong enough that one would expect it to form some bicarbonates in the presence of any adventitious water and CO<sub>2</sub>), but it is a highly sterically hindered base in which the central nitrogen atom is essentially inaccessible to all but a proton, so no direct covalent interaction with CO<sub>2</sub> would be expected. It was hoped that comparing the performance of DIPEA in place of DBU would reveal some interesting data which could shed further light on this as-yet undecided mechanistic debate.

Finally, four solutions were selected to screen secondary and tertiary amines with and without the addition of DBU: **2° amine** (*N*-methylbenzylamine); **DBU/2° amine**; **3° amine** (*N,N*-dimethylbenzylamine) ; and **DBU/3° amine**. These solutions were included a check that the basic assumptions of our hypothesis were valid, since a relatively sterically unhindered 2° amine would be expected to trap [<sup>13</sup>C]CO<sub>2</sub> in a similar manner

to the 1° counterpart. Whereas one would not expect a 3° amine to trap [<sup>11</sup>C]CO<sub>2</sub> to any significant degree: the absence of a labile proton on the basic nitrogen means that the Zwitterionic carbamate could potentially be expected to form, but it would not be expected to proceed through to the formation of a stable carbamate salt.

It was hoped that these 10 solutions could provide an insight into the fundamental reaction mechanistic details underpinning this fairly standard [<sup>11</sup>C]CO<sub>2</sub> fixation chemistry. On a more pragmatic note, it also allowed familiarisation with the apparatus and identification of any operational issues and recurrent flaws with the design. The results from screening these ten solutions are presented in Figure 2.4 below. It should be noted that for these preliminary experiments the discussion primarily focuses on the total-solution fixation values ( $F_{\text{tot}}$ ), as this is the result that reflects the fixation chemistry itself (the in-loop results – which reflect physical factors as well as chemical – are still presented for completeness).

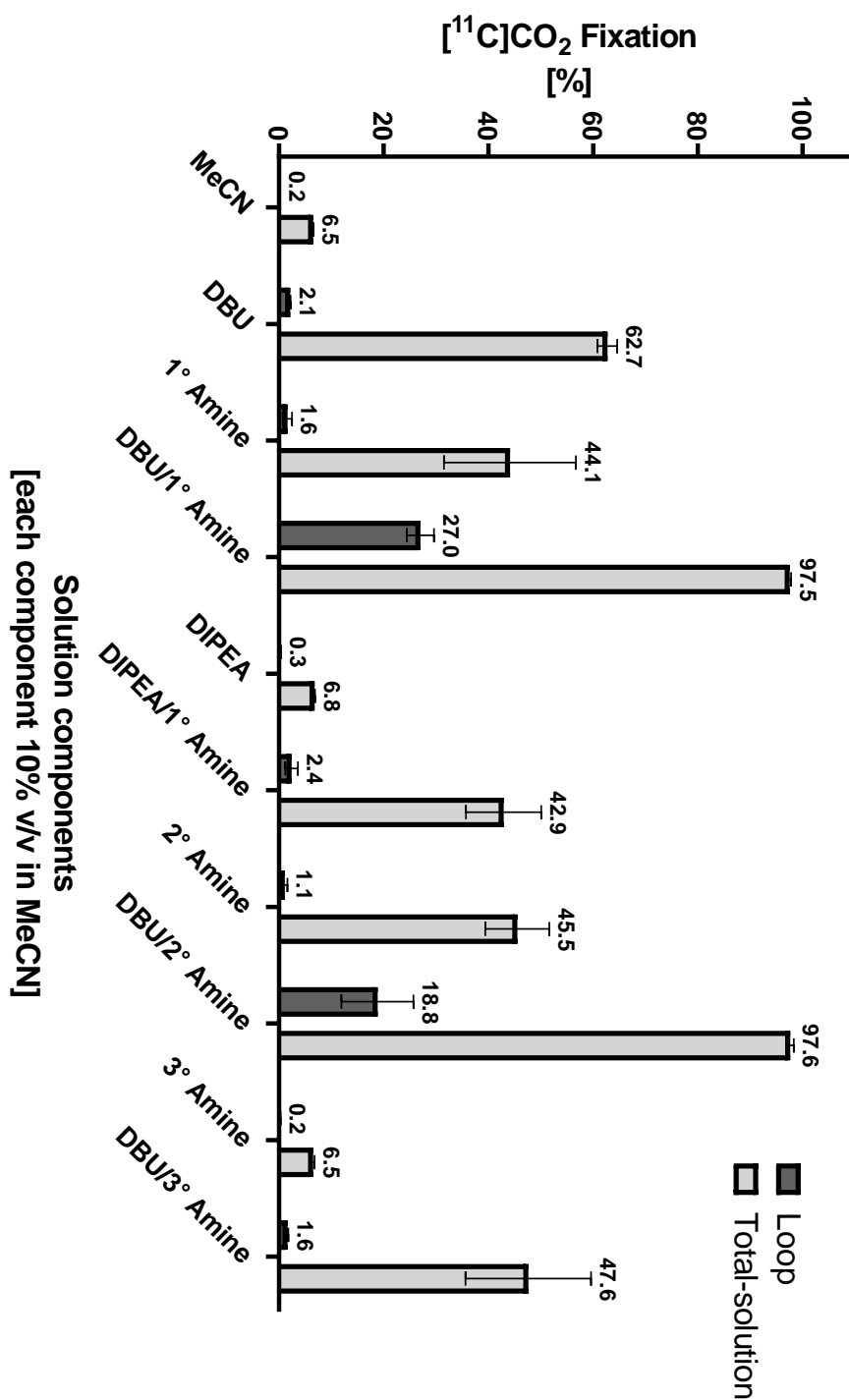


**Figure 2.4** Exploration of [ $^{11}\text{C}$ ]CO $_2$  fixation chemistry with three component apparatus

1°, 2°, and 3° amines were benzylamine, *N*-methylbenzylamine, and *N,N*-dimethylbenzylamine respectively (n=3 for all entries)

### 2.2.2.3 Results – Acetonitrile

The result for the pure acetonitrile fixation was largely as expected, with little  $F_{\text{tot}}$  observed ( $6.5 \pm 0.1\%$ ), with a small S.D between results. This can be simply explained due to the poor solubility of CO<sub>2</sub> in organic solvents, and considering the absence of any other nucleophilic CO<sub>2</sub> fixation reagents. This very low overall [<sup>13</sup>C]CO<sub>2</sub> fixation was ideal as it provided an easy background against which other results could be compared, particularly given the small S.D., meaning that there is a low run-to-run variability in terms of [<sup>13</sup>C]CO<sub>2</sub> fixation in pure solvent.

### 2.2.2.4 Results - 1° Amine, DBU, and DIPEA

These were the key solutions of interest in this work as it was hoped that they would potentially shed more light on the exact mechanistic role of the fixation base (DBU) in these [<sup>13</sup>C]CO<sub>2</sub> fixation reactions.

The first question we hoped to address was the nature of the well-documented DBU-CO<sub>2</sub> adduct, whether it can form the hypothesised covalently bonded Zwitterionic carbamate or whether it simply forms the [DBU-H]<sup>+</sup> [HCO<sub>3</sub>]<sup>-</sup> bicarbonate form in the presence of adventitious water. The **DBU** solution exhibited a reasonably high degree of [<sup>13</sup>C]CO<sub>2</sub> fixation ( $F_{\text{tot}} = 62.7 \pm 1.9\%$ ), which clearly confirms some interaction between DBU and CO<sub>2</sub>, and the small S.D supports the conclusion that this adduct is fairly stable. However by itself this result could be explained by either a covalent adduct or the formation of a bicarbonate salt. The solvent used was a commercially supplied 99.9+% extra dry acetonitrile stored over molecular sieves, and a fresh unopened bottle of solvent was used each time solutions were prepared, so one would not expect a significant amount of water to be present to allow bicarbonate formation to any significant degree. However it would not be surprising if a small quantity of water had still contaminated the solution, allowing a bicarbonate salt to form.

The **DIPEA** solution that was tested used the same solvent as the **DBU** solution, but in this case, no [<sup>13</sup>C]CO<sub>2</sub> fixation was observed at all ( $F_{\text{tot}} = 6.8 \pm 0.1\%$ ) above the baseline solvent trapping. DIPEA should be sufficiently basic to form the bicarbonate salt with [<sup>13</sup>C]CO<sub>2</sub> in the presence of water: in the pH ~ 12 environment of a 10% v/v solution of

DIPEA in MeCN, any [<sup>13</sup>C]carbonic acid ([<sup>13</sup>C]H<sub>2</sub>CO<sub>3</sub>, pK<sub>a</sub> = 6.8) formed from the reaction of CO<sub>2</sub> with H<sub>2</sub>O would be almost entirely deprotonated and thus present in its [<sup>13</sup>C]bicarbonate form [[<sup>13</sup>C]HCO<sub>3</sub>]<sup>-</sup>, as the salt counterion to the DIPEA-derived diisopropylethylammonium species, trapping the [<sup>13</sup>C]CO<sub>2</sub> in solution. However, since no trapping is observed, one can conclude that the solvent was sufficiently anhydrous so as to preclude this bicarbonate formation. This suggests therefore, that the interaction seen between DBU and CO<sub>2</sub> was not bicarbonate formation, but potentially a covalent interaction instead (possibly the Zwitterionic carbamate).

The key difference between DIPEA and DBU is the steric bulk around the basic nitrogen atom influencing their nucleophilicities. While DBU has sometimes been referred to as a “sterically hindered base”<sup>162</sup>, the location of the tertiary amine nitrogen within the ring structure (as in pyridine) means that the substituents are essentially pulled back from the nitrogen, leaving the lewis-basic lone-pair of electrons relatively sterically accessible. This possibly gives DBU a degree of nucleophilicity, particularly with a fairly small molecule such as CO<sub>2</sub>. DIPEA by comparison, is significantly more hindered than DBU, as the nitrogen is *sp*<sup>3</sup> hybridised, with three bulky substituents evenly distributed around it. This difference in steric hindrance likely explains the huge difference in trapping ability between DBU and DIPEA. It should be noted of course, that DBU is significantly more basic than DIPEA (pK<sub>a</sub>H = 24.3 vs 18.7), however as will be seen shortly, amines with even lower basicities than DIPEA (benzylamine and *N*-methylbenzylamine) are very capable of trapping CO<sub>2</sub> in carbamate species by themselves. These results therefore support the assertion that DBU’s ability to trap [<sup>13</sup>C]CO<sub>2</sub> by-itself cannot simply be explained by the formation of <sup>13</sup>C-bicarbonate salts, and is likely due to some covalent interaction between DBU and CO<sub>2</sub> itself forming a Zwitterionic carbamate species.

As is illustrated in Fig 2.4, the likely formed Zwitterionic species in the **DBU** solution is unable to proceed *via* proton exchange towards the formation of a stable carbamate salt, due to the lack of labile protons. This explains the fact that a solution of 10% DBU is insufficient to quantitatively and stably trap the [<sup>13</sup>C]CO<sub>2</sub> passed through it, since this Zwitterionic carbamate is in direct equilibrium with CO<sub>2</sub> release. However, this carbamate does exhibit some resonance stabilisation due to the amidine structure of DBU (which also confers its high basicity). This stability is enough to allow this intermediate

level of [<sup>13</sup>C]CO<sub>2</sub> fixation to be observed, by balancing an equilibrium which otherwise would heavily favour the reversed, decarboxylation reaction.

The second question addressed by these solutions pertained to the fixation-role of DBU in conjunction with an amine substrate. The first solution to consider here was benzylamine with no additional fixation bases added: the **1° amine** solution. The amine by itself still exhibited a reasonable fixation ability ( $F_{\text{tot}} = 44.1 \pm 12.6\%$ ), although with a high S.D. there was a high degree of variability between runs. This suggests that whatever form the species is trapped in, the equilibria *i*, *ii*, and *iii* are not heavily balanced towards the formation of the carbamate salt. The formation of alkylammonium alkylcarbamates in a 2:1 amine:CO<sub>2</sub> ratio, whereby a second molecule of the amine acts as a base to form the carbamate salt counterion, has been well documented before;<sup>154,164,167,414</sup> but so too has their relative instability.<sup>154,164,167,414</sup> This equilibrium process is illustrated in section C of Fig 2.4, and it is likely that the instability of this final carbamate salt product can be attributed to the insufficient basicity of benzylamine itself, meaning that the equilibrium in *iii* has no major significant driving force for the forward salt-forming reaction. The salt can easily undergo the reverse reaction, and therefore the final carbamate salt is in a relatively balanced equilibrium with the decarboxylative decomposition process.

Compared with the **1° amine** solution, the **DBU/1° amine** solution exhibited much improved – essentially quantitative – [<sup>13</sup>C]CO<sub>2</sub> fixation ( $F_{\text{tot}} = 97.5 \pm 0.3\%$ ). This fits exactly with our hypothesis, in that the much stronger basicity of DBU (*versus* a second benzylamine molecule) easily deprotonates the carbamic acid intermediate, forming a stronger and more stable amidinium carbamate species. Compared with the reaction in the **1° amine** solution, the underlying fixation mechanisms in this **DBU/1° amine** solution are nearly identical, except that the equilibrium concentration of the amidinium carbamate salt product is much higher in step *iii* (Fig 2.4, section D) because of the many-orders-of-magnitude stronger base used. The formation of this highly stabilised carbamate salt results in a highly efficient [<sup>13</sup>C]CO<sub>2</sub> fixation solution with good reproducibility due to a strong reduction in the rate of decarboxylative decomposition.

For the **DIPEA/1° amine** solution, no significant improvement in  $F_{\text{tot}}$  ( $42.9 \pm 7.2\%$ ) was observed over the **1° amine** solution without fixation base. This largely concurs with the

hypothesis regarding base strength driving carbamate salt stability and by-extension, fixation efficiency and stability. DIPEA is only a marginally stronger base than benzylamine itself ( $pK_{\text{aH}} = 18.7$  versus 16.9) and would not confer a major increase in salt stability. This results in a fixation efficiency that in these experiments, is indistinguishable from the **1° amine** itself.

These results fit with the major hypothesis of this section of work: that [<sup>13</sup>C]CO<sub>2</sub> fixation efficiency and stability are driven by the formation of a <sup>13</sup>C-carbamate salt, the stability of which is determined by the basicity of the species acting as the cationic protonated counter-ion. Some have posited that the fixation ability of superbases such as DBU involves the trapping and activation of the [<sup>13</sup>C]CO<sub>2</sub> directly, before transferring the now-activated carboxylate group to the desired amine substrate.<sup>132,185,186,415</sup> While this could still be possible in the light of these results, there has been no published evidence to support this theoretical mechanistic activation/transfer role. It could be argued in fact, that DBU's ability to trap CO<sub>2</sub> (in whatever form) is simply a diverting but ultimately irrelevant coincidence. It happens to be that a highly basic reagent (e.g. DBU), will often also be a highly nucleophilic compound in its own right (depending on the sterics). In the absence of any further evidence it seems reasonable to choose the explanation that does not invoke unproven mechanistic theories. This salt stability explanation, by contrast, invokes well understood acid-base equilibria and can equally sufficiently explain how a base which is better-able to stabilise a positive charge (by delocalisation) will tend to drive the formation of these stable carbamate salts and by extension, drive efficient and stable [<sup>13</sup>C]CO<sub>2</sub> fixation.

Further exploration of this mechanism could use this three-component system to compare DBU with the reportedly less nucleophilic but similarly basic 1,1,3,3-tetramethylguanidine (TMG). In non-radioactive work (monitored with FT-IR) by Nicholls *et al.*, it was shown that while TMG was unable to form a complex or bicarbonate salt with CO<sub>2</sub>, it exhibited similar efficacy to DBU and other superbases in mediating CO<sub>2</sub> fixation on amines.<sup>200</sup> In this work, the authors concluded that basicity was a stronger predictor of efficacy in promotion of CO<sub>2</sub> fixation than a compound's ability to directly interact with CO<sub>2</sub>. It would be interesting to attempt to replicate these results with [<sup>13</sup>C]CO<sub>2</sub>, as it could provide further confirmation of our proposed mechanism whereby

DBU primarily acts as a strong base to stabilise <sup>11</sup>C-carbamate salts instead of this widely-proposed CO<sub>2</sub>-activation role.

#### 2.2.2.5 2° and 3° amines

These final screened solutions were of less fundamental interest in this work, since the end goal was to dehydrate any <sup>11</sup>C-carbamate formed, producing a reactive isocyanate. 2° or 3° isocyanates cannot form and as such, even if these amines have fantastic [<sup>11</sup>C]CO<sub>2</sub> fixation abilities, it is ultimately of no use in further application. However, since these screening experiments were quick and easy to perform, it was decided that screening a 2° and 3° amine could help to inform our understanding of the chemistry underlying the [<sup>11</sup>C]CO<sub>2</sub> fixation process. The **2° amine** (*N*-methylbenzylamine) exhibited an almost identical fixation performance ( $F_{\text{tot}} = 45.5 \pm 6.1\%$ ) to the corresponding **1° amine**. This is to be expected as they both have very similar basicities, and the addition of a small methyl group would not be expected to significantly hamper the nucleophilicity of the basic nitrogen. Accordingly, the DBU/2° amine solution also exhibited almost identical performance ( $F_{\text{tot}} = 97.6 \pm 0.7\%$ ) to the corresponding DBU/1° amine solution. Again, the strongly basic DBU provides a significant driving force to the carbamate salt formation equilibrium.

As the hypothesis predicted, the **3° amine** (*N,N*-dimethylbenzylamine) exhibits no [<sup>11</sup>C]CO<sub>2</sub> fixation above baseline ( $F_{\text{tot}} = 6.5 \pm 0.3\%$ ), which can be attributed to the steric hindrance of *sp*<sup>3</sup> hybridised tertiary amines preventing the formation of a covalently-bonded Zwitterionic carbamate. Even if a small amount of this covalent species were able to form, the absence of an exchangeable proton on the nitrogen precludes this carbamate species from further equilibration to form a carbamate salt species. The **DBU/3° amine** solution does exhibit a reasonable fixation ability ( $F_{\text{tot}} = 47.6 \pm 12.0\%$ ), but on comparison with the other results it is less efficient than **DBU** in isolation, and in fact results in more variable fixation performance.



### 2.2.3 Optimisation of in-loop [<sup>13</sup>C]CO<sub>2</sub> fixation – towards the radiosynthesis of *N,N'*-[<sup>13</sup>C]dibenzylurea

#### 2.2.3.1 *Components of fixation solutions.*

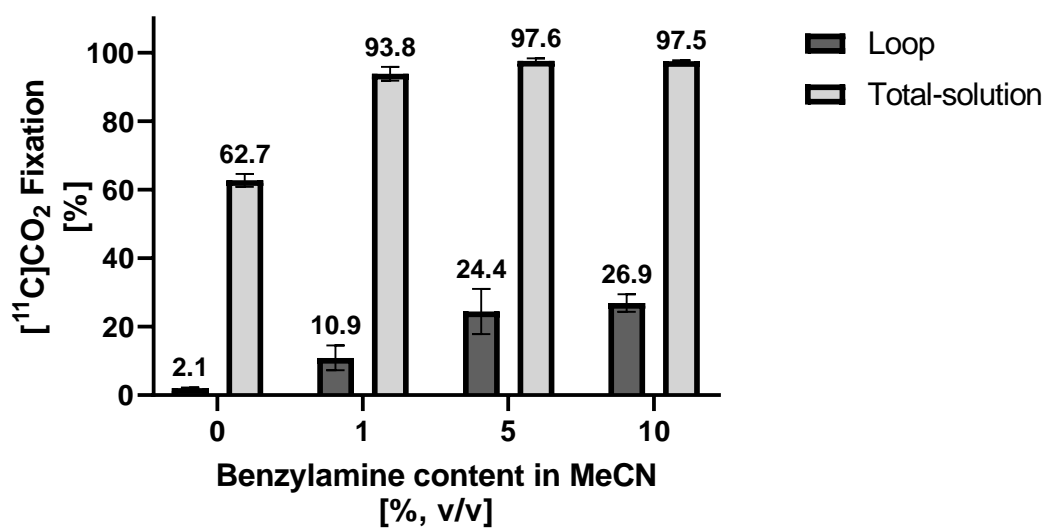
The previous section focused on the fixation ability of the solutions themselves ( $F_{\text{tot}}$ ), and while this is informative in exploring the underlying chemistry behind [<sup>13</sup>C]CO<sub>2</sub> fixation, the primary focus for this work was to adapt these [<sup>13</sup>C]CO<sub>2</sub> fixation reactions into a reaction that could be performed in-loop. For this application, a highly efficient [<sup>13</sup>C]CO<sub>2</sub> fixation solution (i.e. high  $F_{\text{tot}}$ ) does not necessarily efficiently perform this fixation well in-loop. As was discussed in the introduction, in-loop procedures involve a thin-film of captive-solvent coating the interior of a loop where it provides a high surface area for gas-liquid mass transfer. Essentially enabling ultra-efficient trapping of gaseous <sup>13</sup>C-reagents in the microlitre volumes of captive-solvent which make up the thin-film. Therefore we cannot simply optimise for solutions with highly-efficient [<sup>13</sup>C]CO<sub>2</sub> fixation without also paying attention to the factors which influence its retention in-loop; we need to investigate whether a given solution can be sufficiently retained as a thin-film in-loop. Optimising for  $F_{\text{tot}}$  is a prerequisite, but it is not sufficient in itself, we must also optimise for  $F_{\text{loop}}$ .

Once this  $F_{\text{loop}}$  optimisation was complete, the plan was to implement this in a more elaborate in-loop flow radiosynthesis of <sup>13</sup>C-urea compounds. As such, a model substrate had to be chosen for this initial fixation optimisation that could also be used as the amine substrate for any subsequent urea synthesis. Benzylamine was eventually selected since it is cheap and readily available; it is not abnormally nucleophilically “activated” with electron donating groups, so we can expect it to be fairly representative of many of the amines used in [<sup>13</sup>C]CO<sub>2</sub> fixation chemistry; and finally the aromatic phenyl ring provides an easy-to-detect UV-active chromophore which should absorb at 254 nm in any subsequent HPLC analysis.

Now that the amine substrate was selected, a variety of different solutions could be screened with varying DBU and amine compositions. Since there was no precise control over exact quantities of solution that would be retained in-loop anyway. It was decided, in the first instance, that solutions would be more easily made-up volumetrically (in terms of % v/v in MeCN) as opposed to the more time-consuming task of preparing solutions

with defined stoichiometric ratios. If it appears that the chemistry was especially sensitive to exact stoichiometry, the ratios of the components in these solutions could be subsequently calculated where necessary. However for these first exploratory screening experiments, solutions were simply prepared with varying volumetric percentages of both benzylamine and DBU. The results are presented below in Figure 2.5.

i



ii

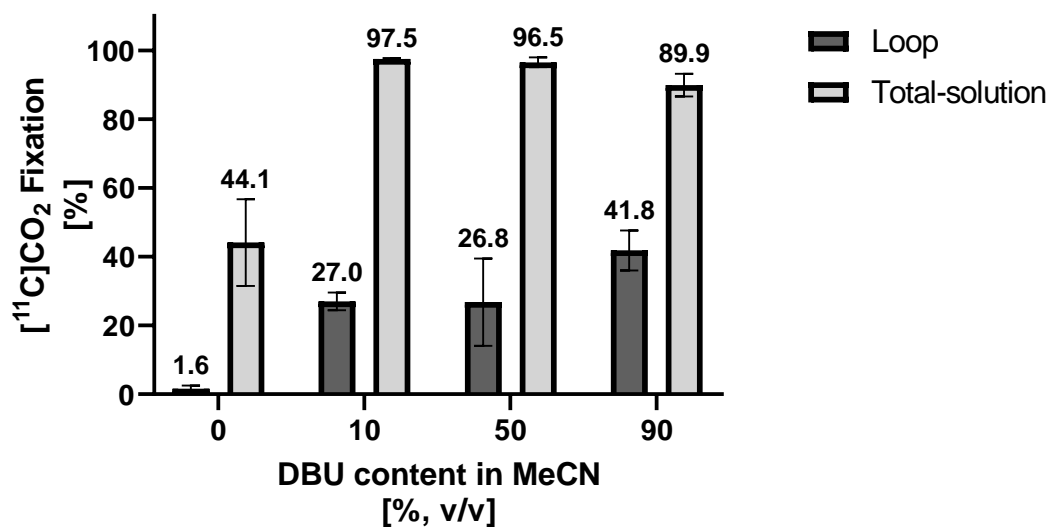


**Figure 2.5 Loop and total-solution [ $^{11}\text{C}$ ]CO $_2$  fixation as solution composition varies**  
i) Varying benzylamine content, with fixed 10 % DBU in MeCN [v/v]. ii) Varying DBU content, with fixed 10% benzylamine in MeCN [v/v]. Total volume of all solutions injected into loop was 75  $\mu\text{L}$

### 2.2.3.2 Varying benzylamine content

Initially the percentage of amine content was varied with respect to a fixed volumetric percentage of DBU (10% v/v). This 10% choice was based on a consideration of the estimated DBU of a thin film in-loop. Initial experiments showed that of the 75 μL of pure MeCN loaded into a loop, approximately 5 μL is retained after 3 minutes of flushing. Therefore in a 10% solution of DBU, assuming a similar retention to the pure MeCN solution, the loop would contain approximately 0.5 μL (3.3 μmol) of DBU. From previous experience with [<sup>11</sup>C]CO<sub>2</sub> fixation chemistry in our group, it was found that the total quantity of [<sup>11/12</sup>C]CO<sub>2</sub> delivered (from the cyclotron or through environmental contamination) was in the region of 0.3 μmol. As discussed fully in the introduction, due to the relatively sluggish kinetics of organic chemistry (when compared with radiometal chelation), carbon-11 reactions generally tend to require a significant excess (on the order of 10-100-fold) of the radiolabeling precursor, relative to the total quantity of [<sup>11/12</sup>C]CH<sub>3</sub>I. This ensures that the reaction produces sufficient product on a timescale that is compatible with the half-life of <sup>11</sup>C. Therefore, a loop containing 3.3 μmol would give a roughly 10-fold excess of DBU relative to the ~ 0.3 μmol of [<sup>11/12</sup>C]CO<sub>2</sub>. This seemed a reasonable place from which optimisation could begin.

The first result was simply 10% DBU in MeCN with no benzylamine added, and as was observed and discussed previously, the DBU by itself gives a reasonable  $F_{\text{tot}}$  of  $62.7 \pm 1.9$  %. However it is important to consider this is only a measure of the radioactive trapping efficiency of the solution in general, the more relevant value for our applications was the  $F_{\text{loop}}$ , the measure of the percentage of [<sup>11</sup>C]CO<sub>2</sub> that is trapped within the loop. For this solution, while it exhibited a reasonable  $F_{\text{tot}}$ , its  $F_{\text{loop}}$  was just  $2.1 \pm 0.1$ %. Demonstrating in-practice the concept that just because a solution can trap efficiently, it does not necessarily make for an efficient in-loop captive solvent.

The next solution screened contained 1% v/v benzylamine in MeCN (with 10% v/v DBU) and exhibited a much improved  $F_{\text{tot}}$  ( $93.8 \pm 2.0$ %) with a marginally improved  $F_{\text{loop}}$  ( $10.9 \pm 3.6$ %). The solution is now capable of near quantitatively trapping [<sup>11</sup>C]CO<sub>2</sub> with just 1% benzylamine added, however it is still a poor solvent for in-loop fixation.

The final two solutions screened here contained 5% and 10% benzylamine in MeCN (with 10% v/v DBU) and exhibited again a near-quantitative  $F_{\text{tot}}$  ( $97.6 \pm 0.7\%$  and  $97.5 \pm 0.3\%$ , respectively), with improved values of  $F_{\text{loop}}$  ( $24.4 \pm 6.6\%$  and  $26.9 \pm 2.6\%$ , respectively). These results revealed that while just 1% benzylamine content was sufficient to ensure efficient [<sup>13</sup>C]CO<sub>2</sub> fixation in solution, the in-loop fixation ability of a solution could be further enhanced by increasing the amine content of the solution.

If these amine DBU solutions (1%, 5% and 10% benzylamine content) were all essentially equally efficient for [<sup>13</sup>C]CO<sub>2</sub> fixation, the the key question to address was what was leading to this variability in in-loop fixation performance. If an equal quantity of these solutions was retained in-loop as a thin-film, then one would expect them to perform equally well in-loop. The fact that a difference is observed leads to the conclusion that there must be a difference in the quantity of solution retained in-loop after flushing, and that the degree of solution retention is correlated with the benzylamine content of the solutions. Therefore it seemed likely that this effect was due to either some purely mechanical property of the amine (e.g. viscosity), or a more complex attractive interaction between the amine and the polymer of the loop, increasing its wettability and subsequently its retention on the internal surface of the loop.

From these results it appeared that there was only a very minor increase in  $F_{\text{loop}}$  on moving from 5% to 10% benzylamine, and as such a significant increase from increasing this further was not expected. Therefore, 10% benzylamine content was chosen for the DBU optimisation experiments.

### ***2.2.3.3 Varying DBU content***

In these experiments (Figure 2.5, *ii*), solutions of varying quantities of DBU in MeCN (with a fixed 10% v/v benzylamine) were screened. The initially screened control solution without the addition of any DBU, demonstrated again that a simple amine solution is capable of trapping [<sup>13</sup>C]CO<sub>2</sub> to a reasonable degree ( $F_{\text{tot}} = 44.1 \pm 12.6$ ), but similarly to the control experiment in the previous section, very little activity was trapped in the loop at all ( $F_{\text{loop}} = 1.6 \pm 0.9\%$ ). However in the presence of DBU (10%), the solution now exhibited both highly efficient total [<sup>13</sup>C]CO<sub>2</sub> fixation ability ( $F_{\text{tot}} = 97.5 \pm 0.3\%$ ) as well as, crucially, a significantly higher in-loop fixation performance ( $F_{\text{loop}} = 27.0 \pm 2.6\%$ ).

While the  $F_{\text{tot}}$  roughly doubled on addition of DBU, the  $F_{\text{loop}}$  saw a more-than 15-fold increase, demonstrating that the increase in  $F_{\text{loop}}$  for these solutions cannot be simply attributed to the use of a more chemically efficient solution, and that there must be a greater retention of solution inside the loop itself.

In accordance with this, the DBU content was further increased to 50% but no significant increase in fixation ability was achieved ( $F_{\text{tot}} = 96.5 \pm 1.4\%$ ,  $F_{\text{loop}} = 26.8 \pm 12.7\%$ ), suggesting that this increased DBU content had not resulted in an improved retention of solution in the loop. The final solution screened increased the DBU content even further, entirely eliminating the MeCN solvent yielding a solvent-free solution consisting of 90% DBU and 10% benzylamine (v/v). This solution achieved a similar  $F_{\text{tot}}$  ( $89.9 \pm 3.3\%$ ) while giving a significantly increased  $F_{\text{loop}}$  ( $41.8 \pm 5.8\%$ ). Without any solvent added, this solution is clearly much better retained in the loop which leads to a much better in-loop fixation performance ( $F_{\text{loop}}$ ), even with the slightly reduction overall chemical efficiency ( $F_{\text{tot}}$ ). This was a surprising result initially because no major increase in performance was achieved on increasing DBU content from 10% to 50%. However, on the preparation and drawing into syringe of these solutions, it was noted that the solvent free 90% DBU solution seemed significantly more viscous than the other screened solutions. For the solutions with similar  $F_{\text{tot}}$  but a variable  $F_{\text{loop}}$ , it seemed reasonable to consider that this variability could be attributed to the variable viscosity of these solutions.

#### 2.2.4 Solution viscosity and its relation to in-loop retention

When discussing the factors dictating solution retention in-loop, it is important to first consider the likely flow regimes in operation within the loop, and therefore the effects upon these flow regimes that a change in solution viscosity might have, if any. In our tubing loop, a bolus of liquid is preloaded and then the tubing is flushed for 3 minutes with helium at a flow rate of 70 mL/min (in 0.75mm I.D. tubing, this equates to 2.64 m/s), the aim being to deposit a thin-film of the captive solvent on its inner surface. In this case, we have a two-component gas-liquid flow, where the gas flow-rate is significantly higher than the liquid flow rate. Under these conditions one would expect to observe an annular-type flow regime.<sup>416-418</sup> An annular flow regime consists of a fast moving gas core moving through a tube, with the much more slowly moving liquid being forced outwards to form a relatively uniform thin-film of the liquid on the inside walls of the solution. This can be contrasted to a slug-flow regime (for example) which is characterised by discrete and alternating “slugs” of gas or liquid sequentially flowing through the tube, and would arise in a situation where gas and liquid flow rates are more equal. In the radiochemistry literature, there has been very little discussion of the fluid mechanics underpinning radiochemistry performed in-loop, but it seems reasonable to assume that in a situation where a static bolus of liquid is purged from a length of tubing with a fast gas flow, the flow regime during this process will best resemble an annular-type flow. It is this annular flow which enables the formation of a thin-film of the captive-solvent on the walls of the loop.

If the helium purge of the loop in this three-component setup results in an annular flow regime, how could viscosity affect the quantity of solution retained in the loop? In an annular flow regime, the fraction of the cross sectional area of the tubing that contains the gaseous phase is referred to as the “void fraction”, so as the thickness of the thin-film of liquid increases, the void fraction consequently decreases. If a solution is better retained in the loop, then it must be retained in a thicker film, and therefore the void fraction for this particular case must be lower. While the exact factors governing the magnitude of the void fraction are difficult to predict precisely, some empirical correlations (beginning with the Lockhart-Martinelli correlation<sup>419</sup>) have been established which demonstrate a general inverse proportionality between solution viscosity and void fraction in 2-phase

gas-liquid flow.<sup>419–422</sup> In other words, under annular flow conditions, a more-viscous solution will form a thicker film on the walls of the tubing loop, and assuming that all solutions have the same (near-quantitative) fixation ability in bulk solution ( $F_{\text{tot}}$ ), those solutions with higher viscosities will therefore result in an increased  $F_{\text{loop}}$ .

The three solution components used in these screening experiments have varying viscosities (as a single component): acetonitrile (0.34 mPa.s),<sup>423</sup> benzylamine (1.49 mPa.s),<sup>424</sup> and DBU (11.76 mPa.s).<sup>425</sup> So by referring to the results presented in Figure 2.5 above, it can be seen that there is a general trend towards increased  $F_{\text{loop}}$  values for solutions where the much-less viscous acetonitrile solvent is replaced with the more viscous benzylamine and DBU; however this is not a simple linear relationship. The viscosities of multi-component solutions are governed by many complex intermolecular interactions, and as such, cannot simply be calculated (or necessarily even predicted with reasonable accuracy) based upon the measured viscosities of their pure components. Put simply, the viscosities of multi-component solutions are more than the sum of their parts, and as such, one could not necessarily expect to see a linear relationship between the percentage of DBU/benzylamine in MeCN, and the  $F_{\text{loop}}$  of any given solution. However, it was also clear on preparation of these solutions that the solvent free (90% DBU/10% benzylamine) solution was significantly more viscous than any others screened, although the absolute viscosity was not directly measured since we do not have access to the apparatus required to measure viscosities accurately.

While for many applications of in-loop radiochemistry, another plausible way to increase  $F_{\text{loop}}$  for a given solution would simply be to use a longer loop, which should lead to higher in-loop retention of a solution. For some applications, this may be possible, but it is possible to foresee applications where this may not be so simple. These could be instances where the architecture and dimensions of the fixation-loop are fixed (in a microfluidic device, for example), or for loops which directly interface with an HPLC where the injection volume cannot exceed a certain value without overloading the column. For these occasions, one could seek to improve the loop retention of the solution by increasing its viscosity. Depending on their compatibility with the reaction, one could foresee the addition of sulfolane, 1,4-dioxane, NMP, DMSO, or even glycerol (where the reaction is unaffected by protic solvents); solvents which are substantially more viscous



than MeCN or THF, the more “traditional” <sup>13</sup>C-radiochemistry reaction solvents. Another possible approach to consider could be cooling the loop during fixation to increase solution viscosity, but this is less ideal since it would require modification of the fixation apparatus itself.

### 2.3 Results & Discussion – In-Loop Synthesis of <sup>11</sup>C-Ureas

The previous section successfully demonstrated the feasibility of trapping [<sup>11</sup>C]CO<sub>2</sub> in-loop in a DBU/amine based solution, (in-fact, the best performing solution was a solvent free mixture with a 10% benzylamine and 90% DBU composition). This is the essential first step common to all [<sup>11</sup>C]CO<sub>2</sub> fixation chemistry, whereby the gaseous [<sup>11</sup>C]CO<sub>2</sub> is trapped and functionalised, forming a more reactive amine carbamate salt intermediate [R-N(H)-CO<sub>2</sub>]<sup>-</sup>[DBU-H]<sup>+</sup>. Depending on the secondary reagents added, this amine carbamate can be further transformed to yield ureas, carbamates, and amides. Now that [<sup>11</sup>C]CO<sub>2</sub> fixation in-loop had been demonstrated, the next step for this work was to explore the possibility of incorporating this initial fixation step into a multi-step flow-type reaction scheme. Whereby solutions of these secondary reagents are passed through the tubing loop after the [<sup>11</sup>C]CO<sub>2</sub> fixation step, achieving these aforementioned transformations in-flow.

Flow-chemistry is a highly efficient and operationally simple way to perform certain radiochemical reactions, since reaction volumes can be easily minimised without incurring the significant transfer losses seen for standard vial-based radiochemistry which requires larger solvent volumes to be practical. Furthermore, flow-setups are a more straightforward way to perform microvolume radiochemistry, when compared with the the complex and labour-intensive reaction setups and operator procedures required in microdroplet style chemistry.<sup>222,374</sup> Finally, the major benefit to performing these reactions inside disposable polymer tubing is the fact that it lends itself very well to GMP production of radiopharmaceuticals. If a synthesiser uses fixed reaction architecture (glass vials etc.), a rigorous cleaning process must be implemented to ensure the sterility and purity of the products are not compromised. These cleaning procedures are laborious and time-consuming, incurring labour costs as well as increasing the time before another production can begin using the same synthesiser. If all materials which the reaction solution contacts are sterile, disposable plastic consumables, this cumbersome cleaning process can be entirely obviated. It is this consideration that has also been responsible for – in recent years – the adoption of cassette-based radiosynthesis units for routine radiopharmaceutical production.

### 2.3.1 Apparatus design and development

This in-loop <sup>11</sup>C-urea synthesis setup was built on the Eckert & Ziegler Modular-Lab platform. This synthesis unit has an array of 2-way switching solenoid valves which can be remotely controlled from outside of the hot-cell. These valves are compatible with standard threaded “finger-tight” adapters and as such allow a variety of different tubing/fluidic connections to be connected directly, with minimal dead volume. These switchable valves allow the construction of fairly complex reaction architectures due to their universality and versatility. It should be noted that for these preliminary experiments, using these reusable permanent valves was convenient. Were this to be translated to a GMP procedure, this setup could be simply transferred onto a synthesis unit employing disposable switching valve manifolds (Trasis AllInOne, GE Fastlab 2, E&Z Modular-Lab PharmTracer, etc.).

In this proof-of-concept implementation, the <sup>11</sup>C-carbamate salt (retained in the thin-film on the walls of the loop) was converted to a symmetrical urea by reaction with a pre-prepared Mitsunobu solution (a betaine formed from the reaction of PBu<sub>3</sub>/DBAD). While the previous three-component loop trapping setup is sufficient for the initial in-loop [<sup>11</sup>C]CO<sub>2</sub> fixation step, in order to enable the introduction of this secondary reagent solution into the fixation loop it was necessary to connect the loop input to a remotely switchable valve. Furthermore, the exit of the loop also had to be connected to a switchable valve to allow flushing of the excess captive solvent to a waste vial (as before), before switching the flow direction when passing the Mitsunobu solution through the system.

Additionally, the distribution of the trapped <sup>11</sup>C along the length of the loop was not known to us, and as such there were some concerns that there could be a significant degree of the <sup>11</sup>C-carbamate salt trapped near to the exit of the loop. In this case, upon passing the Mitsunobu solution through the loop there may not be sufficient mixing/residence time in-flow to enable the dehydration/urea formation reaction to fully proceed before exiting the flow setup. To address this, a second empty “reaction” loop was added to the setup. This simply served to ensure an adequate residence time for the reaction mixture, allowing efficient mixing and – theoretically – a greater yield of the final <sup>11</sup>C-urea product.

Finally, the product was eluted from the reaction loop into a collection vial containing water. This water serves two purposes: it acts as a quench step to halt the reaction upon leaving the loop (explained in greater detail in the following section), as well as serving to predilute the reaction mixture for HPLC analysis/purification.

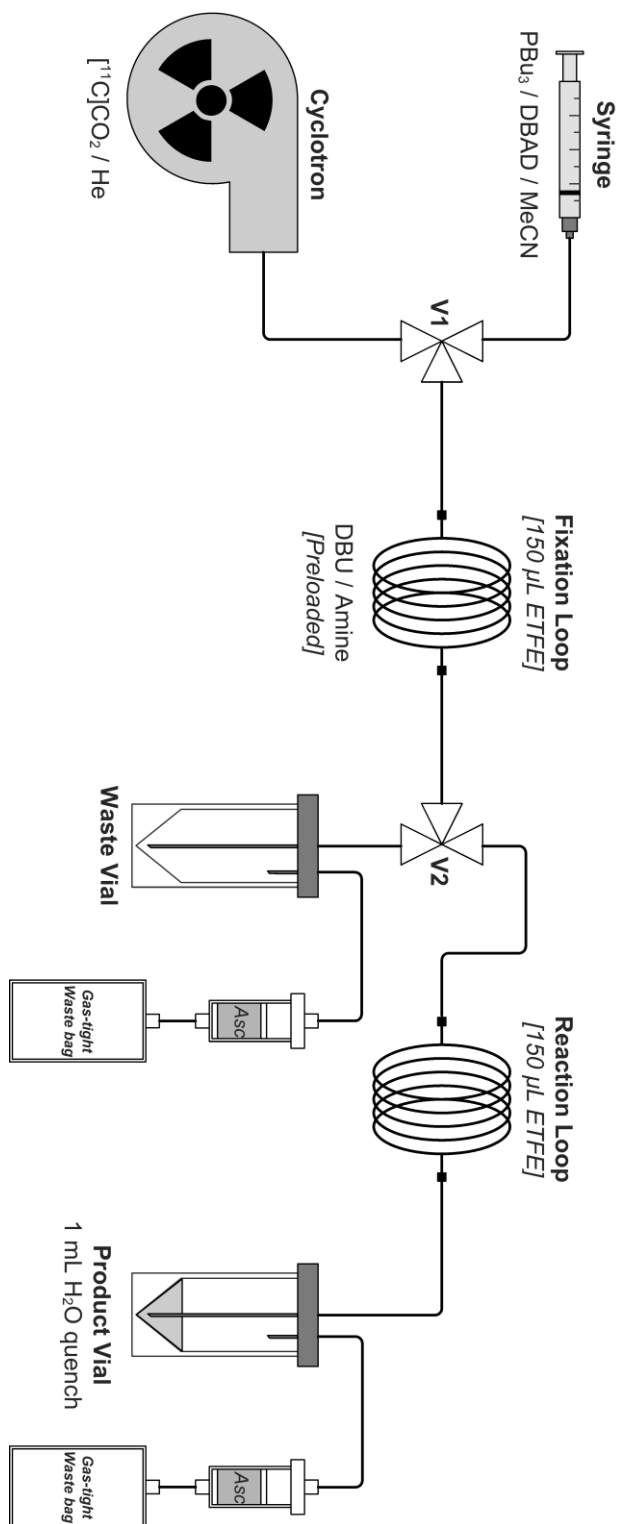


**Figure 2.6 Schematic of apparatus for in-loop synthesis of  $^{11}\text{C}$ -ureas**

Representative process flow diagram describing the apparatus for in-loop fixation of [ $^{11}\text{C}$ ]CO $_2$  and subsequent flow radiosynthesis of  $^{11}\text{C}$ -ureas

Presented above is a representative process flow diagram for the described reaction apparatus setup, and the stepwise operation of this setup for <sup>11</sup>C-urea synthesis proceeds as follows:

1. **Fixation Loop** is preloaded with 75 µL fixation solution and connected to switching valves **V1** and **V2**
  - *Loop is pre-flushed with Helium to remove majority of atmospheric CO<sub>2</sub>*
2. Helium is flushed for 3 minutes at 70 mL/min from the **Cyclotron** via **V1** through the **Fixation Loop** and into the **Waste Vial** via **V2**
  - *Flushes majority of solution through to the vial, leaving a residual thin-film on the walls of the loop*
3. [<sup>11</sup>C]CO<sub>2</sub> is passed from the **Cyclotron** through the **Fixation Loop** and into the **Waste Vial**
  - *[<sup>11</sup>C]CO<sub>2</sub> traps in the thin-film of captive solvent, forming the <sup>11</sup>C-carbamate salt in-situ*
4. **V1** and **V2** are switched and 150 µL Mitsunobu solution is delivered from the **Syringe** into the **Fixation Loop**
  - *Reacts with <sup>11</sup>C-carbamate salt to form the symmetrical <sup>11</sup>C-urea*
5. **V1** is switched and a Helium flush from the **Cyclotron** pushes the contents of the **Fixation Loop** through the **Reaction Loop** and into the **Product Vial**
  - *Ensures a longer residence/mixing time, theoretically maximising the radiochemical yield*
6. The crude reaction products are analysed by radio-HPLC and all washings and component radioactivity levels were measured to determine the total quantity of [<sup>11</sup>C]CO<sub>2</sub> delivered in this instance

The valves are switchable remotely using the E&Z Modular-Lab control software, and the syringe can be remotely operated using a syringe pump. Therefore, while the process was not fully automated, it can be controlled entirely remotely from outside the hot-cell.

### 2.3.2 Quenching

As mentioned previously, the water added to the product vial served to quench the reaction. In the final step of the reaction, the <sup>13</sup>C-carbamate salt and the Mitsunobu reagents are flushed through the reaction loop and into the product vial. In our case, this vial sits for several minutes while the hot-cell is opened, the vial is disconnected, its radioactivity is measured, and a sample is injected into the HPLC for analysis. In the absence of a quenching step, there is a possibility that any urea products observed have simply formed in reactions occurring in the bulk solution within the product vial. The aim of this work however, was to achieve an in-loop flow-synthesis of <sup>13</sup>C-ureas.

By adding a quench in the product vial, it is possible to “freeze-out” the reaction at the point that it leaves the reaction loop. Any products observed in the crude HPLC can be said to have formed solely within the loop as part of the flow process itself. It is particularly important to know whether the reaction occurs in-flow if one were considering either integrating an in-line HPLC purification, or adapting this process for a microfluidic device. Additionally, this allows easier comparison between productions as it gives a precise, reproducible, and easily-measurable total synthesis time.



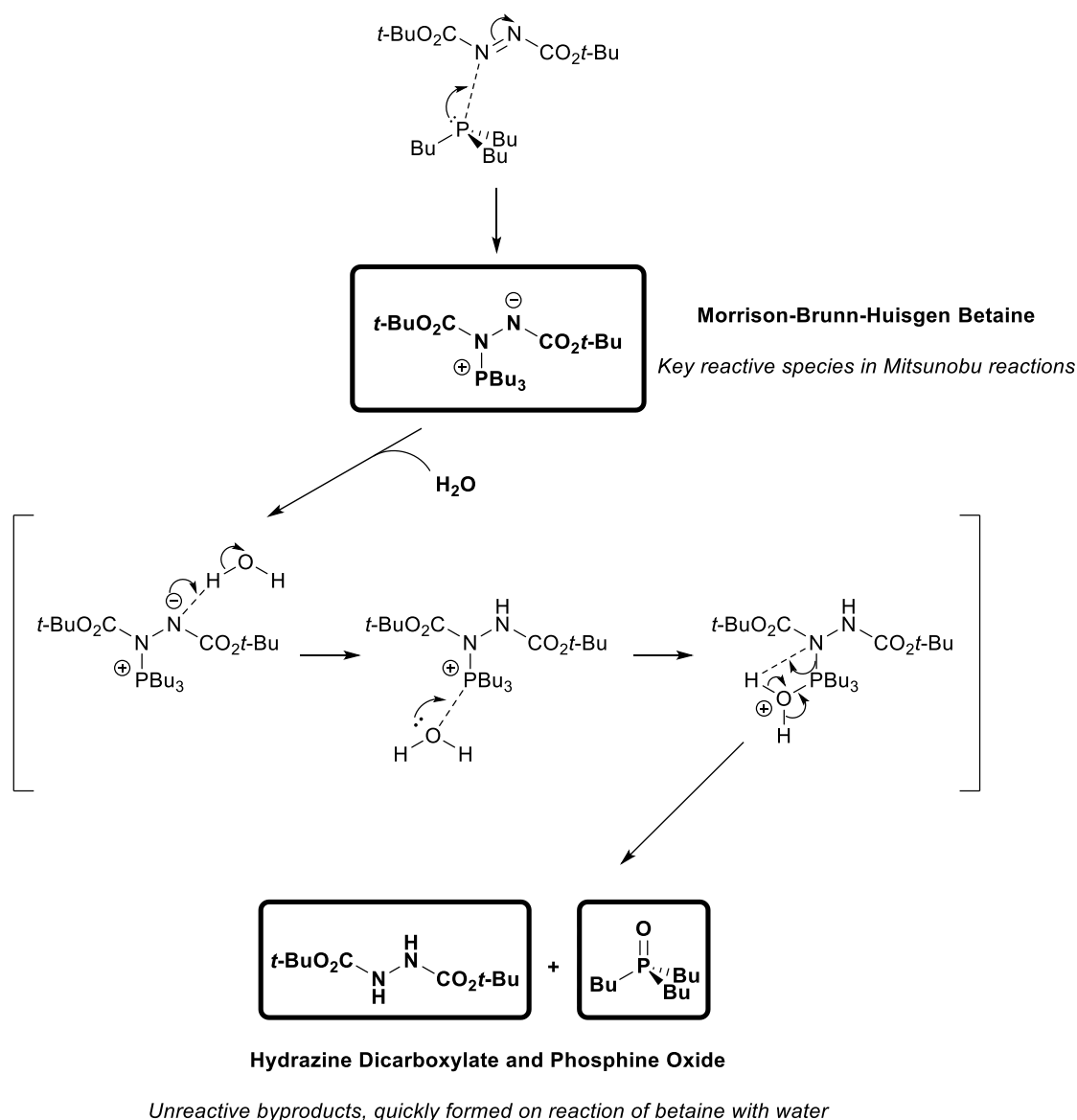


**Figure 2.7 Water quenching mechanism (putative)**

Based on experiments showing addition of water to a solution of  $\text{PBu}_3$ /DBAD in MeCN, rapidly forms the hydrazine dicarboxylate and phosphine oxide products

In order to quench the reaction, it was necessary to consider what is the active species formed by these Mitsunobu reagents. In this case, equimolar amounts of tri-*n*-butylphosphine ( $\text{PBu}_3$ ) and di-*tert*-butyl azodicarboxylate (DBAD) are mixed in acetonitrile. These react near-instantaneously *via* nucleophilic attack of the phosphine on the N=N double bond of the azo compound, to form a zwitterionic species commonly referred to as the Morrison-Brunn-Huisgen betaine.<sup>233,236</sup> A betaine is a subtype of

zwitterion that cannot isomerise by proton exchange to give a neutral form, in this case the positive and negative charges are localised on the phosphorous and nitrogen atoms respectively.

It should be noted that when preparing this reagent, a clear colour change is observed and this can serve as a visual indication that the betaine has formed as desired. Diazo compounds are brightly coloured due to extended  $\pi$ -electron delocalisation across the N=N bond, and at room temperature DBAD exists as a bright yellow crystalline solid which results in a bright yellow solution in acetonitrile, even under high dilution. Upon reaction with a phosphine however, the N=N double bond is broken, interrupting this delocalisation. The resultant betaine is therefore colourless, and this yellow-to-colourless transition is observed rapidly upon addition of the phosphine. Phosphines are highly moisture sensitive however, and rapidly degrade on exposure to atmospheric oxygen and moisture, forming the corresponding phosphine oxide. If the phosphine has degraded to any significant degree, the colour change is not observed and gives a simple indication to the chemist that the betaine has not formed as intended, and a fresh batch of phosphine should be used.

Underpinning this betaine's utility in much of Mitsunobu chemistry is in its reactivity with protic substrates. The negative charge on the nitrogen is readily abstracts a proton from alcohols and carboxylic acid functionalities, and the positively charged phosphonium reacts readily with the electronegative oxygens and nitrogens present in alcohols, carboxylic acids and amines. With this knowledge, one would predict a similar reactivity with water, and so it was hoped that this reaction could simply be quenched with the addition of water to the product vial. Indeed, there are mentions in the literature alluding to the moisture sensitivity of this active betaine species,<sup>234</sup> but few details of this specific hydrolysis reaction have been disclosed thus far.

To confirm whether water was sufficient to quench the reaction by hydrolytic degradation of this betaine, a straightforward experiment was performed. An equimolar solution of PBu<sub>3</sub> and DBAD in acetonitrile was prepared, forming the active betaine *in-situ*, and was added to a large excess of water. An insoluble white precipitate formed immediately upon addition, and TLC of this compared with commercial reference materials indicated the presence of tributylphosphine oxide (PBu<sub>3</sub>O) and the hydrazine byproduct from DBAD

(DBAD-H<sub>2</sub>). These are the standard byproducts formed in the use of this betaine in Mitsunobu chemistry and are also what would theoretically be expected on reaction with water, as is shown in the putative reaction mechanism above. Furthermore, mass spectroscopy confirmed the presence of both of these compounds, and <sup>1</sup>H and <sup>13</sup>C NMR also confirmed that one of the byproducts was indeed the hydrazine byproduct DBAD-H<sub>2</sub>.

This evidence, combined with the previously reported moisture sensitivity, and the well-established reactivity of the betaine with protic substrates, meant that we felt a simple water quench would be sufficient to stop the <sup>13</sup>C-urea formation upon exiting the reaction loop. As such, the resultant distribution of <sup>13</sup>C-labeled products in the radio-HPLC analysis can be fairly-confidently attributed to that formed in the in-loop flow chemistry process itself. This was a simple control to implement but would dramatically improve the reliability and reproducibility of any results obtained.

### 2.3.3 Improved in-loop [ $^{11}\text{C}$ ]CO $_2$ fixation

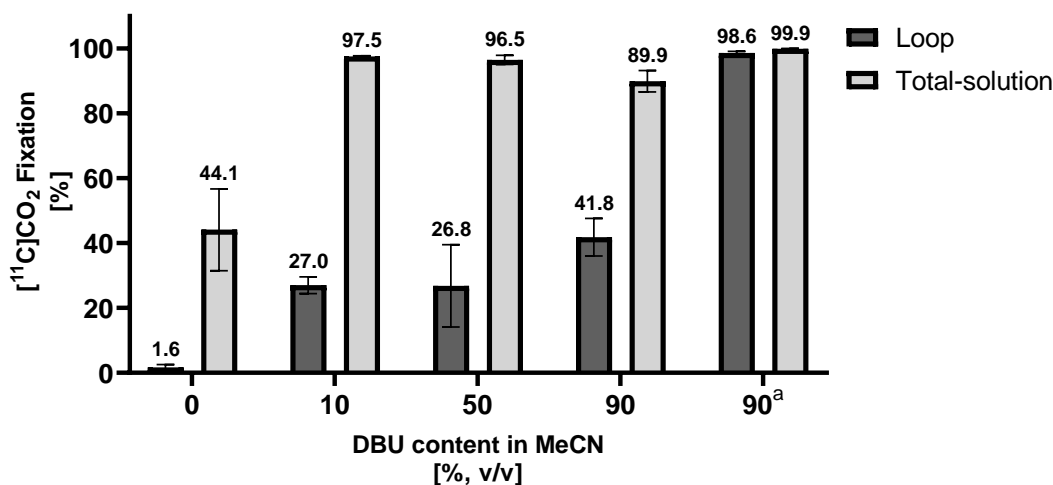


**Figure 2.8** Plot of [ $^{11}\text{C}$ ]CO $_2$  fixation as DBU content in MeCN varies

Entries 0, 10, 50, and 90 % DBU in MeCN [v/v] were obtained using the previously used 3 component fixation apparatus.

a) increased in-loop fixation % of [ $^{11}\text{C}$ ]CO $_2$  in urea synthesis apparatus (using E&Z modular lab switching valves)

During the first full syntheses using this  $^{11}\text{C}$ -urea synthesis setup (on the E&Z Modular-Lab) an interesting and unexpected phenomenon was noted. The trapping solution used in these was the optimal 90% DBU / 10% benzylamine solution that was chosen during the earlier in-loop fixation experiments, using the simple three-component fixation setup. In these earlier instances, the average  $F_{\text{loop}}$  for this solution composition was just  $41.8 \pm 5.8$  %, and while this was less than optimal it was still the best performance seen for any of the screened solutions. However, when this same solution was used in this full  $^{11}\text{C}$ -urea flow setup, the  $F_{\text{loop}}$  more-than-doubled to  $98.6 \pm 0.5$  %. This result was not expected but was highly convenient, meaning that in this new synthetic setup the chosen fixation solution was capable of near-quantitative [ $^{11}\text{C}$ ]CO $_2$  fixation, so any radiochemical yields obtained from the full  $^{11}\text{C}$ -urea synthesis should not be hindered by an inefficient [ $^{11}\text{C}$ ]CO $_2$  fixation step.

From the previous sections discussing in-loop fixation, it has been shown that for solutions with a comparable  $F_{\text{tot}}$ , the major factor governing its  $F_{\text{loop}}$  is the degree of solution retention in-loop. In the previous examples, the solution retention was increased

by increasing the solution's viscosity. For this case however, the solution composition – and therefore its viscosity – remain unchanged. It is necessary therefore, to consider what other factors could influence solution retention, and therefore could be responsible for this significant improvement in  $F_{loop}$ .

In the flushing step, the prefilled loop is flushed from the input with a flow of helium gas, causing the solution to flow through the tubing (likely in an annular flow regime). The Hagen-Poiseuille law states that flow rate through a cylindrical pipe is proportional to the pressure drop along the pipe, where the pressure drop is the difference between the pressures at the input and exit of the pipe.<sup>426</sup> In the case of the simple three-component fixation apparatus, the elevated pressure at the input is provided by the helium flush, while the exit from the tubing is unrestricted as it flows directly into the waste vial without additional needles or fittings. In the case of the urea synthesis setup however, while the elevated pressure at the input remains the same, the exit from the tubing to the waste vial is necessarily directed *via* a switching valve. These switching valves have a very low dead volume so the diameter of the channel through the valve is smaller than the diameter of the loop itself. As such, this will cause a backpressure build-up at the exit of the loop, and so the pressure drop along the tubing will be decreased when compared with the unimpeded three-component setup. Since the pressure drop is decreased, the flow rate of the captive-solvent through the loop during this flushing period will also decrease accordingly. Since the flushing time remained the same for all experiments, the lower flow rate in the urea synthesis setup would likely result in a higher degree of solution retention in-loop, as well as a correspondingly higher  $F_{loop}$ .

Another compounding effect of the increased backpressure due to the switching valve is the corresponding decrease in [<sup>13</sup>C]CO<sub>2</sub> flow rate during the fixation step. Similarly to what was seen in the flushing step, the reduced pressure drop will result in a reduced gaseous flow-rate and, therefore, in an increased residence time of the [<sup>13</sup>C]CO<sub>2</sub> in the loop. This prolonged gas-liquid contact time should theoretically result in a further-improved  $F_{loop}$ .

The combination of these multiple factors likely led to such a dramatic difference in this result. Simply directing the fixation loop to the waste vial *via* a switching valve caused an increased backpressure with a resultant significant increase in in-loop fixation ( $F_{loop}$ ).

While this dramatic increase in  $F_{loop}$  has only been observed, thus far, for this specific case (solution composition, gas flow rates, valve and loop diameters, etc.) the general principles established here will ideally be useful for future in-loop fixation process development and optimisation. The degree of solution retention – and therefore the in-loop fixation efficiency – can be improved by increasing the viscosity of the captive-solvent as well as by decreasing the flow rates through the loop (either that of the liquid during the flushing step, or that of the [<sup>11</sup>C]CO<sub>2</sub> through the fixation step). The flow rate through the loop is dictated by the magnitude of the pressure drop across it, and the pressure drop can be decreased by either increasing the backpressure at the exit, or by decreasing the gas flow rate at the input of the loop. The increased backpressure we encountered here (as a result of the switching valves on the E&Z module) is fairly application/situation specific, but a more general approach to slowing flow-rates through the loop (that could be more generally applicable to other situations) could be to introduce a needle-valve into the [<sup>11</sup>C]CO<sub>2</sub> delivery inlet line to modulate gas flow. As a caveat again, it remains important to ensure that any slowing of gas flow-rates results in sufficiently large increases in yields so as to make up for the longer reaction times with the concomitant losses due to decay.

In any case, for this proof-of-concept reaction the [<sup>11</sup>C]CO<sub>2</sub> fixation step exhibited a near quantitative in-loop fixation efficiency and so the radiochemical yield was unhindered by the fixation step. Any losses in radioactivity could therefore be attributed to the Mitsunobu-mediated dehydration/urea-synthesis step.

### 2.3.4 In-loop synthesis of $N,N'$ -[ $^{11}\text{C}$ ]dibenzylurea

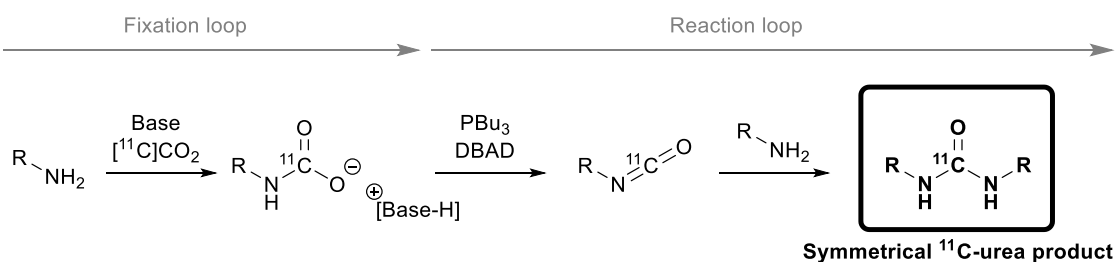


**Figure 2.9** Reaction scheme for in-loop [ $^{11}\text{C}$ ]CO<sub>2</sub> fixation and subsequent flow synthesis of symmetrical  $^{11}\text{C}$ -ureas

Base = non-nucleophilic “superbase” (DBU, BEMP, ..., etc.), R-NH<sub>2</sub> = alkyl/aryl 1° amine

#### 2.3.4.1 Operational discussion

For this full proof-of-concept  $^{11}\text{C}$ -urea synthesis, the reaction can be largely separated into three major mechanistic stages (the details of which are discussed at length in the general introduction to this thesis), depicted in Figure 2.9 above. Stage (1) is the previously discussed [ $^{11}\text{C}$ ]CO<sub>2</sub> fixation step whereby the [ $^{11}\text{C}$ ]CO<sub>2</sub> is incorporated into the [*carbamyl*- $^{11}\text{C}$ ]benzylcarbamate DBU salt retained in a thin-film in-loop. Stage (2) and (3) occur concurrently upon the addition of the active Mitsunobu betaine formed from PBu<sub>3</sub> and DBAD. In stage (2) the  $^{11}\text{C}$ -carbamate is dehydrated by the betaine to yield the [*carbonyl*- $^{11}\text{C}$ ]benzylisocyanate which immediately reacts with the excess unreacted benzylamine in stage (3), yielding the desired  $N,N'$ -[*ureido*- $^{11}\text{C}$ ]dibenzylurea product. Stage (1) occurs entirely in the fixation loop, whereas stages (2) and (3) occur in-flow as the Mitsunobu solution passes sequentially through the fixation and reaction loops.

Practically, this reaction proceeds via the process steps detailed in the earlier *Apparatus Design and Development* section, which are reproduced here for ease of reference:

1. **Fixation Loop** is preloaded with 75  $\mu\text{L}$  fixation solution and connected to switching valves **V1** and **V2**
  - Loop is pre-flushed with Helium to remove majority of atmospheric CO<sub>2</sub>

2. Helium is flushed for 3 minutes at 70 mL/min from the **Cyclotron** via **V1** through the **Fixation Loop** and into the **Waste Vial** via **V2**
  - *Flushes majority of solution through to the vial, leaving a residual thin-film on the walls of the loop*
3. [<sup>11</sup>C]CO<sub>2</sub> is passed from the **Cyclotron** through the **Fixation Loop** and into the **Waste Vial**
  - *[<sup>11</sup>C]CO<sub>2</sub> traps in the thin-film of captive solvent, forming the <sup>11</sup>C-carbamate salt in-situ*
4. **V1** and **V2** are switched and 150 μL Mitsunobu solution is delivered from the **Syringe** into the **Fixation Loop**
  - *Reacts with <sup>11</sup>C-carbamate salt to form the symmetrical <sup>11</sup>C-urea*
5. **V1** is switched and a Helium flush from the **Cyclotron** pushes the contents of the **Fixation Loop** through the **Reaction Loop** and into the **Product Vial**
  - *Ensures a longer residence/mixing time, theoretically maximising the radiochemical yield*
6. The crude reaction products are analysed by radio-HPLC and all washings and component radioactivity levels were measured to determine the total quantity of [<sup>11</sup>C]CO<sub>2</sub> delivered in this instance

*Step 3* begins at the end of bombardment of the <sup>11</sup>C-target in the cyclotron and as such, will be the point from which radiosynthesis reaction times will be calculated, and to which any decay corrections will be made. The process steps from *step 3* onwards will be discussed in turn, giving details of the actual operation as well as any observations made during development.

***Step 3: [<sup>11</sup>C]CO<sub>2</sub> delivery and fixation – 105 seconds***

The [<sup>11</sup>C]CO<sub>2</sub> was delivered directly from the cyclotron target in a helium flush through the reaction loop, taking on average 105 seconds. It was delivered without prior cryogenic



trapping/preconcentration as is employed in much of the [ $^{11}\text{C}$ ]CO<sub>2</sub> chemistry found in the literature. For this process, even highly diluted in the helium carrier gas, the fixation step was still highly efficient ( $F_{\text{loop}} = 98.6 \pm 0.5\%$ ). The radioactivity accumulation in the loop was monitored using the pin-diodes on the E&Z Modular-Lab system, and this confirmed that the radioactivity trapped in-loop reached a maximum at the time that the cyclotron helium flush automatically finished. Additionally, there was no subsequent release of radioactivity from the loop due to desorption. This is a commonly encountered problem seen for [ $^{11}\text{C}$ ]CH<sub>3</sub>I in-loop capture, since in these processes, the in-loop fixation step begins with the passive dissolution of the [ $^{11}\text{C}$ ]CH<sub>3</sub>I in the captive solvent. It is only after sealing the loop and allowing for an extended reaction time that the carbon-11 is incorporated into a more stable  $^{11}\text{C}$ -methylated product.<sup>377</sup> However the [ $^{11}\text{C}$ ]CO<sub>2</sub> fixation reaction here seems to be a more thermodynamically and kinetically favoured process, and hence the fixed  $^{11}\text{C}$ -carbamate species is stabilised which disfavours the reverse [ $^{11}\text{C}$ ]CO<sub>2</sub> release process even on extended helium flushing. As soon as the delivery was complete, no further time was allowed for the fixation reaction to complete and *step 4* was begun immediately.

***Step 4: Mitsunobu solution injected – 30 seconds***

The valves were switched to allow the Mitsunobu solution to be injected into the fixation loop, and to direct the output of the fixation loop towards the reaction loop. In initial experiments, this injection was performed manually by opening the hot-cell and injecting the Mitsunobu quickly into the system. The pre-prepared Mitsunobu solution was stored in a syringe that was already attached to the switching valve at the input of the fixation loop, and so the time-limiting factor for this stage was the time taken to open the hot-cell. Opening the hot-cell took approximately 15 seconds and the injection took another 15 seconds, so this step took approximately 30 seconds total. As soon as the injection of the Mitsunobu solution was complete, *step 5* began.

***Step 5: Reaction solution flows through to product vial – 1 second***

As soon as the loop was filled with 150  $\mu\text{L}$  of the Mitsunobu solution in the previous step, the switching valve on the input was switched back to the cyclotron which provided a flow of helium to push the reaction solution through the fixation and reaction loops into

the product vial where the reaction was quenched. The exact flow rate through the loop was difficult to control and measure, since while the input has a fixed pressure from the compressed helium tank, by the Hagen-Poiseuille law the resultant flow rate of the solution through the loop will vary as a product of backpressure in the system and solution viscosities, amongst other variables. While an accurate figure for the flow rate is therefore impossible to extract from this data, by visual observation of the loops, it took somewhere in the range of 0.5-1 second for all of the solution to pass through the system. Since the combined volume of both loops was 0.3 mL, this equates to an approximate flow rate in the region of 0.5 mL/s or 30 mL/min, but this is likely only accurate to the nearest order of magnitude. A potential remedy to this uncertainty would be to control the solution flow rate with a syringe pump, but this will be discussed in greater detail shortly.

***Total reaction time (from EoB): < 140 seconds***

The reaction is complete in under 3 minutes from EoB and therefore represents an incredibly rapid radiosynthetic procedure which is highly suited to the half-life of carbon-11. The remaining steps were to analyse the reaction mixture by radio-HPLC and to measure the residual radioactivity in all other components and washings. A representative analytical radio-HPLC trace is presented below for the synthesis of the model compound *N,N'*-[ureido-<sup>11</sup>C]dibenzylurea, the crude sample was coinjected with a small quantity of the non-radioactive compound as a reference material to confirm the identity of the radioactive peaks.

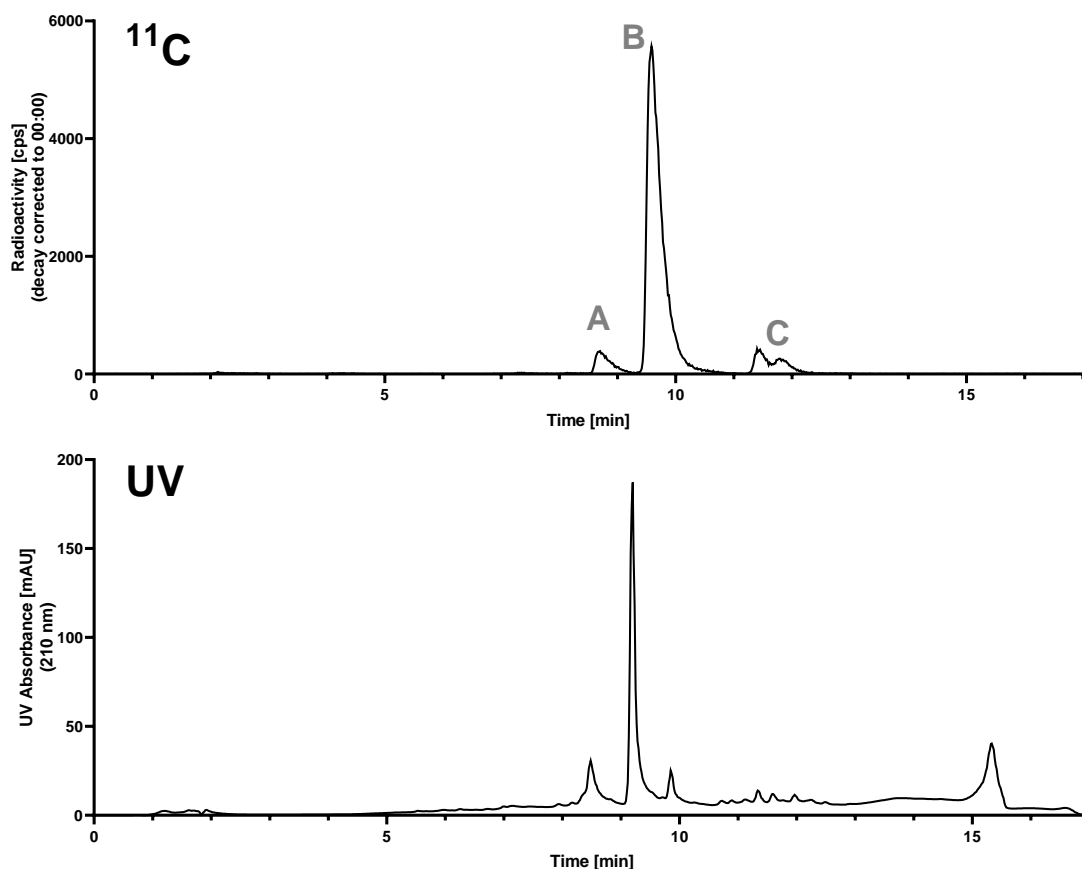


**Figure 2.10** Radio-HPLC trace from in-loop synthesis of  $N,N'$ -[ $^{11}\text{C}$ ]dibenzylurea

Coinjected with non-radioactive reference compound ( $T_R = 9:11$ ). Peaks labeled A, B, and C for future reference purposes.

#### 2.3.4.2 Synthetic results - summary

As the radio-HPLC trace shows above, this reaction proceeded extremely well with a resultant radiochemical purity (RCP) of the crude sample of  $83 \pm 3\%$ . Combining this with the near quantitative loop fixation ( $99 \pm 1\%$ ), the overall non-isolated RCY (decay corrected) for this in-loop flow radiosynthesis of  $N,N'$ -[ureido- $^{11}\text{C}$ ]dibenzylurea was  $82 \pm 3\%$ . This was an impressive achievement, and represented a similar radiochemical yield to traditional vial-based methods, with a significantly reduced reaction time and entirely obviating the need for heating or cooling. The average molar activity for these productions was  $0.75 \pm 0.13 \text{ GBq}/\mu\text{mol}$ , from an initial  $300 \text{ MBq}$  of [ $^{11}\text{C}$ ]CO $_2$ . While this value appears fairly low, this is due in-large-part to the low initial radioactivity

obtained from short, low beam current target bombardments. A more complete discussion of this is presented in the final notes of this section, but in brief, this result is in-line with the molar activities seen for many other [ $^{11}\text{C}$ ]CO<sub>2</sub> fixation reactions performed in both our lab, as well as others.

#### 2.3.4.3 Discussion of crude HPLC – identification of major peaks

The HPLC trace shows three major product peaks, referred to herein as: A, B, and C; in order of elution. Peak B was readily identified by coinjection with the non-radioactive standard as the desired *N,N'*-[ureido- $^{11}\text{C}$ ]dibenzylurea in 83% abundance, with a retention time around 9:34. In order to fully understand and attempt to improve the radiochemical yields, however, it was important to identify the other side-products seen in this radio-HPLC. At this flow-rate through this column, the solvent front passes through the detectors at around 2:30, and it is in this region that any poorly retained and highly polar compounds tend to elute. From previous experiments, it was found that any dissolved-but-unreacted [ $^{11}\text{C}$ ]CO<sub>2</sub> and the charged  $^{11}\text{C}$ -carbamate salt elute in the 2:30 to 3:30 range. The absence of any peaks in this region supports the assumption that all of the [ $^{11}\text{C}$ ]CO<sub>2</sub> has been trapped as the  $^{11}\text{C}$ -carbamate and that this in-turn has been converted to more complex, uncharged organic molecules.

Peak A elutes close-to, but earlier-than the desired product peak B on this reversed-phase C18 column. One would intuitively expect this compound to be similar, but marginally less lipophilic than dibenzylurea. The reaction mechanism involves the intermediate formation of the [isocyanato- $^{11}\text{C}$ ]benzyl isocyanate which reacts with benzylamine to yield the urea product. One would expect this benzyl isocyanate to have a similar degree of lipophilicity to the dibenzylurea on account of their general structural similarities. The urea does however bear two benzyl substituents, to the isocyanate's one, and as such the isocyanate could be expected to be less lipophilic than the corresponding urea. This prediction is further supported by calculating cLogP values in ChemDraw: benzyl isocyanate = 2.314; dibenzylurea = 2.888. Taken together, this reasoning led to the prediction that peak A was the unreacted [ $^{11}\text{C}$ ]benzylisocyanate intermediate. This was subsequently confirmed by injection of a non-radioactive reference standard of benzyl isocyanate, which eluted with a reference time corresponding to that of peak A. The

presence of a significant amount of the intermediate isocyanate implied that the reaction was incomplete, either due to insufficient reaction time or an abundance of amine which could be consuming/quenching the

Peak C elutes significantly later than B and as such was expected to be correspondingly more lipophilic. Where A and B are predicted intermediates and products from this reaction, it's not so clear what peak C could have been, given that it still forms in significant quantities. To begin to explore this, it was necessary to consider what reactive species (radioactive and non-radioactive) are present during this reaction, and therefore what unintended side-reactions could occur. As previously stated, any polar compounds would have eluted much earlier, so this largely rules out any possible hydrolysis products of the urea/isocyanate in the quench vial. It was therefore more likely that this compound was formed by a further reaction on the urea or isocyanate products in-loop. One possible reaction that could theoretically occur, but which has been poorly documented to-date is the reaction of a urea with an isocyanate, forming a biuret (a compound with the general structure R-NH-C(O)-NR-C(O)-NH-R). This reaction has been reported to occur in non-radioactive syntheses at elevated temperatures over extended reaction times.<sup>427-429</sup> It is crucial however to remember that with the pseudo-first-order kinetics encountered within <sup>13</sup>C-radiochemistry, reactions can proceed more readily than would be expected from their non-radioactive counterparts. In these initial experiments, there was a significant degree of atmospheric [<sup>13</sup>C]CO<sub>2</sub> contamination, producing a corresponding quantity of <sup>13</sup>C-isocyanate, evident in the UV trace of the HPLC analyses. The quantities produced would theoretically be sufficient to react with the <sup>13</sup>C-urea to form the [<sup>13</sup>C]1,3,5-tribenzyl-biuret, and this led to a suspicion that this could be the impurity in peak C. The cLogP value for this compound is 5.150, which is more lipophilic than the urea, so again this would fit with the radio-HPLC elution profile. If this biuret formation does require the presence of non-radioactive <sup>13</sup>C-isocyanate, then it would be expected that the RCY of the <sup>13</sup>C-biuret would increase as the molar activity of the reaction decreased (since this implies a larger quantity of atmospheric [<sup>13</sup>C]CO<sub>2</sub> contamination). The data from these in-loop urea syntheses was analysed and it was confirmed that indeed, the RCY of peak C increased as molar activities for the production decreased. This further supports the suggestion that this final peak was the <sup>13</sup>C-biuret, however future work should explore

synthesis of the non-radioactive reference to fully confirm this peak assignment, and to enable a better understanding of the kinetics of this side-reaction.

#### 2.3.4.4 *How to improve RCY*

While this 82% RCY was still impressive for these initial syntheses, the next logical concern was exploring ways in which this reaction could be enhanced to further increase RCYs. Firstly, the absence of any polar species observed in the HPLC suggests that the Mitsunobu-mediated dehydration of the <sup>13</sup>C-carbamate to yield the <sup>13</sup>C-isocyanate had reached completion (due to the strong thermodynamic driving force of the P=O bond formation, as is also seen in the Wittig reaction)<sup>430</sup>. The presence of unreacted <sup>13</sup>C-isocyanate as well in addition to the product <sup>13</sup>C-urea in the radio-HPLC has two plausible explanations. Either: 1) the amine has been totally consumed by Mitsunobu, so the reaction cannot proceed any further; or 2) the reaction is incomplete, and requires elevated temperatures or longer reaction times to reach completeness.

Addressing point (1), this Mitsunobu-mediated chemistry is highly sensitive to the exact reagent stoichiometry, due to the poor chemoselectivity of the Mitsunobu betaine. While it is used in this reaction because of its ability to convert the carbamate into the corresponding isocyanate, it will also react with amines, such as those used in this reaction. Therefore in the presence of a stoichiometric excess of Mitsunobu betaine, in addition to mediating the desired carbamate-to-isocyanate conversion, the remaining amine will be consumed, precluding any subsequent <sup>13</sup>C-urea formation from the <sup>13</sup>C-isocyanate.

It should be noted however, that this phenomenon can also be exploited in cases where an asymmetric urea is to be produced, with careful stoichiometric control allowing selectivity for one urea product over the others. In cases such as this, where the target product is the symmetric urea, the key is to ensure an overall stoichiometric excess of amine, *versus* the Mitsunobu reagent. This should ensure that there remains some unreacted amine present to enable complete conversion of the <sup>13</sup>C-isocyanate to the <sup>13</sup>C-urea. In standard vial-based radiochemistry, this stoichiometric control is relatively trivial. But for in-loop processes, there is an inherent uncertainty introduced in the first loop-flushing stage: it is difficult to control/predict exactly how much amine is retained

in-loop, meaning that it is impossible to precisely control the reaction stoichiometry. This is one plausible reason for the incomplete reaction as observed in the radio-HPLC.

Regarding point (2) – assuming that point (1) is not limiting the maximum theoretical yield – the presence of unreacted <sup>13</sup>C-isocyanate suggests that the reaction has not reached completion. In this case, as with all irreversible reactions such as this, the two logical approaches to improve this radiochemical yield would be to increase either the temperature of the reaction, or the time of reaction. Introducing temperature control to this setup would greatly increase its operational complexity and so where possible should be avoided; increasing the reaction-time was therefore the simpler option to implement.

#### ***2.3.4.5 Attempted RCY increase: flow-rate control***

Up to this point, the loop had been filled manually by syringe before switching the valve at the input and driving the flow through the system with a helium flush. While exact measurements of flow-rates and residence times were difficult to obtain, by visual observation, the solution was seen to be flushed from the system within 0.5-1 second. A 0.5 second residence time for this total 300 µL loop volume equates to a flow-rate of approximately 36 mL/min. To explore the effects of increasing the reaction time, this flow rate would need to be decreased substantially, but control over gas-driven flow rates is difficult to achieve accurately and reliably. The use of a lead-screw driven syringe pump was determined to be the best option, since these provide precise and reliable control of liquid flow rates. Since only small pre-determined amounts of solution were required to be added, larger continuous-flow pumps (HPLC pumps, peristaltic pumps) are less appropriate, since these are better suited for consistent delivery of large volumes of solutions over long periods of time, by drawing from a larger reservoir of solution – a situation that is not appropriate when dealing with small quantities of air-sensitive solutions.

An initial Mitsunobu flow rate of 1 mL/min was chosen, since this would give an 18 second residence time, and represents an order of magnitude difference in reaction time compared with the previous experiments. If the presence of unreacted <sup>13</sup>C-isocyanate was due to an incomplete reaction, then it was expected that this increased reaction time would result in a significant change in the final RCY.

This reduced flow-rate experiment was performed twice, but no significant difference in RCY was noted, since a similar ratio of <sup>13</sup>C-isocyanate and <sup>13</sup>C-urea was observed in the radio-HPLC. This ruled out the possibility that the reaction was incomplete due to insufficient reaction time; it seems in-fact that the <sup>13</sup>C-urea formation reaction under these conditions is fairly instantaneous, and so extended reaction times are largely unnecessary. Given this result, it seemed more likely that a stoichiometric imbalance was the culprit responsible for the incomplete conversion of the <sup>13</sup>C-isocyanate. But as previously discussed, due to the uncertainty introduced by the solution flushing step, controlling this stoichiometry precisely was difficult to achieve. In light of the fact that – even under these sub-optimal conditions – the RCY of *N,N'*-[ureido-<sup>13</sup>C]dibenzylurea was 82 ± 1%, within just 3 minutes from the EoB, it was decided that this RCY was acceptable for our purposes, particularly since this synthesis was intended more as a proof-of-concept. Were this technique to be applied for routine production of a clinically relevant <sup>13</sup>C-urea, this RCY optimisation could of-course be continued in accordance with the principles laid-out herein.

#### **2.3.4.6 Final notes**

One major recurring issue in this chemistry was the highly moisture sensitive nature of the process. As was discussed in the previous section covering the quenching, the active Mitsunobu betaine is a highly moisture sensitive species, and is rapidly deactivated in the presence of small quantities of water. Practically speaking, this occasionally resulted in total failures of the reaction, and it was even (anecdotally) observed that these occurred more often on more humid summer days. This could largely be mitigated by fastidious sample preparation and total exclusion of atmospheric contamination of the system, but even with these precautions in place, these failures were not uncommon.



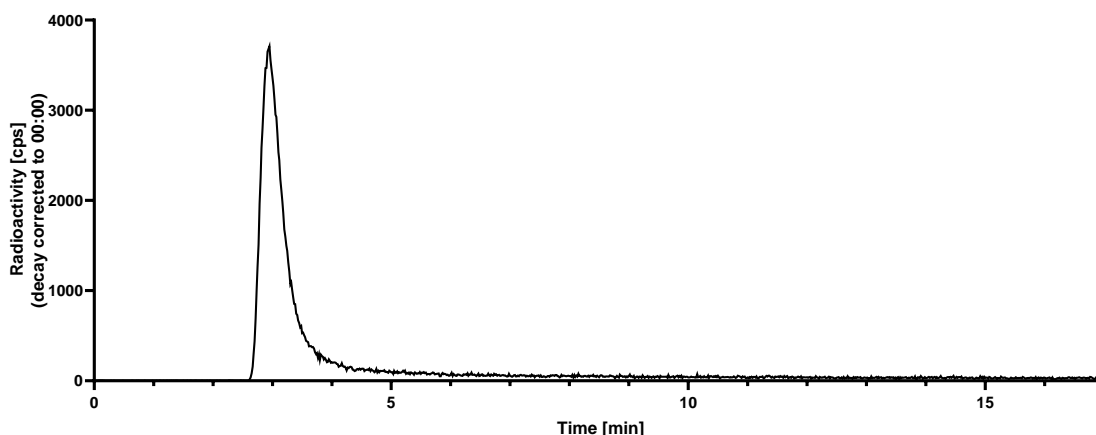


**Figure 2.11 Failed reaction due to moisture contamination**

Single peak corresponds to [ $^{11}\text{C}$ ]H $_2$ CO $_3$  formed due to hydrolytic instability of unconverted  $^{11}\text{C}$ -carbamate salt

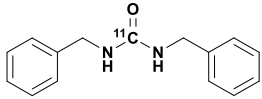
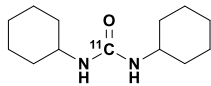
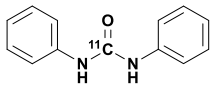
A failure of this nature was simple to identify by radio-HPLC as a single radioactive peak eluting on the solvent front from the C18 column. If the Mitsunobu betaine has been deactivated by moisture, then the  $^{11}\text{C}$ -carbamate salt is not converted to the subsequent  $^{11}\text{C}$ -isocyanate/ $^{11}\text{C}$ -urea products. Upon addition to the water quench in the product vial, this  $^{11}\text{C}$ -carbamate salt is protonated to form the  $^{11}\text{C}$ -carbamic acid. Carbamic acids are highly unstable and will release CO $_2$  spontaneously. In water, this re-released [ $^{11}\text{C}$ ]CO $_2$  reacts to form the polar carbonic acid ([ $^{11}\text{C}$ ]H $_2$ CO $_3$ ), which is what is observed on the radio-HPLC.

Finally, the low molar activity ( $0.75 \pm 0.13$  GBq/ $\mu\text{mol}$ ) of this reaction should be further contextualised. This molar activity was achieved from a 300 MBq production (ca. 1 min, 5  $\mu\text{A}$  target bombardment), as this was the standard level of radioactivity permitted for manually manipulated research productions within our facility. These low-level experiments are ideal for rapid reaction testing/screening, but of course would not be suitable for clinical productions. Were the process automated and therefore allowed to use a higher starting quantity of radioactivity (as an example, routine [ $^{11}\text{C}$ ]acetate production in our facility begins with 30-40 GBq of [ $^{11}\text{C}$ ]CO $_2$ ), the molar activity would be expected to increase proportionally. If the rest of the production process remains the same, then the level of atmospheric carbon-12 contamination would remain constant. Therefore by increasing 100-fold the initial quantity of [ $^{11}\text{C}$ ]CO $_2$  used, from 0.3 GBq to

30 GBq, one would expect a roughly proportional increase in molar activity. This assumption has been previously verified in our laboratory. This would mean that this process would be expected to yield compounds with molar activities in the 70 GBq/μmol range, similar to those seen in other [<sup>13</sup>C]CO<sub>2</sub> fixation processes.

### 2.3.5 Expanded substrate scope

While the general substrate scope for this chemistry has previously been established,<sup>225,226</sup> this method was still applied in the synthesis of other symmetric amine substrates to complete this proof-of-concept work. The two other target compounds synthesised in this section were *N,N'*-[ureido-<sup>11</sup>C]dicyclohexylurea and *N,N'*-[ureido-<sup>11</sup>C]diphenylurea, starting with cyclohexylamine and aniline, respectively. Like dibenzylurea, diphenylurea similarly has no clinical relevance, and was chosen to investigate the applicability of this method to less nucleophilic aromatic amines. Dicyclohexylurea however, was chosen partially since it would allow the investigation of more sterically hindered urea synthesis, but also for its biological activity. Dicyclohexylurea is a potent inhibitor of soluble epoxide hydrolase (sEH, IC<sub>50</sub> = 90 nM)<sup>431</sup>, so this also represents a radiosynthesis of a clinically relevant molecule in addition to further establishing the synthetic substrate scope. While the initial DBU/benzylamine solution was made-up in a *volumetric* 900:100 ratio. To ensure equivalent reaction stoichiometries (and theoretically more comparable results) for these new syntheses, the *molar* ratio of DBU:amine was conserved, which resulted in marginally different volumetric ratios. For dicyclohexylurea, the solution was prepared in a 900:105 ratio, and for aniline, it was prepared in a 900:84 ratio.

			
	<i>N,N'</i> -[ <sup>11</sup> C]dibenzylurea	<i>N,N'</i> -[ <sup>11</sup> C]dicyclohexylurea	<i>N,N'</i> -[ <sup>11</sup> C]diphenylurea
<u>Loop-fixation</u>	99 ± 1%	99 ± 1%	98 ± 1%
<u>RCP (from analytical HPLC)</u>	83 ± 3%	21 ± 6%	25 ± 10%
<b><u>RCY</u></b>	<b>82 ± 3%</b>	<b>21 ± 6%</b>	<b>24 ± 10%</b>

**Figure 2.12 Substrate scope for in-loop synthesis of <sup>11</sup>C-ureas**

Loop fixation calculated as a percentage of the total activity passed through the system. RCP calculated from an analytical HPLC analysis of the crude reaction mixture before any purification. RCY calculated as the product of loop fixation and RCP

### 2.3.5.1 Loop fixation

For both of these syntheses, the in-loop fixation percentages were comparable to those seen for benzylamine, in that [<sup>11</sup>C]CO<sub>2</sub> was trapped near-quantitatively in-loop. So as before, any losses in radiochemical yield can be attributed to incomplete <sup>11</sup>C-urea formation, and not as a result of insufficient fixation efficiency. Aniline is significantly less basic/nucleophilic than cyclohexylamine (pK<sub>aH</sub> in MeCN is 10.64 for aniline *versus* 18.36 for cyclohexylamine, and 16.92 for benzylamine) due to the resonance stability conferred by the aromatic ring. The high loop-fixation even for the less basic aniline supports again the theory discussed earlier and illustrated in Figure 2.2. In this, the fixation mechanism is separated into several equilibrating steps. The initial reaction between the amine and [<sup>11</sup>C]CO<sub>2</sub> – to form the protonated <sup>11</sup>C-carbamic acid – is kinetically disfavoured, with the equilibrium favouring the reverse reaction (and would be even less favoured for the less-nucleophilic aniline). In the presence of DBU however, the second step can occur, whereby the superbasic DBU deprotonates the <sup>11</sup>C-carbamic acid forming a stabilised amidinium carbamate salt. In this step, the highly stabilised product leads the equilibrium to lie strongly to the right, favouring the covalently fixed <sup>11</sup>C-carbamate product. The DBU is so strongly basic that even for less nucleophilic amines like aniline, the resultant amidinium carbamate salt is still sufficiently stabilised as to promote efficient and stable [<sup>11</sup>C]CO<sub>2</sub> fixation. This result supports the idea that the first step of this work – the in-loop superbase-mediated fixation of [<sup>11</sup>C]CO<sub>2</sub> – can be applied to amine substrates with a broad range of nucleophilicities, and as such this should be a fairly generally applicable methodology

### 2.3.5.2 Urea synthesis – lowered radiochemical yields

While the loop-fixation for these substrates was comparable to those seen for *N,N'*-[ureido-<sup>11</sup>C]dibenzylurea, the HPLC-measured radiochemical purities for these reactions were significantly lower, for *N,N'*-[ureido-<sup>11</sup>C]diphenylurea and *N,N'*-[ureido-<sup>11</sup>C]dicyclohexylurea they were 25 ± 10% and 21 ± 6% respectively. Combined with the nearly quantitative loop-fixation, these resulted in similarly reduced radiochemical yields (24 ± 10% and 21 ± 6%, respectively). Representative radio-HPLC traces for these syntheses are presented below, and several significant impurities can be observed.

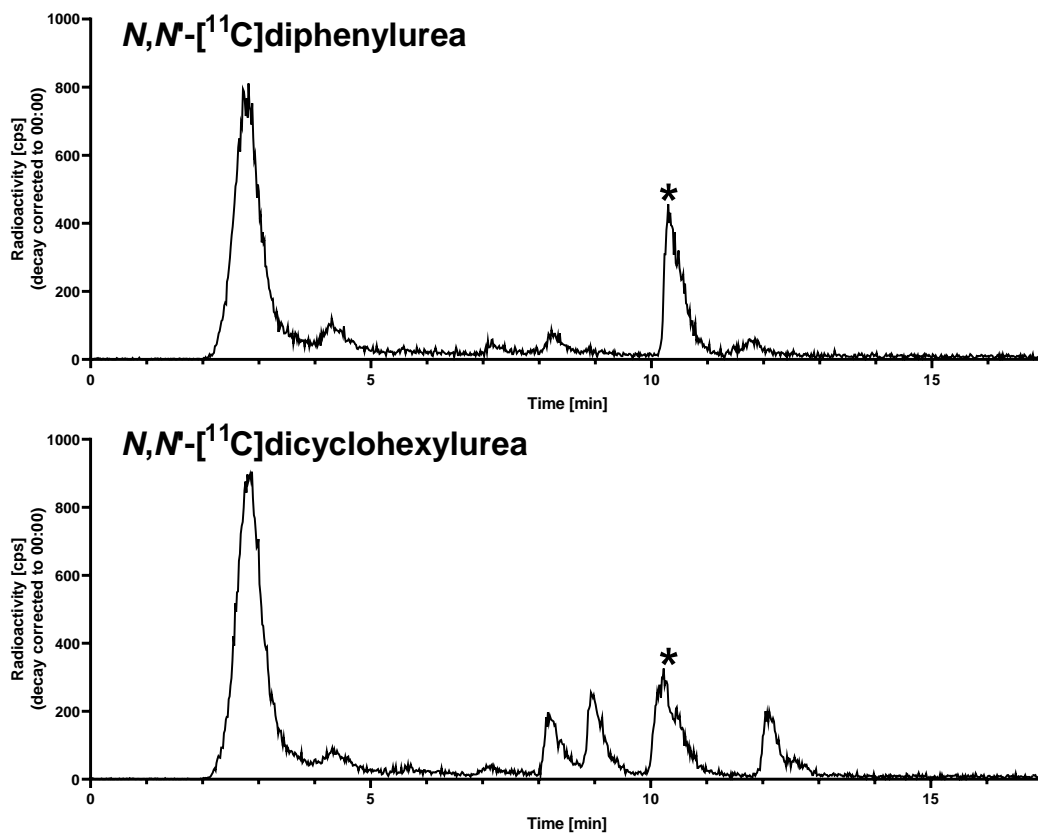


**Figure 2.13** Radio-HPLC trace from in-loop synthesis of alternative  $^{13}\text{C}$ -ureas

\* Indicates the  $^{13}\text{C}$ -urea product peak  
 Upper:  $N,N$ -[ureido- $^{13}\text{C}$ ]diphenylurea;  
 Lower:  $N,N$ -[ureido- $^{13}\text{C}$ ]dicyclohexylurea

By contrast to the earlier presented HPLC trace for  $N,N'$ -[ureido- $^{13}\text{C}$ ]dibenzylurea, in both of these cases the radiochemical purity is significantly reduced, and one clear reason for this is the large quantity of radioactive impurities eluting on or shortly-following the solvent front. As was discussed previously for C18 columns, the compounds which elute early-on (in the chromatographically weakest phase of the gradient) tend to be the most hydrophilic and polar compounds. It was suspected that these hydrophilic compounds were degradation products from partially unreacted [ $^{13}\text{C}$ ]cyclohexyl- and [ $^{13}\text{C}$ ]phenyl-carbamates.

To further support this conclusion, solutions of benzylamine and DBU were used to trap [ $^{13}\text{C}$ ]CO $_2$  from the cyclotron, before injection of these compounds directly into the radio-

HPLC without further chemical reaction. In these experiments, a single broad peak is observed at around 2:30, corresponding roughly to the void volume of the HPLC setup. It should be noted that if compounds are barely retained on the column, there is a significant chance that this peak could contain multiple different co-eluting polar species; if there is little retention on the column stationary phase, then there is little opportunity for sufficient chromatographic resolution of these species. While it is therefore difficult to fully identify and characterise this species at 2:30, some possible suggestions can be made. The amidinium <sup>13</sup>C-carbamate salt should form stably in this fixation solution, but on exposure to the aqueous chromatography solvent this carbamate species would be rapidly protonated. This would likely re-release [<sup>13</sup>C]CO<sub>2</sub> which would subsequently form [<sup>13</sup>C]H<sub>2</sub>CO<sub>3</sub> and in the radio-HPLC trace, this polar species would be expected to elute with the solvent front due to its high degree of hydrophilicity. In any case, this experiment provided confirmation that if an amidinium carbamate species is not completely converted to more-stable isocyanate/urea compounds, its degradation products will be evident at the start of any HPLC analysis.

If these early-eluting hydrophilic peaks were indeed indicative of an incomplete conversion of the amidinium <sup>13</sup>C-carbamates, the logical follow-up question was why was this Mitsunobu-mediated carbamate-to-isocyanate conversion so much less efficient for cyclohexyl- and phenyl-carbamates than for the previous benzyl-carbamate?

From these results it was difficult to adequately explain the difference in reactivity seen for aniline and cyclohexylamine *versus* that seen for benzylamine, although it was suspected that one contributing factor could be the varying degrees of steric hindrance around the amine. As was previously discussed, the basicity of these compounds (pK<sub>aH</sub>) was in the order: cyclohexylamine > benzylamine > aniline, but it is important to note that basicity does not necessarily directly correlate with nucleophilicity. Steric bulk can cause major deviations from the general basicity/nucleophilicity correlation. Of course, this effect is exploited in the usage of “non-nucleophilic” bases such as *N,N*-diisopropylethylamine (DIPEA) which can easily deprotonate many compounds but is very poorly nucleophilic due to the huge steric bulk which blocks the nitrogen from participating as a nucleophile in many reactions. However this effect can still have a more subtle role in influencing the differing reactivities of compounds with otherwise-similar

basicities. Although these three compounds are all primary amines, in the case of cyclohexylamine and aniline, the amine nitrogen is bonded directly to a secondary carbon, giving more steric bulk near to the nitrogen, when compared with the nitrogen in benzylamine which is bonded to the primary benzylic carbon. While there are no direct measurements of the nucleophilic strength of the three amines in question; as an example, one can compare the measured Mayr nucleophilicity parameters (*N*) of *tert*-butylamine (12.35) with those of *iso*-propylamine (13.77), and *n*-propylamine (15.11).<sup>432</sup> These examples demonstrate this effect quite clearly: the linear *n*-propylamine is near to 1000 times more nucleophilic than the sterically crowded – but similarly basic – *tert*-butylamine.

This effect could therefore go some way to explain the comparatively poor performance of these latter amines, but this again leads to the next concern: what approaches could be used to increase the yield? As was explained for the model synthesis of *N,N'*-[<sup>13</sup>C]dibenzylurea, the suggestion of increasing the reaction temperature was rejected due to the hugely increased instrumental complexity this would entail. To increase the reaction time, a syringe pump could again be employed to slow the delivery-rate/residence time of the Mitsunobu solution. Ultimately however, while in-general this Mitsunobu-mediated <sup>13</sup>C-urea synthesis has demonstrated a good substrate scope in our group's previous vial-based implementations<sup>225,226</sup> – with extended reaction-times and elevated temperatures – this in-loop method perhaps requires more substrate-specific optimisation. As such, since these other model <sup>13</sup>C-ureas were simply expanding this proof-of-concept work, it made little sense to fully optimise these particular syntheses any further. In fact, 20+ % RCYs achieved in under 3 minutes from EoB could in some cases still be acceptable; as was covered in the introduction and summarised well by Jewett *et al.*<sup>355</sup> Radiochemistry method development often involves trade-offs; a “sub-optimal” radiochemical yield can sometimes be justified if it leads to sufficient simplification of reaction processes and therefore a reduction of operator workload etc.

## 2.4 Discussion – Recent Developments

### 2.4.1 Comparison with contemporaneous Dahl method

A large portion of the work presented herein – the optimisation of in-loop [<sup>13</sup>C]CO<sub>2</sub> fixation and the proof-of-concept in-loop flow synthesis of *N,N'*-[<sup>13</sup>C]dibenzylurea – was published in 2018.<sup>404</sup> Unbeknownst to us at the time of developing this work, a similar in-loop [<sup>13</sup>C]CO<sub>2</sub> fixation methodology was developed and published near-simultaneously in the same journal issue by Dahl *et al.*<sup>405</sup> In their method, BEMP was used as an alternative fixation base to our DBU, and POCl<sub>3</sub> was employed as an alternative to our Mitsunobu-based dehydration agent, but the method was similarly used to label <sup>13</sup>C-ureas.

In addition to these reagent differences however, the key distinguishing feature of their setup is the use of reusable HPLC injection loops as opposed to our single-use polymer tubing. This is much more similar to the well-known method from Wilson *et al.*,<sup>349</sup> their method employed two separate loops connected to a standard 8-port HPLC injector valve: one loop (1 mL, ETFE) as the “reagent loop”, for storage of POCl<sub>3</sub> solution; and one loop (3.5 mL, stainless steel) as the “reactor loop”, for fixation step and subsequent <sup>13</sup>C-urea synthesis. This “reactor loop” was composed of two separate sections: the first of which was preloaded with an amine/BEMP solution, and the second which was loaded with a solution of a second amine. This was designed to allow for the selective synthesis of asymmetric <sup>13</sup>C-ureas by sequential formation of an isocyanate with the first amine, before “quenching” the reaction with the second amine to form the desired <sup>13</sup>C-isocyanate product. Alternatively, they “quenched” the isocyanate with methanol, forming the corresponding *O*-methyl-<sup>13</sup>C-carbamate product with reasonable selectivity.

This asymmetric urea selectivity was enabled by their use of these much larger-volume loops, their omission of the flushing step, as well as their use of more-wettable stainless steel.<sup>377</sup> These factors meant that small volumes of reagent solutions could be loaded with the knowledge that it would be retained in its entirety on the walls of the loop. This therefore enabled precise stoichiometric control over their reactions, something which was less possible in our method due to the inherent uncertainty regarding solution retention. This is the key criteria in which their methodology is superior to ours: by



controlling their reaction stoichiometries they were able to label more biologically-relevant asymmetric <sup>13</sup>C-ureas.

It should be noted however, that our aim with this work was more to investigate the general possibility of performing [<sup>13</sup>C]CO<sub>2</sub> fixation in-loop, with a particular focus on developing processes that could be easily miniaturised given the increasing prevalence of microfluidic radiosynthesis units as well as disposable cassette-based synthesisers. In this regard, our method was successful in providing a proof-of-concept example, demonstrating that [<sup>13</sup>C]CO<sub>2</sub> fixation could be achieved in very-low volume fluidic settings (our setup had a 300 μL total volume, compared with the more-than-10-times larger 3.5 mL volume in their more traditional “in-loop” setup) and that this could be applied in a simple “model reaction”. The adaptation of our small-volume polymer-loop method for asymmetric <sup>13</sup>C-urea synthesis is certainly one aspect that should be further investigated were this method to be taken forward in the future.

One area where their method is perhaps less well validated is in the absence of any quenching step. The [<sup>13</sup>C]CO<sub>2</sub> fixation occurs in-loop, but then the POCl<sub>3</sub> solution is flushed through the reactor loop and into an empty vial. Without a quench in this vial, it is impossible to determine whether the <sup>13</sup>C-urea synthesis was occurring in-loop or whether it simply occurred in the bulk reaction mixture in the vial prior to injection into the HPLC. It seems likely with the knowledge from our quenching experiments that it would indeed react to some-degree within the loop, but without this vital experimental control, it is difficult to solely attribute the improved radiochemical yields etc. seen here to the benefits from an in-loop flow-type process.

Ultimately, these two otherwise similar methodology development efforts were motivated by slightly different underlying goals. The Dahl method was developed to streamline the production of some of their group’s current radiotracers of interest, and as such, it was optimised with these specific requirements in mind. Their efforts were highly successful, particularly with regards to asymmetric urea selectivity, as well as seeing some significant improvements in RCYs and reaction times, arising from the benefits generally associated with in-loop processes. Our method was a more fundamental and general methodology development effort, with a particular emphasis paid to the in-loop fixation process itself, reflecting on the development and investigation of previous in-loop, thin-film, and

captive-solvent methods in <sup>13</sup>C-radiochemistry. The primary aims were to investigate first whether this recently developed gas-liquid [<sup>13</sup>C]CO<sub>2</sub> fixation chemistry could be adapted to an “in-loop” type synthesis and if-so, what parameters govern this process; the secondary aim was to integrate this process into a relatively straightforward <sup>13</sup>C-urea synthesis as proof-of-concept. Our method was focused more on the process of in-loop fixation itself, with a particular view towards future applications of this chemistry in polymer-based microfluidic synthesisers (such as the PMB iMiLab system); or disposable cassette-based radiosynthesisers (such as the Trasis AllInOne system).

The application to microfluidic settings would require significant amounts of further work, and this work is most useful as a proof-of-concept demonstrating that [<sup>13</sup>C]CO<sub>2</sub> can be trapped in low volume polymer loops at low pressure. By comparison, it is more straightforward to envision the translation of this method onto a system such as the Trasis AllInOne. That system functions by operating a disposable plastic three-way manifold that is compatible with standard fluidic fittings and connections – essentially it is a disposable (and therefore more GMP-suitable) equivalent to the permanent three-way valve manifold of the E&Z ModularLab system used here, so addition of a polymer-tubing loop to the Trasis should be relatively facile.

#### **2.4.2 Recent applications**

In the time since the publication of these two similar methods, there have been a number of articles published detailing their usage of an in-loop [<sup>13</sup>C]CO<sub>2</sub> fixation method in the synthesis of novel <sup>13</sup>C-radiotracers. The first three of these were from Steven Liang’s group (sharing several co-authors from the original Dahl paper), and had varying levels of success. The final example that will be discussed is the recent publication from Jean DaSilva’s group, which was highly successful. Figure 2.14 below illustrates some of the compounds radiolabeled using these methodologies.

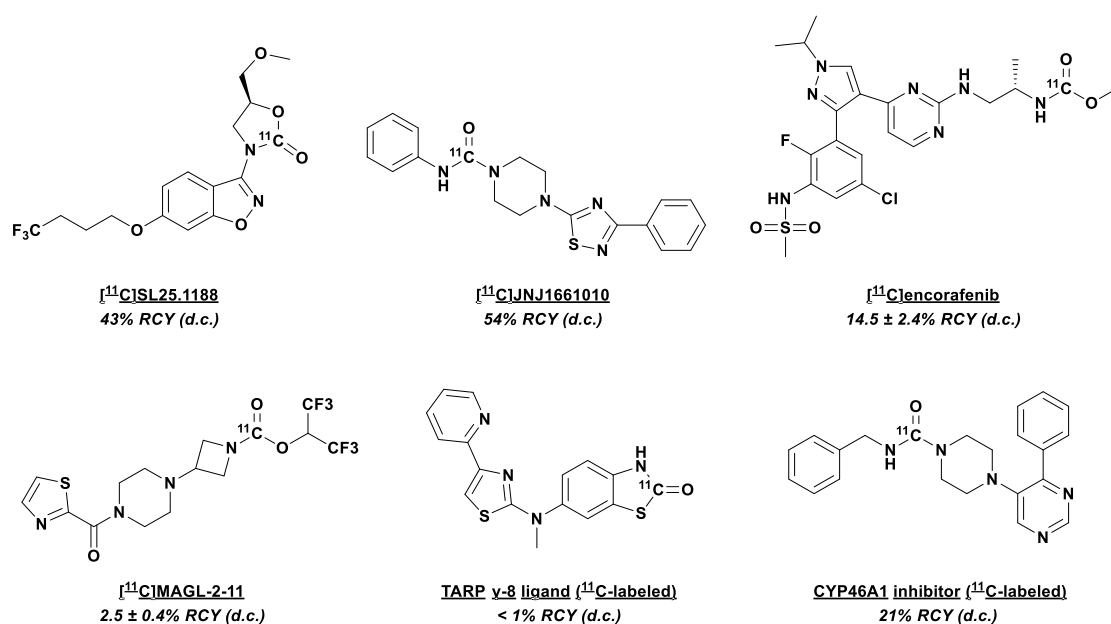


**Figure 2.14 Radiotracers synthesised using in-loop [ $^{11}\text{C}$ ]CO $_2$  fixation**

[ $^{11}\text{C}$ ]SL25.1188 and [ $^{11}\text{C}$ ]JNJ1661010 were both synthesised by Dahl *et al.*;<sup>405</sup> [ $^{11}\text{C}$ ]encorafenib was synthesised by Dornan *et al.*;<sup>406</sup> [ $^{11}\text{C}$ ]MAGL-2-11 and the CYP46A1 inhibitor were both synthesised by Chen *et al.*;<sup>245,248</sup> and the synthesis of the TARP  $\gamma$ -8 ligand was attempted by Yu *et al.*<sup>206</sup>

#### 2.4.2.1 MAGL inhibitor

The first to be discussed is Chen *et al.*'s synthesis of an  $^{11}\text{C}$ -labeled monoacylglycerol lipase inhibitor, radiolabeled at the carbonyl of a [*carbonyl*- $^{11}\text{C}$ ]alkylcarbamate.<sup>248</sup> For this work, they implemented the HPLC-loop setup from Dahl's method, performing the [ $^{11}\text{C}$ ]CO $_2$  fixation on a piperazinyl amine substrate with BEMP, reacting this with POCl $_3$ , and condensing the intermediate product with hexafluoroisopropanol to yield the desired radiotracer. While the molar activity and overall activity yields were sufficiently high for small-animal PET imaging, the compound was produced in a concerningly-low RCY of 2.5 ± 0.4% (decay-corrected), but this receives little discussion. It is not clear whether there were significant losses of  $^{11}\text{C}$  in the fixation stage, or whether the radiochemistry itself produced a large quantity of byproducts etc. To speculate however, it should be noted that the piperazinyl substrate used was a secondary amine. It would be expected (from our earlier fixation experiments) that the secondary amine could participate efficiently in the [ $^{11}\text{C}$ ]CO $_2$  fixation process to form the  $^{11}\text{C}$ -carbamate salt. However, the POCl $_3$  has generally been thought to act on the  $^{11}\text{C}$ -carbamate salt as a dehydrating agent

to form the highly reactive isocyanate intermediate, but the formation of an isocyanate in this manner is only possible on primary amine substrates and so would not be expected to proceed with this particular substrate. The hugely reduced RCY in this paper, compared to the examples from Dahl's original work, therefore suggests that this pathway is in-fact severely hampered as predicted. But it is also key to note that some <sup>11</sup>C-labeled product is still formed in small amounts. In fact, in a much earlier paper from Wilson *et al.*, this topic is discussed in light of their observation of a similar secondary amine fixation product.<sup>433</sup> In it they posit the potential formation of an intermediate carbamoyl chloride species which could be capable of undergoing nucleophilic substitution with an amine/alcohol to yield the corresponding urea/carbamate. Perhaps this is the mechanism by which the MAGL inhibitor was radiolabeled in this more recent case, but it is difficult to draw any more conclusions from the information provided in the paper. In any case, it is clear that an in-loop [<sup>11</sup>C]CO<sub>2</sub> fixation strategy was successfully applied to the synthesis of a novel radiotracer, and – it should be noted – the alternative radiosynthetic route they employed involved the use of [<sup>11</sup>C]COCl<sub>2</sub>; a much more labour intensive and complex production method.

#### 2.4.2.2 TARP inhibitor

Their second implementation of this method was in their radiolabeling of a novel transmembrane AMPA receptor regulatory protein (TARP) inhibitor.<sup>206</sup> This particular target compound was to be labeled at the carbonyl of a benzothiazolone motif, and was therefore an attempt to radiolabel an *S*-[carbonyl-<sup>11</sup>C]thiocarbamate. The authors state that their attempts resulted in very poor yields (RCY < 1%), and that this was “in spite of several attempts using reported [<sup>11</sup>C]CO<sub>2</sub> fixation conditions”, including both our method and the similar Dahl method. Similarly to their previous paper, few other details are provided describing the exact nature of this failure, since no [<sup>11</sup>C]CO<sub>2</sub> trapping efficiencies are disclosed, nor are any crude radio-HPLC traces included. As before, however, it is still possible to speculate on some of the potential reasons for this failure.

It should first be noted that the radiolabeling of this particular motif – the *S*-[carbonyl-<sup>11</sup>C]thiocarbamate – from [<sup>11</sup>C]CO<sub>2</sub>, has yet to be published at the time of writing. However it does not seem such a stretch to imagine how this could be approached. Given

that thiols exhibit broadly similar reactivity to the analogous alcohols, one could foresee a correspondingly analogous radiosynthesis to that already developed for [*carbonyl*-<sup>11</sup>C]alkylcarbamates:<sup>405,433</sup> a standard [<sup>11</sup>C]CO<sub>2</sub> fixation would yield an <sup>11</sup>C-carbamate salt which would be converted to the <sup>11</sup>C-isocyanate with POCl<sub>3</sub>, at which point the nucleophilic sulfur in the thiol could attack at the relatively electrophilic isocyanato-carbon to form the S-thiocarbamate product. In fact this seems such a logical extension from Dahl's original in-loop radiolabeling of [*carbonyl*-<sup>11</sup>C]alkylcarbamates, that it was initially assumed that this was the methodology that was implemented here.

Curiously however, upon closer inspection of the experimental details, they actually attempted this in-loop synthesis using a very different chemical approach. Firstly, the precursor is synthesised as a disulfide-bridged dimer. Immediately preceding radiolabeling, PBu<sub>3</sub> is added to a solution of this precursor to reduce the disulfide and form the active thiol species *in-situ*. The "reactor loop" is filled with a solution of BEMP in toluene, without any other amine precursor, and the [<sup>11</sup>C]CO<sub>2</sub> is passed through the loop to form a "BEMP-[<sup>11</sup>C]CO<sub>2</sub> complex". Then the precursor/PBu<sub>3</sub> solution was injected to the reactor loop, the loop was sealed, before heating at 100°C for 5 minutes. Finally, the product was eluted to a quench vial before injection into an HPLC for analysis.

Several aspects of this procedure warrant comment. From a practical consideration, one of the key advantages to most in-loop radiolabeling methods is that they can be run at ambient temperatures. If this methodology required heating, then one of the major benefits from in-loop radiochemistry – the simple setup/implementation – is somewhat diminished. Secondly, it is not clear exactly how this reaction was expected to proceed at all in the absence of any dehydrating reagents (POCl<sub>3</sub>, or Mitsunobu). They do refer to a method from Coelho *et al.* whereby 2-aminothiophenol – formed by *in-situ* disulfide reduction with PBu<sub>3</sub> – is condensed with carboxylic acids to form benzothiazoles.<sup>434</sup> The link between this methodology and their attempted reaction is not discussed further, and to-date there is no literature precedent for the use of a similar methodology in the radiosynthesis of [*carbonyl*-<sup>11</sup>C]alkylcarbamates *via* [<sup>11</sup>C]CO<sub>2</sub> fixation. So the fact that this reaction was unsuccessful in-loop is not necessarily surprising.

Finally however, the order of operations should be considered; in that they first attempt to form the “BEMP-[<sup>11</sup>C]CO<sub>2</sub> complex” in-loop, *before* adding the amino substrate. While some have suggested that the BEMP acts to trap, activate, and transfer CO<sub>2</sub> to an amine,<sup>435</sup> precious little evidence has ever been presented to support this putative mechanistic role. Of course the ability of BEMP to trap [<sup>11</sup>C]CO<sub>2</sub> is not disputed, but it has yet to be proven whether this BEMP-CO<sub>2</sub> species is capable of “activating” and transferring this CO<sub>2</sub> onto an amine to form the carbamate intermediate. It seems more likely that BEMP simply acts in an analogous manner to DBU – as was discussed previously – whereby the amine precursor itself traps the [<sup>11</sup>C]CO<sub>2</sub> as a <sup>11</sup>C-carbamic acid which BEMP subsequently deprotonates and stabilises as the phosphazanium <sup>11</sup>C-carbamate salt.

In fact, in work by Courtemanche *et al.*, the nature of this BEMP-CO<sub>2</sub> interaction was better elucidated.<sup>436</sup> They demonstrated that a 2+2 rearrangement occurs between a C=O bond in CO<sub>2</sub> and the P=N phosphazene bond of BEMP – analogous to that seen in the Wittig reaction – resulting in the formation of the phosphine-oxide and the release of *tert*-butyl isocyanate. This proceeds *via* a relatively long-lived cyclic BEMP-CO<sub>2</sub> intermediate, and it is this that was likely formed in-loop in this method. There are two issues with this: the first being that it is not clear how this cyclic BEMP-CO<sub>2</sub> adduct could transfer CO<sub>2</sub> to an amine at all, one would expect that the formation of the strong P=O bond would strongly favour the cycloreversion over the release of the CO<sub>2</sub> to an amine. Additionally, since Courtemanche’s work demonstrated that the BEMP-CO<sub>2</sub> adduct eventually transforms to yield *tert*-butyl isocyanate, it should be considered whether this would happen similarly in this radiochemical application. If the BEMP-[<sup>11</sup>C]CO<sub>2</sub> complex was formed in loop first, it seems possible that [<sup>11</sup>C]<sup>t</sup>Bu-NCO could have been produced in significant quantities. Once the aminothiols precursor was added one could envisage the formation of a number of <sup>11</sup>C-urea and *S*-alkyl-<sup>11</sup>C-thiocarbamate impurities. Without viewing the radio-HPLC data however, it is not possible to confirm or further explore this possibility, but it offers a potential explanation for the low radiochemical yields in this case. Since the [<sup>11</sup>C]CO<sub>2</sub> was trapped by BEMP before addition of the amine, there was no opportunity for the formation of the crucial amine-carbamate intermediate to form.

To conclude, the chemistry in this particular example of an in-loop [<sup>13</sup>C]CO<sub>2</sub> fixation was employed without much literature precedent and possibly with an incorrect order of operation. As such, the fact that this particular implementation was unsuccessful does not necessarily reflect upon a flaw within the in-loop fixation concept itself, and perhaps with sufficient modification, this desired radiotracer could have been produced in an in-loop setup.

#### 2.4.2.3 *Cholesterol 24-hydroxylase inhibitor*

The most recent application of an in-loop [<sup>13</sup>C]CO<sub>2</sub> fixation methodology from Liang and co-workers is in their reported synthesis of an <sup>13</sup>C-labeled inhibitor of cholesterol 24-hydroxylase (CYP46A1).<sup>245</sup> The target compound in this case was an asymmetric urea, and the method from Dahl's in-loop [<sup>13</sup>C]CO<sub>2</sub> fixation paper was applied without significant modification. As in this earlier paper, they again demonstrated the importance in this case of controlling the reaction stoichiometry. By reducing the quantity of the first amine (used for the fixation step), relative to that of the POCl<sub>3</sub> and the second amine, they were able to increase the selectivity for the desired asymmetric urea over the undesired symmetric urea.

This again highlights an advantage of the Dahl method over our own. By using larger volume loops, they can avoid any flushing of reagents from the loop, and thus the reaction stoichiometry can be better controlled. This allows the selective formation of one urea product over another. Additionally, it is interesting to note that they transferred their optimal conditions to a vial-based synthesis and saw a reduced [<sup>13</sup>C]CO<sub>2</sub> fixation (90% *versus* >99%), and only trace product formation was observed. The reduced fixation was possibly due to the reduced gas-liquid interfacial contact that is inherent in vial-based syntheses when compared with in-loop processes. The lack of significant product formation is more puzzling, but this could be related to the much lower quantity of reagents that in-loop processes allow. Since the reaction solvent volumes are sufficiently reduced, the effective concentration of reagents is increased, while still allowing a reduction in the absolute quantities of these reagents used. Ultimately the final product was obtained in a 21% RCY, and with reasonably high molar activities, enabling *in-vivo* PET imaging with this radiotracer, for the visualisation of brain CYP46A1 in mice. This

served as an excellent example of the viability of in-loop [<sup>11</sup>C]CO<sub>2</sub> fixation methods for radiotracer synthesis.

#### 2.4.2.4 Encorafenib

As a final example of the recent application of these in-loop [<sup>11</sup>C]CO<sub>2</sub> fixation methodologies was the work from Dornan *et al.* in their synthesis of [<sup>11</sup>C]encorafenib, a B-Raf-selective inhibitor.<sup>406</sup> It was radiolabeled at its *O*-methyl-carbamate moiety by [<sup>11</sup>C]CO<sub>2</sub> fixation on the amine precursor followed by methylation of the resultant carbamate salt with a solution of iodomethane. The setup they employed was more of a hybrid of both Dahl's and ours: the apparatus was based around a stainless-steel HPLC injector and used BEMP as the fixation agent; but it was more simplified in a manner closer to our apparatus, the loop was not separated into two sections, and the reaction solution was also flushed directly into a quench vial. The authors incorporated a quench vial to stop the reaction upon exiting the loop. And similarly to our method, this allowed them to confirm that the product – as well as the major impurities – observed in the radio-HPLC were formed in-loop. As in our method, this was a simple but powerful control, and also helps to demonstrate the speed of most radiochemical reactions performed in-loop, even those performed at ambient temperatures.

The end result, after the BEMP:precursor ratio was optimised, and the iodomethane solution concentration was lowered (to suppress over-alkylation of the desired <sup>11</sup>C-labeled product), was that they successfully synthesised [<sup>11</sup>C]encorafenib in a 14% RCY (in just 30-35 mins from EOB) with a very high molar activity (177 GBq/μmol, from a 144 GBq production). In addition, the authors commented that they found the method to be both robust and reliable, and it is clear that the use of an in-loop method is well suited for automation.

#### 2.4.3 Other recent in-loop radiochemistry

In addition to the aforementioned adaptations of our and Dahl's in-loop [<sup>11</sup>C]CO<sub>2</sub> fixation methodologies, several other gas-liquid radiochemistry processes have since been applied in an in-loop setting, possibly due to the renewed interest in these methods that these publications have generated.



### 2.4.3.1 <sup>11</sup>C-Carbonylation with [<sup>11</sup>C]CO

In their publication from 2019, Ferrat *et al.* described their method for in-loop transition-metal-mediated <sup>11</sup>C-carbonylation using [<sup>11</sup>C]CO. Carbon monoxide has traditionally been a difficult <sup>11</sup>C-synthon to work with due to its low reactivity and poor organic solubility, and as such, a number of different approaches have been employed to overcome these drawbacks; focusing on either high pressure reactions or the use of more efficient and powerful chemical trapping reagents.<sup>437</sup> The reaction used in this work – the Pd-mediated carbonylative cross-coupling of an aryl-halide and a nucleophile – was ideal for adaptation to be performed in loop. The reaction involves a single step, as the reagents are tolerant of one another and only react upon the addition of the [<sup>11</sup>C]CO.

In this method, a standard stainless steel HPLC sample-loop and injector setup was used – as was implemented in the original <sup>11</sup>C-methylation “loop method” from Wilson *et al.* – whereby the loop was coated with the reaction solution containing the aryl halide, nucleophile, palladium source, and the supporting ligand. The [<sup>11</sup>C]CO produced in a molybdenum oven was passed slowly through the loop where it trapped and reacted *in-situ* forming the desired <sup>11</sup>C-carbonylation product which was subsequently flushed onto a semi-prep HPLC column for purification. They applied this method to amides, lactones, esters and carboxylic acids with varying degrees of success. Notably, while the simple test compounds [<sup>11</sup>C]*N*-benzylbenzamide and [<sup>11</sup>C]benzoic acid were formed in reasonable yields at room temperature, the more complex drug-like molecules ([<sup>11</sup>C]olaparib, [<sup>11</sup>C]raclopride, [<sup>11</sup>C]FLB457, [<sup>11</sup>C]AZ13198083) required heating at temperatures above 75°C to achieve significant product yields. While the method appears a promising first application of the standard in-loop methodology to [<sup>11</sup>C]CO chemistry, the requirement for heating in-loop certainly presents some limitations to the wider implementation of the work.

Although this work is the first report of a recognisable in-loop <sup>11</sup>C-carbonylation with [<sup>11</sup>C]CO, it is useful to compare this work to the previous microfluidic <sup>11</sup>C-carbonylation in an annular-flow “pseudo-thin-film” regime, as reported by Miller *et al.*, in which [<sup>11</sup>C]CO was trapped and reacted in the channel of a glass-fabricated microfluidic reactor chip.<sup>438</sup> The high gas-liquid interfacial contact in this example was achieved by establishing an annular-flow regime within the channel. This consisted of a core of fast

flowing [<sup>13</sup>C]CO-containing gas, surrounded by a slower-moving thin-film of reaction solvent (forced to the walls of the channel by the higher-velocity gas flow). While this is undoubtedly a more complex apparatus setup, this annular-flow regime bears some similarities to the sorts of flow-regimes that exist in the previously discussed in-loop gas-liquid processes.

In Miller's microfluidic example, a number of simple amides were labeled, including the same model substrate [<sup>13</sup>C]*N*-benzylbenzamide, however these all required heating to over 100°C. By comparison, Ferrat's in-loop method produced [<sup>13</sup>C]*N*-benzylbenzamide in near quantitative RCYs at room-temperature, although as-discussed, more drug-like amides required heating to at least 75°C. So while the in-loop method has an advantage over Miller's microfluidic method in that it was demonstrated to operate at ambient temperatures in some select cases, for more complex molecules, both methods require heating. As a direct comparison, both papers describe the synthesis of [<sup>13</sup>C]phthalide, and in this case the methods show similar performance. The microfluidic synthesis of [<sup>13</sup>C]phthalide is performed at 110°C, whereas the in-loop method required heating to 75°C. This example suggests that there is little difference between the realistic operation of these two processes, since they both require heating significantly above ambient temperature to synthesise a clinically-relevant compound. While these methods are vastly different in terms of physical setup/implementation, they both demonstrate the power that a thin-film methodology can have in simplifying radiochemistry using [<sup>13</sup>C]CO. The wide-usage of which to-date has thus-far been hampered by [<sup>13</sup>C]CO's sluggish reactivity, poor organic-solubility, and low concentration in its carrier gas.

Even at this very small scale (200 μm channel diameter, 5m channel length), <sup>13</sup>C-amides were obtained in reasonable RCYs (~ 50%). This comparison serves to demonstrate that there is significant scope for the future modification and miniaturisation of Ferrat's in-loop methodology, and it is hoped that if these thin-film methodologies can be reproducibly applied by other labs, otherwise difficult <sup>13</sup>C-carbonylation chemistry may be further-improved and more widely applied.

#### 2.4.3.2 <sup>18</sup>F-Fluorination with [<sup>18</sup>F]triflyl fluoride

From a reaction process-development perspective, <sup>18</sup>F-radiochemistry has traditionally been fairly straightforward when compared with the processes described in this chapter. This is because the vast majority of <sup>18</sup>F-radiolabeling synthons are produced in solution, which of course obviates the need for any gas-liquid trapping apparatus. Recently however, Pees *et al.* published an interesting and potentially highly-valuable method for the production and use of [<sup>18</sup>F]triflyl fluoride, a gaseous [<sup>18</sup>F]fluoride source.<sup>439</sup> This synthon omits the time-consuming and occasionally unreliable azeotropic drying process common to most [<sup>18</sup>F]fluoride chemistry, and unlike some other “azeotropic-drying-free” methods, it can be applied near-universally, without the common incompatibilities (base sensitivity etc.) that can commonly limit the applicability of these other methods. The fact that the pure [<sup>18</sup>F]triflyl fluoride is produced as a gas and distilled from the production vial into a second reaction vial allows for this increased substrate scope. However this does potentially introduce many of the standard issues associated with heterogenous gas-liquid phase radiochemistry and to address this, Dahl and co-workers recently reported their use of [<sup>18</sup>F]triflyl fluoride in the first reported in-loop <sup>18</sup>F-fluorination.<sup>440</sup>

In this work, [<sup>18</sup>F]triflyl fluoride was produced in the manner described by Pees *et al.*, but instead of distilling the synthon into a second reaction vial (*via* a P<sub>2</sub>O<sub>5</sub> drying tube), it was distilled through an HPLC injector loop that had been pre-loaded with a fluorination reaction solution containing a precursor as well as a base and/or cryptand (substrate specific). After some optimisation, this method resulted in quantitative trapping efficiency (>99%), and comparable radiochemical yields of two model radiotracers: [<sup>18</sup>F]FEPPA and [<sup>18</sup>F]T807. The chemistry is still in its infancy, but this application demonstrates the power and versatility of radiochemical methods using thin-films of captive solvents in-loop when applied to otherwise fairly complex reactions requiring gas-liquid trapping.

## 2.5 Summary and Conclusion

As was fully explained in the introduction to this section, the aim in this work was to investigate the feasibility of transferring the recently-developed superbase-mediated [<sup>11</sup>C]CO<sub>2</sub> fixation methods into an in-loop thin-film fixation process. Once this was established, the aim was to integrate this in-loop [<sup>11</sup>C]CO<sub>2</sub> fixation into a simple proof-of-concept radiosynthesis of some <sup>11</sup>C-ureas. In our particular case, this was done with a particular view towards further miniaturisation still, in alignment with our industrial partner's ongoing development of a microfluidic radiosynthesis unit. The eventual aim being to develop a streamlined [<sup>11</sup>C]CO<sub>2</sub> fixation process that could be implemented in the future as part of their "cyclotron-to-syringe" microfluidic production platform.

Two separate apparatus setups were developed in this work, one to initially assess in-loop fixation performance, and the other for the full proof-of-concept <sup>11</sup>C-urea synthesis. The first of these was the simplified three-component in-loop fixation apparatus: a single-use polymer tubing-based setup, which was modular in design. This setup allowed rapid-throughput screening of a variety of different fixation solution compositions, and in addition to allowing the determination of loop-fixation efficiencies, it also gave an insight into the fixation abilities of the bulk solutions, shedding further light on the not fully-understood mechanism underlying superbase-mediated [<sup>11</sup>C]CO<sub>2</sub> fixation. The second of these built upon the three-component setup, and integrated it into the remotely-operable switching valves of an E&Z ModularLab system, allowing for the addition of secondary reagents solutions for the full <sup>11</sup>C-urea synthesis.

The fixation-solution screening experiments revealed that while many solution compositions are efficient at performing [<sup>11</sup>C]CO<sub>2</sub>-fixation in the traditional vial-based manner, this does not necessarily guarantee success in-loop. The in-loop fixation performance was found to be a product of both the total solution efficiency as well as the degree to which the solution is retained on the walls of the loop. This retention was found in-part to be a product of the solution's viscosity, with more viscous solutions being better retained, resulting in an increased in-loop fixation efficiency.

The optimal solution composition – as determined in this screening – was used in the full urea-synthesis setup. Surprisingly it was found that the in-loop fixation performance

increased substantially in this setup (almost 100% of the [<sup>11</sup>C]CO<sub>2</sub> was trapped in-loop), and it seems likely that this can be attributed to the increased backpressure from the switching valves decreasing the flow-rate through the loop and therefore further increasing the solution retention. Applying this solution to the proof-of-concept synthesis of *N,N'*-[ureido-<sup>11</sup>C]dibenzylurea was highly successful, with an average RCY of 82 ± 3% and a promising molar activity of 0.75 ± 0.13 GBq/μmol (from a 300 MBq production). Crucially, the reaction itself was complete (non-isolated) in under 2.5 min from EoB at ambient temperature and pressure. The [<sup>11</sup>C]CO<sub>2</sub> did not require cryogenic pre-concentration, nor did the delivery to the loop require slowing to increase fixation efficiency. Furthermore, the setup was composed of single-use disposable plastic components, which is ideal from a GMP standpoint. Additionally it would be straightforward to translate onto the latest cassette-based radiosynthesisers, as well as reducing the laborious cleaning requirements that vial-based synthesis entails.

The method was successfully applied in the synthesis of two other model substrates, albeit with reduced RCYs (however loop-fixation remained consistently high). It was not clear exactly what was the cause for these reduced yields, although it was hypothesised that the amines used in these cases were less reactive due to steric hindrance around the primary amine. However, since these were still non-clinically-relevant compounds included only to demonstrate substrate scope, these yields were accepted without further optimisation. Were this method to be applied for the routine synthesis of a radiotracer, it would likely require some optimisation as is fairly standard for any radiosynthetic method.

The concept of “captive solvent” radiochemistry was originally described by Jewett; improved by Iwata and Pascali in their work detailing their “on-line” and “on-column” radiosyntheses; further advanced by Davenport, McCarron, and Pike in their <sup>11</sup>C-carboxylations in PTFE tubing; and finally simplified, refined and ultimately popularised by Wilson in the landmark publication describing a “remarkably simple” method for captive solvent <sup>11</sup>C-methylations inside an HPLC injector loop, commonly referred to as the “loop method”. The work presented here built upon the lessons learnt and methodological developmental criteria established in these preceding publications. The result was a demonstration that [<sup>11</sup>C]CO<sub>2</sub> fixation reactions can be readily adapted to an analogous thin-film captive-solvent method for radiosynthesis in-loop. The method

proceeded rapidly under ambient temperatures and pressures, giving an improved performance over similar processes described in-vial. This could be attributed both to the advantages that an in-loop process brings as well as potentially suggesting – as Wilson commented for [<sup>13</sup>C]CH<sub>3</sub>I<sup>441</sup> – that perhaps radiochemists can tend to use longer reaction times and higher temperatures than strictly necessary, when considering the highly reactive nature of the reagents employed in superbase-mediated [<sup>13</sup>C]CO<sub>2</sub> fixation chemistry.

## 2.6 Materials & Methods

### 2.6.1 General

Anhydrous acetonitrile (MeCN, 99.8%), ascarite, benzylamine (99%), di-*tert*-butylazodicarboxylate (DBAD, 98%), triethylamine (Et<sub>3</sub>N, ≥ 99.5%) and tri-*n*-butyl phosphine (PBU<sub>3</sub>, 99%) were purchased from Sigma-Aldrich. Ethyl acetate (EtOAc, ≥ 99.5%) was purchased from Fisher Scientific. Anhydrous magnesium sulfate (MgSO<sub>4</sub>, 98%) was purchased from Fluka. 1,8-Diazabicyclo[5.4.0]undec-7-ene (DBU, 99%) and benzyl isocyanate (98%) were purchased from Alfa Aesar. Carbon dioxide (CO<sub>2</sub>) was purchased from BOC Gases.

ETFE tubing (1/16" O.D. x 0.75 mm I.D., 25 m/pkg) was obtained from VICI Jour. The ascarite traps were constructed from empty SPE-ED cartridges, obtained from Biosys Solutions Ltd: Fritted Empty MiniSPE-ED Cartridges, part # 2447. All fluidic connections were obtained from Upchurch Scientific, the product codes are as follows: fingertight flangeless fitting short, PEEK, XP-235X; female to male quick-connect Luer adapter, P-675-01.

[<sup>13</sup>C]CO<sub>2</sub> was produced using a Siemens RDS112 cyclotron in a <sup>14</sup>N(p,α)<sup>13</sup>C reaction, by the 11 MeV proton bombardment of nitrogen (+ 1% O<sub>2</sub>) gas. The cyclotron produced [<sup>13</sup>C]CO<sub>2</sub> was transferred in a stream of helium gas at 70 mL/min through a P<sub>2</sub>O<sub>5</sub> drying tube into a switching valve of an E&Z Modular Lab automated synthesis unit. Unless otherwise specified, all radioactive experiments used a 5 μA bombardment for 1 min, giving on average 300-350 MBq [<sup>13</sup>C]CO<sub>2</sub> at EOB. Radiochemical yields (RCY) reported are calculated as a percentage of the total radioactivity delivered from the cyclotron. Unless otherwise stated, all experiments were repeated three times (n = 3).

<sup>1</sup>H and <sup>13</sup>C{<sup>1</sup>H} NMR spectra were recorded on a Bruker Avance DRX 400 MHz spectrometer at 294 K. Chemical shifts are reported in parts per million (ppm) relative to the residual solvent proton impurities (<sup>1</sup>H) or the residual solvent carbon impurities (<sup>13</sup>C), as internal standards.

HPLC analysis was performed on an Agilent 1200 system, with a variable wavelength UV detector and a LabLogic Flow-RAM β<sup>+</sup> detector equipped in series. Analytical

reverse-phase column: Agilent XDB-C18, 5 μm, 4.6 x 150 mm. Gradient used: 95% H<sub>2</sub>O, 5% MeCN; to 5% H<sub>2</sub>O, 95% MeCN; over 9 min. Identity of radioactive products was confirmed by co-elution with the non-radioactive standard compounds (*N,N'*-dibenzylurea was synthesised, *N,N'*-diphenylurea and *N, N'*-dicyclohexylurea were commercially obtained). HPLC was used to determine molar radioactivities, by reference to a variable dilution calibration curve.



## 2.6.2 Radiolabeling solution preparation

All of the solutions described herein were prepared under a positive pressure of nitrogen within a dry-box. The solutions are made-up in 1.5 mL v-shaped glass vials which are subsequently crimp-sealed with a PTFE/silicone septum before wrapping the cap with PTFE tape to prevent any atmospheric contamination. Solutions are prepared no more than 3 hours prior to radiolabeling to minimise any degradation of reagents.

### 2.6.2.1 Fixation solutions

*For optimisation:* fixation solutions were prepared as 1 mL solutions by diluting the corresponding percentages (v/v) of DBU and benzylamine in MeCN.

*Optimal composition:* fixation solution was prepared as a 1 mL solvent-free mixture, consisting of DBU (900 µL) and amine substrate (100 µL).

### 2.6.2.2 Mitsunobu solutions

Mitsunobu solutions were prepared by dissolving DBAD (21.1 mg, 91.6 µmol, 3 eq.) in 1 mL MeCN (anhydrous). PBu<sub>3</sub> (22.9 µL, 91.6 µmol, 3 eq.) was added and the mixture was briefly shaken. A colour change from pale yellow-to-colourless was observed on successful formation of the active Mitsunobu intermediate.

## 2.6.3 Radiochemistry apparatus setups

### 2.6.3.1 Three-component [<sup>13</sup>C]CO<sub>2</sub> trapping

The trapping apparatus setup is shown in Figure 2.1. One end of a 350 mm length of ETFE tubing (**loop**, 1/16" O.D., 0.75mm I.D., 150 μL volume) was fitted with a fingertight screw fitting, and the other end was cleanly cut at a 45° taper. The loop was tightly coiled and placed inside a 10 mL glass vial for ease of handling. The tapered end was inserted through the rubber septum of a sealed crimped 10 mL **vial**. This vial was vented *via* a needle through an **ascarite** cartridge into a gas waste bag. The loop was half-filled with 75 μL fixation solution, using a 100 μL syringe, and connected *via* a luer slip fitting to the [<sup>13</sup>C]CO<sub>2</sub> outlet line from the E&Z Modular Lab.

### 2.6.3.2 <sup>13</sup>C-urea derivative flow synthesis

The <sup>13</sup>C-urea synthesis apparatus builds upon the trapping apparatus proof-of-concept, and is shown in Figure 2.6. The cyclotron [<sup>13</sup>C]CO<sub>2</sub> outlet line was connected to switching valve 1 (**V1**) as was a syringe containing Mitsunobu reagents (PBU<sub>3</sub> and DBAD in MeCN). Both ends of a 35 cm length of ETFE tubing (**fixation loop**, 1/16" O.D., 0.75mm I.D., 150 μL volume) were fitted with fingertight screw fittings, and the loop was half filled with 75 μL trapping solution. One end was attached to the outlet of **V1** and the other to the inlet of switching valve 2 (**V2**). To one outlet of **V2**, a short length of ETFE tubing was connected to a **waste vial**, vented *via* an **ascarite** cartridge. To the other outlet is connected a second 35 cm length of coiled ETFE tubing (**reaction loop**, 1/16" O.D., 0.75mm I.D., 150 μL) routed into a sealed crimped product vial (containing 1 mL water), vented *via* an ascarite trap.

## 2.6.4 Generic radiosynthetic procedures

### 2.6.4.1 Three-component [<sup>11</sup>C]CO<sub>2</sub> trapping

The preloaded loop was connected to the [<sup>11</sup>C]CO<sub>2</sub> delivery line from the cyclotron and helium was flushed through the system for 3 min at 70 mL/min, leaving a just a small, residual amount of trapping solution coating the walls of the trapping loop, and flushing the bulk of the trapping solution into the waste vial. The cyclotron produced [<sup>11</sup>C]CO<sub>2</sub> was then directly delivered diluted in carrier helium gas (without prior trapping and concentration) at 70 mL/min into the E&Z Modular Lab and subsequently through the three-component trapping apparatus. Since all [<sup>11</sup>C]CO<sub>2</sub> is trapped within either the trapping loop, the waste vial, or the ascarite trap, these three components are quickly separated and their radioactivities measured within a Capintec<sup>®</sup> dose calibrator. Comparison of the distribution of radioactivity within this apparatus allowed calculation of different solvent trapping efficiencies.

### 2.6.4.2 <sup>11</sup>C-Urea derivative flow synthesis

1) Helium was flushed through the preloaded trapping loop to the waste vial for 3 min at 70 mL/min. 2) Cyclotron produced [<sup>11</sup>C]CO<sub>2</sub> was then directly delivered, diluted in carrier helium gas (without prior trapping or concentration) at 70 mL/min, through the trapping loop, waste vial and ascarite trap. 3) **V1** and **V2** are switched and the trapping loop was filled with 150 μL Mitsunobu solution (PBU<sub>3</sub>/DBAD in MeCN). 4) **V1** was switched and a 70 mL/min helium flush from the cyclotron transferred the contents of the trapping loop through the reaction loop and into the product vial (containing 1 mL water as a quench). 5) The crude products were analysed by radio-HPLC and the system was washed with acetonitrile and all washings and component radioactivities were measured to determine the total [<sup>11</sup>C]CO<sub>2</sub> radioactivity delivered from the cyclotron.

## 2.6.5 Synthesis of *N,N'*-dibenzylurea

Benzylamine (1.2 mmols, 131 μL, 3 eq.) was dissolved in 2 mL EtOAc with stirring at room temperature. To this was added Et<sub>3</sub>N (1.2 mmols, 167 μL, 3 eq.) and benzyl isocyanate (400 μmols, 49.4 μL, 1 eq.). Solution was stirred for 2 hours under ambient

conditions. 1M HCl was added and the solution was extracted three times with EtOAc. The combined organic extracts were washed with brine and dried over MgSO<sub>4</sub>. The solvent was removed by rotary evaporation to yield a white solid (83.5 mg, 87% yield); <sup>1</sup>H NMR (400 MHz, CDCl<sub>3</sub>) δ 7.25-7.1 (m, 10H, CH-*aromatic*), 4.75 (br s, 2H, NH), 4.26 (d, 4H, *J* = 5.8 Hz, CH<sub>2</sub>); <sup>13</sup>C NMR (100 MHz, CDCl<sub>3</sub>) δ 158.1 (NH-CO-NH), 139.0 (C), 128.6 (CH), 127.4 (CH), 127.3 (CH), 44.5 (CH<sub>2</sub>).

### 3 PSMA SECTION 1 – NON-RADIOACTIVE SYNTHESIS

#### 3.1 Introduction

The following three sections of work will discuss the development of our “universal” method for the  $^{11}\text{C}$ -radiolabeling of PSMA-targeted glutamate-ureas *via*  $[^{11}\text{C}]\text{CO}_2$ -fixation. In addition to this, it will cover some unexpected but important-to-discuss discoveries made in the process. This first section primarily concerns the development and optimisation of several non-radioactive synthetic methods to produce a number of functionally diverse glutamate-urea-based reference compounds. These were vital in the subsequent two sections for use as analytical standards; additionally however, this work helped to better understand the fairly complex  $\text{CO}_2$ -fixation-mediated urea synthesis employed, as well as revealing some unexpected reactivity of these glutamate-urea-based ligands.

#### 3.2 PSMA Ligands

The main introduction to this thesis includes a thorough discussion of the development (and current “state-of-the-art”) of glutamate-ureido-based PSMA-targeting PET radioligands. In summary, the vast majority of small-molecule PSMA radiotracers bind at an extracellular enzymatic active site, by virtue of the incorporation of the glutamate-ureido motif. This targeting motif mimics the binding mode of the enzymatic site’s natural ligand NAAG, while importantly resisting any subsequent cleavage. To-date, most of these PET radiotracers have been labeled with gallium-68 or fluorine-18, and in order to incorporate these radionuclides, the amino-acid-sidechain of this glutamate-ureido moiety must be modified to incorporate radiometal chelators or organic prosthetic groups for radiohalogen labeling.

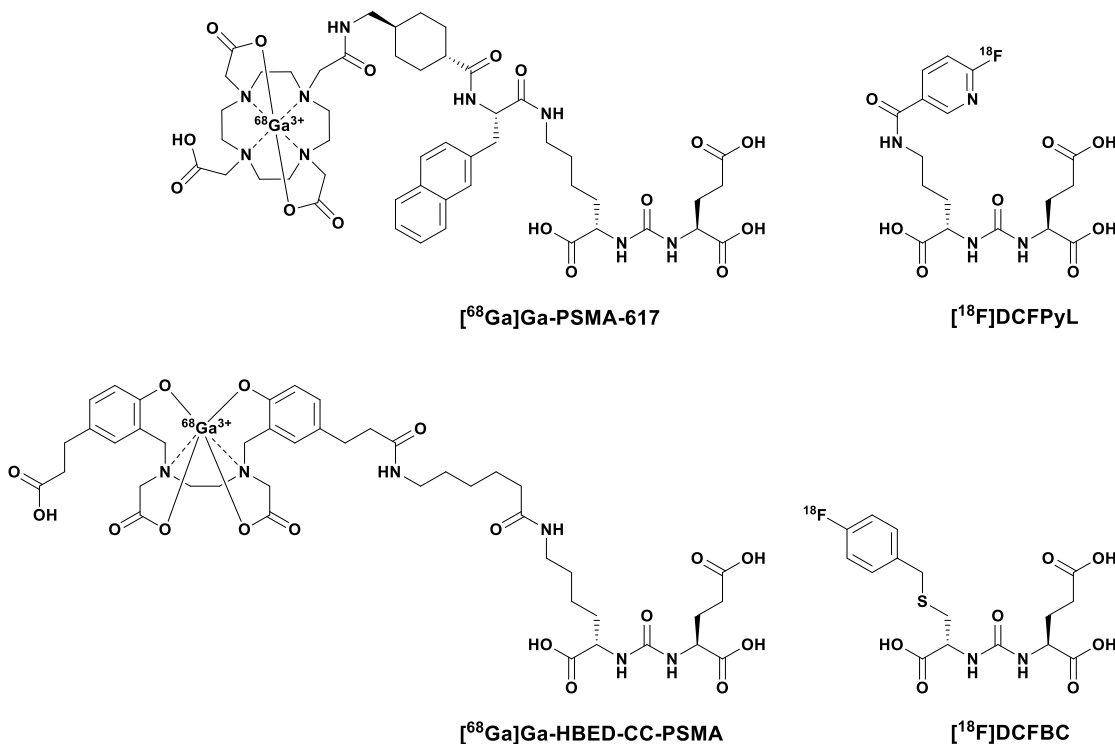


**Figure 3.1 Four examples of <sup>68</sup>Ga- and <sup>18</sup>F-radiolabeled PSMA radiotracers**

Note that all four examples bear the same glutamate-ureido PSMA targeting moiety

These ligands are necessarily structurally elaborate to allow facile radiolabeling without hampering target affinity or otherwise negatively affecting the compound's pharmacokinetics, but they were developed from similarly high-affinity, but structurally simpler glutamate-ureido-amino-acid compounds.<sup>288,300,442</sup> These specific <sup>18</sup>F- and <sup>68</sup>Ga-radiolabeled compounds have been well optimised, but this was not a straightforward effort by any means. The binding site in PSMA is not always tolerant of what can appear to be fairly minor structural changes to previously high affinity compounds.<sup>271</sup> For example, in the development of [<sup>68</sup>Ga]PSMA-617, minor changes in the linker moiety joining the DOTA chelator and the glutamate-ureido targeting motif led to significant and sometimes unpredictable differences in radiotracer performance.<sup>443</sup>

In order to better understand these structure-activity relationships and enable more effective and rational design of newer generation PSMA radioligands, it would be extremely useful to have a widely applicable general method to radiolabel any PSMA-targeted compound. The only structural element which all of these ligands have in

common is the glutamate-ureido pharmacophore, and as such,  $^{11}\text{C}$ -radiochemistry is really the only possibility for isotopologous radiolabeling of any given PSMA ligand. More specifically this could theoretically be achieved through a  $[^{11}\text{C}]\text{CO}_2$ -fixation-mediated urea synthesis, whereby the pharmacophore is  $^{11}\text{C}$ -radiolabeled at the *ureido*-carbon. If this method proved to be general enough, this could theoretically be employed as part of a “library radiosynthesis” strategy,<sup>58,59</sup> as described in the introduction to this thesis. It is hoped that a “universal” method for  $^{11}\text{C}$ -radiolabeling of PSMA-targeted ligands would facilitate the use of exactly this approach in the development of the next generation of PSMA-targeted radioligands, whether they be ultimately intended for imaging or therapy.

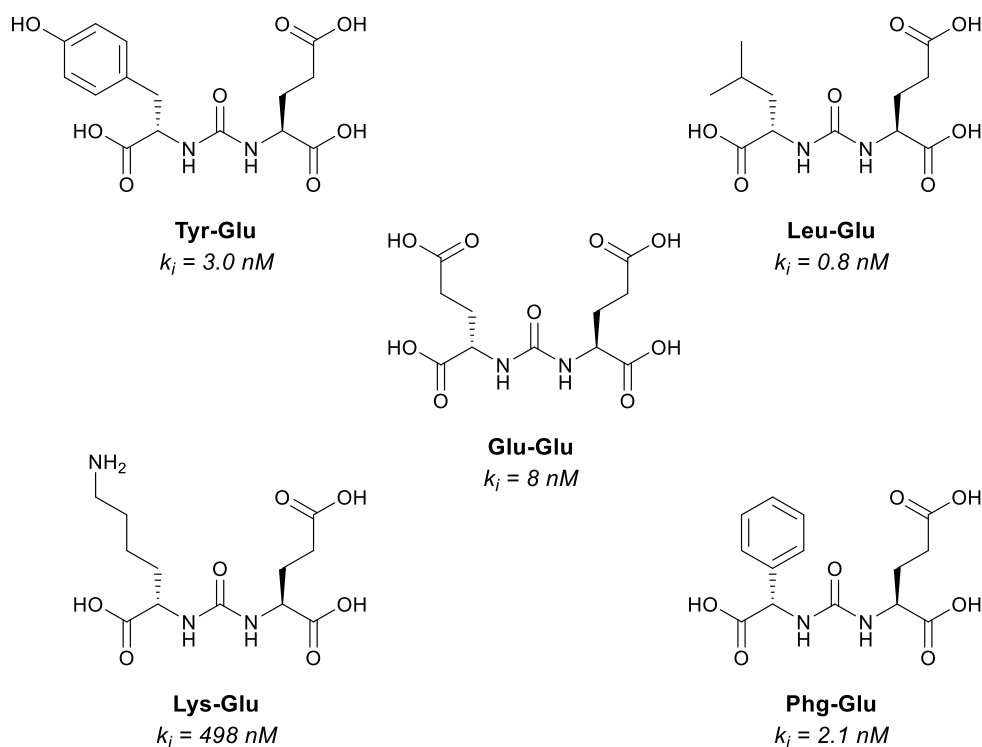


**Figure 3.2 Target compound library - simple AA-ureido-Glu PSMA ligands**

Differing functional groups on the AA sidechains but with all ligands containing common glutamate-ureido motif

For this work therefore, a variety of amino acid-ureido-glutamate (AA-ureido-Glu) target compounds were selected from the literature,<sup>288,300,442</sup> encompassing a range of aromatic and aliphatic sidechains as well as representing a number of common functional groups including amines, alcohols, and carboxylic acids. If a single radiosynthetic method could

be used for the  $^{11}\text{C}$ -radiolabeling of this small but structurally- and functionally-diverse library of high affinity PSMA ligands, then this method could be described as fairly “universal”. The development of such a method would be a valuable tool in the further exploration and understanding of PSMA chemistry and biology. This particular section discusses the development of methods for the non-radioactive synthesis of these reference PSMA ureas (protected and fully-deprotected) as well as exploring some of the unexpected reactivity encountered in the process.



### 3.2.1 Synthetic strategy

#### 3.2.1.1 *Protecting groups*

To facilitate their binding modes in the PSMA internal binding-cavity, these ligands are highly polar and functionalised. They bear at-minimum, three carboxylic acid moieties which bind to arginine residues in the S1 and S1' regions of the cavity, as well as a zinc-binding urea moiety (bioisosteric to the amide linkage in NAAG).<sup>301,444</sup> As is often the issue with highly-pharmacologically active compounds however, these functional groups can present issues to the synthetic chemist: they provide multiple sites for undesired reactivity during synthesis and can be fairly susceptible to degradation even once fully synthesised and isolated.

The majority of urea-forming reactions - including the CO<sub>2</sub>-fixation chemistry which will be used in the <sup>11</sup>C-radiolabeling sections of this work – are not overly chemoselective and will tend to react with most nucleophilic substrates, and as such, any carboxylic acids, alcohols, and amines must be protected during the urea formation stage to avoid a multitude of possible side-reactions. Once the urea synthesis is complete, the intermediate compounds will require deprotection to yield the desired reference compounds. Ideally any protection strategy will ensure that all protecting groups are removed under similar conditions, to ensure only a single deprotection step is required. This will ultimately lead to a 2 stage synthetic strategy: *Stage 1 – Urea Synthesis*; and *Stage 2 – Deprotection*.

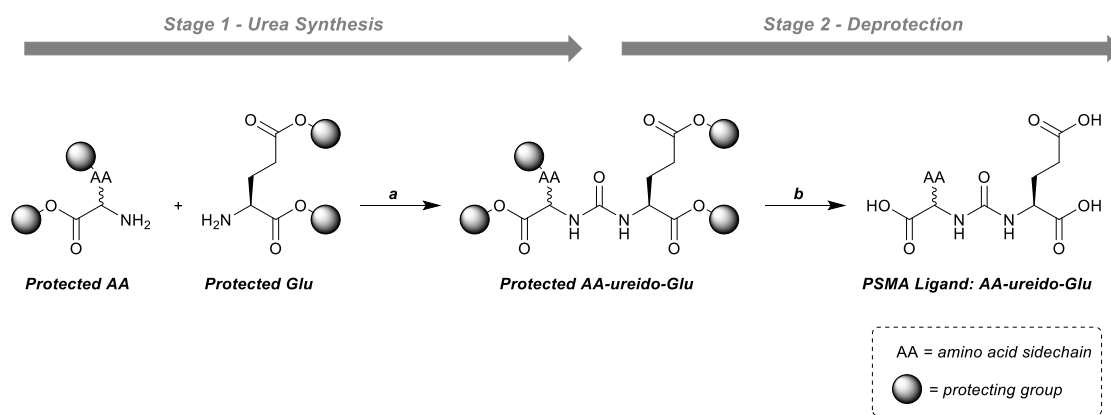


**Figure 3.3 Two stage PSMA ligand synthesis strategy**

**a) urea formation:** multiple options for non-radioactive chemistry; must involve  $[^{14}\text{C}]\text{CO}_2$  fixation for radiolabeling; **b) deprotection:** all protecting groups to be cleanly removed in a single step, must be easy to perform on a standard radiosynthesis platform

In most previous PSMA synthesis, since the glutamate-ureido motif is pre-formed and is instead radiolabeled at the modified AA-sidechain, the protecting group strategy is not of such importance. The urea synthesis and deprotection are both done in a standard synthetic lab without the instrumental limitations and time-constraints that radiochemistry imposes. As such, the standard approach in the literature for the non-radioactive synthesis of small AA-ureido-Glu compounds is to form the benzyl-protected urea from the corresponding benzyl ester-protected amino acids.<sup>288,300</sup> This intermediate urea can subsequently be deprotected in a Pd/C hydrogenation reaction: a fairly straightforward process to perform in an adequately equipped synthetic chemistry laboratory, and so it is appropriate for non-radioactive synthetic approaches. It would be much more difficult however to translate this chemistry into a radiochemical setting: the equipment required is not easily compatible with standard radiosynthesis equipment, the process is fairly hazardous, and the heterogenous nature of the catalysts required does not lend itself well to easy purification.

Given these issues with two of the predominant synthetic approaches, it is clear that the protecting strategy used should avoid any complex heterogenous catalytic deprotection (as for benzyl esters), in favour of simpler solution-phase deprotection chemistry. Furthermore, it is equally important to ensure that the protecting groups are stable enough

under strongly basic conditions (as encountered in CO<sub>2</sub>-fixation chemistry), which precludes any PMB or methyl-ester based protecting group strategies.

From these criteria, a *tert*-butyl-based protection strategy seems most appropriate. This versatile and broadly applicable approach would see carboxylic acids protected as *tert*-butyl esters, alcohols protected as *tert*-butyl ethers, thiols protected as *tert*-butyl thioethers, and amines protected as the *tert*-butyl carbamate derivatives (*N*-Boc).<sup>445</sup> These *tert*-butyl-based protecting groups are highly resistant to decomposition in strongly-basic conditions, but deprotection is theoretically trivial under strongly acidic conditions (TFA or HCl). The solution-phase acidic deprotection should be fast enough to proceed to completion in time-scales appropriate for <sup>11</sup>C-radiochemistry, while being easily compatible with traditional vial-based radiosynthesis units. Furthermore, due to the widespread use of *tert*-butyl protection strategies in standard peptide chemistry,<sup>445</sup> a multitude of *tert*-butyl/Boc protected amino acids (both naturally-occurring as well as synthetic) are commercially available. As such, all of the compounds in the previously-discussed small sample library should theoretically be accessible in two synthetic steps from commercially obtained *tert*-butyl protected amino acid precursors.

### 3.2.1.2 Urea formation

In the radiochemistry sections following this, different [<sup>11</sup>C]CO<sub>2</sub> fixation methodologies are employed for <sup>11</sup>C-urea synthesis. This section by comparison is concerned with the non-radioactive, more “traditional” synthesis of these reference ureas. In this instance therefore, we were not limited to CO<sub>2</sub>-based chemistry and so CO<sub>2</sub>-fixation is not the only possible route to the formation of the urea-linkage in our glutamate-ureido compounds.

Where precursors can be commercially obtained, the simplest method for the synthesis of asymmetric ureas is by reaction of isocyanates with a primary or secondary amine substrate. The absence of two competing amines ensures complete selectivity for the desired asymmetric urea, the conditions are mild (it simply requires the addition of a non-nucleophilic base – commonly DIPEA – as a proton scavenger), the reaction usually proceeds easily to completion, and any required purification can often be relatively minimal after acidic extraction of the starting amine. Unfortunately in the case of these PSMA ligands, both constituent amine building-blocks are generally amino acids, and

amino acid isocyanates cannot be obtained commercially. The obvious alternative therefore is to generate these amino-acid isocyanates *in situ*, and a number of different approaches have been used to achieve this.

Phosgene ( $\text{COCl}_2$ ) has traditionally been used in synthetic chemistry as, effectively, a  $[\text{C}=\text{O}]$  source for carbonylation reactions. It reacts stoichiometrically with amines to form isocyanates, and by extension can be used for the synthesis of ureas. It is however more commonly known to the public as an agent of chemical warfare, due to its high toxicity ( $\text{LCt}_{50} = 500 \text{ ppm/min}$ )<sup>446</sup> and corrosive nature on contact with the skin. It exists as a gas under standard atmospheric conditions, so accidental exposure by inhalation is a major risk, and such incidents can cause both acute and chronic pulmonary damage. The high risk of accidental exposure, as well as the difficulty of handling gaseous reagents (controlling reagent stoichiometry is especially hard on a small scale) has generally lead to an increased demand for safer phosgene alternatives.

The most commonly used phosgene substitute is the derivative reagent triphosgene (bis(trichloromethyl) bicarbonate). It has a roughly analogous reactivity to that of phosgene, although for the purposes of reaction stoichiometry, 1 molecule of triphosgene is equivalent to 3 molecules of phosgene. Crucially, triphosgene exists as a solid under standard conditions and as such it is much more convenient to use than the gaseous phosgene, particularly in cases of standard synthetic laboratory-scale synthesis. As such, triphosgene has been commonly referred to as a safer alternative to the routine use of phosgene in organic carbonylation reactions.<sup>447,448</sup> It is likely for this reason that the most common methods for the production of PSMA ligands use triphosgene to convert two amino acids to the desired asymmetric urea *via* the *in situ* generated isocyanate intermediate.<sup>288,449,450</sup>

Following this example for our reference urea synthesis was theoretically an option available to us, but upon further reflection and research it became apparent that any triphosgene usage would still be far from straightforward in our case. The consensus regarding triphosgene usage has begun to change in recent years, and a number of warnings have been published advising that the concept of triphosgene as a “safer alternative to phosgene” ought to be reconsidered.<sup>451,452</sup> They in fact argue that triphosgene is “at least as hazardous” as phosgene for several key reasons: exposure to

nucleophiles – *including water* – releases gaseous phosgene; furthermore, it is intrinsically toxic in its own right (in addition to its propensity to release phosgene); and while it is a solid, its vapour pressure is high enough to cause hazardous vapour concentrations inside closed containers. As a result of these hazards, the reaction waste streams must be managed carefully to avoid unintended release and exposure. It is for this reason that a “safer” reliable route to the synthesis of glutamate-ureido compounds was sought; one which was much more amenable to the regular and reliable synthetic repetition that library synthesis requires.

### 3.2.2 Section overview

Given these considerations regarding protecting group strategies, as well as the difficulties with traditional methods for urea synthesis a general work plan emerged. The first goal of this section of work was the development of a milder method for the general synthesis of a variety of *tert*-butyl protected AA-ureido-Glu compounds, avoiding the usage of triphosgene where possible.

This began with the investigation and refinement of a one-pot urea synthesis method, using 1,1'-carbonyldiimidazole (CDI) as a phosgene mimic. CDI had been used in previous PSMA chemistry, but the methods involved the isolation/purification of the imidazole intermediate followed by the activation of this intermediate with methyl triflate (a highly hazardous reagent in its own right), before the final condensation with a second amine to form the urea.<sup>305,329,453</sup> This approach seemed overly complex and as such was still unsuitable for routine and rapid synthesis of AA-ureido-Glu compounds. This section describes the adaptation and significant simplification of this chemistry, resulting in our rapid and robust “one-pot” method for the synthesis of asymmetric ureas.

Once this robust urea synthesis method had been established, the deprotection process had to be developed. The removal of *tert*-butyl ester/ether and *N*-Boc protecting groups is usually cleanly-effected with the use of concentrated solutions of TFA (aqueous or in DCM, occasionally with added scavengers to remove the isobutylene byproducts). In our case, while this generally seemed to proceed as expected, there were a number of instances in which significant quantities of an unexpected impurity was obtained. Upon further investigation and analysis, it was deduced that the culprit was likely a cyclic pyroglutamate product formed by the acid-promoted cyclocondensation of the glutamic acid moiety. This reactivity has thus-far not been reported in the literature, which is surprising in light of the recent popularity of the use of *tert*-butyl protected intermediates in PSMA chemistry. As such this effect was further investigated to better understand the conditions which promote its formation, as well as comparing the reaction kinetics relative to those of the deprotection itself. Finally, a general method was developed to effect complete deprotection of the urea substrates while minimising the formation of any cylocondensation products.

### 3.3 Results & Discussion – Urea Synthesis

#### 3.3.1 Mitsunobu-mediated CO<sub>2</sub> fixation

The method developed in our group for the Mitsunobu-mediated <sup>11</sup>C-urea synthesis *via* [<sup>11</sup>C]CO<sub>2</sub> fixation<sup>225,226</sup> was an adaptation of an earlier non-radioactive method developed by Peterson *et al.* from the Merck Research Laboratories.<sup>454</sup> This method was first attempted in our hands for the synthesis of these protected glutamate-urea intermediates, however we achieved disappointing yields (< 15%), and the synthesis required tedious purification protocols to remove the hydrazine and phosphine oxide byproducts.

This CO<sub>2</sub> fixation methodology was of course highly appealing for application in <sup>11</sup>C-radiochemistry as it can be applied directly with [<sup>11</sup>C]CO<sub>2</sub> (generally the starting material for most <sup>11</sup>C-radiochemistry). However since we were not restricted to CO<sub>2</sub> fixation approaches in the synthesis of non-radioactive reference compounds, we sought to use the more energetic reagent CDI (essentially as an “activated” CO<sub>2</sub> surrogate).

#### 3.3.2 Urea synthesis – CDI-method

Although less common than triphosgene, some other groups have synthesised protected amino acid ureas using carbonyldiimidazole (CDI) as a surrogate for phosgene. The first example of such an approach was that reported by Maresca *et al.* in 2009.<sup>305,453</sup> In this, Glu-(OtBu)<sub>2</sub>-NH<sub>2</sub> was reacted with CDI to form the corresponding acylimidazole derivative which was isolated and purified. Secondly this acylimidazole was activated *via* methylation of the imidazole moiety with methyl triflate (MeOTf), before addition of a second protected amino acid to yield the desired urea product. Whilst reportedly effective, the substitution of triphosgene with a method using MeOTf was hardly attractive either, with it posing its own substantial risks to the user.<sup>455</sup> Fortunately, the MeOTf activation step has been omitted by several others<sup>329,335,456</sup> with no noticeable adverse effect. In these methods as previously, the amine is reacted with CDI to form the acylimidazole derivative, which is subsequently isolated and purified. However unlike previously, this was reacted directly (without MeOTf activation) with a second protected amino acid and non-nucleophilic base (Et<sub>3</sub>N) to produce the urea in good yields.

However, we still suspected that the interim isolation and purification of this acylimidazole intermediate was likely unnecessary, if stoichiometries were judiciously controlled. Whilst no such “one-pot” method has been applied to PSMA-targeted compounds thus far, literature reports of one-pot CDI-mediated urea syntheses were found applied to other substrates, and it was hoped that such an approach could be applicable in our case.<sup>457</sup>

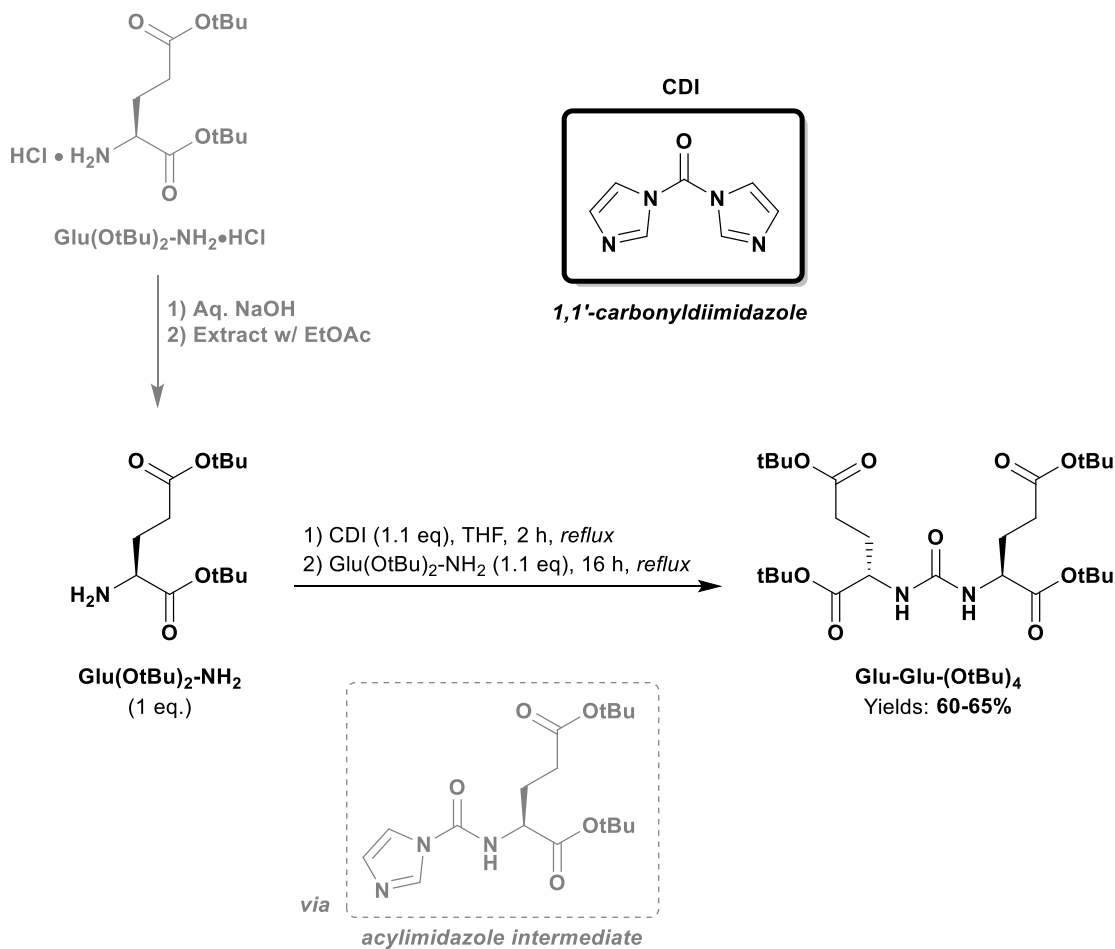


**Figure 3.4**  $\text{Glu-Glu-(OtBu)}_4$  synthesis with CDI (from free base)

Free base is first produced from the corresponding hydrochloride salt by extraction from an aqueous hydroxide solution. Following the general procedure from Frizler *et al.*<sup>457</sup>

Our first attempted CDI-mediated urea synthesis was implemented in strict accordance with the methodology reported by Frizler *et al.*, in their synthesis of non-PSMA-related ureas. The method called for the prior conversion of amine hydrochloride salts to their free base form, and accordingly we returned the  $\text{Glu(OtBu)}_2\text{-NH}_2 \cdot \text{HCl}$  to its free base



form by extraction from aqueous sodium hydroxide. It should be noted that in practical terms, this process was somewhat inefficient, resulting in 10-20% loss of starting material. As a result, the other reagent quantities had to be adjusted on a case-by-case basis to ensure consistent and accurate reaction stoichiometries.

Once the amine was obtained in its free base form, the synthesis was very straightforward:

- 1) The amine and CDI were added to dry THF and heated to reflux with stirring for 2 h.
- 2) The second amine (as free base) in THF was added to the refluxing mixture and the reaction was stirred overnight (approx. 16 h).

After cooling, and evaporation of the THF, the crude was worked-up with aqueous HCl and extracted with EtOAc (leaving the imidazole and any unreacted amines in the aqueous portion). If the product was an asymmetric urea, it could be isolated from any incidentally-formed symmetric urea products by flash column chromatography. The symmetric urea, due to the absence of any other amines in solution, was typically isolated in acceptable purities without the need for any chromatographic purification at all.

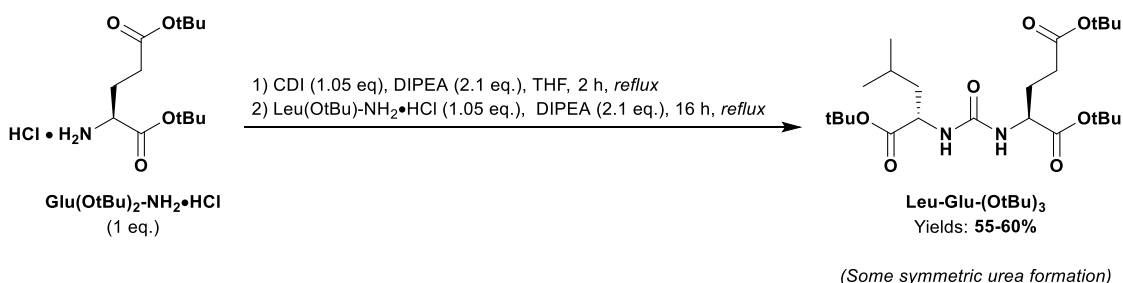


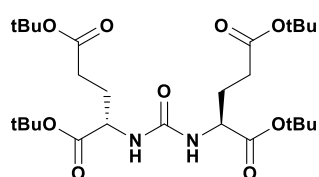
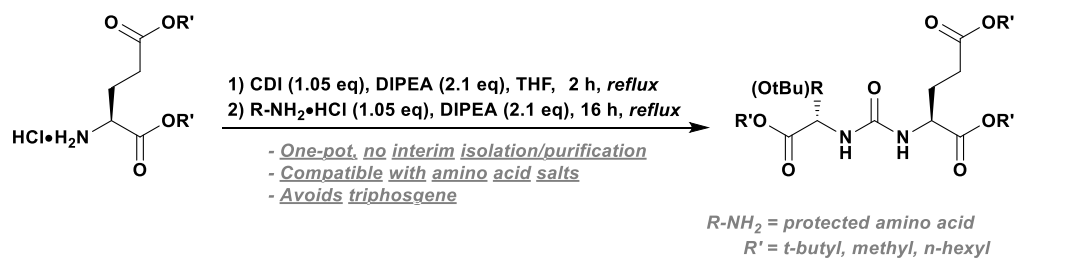
**Figure 3.5 Asymmetric Leu-Glu-(OtBu)<sub>4</sub> synthesis with CDI (direct from HCl salts)**

This is the *tert*-butyl protected precursor to ZJ43, a ligand with sub-nanomolar affinity for PSMA

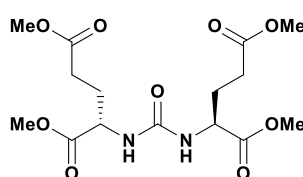
This “one-pot” method was impressive in its simplicity, but was still occasionally complicated by the inefficient HCl salt-to-free base conversion process. In an attempt to mitigate this, we explored the direct reaction of the protected amino acid hydrochloride salts directly, with the addition of two equivalents of the non-nucleophilic organic base *N,N*-diisopropylethylamine (DIPEA). This was added for two purposes: it was intended primarily to mediate the *in situ* free base formation, but also to act as a proton acceptor

during the reaction. Other than the presence of the base, this reaction proceeded as before in a 2-step one-pot manner, producing the urea product in reasonable yields.

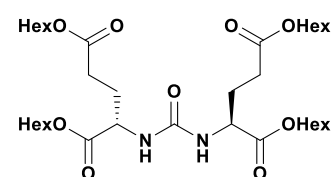
## 3.3.3 Final library of compounds synthesised



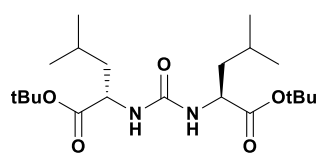
Glu-Glu-(OtBu)<sub>4</sub>  
Yield: 74%



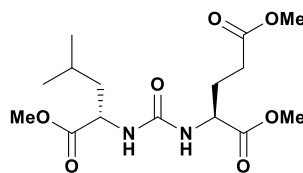
Glu-Glu-(OMe)<sub>4</sub>  
Yield: 68%



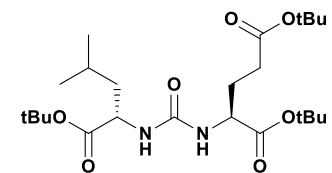
Glu-Glu-(OHex)<sub>4</sub>  
Yield: 63%



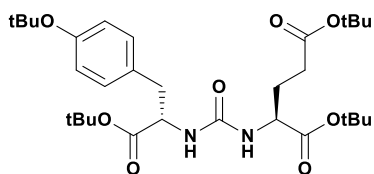
Leu-Leu-(OtBu)<sub>2</sub>  
Yield: 67%



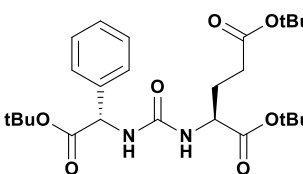
Leu-Glu-(OMe)<sub>3</sub>  
Yield: 61%



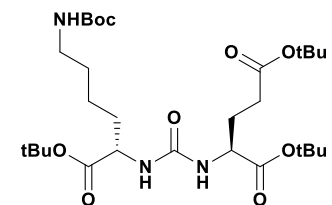
Leu-Glu-(OtBu)<sub>3</sub>  
Yield: 55%



Tyr-Glu-(OtBu)<sub>3</sub>  
Yield: 80%



Phg-Glu-(OMe)<sub>3</sub>  
Yield: 72%



Lys(N-ε-Boc)-Glu-(OtBu)<sub>3</sub>  
Yield: 77%

**Figure 3.6 Simplified method for synthesis of protected ureas with CDI**

All produced from the corresponding protected amino acid hydrochloride salts (except Glu-Glu-(OHex)<sub>4</sub> which was produced from the corresponding *p*-toluenesulfonate salt)

This one-pot methodology was applied to a number of different urea substrates (depicted in Figure 3.6 above), the majority of the substrates were *tert*-butyl protected symmetric and asymmetric glutamate ureas, but there are a few examples of methyl and hexyl protected products (synthesised for a separate application). In all cases, the same one-pot procedure was applied directly with the hydrochloride salts of the protected amino acids (except in the case of the glutamic acid dihexyl ester which was formed from the

corresponding p-toluenesulfonate salt). The various ureas were obtained in yields ranging from 55 to 80%, and product purification was relatively straightforward due to the absence of many troublesome byproducts. Importantly the methodology obviates the previously-common usage of triphosgene for the synthesis of these protected glutamic acid ureas. Additionally it represents a step forward from the previously implemented CDI methodologies: both in avoiding any MeOTf usage, as well as telescoping the procedure into a “one-pot” method, avoiding any interim isolation or purification of the acylimidazole intermediate.

It is hoped that this simplified synthetic methodology could be applied widely in the synthesis of these commonly-encountered protected glutamate ureas, it is arguably superior to the existing methods both from a safety perspective as well as from the perspective of reaction simplicity and ease of use.

### 3.4 Results & Discussion – Deprotection

#### 3.4.1 Initial attempt at TFA deprotection

Now that a reliable and reasonably efficient method had been developed for the synthesis of *tert*-butyl protected amino acid ureas, attention turned to deprotection methods. Trifluoroacetic acid (TFA) is typically employed for this purpose, for a number of reasons: firstly, as a strong acid (by virtue of the strongly electron-withdrawing trifluoromethyl group) TFA is easily capable of mediating the deprotective cleavage reaction; additionally, it can also act as the primary solvent for the reaction due to its ability to directly dissolve most peptides; and finally its high volatility lends itself well to facile removal by evaporation.<sup>458</sup> Cleavage of the *tert*-butyl moieties involves protonation of the oxygen, leading to release of the relatively stable *tert*-butyl cation ( $^+[\text{C}(\text{CH}_3)_3]$ ), which typically is deprotonated by a trifluoroacetate anion, producing the volatile isobutylene byproduct. The *N*-Boc (*tert*-butoxycarbamate moiety) deprotection involves a further mechanistic step: the initial cleavage of the *tert*-butyl moiety yields a carbamic acid intermediate, which rapidly undergoes decarboxylative decomposition (particularly under acidic conditions), to yield the fully deprotected amine. This chemistry is generally well established,<sup>445,459,460</sup> and it was not expected to require substantial optimisation.

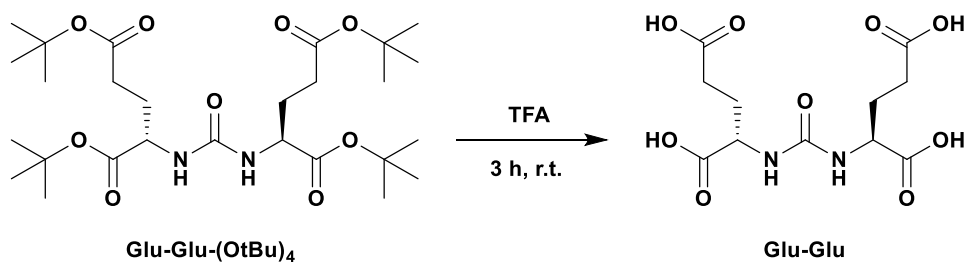


**Figure 3.7 Initial attempted deprotection of Glu-Glu-(OtBu)<sub>4</sub> with TFA**

Neat TFA (no water/scavengers) for 3 h, ~ **80% yield** due to formation of various confounding impurities (quantified by NMR as detailed in Section 3.4.2.3 below)

To begin with, the deprotection of the symmetric Glu-Glu-(OtBu)<sub>4</sub> was performed in 100% TFA for 3 h at rt. At the end of the 3 h stirring, the volatile TFA was simply removed with a stream of nitrogen and the crude product taken up in D<sub>2</sub>O and analysed by NMR. Curiously, while we observed substantial formation of our desired fully

deprotected product, there were a number of impurities identified in the NMR spectrum that were difficult to identify. It was clear that these were not re-alkylation products (from reaction with a liberated *tert*-butyl cation) due to the the absence of the characteristic *tert*-butyl proton signals.

### 3.4.2 Glutamate cyclisation: pyroglutamate impurity

During the investigation of this troublesome impurity, analysis by low-resolution mass spectrometry (APCI) – whilst observing the expected molecular ion – also found a significant peak corresponding to an  $[M-18]$  ion, typically associated with a loss of water. On this basis, we theorised that this impurity commonly observed by NMR could in fact be a dehydration product that was forming in this strongly acidic environment. While we could not find mention of such an impurity forming within the PSMA literature, we initially speculated that what was observed was the formation of a “pyroglutamate” moiety via an intramolecular cyclisation process.

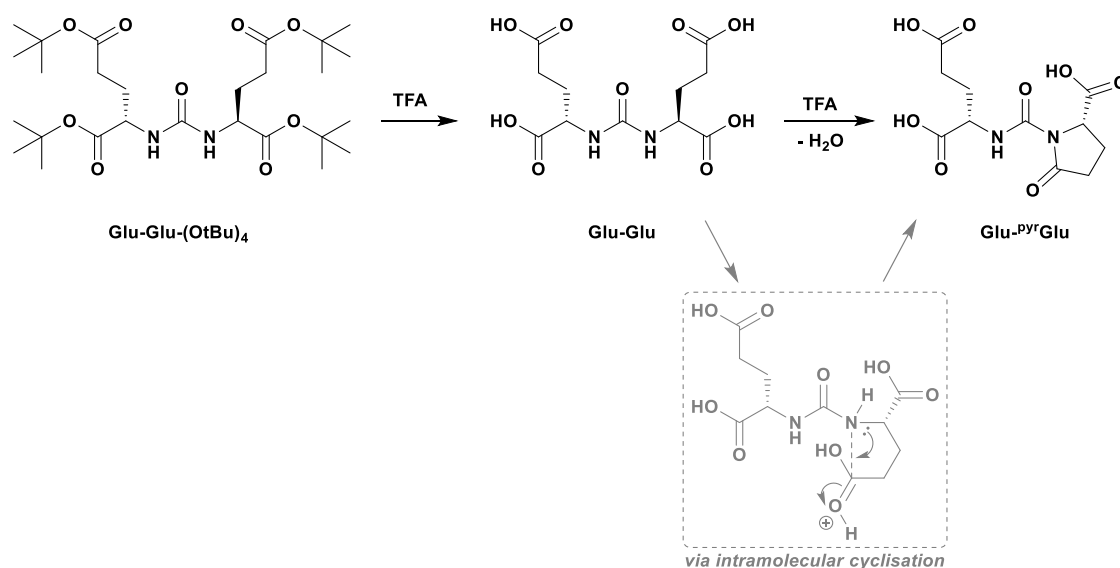


**Figure 3.8 Dehydrative cyclisation of a glutamate moiety to pyroglutamate**

<sup>Pyr</sup>Glu = pyroglutamate. Speculative mechanism, based upon similar mechanisms proposed in the literature<sup>461,462</sup>

This cyclic pyroglutamate formation is commonly observed in larger peptides, with many peptides containing a pyroglutamate moiety at their *N*-terminus. Typically, these are enzymatically formed from either glutamic acid or, more commonly, glutamine.<sup>463</sup> With some suggestions that these are more resistant to enzymatic cleavage, and accordingly serve to render the peptides more resistant to *N*-terminal degradation.<sup>463</sup> In small molecule synthetic chemistry terms, there has been some description of pyroglutamate formation from glutamic acid under both acidic and basic conditions, as well as through direct

heating of glutamic acid, and through intermediate activation of glutamic acid, although investigations in this area remain limited.<sup>461,462,464,465</sup>

A potential mechanism can be proposed for this cyclisation under our conditions, based upon similar reports from the literature.<sup>461,462,466</sup> In mixtures containing 95-100% TFA, this cyclisation likely occurs via initial protonation of the carbonyl oxygen in the  $\gamma$ -carboxylic acid moiety, followed by intramolecular nucleophilic attack at this  $\gamma$ -carbon by the urea nitrogen. This would form a cyclic intermediate that would subsequently eliminate water, resulting in the formation of the Glu-<sup>pyr</sup>Glu dehydrative decomposition product. However based solely upon the observation of an [M-18] ion this was still largely speculative.

#### **3.4.2.1 HRMS evidence**

Some more definitive evidence of this pyroglutamate cyclisation was found during high-resolution LC mass spectrometry (HR-LCMS) of this product. In the negative-mode electrospray ionisation (ESI) method, ammonium hydroxide (NH<sub>4</sub>OH) is added as a modifier to aid in the deprotonation of acidic analytes, to ensure they acquire a sufficient negative charge for ion detection (in the same manner that formic acid is typically employed in positive-mode ESI). Under these conditions, while we observed the expected [M-H]<sup>-</sup> molecular ion, and the [M-H-18]<sup>-</sup> ion we tentatively attributed to the pyroglutamate formation, a number of other highly abundant species were obtained in the spectrum. As this was obtained using ESI, generally considered a “soft” ionisation method, one would expect relatively little ion fragmentation, and as such it is reasonable to assume that these peaks corresponded to species actually present in solution.<sup>467</sup> Interestingly, these observed ions can plausibly be attributed to the hydroxide-induced decomposition of Glu-<sup>pyr</sup>Glu, as is presented in Figure 3.9 below.



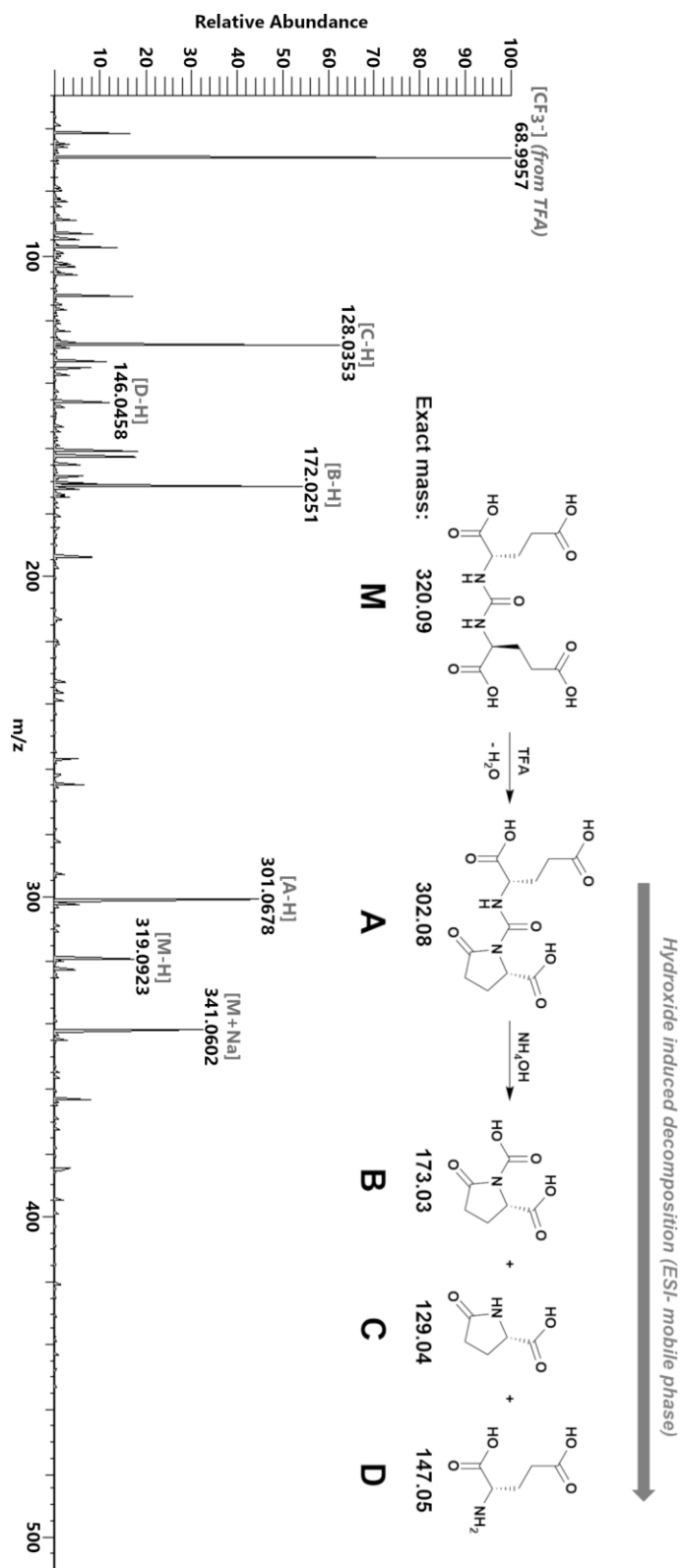


**Figure 3.9 Negative-mode ESI (with  $NH_4OH$  modifier) of deprotection products**

The major unexpected ionic species can all be attributed to hydroxide-induced decomposition products of Glu-<sup>pyr</sup>Glu (**B**, **C**, and **D**)

This mass spectrum (shown in Figure 3.9 above) exhibits three characteristic peaks that, crucially, are not present in the positive-mode ESI spectrum (where  $\text{NH}_4\text{OH}$  is replaced with formic acid as the modifier). It is proposed that these correspond to the three expected products from the nucleophilic attack at the *ureido*-carbonyl by the hydroxide ion from the  $\text{NH}_4\text{OH}$  modifier. **D** is simply the free glutamic acid, and so less important with regards to proving pyroglutamate formation, however the species labeled **B** and **C** are more interesting. The peak at  $m/z$  172.0251 has been assigned as the  $[\mathbf{B-H}]^-$  ion, where **B** is the *N*-carboxy-pyroglutamic acid species (monoisotopic mass = 173.0324), likely formed by the hydroxide addition-elimination at the *ureido*-carbonyl of  $\text{Glu}^{\text{pyr}}\text{Glu}$  (**A**). Furthermore, one would expect this carbamic acid species to spontaneously decompose releasing  $\text{CO}_2$  and the free pyroglutamic acid, **C**. This is also seen in the spectrum, with a major peak observed at  $m/z$  128.0353 corresponding to  $[\mathbf{C-H}]^-$  (monoisotopic mass = 129.0426). The only other major peak seen in the spectrum is that at  $m/z$  68.9957, which corresponds to the  $\text{CF}_3^-$  anion typically characteristic of TFA (likely residual contamination from the deprotection process).

Altogether, the observation of these characteristic species in the negative mode ESI spectrum (compared with their absence in the positive mode) makes a reasonably convincing case that this persistent impurity obtained in the acidic deprotection of  $\text{Glu-Glu}$  is in fact the cyclised  $\text{Glu}^{\text{pyr}}\text{Glu}$  species. With this in mind, the NMR was re-examined in an attempt to rationalise what was previously an unidentified impurity.

## 3.4.2.2 NMR evidence

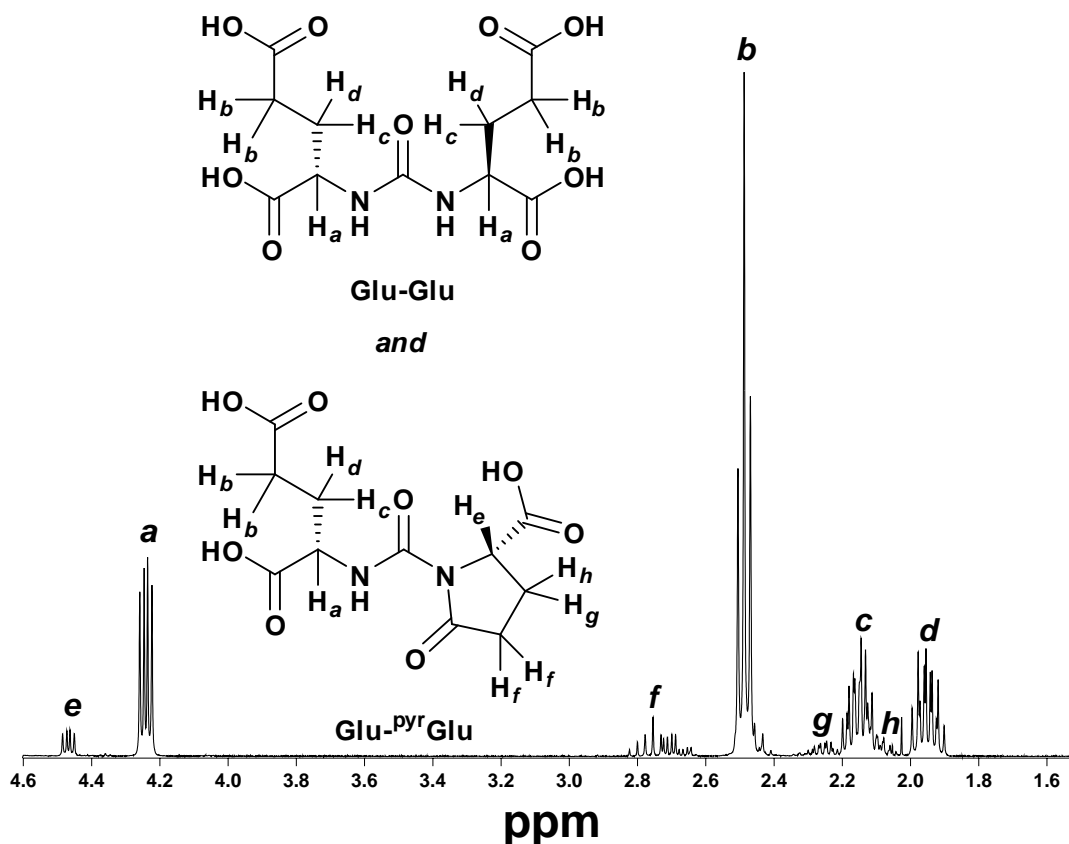


**Figure 3.10**  $^1\text{H}$  NMR of  $\text{Glu-Glu-(OtBu)}_4$  deprotection products

Peaks **a**, **b**, **c**, and **d** are from the Glu-Glu (and the uncyclised glutamate of Glu-<sup>pyr</sup>Glu), with the minor peaks **e**, **f**, **g**, and **h** corresponding to the pyroglutamate protons on Glu-<sup>pyr</sup>Glu

Figure 3.10 above shows the  $^1\text{H}$  NMR spectrum of the crude product obtained after TFA deprotection of  $\text{Glu-Glu-(OtBu)}_4$ , along with the structures of Glu-Glu and Glu-<sup>pyr</sup>Glu with the protons labeled (amine and carboxylic acid protons are not observed due to exchange with the  $\text{D}_2\text{O}$  solvent). The expected Glu-Glu protons were observed, with the proton bonded to the  $\alpha$ -carbon (**a**) being the most de-shielded due to its proximity to both the  $\alpha$ -carboxylate as well as the urea moieties, both electron withdrawing groups. Protons **b**, **c**, and **d** were assigned and distinguished due to the fact that **c** and **d** are diastereopic (due to their adjacency to a chiral carbon), and this chemical inequivalence gives rise to two different chemical shifts, each integrating to 2H. Whereas the **b** protons are not

adjacent to a chiral carbon, so all are chemically equivalent which leads to the 4H integration.

The previously unidentified impurity peaks *e*, *f*, *g*, and *h* (partially overlapping with *c*) are assigned to the pyroglutamate moiety, and represent the comparative downfield shift of protons *a*, *b*, *c*, and *d* (respectively) as a result of cyclisation. This is caused by the marginally more electron withdrawing nature of the  $\gamma$ -amide moiety in pyroglutamate, compared with the  $\gamma$ -carboxylate in the original glutamic acid, leading to comparatively more deshielded protons. These assignments were informed by  $^{13}\text{C}$ ,  $^1\text{H}$ - $^{13}\text{C}$  HSQC-DEPT, and COSY experiments, with reference to analysis of similar pyroglutamate products in the literature.<sup>461,464,468,469</sup>

### 3.4.2.3 NMR quantitation

One key advantage of this NMR analysis is that it also allows quantification of the extent of cyclisation by comparative integration of key peaks, as  $^1\text{H}$  NMR is a fully quantitative analytical technique. This analysis exploits the well separated and differentiated signals of protons *a* and *e*: where *e* represents only the  $\alpha$ -proton in the pyroglutamate moiety of Glu-<sup>pyr</sup>Glu, but *a* represents the combined sum of the  $\alpha$ -protons of both of the glutamate moieties in Glu-Glu as well as that in Glu-<sup>pyr</sup>Glu. Since Glu-<sup>pyr</sup>Glu contains equal amounts of both  $\alpha$ -protons *a* and *e*, the partial contribution of Glu-<sup>pyr</sup>Glu to the total integral of signal *a* (*[a]*) is equal to the total integral of signal *e* (*[e]*). This relationship allows the formulation of an equation that quantifies the degree to which a sample has converted from the intended Glu-Glu to the degradation product Glu-<sup>pyr</sup>Glu:

$$100 \times \frac{[e]}{[e] + 0.5([a] - [e])} = \% \text{ Glu-}^{\text{pyr}}\text{Glu conversion}$$

As an example, in the spectrum shown in Figure 3.10 above, if the integral of peak *e* is set to 1 then peak *a* integrates to 5.8. Inserting these figures into the equation tells us that 29% of the Glu-Glu has degraded to form the Glu-<sup>pyr</sup>Glu. A similar integrative analysis could be performed using other proton signals in the NMR spectra, but these  $\alpha$ -protons lend themselves to it particularly well by virtue of the absence of any nearby confounding signals as well as the inambiguity of their structural assignments (as a result of their high downfield chemical shift compared to all other observed protons).

**Table 3.1 Exploration of deprotection conditions**

	TFA (% v/v)	H <sub>2</sub> O (% v/v)	Time (h)	Signal integration		Glu-Glu to Glu- <sup>pyr</sup> Glu Conversion
				[e]	[a]	
<b>A</b>	<b>100</b>	<b>-</b>	<b>24</b>	1	1.4	<b>83 %</b>
<b>B</b>	<b>90</b>	<b>10</b>	<b>24</b>	1	5.8	<b>29 %</b>
<b>C</b>	<b>90</b>	<b>10</b>	<b>3</b>	1	27.3	<b>7 %</b>
<b>D</b>	<b>90</b>	<b>10</b>	<b>1</b>	1	54	<b>3.6 %</b>
<b>E<sup>†</sup></b>	<b>90</b>	<b>10</b>	<b>0.5</b>	<i>n.d.</i>	-	<b>&lt; 1 %</b>

General procedure: 20 mg Glu-Glu dissolved in 500  $\mu$ L deprotection solution. Solution stirred for varying time periods (at rt) before removal of TFA with N<sub>2</sub> stream. Residue was dissolved in 1 mL cold H<sub>2</sub>O, passed through a 5  $\mu$ m filter (removing insoluble *tert*-butyl protected impurities), and lyophilised. NMR recorded in D<sub>2</sub>O and peaks **e** and **a** were integrated to calculate conversions.

*n.d.* indicates no signal detected in the expected region of the spectrum.

<sup>†</sup> no signal for **e** was detected, so it was determined that little cyclisation had occurred.

This quantitative technique was used to evaluate a number of different deprotection methods, and the results are summarised in Table 3.1 above. Firstly, the solution composition was explored: deprotection in neat TFA for 24 hours (entry **A**) resulted in an extremely high rate of product cyclisation (83% of Glu-Glu had converted to Glu-<sup>pyr</sup>Glu); whereas the addition of just 10% (v/v) water (entry **B**) led to a significantly decreased cyclisation rate. This result was a clear demonstration that the addition of small amounts of water to a deprotection solution helps to suppress the cyclisation process. Since the reaction is a dehydration process (eliminating water) this is to be expected. It was clear that by itself, however, the addition of water is insufficient to suppress the cyclisation over this long time period (24 h). Accordingly, the reaction time was modified: a 3 h deprotection reduced the cyclisation to 7% (entry **C**), and a further reduction to 1 h led to just 3.6% of the Glu-Glu converting to Glu-<sup>pyr</sup>Glu (entry **D**). Ultimately the best results were obtained in just a 30 min deprotection (90% TFA, 10% H<sub>2</sub>O, v/v): under these conditions (entry **E**), no **e** signal was detected in the region expected, giving a clean NMR spectrum free from this troublesome impurity.

Under this modified deprotection protocol, some of the starting-material (Glu-Glu-(OtBu)<sub>4</sub>) remains unreacted or only partially deprotected (typically 10-15%). However due to its extreme aqueous insolubility compared with the highly-polar tetracarboxylic acid product (Glu-Glu), this can be separated from the product in a relatively trivial

trituration. After removal of the TFA in a stream of nitrogen an oily residue remains, this is taken up in a small quantity (approx. 1 mL) of cold water. While the polar deprotected products dissolve, the starting materials remain as an insoluble precipitate. The resultant suspension is passed through a 5 µm filter removing any of these insoluble impurities. After lyophilising overnight, the resultant product is a hygroscopic white solid.

It is important to note that these lyophilised products are relatively unstable in storage, with significant levels of cyclisation observed only two days after deprotection (possibly due to their hygroscopicity and residual TFA contamination). As a result, these glutamate ureas were generally stored in their much more stable *tert*-butyl protected forms, and only small portions of this “stock” (10-20 mg) are deprotected in a single instance, as and when required.

#### **3.4.2.4 Outlook and implications**

This observed cyclisation (particularly under storage) arguably warrants further investigation, particularly in light of recent studies demonstrating *N*-terminal pyroglutamate formation in peptides during short-medium term storage (over several weeks) in both solution and lyophilised solids.<sup>462</sup> There is considerable interest in the development of “kits” for simplified radiolabeling of PSMA-targeted ligands with radiometals (<sup>68</sup>Ga, <sup>177</sup>Lu, etc.).<sup>470</sup> These are typically lyophilised mixtures containing excipients such as antioxidants for radiolysis inhibition, as well the actual radiolabeling precursor itself, a bifunctional molecule consisting of an appropriate chelator linked to a glutamate-urea targeting pharmacophore.<sup>471–473</sup> While most of the focus has been on ensuring appropriately simple but efficient radiolabeling performance (kit-based radiopharmaceuticals are typically intended to radiolabel cleanly upon addition of a radiometal, without significant further operator intervention), as well as on the use of excipients for minimisation of radiolytic degradation after formulation.<sup>474</sup> However less discussion is given in the literature regarding the “shelf life” of the cold-kits themselves. One brief mention could be found in the literature from Ebenhan *et al.*, concerning their development of a kit for [<sup>68</sup>Ga]PSMA-11 radiolabeling.<sup>472</sup> In their work, they found that their kit preparation gave 97% RCYs for fresh preparations, but after 2 months storage of the kit at r.t., this dropped to a RCY of just 77%. However, the authors do not give more

details regarding the identities of the radiochemical species making up the remaining 23%, so it is not possible to determine whether the lowered yield was due to a pyroglutamate formation analogous to our observations, or whether it was a separate decomposition mechanism related to the chelator or linker moieties within the molecule.

In any case, it is unusual that this has yet to be discussed by any others within the PSMA literature, and it would be particularly interesting to check for pyroglutamate formation in kits intended for long-term storage. In the case of the Ebenhan paper, they were able to largely mitigate this by storing the kits at  $-50^{\circ}\text{C}$ , but it would still be useful to understand in-general the mechanism of kit degradation, to better control and monitor for this going forwards. As the glutamate moiety is utterly essential for PSMA targeting, the degradation of this by dehydrative cyclisation would be expected to entirely compromise any target binding affinity of these species. Preparation and administration of a kit with even a small proportion of the glutamate residues cyclised could result in significant non-specific background signal, compromising imaging performance.

## 3.4.3 Final method

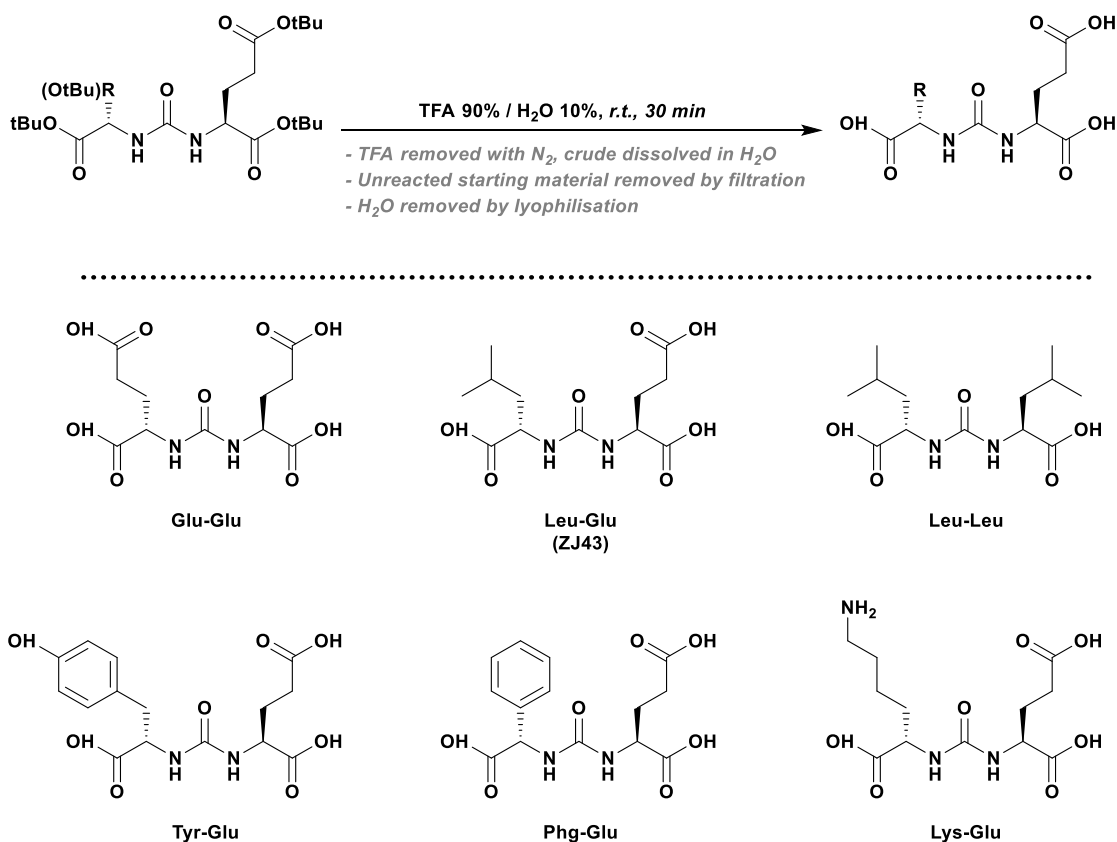


**Figure 3.11 General deprotection scheme and successful substrates**

The method was successfully applied to the deprotection of *tert*-butyl esters, *tert*-butyl ethers (Tyr-Glu), and N-Boc moieties (Lys-Glu). 10%  $\text{H}_2\text{O}$  and limited reaction times were successful in suppressing undesired pyroglutamate cyclisation

The optimal method (90% TFA / 10%  $\text{H}_2\text{O}$ , 30 min, r.t.) was successfully applied to the deprotection of a number of symmetric and asymmetric amino acid ureas, as depicted in Figure 3.11 above. The precursors were protected as *tert*-butyl esters, *tert*-butyl ethers, and N-Boc moieties, all of which were successfully removed under these conditions. Furthermore, the addition of 10%  $\text{H}_2\text{O}$  and the limited reaction time were both successful in suppressing the undesired pyroglutamate formation that had been observed under harsher conditions. The purification of these from any unreacted starting material was relatively straightforward, by virtue of the large polarity difference between the multi-carboxylate bearing products and the corresponding *tert*-butyl-bearing precursors. This allowed a trituration in  $\text{H}_2\text{O}$  to dissolve the product, but leave any unreacted starting materials as an insoluble precipitate. Filtration (typically through syringe filters due to



the small scale of these processes) was quick and effective, and lyophilisation of the aqueous filtrate rendered highly-pure glutamate ureas for use as reference compounds in the forthcoming radiolabeling of PSMA-binding ligands.

### 3.5 Materials & Methods

#### 3.5.1 General

Anhydrous acetonitrile (MeCN, 99.8%), anhydrous tetrahydrofuran (THF,  $\geq 99.9\%$ ), benzylamine (99%), di-*tert*-butyl-azodicarboxylate (DBAD, 98%), diethylazodicarboxylate (DEAD, 98%), triethylamine (Et<sub>3</sub>N,  $\geq 99.5\%$ ), *N,N*-diisopropylethylamine (DIPEA,  $\geq 99\%$ ) tri-*n*-butyl phosphine (PBU<sub>3</sub>, 99%), carbonyldiimidazole (CDI,  $\geq 90\%$ ), chloroform-*d* (CDCl<sub>3</sub>,  $\geq 99\%$ ), and deuterium oxide (D<sub>2</sub>O, 99.9%) were purchased from Sigma-Aldrich. Ethyl acetate (EtOAc,  $\geq 99.5\%$ ), *n*-hexane (95%), and all protected amino acid hydrochloride salts ( $\geq 95\%$ ) were purchased from Fisher Scientific. Anhydrous magnesium sulfate (MgSO<sub>4</sub>, 98%) was purchased from Fluka. 1,8-Diazabicyclo[5.4.0]undec-7-ene (DBU, 99%) was purchased from Alfa Aesar. Carbon dioxide (CO<sub>2</sub>) was purchased from BOC Gases.

<sup>1</sup>H, <sup>13</sup>C{<sup>1</sup>H}, <sup>1</sup>H-<sup>13</sup>C HSQC-DEPT, and COSY NMR spectra were recorded on a Bruker Avance DRX 400 MHz spectrometer at 294 K. Chemical shifts are reported in parts per million (ppm) relative to the residual solvent proton impurities (<sup>1</sup>H) or the residual solvent carbon impurities (<sup>13</sup>C), as internal standards.

#### 3.5.2 General protocol for CDI-mediated urea synthesis: Leu-Glu-(OtBu)<sub>3</sub>

The hydrochloride salt of *L*-glutamic acid di-*tert*-butyl ester (Glu-(OtBu)<sub>2</sub>.HCl) (500 mg, 1.69 mmol) and DIPEA (611  $\mu$ L, 3.55 mmol) were added to anhydrous THF (5 mL) and stirred to dissolve. CDI (288mg, 1.77 mmol) was added and the reaction was heated to reflux for 2 h. A second solution was prepared, in which the hydrochloride salt of *L*-leucine *tert*-butyl ester (Leu-(OtBu).HCl) (397 mg, 1.69 mmol) and DIPEA (611  $\mu$ L, 3.55 mmol) were added to anhydrous THF (5 mL) and stirred to dissolve. This solution was added to the refluxing reaction mixture and the stirring was continued at reflux for a further 16 h. The solvent was removed by rotary evaporation, the crude was acidified with an aqueous solution of 0.5M HCl (40 mL) and extracted with EtOAc (3 x 20 mL). The combined organic extracts were washed with brine (20 mL), dried over MgSO<sub>4</sub>, and removed by rotary evaporation to yield the crude products as a white solid. The crude was purified by flash column chromatography on silica gel, using *n*-hexane/EtOAc (70:30) as

eluent, to obtain the product as a white solid (439 mg, 55%).  $^1\text{H}$  NMR (400 MHz,  $\text{CDCl}_3$ )  $\delta$  5.06 (br d, 1H,  $J = 8.0$  Hz, Glu-NH), 4.91 (br d, 1H,  $J = 8.5$  Hz, Leu-NH), 4.33 (m, 2H, Glu- $\alpha$ -CH & Leu- $\alpha$ -CH *overlapping*), 2.30 (m, 2H, Glu- $\gamma$ -CH<sub>2</sub>), 2.06 (m, 1H, Glu- $\beta$ -CH<sub>2</sub>), 1.85 (m, 1H, Glu- $\beta$ -CH<sub>2</sub>), 1.70 (m, 2H, Leu- $\beta$ -CH<sub>2</sub>), 1.55 (m, 1H, Leu- $\gamma$ -CH), 1.45 (s, 18H, Glu/Leu- $\alpha$ -COOtBu), 1.42 (s, 9H, Glu- $\gamma$ -COOtBu), 0.93 (d, 6H,  $J = 6.4$  Hz, Leu-C(CH<sub>3</sub>)<sub>2</sub>);  $^{13}\text{C}$  NMR (100 MHz,  $\text{CDCl}_3$ ) 173.22 (Glu- $\alpha$ -COOR), 172.46 (Leu- $\alpha$ -COOR), 172.13 (Glu- $\gamma$ -COOR), 156.81 (NH-C(O)-NH), 82.03 (Glu- $\alpha$ -COOC(CH<sub>3</sub>)<sub>3</sub>), 81.54 (Leu- $\alpha$ -COOC(CH<sub>3</sub>)<sub>3</sub>), 80.48 (Glu- $\gamma$ -COOC(CH<sub>3</sub>)<sub>3</sub>), 53.04 (Glu- $\alpha$ -CH), 52.28 (Leu- $\alpha$ -CH), 42.44 (Leu- $\gamma$ -CH), 31.56 (Glu- $\gamma$ -CH<sub>2</sub>), 28.50 (Glu- $\beta$ -CH<sub>2</sub>), 28.07 (Glu- $\gamma$ -COOC(CH<sub>3</sub>)<sub>3</sub>), 28.00 (Glu- $\alpha$ -COOC(CH<sub>3</sub>)<sub>3</sub>), 27.99 (Leu- $\alpha$ -COOC(CH<sub>3</sub>)<sub>3</sub>), 24.80 (Leu- $\beta$ -CH<sub>2</sub>), 22.81, 22.15 (Leu-C(CH<sub>3</sub>)<sub>2</sub>). Assignments informed by  $^1\text{H}$ - $^{13}\text{C}$  HSQC-DEPT and COSY experiments.

### 3.5.3 General protocol for deprotection: Leu-Glu (*aka ZJ43*)

A solution was prepared consisting of TFA (450  $\mu\text{L}$ ) and deionised water (50  $\mu\text{L}$ ). To this solution, the fully protected precursor, Leu-Glu-(OtBu)<sub>3</sub> (20 mg, 42  $\mu\text{mol}$ ), was added and the solution stirred at rt for 30 min. The TFA was removed with a stream of N<sub>2</sub> to yield an oily residue. To this residue, deionised water (1 mL) was added, and the solution passed through a 5 $\mu\text{m}$  syringe filter. The filtrate was frozen in liquid N<sub>2</sub> and lyophilised overnight to yield the product as a hygroscopic white solid (10.4 mg, 81%).  $^1\text{H}$  NMR (400 MHz, D<sub>2</sub>O)  $\delta$  4.20 (m, 2H, Glu- $\alpha$ -CH & Leu- $\alpha$ -CH *overlapping*), 2.47 (t, 2H,  $J = 7.3$  Hz, Glu- $\gamma$ -CH<sub>2</sub>), 2.14 (m, 1H, Glu- $\beta$ -CH<sub>2</sub>), 1.94 (m, 1H, Glu- $\beta$ -CH<sub>2</sub>), 1.67 (m, 1H, Leu- $\gamma$ -CH), 1.58 (t, 2H,  $J = 7.2$  Hz, Leu- $\beta$ -CH<sub>2</sub>), 0.89 (d, 3H,  $J = 6.5$  Hz, Leu-C(CH<sub>3</sub>)<sub>2</sub>), 0.85 (d, 3H,  $J = 6.4$  Hz, Leu-C(CH<sub>3</sub>)<sub>2</sub>);  $^{13}\text{C}$  NMR (100 MHz, D<sub>2</sub>O)  $\delta$  177.04 (Glu- $\alpha$ -COOH), 176.41 (Leu- $\alpha$ -COOH), 175.39 (Glu- $\gamma$ -COOH), 158.54 (NH-C(O)-NH), 51.71 (Glu- $\alpha$ -CH), 51.08 (Leu- $\alpha$ -CH), 38.98 (Leu- $\beta$ -CH<sub>2</sub>), 29.20 (Glu- $\gamma$ -CH<sub>2</sub>), 25.35 (Glu- $\beta$ -CH<sub>2</sub>), 23.54 (Leu- $\gamma$ -CH), 21.34, 19.76 (Leu-C(CH<sub>3</sub>)<sub>2</sub>).

### 3.5.4 Characterisation of protected ureas

All produced according to the general protocol in 3.5.2 using the respective protected amino acid hydrochloride salt precursors. All assignments informed by  $^1\text{H}$ - $^{13}\text{C}$  HSQC-DEPT and COSY experiments.

**3.5.4.1 Glu-Glu-(OtBu)<sub>4</sub>**

<sup>1</sup>H NMR (400 MHz, CDCl<sub>3</sub>) δ 5.05 (br d, 2H, *J* = 7.9 Hz, NH), 4.33 (m, 2H, α-CH), 2.30 (m, 4H, γ-CH<sub>2</sub>), 2.06 (m, 2H, β-CH<sub>2</sub>), 1.86 (m, 2H, β-CH<sub>2</sub>), 1.46 (s, 18H, α-CO<sub>2</sub>tBu), 1.43 (s, 18H, γ-CO<sub>2</sub>tBu); <sup>13</sup>C NMR (100 MHz, CDCl<sub>3</sub>) 172.48 (α-COOR), 171.95 (γ-COOR), 156.67 (NH-C(O)-NH), 82.08 (α-COOC(CH<sub>3</sub>)<sub>3</sub>), 80.55 (γ-COOC(CH<sub>3</sub>)<sub>3</sub>), 53.05 (α-CH), 31.54 (γ-CH<sub>2</sub>), 28.41 (β-CH<sub>2</sub>), 28.07 (γ-COOC(CH<sub>3</sub>)<sub>3</sub>), 28.00 (α-COOC(CH<sub>3</sub>)<sub>3</sub>).

**3.5.4.2 Leu-Leu-(OtBu)<sub>2</sub>**

<sup>1</sup>H NMR (400 MHz, CDCl<sub>3</sub>) δ 4.89 (br d, 2H, *J* = 8.5 Hz, NH), 4.34 (m, 2H, α-CH), 1.69 (m, 4H, β-CH<sub>2</sub>), 1.54 (m, 2H, γ-CH), 1.45 (s, 18H, CO<sub>2</sub>tBu), 0.93 (d, 12H, *J* = 6.6 Hz, C(CH<sub>3</sub>)<sub>2</sub>); <sup>13</sup>C NMR (100 MHz, CDCl<sub>3</sub>) 173.40 (α-COOR), 156.86 (NH-C(O)-NH), 81.55 (α-COOC(CH<sub>3</sub>)<sub>3</sub>), 52.25 (α-CH), 42.51 (γ-CH), 27.99 (α-COOC(CH<sub>3</sub>)<sub>3</sub>), 24.81 (β-CH<sub>2</sub>), 22.84, 22.17 (C(CH<sub>3</sub>)<sub>2</sub>).

**3.5.4.3 Tyr-Glu-(OtBu)<sub>4</sub>**

<sup>1</sup>H NMR (400 MHz, CDCl<sub>3</sub>) δ 7.08 (d, 2H, *J* = 8.5 Hz, Tyr-*aromatic*) 6.88 (d, 2H, *J* = 8.6 Hz, Tyr-*aromatic*), 5.06 (br d, 1H, *J* = 7.9 Hz, Glu-NH), 4.98 (br d, 1H, *J* = 8.3 Hz, Tyr-NH) 4.54 (m, 1H, Tyr-α-CH) 4.33 (m, 1H, Glu-α-CH), 2.96 (m, 1H, Tyr-β-CH<sub>2</sub>), 2.82 (m, 1H, Tyr-β-CH<sub>2</sub>), 2.30 (m, 2H, Glu-γ-CH<sub>2</sub>), 2.06 (m, 1H, Glu-β-CH<sub>2</sub>), 1.85 (m, 1H, Glu-β-CH<sub>2</sub>), 1.45 (s, 18H, Glu/Tyr-α-CO<sub>2</sub>tBu), 1.42 (s, 9H, Glu-γ-CO<sub>2</sub>tBu), 1.33 (s, 9H, Tyr-OtBu); <sup>13</sup>C NMR (100 MHz, CDCl<sub>3</sub>) 173.22 (Glu-α-COOR), 172.38 (Tyr-α-COOR), 172.13 (Glu-γ-COOR), 156.81 (NH-C(O)-NH), 152.31 (Tyr-*aromatic*), 133.24 (Tyr-*aromatic*), 130.82 (Tyr-*aromatic*), 118.76 (Tyr-*aromatic*), 82.03 (Glu-α-COOC(CH<sub>3</sub>)<sub>3</sub>), 81.62 (Tyr-α-COOC(CH<sub>3</sub>)<sub>3</sub>), 80.48 (Glu-γ-COOC(CH<sub>3</sub>)<sub>3</sub>), 76.54 (Tyr-COOC(CH<sub>3</sub>)<sub>3</sub>), 53.04 (Glu-α-CH), 52.34 (Tyr-α-CH), 36.43 (Tyr-β-CH), 31.56 (Glu-γ-CH<sub>2</sub>), 28.50 (Glu-β-CH<sub>2</sub>), 28.07 (Glu-γ-COOC(CH<sub>3</sub>)<sub>3</sub>), 28.00 (Glu-α-COOC(CH<sub>3</sub>)<sub>3</sub>), 27.99 (Tyr-α-COOC(CH<sub>3</sub>)<sub>3</sub>), 27.28 (Tyr-COOC(CH<sub>3</sub>)<sub>3</sub>).

#### 3.5.4.4 Phg-Glu-(OtBu)<sub>3</sub>

<sup>1</sup>H NMR (400 MHz, CDCl<sub>3</sub>) δ 7.42 (m, 5H, Phg-*aromatic*), 5.27 (s, 1H, Phg-α-CH) 5.06 (br d, 1H, *J* = 7.9 Hz, Glu-NH), 4.96 (br d, 1H, *J* = 8.2 Hz, Phg-NH), 4.33 (m, 1H, Glu-α-CH), 2.30 (m, 2H, Glu-γ-CH<sub>2</sub>), 2.06 (m, 1H, Glu-β-CH<sub>2</sub>), 1.85 (m, 1H, Glu-β-CH<sub>2</sub>), 1.45 (s, 18H, Glu/Phg-α-COOCtBu), 1.42 (s, 9H, Glu-γ-COOCtBu); <sup>13</sup>C NMR (100 MHz, CDCl<sub>3</sub>) 173.22 (Glu-α-COOR), 172.19 (Phg-α-COOR), 172.11 (Glu-γ-COOR), 156.72 (NH-C(O)-NH), 137.01 (Phg-*aromatic*), 129.22 (Phg-*aromatic*), 128.78 (Phg-*aromatic*), 127.38 (Phg-*aromatic*), 81.99 (Glu-α-COOC(CH<sub>3</sub>)<sub>3</sub>), 81.47 (Phg-α-COOC(CH<sub>3</sub>)<sub>3</sub>), 80.46 (Glu-γ-COOC(CH<sub>3</sub>)<sub>3</sub>), 53.04 (Glu-α-CH), 31.56 (Glu-γ-CH<sub>2</sub>), 28.50 (Glu-β-CH<sub>2</sub>), 28.07 (Glu-γ-COOC(CH<sub>3</sub>)<sub>3</sub>), 28.00 (Glu-α-COOC(CH<sub>3</sub>)<sub>3</sub>), 27.96 (Phg-α-COOC(CH<sub>3</sub>)<sub>3</sub>).

#### 3.5.4.5 Lys(N-ε-Boc)-Glu-(OtBu)<sub>3</sub>

<sup>1</sup>H NMR (400 MHz, CDCl<sub>3</sub>) δ 5.06 (m, 2H, Glu-NH/Lys-α-NH *overlapping*), 4.70 (s, 1H, Lys-ε-NH), 4.33 (m, 2H, Glu-α-CH/Lys-α-CH *overlapping*), 3.09 (m, 2H, Lys-ε-CH<sub>2</sub>), 2.30 (m, 2H, Glu-γ-CH<sub>2</sub>), 2.06 (m, 1H, Glu-β-CH<sub>2</sub>), 1.85 (m, 1H, Glu-β-CH<sub>2</sub>), 1.75 (m, 1H, Lys-β-CH<sub>2</sub>), 1.62 (m, 1H, Lys-β-CH<sub>2</sub>), 1.52-1.18 (m, 40H, Lys-γ-CH<sub>2</sub>/Lys-δ-CH<sub>2</sub>/Glu-α-COOCtBu/Lys-α-COOCtBu/Glu-γ-COOCtBu/Lys-Boc *overlapping*); <sup>13</sup>C NMR (100 MHz, CDCl<sub>3</sub>) 173.77 (Lys-NHCOOR), 173.22 (Glu-α-COOR), 172.40 (Lys-α-COOR), 172.13 (Glu-γ-COOR), 156.92 (NH-C(O)-NH), 83.22 (Lys-NHCOOC(CH<sub>3</sub>)<sub>3</sub>), 82.03 (Glu-α-COOC(CH<sub>3</sub>)<sub>3</sub>), 81.50 (Lys-α-COOC(CH<sub>3</sub>)<sub>3</sub>), 80.48 (Glu-γ-COOC(CH<sub>3</sub>)<sub>3</sub>), 53.64 (Lys-α-CH) 53.04 (Glu-α-CH), 38.2 (Lys-ε-CH<sub>2</sub>), 31.56 (Glu-γ-CH<sub>2</sub>), 28.50 (Glu-β-CH<sub>2</sub>), 28.39 (Lys-δ-CH<sub>2</sub>), 28.26 (Lys-β-CH<sub>2</sub>), 28.18 (Lys-NHCOOC(CH<sub>3</sub>)<sub>3</sub>), 28.07 (Glu-γ-COOC(CH<sub>3</sub>)<sub>3</sub>), 28.00 (Glu-α-COOC(CH<sub>3</sub>)<sub>3</sub>), 27.99 (Lys-α-COOC(CH<sub>3</sub>)<sub>3</sub>), 27.78 (Lys-γ-CH<sub>2</sub>).

#### 3.5.5 Characterisation of deprotected ureas

All deprotected according to the general protocol in 3.5.3 from the respective fully-protected precursor urea. All assignments informed by <sup>1</sup>H-<sup>13</sup>C HSQC-DEPT and COSY experiments.

**3.5.5.1 Glu-Glu**

$^1\text{H}$  NMR (400 MHz,  $\text{D}_2\text{O}$ )  $\delta$  4.24 (dd, 2H,  $J_1 = 9.2$  Hz,  $J_2 = 5.1$  Hz,  $\alpha$ -CH), 2.48 (t, 4H,  $J = 7.3$  Hz,  $\gamma$ - $\text{CH}_2$ ), 2.14 (m, 1H,  $\beta$ - $\text{CH}_2$ ), 1.94 (m, 1H,  $\beta$ - $\text{CH}_2$ );  $^{13}\text{C}$  NMR (100 MHz,  $\text{D}_2\text{O}$ )  $\delta$  177.26 ( $\alpha$ -COOH), 176.22 ( $\gamma$ -COOH), 159.25 (NH-C(O)-NH), 52.53 ( $\alpha$ -CH), 30.01 ( $\gamma$ - $\text{CH}_2$ ), 26.14 ( $\beta$ - $\text{CH}_2$ ).

**3.5.5.2 Leu-Leu**

$^1\text{H}$  NMR (400 MHz,  $\text{D}_2\text{O}$ )  $\delta$  4.20 (m, 2H,  $\alpha$ -CH), 1.67 (m, 1H,  $\gamma$ -CH), 1.58 (t, 2H,  $J = 7.2$  Hz,  $\beta$ - $\text{CH}_2$ ), 0.89 (d, 3H,  $J = 6.5$  Hz,  $\text{C}(\text{CH}_3)_2$ ), 0.85 (d, 3H,  $J = 6.4$  Hz,  $\text{C}(\text{CH}_3)_2$ );  $^{13}\text{C}$  NMR (100 MHz,  $\text{D}_2\text{O}$ )  $\delta$  176.41 ( $\alpha$ -COOH), 158.54 (NH-C(O)-NH), 51.08 ( $\alpha$ -CH), 38.98 ( $\beta$ - $\text{CH}_2$ ), 23.54 ( $\gamma$ -CH), 21.34, 19.76 ( $\text{C}(\text{CH}_3)_2$ ).

**3.5.5.3 Tyr-Glu**

$^1\text{H}$  NMR (400 MHz,  $\text{D}_2\text{O}$ )  $\delta$  7.10 (d, 2H,  $J = 8.4$  Hz, Tyr-*aromatic*), 6.79 (d, 2H,  $J = 8.5$  Hz, Tyr-*aromatic*), 4.40 (dd, 1H,  $J_1 = 7.8$  Hz,  $J_2 = 5.6$  Hz, Tyr- $\alpha$ -CH), 4.14 (dd, 1H,  $J_1 = 9.2$  Hz,  $J_2 = 5.1$  Hz, Glu- $\alpha$ -CH), 3.04 (m, 1H, Tyr- $\beta$ - $\text{CH}_2$ ), 2.90 (m, 1H, Tyr- $\beta$ - $\text{CH}_2$ ), 2.39 (t, 2H,  $J = 7.3$  Hz, Glu- $\gamma$ - $\text{CH}_2$ ), 2.07 (m, 1H, Glu- $\beta$ - $\text{CH}_2$ ), 1.86 (m, 1H, Glu- $\beta$ - $\text{CH}_2$ );  $^{13}\text{C}$  NMR (100 MHz,  $\text{D}_2\text{O}$ )  $\delta$  177.22 (Glu- $\alpha$ -COOH), 176.14 (Glu- $\gamma$ -COOH), 176.07 (Tyr- $\alpha$ -COOH), 158.91 (NH-C(O)-NH), 130.61 (Tyr-*aromatic*), 115.38 (Tyr-*aromatic*), 54.65 (Tyr- $\alpha$ -CH), 52.413 (Glu- $\alpha$ -CH), 36.23 (Tyr- $\beta$ - $\text{CH}_2$ ), 29.93 (Glu- $\gamma$ - $\text{CH}_2$ ), 26.14 (Glu- $\beta$ - $\text{CH}_2$ ).

**3.5.5.4 Phg-Glu**

$^1\text{H}$  NMR (400 MHz,  $\text{D}_2\text{O}$ )  $\delta$  7.40 (m, 5H, Phg-*aromatic*), 5.26 (s, 1H, Phg- $\alpha$ -CH), 4.23 (dd, 1H,  $J_1 = 9.2$  Hz,  $J_2 = 5.1$  Hz, Glu- $\alpha$ -CH), 2.45 (t, 2H,  $J = 7.3$  Hz, Glu- $\gamma$ - $\text{CH}_2$ ), 2.13 (m, 1H, Glu- $\beta$ - $\text{CH}_2$ ), 1.92 (m, 1H, Glu- $\beta$ - $\text{CH}_2$ );  $^{13}\text{C}$  NMR (100 MHz,  $\text{D}_2\text{O}$ )  $\delta$  177.26 (Glu- $\alpha$ -COOH), 176.22 (Glu- $\gamma$ -COOH), 175.28 (Phg- $\alpha$ -COOH), 158.90 (NH-C(O)-NH), 137.25 (Phg-*aromatic*), 129.56 (Phg-*aromatic*), 128.97 (Phg-*aromatic*), 127.43 (Phg-*aromatic*), 58.48 (Phg- $\alpha$ -CH), 52.56 (Glu- $\alpha$ -CH), 30.08 (Glu- $\gamma$ - $\text{CH}_2$ ), 26.20 (Glu- $\beta$ - $\text{CH}_2$ ).

**3.5.5.5 Lys-Glu**

$^1\text{H}$  NMR (400 MHz,  $\text{D}_2\text{O}$ )  $\delta$  4.16 (m, 2H, Glu- $\alpha$ -CH/Lys- $\alpha$ -CH), 2.91 (t, 2H,  $J = 7.5$  Hz, Lys- $\epsilon$ - $\text{CH}_2$ ), 2.44 (t, 2H,  $J = 7.3$  Hz, Glu- $\gamma$ - $\text{CH}_2$ ), 2.10 (m, 1H, Glu- $\beta$ - $\text{CH}_2$ ), 1.90 (m, 1H, Glu- $\beta$ - $\text{CH}_2$ ), 1.80 (m, 1H, Lys- $\beta$ - $\text{CH}_2$ ), 1.67 (m, 1H, Lys- $\beta$ - $\text{CH}_2$ ), 1.61 (m, 2H, Lys- $\delta$ - $\text{CH}_2$ ), 1.39 (m, 2H, Lys- $\gamma$ - $\text{CH}_2$ );  $^{13}\text{C}$  NMR (100 MHz,  $\text{D}_2\text{O}$ )  $\delta$  177.24 (Glu- $\alpha$ -COOH), 177.13 (Lys- $\alpha$ -COOH), 176.20 (Glu- $\gamma$ -COOH), 162.98 (NH-C(O)-NH), 52.91 (Lys- $\alpha$ -CH), 52.47 (Glu- $\alpha$ -CH), 39.20 (Lys- $\epsilon$ - $\text{CH}_2$ ), 30.33 (Glu- $\gamma$ - $\text{CH}_2$ ), 29.95 (Lys- $\beta$ - $\text{CH}_2$ ), 26.08 (Glu- $\beta$ - $\text{CH}_2$ ), 22.02 (Lys- $\delta$ - $\text{CH}_2$ ), 20.52 (Lys- $\gamma$ - $\text{CH}_2$ ).

## 4 PSMA SECTION 2 – MITSUNOBU-BASED <sup>11</sup>C-RADIOLABELING

### 4.1 Introduction

This chapter covers our first attempts at <sup>11</sup>C-radiolabeling a PSMA ligand. In this short introduction our initial target molecule selection is discussed, with reference to the historical development of the PSMA-targeting glutamate-ureido scaffold, as well as with consideration given to the theoretical radiosynthetic accessibility of different candidates.

#### 4.1.1 Choice of target

As was discussed in section 1.5 (page 90), prostate specific membrane antigen (PSMA) is a well validated target for both PET imaging and targeted radionuclide therapy of prostate cancer. However, PSMA is not solely expressed in PCa tissue, but also exists in healthy brain tissue, where it is expressed predominantly on astrocytes.<sup>281,282,292</sup> In this setting it is more commonly referred to as glutamate carboxypeptidase II (GCPII), but the protein is in fact identical to the PSMA found in prostatic tissue.<sup>280</sup> Prior to any major interest in targeting PSMA for PCa imaging/therapy, a number of groups began developing GCPII inhibitors with a view to their potential neurological application. As was covered previously, these molecules are all based around a common glutamate-urea pharmacophore (as seen in Figure 4.1 below).



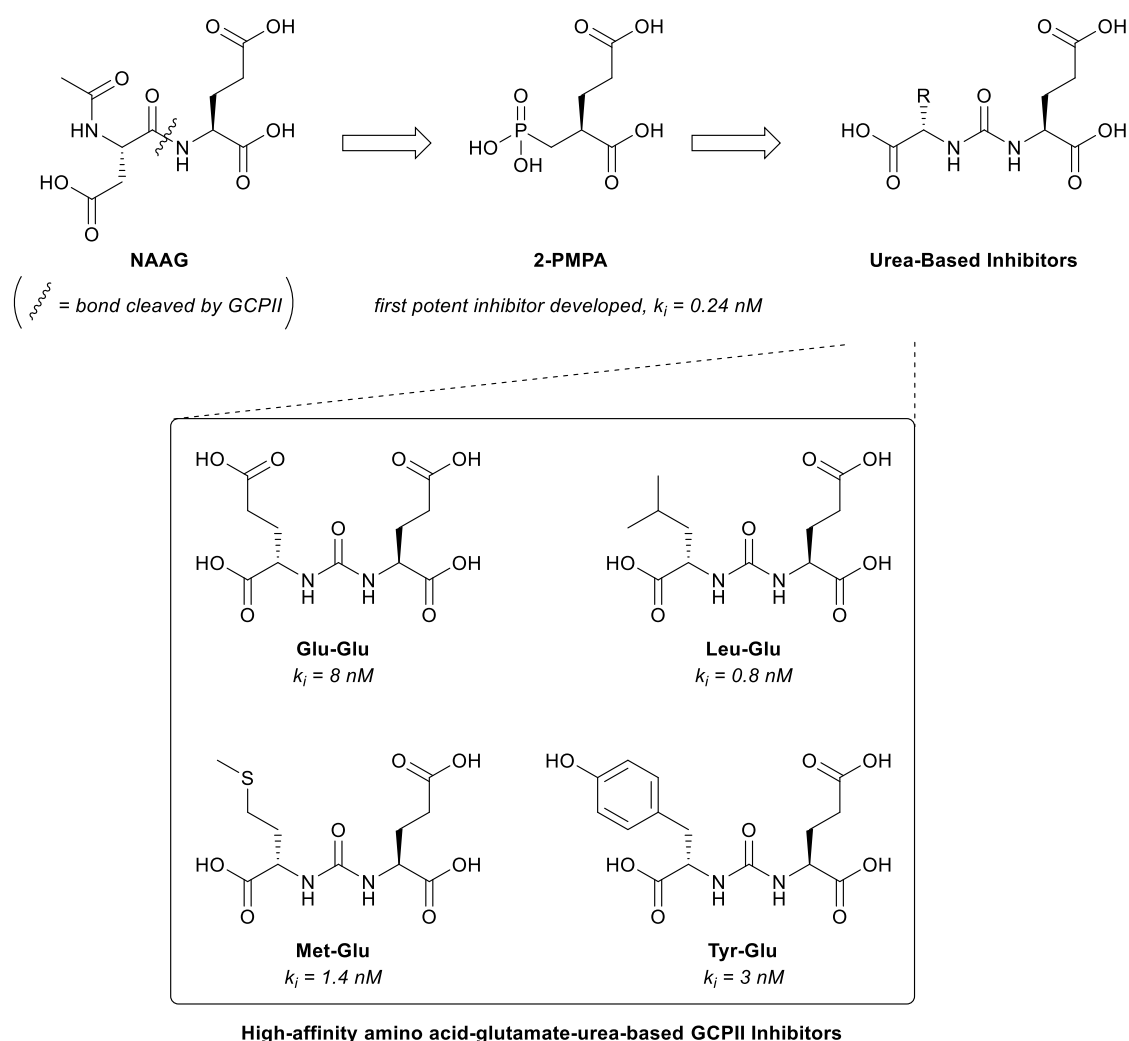


**Figure 4.1 Drug development pathway for GCPII/PSMA inhibitors**

Started with NAAG – the natural neurotransmitter ligand cleaved by GCPII. The example glutamate-ureido GCPII inhibitors presented here were all developed by Kozikowski *et al.*

In light of the more recently developed methods for the rapid <sup>11</sup>C-radiolabeling of ureas via [<sup>11</sup>C]CO<sub>2</sub> fixation chemistry, we wondered whether these original amino acid-glutamate-urea GCPII inhibitors could now be accessible for direct isotopologous ureido-<sup>11</sup>C-radiolabeling for use as potential clinical PSMA imaging agents. While the 20.4 min half-life often precludes widespread diagnostic application of <sup>11</sup>C-radiotracers, one promising use case of an <sup>11</sup>C-PSMA radiotracer would be as part of a multiplexed scanning regime. Multiplexing is the practice whereby a number of different radiotracers can be used with the same patient, this gives multiple different insights into the course of a disease/therapy by combining the benefits of different radiotracers which image

different physiological processes or receptor expression levels.<sup>475</sup> For example in PC, while PSMA-PET is highly accurate at detecting metastatic lesions, it gives no insight into the metabolic activity of a given lesion. The complementary use of <sup>18</sup>F/<sup>11</sup>C-choline or <sup>11</sup>C-acetate (with a lower overall lesion detection rate than PSMA) in the same patient could give this equally important insight into a given lesion's metabolic activity – a physiological change which can be important to monitor, particularly when tracking treatment response.<sup>476,477</sup> To achieve this, the scans must be done as close to one another as possible to ensure that they can be reasonably correlated, but enough time must be left to allow the previous radiotracer to have fully decayed, so as to not interfere with the subsequent scan. If two <sup>18</sup>F-radiotracers (half life 109.7 mins) were to be used in this manner, a significant gap (possibly up to 24 hours) would be required to allow for the first radiotracer to fully decay before administration of the second radiotracer. By contrast, two <sup>11</sup>C-radiotracers, with a 5 times shorter half life (20.4 mins), would potentially allow for two scans within the same day. This would allow multiplexed scanning regimes (perhaps <sup>11</sup>C-PSMA and <sup>11</sup>C-choline) to be completed within a single hospital visit, something that would not be possible with the combination of two <sup>18</sup>F-radiotracers.

Initially we decided to employ the DBU/Mitsunobu-mediated [<sup>11</sup>C]CO<sub>2</sub> fixation methodology to <sup>11</sup>C-radiolabel a candidate molecule from this series of small-molecule GCPII inhibitors. Initially the candidate which stood out to us was the symmetric glutamate urea, Glu-Glu. While its receptor affinity ( $k_i = 8$  nM) was not as high as that of the best in this series (Leu-Glu  $k_i = 0.8$  nM), Glu-Glu was considered more straightforward to radiolabel (theoretically) since there would be no concerns with asymmetric selectivity.

#### 4.1.2 Mitsunobu-mediated symmetric <sup>11</sup>C-urea radiolabeling

The target compound chosen for this initial section of radiochemistry was therefore the symmetrical glutamate urea, (<sup>11</sup>C]Glu-Glu), and the general approach decided upon was a two phase synthesis. The first of these being the synthesis of the *tert*-butyl-ester protected <sup>11</sup>C-urea (<sup>11</sup>C]Glu-Glu-(*O*<sup>t</sup>Bu)<sub>4</sub>) via DBU/Mitsunobu-mediated [<sup>11</sup>C]CO<sub>2</sub> fixation chemistry.<sup>225,226</sup> Once this step had been well optimised, the follow-up step would be the full deprotection of this urea to yield the desired tetracarboxylic acidic product (<sup>11</sup>C]Glu-Glu). The first R&D section will discuss the adaptation of our group's previously developed general method for the synthesis of symmetrical <sup>11</sup>C-ureas,<sup>226</sup> to this particular protected amino-acid substrate.

As is illustrated in the radiosynthetic scheme below, [<sup>11</sup>C]CO<sub>2</sub> is fixed on an amine substrate with DBU, forming an amidinium <sup>11</sup>C-carbamate *in situ*. This is reacted with a pre-formed Mitsunobu betaine (PBu<sub>3</sub>/DBAD) to dehydrate the carbamate, yielding an *in situ* <sup>11</sup>C-isocyanate. This <sup>11</sup>C-isocyanate reacts with any remaining unreacted amine substrate to form the symmetric <sup>11</sup>C-urea product. This method was developed using fairly simple “building block” amines to demonstrate its synthetic scope, and the conditions reported are correspondingly generic; they were developed to effect a broad range of urea syntheses. However when these conditions were applied to our specific substrate, the yields and conversion rates were less than stellar (as will be presented herein). The conditions were then rationally modified to optimise the reaction as best as possible, but for reference, it is useful to summarise here what are henceforth referred to as the “literature conditions”.

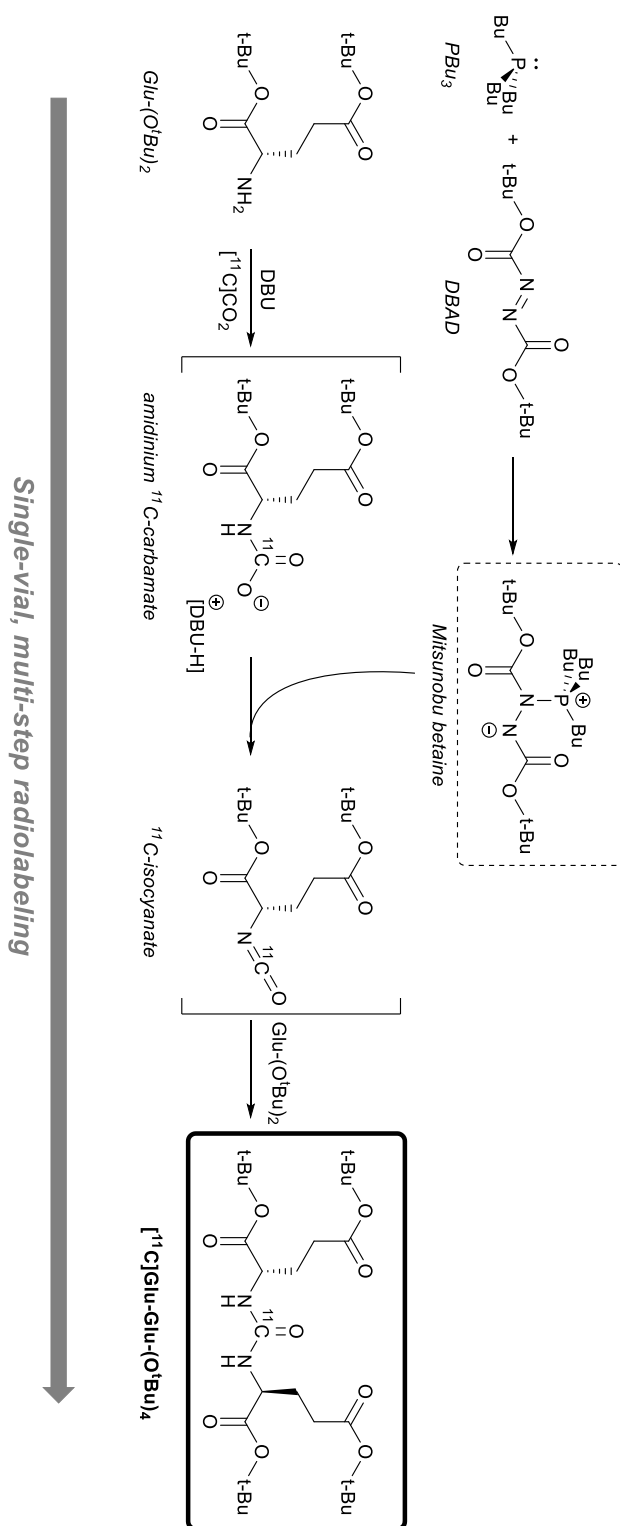


**Figure 4.2 Proposed radiosynthesis of key intermediate  $[^{11}\text{C}]\text{Glu-Glu-(O}^t\text{Bu)}_4$**

Mitsunobu betaine is pre-formed from  $\text{PBu}_3$  and  $\text{DBAD}$ . Reaction proceeds in a “one-pot” manner from  $[^{11}\text{C}]\text{CO}_2$  via the *in situ* formation of the  $^{11}\text{C}$ -carbamate and  $^{11}\text{C}$ -isocyanate intermediates

**4.1.2.1 The “literature conditions”**

1. [<sup>11</sup>C]CO<sub>2</sub> is bubbled through a vial containing **18.3 μmol amine** and **3.4 μmol DBU** at **0°C**
2. The solution temperature is increased to **50°C** before addition of the previously-prepared Mitsunobu reagents (**36.6 μmol DBAD/PBu<sub>3</sub>**) and the reaction is stirred for **2 mins**
3. The reaction is quenched with addition of water before HPLC analysis

## 4.2 Results & Discussion – Mitsunobu-Mediated <sup>11</sup>C-Urea Synthesis

In this section, we aimed to take a rational approach to radiochemical reaction optimisation, guided by a thorough characterisation and understanding of a typical radio-HPLC profile for this reaction. In many reported radiosyntheses, analytical radio-HPLC is largely used to simply assess the RCY of a reaction by integrating the area under the product peak. While there is nothing inherently incorrect with this approach, there is a wealth of data contained in any given radio-HPLC elution profile, and this approach can often disregard much of this information. In the absence of any other commonplace analytical techniques (NMR and MS are not possible with radiochemistry on this scale), it makes sense to obtain the maximum possible insight from the chromatography. By better characterising the typical peaks, and observing under which conditions their respective RCYs increase or decrease, a much deeper insight into the chemistry can be gained. If a peak is identified as a likely reaction intermediate, the conditions can be rationally adjusted to drive the reaction further to completion. Conversely, if an identified peak represents a degradation product (resulting from breakdown of the desired product), the conditions can again be altered accordingly to disfavour this degradative pathway. Such an approach is not always necessary, but in our busy facility with one cyclotron serving both clinical production as well as a team of researchers, a rational radio-HPLC-guided optimisation approach was deemed the most efficient approach. The aim was to maximise the utility of every experiment performed: to streamline the optimisation of this particular radiosynthesis, in addition to furthering our general understanding of this still incompletely-understood, but increasingly widely-used chemistry.

#### 4.2.1 Ammonium-salt precursor: aqueous extraction *versus* deprotonation *in-situ*

Unlike the simpler amines used in our group's earlier development of this method, our desired substrate amine (*L*-glutamic acid di-*tert*-butyl ester) is not available commercially as the free amine (the conjugate base), and is instead obtained as the corresponding hydrochloride salt. This is common for virtually all commercially-obtained amino acid building blocks, whether it be to enhance water solubility, compound stability, or as a byproduct of their synthesis involving strong acids. The problem this presents is that hydrochloride salts are often insoluble in the intended reaction solvent acetonitrile; and even in those cases where they are soluble, one would not expect these protonated ammonium functionalities to exhibit the same reactivity as the corresponding free amines.

Therefore, prior to any further optimisation of this method for our specific usage, it was important to address this specific issue. The two main approaches generally used to overcome this issue in non-radioactive synthetic chemistry are: i) dissolving the hydrochloride salt in a basic aqueous solution (typically dilute NaOH) and extracting the resultant deprotonated free-amine into an appropriate organic solvent; and ii) adding an equimolar quantity of a non-nucleophilic organic base (Et<sub>3</sub>N, DiPEA, etc.) directly to the reaction solution to deprotonate the hydrochloride salt, releasing the free-amine *in-situ*.

To compare these approaches, two test <sup>11</sup>C-urea syntheses were performed and, except for the method of preparation of the starting amine, the previously described literature conditions were implemented identically in both cases.

##### 4.2.1.1 Experiment 1 preparation: the free-amine extraction method

*L*-Glutamic acid di-*tert*-butyl ester hydrochloride was added to 0.1M NaOH and this was extracted with a portion of ethyl acetate. The organic layer was separated and the aqueous layer was extracted three more times with ethyl acetate before these organic extracts were combined, washed with saturated brine solution, and dried with anhydrous magnesium sulfate. The ethyl acetate was removed under reduced pressure to yield the free-amine precursor (*L*-glutamic acid di-*tert*-butyl ester) as a sticky oil. 18.3 μmol of this precursor was dissolved in 300 μL of dry MeCN, and to this solution, 3.4 μmol DBU was added. This solution was prepared and crimp-sealed under an inert atmosphere.

#### 4.2.1.2 *Experiment 2 preparation: in-situ deprotonation method*

18.3 μmol of the corresponding precursor hydrochloride salt was added directly to 300 μL MeCN, forming a suspension of the insoluble amine salt. To this suspension, 21.7 μmol DBU was added (3.4 μmol [for <sup>11</sup>C]CO<sub>2</sub> fixation] + 18.3 μmol [for ammonium salt deprotonation]), where – upon agitation – the previously insoluble material fully dissolved, resulting in a visibly clear solution free of any insoluble material. This served as confirmation that the DBU was deprotonating the ammonium salt, releasing the free-amine into solution. Again, this solution was prepared and crimp-sealed under an inert atmosphere.

#### 4.2.1.3 *Results*

In both of these experiments, the results were broadly similar: both solutions exhibited excellent trapping (>90%) of the delivered [<sup>11</sup>C]CO<sub>2</sub>, and when analysed by radio-HPLC the non-isolated radiochemical yields were found to be 14% and 19% (for experiments **1** and **2**, respectively). In addition, there were no significant differences observed between the two reactions upon radio-HPLC analysis of the crude reaction mixtures: they both exhibited a similar profile of radiolabeled impurities, with no notably different peaks which could have corresponded to degradation products specifically resulting from the differential preparations of the amine precursor solution.

Since there were no major differences between the differentially prepared radiolabeling solutions, the decision to make regarding which approach to adopt going forward was made relatively straightforward. The *in situ* deprotonation method used in experiment **2** is markedly more operationally simple – and by extension theoretically much more reliable – than the alternative aqueous extraction method. It adds no extra steps to the solution preparation workflow, simply requiring the pipetting of 21.7 μmol of DBU instead of 3.4 μmol, and it entirely avoids the time-consuming and potentially error-prone (as detailed earlier) process of liquid-liquid extraction.



#### 4.2.2 Representative HPLC trace – common peaks identified

The following section concerns the optimisation of this <sup>11</sup>C-urea synthesis process, and it involves in depth discussions/comparisons of the radio-HPLC chromatograms of different crude reaction mixtures. Upon first inspection they can appear broadly similar, and so to facilitate this discussion a representative sample chromatogram will be presented. The major peaks will be identified and their significance (with respect to reaction optimisation) will be discussed.

The HPLC method in these cases was a standard reversed-phase C18 stationary phase, eluted with an isocratic solvent mixture (30% H<sub>2</sub>O / 70% MeCN), and the void time (the time at which unretained solvents are eluted, on the “solvent front”) in these cases was 2 minutes and 10 seconds after the sample injection. Additionally, for the purpose of identifying peaks by coinjection with a non-radioactive reference sample, it should be noted that in this system at 1 mL/min, there is a 20 second dead-time between the UV flow-cell and the radiation detector. Under these reversed-phase conditions, one would expect the best retained compounds (*i.e.* those eluting latest) to be the least polar compounds, and the compounds eluting close to the void time to be more polar/hydrophilic.

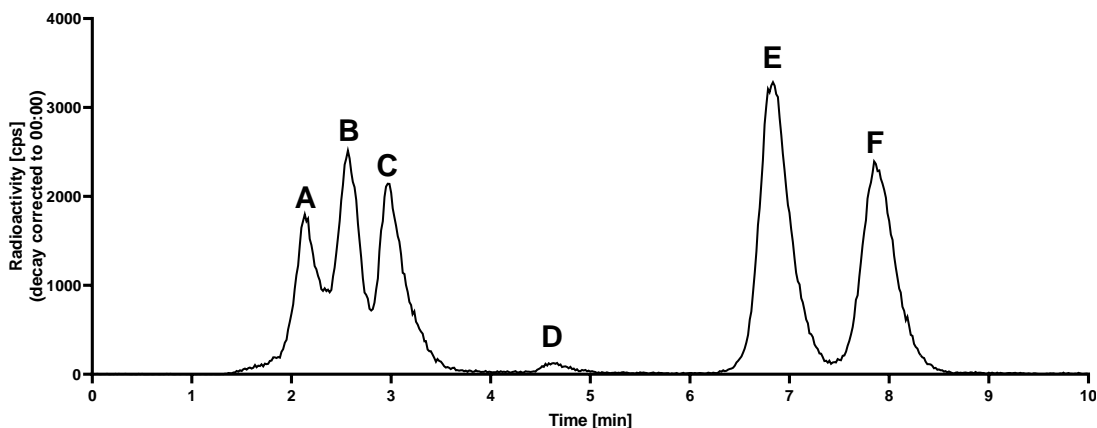


**Figure 4.3 Representative radio-HPLC chromatogram**

Crude reaction mixture from DBU/Mitsunobu-mediated synthesis of  $[^{11}\text{C}]\text{Glu-Glu-(O}^t\text{Bu)}_4$  via  $[^{11}\text{C}]\text{CO}_2$  fixation. The column used was an Agilent Zorbax Eclipse XDB-C18 (5  $\mu\text{m}$ , 4.6 x 150 mm), using a 1 mL/min isocratic elution method (30%  $\text{H}_2\text{O}$  / 70% MeCN). The void time of the system under these conditions was 2:10. The key peaks are labeled for reference.

As can be seen in the chromatogram above, the products of the reaction tend to fall into 2 major categories (**D** excluded, it will be discussed separately as it is a more minor impurity). **A**, **B**, and **C** generally elute within 2 minutes of the void time, suggesting that these are more polar/hydrophilic compounds, possibly even charged/ionised species. **E** and **F** by comparison elute significantly later, corresponding to significantly less polar compounds.

In this work these two categories can be broadly distinguished as either “trapped” or “fixed”  $[^{11}\text{C}]\text{CO}_2$ -derived products and the distinction between  $\text{CO}_2$  “trapping” and “fixation” in this work is subtle but important. The term “trapping” is used herein to refer to any process whereby the gaseous  $[^{11}\text{C}]\text{CO}_2$  is removed from the flow of helium carrier-gas and transferred into the reaction mixture; this could be by simple solvation ( $\text{CO}_2$  is only sparingly soluble in MeCN, but this is not insignificant when considering the general nanomolar scale on which carbon-11 radiochemistry operates) or by transformation into the other so-called “inorganic” carbon species (carbonic acid, bicarbonate, and carbonate ions). These contribute towards the total trapping efficiency of a solution by removing  $[^{11}\text{C}]\text{CO}_2$  from the gas stream, but they do not necessarily contribute to the

more-permanent covalent incorporation of the  $[^{11}\text{C}]\text{CO}_2$  into more complex organic molecules. This process, by comparison, is what is referred to herein as  $\text{CO}_2$  “fixation”. These are processes which, as well as removing the  $[^{11}\text{C}]\text{CO}_2$  from the gas stream, actually further incorporate the  $[^{11}\text{C}]\text{CO}_2$  into covalently-bonded organic compounds. For example in this work, the conversion of  $[^{11}\text{C}]\text{CO}_2$  into  $^{11}\text{C}$ -ureas constitutes a  $[^{11}\text{C}]\text{CO}_2$  fixation process.

The simple trapping products will tend to be highly polar and often (in the case of bicarbonate/carbonate ions) charged in solution. Therefore, it is expected that these products will be poorly retained on a reversed-phase column, and will accordingly elute early (*i.e.* with or shortly following the solvent front). This is the underlying rationale for the suggestion that peaks **A**, **B**, and **C** represent inorganic trapping products. In addition, this is supported by simple experiments whereby  $[^{11}\text{C}]\text{CO}_2$  is bubbled through vials containing only MeCN, or a solution of DBU in MeCN. Upon injection into the radio-HPLC, a single peak elutes with the solvent front, at 2:35. In these cases there is no possibility of a “fixation” product forming, as there are no nucleophilic amines present in solution. The only realistic possible identities of these peaks are either dissolved  $[^{11}\text{C}]\text{CO}_2$  or a bicarbonate species formed by reaction with adventitious water (a process which would be enhanced in the presence of the strongly basic DBU). The specific identities of these three peaks are difficult to speculate upon however, since these species tend to be more transient in solution, and some even exist in an equilibrium with one another. Furthermore, the water present in the HPLC mobile phase means that these specific observed peaks may not necessarily be indicative of the exact species actually present in the nominally anhydrous reaction solution, and it is more useful to just recognise these as “trapping” species, but to avoid the temptation to individually analyse these in any great depth.

Another revealing experiment was the gas-purging of the final reaction solvent. This involved an otherwise standard synthesis of  $[^{11}\text{C}]\text{Glu-Glu}(\text{O}^t\text{Bu})_4$ , but before radio-HPLC analysis, the solution was purged for several minutes with a stream of helium. The intention was that it would act to degas the solution and partially evaporate the reversibly “trapped”  $[^{11}\text{C}]\text{CO}_2$  products, while the significantly less volatile organic  $[^{11}\text{C}]\text{CO}_2$  fixation products would remain relatively unchanged. These were exactly the results

obtained, the relative percentage of total radioactivity retained in the reaction vial decreased (this loss of trapped radioactivity could be observed in real-time *via* the pin-diode detector on the E&Z system). Upon analysis of the resultant solution in the radio-HPLC, the relative percentage of radioactivity in peaks **A**, **B**, and **C** had dropped, and thus the relative amounts of radioactivity in the (less volatile, by our hypothesis) peaks **E** and **F** increased.

By comparison, the fixation products are less-polar small organic molecules, and would accordingly be expected to exhibit a better degree of retention on the C18 column. This is the underlying rationale for the suggestion that peaks **E** and **F** are organic fixation products. This is supported by the injection of the previously synthesised non-radioactive reference urea compound **Glu-Glu-(O<sup>t</sup>Bu)<sub>4</sub>**, which elutes with a retention time (in the UV trace) of 6:30, which corresponds exactly to the 6:50 elution (in the radiation trace) of peak **E**. It could therefore be said with some confidence that this peak corresponds to our desired symmetrical <sup>11</sup>C-urea product.

The identity of **F** was somewhat more difficult to confirm with certainty, although the general absence of significant possible side-reactions in this case (the absence of other amines precluding the formation of any asymmetric urea products) made it relatively easy to speculate regarding its identity. Under most screened conditions (as will be seen) **F** is formed in significant quantities and it has a similar retention time to the urea product, although it is slightly less polar still. Our initial speculation was that this was the intermediate <sup>11</sup>C-isocyanate. This would fit with the observed retention on C18, since it still bears the highly lipophilic *tert*-butyl ester groups as in the urea compound, but where the urea can act as a hydrogen-bond donor and acceptor, the isocyanate can only accept hydrogen bonds. This would possibly lead to a degree more retention under these reversed-phase conditions.<sup>478</sup> Additionally, as will be revealed and discussed in depth in the following sections, the relative amounts of **F** present in the reactions decreased as reaction times and temperatures increased, suggesting that this was a reaction intermediate, and not a product formed from the degradation of the urea **E** (if this were the case, one would expect increased time/temperature to result in the increased formation of **F**). One final confirmation of this is the observation that the relative amount of **F** decreases further-still as the stoichiometry (relative to the amine substrate) of Mitsunobu

reagents decreases. Where there is a relative excess of Mitsunobu reagents, this would be expected to consume significant quantities of the amine substrate, reducing the amount that is available to react with the isocyanate intermediate, in-effect isolating this isocyanate by removing any amines with which it can form the desired urea. By reducing the quantity of the Mitsunobu reagents, more amine is free to react with the isocyanate and so the formation of the urea product is favoured. Again, in practice this is what is observed, decreasing the quantities of PBu<sub>3</sub>/DBAD results in an increased amount of **E** relative to that of **F**. Taken with the other evidence presented here, it can be said with some confidence that **F** corresponds to a reaction intermediate from the Mitsunobu process, and by our understanding of the reaction mechanism, this is most likely to be the corresponding <sup>11</sup>C-isocyanate.

Finally peak **D** must be discussed, although from our investigations it was not possible to speculate on its identity with much confidence. While it is observed in most experiments, it is rarely formed in amounts approaching even 1% of the total detected radioactivity. Setting aside for a moment the issues with inferring causal relationships from such small changes in yield (given the tiny quantities in which this is observed under any conditions), there were no discernible trends observed with changes in temperature, reaction time, or stoichiometry. It was therefore not possible to speculate in the same way as it was for peak **F**, the only information available to us was its degree of retention on the C18 HPLC column. Its retention time ( $t_R = 4:38$ ) suggests that it is significantly more lipophilic than the “trapping” products ( $t_R \sim 2-3$  min), but it is somewhat less lipophilic than the better characterised “fixation” products ( $t_R > 6$  min). The fact that it doesn’t elute from the column with the solvent front at around 2 min suggests that the compound at least has some significant interaction with the octadecyl stationary phase and so it seems likely that it is a neutrally-charged organic “fixation” product, as opposed to an inorganic carbon “trapping” species. The lesser degree of retention compared to these, however, suggests that the molecule is significantly more hydrophilic than **E** and **F**, possibly the intermediate <sup>11</sup>C-carbamic acid (or <sup>11</sup>C-carbamate salt). In any case, **D** is only present in very small quantities and so it is not significantly subtracting from the yield of the desired <sup>11</sup>C-urea product; therefore, identifying it is of less importance for the optimisation process.

Fully identifying (as far as was possible) the radio-HPLC chromatograms greatly helped in guiding the optimisation process, as a great deal of information could be extracted from a single analysis: informing us about multiple aspects of the [<sup>11</sup>C]CO<sub>2</sub> fixation step, as well as the subsequent Mitsunobu-mediated <sup>11</sup>C-urea synthesis. The peaks and their suggested identities are summarised in Table 4.1 below. Additionally, were this work to be extended, the synthesis could be run “carrier-added” with additional [<sup>12</sup>C]CO<sub>2</sub> added to the reaction to allow for more confident identification of the various peaks by mass-spectroscopic analysis.

**Table 4.1 Summary of major HPLC peaks and their assigned identities**

	<b>t<sub>R</sub></b>	<b>Identification</b>	<b>Trapping/Fixation</b>
<b>A</b>	<b>2:10</b>	<i>CO<sub>2</sub>/Carbonic acid/Bicarbonate/DBU-CO<sub>2</sub></i>	<b>Trapping</b>
<b>B</b>	<b>2:35</b>	<i>CO<sub>2</sub>/Carbonic acid/Bicarbonate/DBU-CO<sub>2</sub></i>	<b>Trapping</b>
<b>C</b>	<b>2:58</b>	<i>CO<sub>2</sub>/Carbonic acid/Bicarbonate/DBU-CO<sub>2</sub></i>	<b>Trapping</b>
<b>D</b>	<b>4:38</b>	<b>Glu-(O<sup>t</sup>Bu)<sub>2</sub>-CO<sub>2</sub><sup>-</sup> – Carbamate intermediate (?)</b>	<b>Fixation</b>
<b>E</b>	<b>6:50</b>	<b>Glu-Glu-(O<sup>t</sup>Bu)<sub>4</sub> – Symmetrical urea product*</b>	<b>Fixation</b>
<b>F</b>	<b>7:52</b>	<b>Glu-(O<sup>t</sup>Bu)<sub>4</sub>-NCO – Isocyanate intermediate</b>	<b>Fixation</b>

(?) indicates less certain assignments

\* indicates confirmation by coinjection with non-radioactive reference

### 4.2.3 General optimisation

The overall radiochemical yield of this reaction – the parameter which we were attempting to maximise here – is governed by two relatively separate factors. The first of these is the efficiency of the fixation process itself whereby the [<sup>11</sup>C]CO<sub>2</sub> traps on the amine substrate and is stabilised by DBU, forming the amidinium carbamate salt. This is measured by comparing the relative proportion of radioactivity in the earlier-eluting “trapping” peaks (**A**, **B**, and **C**) with that in the later-eluting “fixation” peaks (**E** and **F**). The second factor is the radiochemical efficiency of the Mitsunobu-mediated urea synthesis reaction. This proceeds by first converting the amidinium carbamate intermediate to form the isocyanate intermediate, **F**, which in turn reacts with a second molecule of amine to form the desired urea product, **E**. This is measured by comparing the relative quantities of radioactivity in these two peaks, where a more efficient reaction will result in a greater proportion of radioactivity in **E** *versus* **F**.

As will be seen in this section, under most circumstances the fixation efficiency remains roughly constant throughout the optimisation experiments. With roughly 70-90% of the initially produced [<sup>11</sup>C]CO<sub>2</sub> being incorporated into fixation products **E** and **F**. This consistently high fixation efficiency meant that the primary focus of our optimisation experiments was to improve the second of the two aforementioned factors: the radiochemical efficiency of the urea formation reaction. As discussed above, this is measured by the relative proportions of radioactivity in peaks **E** and **F**, and so unless stated otherwise, the example radio-HPLC traces in this section will be labeled with the percentages of these two peaks, relative to the total quantity of “fixed” radioactivity. This gives the best insight into the effects of any changes in conditions, by focusing on only the “fixation” peaks.

#### 4.2.3.1 Literature conditions

To begin this work, the initial conditions employed were those previously optimised by others in our laboratory in the course of their development of this Mitsunobu-based [<sup>11</sup>C]CO<sub>2</sub> fixation chemistry.<sup>226</sup> This method was developed using much simpler non-pharmacologically-relevant amine substrates, but it was shown to be relatively successful with a variety of both aliphatic and aromatic substrates, and so the possibility of success

in translating this method to our more-complex substrate seemed fairly promising on first inspection. The only modification made from this described literature method was the previously-discussed use of an additional equimolar 18.3  $\mu\text{mol}$  to deprotonate the precursor amine hydrochloride salt *in situ*, rather than producing the free-amine beforehand and using this to prepare the solution with DBU for radiochemistry. This meant that instead of just 3.4  $\mu\text{mol}$  of DBU in the reaction solution, 21.7  $\mu\text{mol}$  was added (18.3  $\mu\text{mol}$  to deprotonate the amine + 3.4  $\mu\text{mol}$  for fixation). The overall effect of this change was previously shown to have a negligible effect on the performance of the reaction, while vastly improving its operational simplicity.

Expt	Amine		DBU		Mitsunobu		Temp (°C)	Time (min)
	$\mu\text{mol}$	equiv.	$\mu\text{mol}$	equiv.	$\mu\text{mol}$	equiv.		
Lit. conditions	18.3	1	21.7	1.19	36.6	2	50	2

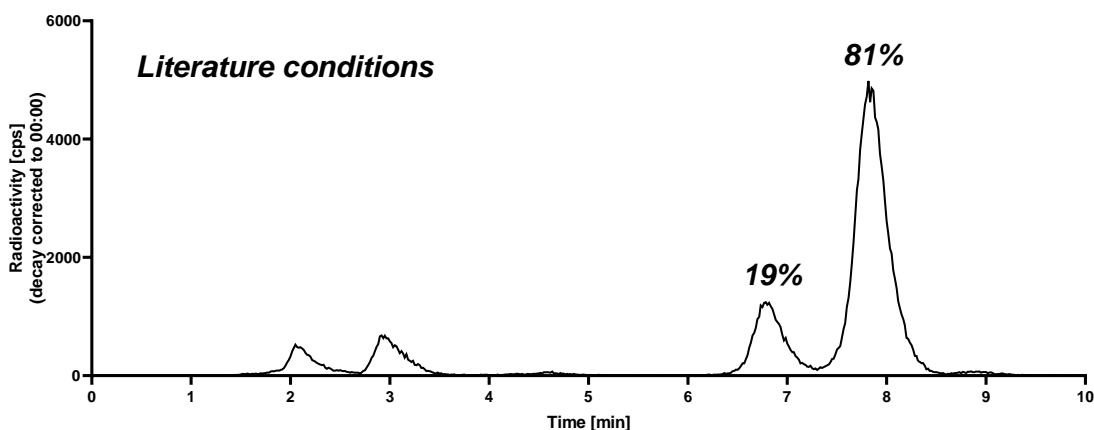


**Figure 4.4 Initial results – replication of literature conditions**

Radio-HPLC analysis of crude reaction mixture from DBU/Mitsunobu-mediated syntheses of [<sup>11</sup>C]Glu-Glu-(O<sup>t</sup>Bu)<sub>4</sub> via [<sup>11</sup>C]CO<sub>2</sub> fixation. Analysed using the standard isocratic method for this compound, as detailed in the methods section. The labeled percentages here refer to the relative abundances of these “fixation” products (i.e.  $t_R > 6$  min)

This replication of literature conditions had a moderate degree of success: 97% of the total carbon-11 radioactivity was retained within the vial and of this, 83% was converted into “fixation” products while the remainder was simply “trapped” in solution. The



fixation process was therefore highly successful, indicating that the amine substrate was sufficiently nucleophilic to form the initial  $^{11}\text{C}$ -carbamate fixation species and that the DBU was able to stabilise this long enough to allow further transformation. This was an initially encouraging observation for the first attempted radiosynthesis of this product.

The less impressive aspect of this reaction was the  $^{11}\text{C}$ -urea synthesis process, with only 19% of the fixed carbon-11 being incorporated into the desired  $^{11}\text{C}$ -urea product (peak **E**). The other 81% remained as the intermediate  $^{11}\text{C}$ -isocyanate, indicating that the reaction had not been able to proceed to completion. This was initially surprising since other  $^{11}\text{C}$ -ureas synthesised with this method had been produced with overall RCYs in excess of 70 %. While the cause for this disappointing yield was not initially obvious, a number of possible explanations were hypothesised.

Firstly, there was the possibility that the reaction had just not reached completion within the 2 min reaction time; the solutions in this case would involve raising the temperature to increase the rate of reaction, or simply extending the reaction time to allow the reaction to proceed further.

One alternative, more-complex explanation would be an unfavourable reaction stoichiometry. In these literature conditions, 2 equiv. of Mitsunobu reagents are used, compared with only 1 equiv. of the substrate amine; presenting a potential problem. This is similar to that encountered in the non-radioactive model reactions described in the previous section. Once the  $^{11}\text{C}$  is fixed as the carbamate salt, the Mitsunobu reagents are added to convert this to the isocyanate, but the unreacted Mitsunobu betaine that remains is still able to react with any other amines present in solution.<sup>238–240,479,480</sup> In this case, this will therefore compete with the newly-formed  $^{11}\text{C}$ -isocyanate for the remaining amine substrate. The 2:1 molar ratio of Mitsunobu to amine would be expected to favour the former (undesired) reaction, potentially at the cost of the intended  $^{11}\text{C}$ -urea forming process. This would result in the total consumption of the amine, leaving the intermediate  $^{11}\text{C}$ -isocyanate unable to proceed to the  $^{11}\text{C}$ -urea. To investigate this hypothesis, various different stoichiometries could be explored, by lowering the aforementioned molar ratio, to increasingly favour the latter reaction.

With a majority of the fixed carbon-11 in the form of a suspected reaction intermediate, the logical optimisation steps were first to attempt to drive the reaction further towards completion by increasing the reaction time and/or temperature. In addition to these steps, the reaction stoichiometry seemed a theoretically promising area for improvement over the standard literature conditions by allowing us to selectively favour the productive <sup>11</sup>C-urea forming reaction over an undesired side-reaction.

## 4.2.3.2 Effect of reaction time

Expt	Amine		DBU		Mitsunobu		Temp (°C)	Time (min)
	μmol	equiv.	μmol	equiv.	μmol	equiv.		
2 mins	18.3	1	21.7	1.19	36.6	2	50	2
10 mins	18.3	1	21.7	1.19	36.6	2	50	10

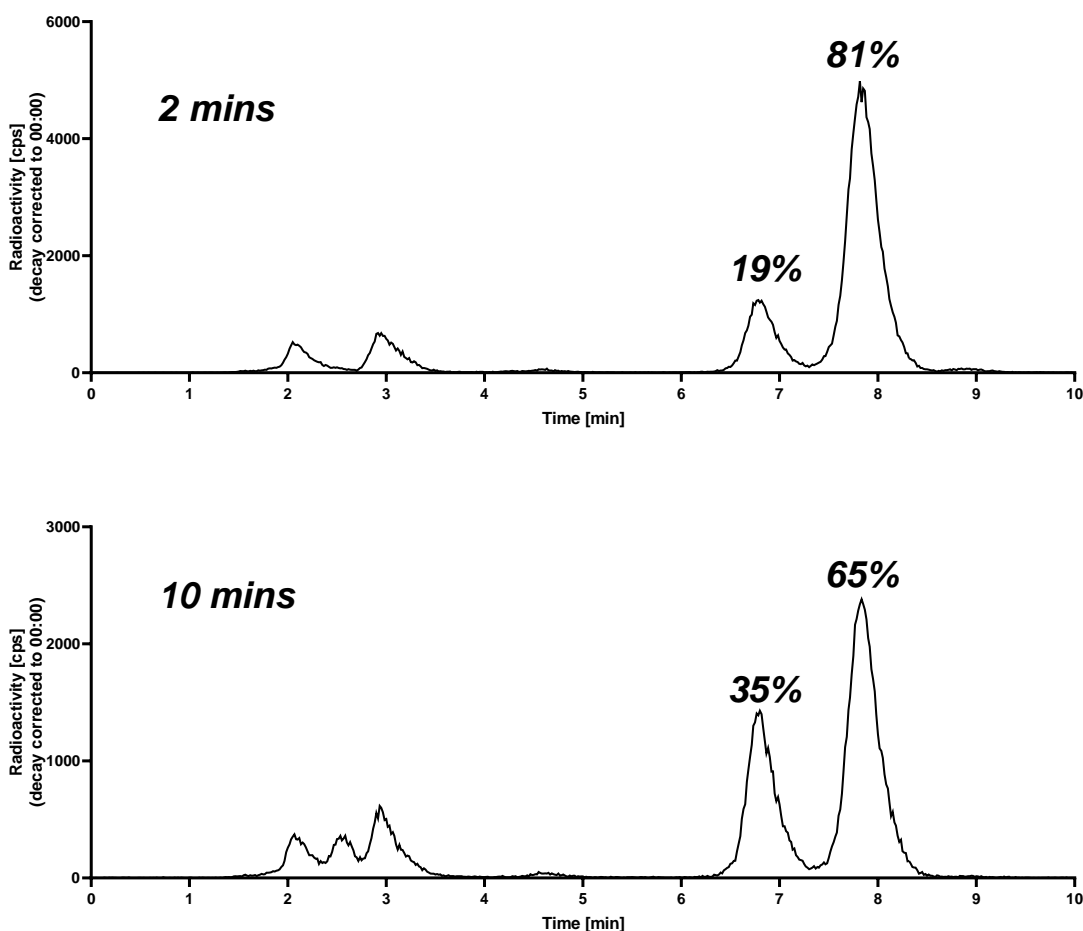


**Figure 4.5 Varying reaction time (after addition of PBU<sub>3</sub>/DBAD)**

Radio-HPLC analyses of crude reaction mixtures from DBU/Mitsunobu-mediated syntheses of [<sup>11</sup>C]Glu-Glu-(O<sup>t</sup>Bu)<sub>4</sub> via [<sup>11</sup>C]CO<sub>2</sub> fixation. Analysed using the standard isocratic method for this compound, as detailed in the methods section. The labeled percentages here refer to the relative abundances of these “fixation” products (i.e. t<sub>R</sub> > 6 min)

Increasing the reaction time from 2 to 10 minutes did result in an increased quantity of peak **E** relative to that of **F**. With a similar fixation efficiency in both cases (since the initial quantities of amine/DBU remained constant in both experiments), the resultant

overall RCY of the <sup>11</sup>C-urea was therefore improved as a result of the longer reaction time. It is important to bear-in-mind however, that RCY is a decay-corrected measure, and does not account for the radioactivity losses due to decay. As has been discussed elsewhere in this thesis, where a straightforward non-radioactive chemical reaction may benefit from greatly extended reaction times in an effort to maximise chemical yields, this does not always apply in the case of radiochemistry. The improvement in chemical efficiency must be sufficiently great to at-least compensate for the decay losses. The shorter the half-life of the radionuclide in question, the more this becomes a more pressing concern. In this case, with carbon-11's very short half-life ( $t_{1/2} = 20.4$  min), this is almost always an important consideration.

For these two examples, both involved the same 105 second [<sup>11</sup>C]CO<sub>2</sub> trapping period, but whilst one was reacted for a further 2 min, while the other was reacted for a further 10 min. This resulted in total synthesis times (from EoB) of approximately 4 and 12 min respectively, corresponding to a difference of 8 min between these two methods. Decay calculations tell us that for two radiolabeling reactions with otherwise identical RCYs, an additional 8 min reaction time corresponds to a 24% reduction in the final "real-world" radioactivity yield. This is a potentially significant difference arising from what could initially appear to be a small absolute difference in reaction time, and highlights the importance of considering radioactivity yield as well as RCY when optimising radiosyntheses.

In this case, the gain in RCY achieved by increasing the reaction time was so large that it did overcome the additional 24% loss due to decay, indicating that it could be of benefit to incorporate a longer reaction-time into the final optimised process. However, because of the unavoidable decay-losses, the decision was to initially attempt to optimise the other factors which do not incur such inherent drawbacks, and only if it was still deemed beneficial after other alterations would the reaction time be increased.

## 4.2.3.3 Effect of reaction temperature

Expt	Amine		DBU		Mitsunobu		Temp (°C)	Time (min)
	μmol	equiv.	μmol	equiv.	μmol	equiv.		
50°C	18.3	1	21.7	1.19	36.6	2	50	10
80°C	18.3	1	21.7	1.19	36.6	2	80	10

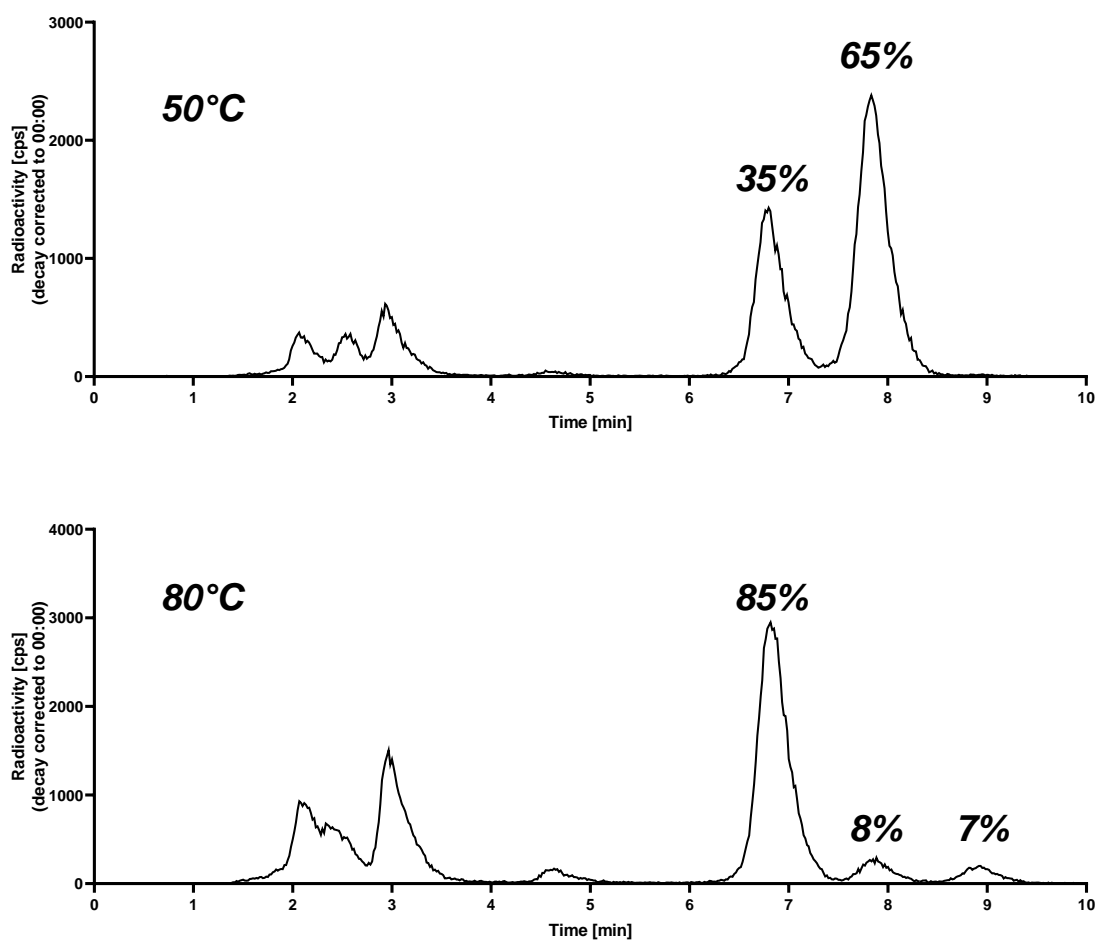


**Figure 4.6 Varying reaction temperature**

Radio-HPLC analyses of crude reaction mixtures from DBU/Mitsunobu-mediated syntheses of [<sup>11</sup>C]Glu-Glu-(O<sup>t</sup>Bu)<sub>4</sub> via [<sup>11</sup>C]CO<sub>2</sub> fixation. Analysed using the standard isocratic method for this compound, as detailed in the methods section. The labeled percentages here refer to the relative abundances of these “fixation” products (i.e. t<sub>R</sub> > 6 min)

Increasing the reaction temperature from 50°C to 80°C led to a significantly improved conversion of the fixed carbon-11 into the desired <sup>11</sup>C-urea product. At 50°C for 10 min,

the reaction was still less than halfway to completion, with the <sup>11</sup>C-urea representing only 35% of the fixation products. By increasing the reaction temperature to 80°C, the reaction had reached 85% conversion in the same time-frame. This was highly promising, and further supported the suggestion that peak **F** was the intermediate <sup>11</sup>C-isocyanate, as implementing these more forcing reaction conditions served to reduce its relative population in the final reaction mixture, this would be expected were this peak an intermediate instead of a product resulting from the degradation of the <sup>11</sup>C-urea.

One final aspect worthy of comment is the extra peak (eluting after peak **F** at approx. 9 min) seen only in this elevated temperature/extended time reaction. While it is only formed in small amounts (7% of the fixed carbon-11) it was an unexpected observation. As it was not observed in amounts exceeding even 1% abundance under other conditions, less attention was paid to this peak, but it is possible to speculate upon its identity. One suggestion was that this could possibly be a <sup>11</sup>C-biuret (also commonly referred to as a carbamylurea), a molecule with an [RN(H)C(O)]<sub>2</sub>NR motif which could result from the reaction of a urea with an isocyanate and have been encountered during urea syntheses at elevated temperatures.<sup>427,481</sup> In any case, this byproduct was only observed under the harshest conditions we employed (80°C for 10 min), therefore it was not investigated further.

## 4.2.3.4 Mitsunobu stoichiometry

Expt	Amine		DBU		Mitsunobu		Temp (°C)	Time (min)
	μmol	equiv.	μmol	equiv.	μmol	equiv.		
2 equiv.	18.3	1	21.7	1.19	36.6	2	50	2
1 equiv.	18.3	1	21.7	1.19	18.3	1	50	2

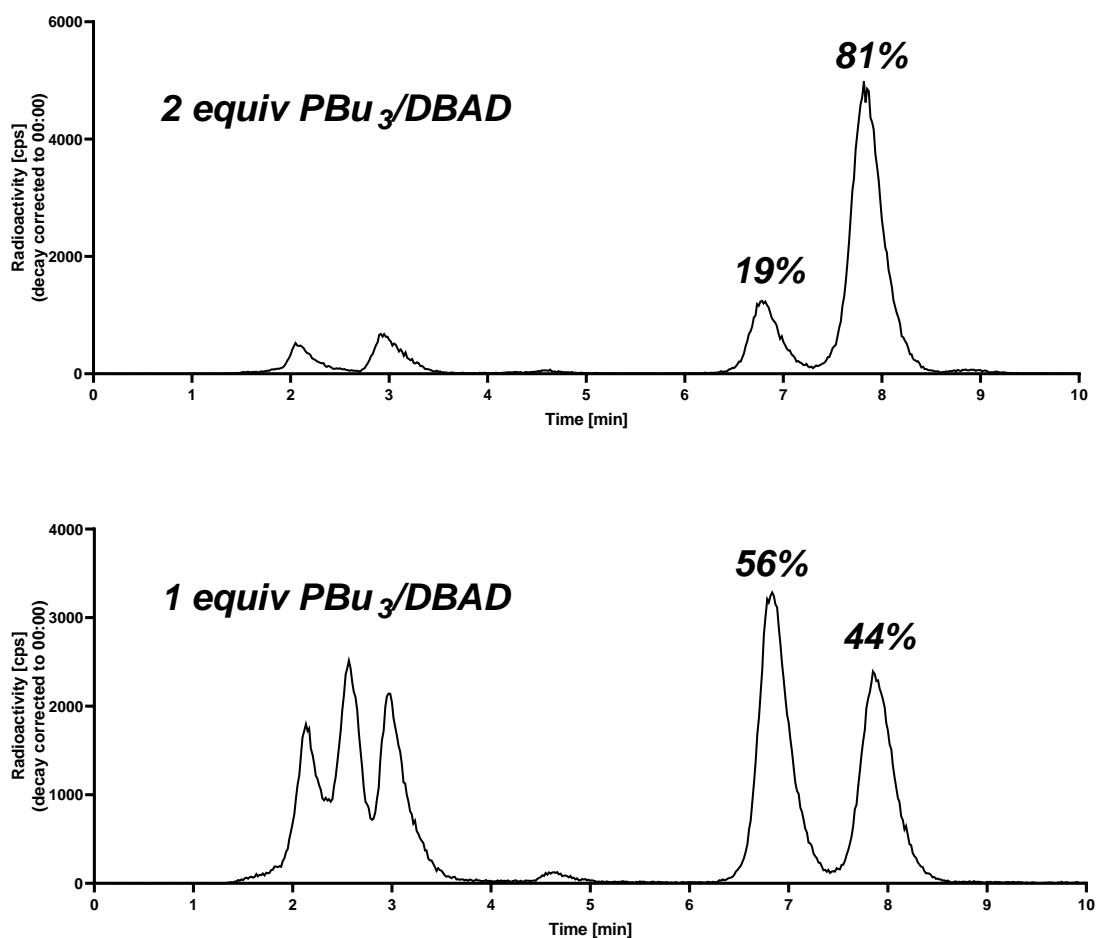


**Figure 4.7 Varying reagent stoichiometry**

Radio-HPLC analyses of crude reaction mixtures from DBU/Mitsunobu-mediated syntheses of [<sup>11</sup>C]Glu-Glu-(O<sup>t</sup>Bu)<sub>4</sub> via [<sup>11</sup>C]CO<sub>2</sub> fixation. Analysed using the standard isocratic method for this compound, as detailed in the methods section. The labeled percentages here refer to the relative abundances of these “fixation” products (i.e. t<sub>R</sub> > 6 min)

Addressing our concerns regarding the 2:1 Mitsunobu:amine stoichiometry, we compared the literature conditions to those employing half of the amount of Mitsunobu reagents (a

1:1 stoichiometric ratio). The results were clear, by reducing the amount of Mitsunobu betaine present in solution, we were able to achieve an improved conversion of the <sup>11</sup>C-isocyanate into the <sup>11</sup>C-urea (19% conversion for 2:1 *versus* 56% conversion for 1:1). This was encouraging evidence supporting the theory that the betaine was competing with the <sup>11</sup>C-isocyanate to react with the amine. By reducing the relative amount of betaine present, we were able to preferentially promote the reaction of the amine with the <sup>11</sup>C-isocyanate over the undesired and unproductive side-reaction between the betaine and the amine substrate. This was a highly promising result for this optimisation exercise and also served to validate our mechanistic understanding of this Mitsunobu-based <sup>11</sup>C-urea synthesis method.

Interestingly, we did note a reduction in the fixation efficiency of the reaction with more of the carbon-11 simply trapping, as opposed to being incorporated into the desired fixation products. This was a surprising result, because the initial fixation step (bubbling [<sup>11</sup>C]CO<sub>2</sub> through a solution of amine and DBU) was identical for both of these experiments. Perhaps a lowered concentration of the Mitsunobu betaine in solution could have meant that the conversion of <sup>11</sup>C-carbamate to <sup>11</sup>C-isocyanate was slower, and therefore there was increased opportunity for the less-stable <sup>11</sup>C-carbamate salt to undergo decarboxylative degradation, re-releasing the [<sup>11</sup>C]CO<sub>2</sub> back into solution. But despite our investigations, we were unable to support this with any additional data, and it was ultimately decided to ensure that this was accounted for when deciding which method was considered “optimal”.



## 4.2.3.5 DBU quantity

Expt	Amine		DBU		Mitsunobu		Temp (°C)	Time (min)
	μmol	equiv.	μmol	equiv.	μmol	equiv.		
3.4 μmol	18.3	1	21.7	1.19	9.2	0.5	80	2
6.8 μmol	18.3	1	25.1	1.37	9.2	0.5	80	2

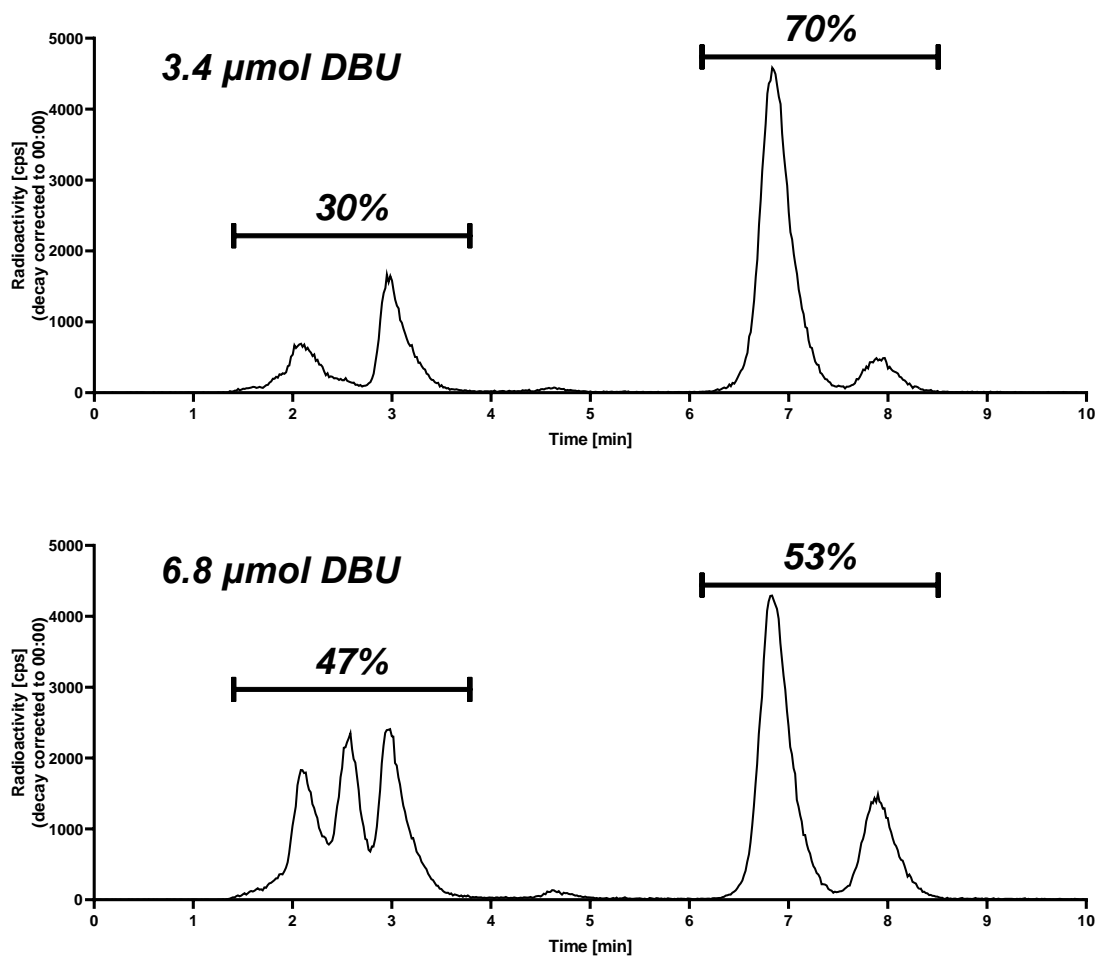


**Figure 4.8 Varying DBU amount**

Radio-HPLC analyses of crude reaction mixtures from DBU/Mitsunobu-mediated syntheses of [<sup>11</sup>C]Glu-Glu-(O<sup>t</sup>Bu)<sub>4</sub> via [<sup>11</sup>C]CO<sub>2</sub> fixation. Analysed using the standard isocratic method for this compound, as detailed in the methods section. Unlike in other comparisons in this section, the percentages here refer to the relative quantities of “trapping” and “fixation” products. This helps demonstrate that additional DBU does not lead to increased [<sup>11</sup>C]CO<sub>2</sub> “fixation”, but in fact shifts the balance more in favour of the less-favourable “trapping” products.

The final investigation regarded the quantity of DBU used for fixation. Until this point, 3.4  $\mu\text{mol}$  of DBU had been used to mediate the  $[^{11}\text{C}]\text{CO}_2$  fixation process, as this was the optimal amount used in the literature method. We were interested to know whether for our application, increasing the amount used would have any significant effect on driving the  $[^{11}\text{C}]\text{CO}_2$  fixation efficiency beyond the 70% value we had obtained thus far. The quantity of DBU was doubled from 3.4 to 6.8  $\mu\text{mol}$ s, but the inverse effect was observed: the fixation products (as a percentage of the total radioactivity in solution) decreased. The original solution containing 3.4  $\mu\text{mol}$  DBU exhibited a 30% trapping and 70% fixation distribution, but upon doubling the DBU content to 6.8  $\mu\text{mol}$ , the fixation performance dropped, exhibiting a 47% trapping and 53% fixation distribution.

This result suggested that the 3.4  $\mu\text{mol}$  (0.19 equiv) DBU was already more than sufficient to mediate  $[^{11}\text{C}]\text{CO}_2$  fixation on the amine, which is in fact consistent with our understanding of the mechanism. DBU acts stoichiometrically to stabilise the initially-formed  $^{11}\text{C}$ -carbamic acid by deprotonation and subsequent formation of the amidinium  $^{11}\text{C}$ -carbamate salt. Therefore – even allowing for a particularly poor molar activity – at most  $\sim 1$   $\mu\text{mol}$   $[^{11/12}\text{C}]\text{CO}_2$  would be introduced into the vial, meaning that the 3.4  $\mu\text{mol}$  DBU is in a significant excess. As has already been shown elsewhere in this thesis and in the literature, it would appear that DBU itself is also capable of interacting directly with  $\text{CO}_2$  in some manner (perhaps forming a charged carbamate species of its own, which we would expect to elute within the “trapping” region on the HPLC), and this stoichiometric excess of DBU could therefore possibly be competing with the amine substrate for the available  $\text{CO}_2$  during the fixation stage of the reaction. Were this true, an increase beyond this 3.4  $\mu\text{mol}$  quantity would simply add to the excess (competing) DBU quantity, resulting in a relative drop in the efficiency of the desired fixation reaction with the amine. Conversely, if DBU was acting as a catalyst which traps  $[^{11}\text{C}]\text{CO}_2$  and acts to transfer it to the amine (as has been suggested previously), then one could possibly expect an increased concentration of DBU to result in a higher fixation efficiency (within a given time). This evidence seems to support our understanding of the reaction mechanism, and demonstrates that increasing the relative quantity of DBU in a given fixation reaction does not necessarily guarantee an improved  $[^{11}\text{C}]\text{CO}_2$  fixation efficiency, in fact the opposite seems to be the case.

This conclusion does potentially raise the question of whether the amount of DBU could be lowered further still, to improve the fixation efficiency by reducing the amount of excess DBU competing with the amine for the CO<sub>2</sub>. This has yet to be fully explored in our hands, but would be a compelling future investigation to shed yet-more light on the operating principles of this chemistry.

## 4.2.3.6 Optimised conditions

Expt	Amine		DBU		Mitsunobu		Temp (°C)	Time (min)
	μmol	equiv.	μmol	equiv.	μmol	equiv.		
Literature	18.3	1	21.7	1.19	36.6	2	50	2
Optimised	18.3	1	21.7	1.19	9.2	0.5	80	2

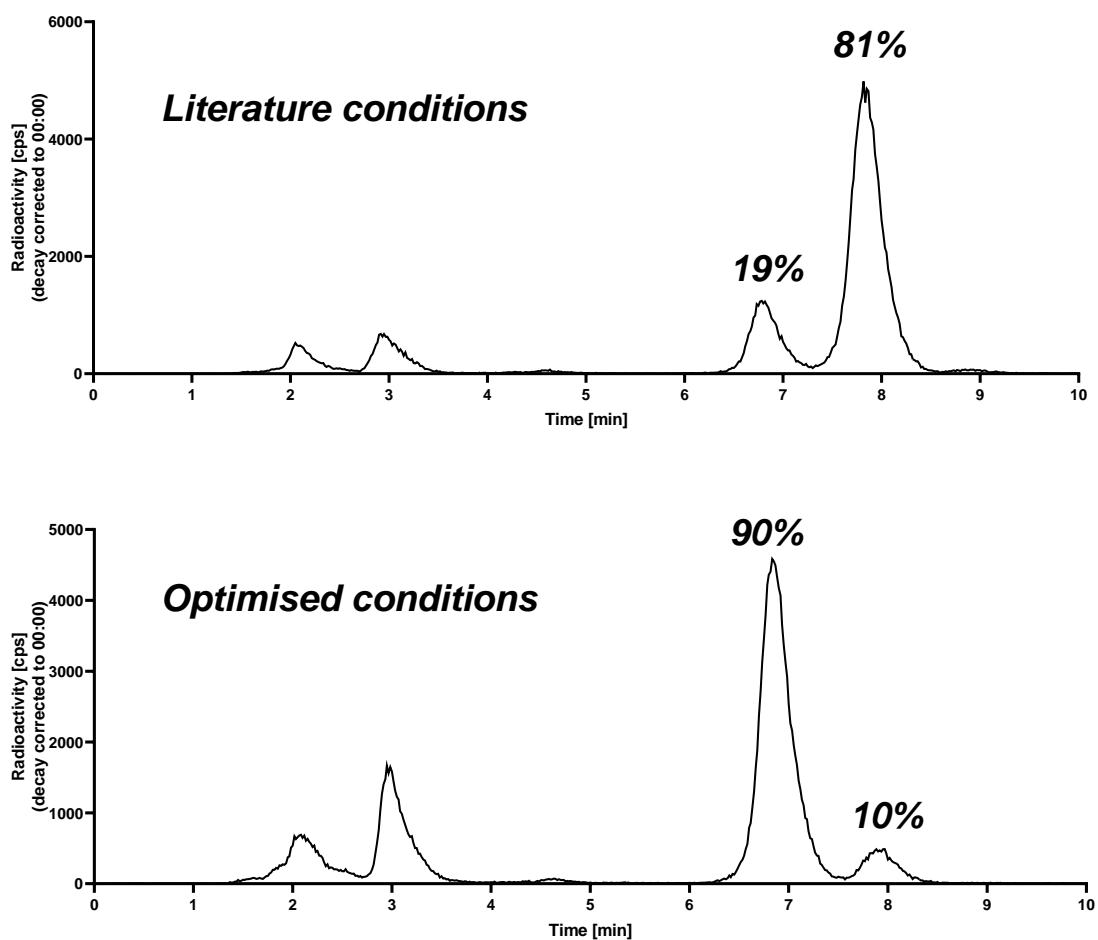


**Figure 4.9 Original conditions from literature versus final optimised conditions**

Radio-HPLC analyses of crude reaction mixtures from DBU/Mitsunobu-mediated syntheses of [<sup>11</sup>C]Glu-Glu-(O<sup>t</sup>Bu)<sub>4</sub> via [<sup>11</sup>C]CO<sub>2</sub> fixation. Analysed using the standard isocratic method for this compound, as detailed in the methods section. The labeled percentages here refer to the relative abundances of these "fixation" products (i.e. t<sub>R</sub> > 6 min)

Following the principles established in these optimisation experiments, the optimal conditions arrived at were: 18.3 μmol amine (1 equiv), 21.7 μmol DBU (1.19 equiv), 9.2 μmol Mitsunobu reagents (0.5 equiv), at 80°C for 2 min. Compared to the “literature conditions”, this represented a reduction in the quantity of Mitsunobu reagents used, as well as an increase in reaction temperature. The reaction under these conditions gives a (radio-HPLC determined) RCP of 60%, with 93% of the total [<sup>11</sup>C]CO<sub>2</sub> being retained in this solution, giving an overall RCY of 56% (decay-corrected, non-isolated). In addition, because the reaction was so quick, being complete within 4 min from EoB, this resulted in an impressive 49% radioactivity yield (non-isolated). By comparison, the equivalent radioactivity yield obtained using the original literature conditions was just 13%, so this optimisation process clearly represents a major improvement.

It should be noted that the earlier optimisation experiments showed a benefit to the <sup>11</sup>C-isocyanate (**F**) to <sup>11</sup>C-urea (**E**) conversion efficiency by increasing the duration of reaction, but in our final conditions, a 2 min reaction time is still used. This is due to the aforementioned offsetting competition between chemical efficiency and radioactive decay. The additional 8 minutes of reaction time corresponds to a further 24% drop in “real-world” radioactivity yield, and so the resultant increase in conversion must be sufficiently large to outweigh this loss due to decay. In the prior example, the efficiency of the poorly-optimised reaction increased from 19% to 31% in switching from a 2 to 10 min reaction; so even with accounting for radioactive decay, there was still a benefit to extending the time of reaction. By comparison, these better-optimised conditions meant that even if the <sup>11</sup>C-isocyanate to <sup>11</sup>C-urea conversion was improved all the way from 90% to 100% efficiency with a 10 min reaction, this would not be sufficient to overcome the losses due to decay. Where the 90% efficient conversion of the 2 min reaction results in a “real world” radioactivity yield of 49%, the hypothetical 100% efficient conversion of a 10 min reaction would result in an inferior “real world” radioactivity yield of 43%. Hence our decision to remain with a less chemically-efficient but more radiochemically-efficient 2 min reaction time. This is an example of the offsetting competition between chemical yield and radiochemical yield that was discussed in section 1.2.2.2 (page 19).

### 4.3 Results & Discussion – HILIC: an alternative to RP-HPLC?

#### 4.3.1 Why HILIC?

Now that a reliable and efficient method had been developed for the radiosynthesis of the *tert*-butyl ester protected urea ( $[^{11}\text{C}]\text{Glu-Glu-(O}^t\text{Bu)}_4$ ), the next step was the deprotection of this intermediate: removing the *tert*-butyl ester groups to yield the free carboxylic acid moieties. An HPLC analysis would be required to confirm and quantify the results of this deprotection reaction, so this section focuses on the development of this analytical method.

As has become largely routine for the majority of carbon-11 radiosynthesis, the initial intention was to develop an analytical method using a standard reversed-phase C18 HPLC column. These columns are robust, widely available, and the retention mechanisms are well understood; which usually means that method development using these stationary phases is a relatively straightforward process. The dominant feature governing a compound's retention is its lipophilicity, as this gives rise to its preferential affinity (by adsorption/partition) for the nonpolar octadecyl stationary phase over that of the more polar aqueous mobile phase. In general, the mobile phase is a two-component solution of an aqueous “weak” solvent (usually pure water or a buffer), with an organic modifier (commonly MeCN or MeOH) as the “strong” solvent. For a given C18 column, the greater the relative aqueous content of a mobile phase, the stronger the compounds will be retained on the stationary phase (therefore eluting later). By increasing the “strength” of this mobile phase (by increasing the relative organic content), the same compound will elute from the column earlier, due to a decreased retention on the stationary phase. Following this general principle, HPLC elution profiles can be rationally designed in a fairly straightforward manner to allow adequate resolution of peaks of interest, while ensuring retention times are otherwise kept to a minimum (particularly crucial for radiochemists, for whom radioactive decay is a primary concern). For the majority of organic small-molecule radiotracers, the compounds of interest will exhibit a sufficient degree of lipophilicity/hydrophobicity so as to allow some retentive interactions with the stationary phase, and so reversed-phase HPLC is usually sufficient for the separation and identification of products and byproducts of these radiolabeling reactions. This was clearly demonstrated in our optimisation of the <sup>11</sup>C-urea synthesis step, where the *tert*-

butyl ester protected intermediate was well retained ( $t_R = 6:50$ ) even under a relatively strong isocratic elution regime (30% H<sub>2</sub>O / 70% MeCN / 0.1% TFA v/v).

Our efforts to develop such a reversed-phase HPLC method for the identification/purification of the deprotected [<sup>11</sup>C]Glu-Glu (a tetracarboxylic acid) were entirely unsuccessful. The previously-synthesised non-radioactive standard was initially screened across a range of isocratic elution profiles ranging from the strongest composition, 50:50 (H<sub>2</sub>O:MeCN with 0.1% TFA), up to the significantly weaker 98:2 composition without any success. In all cases, the compound eluted with the “solvent front” at the column’s void time of approx. 2:10 at 1 mL/min: the compound would not retain on the stationary phase at all, at even the weakest permissible solvent composition. Running standard C18 columns such as ours in 100% aqueous phases is not advised due to the risk of column dewetting (also previously referred-to as phase collapse). This can result in a general loss in the column’s retention of analytes, poor reproducibility, and a general overall degradation of chromatographic performance.<sup>482–485</sup> Therefore, it was clear that standard C18 reversed-phase chromatography would be insufficient for our purposes due to insufficient retention of our target compound under even the most favourable conditions permissible.

The likely explanation for this poor retention on the highly non-polar reversed-phase stationary phase is the highly polar nature of the deprotected symmetrical glutamate urea. It is a highly compact tetracarboxylic acid, lacking much in the way of any hydrophobic character, and at neutral pH, the acidic groups would be expected to be largely dissociated with the compound existing in its ionised carboxylate form. Even with the addition of 0.1% TFA (v/v) to reduce the mobile phase pH to ~ 2 – which would be expected to fully protonate these acidic groups, rendering an uncharged compound – it does not sufficiently retain on the C18 column. Therefore, an alternative column stationary phase was required.

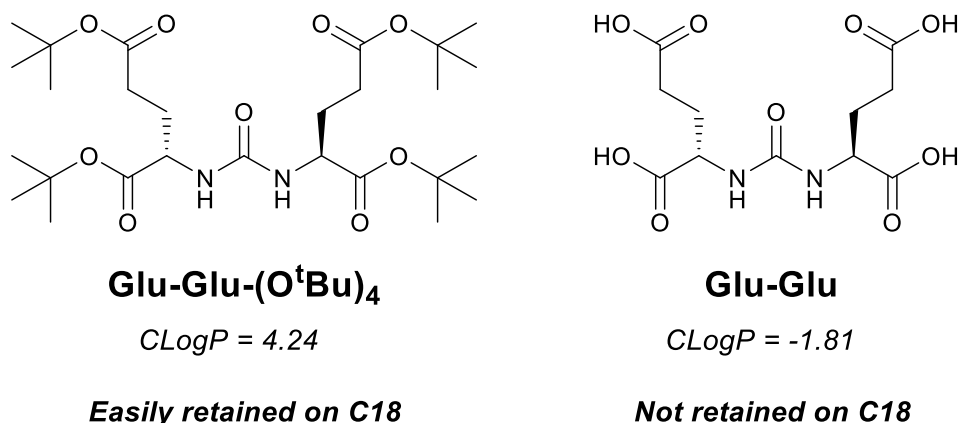


**Figure 4.10 Comparison of *tert*-butyl ester and free acid lipophilicities**

CLogP values calculated with ChemDraw software, used to simply demonstrate the significant difference in the compounds' lipophilicities before and after ester hydrolysis. Tertiary butyl moieties confer a significant degree of lipophilicity to the protected intermediate, allowing it to retain much better on the reversed-phase HPLC column than the deprotected product.

Upon consultation with Phenomenex, a suggested alternative approach was to use a HILIC (hydrophilic interaction liquid chromatography) column. To briefly summarise HILIC, it can be described as roughly the opposite of reversed-phase chromatography (but should also be distinguished from normal phase chromatography as will be discussed shortly). The stationary phase of our Luna HILIC column is a porous silica support with a bonded dihydroxypropane diol coating, instead of the bonded octadecyl chains seen in C18 columns. This means that the stationary phase of HILIC columns is significantly more polar, and so equilibrating the column with a mixed water/acetonitrile solvent system establishes a relatively fixed layer of water coating this polar surface.<sup>486–491</sup> In effect, this means that in HILIC, the effective stationary phase is actually this immobilised water layer. As a result, the mixed water/acetonitrile mobile phase is less polar than the stationary phase, and so in general, the order of retention seen in HILIC elutions is flipped from what would be expected in reversed-phase chromatography. Compounds which do not retain well on C18 columns will be strongly retained on HILIC columns (and *vice versa*); MeCN becomes the weak solvent, with water now becoming the strong solvent capable of driving the elution of more strongly retained analytes.



It should be noted that this flipped polarity (polar stationary-phase and less-polar mobile phase) is similar to that seen in “normal-phase” chromatography, which is another option for polar analyte retention – in fact, the same columns can theoretically be used in normal-phase and HILIC modes – but there is one key difference: the mobile-phase composition. In normal phase chromatography, the polar stationary phase (often bare silica) is eluted with pure organic solvents without any added water, compared to the significant aqueous content (>50%) of HILIC mobile phases. As a result, there is no immobilised aqueous layer to act as a pseudo-stationary phase as in HILIC, instead in normal-phase chromatography the analyte directly interacts with the polar stationary phase. Consequently, small amounts of water contamination in the organic mobile phase can significantly affect a compound’s retention behaviour in a normal-phase elution, and can lead to much more difficult-to-reproduce analytical methods than reversed-phase or HILIC methods. In addition, the bare silica columns often used for normal-phase chromatography can be much more susceptible to chemical degradation and so these columns are much less robust compared to the bonded and endcapped phases common in reversed-phase and HILIC. HILIC is in-effect a more-refined and better-controlled alternative to normal-phase chromatography.

In any case, because of this improved retention of polar and ionised analytes, HILIC has become increasingly widely applied in fields such as metabolomics; it easily allows chromatographic resolution of multiple structurally-similar and highly-polar metabolites, an application which would be significantly more challenging for a standard reversed-phase technique.<sup>492</sup> Encouraged by these metabolomic applications, as well as other examples of the successful application of this technique to the separation of similar polycarboxylic compounds,<sup>493,494</sup> this was the approach decided upon for our purposes.

### **4.3.2 Role of buffers in HILIC**

Compared with the predominant lipophilic retention mechanism for reversed-phase HPLC, HILIC has multiple retention mechanisms which can contribute to an analyte’s retention. While the major retentive interaction is a hydrophilic interaction between the polar analyte and the immobilised water-layer (hydrogen-bonding as well as dipolar interactions), there is also the contributing potential for the same hydrogen-bonding and dipolar interactions between the analyte and the bonded diol phase, as well as potential

ion exchange electrostatic interactions (repulsive/retentive) with the underlying silica (which can be deprotonated depending on mobile phase pH). The strength of these retentive polar interactions will consequently increase if a compound bears a charge, which can result in a strongly pH-dependent retention behaviour for acidic/basic analytes. To ensure consistency therefore, the vast majority of HILIC methods are buffered to control the pH. The manufacturers of our column recommend the use of either ammonium formate (pH 3.2) or ammonium acetate (pH 5.8) buffers of at least 5mM ionic strength. Unlike in C18, where using TFA or formic acid in the mobile phase is generally sufficient to control ion speciation – true salt-based buffers are required to give reproducible polar analyte retention. In addition to the pH control that a buffer gives, its ionic strength (salt concentration) must also be carefully controlled to ensure reproducibility.

One reason for this is the potential for electrostatic ion-exchange-type interactions between charged analytes and the stationary phase's underlying silica support. In our column (as with most non-encapped HILIC columns), while the majority of the silica support is coated with a neutrally charged polymeric crosslinked diol phase, a significant quantity of the underlying silica remains exposed. The acidic silanols (pKa ~ 4.4) on the silica surface will be partially dissociated in the suggested ammonium formate buffer (pH 3.2) and will be almost fully dissociated in the ammonium acetate buffer (pH 5.8). This underlying exposed silica can give these columns a degree of cation-exchange behaviour: positively charged analytes will be more-strongly retained due to positive electrostatic interactions, whereas negatively charged analytes will experience a contrasting repulsive force, decreasing their retention on the column.<sup>491,495,496</sup> This effect is moderated by the buffer: the ammonium cation associates with the negatively charged silica surface, forming – in effect – an electrical double layer on the silica surface which shields the analytes from directly interacting with the charged stationary phase. However, experimental data suggests that even on nominally “neutral” but non-encapped HILIC stationary phases (such as ours), this double layer is only saturated at buffer concentrations exceeding 20-40 mM.<sup>491,497</sup> As a result, at concentrations lower than this, the retention of charged analytes can be strongly dependent on buffer concentration.

Additionally, it is well documented that at low salt concentrations (such as the millimolar range in which HILIC operates), small changes in salt concentration can act to modulate

a molecule's aqueous solubility (either "salting-in" or "salting-out").<sup>498</sup> Although accurate prediction of the direction of this effect can be difficult; it depends on the specific combination of the salt and analyte, due to a number of competing mechanisms contributing to this behaviour. In any case, modulating the buffer's ionic strength can have a resultant effect on the analytes' ability to partition into the aqueous stationary phase; ultimately meaning that an analyte's retention in HILIC can be strongly dependent on the ionic strength of the mobile phase.<sup>491,495,499</sup>

Finally, whilst in this case the use of buffers with non-ammonium cations is not recommended by Phenomenex (possibly due to the poorer organic solubility of sodium and potassium based buffers), it is known in general that the nature of this cation can strongly affect a compound's retention on a HILIC column.<sup>491</sup> This can be due to differences in the cations' abilities to titrate the negative charge of the non-encapped silica stationary-phase, or possibly due to direct interaction with charged moieties on the analyte itself. Alpert has demonstrated that well hydrated counterions promote partitioning of charged analytes into the aqueous pseudo-stationary-phase better than poorly hydrated counterions.<sup>491</sup> Consequently, it is possible to explore the use of better hydrated counterions than  $[\text{NH}_4]^+$  such as  $\text{Na}^+$  or  $\text{K}^+$ ,<sup>500</sup> to further modify analyte retention.

The end result is that while buffers are crucial for the control of ionic speciation of the analyte due to the predominant hydrophilic retention mechanism in operation, small variations in buffer concentration (even at the same pH) can result in large variations in the analyte retention as a result of minor but contributory electrostatic retention mechanisms. As such, when developing any methods for HILIC, care must be taken to ensure highly-consistent buffer concentrations to guarantee reproducible chromatography.

### 4.3.3 Ammonium formate (pH 3.2)

The aim for our elution method was to achieve an analyte retention time in approximately the 6-10 min range. Longer than ~ 6 min would ensure that the analyte was sufficiently resolved from the “solvent front” void peak at approx. 2 min (where the non-polar protected intermediate would elute), guaranteeing a significant chromatographic interaction with the stationary phase. Keeping the retention to under ~ 10 min avoids inconveniently long analyses, mitigates losses due to radioactive decay, and minimises the peak broadening which results from longitudinal diffusion. This latter process is the phenomenon whereby analyte molecules moving slower or faster than the average analyte velocity along the longitudinal direction of a column leads to peak broadening. This effect is cumulative, and the longer a compound resides in the column, the broader its peak becomes as a result of increased longitudinal diffusion. This is particularly observed in isocratic chromatography because it lacks the “focusing” effect that a gradient elution can introduce. Because of the need to balance these offsetting concerns, the intermediate 6-10 min range was our initial “target” range for analyte elution.

In screening experiments from 100% **B** through to 50% **B** isocratic elutions, the product eluted with the solvent front ( $t_R = 2:05$ ), and it was only on further decreasing the composition strength to 40% **B** that it was first retained on the column to a small degree ( $t_R = 2:30$ ). This elution so close to the void peak was still not ideal (for the aforementioned reasons) and so the composition strength was decreased further to 20% **B** ( $t_R = 3:30$ ) and then to 10% **B** ( $t_R = 8:40$ ). At this point, the analyte’s retention time was within the target region and so this theoretically should have been an acceptable isocratic method for the identification and quantification of our target radiolabeled compound. However, the product peak was excessively broad (~ 2:20 at the baseline) and highly asymmetric (strongly fronting), as can be seen in the example chromatogram below.

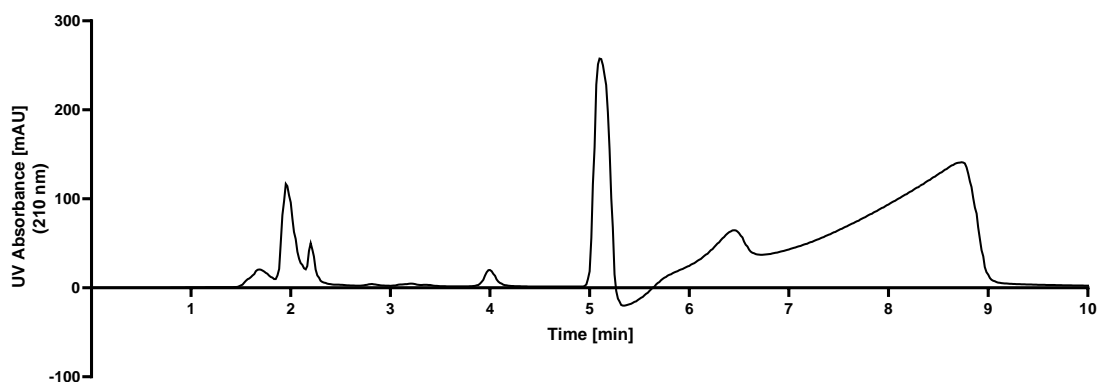


**Figure 4.11 10% B Isocratic (5mM ammonium formate, pH 3.2)**

Chromatogram of Glu-Glu (with impurities). Note significant peak broadening for later eluting peaks.

*TFA* (5:05), *Glu-<sup>DVT</sup>Glu* (6:25), *Glu-Glu* (8:40)

It was noted that upon further decreasing the eluotropic strength, while the retention time decreased further (as expected), the product peak was even broader still. The table below summarises the different solvent compositions screened and illustrates the trend towards broader peaks with increased retention on the column.

**Table 4.2 Table summarising Glu-Glu retention/width with solvent strength (pH 3.2)**

A / B (% / %)	Eff. % H <sub>2</sub> O	t <sub>R</sub> (m:ss)	Peak width at baseline (sec)	Peak shape (S/F/T)
50 / 50	30	2:05*	10	S
60 / 40	26	2:30	20	S
80 / 20	18	3:30	60	T
90 / 10	14	8:40	140	F
95 / 5	12	17:30	300	F

**A:** 90% MeCN, 10% H<sub>2</sub>O. **B:** 50% MeCN, 50% H<sub>2</sub>O. (Both 5 mM ammonium formate)

**Eff. % H<sub>2</sub>O** is the resultant effective H<sub>2</sub>O percentage in the mobile phase

Peak shapes: **S** – symmetrical; **F** – fronting; **T** – tailing

\* elutes with the void peak – not retained on the column

While, as was discussed earlier, some peak broadening is expected in isocratic methods due to longitudinal diffusion, broadening to this extent is highly uncommon. The reasons for this were initially unclear, but it was important to explore this further. Further investigation would be both practical – the method in its current state was almost entirely unusable – as well as useful to give better insights of the intricacies of HILIC: a potentially

valuable complementary analytical technique. Were other factors influencing this peak-broadening beyond the expected longitudinal diffusion?

## 4.3.4 Microspecies distribution

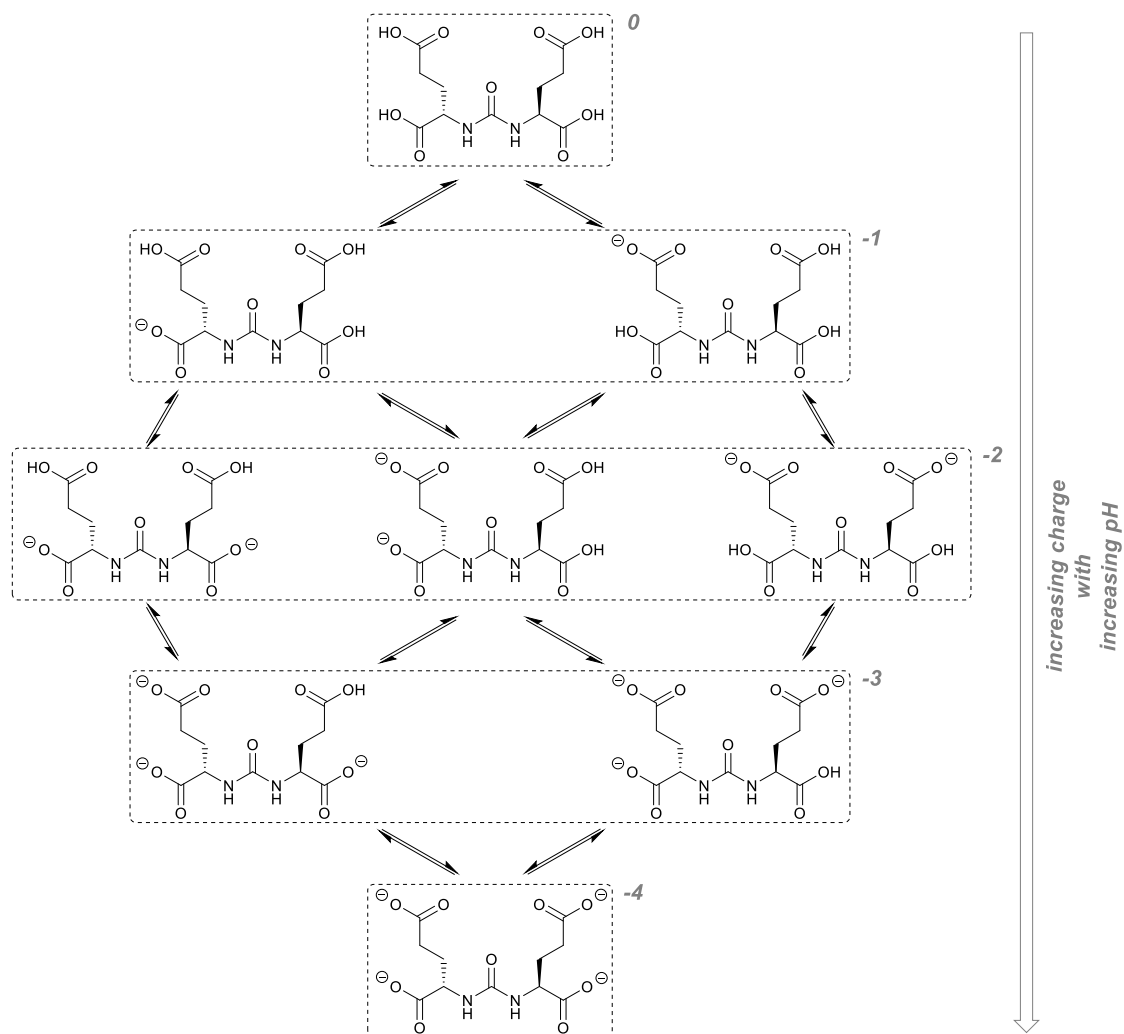


**Figure 4.12** Equilibrating ionised forms of Glu-Glu

Non-exhaustive example of equilibrating species dependent on pH

Due to HILIC's predominant hydrophilic retention mechanism, a given analyte's retention can be strongly dependent on its charge, hence the necessity of pH buffering in the mobile phase in an attempt to ensure consistently protonated (or deprotonated) species. However until this point, we had not considered the effect of this specific pH 3.2 buffer on our specific analyte, the symmetric glutamate urea. In glutamic acid, the  $\alpha$ -carboxylate pKa is 2.16, while the pKa of the  $\gamma$ -carboxylate is 4.15, and while one would expect these to vary slightly as the amino group is incorporated into the urea, these are

still roughly the pKas one would expect for the four ionisable carboxylates in the Glu-Glu urea.

The buffer pH used initially (pH 3.2) is inbetween these two pKa values. As it is approx. 1 pH unit *higher* than the  $\alpha$ -carboxylate pKa (~2.16) one would expect approx. 90% of these to be dissociated. Conversely, as it is approx. 1 pH unit *lower* than the  $\gamma$ -carboxylate pKa (~4.15), one would expect approx. 90% of these functionalities to be protonated. It would be a mistake however, to view this as a fixed/static distribution: at room temperature, these differently ionised forms can rapidly equilibrate (by protonation/deprotonation) with one another; this equilibration is illustrated in the figure above.

Any given species' relative affinity for the aqueous stationary phase will depend on: its overall charge, its specific dipole moment, as well as the number of H-bonds it can donate/accept. Since a given analyte molecule can rapidly interconvert between these differently ionised species as it travels through the column, at different times it will travel significantly slower or quicker than the average analyte velocity. This results in peak broadening and due to the strength of these hydrophilic interactions, it occurs on a significantly greater scale than the broadening which results from longitudinal diffusion. Similarly to the case of longitudinal diffusion-induced peak broadening however, the effect is cumulative: the longer that a given analyte is resident within the column (dependent on the overall elutropic strength of the isocratic mobile phase), the greater the broadening effect becomes. This explains why in the earlier examples with ammonium formate (pH 3.2): the strongest isocratic elution (40% **B**) – where the  $t_R$  was only 0:25 greater than the void peak – the peak was approx. 20 secs wide; whereas for a significantly weaker isocratic elution (10% **B**) – where the  $t_R$  was 6:35 greater than the void peak – the peak was approx. 140 secs wide.



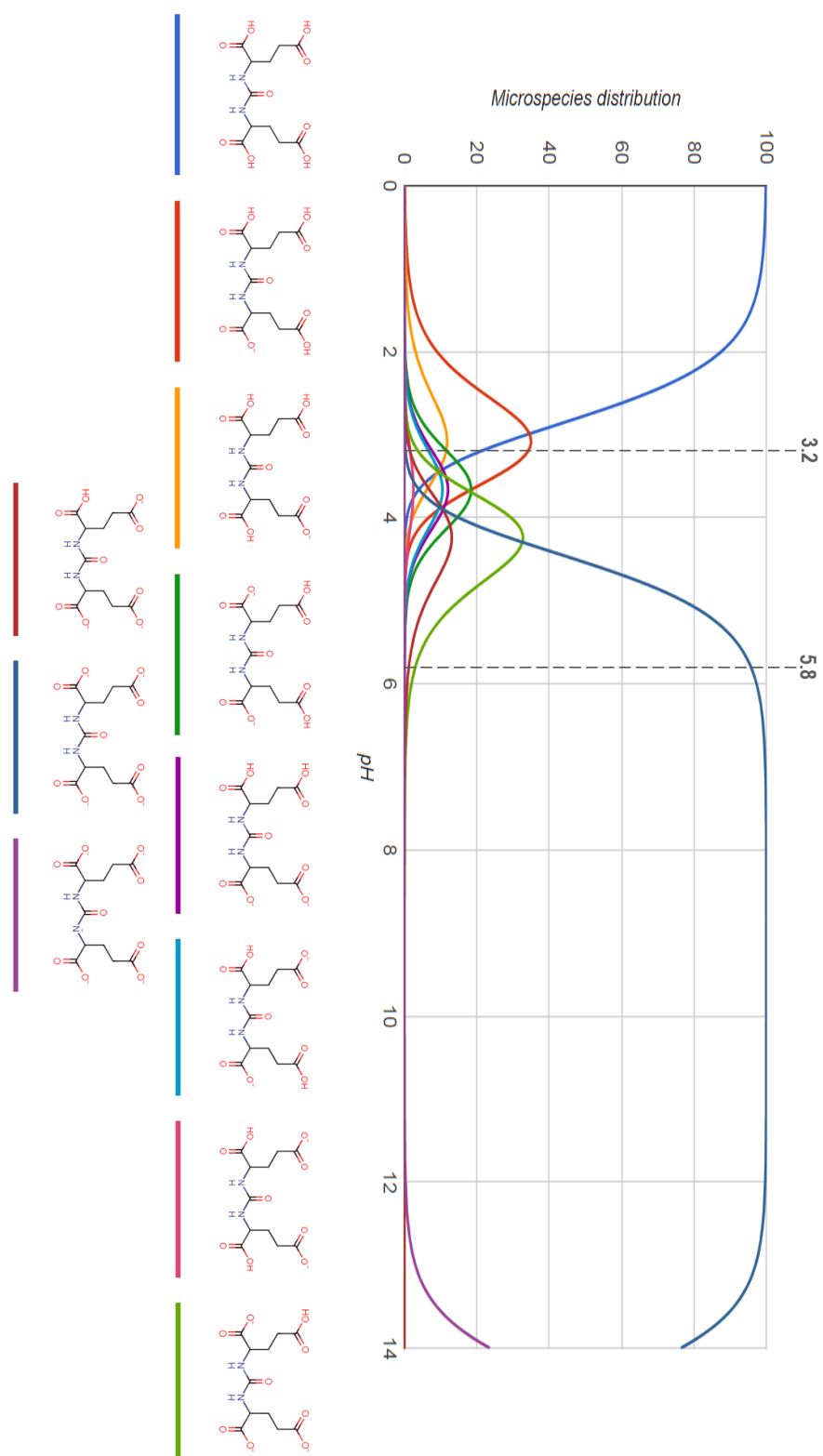


**Figure 4.13 Microspeciation plot**  
 Prediction from ChemAxon's Chemicalize pKa prediction function

Using ChemAxon's Chemicalize pKa prediction function, the microspecies distribution *versus* pH was plotted for the Glu-Glu urea (in the figure below). These microspeciation plots can be extremely useful for a number of different chemical/pharmaceutical applications,<sup>501–503</sup> and in our case it is highly enlightening; demonstrating the large number of differently ionised species present in the sample at pH 3.2. The predominant form according to the prediction (~34% abundant) is the singly-charged species with a single dissociated  $\alpha$ -carboxylate, after this comes the fully protonated neutral species (~21% abundant), and shortly following are: the singly-charged species dissociated at a  $\gamma$ -carboxylate; as well as the doubly-charged species with both  $\alpha$ -carboxylates dissociated; (both of which are ~12% abundant). In addition to these major contributors, the remaining 21% consists of 5 other minor but not insignificant (1-10% abundant) species. Of course this is a fairly-crude software prediction and so the exact abundances are unlikely to be completely accurate, but as a qualitative tool it is highly illustrative of the issue at hand. For our particular tetracarboxylic analyte, a buffer at pH 3.2 was close to the worst possible choice for ensuring uniform behaviour in HILIC. At this pH the analyte exists to some significant extent as one of 9 possible rapidly interconverting microspecies, each of which will be retained differently on the stationary phase. This is almost certainly the underlying cause of this extreme peak broadening behaviour in the isocratic (pH 3.2) ammonium formate-buffered methods.

The other manufacturer-suggested buffering system is ammonium acetate (pH 5.8) and by reference to the same microspeciation plot, it can be seen that this initially seems a more promising option. According to the prediction, at pH 5.8, the vast majority (~96%) of the analyte will exist as the quadruply-charged, fully-dissociated species, as the pH is ~1.5 units higher than even the least acidic carboxylates present. While there are still 2 other species predicted to be present in 1-3% abundance, having the microspeciation equilibrium highly favour one major species is clearly a better situation than the situation seen for pH 3.2. As before, the exact values presented here ought not be taken exactly, and in addition, it should be noted that these predictions are based on pKa values in water. These can vary relatively significantly in organic solvents, and so in our organic-rich mobile phase both our buffer pH as well as analyte pKa values can potentially deviate from their aqueous values.<sup>504</sup>

While the 96% fully-ionised prediction was encouraging, the inherent uncertainty of such predictions combined with the additional uncertainty introduced by our strongly-organic conditions meant that ideally a buffer with an even higher pH than 5.8 would be preferred where possible. This was because even if the prediction were fully accurate, it was not clear what sort of peak broadening could be expected from the ~4% abundant alternative microspecies, and the hope was that by raising the pH further-still, any microspeciation could be completely suppressed. However, HILIC columns are not as robust as many of the newer-generation C18 columns and the upper pH stability limit of the underlying silica is ~ pH 7. The barrier here was that at pH 5.8, the buffering capacity of ammonium acetate is close to its limit, and adjusting the pH much higher would reduce the capacity further, reducing its ability to actually maintain a steady pH. Other buffers could theoretically have been an option, but it would have been important to ensure that the ammonium cation remained constant to ensure adequate silanol shielding. On consultation with Phenomenex however, they were reluctant to recommend any alternative buffer systems due to a lack of compatibility testing on their HILIC columns with any buffers other than the suggested ammonium formate/acetate options.

A further approach to modifying analyte retention behaviour could involve the use of non ammonium-based buffers, perhaps Na<sup>+</sup> or K<sup>+</sup> based buffers instead, due to their documented effects in modifying the retention of charged analytes (as was previously mentioned in section 4.3.2). These metal cations should interact with the multiple deprotonated acidic groups present on this tetracarboxylate analyte and as was discussed, their increased hydration spheres (relative to the ammonium cation) could possibly lead to increased retention of these charged analytes and consequently better separation/resolution. However, the multiple different retention mechanisms at play in HILIC mean that rationally predicting the effects of different buffer types/compositions is entirely non-trivial and was out of scope for this work. Nevertheless, this effect could be investigated to modify the retention of problematic analytes where other options have been unsuccessful.

Ultimately, we proceeded to use the approved ammonium acetate (pH 5.8) buffer as suggested. Even if it was unable to achieve a single fully-ionised species in solution, the situation was still expected to be a major improvement over the chromatography at pH

3.2. In fact, it could hopefully serve as validation of our understanding of the retention mechanisms governing HILIC as well as our predictions regarding microspeciation; and any results obtained could help to inform future buffer selection if required. Since we expect the analyte to exist predominantly as the quadruply-ionised (-4) species, we expected that: the peak shape would be significantly improved (narrower and more symmetrical) because of the microspeciation suppression; and for a given solvent strength (% **B**) the analyte would be retained more strongly (longer  $t_R$ ) than for pH 3.2 ammonium formate, due to the enhanced hydrophilicity of multiply-charged analytes.

### 4.3.5 Ammonium acetate (pH 5.8)

While the buffer used in this section was ammonium acetate (pH 5.8), the method development principles applied here were the same as those applied for the ammonium formate method. The two solvent mixtures **A** and **B** were prepared as before to ensure a consistent 5 mM ionic strength regardless of the mobile phase composition:

**A:** 450 mL MeCN, 25 mL water, 25 mL 100 mM ammonium acetate (pH 5.8)

**B:** 250 mL MeCN, 225 mL water, 25 mL 100 mM ammonium acetate (pH 5.8)

In a similar manner to before, differing solvent compositions were sequentially screened beginning from the strongest conditions (100% **B**), moving to gradually weaker compositions until the analyte began to retain on the column. At 100% **B** all analytes eluted with the void peak ( $t_R = 2:00$ ), however at 50% **B**, the Glu-Glu analyte began to retain slightly ( $t_R = 2:30$ ), and from this point on, each subsequently weakened solvent composition shifted the elution time to sequentially larger values, as expected. The full results of this screening are presented in the table below:

**Table 4.3 Table summarising Glu-Glu retention/width with solvent strength (pH 5.8)**

<b>A / B (% / %)</b>	<b>Eff. % H<sub>2</sub>O</b>	<b><math>t_R</math> (m:ss)</b>	<b>Peak width at baseline (sec)</b>	<b>Peak shape (S/F/T)</b>
<b>50 / 50</b>	<b>30</b>	<b>2:30</b>	<b>~ 30</b>	<b>S</b>
<b>70 / 30</b>	<b>22</b>	<b>4:45</b>	<b>~ 50</b>	<b>S</b>
<b>75 / 25</b>	<b>20</b>	<b>8:00</b>	<b>~ 60</b>	<b>S</b>
<b>80 / 20</b>	<b>18</b>	<b>14:15</b>	<b>~ 80</b>	<b>S</b>

**A:** 90% MeCN, 10% H<sub>2</sub>O. **B:** 50% MeCN, 50% H<sub>2</sub>O. (Both 5 mM ammonium acetate)

**Eff. % H<sub>2</sub>O** is the resultant effective H<sub>2</sub>O percentage in the mobile phase

Peak shapes: **S** – symmetrical; **F** – fronting; **T** – tailing

Peak widths difficult to measure exactly, due to coelution with Glu-<sup>pyr</sup>Glu impurity

Our two predictions (based in-part on the microspeciation plot) were that: i) the analyte would be more strongly retained at this elevated pH, due to a greater degree of carboxylate dissociation; and ii) the peak broadening would be significantly reduced due to the relative predominance of a single species, compared with the wider range of microspeciation at pH 3.2. To summarise briefly: both of these predictions were borne

out in the above-presented evidence, which supported our understanding of the mechanisms underpinning HILIC and our hypothesis regarding the link between pH-related microspecies distribution and peak shape. But it should also be noted that the results here were still ultimately unsatisfactory due to issues with resolving the Glu-Glu peak from the key cyclised byproduct Glu-<sup>Pyr</sup>Glu.

#### 4.3.5.1 Improved retention

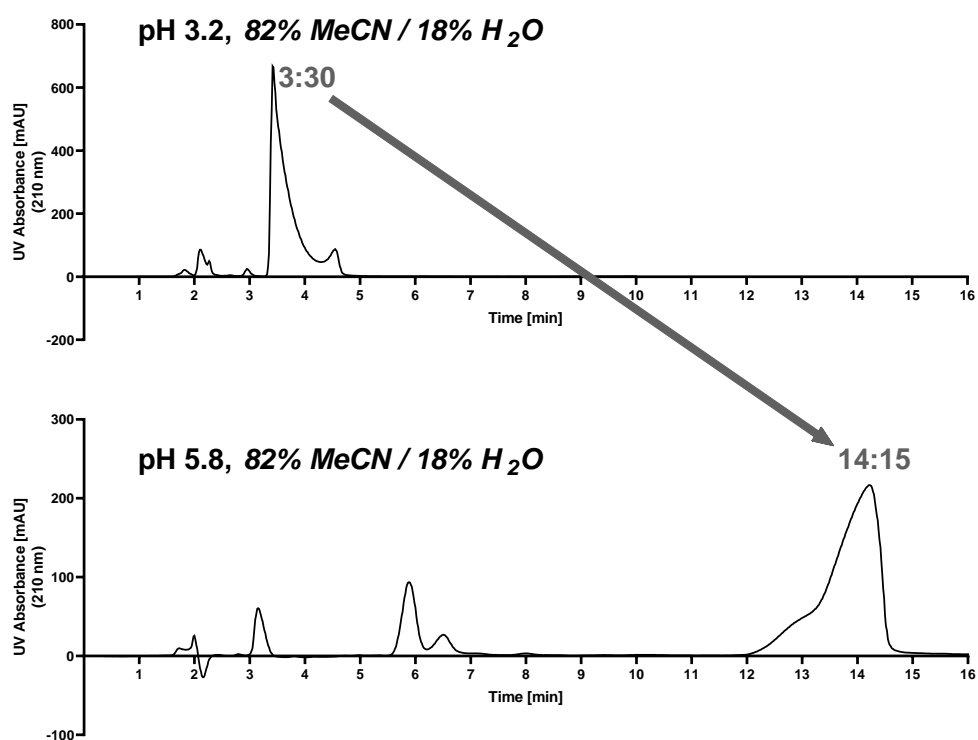


**Figure 4.14 Changing pH while maintaining identical solvent strength**

Isocratic elutions at 20% B (82% MeCN / 18% H<sub>2</sub>O) w/ constant 5 mM ammonium formate (pH 3.2) or acetate (pH 5.8) buffers

The figure above presents two contrasting chromatograms, with the only differences between the two methods being the pH of the ammonium buffer in the mobile phase. Both were isocratic elutions of the same reference sample at the same 20% **B** solvent strength (82% MeCN / 18% H<sub>2</sub>O), both with a constant 5 mM ammonium salt buffer (pH 3.2 – formate; pH 5.8 – acetate). The differences between the two are stark, while the

major analyte peak elutes at around 3:30 for pH 3.2, the same analyte is significantly more strongly retained (14:15) at pH 5.8.

This illustrates the extreme pH dependence of HILIC, as was discussed earlier. Due to the dominant hydrophilic retention mechanism, ionisable functionalities (carboxylates, amines, some hydroxyls, etc.) can exist in a weakly-retained form (neutral – capable of H-bonding) or in a strongly-retained form (charged – capable of forming much stronger electrostatic/ionic interactions), according to their pH-dependent protonation state. This can make HILIC a very powerful tool due to the control that can be exerted over analyte retention behaviour by careful selection of appropriate pH, particularly for the analysis of highly polar compounds which may be difficult to retain on other stationary phases. However, the drawback to this is that it can be a relatively delicate and fickle HPLC technique, at least by comparison to the reversed-phase approach more familiar to most radiochemists. Small changes in mobile phase pH which might not be noticed in a fairly robust C18 method could completely change the profile of a HILIC elution, and as-such, meticulous control of buffer preparation is crucial to ensuring reliable and reproducible chromatography.

In our case, the increased retention as a result of increasing the pH was exactly as predicted. Our tetracarboxylic analyte is likely to be significantly more charged at this elevated pH and we saw the expected increase in retention as a result. This served to partially validate our understanding of the pH-dependent retention behaviour of our analyte, as well as the general mechanisms governing HILIC selectivity/retention.

## 4.3.5.2 Improved peak width/shape

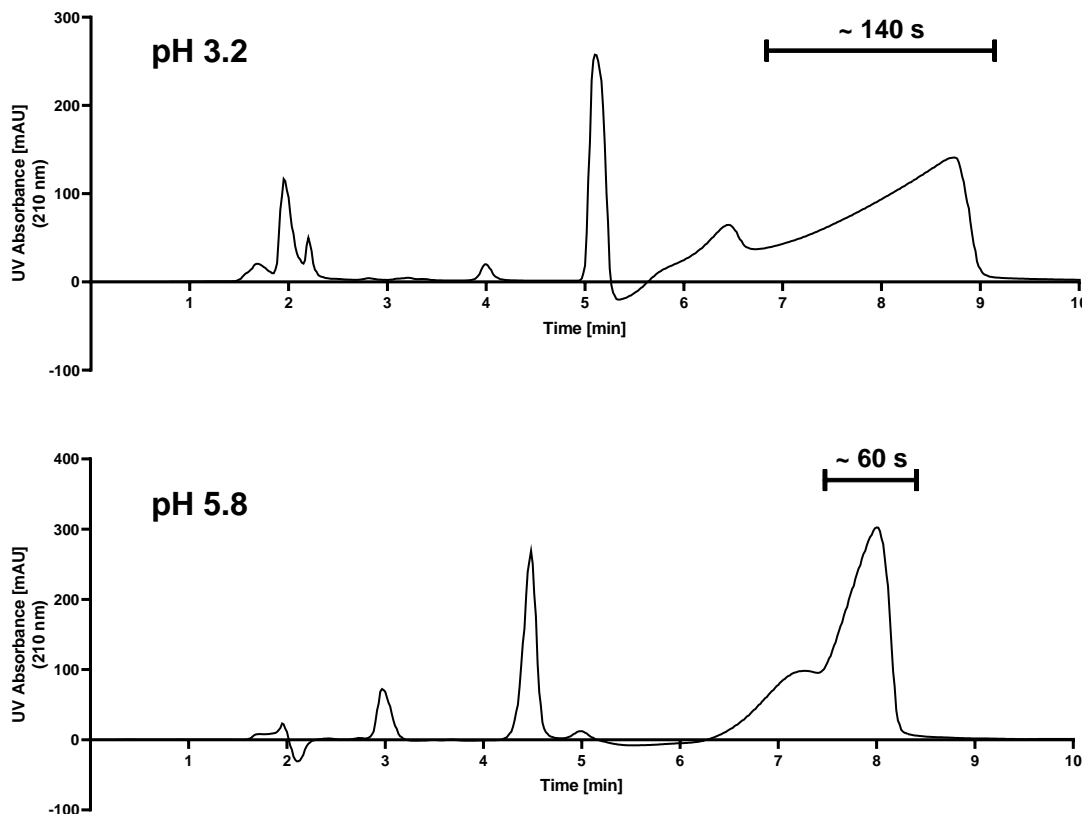


**Figure 4.15 Changing peak width at same retention time**

Both isocratic elutions give comparable retention times for the same analyte. However elution at pH 3.2 gave a much broader peak (~140 s) than at pH 5.8 (~60 s).

pH 3.2 method: 10% B (86% MeCN / 14% H<sub>2</sub>O) w/ constant 5 mM ammonium formate (pH 3.2)

pH 5.8 method: 25% B (80% MeCN / 20% H<sub>2</sub>O) w/ constant 5 mM ammonium acetate (pH 5.8)

This figure presents two contrasting chromatograms (at pH 3.2 and 5.8) in which the Glu-Glu analyte exhibited comparable retention times ( $t_R \sim 8:00-9:00$ ), and so represent examples in which the analyte had similar residence times within the HILIC column. Due to the fact that the analyses were both isocratic methods on the same column, at the same temperature and flow-rate, the expected peak-broadening due to longitudinal diffusion (a factor of residence-time and temperature) was therefore expected to be roughly equivalent in both cases. Any differences in peak broadening can therefore be attributed to different analyte behaviour within the columns.



In the pH 3.2 example, the peak was extremely broad (~ 140 secs) and highly asymmetrical (strongly fronting), whereas at pH 5.8 by comparison, the peak was significantly narrower (~ 60 secs) and more symmetrical, although it is still obscured in part by the closely eluting overlapping Glu-<sup>Pyr</sup>Glu impurity (as will be discussed shortly).

Our prediction was that at pH 5.8, the analyte should exhibit significantly less broadening due to the predominance of one major species (> 96% abundant according to the software prediction), compared with the wider microspecies distribution expected at pH 3.2 (4 species with > 10% abundance, with 5 more species in the 1-10 % abundance range). This result is broadly in line with this prediction, lending further support to this hypothesis. As will be discussed shortly, the peak at pH 5.8 is still significantly more broad than would be expected for a single species (compare with the earlier eluting TFA peak) which does suggest that the predicted >96 % abundance of a single species was perhaps a slight overestimate. However, the general observation of a narrower peak profile supports the prediction of a tighter microspecies distribution at pH 5.8, an important result which could help in guiding future HILIC method development for similarly acidic analytes.

#### 4.3.5.3 Critical pair resolution

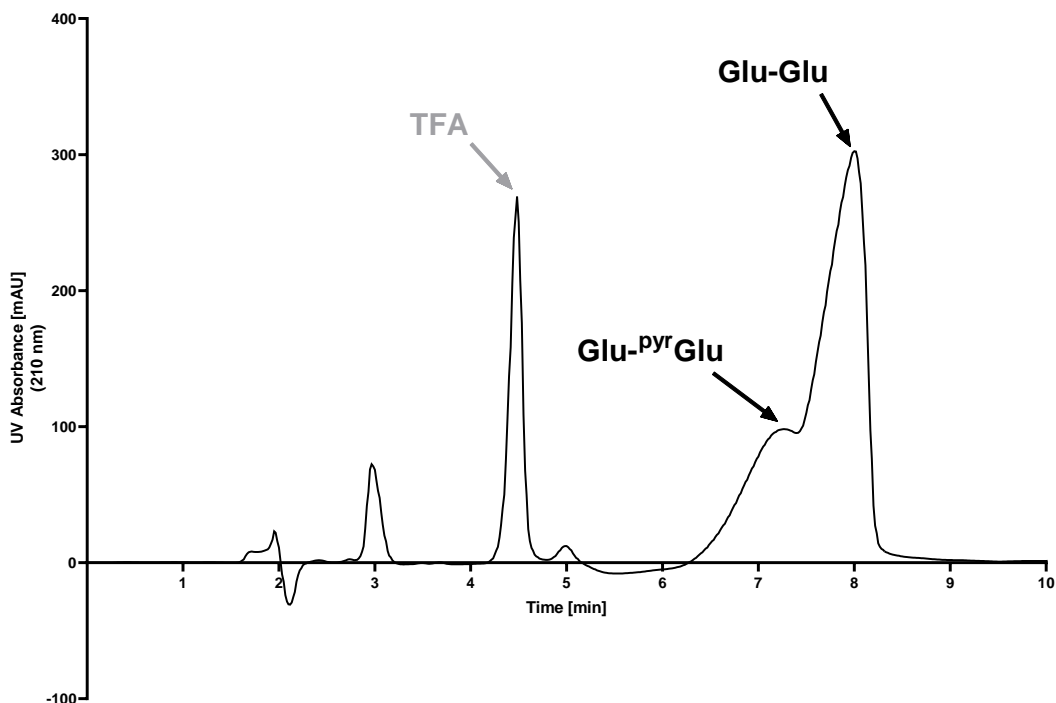


**Figure 4.16** Example chromatogram demonstrating poor critical-pair resolution

Isocratic elution at 25% B (80% MeCN / 20% H<sub>2</sub>O) w/ constant 5 mM ammonium acetate (pH 5.8)

To further contextualise the chromatograms which are presented in the previous sections, while the overall chromatographic performance had improved upon moving to a higher buffer pH, the individual peak resolution was still poor. Our reference sample contained a significant quantity of the cyclised pyroglutamate variant (Glu-pyrGlu), the formation of which is discussed in the section 3.4.2. This molecule still bears three ionisable carboxylate moieties and would be expected to retain similarly to Glu-Glu. There is a significant chance that this impurity could form in any radiochemistry, requiring identification and separation. As such, these two compounds can be considered the “critical pair” which any HILIC method needs to resolve adequately to be successful.

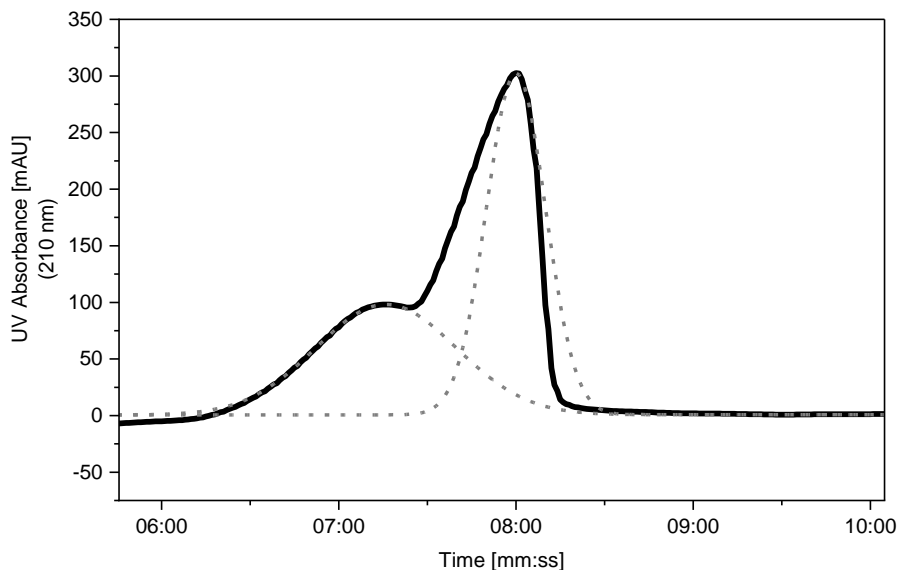


**Figure 4.17 Deconvolved overlapping peaks**

Deconvolution calculation from OriginPro software, using peak deconvolution plugin. Solid line is the real UV absorbance, dashed lines are idealised Gaussian peaks iteratively fitted to match this UV absorbance. Presented to illustrate the approximate extent of the overlapping peaks, not for further numerical calculation. This was the same isocratic elution as presented in previous figure (25% B (80% MeCN / 20% H<sub>2</sub>O) w/ constant 5 mM ammonium acetate (pH 5.8))

In the example chromatogram presented above, Glu-Glu elutes in the target region ( $t_R \sim 8:00$ ), with a reasonably symmetrical profile and significantly reduced broadening *versus* the pH 3.2 methods, as will shortly be discussed more thoroughly. However, the Glu-<sup>pyr</sup>Glu impurity elutes only 45 secs earlier ( $t_R \sim 7:15$ ), and the broad peaks overlap very significantly.

This overlapping critical pair was deconvolved (using OriginPro software) to illustrate the extent of this overlap. The relatively-basic deconvolution algorithm it implements attempts to fit reasonable (Gaussian) peak shapes which could contribute to the overall combined UV absorption. The result presented seems to be a relatively reasonable approximation, but this technique is highly complex and without further verification of these results, no further numerical analyses (resolution calculations etc.) were performed with this data. It is simply presented here to qualitatively illustrate the significantly overlapping coelution of Glu-<sup>pyr</sup>Glu and Glu-Glu. As a result of this overlap between the two peaks, this critical pair remains insufficiently resolved under these conditions and

this is clearly still an unusable method, regardless of how much it improves on the pH 3.2 results.

By comparison, the TFA impurity ( $t_R \sim 4:30$ ,  $\sim 20$  secs width) exhibits a much more desirable (near-gaussian) peak shape/width. This is because it bears just a single, strongly-acidic ( $pK_a \sim 0.2$ ) carboxylate functionality which would be overwhelmingly ( $> 99.9\%$ ) dissociated at pH 5.8 and as a result it elutes in a sharp peak with minimal broadening. If the critical pair analytes eluted with similar peak shapes/widths to this, the method would be entirely acceptable. This issue (and potential solutions) can be better explained with reference to the equation which mathematically defines chromatographic resolution.<sup>505</sup>

$$Resolution = \frac{\Delta t_R}{W_{ave}}$$

Where  $\Delta t_R$  is the difference in retention times, and  $W_{ave}$  is the average baseline-width of the two peaks. A pair of peaks with resolution  $> 1.5$  can be considered well-resolved ( $< 0.15\%$  overlap between peaks). Accordingly, the resolution of two peaks is proportional to  $\Delta t_R$ , but inversely proportional to  $W_{ave}$ . It should be noted that this equation assumes Gaussian peak shapes.

In our situation (isocratic elution) it is difficult to further improve  $\Delta t_R$  without also increasing the retention times of both analytes significantly – a solution which is not possible to any major degree, due to the limitations imposed by radioactive decay. As such, if the  $\Delta t_R$  term cannot be altered, the  $W_{ave}$  term must be decreased further. As an example, if the two peaks of our critical pair ( $t_R \sim 7:15$  and  $8:00$ ,  $\Delta t_R \sim 45$  secs) eluted at the same retention times but with the same widths as the earlier eluting TFA peak ( $W_{ave} \sim 20$  secs), then the resolution of these two peaks would be perfectly acceptable (2.25). It was clear therefore that the selectivity of this HILIC column is appropriate for our purpose – it was able to separate two highly-similar polar analytes (separation factor  $\alpha = 1.14$ ) – but the major confounding factor in the application of this HILIC method is the peak broadening caused by analyte microspeciation as a result of inappropriate selection of mobile phase pH.

#### 4.3.6 Equilibration

It should also be noted that for HILIC columns, the equilibration process is a more critical determinant of reliable chromatography and so the equilibration times are substantially longer than those required for reversed-phase HPLC. The origin of this difference is the different nature of the stationary phases in HILIC and reversed-phase columns. In reversed-phase C18 columns the stationary phase is the bonded non-polar octadecyl phase itself, whereas for HILIC columns (as previously discussed), the effective stationary phase is the water-rich layer immobilised on the bonded diol phase. This water layer takes time to establish and stabilise at the start of any work or between experiments: the column manufacturers advise a minimum equilibration of 20 column volumes. In our case, this equated to a minimum 40 min equilibration required between experiments, and in practice it was often the case that up to 60 min equilibrations were required to ensure the most reproducible results. This can be a significant inconvenience, particularly when performing multiple sequential analyses as is required during method development, and it makes it difficult to envisage many situations in which such a long column equilibration would be compatible with a routine production schedule in a busy radiopharmacy that produces multiple different radiotracers daily.

#### 4.3.7 Summary and alternative HPLC options

The target molecule of this section of work (the symmetrical glutamate urea, Glu-Glu) was too polar to be retained on our standard reversed-phase C18 HPLC columns, even when run at the limits of their aqueous mobile-phase tolerances. So to develop an appropriate QC/purification method for this compound, in-part informed by advice from Phenomenex, we investigated the use of HILIC as an alternative HPLC technique.

In brief, while HILIC overcame the issues related to non-retention of the analyte (Glu-Glu is strongly retained on the column's polar stationary phase), it introduced several more issues of its own. Because HILIC relies on hydrophilic interactions to achieve analyte retention, the exact ionic microspeciation of a particular analyte can be strongly determinant of a compound's retention. This is not an issue for ionisable analytes which can be entirely protonated/deprotonated at a pH within the column's acceptable stability range. However due to the high number of ionisable carboxylates on our particular target

analyte, it was difficult to develop a method (within the stated pH range of the column) that gave acceptable chromatography (symmetrical well-defined peaks, critical-pair resolution), within a timeframe compatible with <sup>11</sup>C-radiochemistry.

On top of this, as a less well-developed or widely-employed HPLC technique (by comparison with the routine reversed-phase C18 columns familiar to almost any radiochemist), HILIC is a relatively difficult technique to envisage employing routinely in a radiosynthetic procedure. While in theory it can be an extremely powerful alternative chromatographic technique, in practice: the columns are expensive and easy to damage; their performance can be incredibly sensitive to minor changes in mobile phase ionic strength and/or pH; method development can be a relatively complex endeavour (due to HILIC's sometimes conflicting mixed-mode retention behaviours); and tediously long equilibration times (up to an hour) are required between injections to achieve reproducible results. All of these problems severely limit the potential for routine use of this technique in any <sup>11</sup>C-radiochemistry applications. Of course, in certain cases, HILIC may still be the best option where no other stationary phases have been able to achieve sufficient retention/resolution of the target molecule and any likely impurities. Additionally, the reliability and robustness of commercially available columns will likely improve in the coming years with further development.

In hindsight however, for our particular purposes the use of other stationary phases may have been more appropriate and could warrant further investigation were this particular work to be continued. For example, polar-embedded reversed-phase columns are compatible with 100% aqueous conditions, while still retaining the stability and ease of method development associated with reversed-phase HPLC. A 100% aqueous mobile phase composition could possibly have been sufficiently eluotopically weak to achieve some retention of the analyte. Another alternative that could have been considered would have been a PFP (pentafluorophenyl) reversed-phase column. This stationary phase consists of both standard C18 octadecyl chains as well as PFP functionalities, which can give the column an additional degree of selectivity for polar functional groups while still retaining a general reversed-phase character and column robustness.

Ultimately, while HILIC can theoretically represent an appealing alternative to reversed-phase chromatography, switching to an entirely orthogonal retention mode was perhaps

unnecessary in our case where modified reversed-phase columns could have sufficed. This would not necessarily have been a such an issue except for the myriad additional difficulties encountered in the “real-world” implementation of a HILIC technique, the result of which was a still largely-unsatisfactory method for identification and purification of the desired Glu-Glu compound of interest.

#### 4.4 Discontinuation and future direction

The numerous difficulties encountered in developing a good QC/purification method for Glu-Glu prompted us to reconsider the initial thought process that led to the selection of this particular target molecule: while it was theoretically simpler to radiolabel this symmetric  $^{11}\text{C}$ -urea, the particular chemical characteristics of the final deprotected tetracarboxylic compound meant that this was actually a much more practically-inaccessible target than first hoped. As a result, we considered instead the possibility of  $^{11}\text{C}$ -radiolabeling an asymmetric PSMA-targeted  $^{11}\text{C}$ -urea; whilst the asymmetric  $^{11}\text{C}$ -urea synthesis may be a more challenging procedure, the additional degree of sidechain-lipophilicity of these compounds ought to make straightforward reversed-phase HPLC a more realistic prospect for analysis/purification.

Our initial intention was to develop a straightforward diagnostic  $^{11}\text{C}$ -radiotracer, and there are a number of alternative asymmetrically substituted glutamate-urea compounds documented with significantly higher PSMA binding affinities (and thus theoretically superior imaging characteristics); ranging from simple natural amino acid ureas (Leu-Glu, or Tyr-Glu, for example),<sup>288,300</sup> to the potentially appealing more-potent chlorinated and brominated analogues of radiohalogenated (labeled with  $^{18}\text{F}$  and  $^{123/131}\text{I}$ ) PSMA radiotracers.<sup>305</sup> In order to produce any of these alternative PSMA-radioligands, a “general” method for  $^{11}\text{C}$ -radiolabeling of the asymmetric glutamate-ureido scaffold would be required. While this would require more work to develop a robust and universally-applicable method, it is possible to imagine a number of potentially highly-valuable applications of such a tool beyond just clinical application of  $^{11}\text{C}$ -PSMA diagnostics; these will be further elaborated upon in the introduction to chapter 5.

Ultimately, in combination with the practical difficulties encountered in developing a method for the radiosynthesis of the symmetrical  $^{11}\text{C}$ -urea, the potential benefits of a more general method for  $^{11}\text{C}$ -radiolabeling PSMA ligands made a convincing case for discontinuing this particular course of work in developing a non-transferable more-specific method for  $^{11}\text{C}$ -radiolabeling only the symmetrical Glu-Glu urea.



## 4.5 Conclusions

In this section of work the overall aim was to develop a method to <sup>11</sup>C-radiolabel the high-affinity PSMA ligand [*ureido*-<sup>11</sup>C]Glu-Glu. The approach to this was broken down into two key synthetic steps: 1) symmetrical <sup>11</sup>C-urea formation *via* DBU/Mitsunobu-mediated [<sup>11</sup>C]CO<sub>2</sub> fixation, to produce the *tert*-butyl ester tetraprotected urea, [*ureido*-<sup>11</sup>C]Glu-Glu-(O<sup>t</sup>Bu)<sub>4</sub>; and 2) acidic cleavage of the ester protecting groups on [*ureido*-<sup>11</sup>C]Glu-Glu-(O<sup>t</sup>Bu)<sub>4</sub> to yield the desired tetracarboxylic [*ureido*-<sup>11</sup>C]Glu-Glu product. The first of these two steps was highly successful, while the second encountered some challenging analytic/purification obstacles which ultimately led to the decision to discontinue this particular course of work.

### 4.5.1 Step 1 – <sup>11</sup>C-urea synthesis

As stated above, the first of these two key steps – the symmetrical <sup>11</sup>C-urea formation *via* an [<sup>11</sup>C]CO<sub>2</sub> fixation approach to produce the intermediate [*ureido*-<sup>11</sup>C]Glu-Glu-(O<sup>t</sup>Bu)<sub>4</sub> – was highly successful. Our synthetic approach was adapted from the earlier published method – developed by others in our group – for the radiosynthesis of symmetrical <sup>11</sup>C-ureas from [<sup>11</sup>C]CO<sub>2</sub>.<sup>226</sup> This proceeds *via* the DBU-mediated [<sup>11</sup>C]CO<sub>2</sub> fixation on the amine substrate followed by Mitsunobu-mediated dehydration to produce the <sup>11</sup>C-isocyanate *in situ*, this finally reacts with another amine molecule to produce the desired symmetrical <sup>11</sup>C-urea (herein referred to as “literature method”). This was developed as a general method using a wide range of simple aliphatic and aromatic building-block amines, and the conditions were generalised to give acceptable yields for this wide range of substrates. For our purposes however, we aimed to apply this method to one specific protected amino-acid substrate, and these more general literature conditions resulted in a rather disappointing 13% radioactivity yield. As such, our first goal was to tailor and optimise these conditions to give a much more efficient synthesis of our target [*ureido*-<sup>11</sup>C]Glu-Glu-(O<sup>t</sup>Bu)<sub>4</sub> intermediate compound.

The commercially available amine substrate is provided as the amine hydrochloride salt, and in one of the first optimisation steps it was shown that this salt could be used directly (without prior basic extraction to yield the free-amine), by increasing the DBU quantity to produce the reactive free-amine *in situ* while leaving the remaining DBU that was

required to facilitate  $[^{11}\text{C}]\text{CO}_2$  fixation. This was a small but important result which could hopefully be extended to other similar amine salts, streamlining their use in these reactions.

The bulk of this reaction optimisation relied on a thorough characterisation of a typical crude radio-HPLC trace for this reaction. The overall goal of such an approach was to maximise the utility of every experiment performed: to streamline the optimisation of this particular radiosynthesis, in addition to furthering our general comprehension of this still incompletely-understood chemistry. In characterising the radio-HPLC, a distinction was drawn between  $[^{11}\text{C}]\text{CO}_2$  “trapping” and “fixation”; the latter is the productive process wherein carbon-11 is covalently incorporated onto the amine substrate as the  $^{11}\text{C}$ -carbamate, which is subsequently converted to the key  $^{11}\text{C}$ -isocyanate intermediate before the final conversion into the  $^{11}\text{C}$ -urea. It was found that while the  $[^{11}\text{C}]\text{CO}_2$  trapping/fixation ratio was more difficult to significantly optimise, the key area with sufficient scope for further optimisation was in the  $^{11}\text{C}$ -isocyanate to  $^{11}\text{C}$ -urea conversion rate. Under the literature conditions, 81% of the “fixed”  $^{11}\text{C}$  existed as the intermediate  $^{11}\text{C}$ -isocyanate. This told us that while the  $^{11}\text{C}$ -carbamate to  $^{11}\text{C}$ -isocyanate conversion was successful, there were issues in driving the final  $^{11}\text{C}$ -urea-forming reaction of this  $^{11}\text{C}$ -isocyanate with a second molecule of the amine substrate. With this in mind, appropriate rational modifications could be made to drive the reaction further towards completion.

In this process, it was shown that increasing the reaction temperature from  $50^\circ\text{C}$  to  $80^\circ\text{C}$  resulted in a significantly enhanced  $^{11}\text{C}$ -isocyanate to  $^{11}\text{C}$ -urea conversion rate, and increasing the reaction time from 2 to 10 mins allowed the reaction to proceed further towards completion, increasing the overall RCY (although to a lesser extent than that resulting from increased temperature, due to the offsetting losses attributed to increased radioactive decay). The most significant modification regarded the stoichiometry of the added Mitsunobu reagents. It was hypothesised that the 2:1 ratio of Mitsunobu:amine as used in the literature conditions served to isolate the intermediate  $^{11}\text{C}$ -isocyanate by competing with it for the limited remaining amine substrate. There were two competing reaction pathways: the productive pathway involved the condensation of the  $^{11}\text{C}$ -isocyanate with the remaining amine to produce the  $^{11}\text{C}$ -urea; but the unproductive

pathway involved the reaction of the Mitsunobu betaine with the amine (likely forming an undesired iminophosphorane).<sup>238–240,479,480</sup> If this second reaction pathway dominated, a significant quantity of the intermediate <sup>11</sup>C-isocyanate would be left without any amine with which it could further react. Accordingly, reducing the Mitsunobu:amine ratios from 2:1 down to 1:1 and even to 0.5:1 led to a significantly improved conversion of the <sup>11</sup>C-isocyanate to the final <sup>11</sup>C-urea.

In addition to giving a deeper understanding regarding this increasingly-widely-used chemistry, this radio-HPLC-informed rational optimisation approach was highly successful. The initial literature conditions resulted in a 97% [<sup>11</sup>C]CO<sub>2</sub> trapping efficiency and a 16% radiochemical conversion (measured by crude radio-HPLC); this gave an overall RCY of 15% (d.c.) in a total 4 min reaction time, equivalent to a radioactivity yield of 13%. By comparison, our final optimised conditions gave a 93% [<sup>11</sup>C]CO<sub>2</sub> trapping efficiency and a 60% radiochemical conversion (measured by crude radio-HPLC); this gave a dramatically improved overall RCY of 56% (d.c.) in a 4 min reaction time, equivalent to a radioactivity yield of 49%.

#### 4.5.2 Step 2 – acidic deprotection

The aim of this second step was to achieve the cleavage of the *tert*-butyl ester protecting groups on the intermediate to yield the final tetracarboxylic urea product, [*ureido*-<sup>11</sup>C]Glu-Glu. Before investigating this cleavage process however, an analytic radio-HPLC method had to be developed to allow assessment of the reaction to guide any further optimisation, as in step 1. The development of such an analytical method is generally a routine step, which does not require a significant amount of work. However, the highly polar nature of the tetracarboxylic compound led to its lack of retention on the standard C18 stationary phase of our reversed-phase HPLC column. Under the eluotropeically weakest solvent strength permissible (without causing irreversible damage to the column), the highly polar reference compound would still elute with the void volume of the column due to a lack of any significant retentive lipophilic interactions with the stationary phase.

To remedy this, we attempted to develop an analytical method using a different column stationary phase (crosslinked-diol) with a roughly orthogonal retention behaviour to

reversed-phase chromatography (HILIC). While the goal of increasing the HPLC retention of Glu-Glu with the use of a polar stationary phase was achieved, in practice, the operational intricacies of HILIC instead posed a number of different barriers to the development of a reliable chromatographic method. These arose in large-part as a result of the strongly pH-dependent retention behaviour of HILIC columns, which in-turn is attributed to the big differences in hydrophilic interaction strength between ionised and non-ionised analytes. To control this behaviour, HILIC methods are generally buffered to ensure one specific ionic species of an analyte predominates. The presence of four ionisable carboxylate moieties on Glu-Glu complicated this further, and microspeciation predictions revealed that at both manufacturer-recommended ammonium buffer pH levels (formate at 3.2 and acetate at 5.8), Glu-Glu exists to a significant degree as one of several different ionic species. The overall result of this microspeciation was unacceptably broad and asymmetric peaks which also overlapped significantly with other similarly-broad multiply-ionisable impurities.

Our microspeciation predictions fit well with the observed results, whereby stronger compound retention with narrower peaks was expected at the higher pH (5.8) as a result of a smaller number of more fully-ionised species predominating. This was the result observed in practice, and served to validate our understanding of the complex retention behaviour of HILIC as well as partially confirming our explanation of the microspeciation-based origins of this peak broadening behaviour. However, the remaining peak-broadening effects still led to significant overlaps with the key cyclised Glu-<sup>Pyr</sup>Glu impurity. In combination with the unavoidable and inconvenient general requirements of HILIC: tediously long column equilibration is required, and the fact that method reproducibility is highly dependent on extremely careful control of buffer pH and ionic strength; the best optimised method we produced was still deemed to be unacceptable for our purposes.

The myriad struggles encountered in the development of either a reversed-phase or HILIC-based method for analytic radio-HPLC of [*ureido*-<sup>11</sup>C]Glu-Glu prevented any further development of a radiochemical deprotection method, and so the decision was made to discontinue this particular line of investigation. While the efforts at radiolabeling [*ureido*-<sup>11</sup>C]Glu-Glu were discontinued at this point, the development of a general

method for  $^{11}\text{C}$ -radiolabeling PSMA ligands continued and it is this method development process which is presented in chapter 5.

## 4.6 Materials & Methods

### 4.6.1 General

Anhydrous acetonitrile (MeCN, 99.8%), Ascarite, L-glutamic acid di-*tert*-butyl ester hydrochloride ( $\geq 98\%$ ), di-*tert*-butyl-azodicarboxylate (DBAD, 98%), triethylamine (Et<sub>3</sub>N,  $\geq 99.5\%$ ), tri-*n*-butyl phosphine (PBu<sub>3</sub>, 99%), sodium hydroxide pellets (NaOH,  $\geq 98\%$ ), ammonium formate (LC-MS grade,  $\geq 99\%$ ), ammonium acetate (LC-MS grade,  $\geq 99\%$ ) formic acid ( $\geq 95\%$ ), acetic acid (glacial,  $\geq 99\%$ ), and trifluoroacetic acid (TFA,  $\geq 99\%$ ), were purchased from Sigma-Aldrich. Ethyl acetate (EtOAc,  $\geq 99.5\%$ ) was purchased from Fisher Scientific. Anhydrous magnesium sulfate (MgSO<sub>4</sub>, 98%) was purchased from Fluka. 1,8-Diazabicyclo[5.4.0]undec-7-ene (DBU, 99%) was purchased from Alfa Aesar. Deionised water (18.2 M $\Omega$ .cm) was produced in a Milli-Q Reference Water Purification System.

[<sup>11</sup>C]CO<sub>2</sub> was produced using a Siemens RDS112 cyclotron in a <sup>14</sup>N(p, $\alpha$ )<sup>11</sup>C reaction, by the 11 MeV proton bombardment of nitrogen (+ 1% O<sub>2</sub>) gas. The cyclotron produced [<sup>11</sup>C]CO<sub>2</sub> was transferred in a stream of helium gas at 70 mL/min through a P<sub>2</sub>O<sub>5</sub> drying tube (without further cryogenic trapping/preconcentration) into a switching valve of an Eckert & Ziegler Modular-Lab automated synthesis unit. Unless otherwise specified, all radioactive experiments used a 5 $\mu$ A bombardment for 1 min, producing on average 300-350 MBq [<sup>11</sup>C]CO<sub>2</sub> at the end of bombardment (EoB). The radioactivity contents of reaction vials and ascarite cartridges were all measured (along with the measurement time since EoB) in a Capintec® dose calibrator. Decay correcting these to the EoB allows for the accurate calculation of both the total amount of delivered radioactivity as well as the reaction trapping efficiencies. Radiochemical yields (RCY) reported are calculated as a percentage of the total radioactivity delivered from the cyclotron and are decay corrected to the EoB. Where RCY is non-decay-corrected, this is reported instead as the *radioactivity yield*.

Where solutions were prepared under inert atmospheres (argon or nitrogen) a dry-box apparatus was used. By maintaining a positive pressure of inert gas inside the box, an acceptable CO<sub>2</sub>-free atmosphere could be established for preparing CO<sub>2</sub>-sensitive radiolabeling solutions.

## 4.6.2 HILIC buffers and mobile phase preparation

### 4.6.2.1 Ammonium formate (pH 3.2) stock buffer (100 mM)

Ammonium formate (3.16 g, 50 mmol) was dissolved in 475 mL deionised water. The pH was adjusted to pH 3.2 with ~ 5.25 mL formic acid and mixed well. The total volume was adjusted to 500 mL with additional deionised water.

### 4.6.2.2 Ammonium acetate (pH 5.8) stock buffer (100 mM)

Ammonium acetate (3.86 g, 50 mmol) was dissolved in 475 mL deionised water. The pH was adjusted to pH 5.8 with ~ 0.25 mL acetic acid and mixed well. The total volume was adjusted to 500 mL with additional deionised water.

### 4.6.2.3 Weak mobile phase, A (90% MeCN, 10% water, 5 mM ionic strength)

450 mL MeCN, 25 mL deionised water, and 25 mL stock buffer (100 mM pH 3.2 ammonium formate, or 100 mM pH 5.8 ammonium acetate) were mixed before thorough ultrasonic degassing for 30 min.

### 4.6.2.4 Strong mobile phase, B (50% MeCN, 50% water, 5 mM ionic strength)

250 mL MeCN, 225 mL deionised water, and 25 mL stock buffer (100 mM pH 3.2 ammonium formate, or 100 mM pH 5.8 ammonium acetate) were mixed before thorough ultrasonic degassing for 30 min.

## 4.6.3 HPLC details

Both reversed-phase and HILIC HPLC analyses were performed on an Agilent 1200 system, with a variable wavelength UV detector and a LabLogic Flow-RAM  $\beta^+$  detector equipped in series. All non-radioactive reference compounds were previously synthesised, as detailed in an earlier section of this thesis.

### 4.6.3.1 Reversed-phase HPLC methods

*Column:* Agilent Zorbax Eclipse XDB-C18, 5  $\mu$ m, 4.6 x 150 mm

*UV detector wavelength:* 210 nm

*Isocratic method A:* 30% H<sub>2</sub>O, 70% MeCN (0.1% TFA) at 1mL/min for 10 min

#### **4.6.3.2 HILIC HPLC methods**

*Column:* Phenomenex Luna HILIC 200Å, 5 µm, 4.6 x 150 mm

*UV detector wavelength:* 210 nm

*Scouting gradient:* 100% **A** isocratic [0-3 min]; 100% **A** to 100% **B** gradient [3-12 min]; 100% **B** isocratic [12-15 min]; at 1mL/min

*Isocratic methods:* All isocratic analyses were performed using the pre-prepared 5 mM buffered mobile phases (weak, **A**; and strong, **B**) as detailed above. The binary pump of our HPLC system was used to combine these two mobile phases and deliver the desired mobile phase composition to the column (at 1mL/min), allowing a wide range of isocratic solvent compositions to be screened

#### **4.6.4 Radiolabeling solution preparations**

The radiolabeling solutions described herein are representative examples taken from the unoptimised “literature conditions” syntheses. The exact quantities of reagents/solvents used were varied throughout the optimisation process, but the methods of solution preparation remained constant.

##### **4.6.4.1 Trapping solution A (with free amine)**

L-glutamic acid di-*tert*-butyl ester hydrochloride (8.9 mg, 30 µmol) was dissolved in 20 mL 0.1M NaOH solution in a separatory funnel. 10 mL EtOAc was added and shaken before separation of the organic layer. The aqueous layer was extracted a further 3 times with 10 mL portions of EtOAc and these organic extracts were combined. This solution was washed with saturated NaCl solution before drying over MgSO<sub>4</sub>. The EtOAc was removed under reduced pressure on a rotary evaporator to yield the free amine as a clear viscous oil (7 mg, ~ 90% extraction efficiency). The oil was dissolved in an appropriate quantity of anhydrous MeCN, which varies depending on extraction efficiency, in this



case: 441  $\mu\text{L}$  was required. 300  $\mu\text{L}$  of this solution (containing 18.3  $\mu\text{mol}$  of L-glutamic acid di-*tert*-butyl ester) was transferred to a 1.5 mL v-shaped glass vial containing a micro stirrer-bar under argon and the vial headspace was purged thoroughly to remove any atmospheric contamination. To this solution, DBU (0.51  $\mu\text{L}$ , 3.4  $\mu\text{mol}$ ) was added and the vial was crimp-sealed with a PTFE/silicone septum.

#### 4.6.4.2 *Trapping solution B (with amine hydrochloride salt)*

L-glutamic acid di-*tert*-butyl ester hydrochloride (5.4 mg, 18.3  $\mu\text{mol}$ ) was suspended in 300  $\mu\text{L}$  anhydrous MeCN in a 1.5 mL v-shaped glass vial containing a micro stirrer-bar under argon and the vial headspace was purged thoroughly to remove any atmospheric contamination. To this suspension, DBU (3.25  $\mu\text{L}$ , 21.7  $\mu\text{mol}$ ) was added, where upon agitation, the suspended hydrochloride salt fully dissolved to yield a clear, colourless solution. Finally, the vial was crimp-sealed with a PTFE/silicone septum.

#### 4.6.4.3 *Mitsunobu solution*

Under argon, DBAD (8.4 mg, 36.6  $\mu\text{mol}$ ) was dissolved in 100  $\mu\text{L}$  anhydrous MeCN in a 1.5 mL v-shaped glass vial forming a clear yellow solution.  $\text{PBU}_3$  (9.2  $\mu\text{L}$ , 36.6  $\mu\text{mol}$ ) was added, the vial was crimp-sealed with a PTFE/silicone septum and the mixture was briefly agitated. A colour change of the solution from pale yellow-to-colourless was observed on successful formation of the active betaine species.

#### 4.6.5 **Radiochemistry: synthesis of [ureido-<sup>11</sup>C]Glu-Glu-(O<sup>t</sup>Bu)<sub>4</sub>**

This target compound was synthesised many times in this optimisation process, the procedures described herein represent the initial “literature conditions” as well as the final optimised conditions. The overall method was kept constant throughout the optimisation process, with only temperatures, reaction times, and reagent quantities/stoichiometries varied accordingly.

##### 4.6.5.1 *Radiolabeling according to “literature conditions”*

Trapping vial A (18.3  $\mu\text{mol}$  free amine, 3.4  $\mu\text{mol}$  DBU, 300  $\mu\text{L}$  MeCN) was placed in the temperature-controlled vial-holder of the Modular-Lab system. A short vent needle

was inserted through the septum (into the vial headspace), and connected to a gas waste bag *via* an ascarite cartridge (to capture any unreacted [<sup>11</sup>C]CO<sub>2</sub>). The long gas delivery needle was inserted through the septum and submerged below the level of the trapping solution. The vial was cooled to 0°C, and immediately after the end of cyclotron bombardment, [<sup>11</sup>C]CO<sub>2</sub> was delivered through the solution in a stream of helium over ~ 1 min 45 secs. The end of delivery could be observed by visual confirmation that bubbling had stopped and was correlated with a peak in accumulated radioactivity in the vial, as measured by the pin-diode detectors in the Modular-Lab system. Once delivery was complete, the vial temperature was raised to 50°C (taking approx. 2 min) and once this temperature was reached, the previously prepared Mitsunobu solution (**36.6 μmol DBAD/PBu<sub>3</sub>, 100 μL MeCN**) was added to the reaction solution by injection through the septum. The reaction was stirred at 50°C for 2 min, before 100 μL H<sub>2</sub>O (containing 0.1 % TFA v/v) was injected to quench the reaction. The radioactivity contents in the vial and ascarite cartridge were measured, and a sample from the reaction vial was analysed by reversed-phase radio-HPLC, using the previously described isocratic method **A**.

#### 4.6.5.2 *Optimised radiolabeling conditions*

Trapping vial **B** (**18.3 μmol amine hydrochloride salt, 21.7 μmol DBU, 300 μL MeCN**) was placed in the temperature-controlled vial-holder of the Modular-Lab system. A short vent needle was inserted through the septum (into the vial headspace), and connected to a gas waste bag *via* an ascarite cartridge (to capture any unreacted [<sup>11</sup>C]CO<sub>2</sub>). The long gas delivery needle was inserted through the septum and submerged below the level of the trapping solution. The vial was cooled to 0°C, and immediately after the end of cyclotron bombardment, [<sup>11</sup>C]CO<sub>2</sub> was delivered through the solution in a stream of helium over ~ 1 min 45 secs. The end of delivery could be observed by visual confirmation that bubbling had stopped and was correlated with a peak in accumulated radioactivity in the vial, as measured by the pin-diode detectors in the ModularLab system. Once delivery was complete, the vial temperature was raised to 80°C (taking approx. 2 min 30 secs) and once this temperature was reached, the previously prepared Mitsunobu solution (**9.2 μmol DBAD/PBu<sub>3</sub>, 100 μL MeCN**) was added to the reaction solution by injection through the septum. The reaction was stirred at 80°C for 2 min, before 100 μL H<sub>2</sub>O (containing 0.1 % TFA v/v) was injected to quench the reaction. The

radioactivity contents in the vial and ascarite cartridge were measured, and a sample from the reaction vial was analysed by reversed-phase radio-HPLC, using the previously described isocratic method A.

## 5 PSMA SECTION 3 – GENERALLY-APPLICABLE ASYMMETRIC <sup>11</sup>C-RADIOLABELING METHOD

### 5.1 Introduction

#### 5.1.1 Context & motivations

In chapter 4, we attempted to develop a method for the <sup>11</sup>C-radiolabeling of a symmetrically substituted glutamate urea ([<sup>11</sup>C]Glu-Glu), a high affinity PSMA-ligand. The *tert*-butyl protected intermediate, [<sup>11</sup>C]Glu-Glu-(O<sup>t</sup>Bu)<sub>4</sub>, was successfully produced *via* DBU-mediated [<sup>11</sup>C]CO<sub>2</sub> fixation followed by Mitsunobu-mediated <sup>11</sup>C-urea synthesis. However it was not possible to attempt the deprotection stage due to the difficulties encountered in developing a suitable analytical HPLC method for this compound. These issues forced a reconsideration of our motivations, and it became clear that a *general* method for <sup>11</sup>C-radiolabeling within the common glutamate-urea pharmacophore of PSMA-targeted ligands could be of much greater value than a single <sup>11</sup>C-radiolabeled diagnostic PSMA radiotracer could be. Nearly all small molecule PSMA-targeted compounds are built around this common glutamate-urea core, whether they be diagnostic PET radiotracers, targeted radionuclide therapeutics, or other non-radiation based probes/therapeutics.<sup>270,271,273</sup> The development of PSMA as a biomarker is leading to a real paradigm shift in the diagnosis, monitoring, and treatment of prostate cancer. The research is by no means “settled”; newer-generation radiotracers and radiotherapeutics are in ongoing development. Furthermore, there remain unsolved challenges regarding PSMA distribution outside of prostate cancer tissue: whether it be regarding its presence in healthy non-prostatic tissue (e.g. salivary glands), as well as its presence and possible role in other cancers (e.g. renal cell carcinoma). Accordingly, a general method to isotopologously radiolabel within the core of these PSMA-targeted small-molecules could be a highly valuable tool in a number of different applications.

##### 5.1.1.1 Diagnostic agents – ultra-high affinity <sup>11</sup>C-radiotracers

The most straightforward possible application of such a method would be the radiolabeling of ultra-high-affinity PSMA ligands. There exist a number of compounds

well-documented in the literature that have extremely high affinities for PSMA, but due to the absence of any fluorine/iodine atoms within the structure, isotopologous radiolabeling of these molecules is otherwise impossible. Take, for example, the compounds synthesised by Maresca *et al.* in their work developing halogenated PSMA ligands.<sup>305</sup> In this work, a series of asymmetric glutamate-urea based PSMA ligands were synthesised and their PSMA binding affinities were measured. The highest-affinity iodinated compounds (with  $K_i$  values of 22 and 10 nM) were subsequently <sup>123/131</sup>I-radiolabeled and advanced for further preclinical investigation. However, of the library of halogenated PSMA-ligands they synthesised, the highest affinities were the chlorinated and brominated compounds with 5-10x higher target affinities than the respective iodinated analogues, but these most-promising candidates were radiochemically inaccessible (at least with with traditionally-used and widely-accessible radiohalogens). With a general method for the installation of a carbon-11 radiolabel within the glutamate-urea pharmacophore, all of the ligands reported within this paper could theoretically be radiochemically accessible.

In this example case, the highest affinity compounds developed were still in the nanomolar range, however it is possible to envisage a situation where an ultra-high (picomolar) affinity PSMA-ligand could be developed, but where the incorporation of a radiohalogen serves to compromise its ultra-high binding affinity. In such a situation, the ability to isotopologously radiolabel this ligand could be of great value, and by <sup>11</sup>C-radiolabeling within the near-universally-present glutamate-urea core, this is theoretically possible.

#### **5.1.1.2 Library <sup>11</sup>C-radiosynthesis for candidate <sup>18</sup>F-radiotracers**

In the development of new-generation PSMA-targeted <sup>18</sup>F-radiotracers, each candidate molecule can require unique and lengthy radiolabeling conditions depending on the exact position of the <sup>18</sup>F-label.<sup>506</sup> Since the <sup>18</sup>F-radiolabel is generally incorporated onto a linker scaffold bound to the glutamate-urea pharmacophore through a lysine sidechain, every time that linker or sidechain is modified to improve, for example, the molecule's binding affinity or biodistribution, it also modifies the conditions required for radiolabeling. As a result, the preclinical screening of just three or four <sup>18</sup>F-radiolabeled candidate PSMA

ligands could require a large amount of radiolabeling method-development work. This is an example of a plausible scenario in-which a library <sup>11</sup>C-radiosynthesis could help to significantly streamline the development process. Library <sup>11</sup>C-radiosynthesis is described in the introduction to this thesis (section 1.3.1.3, page 26).

### 5.1.1.3 *Therapeutic dosimetry*

PSMA-PET is rapidly becoming an element of the prostate cancer standard-of-care as a routine diagnostic tool, and in addition to imaging, there are a number of highly promising PSMA-targeted radionuclide therapy approaches. Other than the small number of antibody-based agents, the vast majority of the “state-of-the-art” therapeutic PSMA-radioligands are built upon the glutamate-urea scaffold, which has been labeled with  $\alpha$ ,  $\beta$ , and Auger-electron emitting radionuclides.<sup>332–336,338,507–512</sup> In addition to targeted radionuclide therapy, there are ongoing studies into the development of PSMA targeted boron neutron capture therapy (BNCT),<sup>340</sup> and photodynamic therapy (PDT).<sup>513</sup>

The *in vivo* biodistribution of these targeted therapeutics must be known in order to calculate dosimetry and minimise off-target side-effects. This is particularly important in-light of the non-prostate-cancer-associated incidental PSMA-binding observed in salivary glands and kidneys.<sup>344,514–516</sup> Some of these therapeutics (such as the iodine/copper radiolabeled compounds) have isotopologous theranostic labeling options,<sup>331,507</sup> but many rely on similar but non-identical theranostic pairings (for example, PSMA-I&T has a DOTA chelator incorporated which can be used with <sup>68</sup>Ga for imaging and <sup>177</sup>Lu for therapy).<sup>330</sup> While this may be an acceptable theranostic pair for PET-monitoring of radiotherapy response, because of the differences in their coordination chemistry (Ga is 6-coordinate while Lu is 8-coordinate in DOTA, which could theoretically lead to significant differences in their *in vivo* behaviour) PET imaging cannot predict with 100% accuracy the biodistribution and pharmacokinetics of the <sup>177</sup>Lu-labeled compound, which would be required for the most accurate dosimetry predictions. Additionally in the radiation sensitising therapy examples (BNCT and PDT), while target engagement can be probed with alternative PSMA-targeted radiotracers, there is no alternative method for accurate dosimetry predictions other than preclinical *ex vivo* biodistribution studies.<sup>340</sup>

A method for <sup>11</sup>C-labeling all PSMA-targeted small-molecule therapeutics would allow true *in vivo* biodistribution/pharmacokinetic studies of the exact therapeutic agent, giving the most reliable therapeutic dosimetry data as opposed to that obtained with similar but non-identical radionuclide swaps (e.g. <sup>68</sup>Ga/<sup>177</sup>Lu-PSMA-I&T). This concept whereby the exact same molecule can be radiolabeled with two different radionuclides in different locations has variously been referred to as a “radiohybrid”<sup>517</sup> or a “molecular twin”,<sup>518</sup> and is an appealing prospect for the future of theranostics development beyond this somewhat imperfect <sup>68</sup>Ga/<sup>177</sup>Lu “theranostic pair”. <sup>11</sup>C-radiolabeling of <sup>nat</sup>Ga/<sup>nat</sup>Lu-PSMA-I&T could also help to further explore the differences between compound biodistributions, since the effect of these different metals (with their varying coordination chemistry) on the *in vivo* biodistribution of these complexes is still not well understood and remains a relatively unanswered question in an area of current interest. This could go some way to answering whether the use of these as a “theranostic” pair is indeed appropriate or not.

#### 5.1.1.4 Fundamental PSMA research

In light of the overwhelming popularity of PSMA as a diagnostic and therapeutic target, it is important that the details of the ligand-binding-site interactions, are as completely understood as possible, particularly where this can inform in the development of new-generation PSMA radiotracers. While the first-generation radiotracers were effectively designed to simply maximise PSMA-binding, less consideration was given to the radiotracer’s pharmacokinetics. The second-generation development has focused on addressing the practical shortcomings in the imaging-performance of the first-generation radiotracers: signal-noise ratios have been improved by reducing nonspecific-binding and increasing blood-pool clearance rates,<sup>319,320</sup> and clearance pathways have been altered from the usual renal clearance in favour of hepatobiliary excretion – improving the performance of these radiotracers in the imaging/detection of pelvic lesions.<sup>321,326,443,519,520</sup>

Particular attention has been paid to the structure-activity relationships (SAR) of the group linking the glutamate-ureido PSMA-targeting moiety with the radiometal chelator or <sup>18</sup>F-prosthetic group (PG). Researchers have experimented with different linker

lengths, rigidities, and lipophilicities to alter the binding affinities and internalisation rates of these new radioligands.<sup>271,273,328,443,521–523</sup> However, these SAR investigations are made difficult by the necessity of attaching bulky chelators or PGs on the sidechain to enable radiolabeling. It is therefore difficult to deconvolve the effects of the linker modifications being explored from the incidental but non-benign introduction of an aromatic PG or large chelator.

Ligand-receptor binding interactions, and the imaging implications thereof, are a result of many complex and highly-interdependent factors. Investigating, for example, the effect of increasing linker lipophilicity on the imaging characteristics of a number of <sup>18</sup>F-labeled PSMA ligands may establish an SAR profile for this sub-class of ligands, but the results cannot confidently be extended to other ligand sub-classes labeled in a different manner. The result has been that while there is a great deal of published PSMA-ligand SAR data, these remain only of marginal benefit to the future investigator who seeks to develop a new-generation PSMA ligand. A general method for isotopologously <sup>11</sup>C-radiolabeling the universally-present glutamate-urea moiety in PSMA-targeted compounds could theoretically help to deconvolve these SAR studies. By obviating the need for a potentially-conflicting chelator/PG, it could provide a tool for the rational and systematic exploration of PSMA imaging SAR in enabling true like-for-like comparisons of the effects of differing structural modifications. This should provide a more solid fundamental basis from which any new-generation PSMA-radiotracers can be rationally designed.



## 5.1.2 Synthetic approach

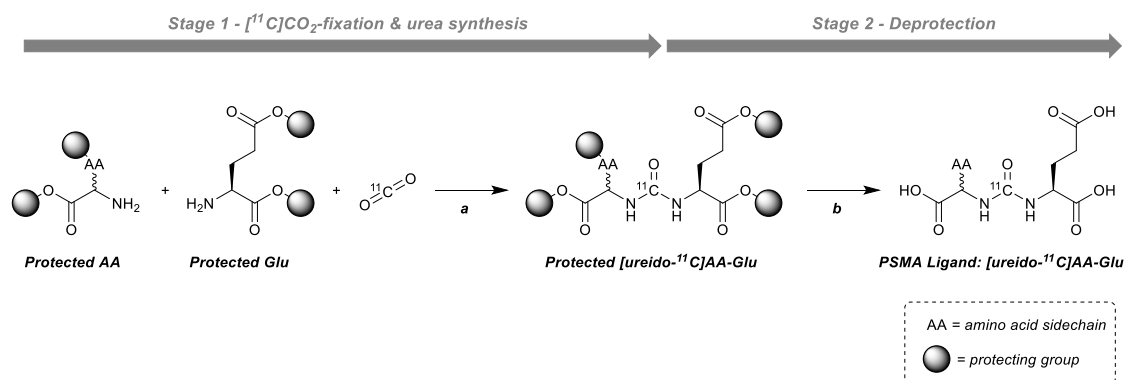


**Figure 5.1 Overall radiosynthetic scheme – separated into two major stages**

a: DBU and PBU<sub>3</sub>/DBAD; or BEMP and POCl<sub>3</sub>

b: Usually strongly acidic or basic conditions (depending on protecting group)

The reaction was intended to proceed *via* two major stages which are shown in the scheme above. Firstly, the fully-protected  $^{11}\text{C}$ -urea intermediate will be produced, before the various protecting groups are cleaved to yield the desired asymmetric  $^{11}\text{C}$ -urea.

Similarly to the approach employed in chapter 4, the radiosynthetic method being adapted in the first stage (the fully-protected  $^{11}\text{C}$ -urea synthesis) is a [ $^{11}\text{C}$ ]CO<sub>2</sub>-fixation method. In this, [ $^{11}\text{C}$ ]CO<sub>2</sub> is fixed onto the *tert*-butyl ester protected glutamic acid precursor amine as the  $^{11}\text{C}$ -carbamate salt intermediate, which is subsequently dehydrated to produce the key  $^{11}\text{C}$ -isocyanate, which reacts again with another protected amino acid precursor amine to form the fully-protected  $^{11}\text{C}$ -urea. In chapter 4, the method adapted was the DBU/Mitsunobu method for  $^{11}\text{C}$ -urea synthesis as was developed by other members of our group.<sup>225,226</sup> By comparison, in this section of work we adapted the BEMP/POCl<sub>3</sub> method originally developed several years previously by Wilson *et al.*<sup>214</sup> In this method, BEMP is used as the fixation-promoting superbases in an analogous role to that of DBU, and POCl<sub>3</sub> serves as the dehydrating agent in place of the Mitsunobu reagents.

We opted to investigate this alternative methodology for several reasons. Firstly, we had intermittently experienced frustrating failures of our Mitsunobu-mediated syntheses due to adventitious water contamination, and we hoped that this method may be more tolerant to trace water contamination, leading to a more reliable reaction. Secondly, as it is known

that the DBU/Mitsunobu method is superior to the BEMP/POCl<sub>3</sub> method for radiolabeling aromatic substrates,<sup>214,225,226</sup> there are clearly some differences in substrate scope between these two reactions. So in the possibility that the BEMP/POCl<sub>3</sub> method was better suited to radiolabeling our target structures for some reason, we opted to initially explore the use of this BEMP/POCl<sub>3</sub> method, with the knowledge that we could return to the use of the Mitsunobu method that had already been demonstrated to produce reasonable yields of the symmetric-glutamate <sup>11</sup>C-urea.

## 5.2 Results & Discussion – Asymmetric <sup>11</sup>C-Urea Synthesis

### 5.2.1 Approach and general considerations

As was explained in the introduction to this chapter, the overall aim of this section of work was to develop a generally-applicable method for the *ureido*-<sup>11</sup>C-radiolabeling of PSMA-targeted ligands incorporating the glutamate-urea pharmacophore. In the course of our method-development efforts, this was broken down into two key reaction stages:

1. Synthesis of fully-protected asymmetric <sup>11</sup>C-urea intermediates
2. Deprotection to yield <sup>11</sup>C-radiolabeled PSMA-targeted ligands

Crucially during this method-development process, it was important to bear-in-mind the envisaged end-use case of this method. It was hoped that this method could be used to easily <sup>11</sup>C-radiolabel a library of structurally/functionally-diverse PSMA-targeted compounds without additional substrate-specific optimisation. Simply-put, another radiochemist should be able to use this as a tool to quickly pre-clinically screen a library of candidates without first optimising the method for each particular substrate. As such, it was important that as many steps as possible in the method were generic (applicable in all cases) and well optimised.

The urea-synthesis stage, discussed in this section, can be further broken-down into two sub-stages which can be controlled and optimised separately from one-another:

1. [<sup>11</sup>C]CO<sub>2</sub>-fixation and dehydration, yielding the <sup>11</sup>C-isocyanate *in situ*
2. Reaction of an amine with the <sup>11</sup>C-isocyanate, yielding the <sup>11</sup>C-urea

The first of these sub-stages is a fairly difficult transformation to achieve: [<sup>11</sup>C]CO<sub>2</sub> is a relatively unreactive (due to the strength of the C=O bonds) gaseous reagent that is sparingly soluble in most organic solvents. So while it is firstly difficult to bring it into solution, driving a reaction which breaks these C=O bonds is even more challenging. As such, a strong fixation superbase (BEMP) is used to help stabilise the otherwise-transient carbamate intermediate formed in solution, and a powerful dehydration agent (POCl<sub>3</sub>) is required to reduce the carbamate to the desired isocyanate. This is a difficult reaction to perform, and due to the strength/reactivity of BEMP and POCl<sub>3</sub>, there are a number of

unproductive side-reactions which can easily occur. This sub-stage of the reaction can therefore be highly substrate-specific and requires much optimisation.

By comparison, the second sub-stage – the nucleophilic attack of an amine on an  $^{11}\text{C}$ -isocyanate – is a much more straightforward process; so much so that it can arguably be considered to meet the definitions of a “click” reaction, in that it is “spring-loaded for a single trajectory”.<sup>221,524</sup> An isocyanate will react rapidly and predictably with an amine to form a urea, without additional heating or significant undesired side reactions (excepting the reaction with water, hence the use of anhydrous solvents/reagents). As a result, this second sub-stage required much less optimisation and attention.

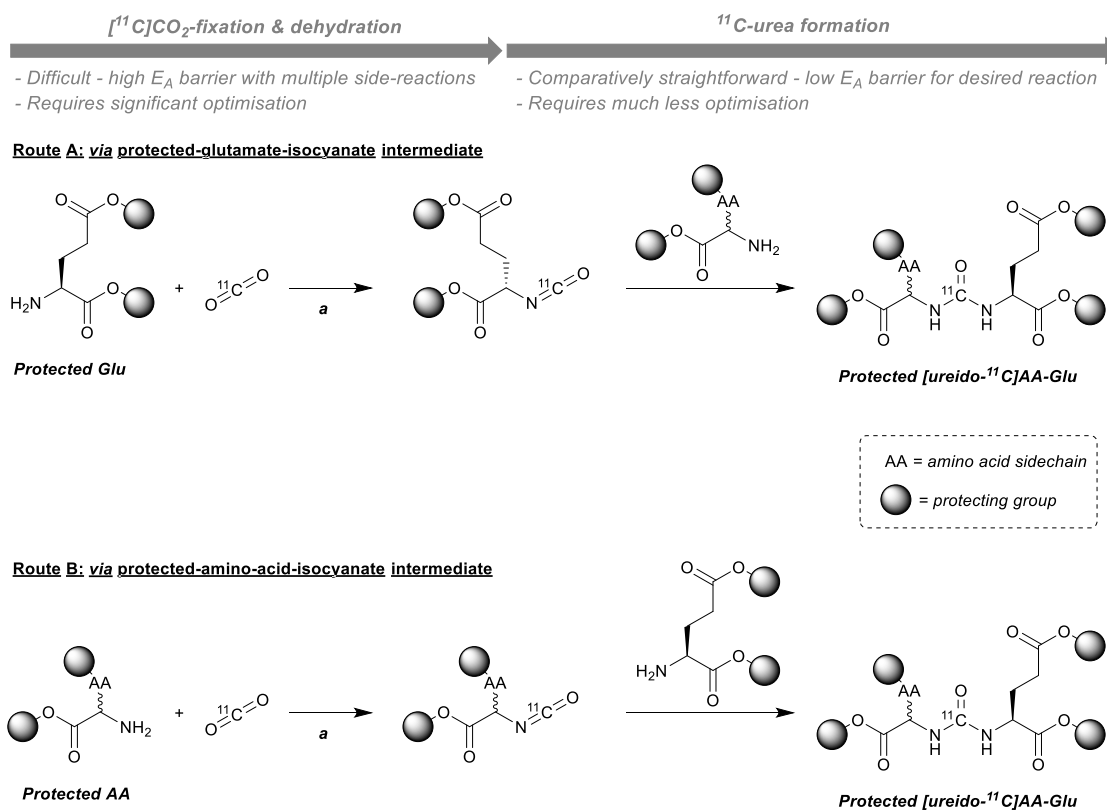


**Figure 5.2 Two possible routes to protected  $^{11}\text{C}$ -ureas**

Same product is obtained in each case, but with route **A**, the  $[^{11}\text{C}]\text{CO}_2$  fixation & dehydration to form the isocyanate will remain constant, regardless of the target  $^{11}\text{C}$ -urea product, whereas route **B** will require separate optimisation for each individual target. **a**) i) BEMP; ii)  $\text{POCl}_3$

The radiosynthesis of asymmetric  $^{11}\text{C}$ -ureas (from two different amines, **1** and **2**) via intermediate  $^{11}\text{C}$ -isocyanate formation can theoretically be achieved by effecting the  $[^{11}\text{C}]\text{CO}_2$  fixation on either amine. This would form a carbamate intermediate which is

converted rapidly to the corresponding isocyanate, and finally this <sup>11</sup>C-isocyanate is reacted with the other amine to give an asymmetric disubstituted urea. Setting aside (for the sake of argument) the consideration of their differential reactivities with [<sup>11</sup>C]CO<sub>2</sub>, it is equally possible to arrive at the same target urea by proceeding *via* the intermediate <sup>11</sup>C-isocyanate derivatives of amine **1** or **2**.

In our application of this reaction to PSMA-ligands, one of these two amine components will always remain fixed (*L*-glutamic acid di-*tert*-butyl ester), while the other is varied depending on the target compound. With this in mind, it was decided that the more-challenging and substrate-specific sub-stage of the reaction ([<sup>11</sup>C]CO<sub>2</sub>-fixation and dehydration, to form the <sup>11</sup>C-isocyanate) should be optimised using the amine component that is common to all possible applications of the method: the protected glutamate derivative (Route **A** depicted in the figure above). While it would still require significant optimisation initially, once optimal conditions are found they should be reproduced in all applications of this method since this amine substrate will remain constant. The second step – the reaction of the amine with the <sup>11</sup>C-isocyanate – is much more “spring-loaded” towards a relatively clean and efficient urea formation reaction, and should be much less substrate-specific, which is crucial due to the wide variety of amine substrates that could theoretically be used at this stage.

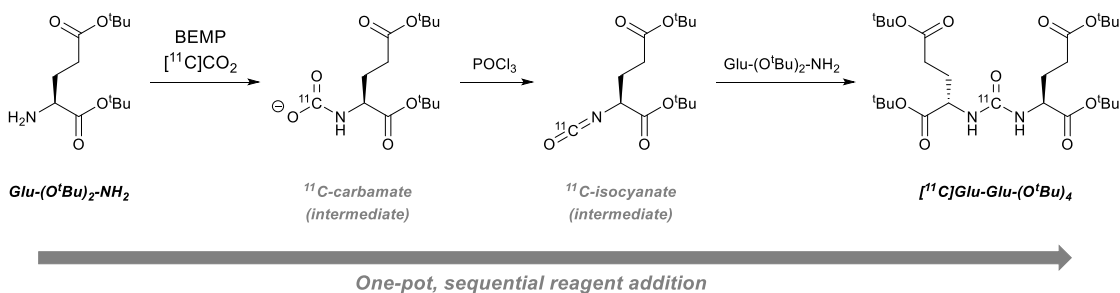
During this optimisation work, the two important aspects of this first stage which received much of our focus were: i) the BEMP-mediated [<sup>11</sup>C]CO<sub>2</sub>-fixation; and ii) the reaction’s asymmetric selectivity.

Firstly, in this reaction BEMP is intended to play the same role as DBU in our earlier Mitsunobu-mediated symmetrical <sup>11</sup>C-urea syntheses: it primarily acts as a strong base to deprotonate and stabilise the transiently formed <sup>11</sup>C-carbamic acid as the <sup>11</sup>C-carbamate salt. However, as is common for these fixation-mediating superbases, it is also capable of directly trapping [<sup>11</sup>C]CO<sub>2</sub> by itself which can introduce complications, unproductive side-reactions, and mechanistic confusion. This potentially conflicting reactivity was explored, leading to some seemingly counter-intuitive results.

Secondly, due to the inherent nano/picomolar quantities of [<sup>11</sup>C]CO<sub>2</sub> produced, all other reagents are used in a multifold stoichiometric excess. As such, a reaction which may be

relatively easy to control on a macro-scale can be more difficult to control in a radiochemical setting; otherwise minor side-reaction pathways can dominate under this stoichiometry. The major issue with these recently-developed <sup>11</sup>C-urea syntheses is that the key <sup>11</sup>C-isocyanate intermediate is formed *in situ*, in the presence of an excess of its own unreacted precursor amine. If this excess amine is not rapidly consumed by another reagent, the <sup>11</sup>C-isocyanate will readily react with it, forming the undesired symmetrical <sup>11</sup>C-urea (this is the downside to the “spring-loaded” reactivity of isocyanates). To suppress this pathway, and achieve a reaction that selectively forms the asymmetric urea product, conditions must be altered to allow the isolation of this intermediate <sup>11</sup>C-isocyanate from any undesired reaction partners (amines/alcohols etc.). After this, the desired reaction partner (the second amine substrate) can be introduced and the intended asymmetric <sup>11</sup>C-urea formation pathway can be selectively promoted.

The majority of the optimisation experiments used the synthesis of the asymmetric [*ureido*-<sup>11</sup>C]Leu-Glu (and its fully protected intermediate, [*ureido*-<sup>11</sup>C]Leu-Glu-(O<sup>t</sup>Bu)<sub>3</sub>) as a model reaction. The asymmetrically-disubstituted leucine-glutamate urea (often referred to in the literature as ZJ43) is an ultra-high affinity ( $k_i = 0.8 \text{ nM}$ )<sup>300</sup> PSMA ligand. It is commonly sold and used (alongside 2-PMPA) as a reference high-affinity PSMA blocker/inhibitor in both the preclinical investigation of other PSMA-targeted diagnostic and therapeutic agents,<sup>525</sup> as well as in the more-fundamental *in vitro/in vivo* investigation of PSMA/GCPII biological function.<sup>526,527</sup> In addition to this well-validated affinity for PSMA, from a more practical-standpoint the molecule itself should be a simple model-substrate. It bears no additional functional groups which could otherwise interfere with the reaction, and the additional degree of lipophilic character provided by the isobutyl sidechain was sufficient to enable facile retention and analysis of the tricarboxylic molecule on a standard reversed-phase HPLC column.

5.2.2 Proof-of-concept symmetric  $^{11}\text{C}$ -urea synthesis: [ $^{11}\text{C}$ ]Glu-Glu-( $\text{O}^t\text{Bu}$ ) $_4$ 

**Figure 5.3** Scheme of [ $^{11}\text{C}$ ]Glu-Glu-( $\text{O}^t\text{Bu}$ ) $_4$  synthesis via BEMP/ $\text{POCl}_3$

$^{11}\text{C}$ -carbamate and  $^{11}\text{C}$ -isocyanate intermediates are not isolated and are simply formed and further reacted *in situ*

The first radiosynthesis in this section of work was a simple proof-of-concept, linking this chapter with the previous. The BEMP/ $\text{POCl}_3$  method was used to radiolabel the fully-protected symmetric urea, [ $^{11}\text{C}$ ]Glu-Glu-( $\text{O}^t\text{Bu}$ ) $_4$ , that was previously radiolabeled with the DBU/Mitsunobu method. Compared with the Mitsunobu method, where the byproducts are fairly innocuous and unreactive (DBAD- $\text{H}_2$  and  $\text{Bu}_3\text{PO}$ ), the BEMP/ $\text{POCl}_3$  method can be somewhat harsher due to the  $\text{HCl}$  byproduct from the decomposition of  $\text{POCl}_3$ , and has led to reported issues with some substrate incompatibilities.<sup>241,242</sup> Whilst we did not expect the  $\text{HCl}$  byproduct to be produced in a sufficiently high concentration as to cause significant decomposition of the precursor or product, it was easier to check for this by testing on a known compound before advancing to any more-novel targets. Additionally, as this target urea is symmetrically substituted, it entirely removes the potentially complicating factors that a second amine precursor would introduce were the target an asymmetric urea

In the absence of any other experience with this reaction, the conditions used for this initial radiosynthesis were adapted from those employed by Wilson *et al.* in their 2010 report detailing the development of this BEMP/ $\text{POCl}_3$  method.<sup>433</sup> In an extension of our work discussed in chapter 4, the hydrochloride salt was used directly without prior deprotonation: the molar excess of BEMP served to deprotonate the ammonium salt and release the active free-amine *in situ*, in addition to its primary role of mediating the [ $^{11}\text{C}$ ]CO $_2$  fixation process.

To briefly summarise the process stages:

1. [<sup>11</sup>C]CO<sub>2</sub> was bubbled (70mL/min) through a pre-prepared solution of amine hydrochloride salt (5 μmol, 1 equiv.) and BEMP (22 μmol, 4.4 equiv.) in 100 μL MeCN
2. Immediately following [<sup>11</sup>C]CO<sub>2</sub> delivery, a solution of POCl<sub>3</sub> (21.5 μmol, 4.3 equiv.) in 100 μL MeCN was added and the vial was stirred for 30 seconds
3. A solution of amine hydrochloride salt (50 μmol, 10 equiv.) and BEMP (50 μmol, 10 equiv.) in MeCN was added and stirred for a further 60 seconds
4. The reaction was quenched with an aliquot of the HPLC eluent (30% H<sub>2</sub>O / 70% MeCN) and immediately injected onto the radio-HPLC for analysis

This initial procedure resulted in a reasonable trapping efficiency (~ 80%) but exhibited a somewhat underwhelming 16% RCC (as measured by radio-HPLC), resulting in an overall RCY of ~ 13%. From the crude radio-HPLC trace, it was clear that the majority of the radioactivity was still in a more-polar trapping product, eluting near to the solvent front. This suggested that the initial POCl<sub>3</sub>-mediated isocyanate formation reaction was still fairly incomplete within the initial 30 second reaction time allowed and suggested that there was easily scope for improvement. The results of these simple optimisation steps are presented in the table below.

**Table 5.1 Preliminary symmetrical <sup>11</sup>C-urea synthesis optimisation**

	Reaction Time [mins]	Reaction Temperature [°C]	RCC [%]	RCY [%]
<b>A</b>	<b>0.5</b>	<b>18</b>	<b>16</b>	<b>13</b>
<b>B</b>	<b>2</b>	<b>18</b>	<b>35</b>	<b>28</b>
<b>C</b>	<b>2</b>	<b>50</b>	<b>57</b>	<b>47</b>

General procedure: [<sup>11</sup>C]CO<sub>2</sub> bubbled through solution of *L*-glutamic acid di-*tert*-butyl ester (5 μmol) and BEMP (22 μmol) in MeCN (100 μL) at 20°C. Then temperature raised to 50°C and POCl<sub>3</sub> in MeCN (100 μL) was added. After 2 mins, solution of *L*-glutamic acid di-*tert*-butyl ester (50 μmol) and BEMP (50 μmol) in MeCN (200 μL) were added before quenching and analysing with radio-HPLC.

RCC was measured by radio-HPLC of crude reaction mixture  
RCY accounts for the ~80% fixation efficiency

Upon increasing the reaction time (in stage **2**) to 2 minutes, the RCC saw a corresponding improvement (35%). As the initial [<sup>11</sup>C]CO<sub>2</sub> trapping stage remained unchanged, the



[<sup>11</sup>C]CO<sub>2</sub> trapping efficiency remained unchanged (~ 80%), but combined with the improved RCC, this 2 minute reaction exhibited an improved RCY of 28%.

Finally, suspecting that these conditions were still insufficient as to allow full conversion of the trapped [<sup>11</sup>C]CO<sub>2</sub> to the desired <sup>11</sup>C-isocyanate intermediate, the reaction temperature in stages **2** and **3** was increased from the previous ambient temperature (~ 18°C) to 50°C. As a result of performing the reaction at 50°C with a 2 min stirring phase in stage **2**, the RCC was significantly improved again (57%), which combined with the reasonable trapping efficiency (80%) resulted in an overall non-isolated RCY of 47%.

These simple adjustments in the stage **2** POCl<sub>3</sub> reaction time (30 secs *versus* 2 mins) and temperature (18°C *versus* 50°C) resulted in a more than threefold increase in RCY (13% *versus* 47%). However, it was notable that these elevated reaction temperatures were not required to achieve reasonable RCYs for most of the example products in the original report of this method by Wilson *et al.*<sup>433</sup> For most of their simple aliphatic model reactions, RCYs in excess of 80-85% were achieved with 2 min reaction times at ambient temperature. The exceptions to this trend were the lowered RCYs encountered when using more-hindered and/or less nucleophilic aromatic amine precursors. It was inferred from this comparison that our protected glutamic acid precursor was a somewhat less-reactive nucleophile (whether it be due to basicity or steric factors) than most of the model aliphatic amines with which this reaction had previously been optimised. Consequently, this underlined the importance of paying close attention to the initial [<sup>11</sup>C]CO<sub>2</sub> fixation and <sup>11</sup>C-carbamate to <sup>11</sup>C-isocyanate conversion phases, to ensure that these are as well optimised and highly-efficient as possible since this is the substrate which will be common to all applications of this method to PSMA-ligands.

No further optimisation was attempted for this symmetrical <sup>11</sup>C-urea target since this was only intended as an exploratory proof-of-concept radiosynthesis and the primary aim of this chapter was to focus on the synthesis of asymmetrically substituted <sup>11</sup>C-ureas. It had successfully demonstrated the compatibility of this reaction with our *tert*-butyl protected glutamic acid precursor, and provided some insight into how this reaction could be expected to perform in general.

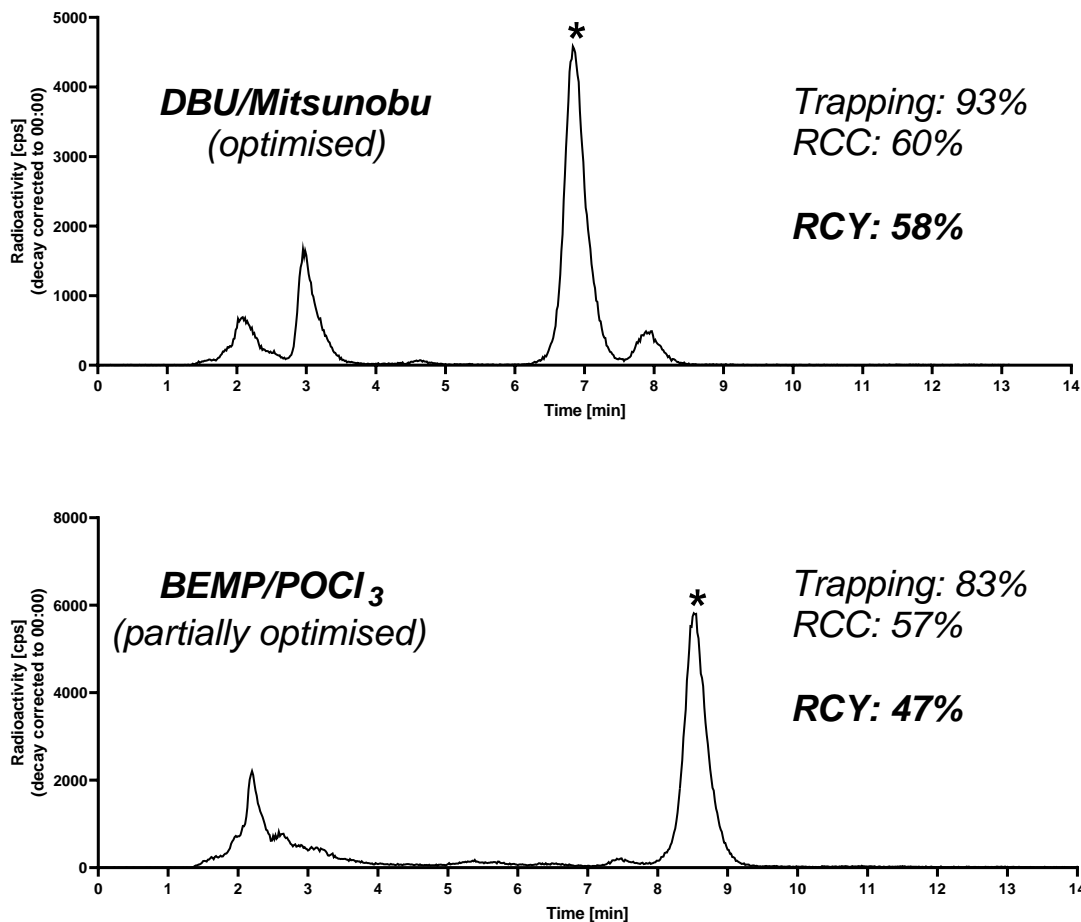


**Figure 5.4 Radiosyntheses of [ureido- $^{11}\text{C}$ ]Glu-Glu-(O<sup>t</sup>Bu)<sub>4</sub> by different methods**

\* Denotes product peak

Retention times vary slightly between the two chromatograms because different C18 columns were used for each analysis:

DBU/Mitsunobu: Agilent Zorbax Eclipse XDB-C18, 5  $\mu\text{m}$ , 4.6 x 150 mm

BEMP/POCl<sub>3</sub>: Phenomenex Luna C18(2), 5  $\mu\text{m}$ , 4.6 x 150 mm

(Both eluted with 30% H<sub>2</sub>O / 70% MeCN (0.1% TFA v/v) at 1 mL/min)

The final insight this provided was a direct comparison of the radiosynthesis of [ $^{11}\text{C}$ ]Glu-Glu-(O<sup>t</sup>Bu)<sub>4</sub> using either this BEMP/POCl<sub>3</sub> method or the DBU/Mitsunobu method as developed in chapter 4. The [ $^{11}\text{C}$ ]CO<sub>2</sub> trapping efficiency was better optimised in the DBU/Mitsunobu example (93%) versus the equivalent process in the BEMP/POCl<sub>3</sub> reaction (80%), but it was hoped that this would be further optimised throughout this scheme of work. In terms of the radio-HPLC profiles, they were broadly similar. The majority of the radioactivity in both cases exists either as an early-eluting polar trapping

product (~ 40%), or as the desired <sup>11</sup>C-urea fixation product (RCCs of ~ 57-60%). In these particular cases, the Mitsunobu method gave a marginally higher RCC (60% *versus* 57%), but the difference between the two methods was so small as to be essentially insignificant. However, one key difference to note was the total absence of any isocyanate intermediate (eluting shortly after the <sup>11</sup>C-urea product) observed in the BEMP/POCl<sub>3</sub> reaction compared to the small <sup>11</sup>C-isocyanate peak observed for the Mitsunobu method. This suggests that under our Mitsunobu conditions, there was still too little amine present to allow full conversion of the <sup>11</sup>C-isocyanate to the <sup>11</sup>C-urea. By comparison, following the literature procedure from Wilson *et al.*, the final stage (after formation of the <sup>11</sup>C-isocyanate with POCl<sub>3</sub>) involved the addition of a large excess of a second amine as this method was developed for asymmetrically disubstituted <sup>11</sup>C-ureas.

On a more pragmatic note, the BEMP/POCl<sub>3</sub> method was somewhat more operationally simple than the Mitsunobu method, due to the fact that the single-component POCl<sub>3</sub> solution (in MeCN) preparation was more straightforward to prepare than the analogous two-component PBu<sub>3</sub>/DBAD solution (in MeCN). It was encouraging that we were able to produce the fully protected [*ureido*-<sup>11</sup>C]Glu-Glu-(O<sup>t</sup>Bu)<sub>4</sub> in reasonably high RCYs within 5-6 mins from EoB, and this was promising for the intended development of a more general method for the BEMP/POCl<sub>3</sub>-mediated <sup>11</sup>C-radiolabeling of PSMA-ligands.

### 5.2.3 Fixation optimisation

#### 5.2.3.1 Mechanistic considerations – the role of BEMP

BEMP, a phosphazene base, has been used in an analogous manner to DBU in [<sup>11</sup>C]CO<sub>2</sub> fixation chemistry and by virtue of its often superior performance it has become arguably the more commonly used fixation base for these radiochemical applications. Similarly to DBU, BEMP can directly trap [<sup>11</sup>C]CO<sub>2</sub> in solution, and so it similarly follows that this [<sup>11</sup>C]CO<sub>2</sub>-trapping ability has led to suggestions that a BEMP-CO<sub>2</sub> species plays a role in the fixation mechanism by trapping, activating, and transferring [<sup>11</sup>C]CO<sub>2</sub> onto an amine substrate to form the amine carbamate product. In the introduction to this thesis, these claims were considered but we ultimately concluded that the formation of a BEMP-CO<sub>2</sub> adduct is incidental to its productive mechanistic role in deprotonating the transiently-formed <sup>11</sup>C-carbamic acid intermediate, to form the stabilised phosphazanium <sup>11</sup>C-carbamate salt.

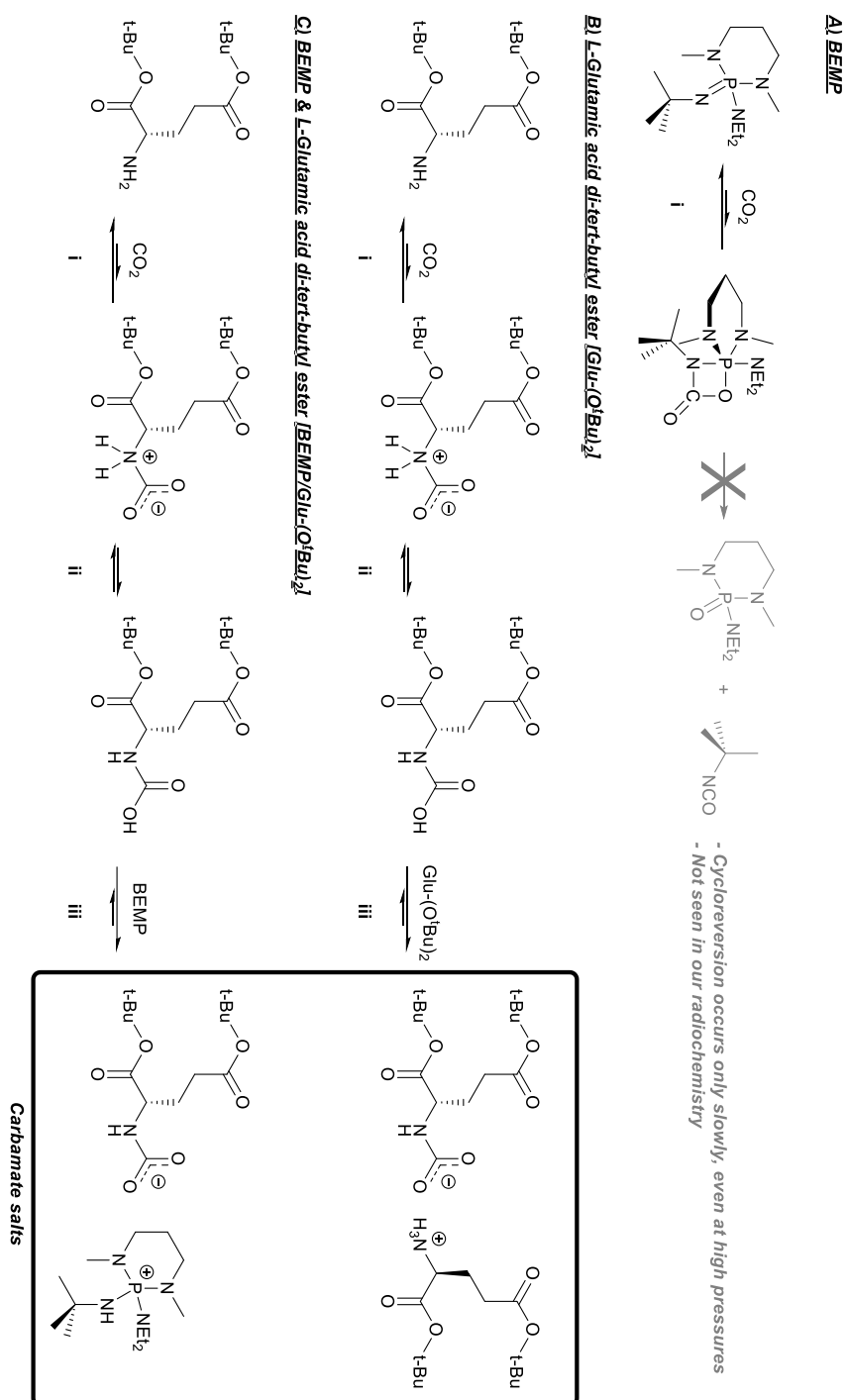


**Figure 5.5 Possible reactions between  $[^{11}\text{C}]\text{CO}_2$  and BEMP/Glu-(O<sup>t</sup>Bu)<sub>2</sub>**

Suggested 4-membered ring intermediate in **A** is adapted from work by Courtemanche *et al.*<sup>172</sup> This theoretically can proceed *via* a cycloreversion to yield the *tert*-butyl isocyanate, but in practice this is too slow due to steric bulk of BEMP and is not observed in our short reaction at atmospheric pressure

The figure above illustrates the major possible reactions which could occur as [<sup>11</sup>C]CO<sub>2</sub> is bubbled through a solution of our precursor amine, *L*-glutamic acid di-*tert*-butyl ester, and BEMP, in MeCN.

- Reaction **A** is the direct reaction of BEMP and CO<sub>2</sub> forming the BEMP-CO<sub>2</sub> covalent adduct.
  - Also shown (in grey) is the subsequent cycloreversion reaction (releasing *tert*-butyl isocyanate) that has been shown in non-radioactive chemistry, to occur under elevated CO<sub>2</sub> pressures (3 atm.) with extended reaction times (>12 hrs).<sup>436</sup> This was not expected to occur to any significant degree during our unpressurised reaction with a sub-10 min total duration, and indeed no sign of this [<sup>11</sup>C]*tert*-butyl isocyanate (or its likely reaction products) were seen in this work.
- Reaction **B** is the reaction of the precursor amine with CO<sub>2</sub>, forming the carbamic acid intermediate, followed by deprotonation by a second molecule of the precursor amine to yield a stabilised ammonium carbamate salt.
  - The precursor amine is relatively poorly basic and so this would not be expected to yield a particularly stable fixation product.
- Reaction **C** is the reaction of the precursor amine with CO<sub>2</sub>, forming the carbamic acid intermediate, followed by deprotonation by BEMP, yielding a stabilised phosphonium carbamate salt.
  - BEMP is strongly basic, so the stabilisation conferred by this deprotonation and salt formation would be expected to be significant.

It is firstly important to compare reactions **B** and **C** as they are very similar processes, only differing in the final carbamic acid deprotonation stage *iii*. In **B** a second molecule of the precursor amine, *L*-glutamic acid di-*tert*-butyl ester, acts to deprotonate the carbamic acid forming the stabilised ammonium carbamate salt derivative. By comparison, in **C** the carbamic acid is deprotonated by the phosphazene superbases BEMP, forming the respective stabilised phosphonium carbamate salt derivative. In an abundance (relative to the <sup>11</sup>C-carbamic acid intermediate) of both of these two molecules, (as will be the case with radiochemistry), one can predict with some confidence which of these reactions will dominate over the other by comparison of their relative basicities. In this case, BEMP – by virtue of its ability to delocalise a positive charge across the

phosphorous and the four nitrogen atoms – is extremely basic ( $pK_a = 27.6$ )<sup>189</sup> compared to the moderate basicity of the glutamic acid derivative (no  $pK_a$  data for this compound exists, but in general amino acid amino groups have  $pK_a$ s in the 9-10 range). Therefore, the many orders-of-magnitude stronger basicity of BEMP when compared with the precursor amine leads one to presume that reaction **C** would be heavily favoured compared to **B**, and so this can be discounted from any further consideration.

Therefore, during the [<sup>11</sup>C]CO<sub>2</sub> trapping phase, there are two major competing reactions which must be considered: reaction **A**, the unproductive BEMP-[<sup>11</sup>C]CO<sub>2</sub> adduct formation; and reaction **C**, the productive [<sup>11</sup>C]CO<sub>2</sub>-fixation reaction on the precursor amine. By varying different reaction parameters, we attempted to arrive at conditions which favour the latter [<sup>11</sup>C]CO<sub>2</sub>-fixation reaction, while suppressing the direct BEMP-[<sup>11</sup>C]CO<sub>2</sub> interaction. Quantification of these two pathways was straightforward by inspecting the radio-HPLC trace of the <sup>11</sup>C-urea syntheses. Similarly to what was seen in chapter 4, the unproductive [<sup>11</sup>C]CO<sub>2</sub> trapping products eluted towards the start of any HPLC analysis (on or near to the solvent front). By comparison, the organic products from the productive [<sup>11</sup>C]CO<sub>2</sub> fixation pathway (<sup>11</sup>C-isocyanates or <sup>11</sup>C-ureas) elute later, due to their substantially more-lipophilic character. The ability to relatively quantify these two processes enabled us to better pursue a rational [<sup>11</sup>C]CO<sub>2</sub> fixation optimisation.

### 5.2.3.2 Solvent volume

One early optimisation simply concerned the volume of the fixation solution. Initially, we followed the procedure as reported by Wilson *et al.*<sup>433</sup> and prepared our initial radiolabeling solution (containing BEMP and precursor amine) in **100 μL** MeCN. In their original method, [<sup>11</sup>C]CO<sub>2</sub> was cryogenically pre-concentrated before being bubbled through the solution in a stream of N<sub>2</sub> at 10 mL/min. By contrast, in our optimisation experiments, no preconcentration was performed and the [<sup>11</sup>C]CO<sub>2</sub> was flushed directly from the cyclotron (*via* a P<sub>2</sub>O<sub>5</sub> trap) into the reaction vial, in a stream of He at 70 mL/min.

Initial fixation experiments under these conditions gave highly variable trapping efficiencies, between 22% at the lowest and 84% at the highest, with an average across 9 experiments of **45 ± 19%**. Upon observation of the vial (using the inbuilt camera), it became clear that at this very low volume (**100 μL**) in our 1.5 mL v-shaped vials, the liquid level only barely reached above the heel of the gas-delivery needle bevel. At this high gas flow-rate, this resulted in vigorous agitation, causing significant amounts of solution to splash onto the walls of the vial. Our suspicion was that the variable trapping efficiencies of otherwise-identical solutions could be attributed to this behaviour, due to variable solution exposure to the [<sup>11</sup>C]CO<sub>2</sub>.

To investigate this, the solution volumes were increased to **250 μL**, while keeping the quantities of other reagents constant. Observation of these solutions during [<sup>11</sup>C]CO<sub>2</sub> delivery confirmed that with the needle bevel fully submerged below the surface of the liquid, the gas was delivered in a more well-ordered stream of bubbles and resulted in little-to-no splashing of the solution onto the walls of the vial. Fortunately, this also resulted in an improvement in the trapping efficiencies. Not only were they more efficient on average, the run-to-run consistency varied much less, giving an average trapping efficiency (across 8 experiments) of **77 ± 3%** (compared with the less-efficient and significantly more variable trapping of **45 ± 19%** in the 100μL experiments). This highlighted how an unintended physical phenomenon like this can easily have a significant effect on the performance of a reaction; and on a comparable or even-greater degree than the effects of any chemical optimisation. In any case, to avoid this issue going forward, all future trapping/fixation optimisation experiments employed **250 μL** solution volumes.



### 5.2.3.3 *Temperature experiments*

To explore the effects of solution temperature on these competing reactions, we selected the same trapping solution composition as was previously used in the proof-of-concept BEMP/POCl<sub>3</sub> synthesis of [<sup>11</sup>C]Glu-Glu-(O<sup>t</sup>Bu)<sub>4</sub>: a solution of the amine hydrochloride salt (5 μmol, 1 equiv.) and BEMP (22 μmol, 4.4 equiv.) in 250 μL MeCN. 1 molar equivalent of the BEMP is present in the solution to remove the HCl and release the free amine *in situ*, leaving 17 μmol unreacted BEMP (3.4 equiv) in solution.

This solution was then screened at different temperatures (-10°C, 0°C, 20°C and 50°C) to ascertain its overall trapping efficiencies under these conditions. In these screening reactions, [<sup>11</sup>C]CO<sub>2</sub> was bubbled at 70 mL/min through the trapping solution over 105 seconds (the standard delivery time from the cyclotron), and the vial was vented to a gas waste bag via an Ascarite trap. After delivery, the vial and Ascarite cartridges were separated and their radioactivities measured to ascertain the total quantity of [<sup>11</sup>C]CO<sub>2</sub> delivered through the system, and to what extent it was trapped in the solution (its trapping efficiency). This experiment only shows half of the picture, as even 100% trapping efficiency does not guarantee that any of the [<sup>11</sup>C]CO<sub>2</sub> has been incorporated into fixation products. Nevertheless, because these experiments do not require HPLC analysis, they can be screened quickly and were useful to give a wider insight into how these solutions perform as reaction temperature varies.

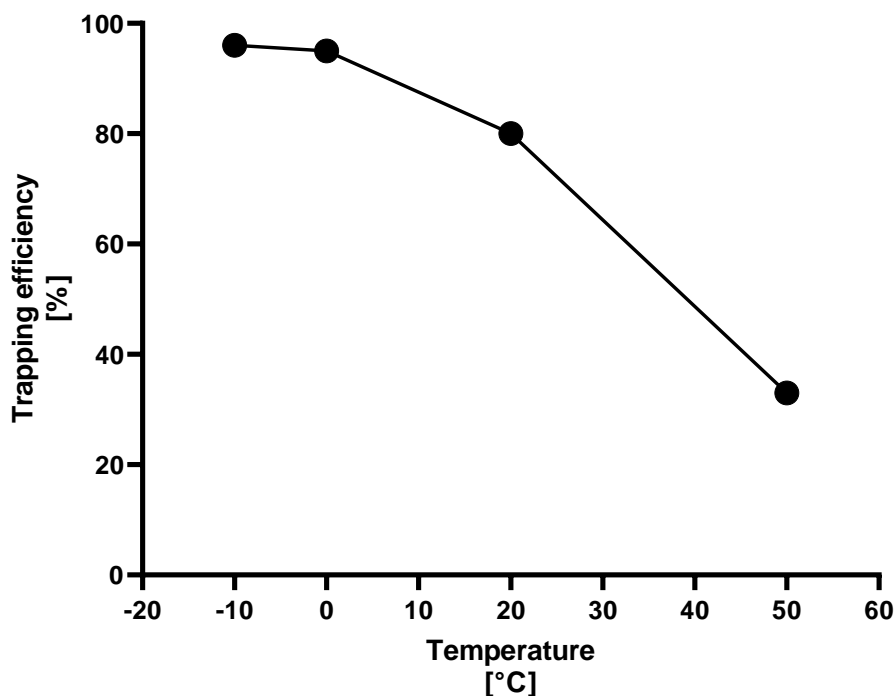


**Figure 5.6 Plot of  $[^{11}\text{C}]\text{CO}_2$  trapping efficiency as a function of temperature**

Temperature dependency of trapping efficiency. As temperature decreases, so does the overall trapping efficiency

As can be seen in the results presented in the figure above, there is a general trend towards higher trapping efficiencies with lower temperatures. The method developed by Wilson *et al.* performed their trapping stage at ambient temperatures ( $\sim 15\text{-}20^\circ\text{C}$ ) and achieved trapping efficiencies of  $>95\%$  with most amines they screened. By comparison, our experiment at  $20^\circ\text{C}$  resulted in a trapping efficiency of  $80\%$ . There are several possible explanations for this discrepancy, but the two most likely culprits are either: a) the precursor amine (a protected amino acid) is less basic (and perhaps moderately more sterically-hindered) than many of the standard aliphatic building block amines used in the Wilson paper; or b) our faster delivery flow rate ( $70\text{ mL/min}$  *versus*  $10\text{ mL/min}$ ) with a more dilute  $[^{11}\text{C}]\text{CO}_2$  content (due to no preconcentration) would both disfavour  $[^{11}\text{C}]\text{CO}_2$  trapping in solution. It should be noted however, considering these limiting factors, that achieving these  $>80\%$  trapping efficiencies at  $70\text{ mL/min}$  was still fairly impressive and is a testament to the robustness of this  $[^{11}\text{C}]\text{CO}_2$  fixation chemistry.

With this evidence to hand, it seemed clear that future reactions should be performed at lower temperatures (0 or  $-10^\circ\text{C}$ ) as under these conditions, superior trapping efficiencies were obtained (95% and 96%, respectively). This could be an appealing conclusion at first, but these experiments by themselves are somewhat misleading, as the results give an incomplete picture. While the experiment explores the ability of a given solution to trap  $^{11}\text{C}$ CO<sub>2</sub> from the gas phase, it does not give any insight regarding the ultimate fate of this trapped  $^{11}\text{C}$ CO<sub>2</sub>, is it trapped unproductively as the BEMP-CO<sub>2</sub> adduct, or is it productively incorporated into the desired  $^{11}\text{C}$ -carbamate salt fixation product?

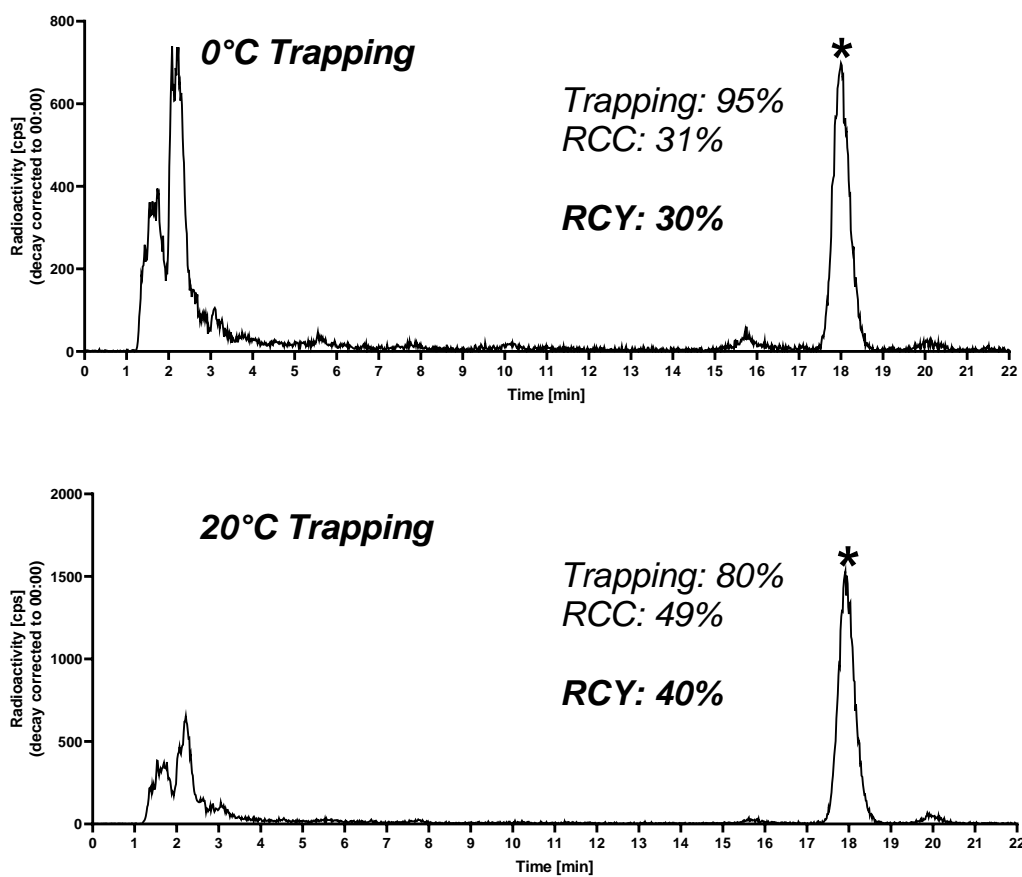


**Figure 5.7 Comparison of two syntheses of  $^{11}\text{C}$ Leu-Glu-(O<sup>t</sup>Bu)<sub>3</sub> with  $^{11}\text{C}$ CO<sub>2</sub> trapping at different temperatures**

\* Denotes product peak

RCY is calculated as a product of both the trapping efficiency and the RCC as measured by radio-HPLC analysis of the crude reaction mixture

To further explore this question, two radiosyntheses of the fully protected asymmetric urea [*ureido*- $^{11}\text{C}$ ]Leu-Glu-(O<sup>t</sup>Bu)<sub>3</sub> were performed, with the initial BEMP-mediated

[<sup>11</sup>C]CO<sub>2</sub>-fixation performed on the protected glutamate precursor at both 0°C and 20°C under the same conditions as the previous trapping screening experiments described. Following these initial trapping steps at 0°C and 20°C, both reactions were performed identically: the solutions were warmed to 50°C, POCl<sub>3</sub> was added, followed shortly by an excess of the protected leucine precursor amine. These reactions were quenched (with HPLC eluent) and analysed by radio-HPLC (shown in the figure above). This otherwise identical treatment means that any difference between the results of these two can be attributed to the temperature during the [<sup>11</sup>C]CO<sub>2</sub> trapping stage, and analysis of these chromatograms should give a useful insight into the chemistry occurring during the initial [<sup>11</sup>C]CO<sub>2</sub> gas bubbling phase.

A comparison of these two chromatograms reveals a surprising result: cooling the solution to 0°C (*versus* 20°C) does indeed capture more of the [<sup>11</sup>C]CO<sub>2</sub> as it passes through (95% *versus* 80%), but the overall non-isolated RCY of these two methods does not follow the same trend. In fact, even accounting for its lower [<sup>11</sup>C]CO<sub>2</sub> trapping efficiency, the reaction with trapping at 20°C resulted in a significantly higher RCY (40%) than was obtained with the 0°C trapping method (30%). It is clear, even on visual inspection of the chromatograms, that a significantly higher proportion of the [<sup>11</sup>C]CO<sub>2</sub> was incorporated into the desired <sup>11</sup>C-urea in the 20°C experiment (49% of the injected radioactivity is in the <sup>11</sup>C-urea peak) compared to when [<sup>11</sup>C]CO<sub>2</sub> trapping was performed at 0°C (only 31% of the injected radioactivity is in the <sup>11</sup>C-urea peak). The product profiles of both reactions are qualitatively the same – i.e. there are no significant unexpected impurity peaks present in only one chromatogram – so it appears that the major cause of this product imbalance between these two reactions is the competition between the unproductive reaction pathway **A** (favoured at 0°C), and the productive reaction pathway **C** (comparatively more favoured at 20°C).

It appears that at these lowered temperatures, the incidental (and unproductive) formation of the BEMP-[<sup>11</sup>C]CO<sub>2</sub> adduct still occurs readily due to a low activation barrier for this pathway (this can therefore be considered the kinetic product), while the mixture is not at a sufficient temperature to adequately drive the intended but more energetically-demanding formation of the (thermodynamically favoured) <sup>11</sup>C-carbamic acid. On the other hand, by raising the temperature to just 20°C, this productive [<sup>11</sup>C]CO<sub>2</sub> fixation

process is now more strongly driven relative to the BEMP-[<sup>11</sup>C]CO<sub>2</sub> adduct formation, and by extension, this unproductive pathway is comparatively suppressed, ultimately resulting in higher RCYs of the desired <sup>11</sup>C-urea product, even when less of the total radioactivity is trapped during this initial stage. At the elevated temperature it is “usefully” trapped in a fixation product, whereas at the lower temperatures, it is trapped in otherwise “useless” BEMP-[<sup>11</sup>C]CO<sub>2</sub> adducts.

This surprising result underscores the sometimes “contradictory” behaviour of these CO<sub>2</sub>-fixation superbases like BEMP and DBU. The direct CO<sub>2</sub> trapping behaviour is purely incidental to their primary function as strong bases, and without careful controls such as this, this behaviour can be actively detrimental to the overall radiochemical yield of a process. In this example, were we to have accepted the temperature screening data on its face, it would have been a logical decision to perform all future trapping at 0°C (or even -10°C) as it is under these conditions that the trapping efficiency was highest, even though it would have ultimately resulted in significantly-decreased final radiochemical yields.

## 5.2.3.4 BEMP quantity

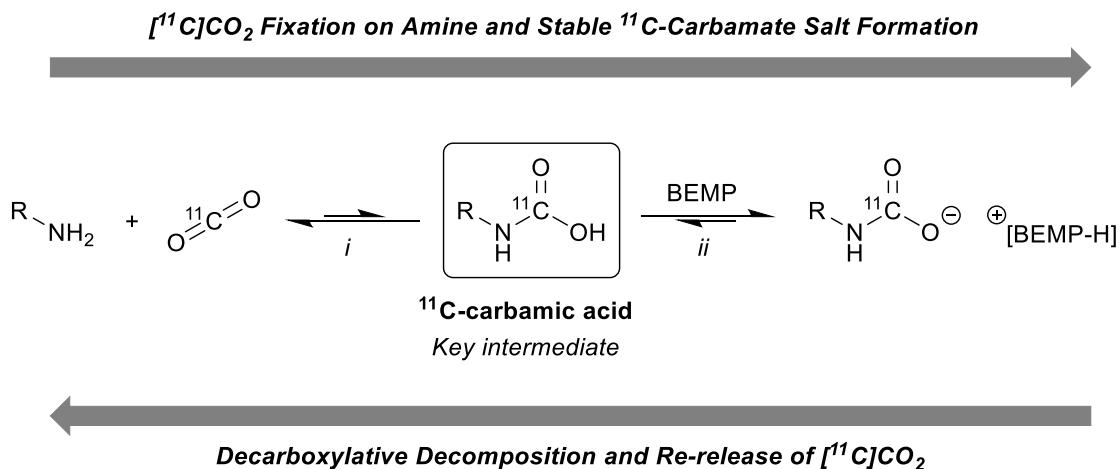


**Figure 5.8** Simplified scheme demonstrating the key  $[^{11}\text{C}]\text{CO}_2$  fixation equilibrium

The forward reaction relies on a sufficient concentration of BEMP in solution to deprotonate (step *ii*) the transient intermediate before it undergoes the reverse reaction, re-releasing the  $[^{11}\text{C}]\text{CO}_2$  (step *i*). The tautomeric zwitterion form of the carbamic acid is not shown here for simplicity.

It was important to understand the effect of varying BEMP/amine stoichiometric ratios and concentrations on fixation efficiency. Based upon our suspected mechanism, BEMP acts stoichiometrically with an amine and  $[^{11}\text{C}]\text{CO}_2$  molecule to form the  $^{11}\text{C}$ -carbamate, with the  $[\text{BEMP-H}]^+$  phosphazanium species serving as the counterion, and so theoretically, even small quantities of reagents should be able to capture the  $[^{11}\text{C}]\text{CO}_2$  effectively. But for practical radiochemistry (a single-pass equilibrium fixation process), significant excesses of reagents are typically required in order to attain acceptable yields within the short synthetic timeframe available. Conversely, BEMP is also able to participate in an unproductive side-reaction which can consume significant quantities of the  $[^{11}\text{C}]\text{CO}_2$ , adversely affecting the overall  $[^{11}\text{C}]\text{CO}_2$ -fixation efficiency.

As a result of these offsetting factors the ratio of BEMP to the amine requires balancing: too little BEMP in solution risks re-release of  $[^{11}\text{C}]\text{CO}_2$  by the  $^{11}\text{C}$ -carbamic acid before it can be deprotonated; too much, and the desired  $[^{11}\text{C}]\text{CO}_2$  fixation reaction could be suppressed by the preferential formation of the BEMP- $[^{11}\text{C}]\text{CO}_2$  adduct.

In our experiments, three solutions with BEMP:amine ratios of **1.2:1**, **4.5:1**, and **11:1** were prepared (5 μmol of the amine was fixed throughout, with the BEMP quantities adjusted accordingly to reach the desired molar ratios) in MeCN. [<sup>11</sup>C]CO<sub>2</sub> was bubbled through these solutions (at 70 mL/min) and the trapping efficiencies were measured. For the solution with the lowest BEMP:amine ratio, the **1.2:1** experiment, only **2.5%** of the total [<sup>11</sup>C]CO<sub>2</sub> was trapped in solution. By comparison, the **4.5:1** experiment resulted in **95%** trapping efficiency, and increasing this to **11:1** resulted in a marginally increased **99%** trapping efficiency.

Low amounts of BEMP (**1.2:1**) resulted in significant release of [<sup>11</sup>C]CO<sub>2</sub> from the solution, likely due to an inability to deprotonate the key <sup>11</sup>C-carbamic acid intermediate before it could re-release the [<sup>11</sup>C]CO<sub>2</sub>. Increasing the BEMP concentration in solution (the **4.5:1** ratio) accordingly gave excellent trapping efficiencies. This could be marginally improved by increasing the ratio to 11:1, but this then risked promoting the undesired and unproductive BEMP-[<sup>11</sup>C]CO<sub>2</sub> adduct formation, decreasing the [<sup>11</sup>C]CO<sub>2</sub> fixation efficiency.

### 5.2.3.5 Summary

In optimising the initial [<sup>11</sup>C]CO<sub>2</sub> fixation stage, the solution volume, trapping temperature, and BEMP:amine ratio were all explored, and as a result, we arrived at some reasonably optimal conditions for the initial [<sup>11</sup>C]CO<sub>2</sub> fixation stage of the intended “generally applicable” method for <sup>11</sup>C-radiolabeling of PSMA-ligands. These conditions were designed so as to ensure that the majority of the [<sup>11</sup>C]CO<sub>2</sub> would trap in a minimal quantity of trapping solution, and once in solution, that it would preferentially react with the desired amine substrate *versus* the undesired and unproductive formation of a BEMP-[<sup>11</sup>C]CO<sub>2</sub> adduct.

Firstly, it was found that at the fast flow rates of our cyclotron delivery of [<sup>11</sup>C]CO<sub>2</sub> (70 mL/min), the use of 100 μL trapping solutions (a common solution volume used in the literature) was insufficient. The vigorous agitation caused by this high flow rate caused the solution to splash onto the walls of the vial, reducing the solution’s interaction with the [<sup>11</sup>C]CO<sub>2</sub>, and ultimately leading to highly variable levels of [<sup>11</sup>C]CO<sub>2</sub> breakthrough. This was simply rectified by increasing the solution volumes to 250 μL: in these conditions, the trapping phase was more consistent, with much less run-to-run variability. This was a simple physical optimisation (no consideration of the chemical reactivity was required), but modifications such as these can be fairly important when performing chemistry on such small-scales, something common to radiochemistry.

Secondly, a balancing point was required for the solution temperature. It was found that lowering the solution temperature preferentially favours the undesired BEMP-[<sup>11</sup>C]CO<sub>2</sub> reaction, and thus cooling the solution resulted in decreased radiochemical yields (even if the trapping efficiency was higher). However, while increasing the temperature to 20°C promotes the fixation reaction, increasing the temperature too far (50°C) favours the re-release of the [<sup>11</sup>C]CO<sub>2</sub> from the solution (reducing both the trapping/fixation yield).

Finally, a similar balancing point was found for the BEMP:amine ratios. Too little BEMP could result in decarboxylative decomposition of the key transient <sup>11</sup>C-carbamic acid intermediate, while it was found that excessively high molar ratios of BEMP:amine could result in preferential formation of the unproductive BEMP-[<sup>11</sup>C]CO<sub>2</sub> adduct. While it was necessary to increase the BEMP:amine ratio to ensure that the transient <sup>11</sup>C-carbamic acid



intermediate was captured/deprotonated by a molecule of BEMP (before undergoing decarboxylative decomposition), it was clear that with 94% of the total [<sup>11</sup>C]CO<sub>2</sub> already trapped at a molar ratio of 4.5:1, any further increase in the BEMP:amine ratio would have minimal effect on the overall trapping efficiency, while simply providing more starting material for the BEMP-[<sup>11</sup>C]CO<sub>2</sub> adduct formation, leading to a relative decrease in the intended fixation reaction.

These careful balancing acts with both temperature and BEMP:amine ratios were required due to the *incidental* dual-reactivity of BEMP, and could possibly benefit from further optimisation. The complex reactivity that can occur during the [<sup>11</sup>C]CO<sub>2</sub> trapping stage of the reaction means that it was difficult to determine with much certainty whether significantly better conditions could have easily been arrived at (as modifying the reaction to favour one factor could result in a detrimental effect elsewhere), but the achieved ~45-50% fixation efficiency within 2 minutes from the EoB was satisfying, and the following conditions were therefore selected for use going forward:

- ***L*-glutamic acid di-*tert*-butyl ester hydrochloride: 1.47 mg (5 μmol, 1 equiv.)**
- **BEMP: 6.47 μL (22 μmol, 4.5 equiv.)**
- **MeCN: 250 μL**
- **Solution temperature: 20°C**
- **[<sup>11</sup>C]CO<sub>2</sub> delivery: 70 mL/min for 105 secs**

## 5.2.4 Dehydration and asymmetric urea formation

### 5.2.4.1 Asymmetric selectivity

Once the [<sup>11</sup>C]CO<sub>2</sub> is fixed onto the amine precursor as the <sup>11</sup>C-carbamate salt (as was optimised in the previous section), the subsequent phase of the urea synthesis mechanism is to dehydrate this using POCl<sub>3</sub> to form the <sup>11</sup>C-isocyanate, which reacts in-turn with an amine substrate to produce the <sup>11</sup>C-urea product. Isocyanates are highly reactive species, susceptible to nucleophilic attack at their electrophilic carbonyl carbon. This “spring-loaded” reactivity towards nucleophiles (commonly amines/alcohols) can also lead to unwanted side-reactions, unless conditions are carefully controlled. These side-reactions are less of a concern in non-radioactive synthetic chemistry, since stoichiometric quantities of isocyanates and amines can be used to somewhat curtail this behaviour. In <sup>11</sup>C-radiochemistry by comparison, the [<sup>11</sup>C]CO<sub>2</sub> starting material (and therefore any subsequently produced <sup>11</sup>C-isocyanate) is produced in nanomolar quantities. As such, in most cases, all other non-radioactive reagents exist in large excesses relative to the <sup>11</sup>C-radiolabeled species (typically on the scale of at least three-to-four orders of magnitude higher concentrations), and this is typically necessary to ensure rapid reactions that are compatible with the 20 min half-life. In the case of the reaction in question however, this can pose a major issue: even if all of the [<sup>11</sup>C]CO<sub>2</sub> is incorporated into the desired <sup>11</sup>C-isocyanate, this excess of reagents will result in a significant quantity of the unreacted amine precursor remaining in solution. In this case, this remaining amine can rapidly react with the <sup>11</sup>C-isocyanate, producing the symmetric <sup>11</sup>C-urea.

If the target molecule is an asymmetrically substituted <sup>11</sup>C-urea (as in any “generally applicable” method for <sup>11</sup>C-radiolabeling PSMA-ligands), this tendency to form the symmetric <sup>11</sup>C-urea by reaction with excess amounts of the precursor amine can be problematic. Generally the approach that has been taken to overcome this issue, both with the Mitsunobu-mediated<sup>225,251</sup> as well as the POCl<sub>3</sub>-mediated methods,<sup>433</sup> has been to use excess quantities of the Mitsunobu or POCl<sub>3</sub> reagents to consume this first amine at the same time as the <sup>11</sup>C-carbamate to <sup>11</sup>C-isocyanate conversion is taking place. If this is done correctly, the end result is that the <sup>11</sup>C-isocyanate can be “isolated” in solution, due to the absence of any nucleophilic potential reaction partners. At this point, a second

amine can be introduced, and the reaction can proceed, producing the desired asymmetrically substituted <sup>11</sup>C-urea.

In reality, even well optimised processes will result in some formation of the symmetrically-substituted <sup>11</sup>C-ureas, and the formation of small amounts of these is not in itself a major concern, as isolation/purification of the desired asymmetric product can generally be achieved in a fairly straightforward manner. Where this can be of concern is in cases where the symmetrically substituted product is formed in such quantities as to significantly affect the overall RCY of the process. In monitoring this in our work, we referred to the asymmetric selectivity ( $S_A$ ) of a given <sup>11</sup>C-urea synthesis process. The  $S_A$  (as measured by crude radio-HPLC) represents the yield of the desired asymmetrically substituted <sup>11</sup>C-urea relative to the total combined yields of the three possible symmetric and asymmetrically substituted <sup>11</sup>C-urea products.

$$S_A = \frac{[AA_1 - C(O) - AA_2]}{[AA_1 - C(O) - AA_1] + [AA_1 - C(O) - AA_2] + [AA_2 - C(O) - AA_2]}$$

[ ] = RCP of a given product (by crude radio-HPLC)

$AA_x - C(O) - AA_y$  = urea disubstituted with amino acid  $x$  and amino acid  $y$

This is not a traditional measure, but it was a useful metric for our purposes in assessing, understanding, and summarising the effects of different conditions on our <sup>11</sup>C-urea synthesis. To assess this accurately, using the synthesis of [<sup>11</sup>C]Leu-Glu-(O<sup>t</sup>Bu)<sub>3</sub> as a model reaction, an analytical radio-HPLC method was developed to achieve reasonable baseline-resolution of the three possible <sup>11</sup>C-urea products: [<sup>11</sup>C]Leu-Leu-(O<sup>t</sup>Bu)<sub>2</sub>, [<sup>11</sup>C]Leu-Glu-(O<sup>t</sup>Bu)<sub>3</sub>, and [<sup>11</sup>C]Glu-Glu-(O<sup>t</sup>Bu)<sub>4</sub>. The challenge in this case was that due to the overall similarities of these three compounds (lipophilicities, sterics, charge, etc.), they tend to behave similarly on the column's standard C18 stationary phase. To overcome their near-co-elution under pre-designed gradient elution conditions, the method developed was an isocratic elution (for maximum resolution between similar analytes), with a relatively eluotropically weak solution employed to achieve greater analyte retention on the column. This resulted in better separation of the products, albeit at the expense of longer retention times – something that is usually best avoided with radiochemistry due to the decay-related implications. However in this case, the method

was purely used for analysis/optimisation, and not for any isolation/purification, so the losses due to decay are irrelevant.

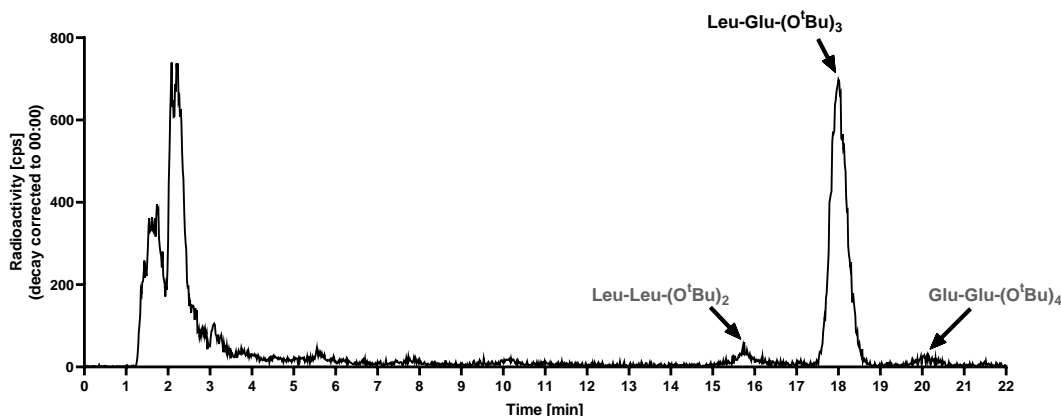


**Figure 5.9** Representative radio-HPLC separation of the three possible  $^{11}\text{C}$ -ureas

Column: Phenomenex Luna C18(2)  $5\mu\text{m}$ ,  $150 \times 4.6 \text{ mm}$

Elution method: 40%  $\text{H}_2\text{O}$  / 60% MeCN (0.1% TFA v/v) *isocratic*, 1 mL/min

A representative trace from this radio-HPLC method is presented in the figure above. The three  $^{11}\text{C}$ -urea peaks are visible and labeled, and as can be seen, all peaks are well resolved at the baseline, allowing for accurate quantification of each product, and in-turn allowing reliable calculations of the reaction  $S_A$ .

The optimisation process in this section was focused on the role of  $\text{POCl}_3$  in the reaction; and similarly to the previous optimisation of the BEMP-mediated fixation stage, several competing reactions had to be balanced. The primary function of  $\text{POCl}_3$  in this reaction is to dehydrate the  $^{11}\text{C}$ -carbamate to yield the corresponding  $^{11}\text{C}$ -isocyanate, however it is also used to consume any of the remaining first amine precursor by directly reacting with it, resulting in an “isolated”  $^{11}\text{C}$ -isocyanate intermediate. However, in addition to these intended roles, it was also important to remember the potential problem with using  $\text{POCl}_3$ : it produces HCl as a byproduct during its reaction with protic substrates, and this can lead to some substrate incompatibilities. While our initial proof-of-concept synthesis of [*ureido*- $^{11}\text{C}$ ]Glu-Glu-( $\text{O}^t\text{Bu}$ ) $_4$  seemed unaffected by this, it was important to check for any possible decomposition of starting materials/products as  $\text{POCl}_3$  quantities were modified during the optimisation process.

Similarly to the previous BEMP optimisation, it was initially expected that a balance would be required in finding an optimal quantity of POCl<sub>3</sub> to be used. Too little POCl<sub>3</sub> would risk incomplete consumption of the first amine, resulting in large quantities of the symmetric <sup>11</sup>C-urea forming, giving an overall low *S<sub>A</sub>* for the reaction. Conversely, too much POCl<sub>3</sub> could lead to decomposition of starting materials/products due to the HCl byproduct. Additionally, the use of an excess of POCl<sub>3</sub> relative to the first amine necessitates the use of an even larger excess of the second amine, to ensure that enough amine remains (after consumption by the remaining POCl<sub>3</sub>) to fully react with the <sup>11</sup>C-isocyanate and form the asymmetric <sup>11</sup>C-urea. It was hoped that this could be avoided, since the use of large quantities of reagents can somewhat complicate purification by overloading HPLC columns/SPE cartridges. Overall, it was expected that finding “optimal” conditions for this POCl<sub>3</sub> dehydration stage would be a tradeoff between these conflicting factors: enough POCl<sub>3</sub> would be required to achieve a high reaction *S<sub>A</sub>* while minimising any deleterious effects of the HCl byproduct formation as well as the relatively high reagent concentrations.

#### 5.2.4.2 POCl<sub>3</sub> optimisation

The method initially used in this section was based on the semi-optimised method developed earlier in section 5.2.2 for the proof-of-concept radiolabeling of the symmetrical <sup>11</sup>C-urea [<sup>11</sup>C]Glu-Glu-(O<sup>t</sup>Bu)<sub>4</sub>.

To summarise, the general method was as follows:

1. [<sup>11</sup>C]CO<sub>2</sub> was bubbled (70mL/min) through a pre-prepared solution of *L*-glutamic acid di-*tert*-butyl ester hydrochloride (5 μmol, 1 equiv.) and BEMP (22 μmol, 4.4 equiv.) in 250 μL MeCN at 20°C
2. Immediately following [<sup>11</sup>C]CO<sub>2</sub> delivery, the temperature was raised to 50°C and upon reaching this temperature, a solution of POCl<sub>3</sub> (varying quantities) in 100 μL MeCN was added and the vial was stirred for 2 min
3. A solution of *L*-leucine *tert*-butyl hydrochloride (50 μmol, 10 equiv.) and BEMP (50 μmol, 10 equiv.) in MeCN was added and stirred for a further 60 seconds
4. The reaction was quenched with an aliquot of the HPLC eluent (40% H<sub>2</sub>O / 60% MeCN) and immediately injected onto the radio-HPLC for analysis

By analysing the results from the reaction using the previously-described isocratic method, the three possible <sup>11</sup>C-ureas could be separated and quantified and from this data, the overall *S<sub>A</sub>* of the reaction was calculated. A number of different reactions were screened, with varying quantities of POCl<sub>3</sub> added in step 2. We suspected that higher ratios of POCl<sub>3</sub> vs amine would likely be required to achieve an acceptable (>90%) asymmetric selectivity, *S<sub>A</sub>*.

**Table 5.2 Varying POCl<sub>3</sub> quantities**

	Amine [μmols]	POCl <sub>3</sub> [μmols]	Ratio [POCl <sub>3</sub> /Amine]	Proportion of urea product			S <sub>A</sub>
				<i>Leu-Leu</i>	<i>Leu-Glu</i>	<i>Glu-Glu</i>	
<b>A</b>	<b>5</b>	<b>2.5</b>	<b>0.5 : 1</b>	8%	19%	73%	<b>19%</b>
<b>B</b>	<b>5</b>	<b>10</b>	<b>2 : 1</b>	2%	71%	27%	<b>71%</b>
<b>C</b>	<b>5</b>	<b>21.4</b>	<b>4.3 : 1</b>	2%	95%	3%	<b>95%</b>
<b>D*</b>	<b>5</b>	<b>50</b>	<b>10 : 1</b>	-	-	-	-
<b>E†</b>	<b>5</b>	<b>21.4</b>	<b>4.3 : 1</b>	12%	55%	33%	<b>55%</b>

General procedure: [<sup>11</sup>C]CO<sub>2</sub> bubbled through solution of amine (*L*-glutamic acid di-*tert*-butyl ester) and BEMP (22 μmol) in MeCN (250 μL) at 20°C. Then temperature raised to 50°C and POCl<sub>3</sub> in MeCN (100 μL) was added. After 2 mins, solution of *L*-leucine *tert*-butyl ester (50 μmol) and BEMP (50 μmol) in MeCN (200 μL) were added before quenching and analysing with radio-HPLC.

*Relative proportions of <sup>11</sup>C-urea products measured by radio-HPLC*

\* Every attempt at this highest POCl<sub>3</sub> concentration resulted in no <sup>11</sup>C-urea product

† POCl<sub>3</sub> added to solution (at 20°C) before temperature raised to 50°C (in step 2)

#### 5.2.4.2.1 Screening experiment A

Entry **A** in the table above shows the results obtained when a **0.5:1** ratio of POCl<sub>3</sub> to the first amine was used, i.e. the first amine was in excess relative to the POCl<sub>3</sub>. Under these conditions, even after all of the POCl<sub>3</sub> had reacted, (yielding the <sup>11</sup>C-isocyanate and consuming some of the amine) there would still be significant quantities of the initial amine present in solution available to react with the <sup>11</sup>C-isocyanate. The results are therefore unsurprising – 73% of the total <sup>11</sup>C-urea product was in the symmetrically substituted [<sup>11</sup>C]Glu-Glu-(O<sup>t</sup>Bu)<sub>4</sub> form. The fact that 19% of the <sup>11</sup>C-urea was in the asymmetric [<sup>11</sup>C]Leu-Glu-(O<sup>t</sup>Bu)<sub>3</sub> form also demonstrates that the <sup>11</sup>C-isocyanate had not totally reacted with the glutamate precursor during the initial 2 minute reaction time, before the 50 μmol excess of the protected leucine precursor was added.

Surprisingly, 8% of the <sup>11</sup>C-urea product was the symmetrically substituted [<sup>11</sup>C]Leu-Leu-(O<sup>t</sup>Bu)<sub>2</sub> form, but according to the order of reagent addition this product would not be expected to form. The [<sup>11</sup>C]CO<sub>2</sub> fixation was performed on the protected glutamic acid precursor amine, so logically all <sup>11</sup>C-urea products would be expected to be at least mono-substituted with the protected glutamic acid. However the existence (in a not insignificant quantity) of this product suggests that none of the reaction steps reach full completion

before the next step begins. While this pathway initially seems comparatively improbable compared to the reaction pathway as designed/intended, the formation of this product in significant quantities served as an indication or reminder that in these rapid and non-stoichiometric radiolabeling reactions, unexpected reaction pathways can sometimes be more prevalent than might be expected “on paper”.

#### **5.2.4.2.2 Screening experiment B**

Increasing the ratio to **2:1** in experiment **B** resulted in an improved but still less than satisfactory  $S_A$  (71%). Clearly, an increase in the POCl<sub>3</sub> concentration had improved the situation by more-rapidly consuming the unreacted amine precursor, and achieving a better isolation of the <sup>11</sup>C-isocyanate intermediate. However, the fact that 27% of the total <sup>11</sup>C-urea products were still in the symmetrical [<sup>11</sup>C]Glu-Glu-(O<sup>t</sup>Bu)<sub>4</sub> form was still less than ideal, as over one quarter of the <sup>11</sup>C-isocyanate reacted with the first amine before the POCl<sub>3</sub> was able to remove it, even in a 2:1 molar excess.

#### **5.2.4.2.3 Screening experiment C**

The **4.3:1** ratio in experiment **C** was the same as that used in our earlier proof-of-concept symmetrical <sup>11</sup>C-urea radiolabeling. This was the lowest ratio reported by Wilson *et al.* to achieve an acceptable isolation of the <sup>11</sup>C-isocyanate (avoiding formation of any symmetrical <sup>11</sup>C-urea byproduct),<sup>433</sup> and so we hoped that it would achieve a similar effect for us. Gratifyingly, under these conditions, the reaction exhibited a vastly improved  $S_A$  of 95%, forming almost-exclusively the target asymmetrically-substituted <sup>11</sup>C-urea. This was a highly promising proof-of-concept; with this result demonstrating that an increased POCl<sub>3</sub> concentration could almost entirely consume the first amine, leaving the key <sup>11</sup>C-isocyanate intermediate ([<sup>11</sup>C]glutamic acid isocyanate di-*tert*-butyl ester) isolated in solution. As a consequence of this successful isolation, the addition of an excess of a second protected amino acid precursor is therefore able to effect a relatively selective, clean, and efficient reaction to produce an asymmetrically-substituted protected-glutamate <sup>11</sup>C-urea compound – the precursor to <sup>11</sup>C-radiolabeled PSMA ligands.



#### 5.2.4.2.4 Screening experiment D

From inspecting the optimisation experiments reported in the original paper disclosing this method, the best selectivity was achieved with a roughly **10:1** ratio, so we screened these conditions (experiment **D**) with the hope that they could improve upon the  $S_A$  of 95% achieved with the **4.3:1** ratio. In our hands surprisingly, despite several attempts using this elevated POCl<sub>3</sub> concentration, no <sup>11</sup>C-urea formation was observed at all. It was confirmed that [<sup>11</sup>C]CO<sub>2</sub> was trapping successfully in solution, but either the subsequent <sup>11</sup>C-isocyanate- or <sup>11</sup>C-urea-formation stages were unsuccessful. There are two suggested explanations for this failure, although neither were further explored/confirmed in the course of this work.

Firstly, from a stoichiometric perspective, the 50 μmol quantity of POCl<sub>3</sub> used in this experiment was potentially too-great an excess. While it would be expected to consume all of the 5 μmol of the original amine, and convert any <sup>11</sup>C-carbamate to the <sup>11</sup>C-isocyanate, approx. 45 μmol POCl<sub>3</sub> would remain unreacted after this stage. Upon addition of the 50 μmol second amine, it is possible to envisage a situation where the POCl<sub>3</sub> consumes the majority of this amine before it has a chance to react with the <sup>11</sup>C-isocyanate, significantly reducing the <sup>11</sup>C-urea yields within the final 1 min reaction time. However, while this could possibly explain a severely decreased RCY, one would still expect to see trace quantities of the <sup>11</sup>C-urea in the radio-HPLC.

Alternatively, it is possible that under these high-concentration POCl<sub>3</sub> conditions, the reagent itself (or more likely the HCl byproduct) caused the decomposition of either the starting materials or the <sup>11</sup>C-radiolabeled intermediates. In fact it has already been documented that these relatively harsh conditions are incompatible with certain more-sensitive precursor amines and reagents.<sup>241,242</sup> While no such substrate incompatibility was discussed in Wilson's original method development publication, it should be noted that the vast majority of the amine substrates with which this method was demonstrated were simple aliphatic and aromatic amines, without many of the chemically-sensitive functionalities present in drug-like molecules. By comparison, the precursor amines used in this application contain *tert*-butyl ester moieties which are (by design) labile under strongly acidic conditions. It is possible that this more chemically-fragile precursor could degrade in a high-concentration solution of POCl<sub>3</sub> at the elevated temperatures and

reaction times (that we had found to be beneficial for other aspects of the reaction). In any case, it was clear that no <sup>11</sup>C-urea product was forming with the use of this **10:1** ratio, and so the decision was taken to proceed with the still highly-acceptable 95%  $S_A$  as previously obtained with a **4.3:1** ratio.

#### 5.2.4.2.5 Screening experiment E

Our final experiment (**E**) in this section concerned the order of reagent addition. In the previous experiments, immediately following the [<sup>11</sup>C]CO<sub>2</sub> trapping stage (at 20°C), the reaction temperature had been raised to 50°C *before* the addition of the POCl<sub>3</sub> solution. We were concerned that raising the temperature before addition of POCl<sub>3</sub> could possibly lead to losses of [<sup>11</sup>C]CO<sub>2</sub> in the time (~40s) taken to raise the temperature. As was shown in the earlier plot demonstrating trapping *versus* temperature, the overall trapping efficiency at 50°C was significantly lower than at 20°C, we suspected because it favoured the decarboxylative decomposition of the <sup>11</sup>C-carbamate. It was therefore of interest to us to screen the “optimal” **4.3:1** ratio with a modified reagent addition protocol.

Fortunately for us, no difference in overall [<sup>11</sup>C]CO<sub>2</sub> trapping/fixation was observed in this experiment; a finding that was corroborated by checking the real-time plots of the vial radioactivity (as measured by the pin-diode built into the Modular-Lab system). The gradual loss in radioactivity due to decay was observed as expected, but no sudden loss of radioactivity was observed during heating, whether it be before or after addition of POCl<sub>3</sub>. By comparison however, what was fairly striking in this experiment was the difference in asymmetric selectivity: where previously this **4.3:1** ratio had resulted in an impressive  $S_A$  of 95%; with the POCl<sub>3</sub> added at 20°C *before* the reaction was heated to 50°C, the reaction was notably less asymmetrically selective ( $S_A = 55%$ ). Instead of the asymmetric product forming almost exclusively, a large proportion of the total <sup>11</sup>C-urea product (33%) was the symmetrical [<sup>11</sup>C]Glu-Glu-(O<sup>t</sup>Bu)<sub>4</sub>, with 12% as the alternative symmetrical [<sup>11</sup>C]Leu-Leu-(O<sup>t</sup>Bu)<sub>2</sub> product.

The origin of this differing selectivity was difficult to ascertain exactly, but it was possible to speculate as to possible causes. Similarly to previous discussion in this section, one plausible explanation requires the consideration of the competing reaction pathways that are possible during this reaction. Initially – before the addition of any POCl<sub>3</sub> – the reaction

solution contains the <sup>11</sup>C-carbamate salt intermediate and a significant quantity of unreacted amine. Upon addition of POCl<sub>3</sub>, two reactions are initially possible: 1) the <sup>11</sup>C-carbamate reacts with the POCl<sub>3</sub> to produce the <sup>11</sup>C-isocyanate; and 2) the POCl<sub>3</sub> can react with the remaining amine to (possibly forming a dichlorophosphoramidate species), this is the process by which the POCl<sub>3</sub> is said to have “consumed” the unreacted amine. As was discussed previously, to ensure a reasonable level of asymmetric selectivity it is crucial that the rates of these two reactions are similar. If reaction (2) is slow relative to (1), significant quantities of the symmetrical <sup>11</sup>C-urea would be produced from the reaction of the <sup>11</sup>C-isocyanate with the unconsumed first amine substrate.

With this principle in mind, it would seem that by adding POCl<sub>3</sub> to the reaction at 20°C *before* it was heated to 50°C, the rate of reaction (2) was disproportionately slowed, relative to (1). In other words: at this lower reaction temperature, the POCl<sub>3</sub>-mediated dehydration reaction remains relatively rapid, while the rate of amine consumption (by POCl<sub>3</sub>) decreased significantly. By comparison, it was clear that at 50°C, the consumption of the amine by POCl<sub>3</sub> is considerably faster than at 20°C, and under these conditions, the <sup>11</sup>C-isocyanate is more-effectively isolated, with the addition of an excess of the second amine substrate producing the desired asymmetric <sup>11</sup>C-urea with high selectivity.

In the paper from Wilson *et al.*, while the concept of asymmetric selectivity is discussed (although not by that name), little attention is paid to the relative temperature dependency of these competing reaction pathways. The difference in reaction performance was striking in this case, and provides another insight into the often conflicting reactivity involved in these reactions as well as offering another parameter to consider when optimising similar processes.

### 5.2.4.3 Epimerisation concerns

The stereochemistry at the  $\alpha$ -carbon of the glutamate moiety within these PSMA ligands is crucial to their high binding affinities. Some early work on the development of these compounds found that the highest affinity glutamate-urea ligands with the naturally occurring (*S*)-glutamic acid motif entirely lost their binding affinity when the stereochemistry at this  $\alpha$ -carbon was switched to give the opposite (*R*)-glutamic acid epimer.<sup>299,528</sup> If a <sup>11</sup>C-radiolabeled PSMA ligand was not produced as the correct stereoisomer, in the best case, a significantly higher level of background activity would degrade imaging quality, but at worst, if the stereochemistry were entirely inverted, the radiotracer would entirely lose its target affinity. It was important, therefore, to ensure that our method produced only the high affinity (*S*),(*S*) epimer, with a particular focus on the retention of stereochemistry at the crucial  $\alpha$ -carbon of the glutamate moiety.

For this reason, all of our methods (radioactive and non-radioactive syntheses) employed enantiomerically-pure starting materials in an effort to ensure that the final products would have the correct stereochemistry for PSMA binding. However, there was some concern that the strongly basic conditions employed as part of the <sup>11</sup>C-urea synthesis could result in the epimerization of our final products. The particular concern was regarding the intermediate species [*isocyanato*-<sup>11</sup>C]glutamic acid isocyanate di-*tert*-butyl ester, as it was suspected that in this form (due to the electron-withdrawing nature of the isocyanate functionality), the proton on the  $\alpha$ -carbon would be most acidically labile. When this was present in solution with significant quantities of a superbases such as BEMP, could this result in the base-catalysed racemisation of this <sup>11</sup>C-isocyanate? If this were to occur, upon addition of the second amine, the resulting product would be a mixture of two <sup>11</sup>C-urea epimers, one (*S*),(*S*) and one (*S*),(*R*). This possible epimerisation is illustrated in the scheme below, and demonstrates the mechanism by which both epimers could be produced even when starting with enantiomerically pure reagents.

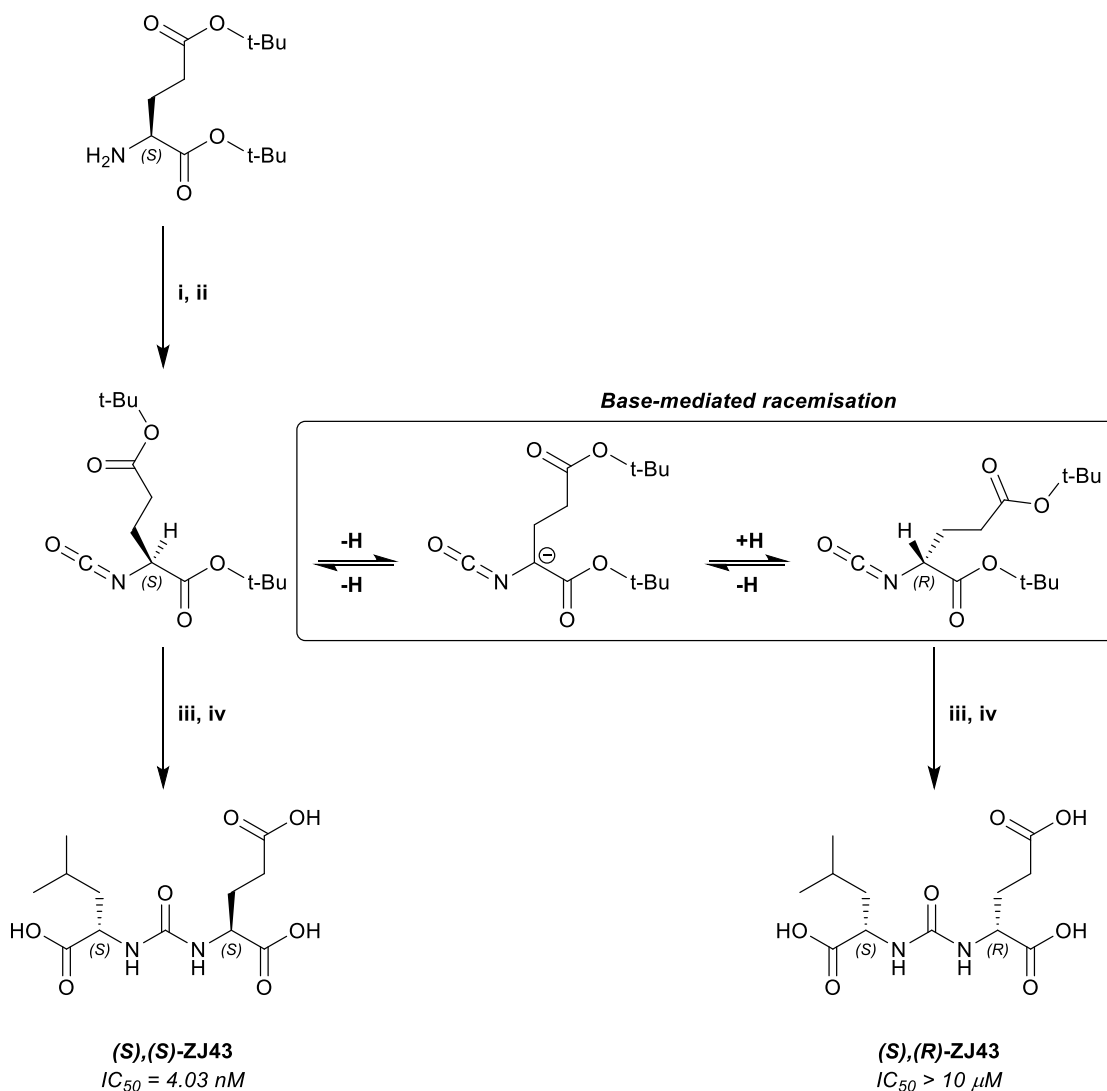


**Figure 5.10 Formation of (S),(S)- and (S),(R)-ZJ43 via base-mediated racemisation**

ZJ43 is a commonly used name for the leucine-glutamate urea  
 Racemisation is not definitely known to occur, but theoretically possible  
 Reagents: i) BEMP, CO<sub>2</sub>; ii) POCl<sub>3</sub>; iii) *L*-leucine *tert*-butyl ester; iv) HCl  
 IC<sub>50</sub> values of the ZJ43 stereoisomers were reported by Kwon *et al.*<sup>528</sup>

To address this concern, it was necessary to check and ensure that no epimerisation was occurring in the course of our reaction. As is shown in the scheme above, the primary theory was that the chirality at the glutamic acid  $\alpha$ -carbon would be affected because it is the amine upon-which the isocyanate is formed, but there was less concern that the chirality at the  $\alpha$ -carbon of the second amino acid (leucine, in this case) would be affected. As a result, the two possible products, the (S),(S)- and the (S),(R)- stereoisomers are in

fact two diastereomers, not enantiomers, of one another. Fortunately, diastereomers are separable by standard reversed-phase HPLC, whereas enantiomers are only separable with the use of much more complex and expensive chiral stationary phases. In fact, a recent publication by Kwon *et al.* discussed their investigation into the SAR of PSMA inhibitors with differing chiralities at the glutamic acid moiety. In this work, they demonstrated that the separation of (*S*),(*S*)- and (*S*),(*R*)-ZJ43 was straightforward. Using a standard analytical (150 x 4.6 mm) Phenomenex C18 column (the same as that used in our work), with an isocratic MeCN/H<sub>2</sub>O elution, they were able to sufficiently separate the two epimers by approximately 1 minute (with the (*S*),(*S*)- epimer eluting at ~ 3:50, and the (*S*),(*R*)- epimer eluting later at ~ 4:50). Accordingly, we expected that if any epimerisation was occurring within our reaction, the product would be separable and observable in the radio-HPLC chromatogram.

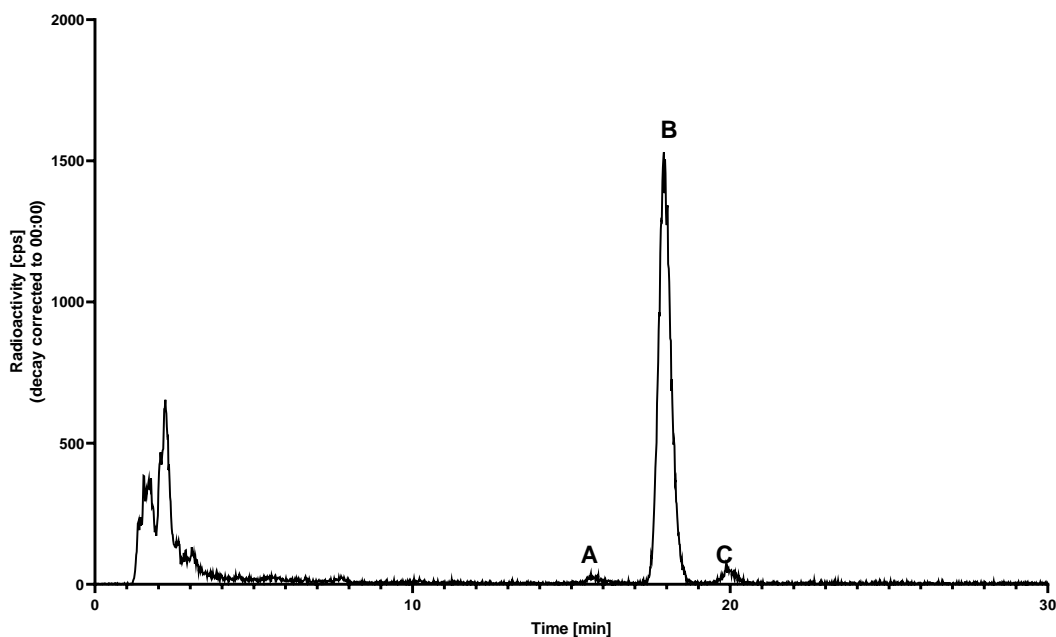


**Figure 5.11** Radiosynthesis of [ $^{11}\text{C}$ ]Leu-Glu-(*O*<sup>t</sup>Bu)<sub>3</sub> using the optimised conditions

**B** is the desired (*S*),(*S*)-form of [ $^{11}\text{C}$ ]Leu-Glu-(*O*<sup>t</sup>Bu)<sub>3</sub>, **A** and **C** are the previously discussed/identified symmetric  $^{11}\text{C}$ -ureas, no other radioactive products elute within 10 mins of **B**

Using the optimal conditions arrived at in the previous section, [ $^{11}\text{C}$ ]Leu-Glu-(*O*<sup>t</sup>Bu)<sub>3</sub> was synthesised and the crude reaction mixture was analysed by radio-HPLC (presented

above). Aside from the two peaks corresponding to the symmetric <sup>11</sup>C-urea byproducts, no other radioactive impurities were observed eluting within even 10 mins of the (*S*),(*S*)-[<sup>11</sup>C]Leu-Glu-(*O*<sup>t</sup>Bu)<sub>3</sub> product, leading us to conclude that no epimerisation had occurred under these conditions.

In the interests of thoroughly developing a robust and generally applicable method, it was important to check for any epimerisation, but the fact that none was observed was not overly surprising. In general, the vast majority of conditions that have been demonstrated to induce amino acid racemisation have required heating (>140°C) for extended durations to achieve measurable levels of conversion.<sup>529-531</sup> Our concern was that the addition of an isocyanate functionality could have increased the acidity of the key  $\alpha$ -proton, however upon reflection it seems unlikely that this could have such an effect as to result in significant levels of racemization in a 2 min reaction at 50°C. In concurrence with this conclusion, previous literature has found that amino acid ester isocyanates are resistant to racemization even in moderately acidic/basic conditions.<sup>532-535</sup>

## 5.3 Results & Discussion – Deprotection

### 5.3.1 Approach and general considerations

Now that a method had been developed for an efficient <sup>11</sup>C-radiosynthesis of the *tert*-butyl ester protected glutamate urea intermediates, the final stage in the method development was to remove the *tert*-butyl ester protecting groups (PGs) to yield the free carboxylic acid-bearing molecules. In designing the synthetic strategy, *tert*-butyl-based PGs were selected because of their general ease of removal under acidic conditions. In non-radioactive synthesis (including our own), such deprotections are generally effected with the use of trifluoroacetic acid (TFA) – as a strong acid it is capable of cleanly removing the PGs, but its volatility makes it easy to remove from the final product. For carbon-11 radiochemistry however, we had some concerns regarding the use of TFA. The demands imposed by radioactive decay meant that a rapid deprotection was required, and as a result, it was desirable to use an acid that could be heated without significant evaporation etc., but TFA boils at 72°C, somewhat limiting the possibilities in this regard. Additionally, if any trace quantities remained in the product, it was unclear what levels of residual TFA or trifluoroacetate byproducts<sup>536</sup> would be permissible in doses intended for use *in vivo*. So the decision was made to avoid the use of TFA where possible in this method.

To address these concerns we looked to aqueous hydrochloric acid as an alternative. As a stronger acid than even TFA it should be able to cleave the esters with equal or superior efficiency, but it should also allow heating of the reaction to higher temperatures without evaporation. Furthermore, HCl is a more biologically acceptable contaminant, particularly as its neutralisation products tend to be chloride salts and water/CO<sub>2</sub>, depending on the bases used, so there were comparatively few concerns relating to residual byproduct limits.

Initially we looked to the literature for inspiration regarding *tert*-butyl deprotection with HCl in <sup>11</sup>C-radiochemistry and found a method recently reported by Pekošak *et al.* as part of their method for the <sup>11</sup>C-radiolabeling of “native” tetrapeptides.<sup>537</sup> In this work a tetrapeptide was radiolabeled with [<sup>11</sup>C]benzyl iodide, and the final stage of the radiosynthesis was to remove the *tert*-butyl-based protecting groups from the molecule to



yield the final fully-protected <sup>11</sup>C-radiolabeled peptide. In their method, the <sup>11</sup>C-radiolabeled protected tetrapeptide was first isolated by HPLC, the mobile phase was removed with evaporation, 100 μL of HCl (12M) was added and heated to 100°C for 2 mins. With this method, the deprotection was cleanly effected, and no racemisation of any of the five stereocentres (the sidechain β-carbon on threonine, in addition to the four amino acid α-carbons) was observed as a result of this protocol. This seemed a simple and highly promising approach that could be applied without much modification to our *tert*-butyl protected molecule, and it was particularly encouraging to see that the use of concentrated HCl at 100°C did not result in racemisation or other decomposition of their product.

The main modification that we hoped to make to this method was to eliminate the time-consuming interim HPLC-purification of the protected intermediate. In the previous section, the method for synthesising the fully-protected <sup>11</sup>C-urea had been well optimised, validated, and found to be reliable, with no other major impurities present in the solution at this stage. As such, we initially saw no reason why this crude reaction mixture could not be used without purification for the deprotection stage – essentially the method would be a “telescoping” synthesis: whereby all reagents are added to a single vial to perform multiple transformations sequentially, without interim purification/isolation.<sup>538</sup> If this were successful, this would be the most operationally simple approach, making this a more attractive and easily-implementable method for the library <sup>11</sup>C-radiosynthesis of PSMA-ligands. In addition, avoiding an interim purification would result in a significantly shorter total radiosynthesis time – an important factor in <sup>11</sup>C-radiochemistry. It should be noted however, that the total volume of the reaction solution containing the fully-protected <sup>11</sup>C-urea intermediate was 550 μL. To achieve a high concentration of HCl in a minimal volume, we intended to fully evaporate the MeCN before addition of HCl (mirroring the approach taken by Pekošak *et al.*).

### 5.3.2 HPLC method development

To evaluate the reaction and determine RCPs (and by extension, RCYs) a reliable HPLC method had to be developed for this reaction. Primarily, it had to retain and separate the highly-polar, fully-deprotected [<sup>11</sup>C]Leu-Glu product from the small amounts of symmetric <sup>11</sup>C-urea products and any of the potentially-formed [<sup>11</sup>C]Leu-<sup>pyr</sup>Glu impurity. Additionally, it was essential to ensure that none of the injected radioactivity was retained on the column with this elution method, otherwise any RCPs calculated from these results would be invalid.

To achieve the retention/separation of the target [<sup>11</sup>C]Leu-Glu it was determined that an isocratic elution would achieve the best chromatographic performance. However, it was clear that any isocratic elution method capable of achieving sufficient retention of the highly-polar tricarboxylic [<sup>11</sup>C]Leu-Glu product, would result in overly strong retention of the significantly more-lipophilic *tert*-butyl ester protected [<sup>11</sup>C]Leu-Glu-(*O*<sup>t</sup>Bu)<sub>3</sub>, some of which would still possibly remain unreacted in solution. To avoid this issue, we designed a 2-phase stepped isocratic elution method. The initial phase of this method was a eluotropically-weak isocratic elution to achieve retention/separation of the target compound, [<sup>11</sup>C]Leu-Glu. Once this has eluted, the solvent mixture is switched (*via* a short ramping-gradient) to a significantly eluotropically-stronger isocratic elution regime. This second phase serves to fully “wash” the column of all radioactive impurities remaining, and is not intended to separate these compounds for analysis, but simply to elute everything from the column, to allow for accurate assessments of radiochemical conversions/purities.

The method developed for the radiosynthesis of [<sup>11</sup>C]Leu-Glu was as follows:

**Phase 1** (*weak isocratic*), 0-10 mins: 85% H<sub>2</sub>O / 15% MeCN

**Ramping** (*gradient*), 10-11 mins: 85% H<sub>2</sub>O / 15% MeCN to 15% H<sub>2</sub>O, 85% MeCN

**Phase 2** (*strong isocratic*), 11-20 mins: 15% H<sub>2</sub>O / 85% MeCN

This method was highly effective, with the target [<sup>11</sup>C]Leu-Glu eluting at ~ 7:25, an impurity (likely [<sup>11</sup>C]Leu-<sup>pyr</sup>Glu) eluting at ~ 11:00, and the remaining more lipophilic impurities coeluting in a sharp peak at ~ 13:25 on the solvent front with the change in

solvent (remember that due to the system void volume, any changes in solvent composition will only reach the detectors ~ 2 mins after the composition is changed at the HPLC pumps). An example radio-HPLC chromatogram is shown in the figure below, with the HPLC method superimposed for clarity.

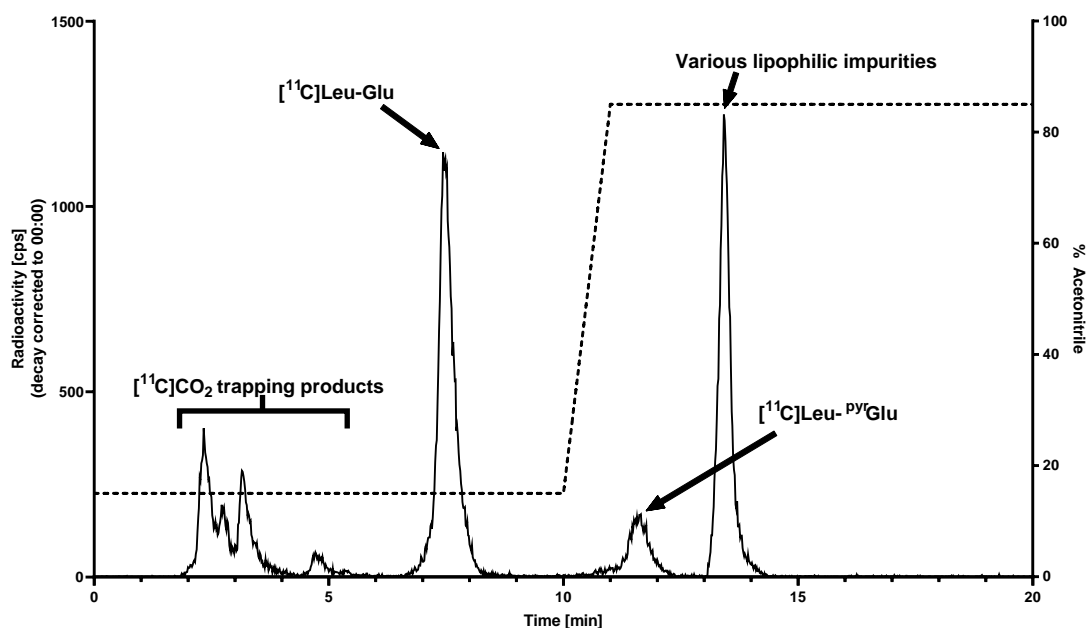


**Figure 5.12 Radiosynthesis of [ $^{11}\text{C}$ ]Leu-Glu with HPLC method superimposed**

Solid line – HPLC trace (radioactivity)

Dashed line – Eluent composition (% MeCN)

Remember, ~ 2 mins void time of the column means any changes in solvent composition will not be seen in chromatogram for ~ 2 mins.

With this stepped isocratic radio-HPLC method, the measurement of the product radiochemical purity in solution was possible. Additionally, the measurement of radioactivity in the reaction-vial and ascarite-cartridge enabled the calculation of [ $^{11}\text{C}$ ]CO $_2$  trapping efficiencies. Combining these two measurements it was possible to calculate accurate non-isolated radiochemical yields for our radiosynthesis of [ $^{11}\text{C}$ ]Leu-Glu. Additionally, as will be discussed shortly, it is trivial to modify this method for the analysis of other  $^{11}\text{C}$ -radiolabeled PSMA ligands.

### 5.3.3 Deprotection: first successful radiosynthesis of [ $^{11}\text{C}$ ]Leu-Glu ([ $^{11}\text{C}$ ]ZJ43)

#### 5.3.3.1 Solvent evaporation

At the end of the  $^{11}\text{C}$ -urea synthesis stage (performed as previously developed but omitting the quench step), the intermediate fully-protected  $^{11}\text{C}$ -urea (and the various minor impurities) exist in a 550 $\mu\text{L}$  solution of MeCN. To remove this solvent, a combination of gas flushing and heating was employed. The vial was heated to 100 $^{\circ}\text{C}$ , well above the 82 $^{\circ}\text{C}$  boiling point of MeCN, and helium was bubbled through the solution at 70 mL/min using the gas-delivery needle (previously used for [ $^{11}\text{C}$ ]CO $_2$  delivery) to evaporate the solution efficiently. A second vial (at room temperature) was placed between the vent needle and the ascarite cartridge to capture (by condensation) the majority of the evaporated MeCN, to avoid condensation in the cartridge itself which could lead to blockages in the system, reducing flow rates. The vial could be observed using the inbuilt camera on the Modular-Lab system, allowing for real-time monitoring of the evaporation process.

In practice, this process resulted in the full evaporation of the MeCN from the reaction vial over approx ~ **5 mins**. During this time, some loss in radioactivity (~ 20%) from the vial was observed (*via* the inbuilt pin-diode detector). We suspected this was selective evaporation of the unfixed [ $^{11}\text{C}$ ]CO $_2$  trapping products, and not loss of the key [ $^{11}\text{C}$ ]CO $_2$ -fixation products. This suspicion was based upon previous experience within our lab that showed that these [ $^{11}\text{C}$ ]CO $_2$  trapping products are relatively volatile (or at least decarboxylatively unstable) and can be selectively evaporated from radiolabeling solutions by heating/helium flushing, without loss of the key  $^{11}\text{C}$ -intermediates. It will be shown (in section 5.3.3.2.1), that while this does indeed result in a lower “trapping” efficiency for the overall procedure (as measured by comparing the radioactivity in the vial to that trapped in the ascarite cartridge), this has no effect on the overall fixation efficiency since these key fixation products are much less volatile and are therefore not lost during this evaporation process.

### 5.3.3.2 Deprotection and first radiosynthesis of $[^{11}\text{C}]\text{Leu-Glu}$ ( $[^{11}\text{C}]\text{ZJ43}$ )

The radiosynthesis of  $[^{11}\text{C}]\text{Leu-Glu-(O}^t\text{Bu)}_3$  was performed as previously described, (but omitting the final quench/HPLC analysis), and this stage was complete within ~ 6m 30s from EoB. Immediately following this, the reaction solvent was evaporated (as described above), taking approximately 5 min to remove the 550 $\mu\text{L}$  of MeCN. Once the solvent had been fully evaporated, the reactor temperature was lowered from 100 $^\circ\text{C}$  to 90 $^\circ\text{C}$ , before 100  $\mu\text{L}$  of conc. HCl (12 M) was added to the vial. The solution was stirred at 90 $^\circ\text{C}$  for 2 min before the reaction was quenched with 500  $\mu\text{L}$  HPLC eluent, the radioactivity in the vial and ascarite cartridges was measured, and an aliquot of the crude reaction mixture was injected and analysed by radio-HPLC, using the method as described above. This entire process took ~14 min from the end of cyclotron bombardment.

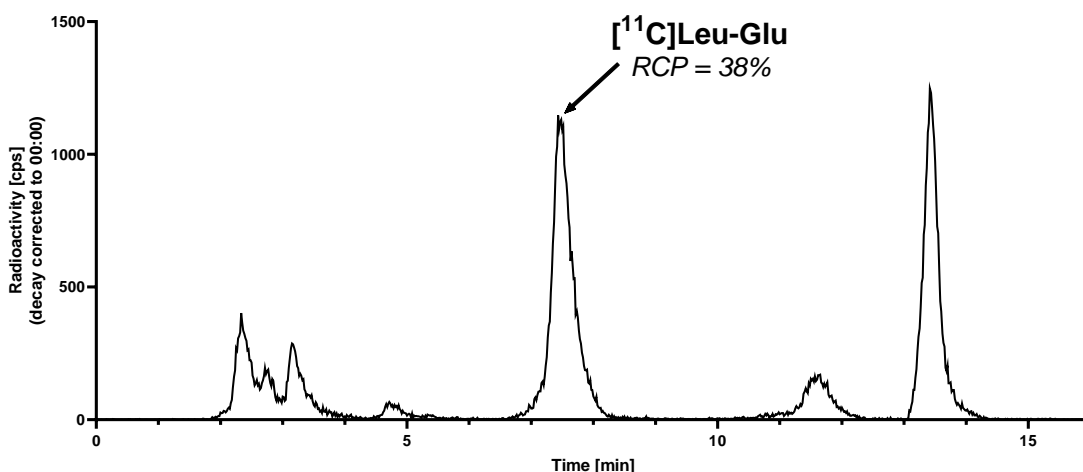


**Figure 5.13  $[^{11}\text{C}]\text{Leu-Glu}$  radiosynthesis radio-HPLC**

Product identity confirmed by co-injection with non-radioactive standard.  
RCP calculated by integration of crude radio-HPLC chromatogram

The target product,  $[^{11}\text{C}]\text{Leu-Glu}$  (aka  $[^{11}\text{C}]\text{ZJ43}$ ) was produced in reasonable yields: the crude RCP was **38%** (measured by radio-HPLC), and the trapping efficiency was **60%**, resulting in an overall **23%** RCY (decay-corrected, non-isolated). With a 14 min total synthesis time, this corresponds to a (non-decay-corrected) radioactivity yield of **14%**, relative to the total quantity of  $[^{11}\text{C}]\text{CO}_2$  delivered from the cyclotron. This was a highly satisfactory result: the model compound  $[^{11}\text{C}]\text{Leu-Glu}$ , a high-affinity PSMA ligand ( $K_i = 0.8 \text{ nM}$ ),<sup>300</sup> had been successfully synthesised, marking the first  $^{11}\text{C}$ -radiolabeling of

the essential glutamate-urea pharmacophore of a PSMA ligand, and bodes well for the translation of this method to the <sup>11</sup>C-radiolabeling of alternative PSMA-ligands.

#### **5.3.3.2.1 Decreased trapping efficiency**

This result was excellent, but one detail which immediately draws attention is the **60%** trapping efficiency. During our earlier optimisation of trapping efficiencies (using the synthesis of [<sup>11</sup>C]Leu-Glu-(O<sup>t</sup>Bu)<sub>3</sub> as a model reaction), these same conditions had trapped the [<sup>11</sup>C]CO<sub>2</sub> with approximately **80%** efficiency; what was the cause of this discrepancy? During the solvent evaporation stage, significant quantities of radioactivity (~20-25%) were lost from the vial. We suspected that this was selective loss of the [<sup>11</sup>C]CO<sub>2</sub> trapping products (inorganic <sup>11</sup>C-carbon species, BEMP-[<sup>11</sup>C]CO<sub>2</sub> adduct, etc.), as these are more volatile and decarboxylatively unstable compared with the <sup>11</sup>C-fixation products (<sup>11</sup>C-ureas, <sup>11</sup>C-isocyanates). If this were true, then this drop in trapping efficiency would not result in an overall drop in RCY of the desired [<sup>11</sup>C]CO<sub>2</sub> fixation products. This appears to be the case, and can be demonstrated by comparison of two radio-HPLC chromatograms in Figure 5.14 below: chromatogram **A** depicts the <sup>11</sup>C-species distribution after <sup>11</sup>C-urea synthesis, and **B** depicts the <sup>11</sup>C-species distribution after <sup>11</sup>C-urea synthesis, solvent evaporation, and deprotection. In both chromatograms, the <sup>11</sup>C-trapping and <sup>11</sup>C-fixation products are labeled, and their peaks integrated/compared to give a trapping vs fixation product distribution for each chromatogram.

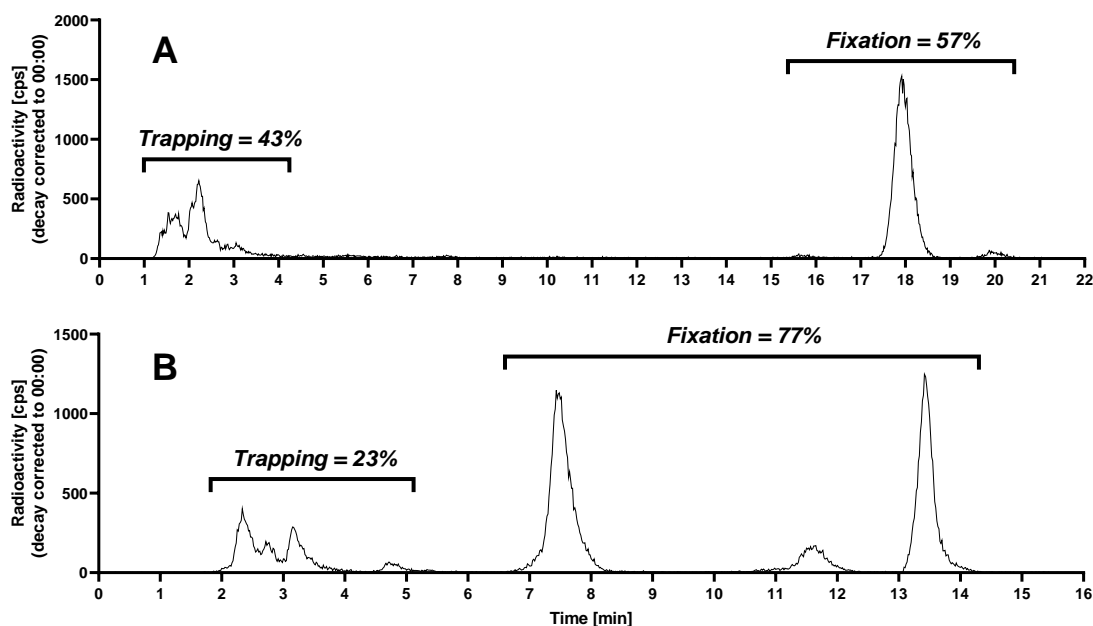


**Figure 5.14 Trapping vs fixation distribution before/after solvent evaporation**

**A** is before solvent evaporation (synthesis of  $[^{11}\text{C}]\text{Leu-Glu-(O}^t\text{Bu)}_3$ )  
**B** is after solvent evaporation (synthesis of  $[^{11}\text{C}]\text{Leu-Glu}$ )

As can be seen by comparing the trapping *versus* fixation distributions in both chromatograms, *after* evaporation (**B**), the fixation products have become comparatively enriched, from 57% to 77%, while the proportion of trapping products have decreased accordingly from 43% to 23%. This would seem to support the assertion that the loss in radioactivity during evaporation is only due to loss of  $^{11}\text{C}$ -trapping products, and not  $^{11}\text{C}$ -fixation products. Furthermore, combining these results with the total  $[^{11}\text{C}]\text{CO}_2$  trapping efficiencies (total radioactivity in vial *versus* ascarite cartridge) to calculate the overall  $[^{11}\text{C}]\text{CO}_2$  fixation efficiency (relative to the total produced  $[^{11}\text{C}]\text{CO}_2$ ) of both of these reactions clarifies the picture further, again supporting this conclusion.

For **A**, the total trapping efficiency was 80%, of which 57% was converted to  $^{11}\text{C}$ -fixation products, giving an overall  $[^{11}\text{C}]\text{CO}_2$  fixation efficiency of ~ 46%.

In **B**, the total trapping efficiency was reduced to 60%, of which 77% was converted to  $^{11}\text{C}$ -fixation products, giving an overall  $[^{11}\text{C}]\text{CO}_2$  fixation efficiency of ~ 46%.

This result confirms that the additional loss of radioactivity during the solvent evaporation stage is not detrimental to the overall [<sup>11</sup>C]CO<sub>2</sub> fixation efficiency, as it is caused by selective evaporation of <sup>11</sup>C-trapping byproducts, with the total <sup>11</sup>C-fixation products (<sup>11</sup>C-urea) fully retained in the vial throughout the evaporation process.

#### **5.3.3.2.2 Impurities**

In the radio-HPLC presented above, it is clear that other than the product peak (7:35) and the previously discussed [<sup>11</sup>C]CO<sub>2</sub> trapping products (2:00-5:00), the major radioactive impurities (that contain significant quantities of the fixed carbon-11, thereby decreasing the product RCY) are those that elute with the strong isocratic solvent front (13:00-14:00). As has been discussed already, the rapid switch to this very eluotopically strong elution regime was intended to “wash” everything from the column to allow accurate RCP calculations, but this is done at the expense of any separation between these different impurities; the eluotopically-strong 85% MeCN elution causes all of the impurities remaining on the column to co-elute. This was confirmed by continuing to run the analysis for an additional 40 minutes with the same isocratic solvent mixture: no further radioactive products elute from the column, and no significant quantities of radiation can be detected on the column with a handheld radiation monitor. So we were fairly certain that this method was accounting for the entirety of the injected radioactive products, although due to this co-elution, this gives very little insight into the chemistry occurring during this final deprotection stage.

Due to their stronger retention on the column than [<sup>11</sup>C]Leu-Glu, it can be deduced that these products have at least a degree more lipophilicity than the highly-polar tricarboxylic product, but this is close to the extent of the information that can be obtained from this chromatography. It is already known that in the <sup>11</sup>C-urea synthesis stage, 95% of the fixed carbon-11 was in the fully-protected [<sup>11</sup>C]Leu-Glu-(O<sup>t</sup>Bu)<sub>3</sub> intermediate, and by extension, if the deprotection had proceeded cleanly to completion then the same distribution within the fixation products would have been expected in the reaction solution after deprotection. In practice however, the fully-deprotected [<sup>11</sup>C]Leu-Glu product accounted for only 49% of the total fixed carbon-11 after the deprotection phase.



Ultimately however, for our purposes in this work, a 24% RCY was more than sufficient. Were this to be synthesised during a library <sup>11</sup>C-radiosynthesis of a variety of PSMA-ligands, a 24% RCY would be more than sufficient to be used in a preclinical imaging screening. If there were a later call for the routine production of [<sup>11</sup>C]Leu-Glu specifically, this final deprotection step could be further investigated and optimised. But at this point, we had no immediate intentions of using this particular molecule in any such studies. [<sup>11</sup>C]Leu-Glu was selected as a “model” compound: a proof-of-concept upon-which we hoped to develop a more generally-applicable method for <sup>11</sup>C-radiolabeling within the glutamate-urea pharmacophore of PSMA ligands. A more pressing concern to us concerned the wider applicability of this method to alternative substrates bearing structurally/functionally diverse sidechains; without such an investigation, this method could not be claimed to be “generally applicable”.

#### **5.3.3.2.3 Epimerisation**

As was discussed earlier, the binding affinity of PSMA-ligands depends strongly upon the stereochemistry at the two  $\alpha$ -carbons of the amino acid residues attached to the central urea functionality. We have already demonstrated that there was no racemisation of the amino-acid <sup>11</sup>C-isocyanate, as evidenced by the absence of any (*S*),(*R*)-epimer in the radio-HPLC analysis of the [<sup>11</sup>C]Leu-Glu-(*O*<sup>t</sup>Bu)<sub>3</sub> intermediate radiosynthesis. This was the most likely stage of the reaction during which epimerisation could have occurred, but we also had some concerns that epimerisation could occur during this acidic deprotection. Although as was noted previously, no epimerisation was noted in the work by Pekořak *et al.*,<sup>537</sup> from which we adapted this protocol.

With reference again to the analytical HPLC method developed by Kwon *et al.*, for the separation of the (*S*),(*S*)- and (*S*),(*R*)-ZJ43 epimers, we expected any of the (*S*),(*R*)-ZJ43, if formed, to elute within ~ 2 mins of the target (*S*),(*S*)-epimer. Upon analysis of the radio-HPLC trace, no such peak was observed, confirming again that this method successfully proceeds with full stereochemical retention. While the conditions at different points throughout the method are relatively harsh (strong acids/bases, high temperatures, etc.), the duration of any of these was so short that if any epimerisation were possible, it is evidently not observed within this short radiochemical timeframe.

## 5.4 Results & Discussion - General Method and Substrate Scope

### 5.4.1 General radiosynthetic methodology

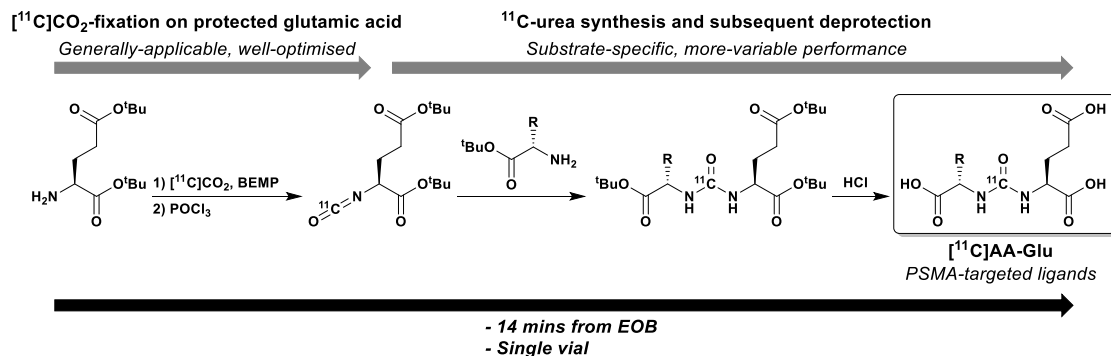


**Figure 5.15**  $^{11}\text{C}$ -radiolabeling of PSMA-targeted glutamate-ureas

Full details of the general protocol are detailed in the Materials and Methods section at the end of this chapter

Throughout this chapter, we have described the various stages of development of our “generally applicable” method for the  $^{11}\text{C}$ -radiolabeling of PSMA-ligands within their essential glutamate-urea pharmacophore (*via*  $^{11}\text{C}$ CO<sub>2</sub> fixation), and a figure summarising the general radiosynthetic approach is presented above. Altogether, the method developed was an impressively chemically complex procedure: a single-vial telescoped reaction, complete within just 14 min from the end of cyclotron bombardment.

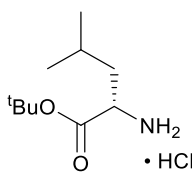
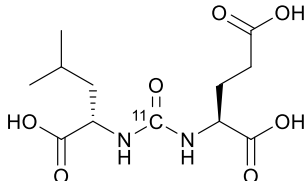
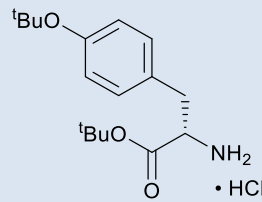
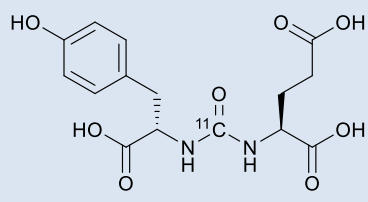
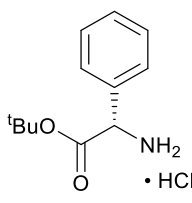
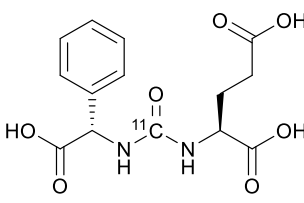
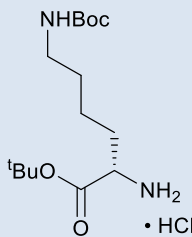
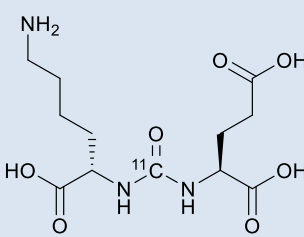
In an effort to ensure that the method was as substrate independent as possible, our approach was to ensure that the reaction steps that are common to all possible applications of this method (the BEMP-mediated  $^{11}\text{C}$ CO<sub>2</sub>-fixation on the protected glutamic acid precursor, and the POCl<sub>3</sub>-mediated formation and isolation of the  $^{11}\text{C}$ -isocyanate intermediate) were as well optimised as possible. In this effort, we optimised the initial  $^{11}\text{C}$ CO<sub>2</sub>-trapping process to promote the productive  $^{11}\text{C}$ CO<sub>2</sub>-fixation reaction over the unproductive BEMP- $^{11}\text{C}$ CO<sub>2</sub> adduct formation. Additionally, the  $^{11}\text{C}$ -carbamate to  $^{11}\text{C}$ -isocyanate conversion stage – mediated by POCl<sub>3</sub> – was optimised to ensure the  $^{11}\text{C}$ -isocyanate remains isolated and unreacted in solution after this stage, leading to high asymmetric selectivity in the subsequent  $^{11}\text{C}$ -urea synthesis. These two stages are common to all possible applications of this methodology, so their thorough optimisation was crucial to ensuring a successful and generally-applicable radiolabeling methodology.

The latter substrate-specific steps are less thoroughly-optimised, but are arguably more-straightforward chemical transformations, and accordingly, less optimisation of these procedures was expected to be necessary. Firstly, the <sup>11</sup>C-isocyanate is comparatively “spring-loaded” towards nucleophilic attack, and the addition of a significant quantity of any other nucleophilic amine should result in a reasonably selective formation of the asymmetric <sup>11</sup>C-urea. Secondly, the *tert*-butyl protection strategy is a well validated approach, used widely in the field of peptide chemistry. The protected functionalities have a good level of general chemical resistance, but cleavage of these protecting groups can generally be effected rapidly and cleanly under acidic conditions. Accordingly, it was hoped that this method would prove to be “generally applicable” to a range of structurally and functionally diverse PSMA-ligands.

### 5.4.2 Substrate scope

To demonstrate the broad substrate scope of this general synthetic method, it was applied to the <sup>11</sup>C-radiolabeling of several structurally/functionally diverse PSMA ligands, and the results of these syntheses are presented in the table below:

**Table 5.3 Substrate scope**

Name	Precursor	Product	Affinity (K <sub>i</sub> )	RCY (d.c.)
[ <sup>11</sup> C]Leu-Glu			<b>0.8 nM<sup>[a]</sup></b>	<b>24%</b>
[ <sup>11</sup> C]Tyr-Glu			<b>3.0 nM<sup>[b]</sup></b>	<b>35%</b>
[ <sup>11</sup> C]Phg-Glu			<b>2.1 nM<sup>[b]</sup></b>	<b>25%</b>
[ <sup>11</sup> C]Lys-Glu			<b>498 nM<sup>[c]</sup></b>	<b>13%</b>

[a] affinity reported by Olszewski *et al.*<sup>300</sup>

[b] affinities reported by Kozikowski *et al.*<sup>288</sup>

[c] affinity reported by Maresca *et al.*<sup>305</sup>

d.c. = decay corrected, (synthesis time = 14 min from EoB)

To ensure successful deprotection of the <sup>11</sup>C-urea, sidechain functionalities on the amino-acid precursors were protected with acid-labile *tert*-butyl-based protecting groups:

- **Amines** are protected as *tert*-butoxycarbamates (**Boc**)
- **Hydroxyls** are protected as *tert*-butyl ethers
- **Carboxylic acids** are protected as *tert*-butyl esters

These protected amino-acid building-blocks are generally cheap and readily available from commercial sources in their hydrochloride salt forms. Fortunately, rather than first requiring basic extraction to yield the free amine, the addition of an equimolar quantity of BEMP to the solution serves to deprotonate these HCl salts *in situ*, allowing the reaction to proceed unhindered.

In general, the results demonstrate this method's functional group tolerance and broad substrate scope. Ligands bearing both aromatic and aliphatic sidechains are successfully radiolabeled with this method. Additionally, due to the use of the generally-applicable *tert*-butyl protection scheme, compounds bearing amines, hydroxyls, and carboxylic acids were all successfully radiolabeled without any obvious signs of unintended adverse reactivity of these functionalities. Some of these substrates could benefit from some optimisation of conditions (particularly the [<sup>11</sup>C]Lys-Glu synthesis, which was only produced in a 13% RCY), however achieving the highest possible yields for each product was not the goal in this work. The aim in this section was to demonstrate how one general method is capable of <sup>11</sup>C-radiolabeling PSMA-ligands, and that even though in this case the RCY was relatively low, such a yield would still be sufficient to enable pre-clinical screening.

Reversed-phase radio-HPLC analysis of all of these radiosyntheses was performed using a stepped isocratic elution method (as described previously). The only substrate-specific modification required was the adjustment of the chromatographic strength of the initial "weak isocratic" phase. By virtue of the 3 (at-minimum) highly-polar carboxylate moieties on these PSMA-ligands, they only retain on reversed-phase C18 columns under highly aqueous conditions. To develop a method for each specific product, the non-radioactive reference standard was analysed (initially) with an 80% aqueous elution, and the solvent composition was accordingly adjusted from there to achieve an analyte retention time in the approximate 6-8 min range (specific solvent compositions for the identification/separation of each product are detailed in the materials and methods

section). Elution in this region ensures that the product is clear from any “trapped” impurities eluting with the column void volume (~2-4 min), but also avoids eluting near to the large impurity peak that elutes (at ~13-14 min) as result of the switch to the eluotropically-strong isocratic “washing” phase. In practice, this analytical method development is a fairly trivial process, and usually enabled a new analytic method to be developed in under 1 hour.

## 5.5 Conclusion

The intention of this method was to develop a simple and generally applicable approach to <sup>11</sup>C-radiolabel within the glutamate-urea pharmacophore of otherwise functionally-diverse PSMA-ligands. Because of the ubiquity of the glutamate-urea fragment within these ligands, the method was developed with a focus on the efficient formation of this common core. This section of the method (<sup>11</sup>C]CO<sub>2</sub>-fixation on a protected glutamic acid precursor, and subsequent <sup>11</sup>C-isocyanate production) proceeds identically, regardless of the second amine substituent later introduced to the urea moiety. The second section was less thoroughly optimised by-comparison, but in this work, we had no specific interest in any one of the PSMA-ligands, so thorough optimisation of any one specific radiosynthesis was not necessary. However, the reaction was demonstrated to have a broad substrate scope: product RCYs in the 13%-35% range were achieved within 14 min from the EoB, which is highly promising for future use as a method for library <sup>11</sup>C-radiosynthesis.

In optimising the different stages of this reaction, a common theme was the issue of competition between productive and unproductive reaction pathways. By consideration of the possible reactivity of all reagents and intermediates present in solution at any particular instance, the rational optimisation of the reaction was made possible by selectively promoting and suppressing the productive and unproductive pathways, respectively. It is hoped that this will also serve to guide future development of similar broad methodologies based on this BEMP/POCl<sub>3</sub>-based [<sup>11</sup>C]CO<sub>2</sub>-fixation chemistry.

There are several different use-cases in which this method could be valuable and so it was developed to be as general an approach as possible. Primarily, we see this as a tool for library <sup>11</sup>C-radiosynthesis for the pre-clinical screening of a variety of candidate new-generation fluorinated PSMA-radiotracers, due to the broad substrate tolerance of this method. Additionally, it is also possible to envision such a method being further-developed for the <sup>11</sup>C-radiolabeling of a particularly promising candidate (perhaps an ultra-high affinity PSMA-ligand) that may be otherwise radiochemically inaccessible (e.g. incorporating <sup>18</sup>F or a radiometal compromises its affinity). For such a use-case, this method hopefully provides a solid and considered foundation from-which conditions can

be further rationally-optimised towards the efficient <sup>11</sup>C-radiolabeling of a particularly promising candidate PSMA-radiotracer.

In any case, it is hoped that the method developed in this work will provide a useful tool in the further development and understanding of PSMA-targeted PET-imaging and radionuclide-therapy. This rapidly developing field is causing a paradigm shift in the diagnosis, monitoring, and treatment of prostate cancer, and there is undoubtedly much-more investigation to come.



## 5.6 Materials & Methods

### 5.6.1 General

Anhydrous acetonitrile (MeCN, 99.8%), Ascarite, *L*-glutamic acid di-*tert*-butyl ester hydrochloride (Glu-(OtBu)<sub>2</sub>.HCl, ≥ 98%), *L*-leucine *tert*-butyl ester hydrochloride (Leu-(OtBu).HCl, ≥ 98%), phosphorous(V) oxychloride (POCl<sub>3</sub>, 99%), hydrochloric acid (HCl, 37%), trifluoroacetic acid (TFA, ≥ 99%), and 2-*tert*-butylimino-2-diethylamino-1,3-dimethylperhydro-1,3,2-diazaphosphorine (BEMP, ≥ 98%) were purchased from Sigma-Aldrich. *O*-*tert*-butyl-*L*-tyrosine *tert*-butyl ester hydrochloride (Tyr(tBu)-(OtBu).HCl, ≥ 98%), *L*-phenylglycine *tert*-butyl ester hydrochloride (Phg-(OtBu).HCl, ≥ 98%), and *N*- $\epsilon$ -Boc-*L*-lysine *tert*-butyl ester hydrochloride (Lys(N- $\epsilon$ -Boc)-(OtBu).HCl, ≥ 98%) were purchased from Santa Cruz Biotechnology. Deionised water (18.2 M $\Omega$ .cm) was produced in a Milli-Q Reference Water Purification System.

[<sup>11</sup>C]CO<sub>2</sub> was produced using a Siemens RDS112 cyclotron in a <sup>14</sup>N(p, $\alpha$ )<sup>11</sup>C reaction, by the 11 MeV proton bombardment of nitrogen (+ 1% O<sub>2</sub>) gas. The cyclotron produced [<sup>11</sup>C]CO<sub>2</sub> was transferred in a stream of helium gas at 70 mL/min through a P<sub>2</sub>O<sub>5</sub> drying tube (without further cryogenic trapping/preconcentration) into a switching valve of an Eckert & Ziegler Modular-Lab automated synthesis unit. Unless otherwise specified, all radioactive experiments used a 5 $\mu$ A bombardment for 1 min, producing on average 300-350 MBq [<sup>11</sup>C]CO<sub>2</sub> at the end of bombardment (EoB). The radioactivity contents of reaction vials and ascarite cartridges were all measured (along with the measurement time since EoB) in a Capintec® dose calibrator. Decay correcting these to the EoB allows for the accurate calculation of both the total amount of delivered radioactivity as well as the reaction trapping efficiencies. Radiochemical yields (RCY) reported are calculated as a percentage of the total radioactivity delivered from the cyclotron and are decay corrected to the EoB. Where RCY is non-decay-corrected, this is reported instead as the *radioactivity yield*.

Where solutions were prepared under inert atmospheres (argon or nitrogen) a dry-box apparatus was used. By maintaining a positive pressure of inert gas inside the box, an acceptable CO<sub>2</sub>-free atmosphere could be established for preparing CO<sub>2</sub>-sensitive radiolabeling solutions.

## 5.6.2 Radiolabeling solution preparation:

All of the solutions described herein were prepared under a positive pressure of nitrogen within a dry-box. The solutions are made-up in 1.5 mL v-shaped glass vials which are subsequently crimp-sealed with a PTFE/silicone septum before wrapping the cap with PTFE tape to prevent any atmospheric contamination. Solutions are prepared no more than 3 hours prior to radiolabeling to minimise any degradation of reagents.

### 5.6.2.1 Fixation solution

Glu-(OtBu)<sub>2</sub>.HCl (1.47 mg, 5 μmol) and BEMP (6.47 μL, 22 μmol) were dissolved in anhydrous MeCN (250 μL) and a micro-stirrer bar was added.

### 5.6.2.2 POCl<sub>3</sub> solution

POCl<sub>3</sub> (2 μL, 21.4 μmol) was dissolved in anhydrous MeCN (100 μL).

### 5.6.2.3 Amine solution

The hydrochloride salt of the relevant *tert*-butyl/N-Boc protected amino acid (50 μmol) and BEMP (14.7 μL, 50 μmol) were dissolved in anhydrous MeCN (200 μL).

### 5.6.3 General radiolabeling procedures

#### 5.6.3.1 Protected <sup>11</sup>C-urea radiolabeling

[<sup>11</sup>C]CO<sub>2</sub> was bubbled through the **fixation solution** vial at 20°C. Following delivery (~ 105 s) the temperature was raised to 50°C and the **POCl<sub>3</sub> solution** was added (*via* a N<sub>2</sub>-flushed syringe) with stirring and left to react for 2 min. Then the **amine solution** was added (*via* a N<sub>2</sub>-flushed syringe), the vial was stirred for a further 1 min before injection of 1 mL HPLC eluent (1 mL) as a quench. The crude reaction mixture was analysed by radio-HPLC according to the procedure described in 5.6.4.1 below.

#### 5.6.3.2 Deprotected <sup>11</sup>C-urea radiolabeling: PSMA-targeted ligands

[<sup>11</sup>C]CO<sub>2</sub> was bubbled through the **fixation solution** vial at 20°C. Following delivery (~ 105 s) the temperature was raised to 50°C and the **POCl<sub>3</sub> solution** was added (*via* a N<sub>2</sub>-flushed syringe) with stirring and left to react for 2 min. Then the **amine solution** was added (*via* a N<sub>2</sub>-flushed syringe), the vial was stirred for a further 1 min. Following this, the temperature was raised to 100°C with He purging the solution to evaporate the MeCN (~ 6 min). The temperature was lowered to 90°C, before HCl (12M, 100µL) was added (*via* a N<sub>2</sub>-flushed syringe) and the reaction stirred for 2 min before injection of HPLC eluent (500 µL) as a quench. The crude reaction mixture was analysed by radio-HPLC according to the procedure described in 5.6.4.2 below.

#### 5.6.4 Radio-HPLC methods

HPLC analyses were performed on an Agilent 1200 system, with a variable wavelength UV detector and a LabLogic Flow-RAM  $\beta^+$  detector equipped in series. All radio-HPLC data was decay-corrected to the time of injection, to ensure accurate quantitation of solution composition (particularly important for longer HPLC analyses used for reaction optimisation).

##### 5.6.4.1 Protected <sup>11</sup>C-urea analytic method

*Column:* Phenomenex Luna C18(2), 5  $\mu$ m, 150 x 4.6 mm

*Isocratic elution:* 40% H<sub>2</sub>O / 60% MeCN (0.1% TFA v/v), 1 mL/min, UV lamp = 210nm

*Protected <sup>11</sup>C-urea retention times:* [<sup>11</sup>C]Leu-Leu-(OtBu)<sub>2</sub> = 15:40; [<sup>11</sup>C]Leu-Glu-(OtBu)<sub>3</sub> = 18:00; [<sup>11</sup>C]Glu-Glu-(OtBu)<sub>4</sub> = 20:00.

##### 5.6.4.2 Deprotected <sup>11</sup>C-urea analytic methods

To tailor these methods for the individual <sup>11</sup>C-urea product, the initial solvent composition (**A**% H<sub>2</sub>O / **B**% MeCN [0-10 min]) was varied, however the eluotropicall strong isocratic phase (15% H<sub>2</sub>O/85% MeCN [11-20 min]) was kept constant across all methods.

*Column:* Phenomenex Luna C18(2), 5  $\mu$ m, 150 x 4.6 mm

*Stepped-isocratic elution:* **A**% H<sub>2</sub>O / **B**% MeCN (0.1% TFA v/v) [0-10 min]; **A**% H<sub>2</sub>O / **B**% MeCN to 15% H<sub>2</sub>O / 85% MeCN (ramping gradient) [10-11 min]; 15% H<sub>2</sub>O / 85% MeCN [11-20 min].

*<sup>11</sup>C-urea products (A, B, retention time [m:ss]):* [<sup>11</sup>C]Leu-Glu (85% H<sub>2</sub>O, 15% MeCN, 7:30); [<sup>11</sup>C]Tyr-Glu (90% H<sub>2</sub>O, 10% MeCN, 8:10); [<sup>11</sup>C]Phg-Glu (85% H<sub>2</sub>O, 15% MeCN, 6:30); [<sup>11</sup>C]Lys-Glu (98% H<sub>2</sub>O, 2% MeCN, 4:40).

## 6 CONCLUSIONS & FUTURE WORK

### 6.1 Summary

This thesis has two main schemes of work – the development of an in-loop [ $^{11}\text{C}$ ]CO<sub>2</sub> fixation methodology, and the development of a generally applicable method for the  $^{11}\text{C}$ -radiolabeling of PSMA targeted ligands – and while there are some thematic overlaps between them, they will largely be addressed separately in this section. For each of these two areas, three aspects will be discussed. Firstly, conclusions will be drawn regarding the results presented herein, with an aim to critically appraise the achievements and highlight important results. Secondly, consideration will be given to the prospect of what future work could be done to further investigate/improve the techniques developed. Finally, the broader outlook for the work will be discussed, with reference to the wider field in which it exists.

### 6.2 In-Loop [ $^{11}\text{C}$ ]CO<sub>2</sub> Fixation

#### 6.2.1 Conclusions

In this first section of the thesis, our aim was to explore the possibility of transferring the relatively-new but increasingly well-established [ $^{11}\text{C}$ ]CO<sub>2</sub>-fixation methodologies to an “in-loop” reaction setup. Whilst these [ $^{11}\text{C}$ ]CO<sub>2</sub> fixation processes are well described and optimised in-vial, as a heterogenous gas-liquid phase reaction involving bubbling of the gaseous [ $^{11}\text{C}$ ]CO<sub>2</sub> through a solution containing the fixation reagents, we hypothesised that the chemistry could benefit from the same improvements commonly encountered for other heterogenous gas-liquid radiolabeling methodologies in transferring to a thin-film/captive-solvent approach in-loop.

The paradigmatic example of such a technique is that published by Wilson *et al.*, in which they described their “remarkably simple captive solvent method” for reactions of [ $^{11}\text{C}$ ]methyl iodide within an HPLC injector assembly.<sup>441</sup> However, it first occurred to us that to develop an analogous methodology to this, it was important to delve beyond this landmark paper. As such, this section begins with a reasonably comprehensive review of

the historic development of these thin-film and captive-solvent methodologies as they are applied to  $^{11}\text{C}$ -radiochemistry, both before and after the Wilson method; and this was used to assemble a list of key criteria by-which a new methodology ought to be measured. At their heart, these methods are intended to be practically applicable and enable easier/wider access to  $^{11}\text{C}$ -radiolabeled molecules. As such, any new method should be designed with significant consideration given to ease of implementation/use, simplified/automatable workflows, broad applicability, and all without significantly compromising the end-results of the chemistry.

A potential hurdle for this work was that while in-loop  $^{11}\text{C}$ -methylations function primarily by virtue of the high solubility of  $[^{11}\text{C}]\text{CH}_3\text{I}$  in organic solvents,  $[^{11}\text{C}]\text{CO}_2$  is sparingly soluble by itself. As such,  $[^{11}\text{C}]\text{CH}_3\text{I}$  can be trapped just by passage through a vessel containing pure solvent: as a result, protocols often call for initial trapping of  $[^{11}\text{C}]\text{CH}_3\text{I}$ , sealing the loop for a certain time to allow reaction to take place, before re-opening the loop to elute the product. By comparison, for reactions with  $[^{11}\text{C}]\text{CO}_2$ , trapping and reaction are essentially one-and-the-same process, so the chemistry has to be better optimised to ensure efficient trapping.

The first key result of this work was therefore the proof-of-concept demonstration that  $[^{11}\text{C}]\text{CO}_2$  can be efficiently trapped (~ 99%) in a small volume (150  $\mu\text{L}$ ) polymer loop, the inner surface of-which is coated with just ~ 10-15  $\mu\text{L}$  fixation solution (amine and DBU). The efficient trapping of  $[^{11}\text{C}]\text{CO}_2$  in such small-volumes in-vial is extremely challenging, but this thin-film in-loop approach enabled easy microvolume  $[^{11}\text{C}]\text{CO}_2$  fixation. The results indicate that while all of these fixation solutions – containing an amine and superbase (DBU in our case) – are highly effective at trapping  $[^{11}\text{C}]\text{CO}_2$  in general, the key determinant of trapping efficiency in-loop is the degree to which the solution is retained on the walls of the loop during gaseous flushing. This in-turn is affected by the solution viscosity as well as the gaseous flow-rate (a product of the pressure drop along the tubing).

The second key result of the work was the proof-of-concept implementation of this in-loop  $[^{11}\text{C}]\text{CO}_2$  fixation into a more-complex in-flow radiolabeling setup, whereby Mitsunobu-mediated  $^{11}\text{C}$ -isocyanate formation produced three symmetric  $^{11}\text{C}$ -ureas ( $N,N'$ - $[^{11}\text{C}]$ dibenzylurea,  $N,N'$ - $[^{11}\text{C}]$ dicyclohexylurea, and  $N,N'$ - $[^{11}\text{C}]$ diphenylurea) in

reasonable radiochemical yields. The standout feature of this technique was its remarkable speed and simplicity: the  $^{11}\text{C}$ -ureas were produced (non isolated) in  $< 3 \text{ min}$  from EoB, at *ambient temperatures and pressures*. Such rapid and simplified access to  $^{11}\text{C}$ -ureas was without precedent, and demonstrated the power of these thin-film in-loop techniques for the streamlining of heterogenous gas-liquid radiochemistry.

### 6.2.2 Future work

On a practical note, while ETFE was a useful polymer type for initial method development (optical transparency, flexibility, cost) it was perhaps not the optimal material for this application. It was shown throughout our work, that key to ensuring a high in-loop trapping efficiency was ensuring sufficient solution retention in-loop after gaseous purging. As was demonstrated by Studenov in their investigation into the underlying mechanisms of in-loop  $^{11}\text{C}$ -methylation,<sup>377</sup> perfluorinated polymers (ETFE, PTFE, etc.) are not effectively wetted by most organic solvents. While this could be beneficial in terms of avoiding significant loss of radioactivity by solution retention in-loop, it could also be responsible for some of the variable in-loop trapping performance that was seen. To address this, a relatively simple modification worth exploring would be the replacement of ETFE with PEEK tubing (as was recommended by Studenov), due to its greater solvent wettability. However it should be borne in mind that this is more difficult to use routinely, due to its optical opacity, comparative stiffness, and general expense.

On a more general note, a clear limitation of the method as presented herein was the relatively-limited number of substrates to-which the methodology was applied. While it was an important proof-of-principle demonstration of such a method, the next steps in further developing this would be to explore its application to a biologically relevant substrate. However there exist few molecules of interest built upon a symmetric urea scaffold, and this clearly justifies the expansion/modification of this methodology for the radiolabeling of asymmetric ureas. Based on the similar work from Dahl *et al.*,<sup>405</sup> it seems that the most promising approach to this would involve loading a second amine substrate into the “reaction loop” segment of the  $^{11}\text{C}$ -urea synthesis setup. In the method presented herein, after  $[^{11}\text{C}]\text{CO}_2$  fixation is complete, the Mitsunobu solution is passed through the fixation loop and through a second empty “reaction loop” to ensure adequate mixing to

allow for efficient  $^{11}\text{C}$ -urea synthesis. It is possible to imagine that a second amine substrate loaded in this reaction loop would be able to capture the intermediate  $^{11}\text{C}$ -isocyanate that has formed *in situ*, forming an asymmetric  $^{11}\text{C}$ -urea product.

Furthermore, an alternative application of this methodology would be in the synthesis of cyclic  $^{11}\text{C}$ -ureas. There are a significant number of promising  $^{11}\text{C}$ -radiotracers bearing [ $^{11}\text{C}$ ]benzimidazolinone and [ $^{11}\text{C}$ ]imidazolinone moieties, that have thus far only been accessible with [ $^{11}\text{C}$ ]COCl<sub>2</sub>, however it is possible to envisage these being produced from the diamino precursors in a similar manner to the symmetric  $^{11}\text{C}$ -ureas described herein, although it would likely require some stoichiometric modifications and general optimisation.

Finally, Jakobsson and Pike have recently described the production and application of [ $^{11}\text{C}$ ]COF<sub>2</sub>, a novel  $^{11}\text{C}$  synthon with seemingly analogous reactivity to [ $^{11}\text{C}$ ]COCl<sub>2</sub> but with a much simpler on-line production route directly from [ $^{11}\text{C}$ ]CO.<sup>142,143</sup> While the production and application of [ $^{11}\text{C}$ ]COF<sub>2</sub> has yet to be reported by others, taken at face value it seems to be a highly promising synthon for  $^{11}\text{C}$ -carbonylation, and has been applied successfully for the formation of both cyclic and linear  $^{11}\text{C}$ -urea derivatives. As a highly-reactive gaseous reagent produced on-line by gas-phase conversions from [ $^{11}\text{C}$ ]CO<sub>2</sub>, it is possible to envisage the integration of this production setup into a larger in-loop style radiosynthesis setup akin to that developed herein. Such an implementation would involve passing the stream of [ $^{11}\text{C}$ ]COF<sub>2</sub> directly through a loop coated with a solution of a diamino precursor, where it would be expected to react directly to form a cyclic  $^{11}\text{C}$ -urea *in situ*.

### 6.2.3 Outlook

Following our publication of this method, along with Dahl's concurrent publication of a similar methodology,<sup>404,405</sup> a number of other groups have attempted to implement [ $^{11}\text{C}$ ]CO<sub>2</sub> fixation chemistry in an in-loop setting, with varying degrees of success. These were summarised in the final discussion section, but broadly speaking, they demonstrated the simple nature of this chemistry, and the ease of setup and reaction efficiency that they can afford. Furthermore, over the previous 2 years, similar in-loop methodologies have been developed for both [ $^{11}\text{C}$ ]CO chemistry,<sup>116</sup> as well as – interestingly – for  $^{18}\text{F}$ -



fluorination using an unusual gaseous  $^{18}\text{F}$ -synthon.<sup>440</sup> These recent applications of our methodology, the development of new in-loop methodologies for other radiolabeling synthons, and the ongoing and widespread usage of in-loop  $^{11}\text{C}$ -methylation techniques serve as proof of the enduring appeal of such simplified radiolabeling setups.

Remote handling of bulk large volumes of solution can be extremely difficult, and can require complex and expensive automation hardware. Compared with this, doing radiochemistry within existing hardware (HPLC injector assemblies) or cheap and versatile disposable hardware (polymer tubing loop reactors) makes the remote operation and automation of these often difficult heterogenous gas-liquid processes significantly easier and cheaper to implement. Additionally, they can often lead to the efficiency benefits that arise as a result of miniaturising the reactions: reduced reagent quantities makes purification more straightforward. Furthermore, the use of high-surface-area inert solid supports for small volumes of solution can achieve highly efficient gas-liquid mass transfer, far surpassing what is practically achievable with gas bubbling through solutions of much larger volumes.

The general trend in radiochemistry automation for clinical GMP applications seems to be moving towards the adoption of sterile single-use cassette-based systems (as implemented by the GE FastLab synthesisers, Trasis AllinOne, IBA Synthera, Scintomics GRP, etc.). In combination with the maturation of these  $[^{11}\text{C}]\text{CO}_2$  fixation methodologies leading to appealing novel *carbonyl*- $^{11}\text{C}$ -radiotracers, it is possible to envisage the integration of a polymer loop-based  $[^{11}\text{C}]\text{CO}_2$  fixation setup into a single-use cassette. The standardised preparation and inert atmosphere storage of these commercially available cassettes could also somewhat mitigate the concerns regarding the molar activity of  $[^{11}\text{C}]\text{CO}_2$ -fixation reactions. It is important to ensure however, that any such cartridges produced are designed to be sufficiently airtight so as to prevent atmospheric contamination once opened and installed on the synthesis unit – this has not generally been a major concern for manufacturers in the development of these cassettes previously: avoiding any atmospheric contamination is less important for radiochemistry using  $[^{11}\text{C}]\text{CH}_3\text{I}$  or  $[^{18}\text{F}]\text{fluoride}$  since it would have no effect on the molar activity of the final product and it does not pose major sterility concerns due to ubiquitous post-synthesis sterile filtration.

### 6.3 Generally Applicable Method for $^{11}\text{C}$ -Radiolabeling PSMA ligands

#### 6.3.1 Conclusions

PSMA is a well-validated molecular target for the radionuclide imaging (PET/SPECT) and – increasingly – for the targeted radionuclide therapy of metastatic prostate cancer. The levels of PSMA expression in prostatic tissue are correlated with both tumour stage and likelihood of biochemical recurrence, and this has ultimately led, arguably, to a paradigm shift in the diagnosis, monitoring, and treatment of prostate cancer. The vast majority of all small-molecule PSMA ligands incorporate a ubiquitous glutamate-urea pharmacophore, which mimics PSMA's glutamate-based natural substrates (folate and NAAG). Accordingly, the only possible approach for radiolabeling PSMA-targeted molecules has been by installation of a radiometal chelator or radiohalogenated prosthetic group onto the sidechain of the second amino acid (typically through the amino-sidechain of lysine or the thiol-sidechain of cysteine), and these approaches can require widely varying radiolabeling conditions/approaches depending on the exact position in-which the radiolabel is to be installed. As an alternative to this, we aimed to develop a *generally applicable method* for the  $^{11}\text{C}$ -radiolabeling of PSMA-binding ligands. This would involve the installation of a  $^{11}\text{C}$ -radiolabel within the core urea linkage of this essential glutamate-urea pharmacophore, *via* [ $^{11}\text{C}$ ]CO<sub>2</sub> fixation.

Prior to any radiochemistry however, we had to synthesise a number of non-radioactive glutamate-urea reference compounds. The first key result of this scheme of work was the development of a simple, reliable, and safe approach for the synthesis of protected amino-acid-glutamate ureas via a “one-pot” CDI-mediated urea formation. Typically, these molecules have been produced using triphosgene, but we hoped to find a similarly broadly-applicable but safer alternative, due to the highly hazardous nature of triphosgene usage. The method developed was reliably applied in the synthesis of many protected glutamate-urea derivatives, and should hopefully allow the elimination of triphosgene from all but the trickiest of urea syntheses. Following this, we sought to deprotect these ureas by cleavage of the *tert*-butyl-based protecting groups, a conversion typically effected with TFA. In the process we encountered the unintended dehydrative cyclisation of the glutamate residue, forming the corresponding pyroglutamate species. Such a conversion has yet to be reported in the PSMA literature, but it was relatively frequent in

our hands, and raises concerns particularly for the long-term stability of “cold-kits” for PSMA radiolabeling. Ultimately we were able to develop a reliable deprotection protocol that suppresses this unintended dehydrative cyclisation with short reaction times and the addition of water.

Regarding the  $^{11}\text{C}$ -radiolabeling of these glutamate-ureas, we explored both the DBU/Mitsunobu<sup>225,226</sup> and BEMP/ $\text{POCl}_3$ <sup>214</sup> mediated approaches to  $^{11}\text{C}$ -urea formation, but ultimately opted to proceed *via* the BEMP/ $\text{POCl}_3$  methodology due to its superior operational simplicity and comparative ease of byproduct removal. Whilst this approach has sometimes been incompatible with sensitive substrates, due to the acidic byproducts of the  $\text{POCl}_3$ , application to these substrates saw no major incompatibilities.

Careful consideration of the radio-HPLC data (including characterisation/identification of both the intended product as well as common byproducts) informed the rational optimisation of the  $[^{11}\text{C}]\text{CO}_2$ -fixation conditions by selectively promoting/suppressing productive/unproductive reaction pathways, giving excellent selectivity for the asymmetric  $^{11}\text{C}$ -urea intermediate (avoiding the formation of significant quantities of the symmetric byproduct, a common pitfall).

This *tert*-butyl-protected  $^{11}\text{C}$ -urea synthesis was followed up with a rapid acidic deprotection, and the two steps were incorporated into a “telescoped” one-pot procedure, with the synthesis complete within 14 min from EoB. This was successfully applied in the proof-of-concept  $^{11}\text{C}$ -radiosynthesis of four high-affinity small-molecule PSMA ligands that were until-now radiochemically inaccessible.

### 6.3.2 Future work

Regarding the future development or implementation of this methodology, there are some clear choices for follow-up investigations. Firstly, it is important to note that one of the compounds produced herein,  $[^{11}\text{C}]\text{ZJ43}$  ( $[^{11}\text{C}]\text{Leu-Glu}$ ) is commonly used (*in vitro* and *in vivo*, in its non-radiolabeled form) as a high-affinity ( $k_i = 0.8 \text{ nM}$ ) blocking agent for PSMA target engagement studies and cell-binding assays. Because of this common reference usage in the assessment of many other PSMA-targeting compounds, it is arguably worthy of investigation in its own right. Imaging the *in vivo*

pharmacokinetics/pharmacodynamics and target uptake of this species could potentially help to better inform its usage as a reference compound in this manner.

In order to produce the quantities of [ $^{11}\text{C}$ ]ZJ43 that would be required for *in vivo* studies, the reaction would require a better-developed semi-automated production protocol to allow fully-remote synthesis (compared to the semi-manual process developed herein). The development of a similar (albeit less complex) automated  $^{11}\text{C}$ -urea synthesis protocol has been achieved by others in our lab recently for the radiolabeling of [ $^{11}\text{C}$ ]biotin, using the same E&Z Modular Lab system as was used throughout this project.<sup>244</sup> While this could provide a basis from which to work, as a cyclic  $^{11}\text{C}$ -urea product which does not require a deprotection step, the synthesis of [ $^{11}\text{C}$ ]biotin – a cyclic  $^{11}\text{C}$ -urea product which does not require a deprotection step – requires two fewer steps than [ $^{11}\text{C}$ ]ZJ43 would and so the method would necessarily be somewhat more elaborate. Nevertheless, due to the demonstrated generality of this method, it is hoped that once this automated method is developed, it should not require significant modification to be applied to a different PSMA-targeted substrate.

Another possible investigation pertains to the radiochemical yields obtained from the deprotection phase of the radiosynthetic protocol. Initially there was less focus on optimising this, as it would be expected to be relatively substrate dependent. This was not deemed of the highest importance; since the method produced reasonable radiochemical yields for all substrates attempted, it was considered sufficient as a proof of the method's "generally-applicable" nature. Nevertheless, it would still be of interest to further-investigate the large lipophilic impurity peak that typically elutes with the "solvent front" of the eluotropically-strong isocratic phase; as it is this peak which accounts for the majority of the remaining non-product radiochemical yield.

As was discussed, the second eluotropically-strong-isocratic phase of this method was intended to ensure the accurate calculation of radiochemical yields by ensuring no radioactivity remained on the column in any form. The disadvantage of this method is that in ensuring all impurities are washed off in a short time-period, it likely causes them to co-elute in one single peak. To address this, it would be interesting to separate and identify the constituent co-eluting radioactive species with a gradient elution. Performing such an analysis for several of these different substrates could help to reveal whether there

is a systematic and predictable mechanistic cause for these impurities (e.g. incomplete deprotection, or acidic hydrolysis of the urea linkage, etc.), or whether the mechanisms behind the formation of these impurities are largely specific to a particular substrate. If these impurities are found to be systematic in nature, then an alteration could be made to the general methodology in an attempt to ameliorate this. However if it is found to be a less-systematic issue, then this is a more difficult issue to resolve.

Finally, to extend the “proof-of-concept”, it could be useful to apply this method to a pre-existing well established fluorinated radiotracer (e.g. [ $^{18}\text{F}$ ]DCFPyL), to better demonstrate the generally-applicable nature of this “general” approach in enabling the radiolabeling of [ $^{11}\text{C}$ ]DCFPyL. This would require custom precursor synthesis of the fluoronicotinamide *tert*-butyl-ester derivative of lysine as the second amine precursor, since this is not commercially available: typically the Lys-Glu urea moiety is pre-formed (often commercially obtained) and the final radiolabeling stage involves the amide condensation between the [ $^{18}\text{F}$ ]fluoronicotinic acid and the lysine amino-sidechain to produce [ $^{18}\text{F}$ ]DCFPyL. However in our  $^{11}\text{C}$ -radiolabeling method, since the  $^{11}\text{C}$ -urea linkage is typically the final bond formed, the synthesis of [ $^{11}\text{C}$ ]DCFPyL would require the lysine to be pre-functionalised at its sidechain.

### 6.3.3 Outlook

In light of the ongoing development of new 2<sup>nd</sup>/3<sup>rd</sup> generation PSMA-targeted radiotracers, in addition to the increasing interest into the use of PSMA as a therapeutic target, the potential applications of this methodology are numerous. It is clear that PSMA is by no means a “settled question”, with multiple ongoing clinical trials in addition to basic research and development.

Firstly, with regards to the development of new radiotracers, this method seems particularly well suited to the preclinical screening and selection of promising candidate  $^{18}\text{F}$ -radiotracers using the library  $^{11}\text{C}$ -radiosynthesis approach, as was extensively discussed in greater depth in section 1.3.1.3 (page 26). Furthermore, while some radiotherapeutics have almost identical companion diagnostic imaging agents (e.g. [ $^{68}\text{Ga}/^{177}\text{Lu}$ ]PSMA-I&T), others rely on the use of similar but non-identical imaging agents to calculate dosimetry or check for target engagement. The ability to

isotopologously radiolabel therapeutics could help in dosimetry calculations, as well as allowing direct measurements of target engagement etc. One particular example where this could be beneficial is in the recently developed PSMA-targeted boron neutron capture therapeutic molecules. As a result of the inability to radiolabel these directly, target engagement is assessed by measuring the *in vivo* displacement of [ $^{68}\text{Ga}$ ]PSMA-11, but *in vivo* non-specific binding and clearance pathways are difficult to ascertain clearly. Furthermore, these  $^{11}\text{C}$ -labeled isotopologues (a concept referred to elsewhere as “radiohybrids” or “molecular twins”)<sup>517,518</sup> of (e.g.)  $^{\text{nat}}\text{Ga}/^{\text{nat}}\text{Lu}$ -PSMA-I&T could allow for more thorough investigation of the differences in biodistribution/pharmacokinetics between the  $^{68}\text{Ga}$ -radiolabeled imaging agent and the  $^{177}\text{Lu}$ -radiolabeled therapeutic. The difference between the *in vivo* behaviour of these two agents is still not fully understood despite the current active interest in PSMA theranostics. From allowing the more accurate assessment of theranostic concepts, to the investigation of newer generation multivalent targeting concepts without the confounding interference of pendant sterically-bulky and charged radiometal complexes; the ability to isotopologously  $^{11}\text{C}$ -radiolabel PSMA ligands could be beneficial from multiple perspectives.

## 7 BIBLIOGRAPHY

- 1 D. L. Bailey, D. W. Townsend, P. E. Valk and M. N. Maisey, *Positron Emission Tomography - Basic Sciences*, Springer-Verlag, London, 1st edn., 2005.
- 2 P. A. Bryant, in *Airborne Radioactive Discharges and Human Health Effects: An introduction*, ed. P. A. Bryant, IOP Publishing, 1st edn., 2019, pp. 1–16.
- 3 C. Amsler, *Nuclear and Particle Physics*, IOP Publishing, 1st edn., 2015.
- 4 N. Long and W.-T. Wong, *The Chemistry of Molecular Imaging*, John Wiley & Sons, Inc, Hoboken, NJ, 1st edn., 2014.
- 5 L. T. Dauer, M. J. Williamson, J. Humm, J. O'Donoghue, R. Ghani, R. Awadallah, J. Carrasquillo, N. Pandit-Taskar, A.-K. Aksnes, C. Biggin, V. Reinton, M. Morris and J. St. Germain, Radiation Safety Considerations for the Use of  $^{223}\text{RaCl}_2$  DE in Men with Castration-resistant Prostate Cancer, *Health Phys.*, 2014, **106**, 494–504.
- 6 J. Maus, File:Annihilation.png, <https://commons.wikimedia.org/wiki/File:Annihilation.png>, (accessed 5 May 2021).
- 7 M. E. Phelps, *PET: Physics, Instrumentation, and Scanners*, Springer Science & Business Media, 2006.
- 8 M. Lubberink, V. Tolmachev, S. Beshara and H. Lundqvist, Quantification aspects of patient studies with  $^{52}\text{Fe}$  in positron emission tomography, *Appl. Radiat. Isot.*, 1999, **51**, 707–715.
- 9 G. Firth, J. E. Blower, J. J. Bartnicka, A. Mishra, A. M. Michaels, A. Rigby, A. Darwesh, F. Al-Saleme and P. J. Blower, Non-invasive radionuclide imaging of trace metal trafficking in health and disease: “PET metallomics”, *RSC Chem. Biol.*, 2022, **3**, 495–518.
- 10 J. O. Juliano, C. W. Kocher, T. D. Nainan and A. C. G. Mitchell, Disintegration of Iron-52 and Iron-53, *Phys. Rev.*, 1959, **113**, 602–608.
- 11 S. Beshara, H. Lundqvist, J. Sundin, M. Lubberink, V. Tolmachev, S. Valind, G. Antoni, B. Långström and B. G. Danielson, Kinetic analysis of  $^{52}\text{Fe}$ -labelled iron(III) hydroxide-sucrose complex following bolus administration using positron emission tomography, *Br. J. Haematol.*, 1999, **104**, 288–295.
- 12 J. Long, Sci. Creat. Q., <https://www.scq.ubc.ca/images/PETschematic.ai>, (accessed 5 May 2021).
- 13 S. Tong, A. M. Alessio and P. E. Kinahan, Image reconstruction for PET/CT scanners: past achievements and future challenges, *Imaging Med.*, 2010, **2**, 529–545.
- 14 M. Conti and L. Eriksson, Physics of pure and non-pure positron emitters for PET: a review and a discussion, *EJNMMI Phys.*, 2016, **3**, 8.
- 15 A. Rahmim and H. Zaidi, PET versus SPECT: strengths, limitations and challenges, *Nucl. Med. Commun.*, 2008, **29**, 193–207.

- 16 W. R. Hendee and E. R. Ritenour, *Medical Imaging Physics*, John Wiley & Sons, Inc., New York, USA, 2002.
- 17 W. W. Moses, Fundamental Limits of Spatial Resolution in PET., *Nucl. Instrum. Methods Phys. Res. A.*, 2011, **648 Supple**, S236–S240.
- 18 A. Sanchez-Crespo, P. Andreo and S. A. Larsson, Positron flight in human tissues and its influence on PET image spatial resolution, *Eur. J. Nucl. Med. Mol. Imaging*, 2004, **31**, 44–51.
- 19 K. Wagatsuma, M. Sakata, K. Ishibashi, A. Hirayama, H. Kawakami, K. Miwa, Y. Suzuki and K. Ishii, Direct comparison of brain [<sup>18</sup>F]FDG images acquired by SiPM-based and PMT-based PET/CT: phantom and clinical studies, *EJNMMI Phys.*, 2020, **7**, 70.
- 20 L. Eriksson, K. Wienhard, M. Eriksson, M. E. Casey, C. Knoess, T. Bruckbauer, J. Hamill, M. Schmand, T. Gremillion, M. Lenox, M. Conti, B. Bendriem, W. D. Heiss and R. Nutt, The ECAT HRRT: NEMA NEC evaluation of the HRRT system, the new high-resolution research tomograph, *IEEE Trans. Nucl. Sci.*, 2002, **49**, 2085–2088.
- 21 J. P. Schmall, J. S. Karp and A. Alavi, The Potential Role of Total Body PET Imaging in Assessment of Atherosclerosis, *PET Clin.*, 2019, **14**, 245–250.
- 22 S. R. Cherry, T. Jones, J. S. Karp, J. Qi, W. W. Moses and R. D. Badawi, Total-Body PET: Maximizing Sensitivity to Create New Opportunities for Clinical Research and Patient Care, *J. Nucl. Med.*, 2018, **59**, 3–12.
- 23 G. Wang, M. Parikh, L. Nardo, Y. Zuo, Y. Abdelhafez, J. Qi, T. Jones, P. Price, S. Cherry, C.-X. Pan and R. Badawi, Total-Body Dynamic PET of Metastatic Cancer: First Patient Results, *J. Nucl. Med.*, 2020, **61**, 208.
- 24 A. I. Kassis, Therapeutic Radionuclides: Biophysical and Radiobiologic Principles, *Semin. Nucl. Med.*, 2008, **38**, 358–366.
- 25 D. R. Dance, S. Christofides, A. D. A. Maidment, I. D. McLean and K. H. Ng, *Diagnostic Radiology Physics: A Handbook for Teachers and Students*, IAEA, Vienna, 2014.
- 26 J. S. Lewis, A. D. Windhorst and B. M. Zeglis, Eds., *Radiopharmaceutical Chemistry*, Springer International Publishing, 2019.
- 27 H. Zhuang and I. Codreanu, Growing applications of FDG PET-CT imaging in non-oncologic conditions, *J. Biomed. Res.*, 2015, **29**, 189–202.
- 28 M. Beheshti, W. Langsteger and A. Rezaee, *PET/CT in Cancer: An Interdisciplinary Approach to Individualized Imaging*, Elsevier, 1st edn., 2018.
- 29 O. Warburg, über den Stoffwechsel der Carcinomzelle, *Klin. Wochenschr.*, 1925, **4**, 534–536.
- 30 T. Z. Wong, A. H. Khandani and A. Sheikh, in *Clinical Radiation Oncology*, Elsevier, 2016, pp. 206–216.
- 31 S. Y. Kim, K.-T. Jang and J. H. Lee, Gastric Adenocarcinoma with Systemic Metastasis Involving the Intraocular Choroid and Duodenum, *Clin. Endosc.*, 2018, **51**, 95–98.



- 32 P. Therasse, S. G. Arbuck, E. A. Eisenhauer, J. Wanders, R. S. Kaplan, L. Rubinstein, J. Verweij, M. Van Glabbeke, A. T. van Oosterom, M. C. Christian and S. G. Gwyther, New guidelines to evaluate the response to treatment in solid tumors. European Organization for Research and Treatment of Cancer, National Cancer Institute of the United States, National Cancer Institute of Canada., *J. Natl. Cancer Inst.*, 2000, **92**, 205–16.
- 33 E. A. Eisenhauer, P. Therasse, J. Bogaerts, L. H. Schwartz, D. Sargent, R. Ford, J. Dancey, S. Arbuck, S. Gwyther, M. Mooney, L. Rubinstein, L. Shankar, L. Dodd, R. Kaplan, D. Lacombe and J. Verweij, New response evaluation criteria in solid tumours: revised RECIST guideline (version 1.1)., *Eur. J. Cancer*, 2009, **45**, 228–47.
- 34 A. D. Van den Abbeele, The lessons of GIST--PET and PET/CT: a new paradigm for imaging., *Oncologist*, 2008, **13 Suppl 2**, 8–13.
- 35 S. Ben-Haim and P. Ell, <sup>18</sup>F-FDG PET and PET/CT in the Evaluation of Cancer Treatment Response, *J. Nucl. Med.*, 2008, **50**, 88–99.
- 36 S. M. Schuetze, L. H. Baker, R. S. Benjamin and R. Canetta, Selection of response criteria for clinical trials of sarcoma treatment., *Oncologist*, 2008, **13 Suppl 2**, 32–40.
- 37 S. J. Finnema, N. B. Nabulsi, T. Eid, K. Detyniecki, S. Lin, M.-K. Chen, R. Dhaher, D. Matuskey, E. Baum, D. Holden, D. D. Spencer, J. Mercier, J. Hannestad, Y. Huang and R. E. Carson, Imaging synaptic density in the living human brain, *Sci. Transl. Med.*
- 38 Z. Cai, S. Li, D. Matuskey, N. Nabulsi and Y. Huang, PET imaging of synaptic density: A new tool for investigation of neuropsychiatric diseases, *Neurosci. Lett.*, 2019, **691**, 44–50.
- 39 P. M. Matthews, E. A. Rabiner, J. Passchier and R. N. Gunn, Positron emission tomography molecular imaging for drug development, *Br. J. Clin. Pharmacol.*, 2012, **73**, 175–186.
- 40 G. Boscutti, M. Huiban and J. Passchier, Use of carbon-11 labelled tool compounds in support of drug development, *Drug Discov. Today Technol.*, 2017, **25**, 3–10.
- 41 M. Bergstrom, A. Grahnen and B. Langstrom, Positron emission tomography microdosing: a new concept with application in tracer and early clinical drug development, *Eur. J. Clin. Pharmacol.*, 2003, **59**, 357–366.
- 42 S. Ashworth, E. A. Rabiner, R. N. Gunn, C. Plisson, A. A. Wilson, R. A. Comley, R. Y. K. Lai, A. D. Gee, M. Laruelle and V. J. Cunningham, Evaluation of <sup>11</sup>C-GSK189254 as a Novel Radioligand for the H3 Receptor in Humans Using PET, *J. Nucl. Med.*, 2010, **51**, 1021–1029.
- 43 M. Bergstrom, The Use of Microdosing in the Development of Small Organic and Protein Therapeutics, *J. Nucl. Med.*, 2017, **58**, 1188–1195.
- 44 T. Burt, G. Young, W. Lee, H. Kusuhara, O. Langer, M. Rowland and Y. Sugiyama, Phase 0/microdosing approaches: time for mainstream application in drug development?, *Nat. Rev. Drug Discov.*, 2020, **19**, 801–818.

- 45 IAEA, *Cyclotron Produced Radionuclides: Principles and Practice, Technical Reports Series No. 465*, Vienna, 2009.
- 46 IAEA, *Cyclotron Produced Radionuclides: Principles and Practice*, 2009.
- 47 R. E. Boyd, Technetium-99m generators—The available options, *Int. J. Appl. Radiat. Isot.*, 1982, **33**, 801–809.
- 48 M. Fani, J. P. André and H. R. Maecke, <sup>68</sup>Ga-PET: a powerful generator-based alternative to cyclotron-based PET radiopharmaceuticals, *Contrast Media Mol. Imaging*, 2008, **3**, 53–63.
- 49 M. Meisenheimer, Y. Saenko and E. Eppard, in *Medical Isotopes*, IntechOpen, 2021.
- 50 J. P. Holland, Chemical Kinetics of Radiolabelling Reactions, *Chem. - A Eur. J.*, 2018, **24**, 16472–16483.
- 51 N. B. Nabulsi, J. Mercier, D. Holden, S. Carre, S. Najafzadeh, M.-C. Vandergeten, S. -f. Lin, A. Deo, N. Price, M. Wood, T. Lara-Jaime, F. Montel, M. Laruelle, R. E. Carson, J. Hannestad and Y. Huang, Synthesis and Preclinical Evaluation of <sup>11</sup>C-UCB-J as a PET Tracer for Imaging the Synaptic Vesicle Glycoprotein 2A in the Brain, *J. Nucl. Med.*, 2016, **57**, 777–784.
- 52 S. J. Finnema, N. B. Nabulsi, T. Eid, K. Detyniecki, S. Lin, M.-K. Chen, R. Dhaher, D. Matuskey, E. Baum, D. Holden, D. D. Spencer, J. Mercier, J. Hannestad, Y. Huang and R. E. Carson, Imaging synaptic density in the living human brain, *Sci. Transl. Med.*, 2016, **8**, 348ra96-348ra96.
- 53 S. Li, Z. Cai, X. Wu, D. Holden, R. Pracitto, M. Kapinos, H. Gao, D. Labaree, N. Nabulsi, R. E. Carson and Y. Huang, Synthesis and in Vivo Evaluation of a Novel PET Radiotracer for Imaging of Synaptic Vesicle Glycoprotein 2A (SV2A) in Nonhuman Primates, *ACS Chem. Neurosci.*, 2019, **10**, 1544–1554.
- 54 C. C. Constantinescu, C. Tresse, M. Zheng, A. Gouasmat, V. M. Carroll, L. Mistico, D. Alagille, C. M. Sandiego, C. Papin, K. Marek, J. P. Seibyl, G. D. Tamagnan and O. Barret, Development and In Vivo Preclinical Imaging of Fluorine-18-Labeled Synaptic Vesicle Protein 2A (SV2A) PET Tracers, *Mol. Imaging Biol.*, 2019, **21**, 509–518.
- 55 B. A. Lynch, N. Lambeng, K. Nocka, P. Kensel-Hammes, S. M. Bajjalieh, A. Matagne and B. Fuks, The synaptic vesicle protein SV2A is the binding site for the antiepileptic drug levetiracetam, *Proc. Natl. Acad. Sci.*, 2004, **101**, 9861–9866.
- 56 J. Mercier, L. Archen, V. Bollu, S. Carré, Y. Evrard, E. Jnoff, B. Kenda, B. Lallemand, P. Michel, F. Montel, F. Moureau, N. Price, Y. Quesnel, X. Sauvage, A. Valade and L. Provins, Discovery of Heterocyclic Nonacetamide Synaptic Vesicle Protein 2A (SV2A) Ligands with Single-Digit Nanomolar Potency: Opening Avenues towards the First SV2A Positron Emission Tomography (PET) Ligands, *ChemMedChem*, 2014, **9**, 693–698.
- 57 F. Chauveau, G. Becker and H. Boutin, Have (R)-[<sup>11</sup>C]PK11195 challengers fulfilled the promise? A scoping review of clinical TSPO PET studies, *Eur. J. Nucl. Med. Mol. Imaging*, , DOI:10.1007/s00259-021-05425-w.
- 58 S. H. Liang and N. Vasdev, Total Radiosynthesis: Thinking Outside ‘the Box’,

- Aust. J. Chem.*, 2015, **68**, 1319–1328.
- 59 A. D. Gee, M. M. Herth, M. L. James, A. Korde, P. J. H. Scott and N. Vasdev, Radionuclide Imaging for Neuroscience: Current Opinion and Future Directions, *Mol. Imaging*, 2020, **19**, 153601212093639.
- 60 B. H. Rotstein, S. H. Liang, M. S. Placzek, J. M. Hooker, A. D. Gee, F. Dollé, A. A. Wilson and N. Vasdev,  $^{11}\text{C}=\text{O}$  bonds made easily for positron emission tomography radiopharmaceuticals, *Chem. Soc. Rev.*, 2016, **45**, 4708–4726.
- 61 A. A. Wilson, J. W. Hicks, O. Sadovski, J. Parkes, J. Tong, S. Houle, C. J. Fowler and N. Vasdev, Radiosynthesis and Evaluation of [ $^{11}\text{C}$ -Carbonyl]-Labeled Carbamates as Fatty Acid Amide Hydrolase Radiotracers for Positron Emission Tomography, *J. Med. Chem.*, 2013, **56**, 201–209.
- 62 O. Sadovski, J. W. Hicks, J. Parkes, R. Raymond, J. Nobrega, S. Houle, M. Cipriano, C. J. Fowler, N. Vasdev and A. A. Wilson, Development and characterization of a promising fluorine-18 labelled radiopharmaceutical for in vivo imaging of fatty acid amide hydrolase, *Bioorg. Med. Chem.*, 2013, **21**, 4351–4357.
- 63 B. H. Rotstein, H.-Y. Wey, T. M. Shoup, A. A. Wilson, S. H. Liang, J. M. Hooker and N. Vasdev, PET Imaging of Fatty Acid Amide Hydrolase with [ $^{18}\text{F}$ ]DOPP in Nonhuman Primates, *Mol. Pharm.*, 2014, **11**, 3832–3838.
- 64 IAEA, *Cyclotron Produced Radionuclides: Operation and Maintenance of Gas and Liquid Targets*, 2012.
- 65 N. Gillings, J. Jøregensen, P. Larsen, J. Kozirowski and H. Jensen, 2012, pp. 181–184.
- 66 L. Yang, P. J. H. Scott and X. Shao, in *Carbon Dioxide Chemistry, Capture and Oil Recovery*, InTech, 2018.
- 67 P. W. Miller, N. J. Long, R. Vilar and A. D. Gee, Synthesis of  $^{11}\text{C}$ ,  $^{18}\text{F}$ ,  $^{15}\text{O}$ , and  $^{13}\text{N}$  Radiolabels for Positron Emission Tomography, *Angew. Chemie Int. Ed.*, 2008, **47**, 8998–9033.
- 68 T. Fukumura, W. Mori, M. Ogawa, M. Fujinaga and M.-R. Zhang, [ $^{11}\text{C}$ ]phosgene: Synthesis and application for development of PET radiotracers, *Nucl. Med. Biol.*, 2021, **92**, 138–148.
- 69 A. K. Ghosh and M. Brindisi, Urea Derivatives in Modern Drug Discovery and Medicinal Chemistry, *J. Med. Chem.*, 2020, **63**, 2751–2788.
- 70 M. Ogawa, Y. Takada, H. Suzuki, K. Nemoto and T. Fukumura, Simple and effective method for producing [ $^{11}\text{C}$ ]phosgene using an environmental  $\text{CCl}_4$  gas detection tube, *Nucl. Med. Biol.*, 2010, **37**, 73–76.
- 71 Y. Bramoullé, D. Roeda and F. Dollé, *A simplified [ $^{11}\text{C}$ ]phosgene synthesis*, 2010, vol. 51.
- 72 F. Wuest, M. Berndt and T. Kniess, in *PET Chemistry*, eds. P. A. Schubiger, L. Lehmann and M. Friebe, Springer, Berlin, 2007, pp. 183–213.
- 73 H. Doi, Pd-mediated rapid cross-couplings using [ $^{11}\text{C}$ ]methyl iodide: groundbreaking labeling methods in  $^{11}\text{C}$  radiochemistry, *J. Label. Compd.*

- Radiopharm.*, 2015, **58**, 73–85.
- 74 C. Marazano, M. Maziere, G. Berger and D. Comar, Synthesis of methyl iodide- $^{11}\text{C}$  and formaldehyde- $^{11}\text{C}$ , *Int. J. Appl. Radiat. Isot.*, 1977, **28**, 49–52.
- 75 B. Långström and H. Lundqvist, The preparation of  $^{11}\text{C}$ -methyl iodide and its use in the synthesis of  $^{11}\text{C}$ -methyl-L-methionine, *Int. J. Appl. Radiat. Isot.*, 1976, **27**, 357–363.
- 76 F. Oberdorfer, M. Hanisch, F. Helus and W. Maier-Borst, A new procedure for the preparation of  $^{11}\text{C}$ -labelled methyl iodide, *Int. J. Appl. Radiat. Isot.*, 1985, **36**, 435–438.
- 77 M. Holschbach and M. Schüller, A new and simple on-line method for the preparation of n.c.a. [ $^{11}\text{C}$ ]methyl iodide, *Appl. Radiat. Isot.*, 1993, **44**, 779–780.
- 78 P. Larsen, J. Ulin, K. Dahlstrøm and M. Jensen, Synthesis of [ $^{11}\text{C}$ ]iodomethane by iodination of [ $^{11}\text{C}$ ]methane, *Appl. Radiat. Isot.*, 1997, **48**, 153–157.
- 79 J. M. Link, K. A. Krohn and J. C. Clark, Production of [ $^{11}\text{C}$ ]CH<sub>3</sub>I by single pass reaction of [ $^{11}\text{C}$ ]CH<sub>4</sub> with I<sub>2</sub>, *Nucl. Med. Biol.*, 1997, **24**, 93–97.
- 80 T. Kniess, K. Rode and F. Wuest, Practical experiences with the synthesis of [ $^{11}\text{C}$ ]CH<sub>3</sub>I through gas phase iodination reaction using a TRACERlabFXC synthesis module, *Appl. Radiat. Isot.*, 2008, **66**, 482–488.
- 81 P. Elsinga, Radiopharmaceutical chemistry for positron emission tomography, *Methods*, 2002, **27**, 208–217.
- 82 D. M. Jewett, A simple synthesis of [ $^{11}\text{C}$ ]methyl triflate, *Int. J. Radiat. Appl. Instrumentation. Part A. Appl. Radiat. Isot.*, 1992, **43**, 1383–1385.
- 83 D. Yokell, R. Neelamegam, P. Rice, D. Vesper and G. El Fakhri, Tips and tricks gained from years of experience with GE Tracerlab FXC Pro, *J. Nucl. Med.*, 2018, **59**, 1038–1038.
- 84 B. Mock, Automated C-11 Methyl Iodide/Triflate Production: Current State of the Art, *Curr. Org. Chem.*, 2013, **17**, 2119–2126.
- 85 Y. Andersson, A. Cheng, B. Långström, K. Zetterberg, B. Nilsson, C. Damberg, T. Bartfai and Ü. Langel, Palladium-promoted Coupling Reactions of [ $^{11}\text{C}$ ]Methyl Iodide with Organotin and Organoboron Compounds., *Acta Chem. Scand.*, 1995, **49**, 683–688.
- 86 M. Suzuki, H. Doi, M. Björkman, Y. Andersson, B. Långström, Y. Watanabe and R. Noyori, Rapid Coupling of Methyl Iodide with Aryltributylstannanes Mediated by Palladium(0) Complexes: A General Protocol for the Synthesis of  $^{11}\text{C}$ -Labeled PET Tracers, *Chem. - A Eur. J.*, 1997, **3**, 2039–2042.
- 87 J. Madsen, P. Merachtsaki, P. Davoodpour, M. Bergström, B. Långström, K. Andersen, C. Thomsen, L. Martiny and G. M. Knudsen, Synthesis and biological evaluation of novel carbon-11-labelled analogues of citalopram as potential radioligands for the serotonin transporter, *Bioorg. Med. Chem.*, 2003, **11**, 3447–3456.
- 88 J. Tarkiainen, J. Vercouillie, P. Emond, J. Sandell, J. Hiltunen, Y. Frangin, D. Guilloteau and C. Halldin, Carbon-11 labelling of MADAM in two different

- positions: a highly selective PET radioligand for the serotonin transporter, *J. Label. Compd. Radiopharm.*, 2001, **44**, 1013–1023.
- 89 J. Prabhakaran, V. J. Majo, N. R. Simpson, R. L. Van Heertum, J. J. Mann and J. S. D. Kumar, Synthesis of [<sup>11</sup>C]celecoxib: a potential PET probe for imaging COX-2 expression, *J. Label. Compd. Radiopharm.*, 2005, **48**, 887–895.
- 90 E. D. Hostetler, G. E. Terry and H. Donald Burns, An improved synthesis of substituted [<sup>11</sup>C]toluenes via Suzuki coupling with [<sup>11</sup>C]methyl iodide, *J. Label. Compd. Radiopharm.*, 2005, **48**, 629–634.
- 91 T. G. Hamill, S. Krause, C. Ryan, C. Bonnefous, S. Govek, T. J. Seiders, N. D. P. Cosford, J. Roppe, T. Kamenecka, S. Patel, R. E. Gibson, S. Sanabria, K. Riffel, W. Eng, C. King, X. Yang, M. D. Green, S. S. O'malley, R. Hargreaves and H. D. Burns, Synthesis, characterization, and first successful monkey imaging studies of metabotropic glutamate receptor subtype 5 (mGluR5) PET radiotracers, *Synapse*, 2005, **56**, 205–216.
- 92 H. Doi, I. Ban, A. Nonoyama, K. Sumi, C. Kuang, T. Hosoya, H. Tsukada and M. Suzuki, Palladium(0)-Mediated Rapid Methylation and Fluoromethylation on Carbon Frameworks by Reacting Methyl and Fluoromethyl Iodide with Aryl and Alkenyl Boronic Acid Esters: Useful for the Synthesis of [<sup>11</sup>C]CH<sub>3</sub> δC- and [<sup>18</sup>F]FCH<sub>2</sub> δC-Containing PET Tracers, *Chem. - A Eur. J.*, 2009, **15**, 4165–4171.
- 93 M. Takashima-Hirano, T. Takashima, Y. Katayama, Y. Wada, Y. Sugiyama, Y. Watanabe, H. Doi and M. Suzuki, Efficient sequential synthesis of PET Probes of the COX-2 inhibitor [<sup>11</sup>C]celecoxib and its major metabolite [<sup>11</sup>C]SC-62807 and in vivo PET evaluation, *Bioorg. Med. Chem.*, 2011, **19**, 2997–3004.
- 94 S. Kealey, J. Passchier and M. Huiban, Negishi coupling reactions as a valuable tool for [<sup>11</sup>C]methyl-arene formation; first proof of principle, *Chem. Commun.*, 2013, **49**, 11326.
- 95 F. Wüst, J. Zessin and B. Johannsen, A new approach for <sup>11</sup>C-C bond formation: Synthesis of 17 α -(3'-[<sup>11</sup>C]prop-1-yn-1-yl)-3-methoxy-3,17 β -estradiol, *J. Label. Compd. Radiopharm.*, 2003, **46**, 333–342.
- 96 R. Liu, X. Li and K. S. Lam, Combinatorial chemistry in drug discovery, *Curr. Opin. Chem. Biol.*, 2017, **38**, 117–126.
- 97 C. Taddei and V. W. Pike, [<sup>11</sup>C]Carbon monoxide: advances in production and application to PET radiotracer development over the past 15 years, *EJNMMI Radiopharm. Chem.*, 2019, **4**, 25.
- 98 J. Eriksson, G. Antoni, B. Långström and O. Itsenko, The development of <sup>11</sup>C-carbonylation chemistry: A systematic view, *Nucl. Med. Biol.*, 2021, **92**, 115–137.
- 99 J.-B. Peng, H.-Q. Geng and X.-F. Wu, The Chemistry of CO: Carbonylation, *Chem*, 2019, **5**, 526–552.
- 100 J. C. Clark and P. D. Buckingham, The preparation and storage of carbon-11 labelled gases for clinical use, *Int. J. Appl. Radiat. Isot.*, 1971, **22**, 639–646.
- 101 Y. Andersson and B. Långström, Synthesis of <sup>11</sup>C-labelled ketones via carbonylative coupling reactions using [<sup>11</sup>C]carbon monoxide, *J. Chem. Soc., Perkin Trans. 1*, 1995, 287–289.

- 102 K. Dahl, J. Ulin, M. Schou and C. Halldin, Reduction of [ $^{11}\text{C}$ ]CO<sub>2</sub> to [ $^{11}\text{C}$ ]CO using solid supported zinc, *J. Label. Compd. Radiopharm.*, 2017, **60**, 624–628.
- 103 S. K. Zeisler, M. Nader, A. Theobald and F. Oberdorfer, Conversion of No-carrier-added [ $^{11}\text{C}$ ]carbon dioxide to [ $^{11}\text{C}$ ]carbon monoxide on molybdenum for the synthesis of  $^{11}\text{C}$ -labelled aromatic ketones, *Appl. Radiat. Isot.*, 1997, **48**, 1091–1095.
- 104 D. Roeda, C. Crouzel and F. Dollé, A rapid, almost quantitative conversion of [ $^{11}\text{C}$ ]carbon dioxide into [ $^{11}\text{C}$ ]carbon monoxide via [ $^{11}\text{C}$ ]formate and [ $^{11}\text{C}$ ]formyl chloride, *Radiochim. Acta*, 2004, **92**, 329–332.
- 105 C. Taddei, S. Bongarzone, A. K. Haji Dheere and A. D. Gee, [ $^{11}\text{C}$ ]CO<sub>2</sub> to [ $^{11}\text{C}$ ]CO conversion mediated by [ $^{11}\text{C}$ ]silanes: a novel route for [ $^{11}\text{C}$ ]carbonylation reactions, *Chem. Commun.*, 2015, **51**, 11795–11797.
- 106 P. Nordeman, S. D. Friis, T. L. Andersen, H. Audrain, M. Larhed, T. Skrydstrup and G. Antoni, Rapid and Efficient Conversion of  $^{11}\text{CO}_2$  to  $^{11}\text{CO}$  through Silacarboxylic Acids: Applications in Pd-Mediated Carbonylations, *Chem. - A Eur. J.*, 2015, **21**, 17601–17604.
- 107 C. Taddei, S. Bongarzone and A. D. Gee, Instantaneous Conversion of [ $^{11}\text{C}$ ]CO<sub>2</sub> to [ $^{11}\text{C}$ ]CO via Fluoride-Activated Disilane Species, *Chem. - A Eur. J.*, 2017, **23**, 7682–7685.
- 108 D. A. Anders, S. Bongarzone, R. Fortt, A. D. Gee and N. J. Long, Electrochemical [ $^{11}\text{C}$ ]CO<sub>2</sub> to [ $^{11}\text{C}$ ]CO conversion for PET imaging, *Chem. Commun.*, 2017, **53**, 2982–2985.
- 109 M. M. T. Khan, S. B. Halligudi and S. Shukla, Solubility of carbon monoxide in water-n-butylamine, ethanol-cyclohexene and water-dimethylformamide mixtures, *J. Chem. Eng. Data*, 1989, **34**, 353–355.
- 110 C. Vogelpohl, C. Brandenbusch and G. Sadowski, High-pressure gas solubility in multicomponent solvent systems for hydroformylation. Part I: Carbon monoxide solubility, *J. Supercrit. Fluids*, 2013, **81**, 23–32.
- 111 R. Koelliker and H. Thies, Solubility of carbon monoxide in n-hexane between 293 and 473 K and carbon monoxide pressures up to 200 bar, *J. Chem. Eng. Data*, 1993, **38**, 437–440.
- 112 H. M. Colquhoun, D. J. Thompson and M. V. Twigg, in *Carbonylation*, Springer US, Boston, MA, 1991, pp. 33–54.
- 113 J. Eriksson, O. Åberg and B. Långström, Synthesis of [ $^{11}\text{C}$ ]/[ $^{13}\text{C}$ ]Acrylamides by Palladium-Mediated Carbonylation, *European J. Org. Chem.*, 2007, **2007**, 455–461.
- 114 S. Y. Chow, L. R. Odell and J. Eriksson, Low-Pressure Radical  $^{11}\text{C}$ -Aminocarbonylation of Alkyl Iodides through Thermal Initiation, *European J. Org. Chem.*, 2016, **2016**, 5980–5989.
- 115 P. W. Miller, H. Audrain, D. Bender, A. J. Demello, A. D. Gee, N. J. Long and R. Vilar, Rapid carbon-11 radiolabelling for PET using microfluidics, *Chem. - A Eur. J.*, 2011, **17**, 460–463.

- 116 M. Ferrat, K. Dahl, C. Halldin and M. Schou, “In-loop” carbonylation-A simplified method for carbon-11 labelling of drugs and radioligands, *J. Label. Compd. Radiopharm.*, 2020, **63**, 100–107.
- 117 S. Kealey, P. W. Miller, N. J. Long, C. Plisson, L. Martarello and A. D. Gee, Copper(i) scorpionate complexes and their application in palladium-mediated [<sup>11</sup>C]carbonylation reactions, *Chem. Commun.*, 2009, 3696.
- 118 P. Lidström, T. Kihlberg and B. Långström, [<sup>11</sup>C]Carbon monoxide in the palladium-mediated synthesis of <sup>11</sup>C-labelled ketones, *J. Chem. Soc. Perkin Trans. 1*, 1997, 2701–2706.
- 119 T. Kihlberg, P. Lidström and B. Långström, Palladium mediated carbonylation reactions using [<sup>11</sup>C]carbon monoxide in a high pressure micro-autoclave, *J. Label. Compd. Radiopharm.*, 1997, **40**, 781–782.
- 120 US20040197257A1, 2002.
- 121 F. Karimi and B. Långström, Synthesis of <sup>11</sup>C-amides using [<sup>11</sup>C]carbon monoxide and in situ activated amines by palladium-mediated carboxaminations, *Org. Biomol. Chem.*, 2003, **1**, 541–546.
- 122 J. Eriksson, J. Hoek and A. D. Windhorst, Transition metal mediated synthesis using [<sup>11</sup>C]CO at low pressure - a simplified method for <sup>11</sup>C-carbonylation, *J. Label. Compd. Radiopharm.*, 2012, **55**, 223–228.
- 123 K. Dahl, M. Schou, J. Ulin, C.-O. Sjöberg, L. Farde and C. Halldin, <sup>11</sup>C-carbonylation reactions using gas–liquid segmented microfluidics, *RSC Adv.*, 2015, **5**, 88886–88889.
- 124 D. J. Donnelly, S. Preshlock, T. Kaur, T. Tran, T. C. Wilson, K. Mhanna, B. D. Henderson, D. Batalla, P. J. H. Scott and X. Shao, Synthesis of Radiopharmaceuticals via “In-Loop” <sup>11</sup>C-Carbonylation as Exemplified by the Radiolabeling of Inhibitors of Bruton’s Tyrosine Kinase, *Front. Nucl. Med.*, , DOI:10.3389/fnume.2021.820235.
- 125 N. Kitajima, T. Koda, S. Hashimoto, T. Kitagawa and Y. Morooka, Synthesis and characterization of the dinuclear copper(II) complexes [Cu(HB(3,5-Me<sub>2</sub>pz)<sub>3</sub>)<sub>2</sub>X] (X = O<sup>2-</sup>, (OH)<sup>2-</sup>, CO<sup>2-</sup>, O<sub>2</sub><sup>2-</sup>), *J. Am. Chem. Soc.*, 1991, **113**, 5664–5671.
- 126 M. Beller and X.-F. Wu, *Transition Metal Catalyzed Carbonylation Reactions*, Springer Berlin Heidelberg, Berlin, Heidelberg, 1st edn., 2013.
- 127 S. Kealey, S. M. Husbands, I. Bennacef, A. D. Gee and J. Passchier, Palladium-mediated oxidative carbonylation reactions for the synthesis of (11) C-radiolabelled ureas., *J. Labelled Comp. Radiopharm.*, 2014, **57**, 202–8.
- 128 M. H. Al-Qahtani and V. W. Pike, Palladium(II)-mediated <sup>11</sup>C-carbonylative coupling of diaryliodonium salts with organostannanes—a new, mild and rapid synthesis of aryl [<sup>11</sup>C]ketones, *J. Chem. Soc. Perkin Trans. 1*, 2000, 1033–1036.
- 129 T. Kihlberg and B. Långström, Biologically Active <sup>11</sup>C-Labeled Amides Using Palladium-Mediated Reactions with Aryl Halides and [<sup>11</sup>C]Carbon Monoxide, *J. Org. Chem.*, 1999, **64**, 9201–9205.
- 130 P. W. Miller, L. E. Jennings, A. J. DeMello, A. D. Gee, N. J. Long and R. Vilar, A

- microfluidic approach to the rapid screening of palladium-catalysed aminocarbonylation reactions, *Adv. Synth. Catal.*, 2009, **351**, 3260–3268.
- 131 S. Roslin, P. Brandt, P. Nordeman, M. Larhed, L. Odell and J. Eriksson, Synthesis of  $^{11}\text{C}$ -Labelled Ureas by Palladium(II)-Mediated Oxidative Carbonylation, *Molecules*, 2017, **22**, 1688.
- 132 B. H. Rotstein, S. H. Liang, J. P. Holland, T. L. Collier, J. M. Hooker, A. A. Wilson and N. Vasdev,  $^{11}\text{CO}_2$  fixation: a renaissance in PET radiochemistry, *Chem. Commun.*, 2013, **49**, 5621.
- 133 D. Roeda and G. Westera, A u.v.-induced on-line synthesis of  $^{11}\text{C}$ -phosgene and the preparation of some of its derivatives, *Int. J. Appl. Radiat. Isot.*, 1981, **32**, 931–932.
- 134 C. Crouzel, D. Roeda, M. Berridge, R. Knipper and D. Comar,  $^{11}\text{C}$ -labelled phosgene: an improved procedure and synthesis device, *Int. J. Appl. Radiat. Isot.*, 1983, **34**, 1558–1559.
- 135 K. Nishijima, Y. Kuge, K. Seki, K. Ohkura, N. Motoki, K. Nagatsu, A. Tanaka, E. Tsukamoto and N. Tamaki, A simplified and improved synthesis of [ $^{11}\text{C}$ ]phosgene with iron and iron (III) oxide, *Nucl. Med. Biol.*, 2002, **29**, 345–350.
- 136 C. Morisseau, M. H. Goodrow, D. Dowdy, J. Zheng, J. F. Greene, J. R. Sanborn and B. D. Hammock, Potent urea and carbamate inhibitors of soluble epoxide hydrolases, *Proc. Natl. Acad. Sci. U. S. A.*, 1999, **96**, 8849–8854.
- 137 F. Brady, S. K. Luthra, H.-J. Tochon-Danguy, C. J. Steel, S. L. Waters, M. J. Kensett, P. Landais, F. Shah, K. A. Jaeggi, A. Drake, J. C. Clark and V. W. Pike, Asymmetric synthesis of a precursor for the automated radiosynthesis of as a preferred radioligand for  $\beta$ -adrenergic receptors, *Int. J. Radiat. Appl. Instrumentation. Part A. Appl. Radiat. Isot.*, 1991, **42**, 621–628.
- 138 K. Nishijima, Y. Kuge, K. Seki, K. Ohkura, K. Morita, K. Nakada and N. Tamaki, Preparation and pharmaceutical evaluation for clinical application of high specific activity S(-), *Nucl. Med. Commun.*, 2004, **25**, 845–849.
- 139 C. Asakawa, M. Ogawa, K. Kumata, M. Fujinaga, T. Yamasaki, L. Xie, J. Yui, K. Kawamura, T. Fukumura and M.-R. Zhang, Radiosynthesis of three [ $^{11}\text{C}$ ]ureido-substituted benzenesulfonamides as PET probes for carbonic anhydrase IX in tumors, *Bioorg. Med. Chem. Lett.*, 2011, **21**, 7017–7020.
- 140 C. Asakawa, M. Ogawa, K. Kumata, M. Fujinaga, K. Kato, T. Yamasaki, J. Yui, K. Kawamura, A. Hatori, T. Fukumura and M.-R. Zhang, [ $^{11}\text{C}$ ]Sorafenib: Radiosynthesis and preliminary PET study of brain uptake in P-gp/Bcrp knockout mice, *Bioorg. Med. Chem. Lett.*, 2011, **21**, 2220–2223.
- 141 G. D. Brown, D. Henderson, C. Steel, S. Luthra, P. M. Price and F. Brady, Two routes to [ $^{11}\text{C}$ -carbonyl]organo-isocyanates utilizing [ $^{11}\text{C}$ ]phosgene ([ $^{11}\text{C}$ ]organo-isocyanates from [ $^{11}\text{C}$ ]phosgene), *Nucl. Med. Biol.*, 2001, **28**, 991–998.
- 142 J. E. Jakobsson, S. Lu, S. Telu and V. W. Pike, [ $^{11}\text{C}$ ]Carbonyl Difluoride—a New and Highly Efficient [ $^{11}\text{C}$ ]Carbonyl Group Transfer Agent, *Angew. Chemie Int. Ed.*, 2020, **59**, 7256–7260.
- 143 J. E. Jakobsson, S. Telu, S. Lu, S. Jana and V. W. Pike, Broad Scope and High-



- yield Access to Unsymmetrical Acyclic [ $^{11}\text{C}$ ]ureas for Biomedical Imaging from [ $^{11}\text{C}$ ]carbonyl Difluoride, *Chem. – A Eur. J.*, 2021, chem.202100690.
- 144 M. Peters, B. Köhler, W. Kuckshinrichs, W. Leitner, P. Markewitz and T. E. Müller, Chemical Technologies for Exploiting and Recycling Carbon Dioxide into the Value Chain, *ChemSusChem*, 2011, **4**, 1216–1240.
- 145 M. B. Winstead, J. F. Lamb and H. S. Winchell, Relationship of Chemical Structure to In vivo Scintigraphic Distribution Patterns of  $^{11}\text{C}$  Compounds: I.  $^{11}\text{C}$ -Carboxylates, *J. Nucl. Med.*, 1973, **14**, 747–754.
- 146 V. W. Pike, M. N. Eakins, R. M. Allan and A. P. Selwyn, Preparation of carbon-11 labelled acetate and palmitic acid for the study of myocardial metabolism by emission-computerised axial tomography, *J. Radioanal. Chem.*, 1981, **64**, 291–297.
- 147 V. W. Pike, M. N. Eakins, R. M. Allan and A. P. Selwyn, Preparation of [ $1-^{11}\text{C}$ ]acetate—An agent for the study of myocardial metabolism by positron emission tomography, *Int. J. Appl. Radiat. Isot.*, 1982, **33**, 505–512.
- 148 M. B. Winstead, H. S. Winchell and R. Fawwaz, The use of sodium  $^{11}\text{C}$ -benzoate in renal visualization, *Int. J. Appl. Radiat. Isot.*, 1969, **20**, 859–863.
- 149 R. J. Davenport, K. Dowsett and V. W. Pike, A simple technique for the automated production of no-carrier-added [ $1-^{11}\text{C}$ ]acetate, *Appl. Radiat. Isot.*, 1997, **48**, 1117–1120.
- 150 H. C. Padgett, G. D. Robinson and J. R. Barrio, [ $1-^{11}\text{C}$ ]Palmitic acid: Improved radiopharmaceutical preparation, *Int. J. Appl. Radiat. Isot.*, 1982, **33**, 1471–1472.
- 151 M. J. Welch, C. S. Dence, D. R. Marshall and M. R. Kilbourn, Remote system for production of carbon-11 labeled palmitic acid, *J. Label. Compd. Radiopharm.*, 1983, **20**, 1087–1095.
- 152 S. Nakao, K. Yogo, K. Goto, T. Kai and H. Yamada, in *Advanced CO<sub>2</sub> Capture Technologies*, Springer, 2019, pp. 3–22.
- 153 P. V. Danckwerts, The reaction of CO<sub>2</sub> with ethanolamines, *Chem. Eng. Sci.*, 1979, **34**, 443–446.
- 154 D. Belli Dell'Amico, F. Calderazzo, L. Labella, F. Marchetti and G. Pampaloni, *Chem. Rev.*, 2003, 103, 3857–3897.
- 155 R. Ben Said, J. M. Kolle, K. Essalah, B. Tangour and A. Sayari, A Unified Approach to CO<sub>2</sub>–Amine Reaction Mechanisms, *ACS Omega*, 2020, **5**, 26125–26133.
- 156 E. F. da Silva and H. F. Svendsen, Ab Initio Study of the Reaction of Carbamate Formation from CO<sub>2</sub> and Alkanolamines, *Ind. Eng. Chem. Res.*, 2004, **43**, 3413–3418.
- 157 E. Orestes, C. Machado Ronconi and J. W. de M. Carneiro, Insights into the interactions of CO<sub>2</sub> with amines: a DFT benchmark study, *Phys. Chem. Chem. Phys.*, 2014, **16**, 17213–17219.
- 158 T. Yamada, P. J. Lukac, T. Yu and R. G. Weiss, Reversible, Room-Temperature, Chiral Ionic Liquids. Amidinium Carbamates Derived from Amidines and Amino-

- Acid Esters with Carbon Dioxide †, *Chem. Mater.*, 2007, **19**, 4761–4768.
- 159 G. Bresciani, L. Biancalana, G. Pampaloni and F. Marchetti, Recent Advances in the Chemistry of Metal Carbamates, *Molecules*, 2020, **25**, 3603.
- 160 M. Hulla and P. J. Dyson, Pivotal Role of the Basic Character of Organic and Salt Catalysts in C–N Bond Forming Reactions of Amines with CO<sub>2</sub>, *Angew. Chemie - Int. Ed.*, 2020, **59**, 1002–1017.
- 161 C. Ma, F. Pietrucci and W. Andreoni, Capture and Release of CO<sub>2</sub> in Monoethanolamine Aqueous Solutions: New Insights from First-Principles Reaction Dynamics, *J. Chem. Theory Comput.*, 2015, **11**, 3189–3198.
- 162 L. Biancalana, G. Bresciani, C. Chiappe, F. Marchetti and G. Pampaloni, Synthesis and study of the stability of amidinium/guanidinium carbamates of amines and  $\alpha$ -amino acids, *New J. Chem.*, 2017, **41**, 1798–1805.
- 163 Y. H. Wang, Z. Y. Cao, Q. H. Li, G. Q. Lin, J. Zhou and P. Tian, *Angew. Chemie - Int. Ed.*, 2019, **59**, 8004–8014.
- 164 W. McGhee, D. Riley, K. Christ, Y. Pan and B. Parnas, Carbon Dioxide as a Phosgene Replacement: Synthesis and Mechanistic Studies of Urethanes from Amines, CO<sub>2</sub>, and Alkyl Chlorides, *J. Org. Chem.*, 1995, **60**, 2820–2830.
- 165 W. D. McGhee, Y. Pan and D. P. Riley, Highly selective generation of urethanes from amines, carbon dioxide and alkyl chlorides, *J. Chem. Soc. Chem. Commun.*, 1994, 699–700.
- 166 A. Schirbel, M. H. Holschbach and H. H. Coenen, N.C.A.[<sup>11</sup>C]CO<sub>2</sub> as a safe substitute for phosgene in the carbonylation of primary amines, *J. Label. Compd. Radiopharm.*, 1999, **42**, 537–551.
- 167 T. E. Waldman and W. D. McGhee, Isocyanates from primary amines and carbon dioxide: ‘Dehydration’ of carbamate anions, *J. Chem. Soc. Chem. Commun.*, 1994, **26**, 957–958.
- 168 S. Tshepelevitsh, A. Kütt, M. Lõkov, I. Kaljurand, J. Saame, A. Heering, P. G. Plieger, R. Vianello and I. Leito, On the Basicity of Organic Bases in Different Media, *European J. Org. Chem.*, 2019, **2019**, 6735–6748.
- 169 D. C. Dean, M. A. Wallace, T. M. Marks and D. G. Melillo, Efficient utilization of [<sup>14</sup>C]carbon dioxide as a phosgene equivalent for labeled synthesis, *Tetrahedron Lett.*, 1997, **38**, 919–922.
- 170 E. W. van Tilburg, A. D. Windhorst, M. van der Mey and J. D. M. Herscheid, One-pot synthesis of [<sup>11</sup>C]ureas via triphenylphosphinimines, *J. Label. Compd. Radiopharm.*, 2006, **49**, 321–330.
- 171 F. P. Cossío, C. Alonso, B. Lecea, M. Ayerbe, G. Rubiales and F. Palacios, Mechanism and Stereoselectivity of the Aza-Wittig Reaction between Phosphazenes and Aldehydes, *J. Org. Chem.*, 2006, **71**, 2839–2847.
- 172 M.-A. Courtemanche, M.-A. Légaré, É. Rochette and F.-G. Fontaine, Phosphazenes: efficient organocatalysts for the catalytic hydrosilylation of carbon dioxide, *Chem. Commun.*, 2015, **51**, 6858–6861.
- 173 J. J. Monagle, T. W. Campbell and H. F. McShane, Carbodiimides. II. Mechanism

- of the Catalytic Formation from Isocyanates, *J. Am. Chem. Soc.*, 1962, **84**, 4288–4295.
- 174 H. Wamhoff, G. Richardt and S. Stölben, 1995, pp. 159–249.
- 175 A. J. Poot, B. van der Wildt, M. Stigter-van Walsum, M. Rongen, R. C. Schuit, N. H. Hendrikse, J. Eriksson, G. A. M. S. van Dongen and A. D. Windhorst, [<sup>11</sup>C]Sorafenib: Radiosynthesis and preclinical evaluation in tumor-bearing mice of a new TKI-PET tracer, *Nucl. Med. Biol.*, 2013, **40**, 488–497.
- 176 U. S. Ismailani, M. Munch, B. A. Mair and B. H. Rotstein, Interrupted aza-Wittig reactions using iminophosphoranes to synthesize <sup>11</sup>C–carbonyls, *Chem. Commun.*, 2021, **57**, 5266–5269.
- 177 A. Del Vecchio, F. Caillé, A. Chevalier, O. Loreau, K. Horkka, C. Halldin, M. Schou, N. Camus, P. Kessler, B. Kuhnast, F. Taran and D. Audisio, Late-stage isotopic carbon labeling of pharmaceutically relevant cyclic ureas directly from CO<sub>2</sub>, *Angew. Chemie Int. Ed.*, , DOI:10.1002/anie.201804838.
- 178 V. Babin, A. Sallustrau, O. Loreau, F. Caillé, A. Goudet, H. Cahuzac, A. Del Vecchio, F. Taran and D. Audisio, A general procedure for carbon isotope labeling of linear urea derivatives with carbon dioxide, *Chem. Commun.*, 2021, **57**, 6680–6683.
- 179 T. Ishikawa, Y. Kondo, H. Kotsuki, T. Kumamoto, D. Margetic, K. Nagasawa and W. Nakanishi, *Superbases for Organic Synthesis: Guanidines, Amidines, Phosphazenes and Related Organocatalysts*, John Wiley & Sons, Ltd, Chichester, UK, 2009.
- 180 T. R. Puleo, S. J. Sujansky, S. E. Wright and J. S. Bandar, Organic Superbases in Recent Synthetic Methodology Research, *Chem. – A Eur. J.*, 2021, **27**, 4216–4229.
- 181 W. D. McGhee, Y. Pan and D. P. Riley, Highly selective generation of urethanes from amines, carbon dioxide and alkyl chlorides, *J. Chem. Soc. Chem. Commun.*, 1994, 699.
- 182 R. F. Weitkamp, B. Neumann, H. Stammmler and B. Hoge, Phosphorus-Containing Superbases: Recent Progress in the Chemistry of Electron-Abundant Phosphines and Phosphazenes, *Chem. – A Eur. J.*, 2021, **27**, 10807–10825.
- 183 R. Schwesinger and H. Schlemper, Peralkylated Polyaminophosphazenes—Extremely Strong, Neutral Nitrogen Bases, *Angew. Chemie Int. Ed. English*, 1987, **26**, 1167–1169.
- 184 J. M. Hooker, A. T. Reibel, S. M. Hill, M. J. Schueller and J. S. Fowler, One-Pot, Direct Incorporation of [<sup>11</sup>C]CO<sub>2</sub> into Carbamates, *Angew. Chemie Int. Ed.*, 2009, **48**, 3482–3485.
- 185 D. J. Heldebrant, P. G. Jessop, C. A. Thomas, C. A. Eckert and C. L. Liotta, The reaction of 1,8-diazabicyclo[5.4.0]undec-7-ene (DBU) with carbon dioxide., *J. Org. Chem.*, 2005, **70**, 5335–8.
- 186 E. R. Pérez, R. H. A. Santos, M. T. P. Gambardella, L. G. M. de Macedo, U. P. Rodrigues-Filho, J.-C. Launay and D. W. Franco, Activation of Carbon Dioxide by Bicyclic Amidines, *J. Org. Chem.*, 2004, **69**, 8005–8011.

- 187 J. M. Valera Lauridsen, S. Y. Cho, H. Y. Bae and J.-W. Lee, CO<sub>2</sub> (De)Activation in Carboxylation Reactions: A Case Study Using Grignard Reagents and Nucleophilic Bases, *Organometallics*, 2020, **39**, 1652–1657.
- 188 A. A. Wilson, A. Garcia, S. Houle and N. Vasdev, Direct fixation of [<sup>11</sup>C]-CO<sub>2</sub> by amines: Formation of [<sup>11</sup>C-carbonyl]-methylcarbamates, *Org. Biomol. Chem.*, 2010, **8**, 428–432.
- 189 R. Schwesinger, J. Willaredt, H. Schlemper, M. Keller, D. Schmitt and H. Fritz, Novel, Very Strong, Uncharged Auxiliary Bases; Design and Synthesis of Monomeric and Polymer-Bound Triaminoiminophosphorane Bases of Broadly Varied Steric Demand, *Chem. Ber.*, 1994, **127**, 2435–2454.
- 190 E. R. Pérez, M. O. da Silva, V. C. Costa, U. P. Rodrigues-Filho and D. W. Franco, Efficient and clean synthesis of N-alkyl carbamates by transcarboxylation and O-alkylation coupled reactions using a DBU–CO<sub>2</sub> zwitterionic carbamic complex in aprotic polar media, *Tetrahedron Lett.*, 2002, **43**, 4091–4093.
- 191 M. Yoshida, Y. Komatsuzaki and M. Ihara, Synthesis of 5-Vinylideneoxazolidin-2-ones by DBU-Mediated CO<sub>2</sub> -Fixation Reaction of 4-(Benzylamino)-2-butynyl Carbonates and Benzoates, *Org. Lett.*, 2008, **10**, 2083–2086.
- 192 X. Gao, Y. Deng, C. Lu, L. Zhang, X. Wang and B. Yu, Organic Base-Catalyzed C–S Bond Construction from CO<sub>2</sub>: A New Route for the Synthesis of Benzothiazolones, *Catalysts*, 2018, **8**, 271.
- 193 M. Brahmayya, S. A. Dai and S.-Y. Suen, Facile synthesis of 2-benzimidazolones via carbonylation of o -phenylenediamines with CO<sub>2</sub>, *J. CO<sub>2</sub> Util.*, 2017, **22**, 135–142.
- 194 M. Lv, P. Wang, D. Yuan and Y. Yao, Conversion of Carbon Dioxide into Oxazolidinones Mediated by Quaternary Ammonium Salts and DBU, *ChemCatChem*, 2017, **9**, 4451–4455.
- 195 M. Marchegiani, M. Nodari, F. Tansini, C. Massera, R. Mancuso, B. Gabriele, M. Costa and N. Della Ca', Urea derivatives from carbon dioxide and amines by guanidine catalysis: Easy access to imidazolidin-2-ones under solvent-free conditions, *J. CO<sub>2</sub> Util.*, 2017, **21**, 553–561.
- 196 Y. Zhao, Y. Wu, G. Yuan, L. Hao, X. Gao, Z. Yang, B. Yu, H. Zhang and Z. Liu, Azole-Anion-Based Aprotic Ionic Liquids: Functional Solvents for Atmospheric CO<sub>2</sub> Transformation into Various Heterocyclic Compounds, *Chem. - An Asian J.*, 2016, **11**, 2735–2740.
- 197 M. Yoshida, T. Mizuguchi and K. Shishido, Synthesis of Oxazolidinones by Efficient Fixation of Atmospheric CO<sub>2</sub> with Propargylic Amines by using a Silver/1,8-Diazabicyclo[5.4.0]undec-7-ene (DBU) Dual-Catalyst System, *Chem. - A Eur. J.*, 2012, **18**, 15578–15581.
- 198 K. Dahl, C. Halldin and M. Schou, New methodologies for the preparation of carbon-11 labeled radiopharmaceuticals, *Clin. Transl. Imaging*, 2017, **5**, 275–289.
- 199 F. S. Pereira, E. R. DeAzevedo, E. F. da Silva, T. J. Bonagamba, D. L. da Silva Agostíni, A. Magalhães, A. E. Job and E. R. Pérez González, Study of the carbon dioxide chemical fixation—activation by guanidines, *Tetrahedron*, 2008, **64**,

- 10097–10106.
- 200 R. Nicholls, S. Kaufhold and B. N. Nguyen, Observation of guanidine–carbon dioxide complexation in solution and its role in the reaction of carbon dioxide and propargylamines, *Catal. Sci. Technol.*, 2014, **4**, 3458–3462.
- 201 C. Villiers, J.-P. Dognon, R. Pollet, P. Thuéry and M. Ephritikhine, An Isolated CO<sub>2</sub> Adduct of a Nitrogen Base: Crystal and Electronic Structures, *Angew. Chemie Int. Ed.*, 2010, **49**, 3465–3468.
- 202 T. Mizuno, T. Nakai and M. Mihara, Is CO<sub>2</sub> fixation promoted through the formation of DBU bicarbonate salt?, *Heteroat. Chem.*, 2012, **23**, 276–280.
- 203 P. V. Kortunov, L. S. Baugh, M. Siskin and D. C. Calabro, In Situ Nuclear Magnetic Resonance Mechanistic Studies of Carbon Dioxide Reactions with Liquid Amines in Mixed Base Systems: The Interplay of Lewis and Brønsted Basicities, *Energy & Fuels*, 2015, **29**, 5967–5989.
- 204 P. V. Kortunov, M. Siskin, L. S. Baugh and D. C. Calabro, In Situ Nuclear Magnetic Resonance Mechanistic Studies of Carbon Dioxide Reactions with Liquid Amines in Non-aqueous Systems: Evidence for the Formation of Carbamic Acids and Zwitterionic Species, *Energy & Fuels*, 2015, **29**, 5940–5966.
- 205 A. F. Eftaiha, A. K. Qaroush, I. K. Okashah, F. Alsoubani, J. Futter, C. Troll, B. Rieger and K. I. Assaf, CO<sub>2</sub> activation through C–N, C–O and C–C bond formation, *Phys. Chem. Chem. Phys.*, 2020, **22**, 1306–1312.
- 206 Q. Yu, K. Kumata, H. Li, Y. Zhang, Z. Chen, X. Zhang, T. Shao, A. Hatori, T. Yamasaki, L. Xie, K. Hu, G. Wang, L. Josephson, S. Sun, M.-R. Zhang and S. H. Liang, Synthesis and evaluation of 6-(<sup>11</sup>C-methyl(4-(pyridin-2-yl)thiazol-2-yl)amino)benzo[d]thiazol-2(3H)-one for imaging  $\gamma$ -8 dependent transmembrane AMPA receptor regulatory protein by PET, *Bioorg. Med. Chem. Lett.*, 2020, **30**, 126879.
- 207 H. H. Coenen, M. Schüller, G. Stöcklin, B. Klatte and A. Knöchel, Preparation of N.C.A. [<sup>17-18</sup>F]-fluoroheptadecanoic acid in high yields via aminopolyether supported, nucleophilic fluorination, *J. Label. Compd. Radiopharm.*, 1986, **23**, 455–466.
- 208 D. Landini, A. Maia, F. Montanari and P. Tundo, Lipophilic [2.2.2] cryptands as phase-transfer catalysts. Activation and nucleophilicity of anions in aqueous-organic two-phase systems and in organic solvents of low polarity, *J. Am. Chem. Soc.*, 1979, **101**, 2526–2530.
- 209 R. Schwesinger, R. Link, G. Thiele, H. Rotter, D. Honert, H.-H. Limbach and F. Männle, Stable Phosphazanium Ions in Synthesis—an Easily Accessible, Extremely Reactive “Naked” Fluoride Salt, *Angew. Chemie Int. Ed. English*, 1991, **30**, 1372–1375.
- 210 R. Schwesinger, R. Link, P. Wenzl and S. Kossek, Anhydrous Phosphazanium Fluorides as Sources for Extremely Reactive Fluoride Ions in Solution, *Chem. - A Eur. J.*, 2006, **12**, 438–445.
- 211 U. Wild, C. Neuhäuser, S. Wiesner, E. Kaifer, H. Wadepohl and H.-J. Himmel, Redox-Controlled Hydrogen Bonding: Turning a Superbase into a Strong

- Hydrogen-Bond Donor, *Chem. - A Eur. J.*, 2014, **20**, 5914–5925.
- 212 D. Jardel, C. Davies, F. Peruch, S. Massip and B. Bibal, Protonated Phosphazenes: Structures and Hydrogen-Bonding Organocatalysts for Carbonyl Bond Activation, *Adv. Synth. Catal.*, 2016, **358**, 1110–1118.
- 213 Y. Manaka, Y. Nagatsuka and K. Motokura, Organic bases catalyze the synthesis of urea from ammonium salts derived from recovered environmental ammonia, *Sci. Rep.*, 2020, **10**, 1–8.
- 214 A. A. Wilson, A. Garcia, S. Houle, O. Sadovski and N. Vasdev, Synthesis and application of isocyanates radiolabeled with carbon-11, *Chem. - A Eur. J.*, 2011, **17**, 259–264.
- 215 M. S. Meier, S. M. Ruder, J. A. Malona and A. J. Frontier, in *Encyclopedia of Reagents for Organic Synthesis*, John Wiley & Sons, Ltd, Chichester, UK, 2008.
- 216 B. Rickborn and F. R. Jensen,  $\alpha$ -Carbon Isomerization in Amide Dehydrations 1, *J. Org. Chem.*, 1962, **27**, 4608–4610.
- 217 J. L. Giner, C. Margot and C. Djerassi, Stereospecificity and regioselectivity of the phosphorus oxychloride dehydration of sterol side chain alcohols, *J. Org. Chem.*, 1989, **54**, 369–373.
- 218 M. B. Smith and J. March, in *March's Advanced Organic Chemistry*, John Wiley & Sons, Inc., Hoboken, NJ, USA, 6th edn., 2006, pp. 1477–1558.
- 219 Z. Li, R. J. Mayer, A. R. Ofial and H. Mayr, From Carbodiimides to Carbon Dioxide: Quantification of the Electrophilic Reactivities of Heteroallenes, *J. Am. Chem. Soc.*, 2020, **142**, 8383–8402.
- 220 R. Ramapanicker and P. Chauhan, in *Click Reactions in Organic Synthesis*, ed. S. Chandrasekaran, Wiley-VCH Verlag GmbH & Co. KGaA, Weinheim, Germany, 1st edn., 2016, pp. 1–24.
- 221 G. Gody, D. A. Roberts, T. Maschmeyer and S. Perrier, A New Methodology for Assessing Macromolecular Click Reactions and Its Application to Amine–Tertiary Isocyanate Coupling for Polymer Ligation, *J. Am. Chem. Soc.*, 2016, **138**, 4061–4068.
- 222 M. Sergeev, M. Lazari, F. Morgia, J. Collins, M. R. Javed, O. Sergeeva, J. Jones, M. E. Phelps, J. T. Lee, P. Y. Keng and R. M. van Dam, Performing radiosynthesis in microvolumes to maximize molar activity of tracers for positron emission tomography, *Commun. Chem.*, 2018, **1**, 10.
- 223 K. Gholivand, Z. Shariatnia and N. Oroujzadeh, Phosphoramides: Synthesis, Spectroscopy, and X-ray Crystallography, *Heteroat. Chem.*, 2013, **24**, 404–412.
- 224 C. Grison, A. Thomas, F. Coutrot and P. Coutrot, New ketone homoenolate anion equivalents derived from (alkenyl)pentamethyl phosphoric triamides, *Tetrahedron*, 2003, **59**, 2101–2123.
- 225 A. K. Haji Dheere, N. Yusuf and A. Gee, Rapid and efficient synthesis of [ $^{11}\text{C}$ ]ureas via the incorporation of [ $^{11}\text{C}$ ]CO $_2$  into aliphatic and aromatic amines., *Chem. Commun. (Camb.)*, 2013, **49**, 8193–5.
- 226 A. Dheere, S. Bongarzone, C. Taddei, R. Yan and A. Gee, Synthesis of  $^{11}\text{C}$ -

- Labelled Symmetrical Ureas via the Rapid Incorporation of [ $^{13}\text{C}$ ]CO<sub>2</sub> into Aliphatic and Aromatic Amines, *Synlett*, 2015, **26**, 2257–2260.
- 227 C. J. Dinsmore and S. P. Mercer, Carboxylation and Mitsunobu Reaction of Amines to Give Carbamates: Retention vs Inversion of Configuration Is Substituent-Dependent, *Org. Lett.*, 2004, **6**, 2885–2888.
- 228 S. L. Peterson, S. M. Stucka and C. J. Dinsmore, Parallel synthesis of ureas and carbamates from amines and CO<sub>2</sub> under mild conditions., *Org. Lett.*, 2010, **12**, 1340–3.
- 229 M. Kodaka, T. Tomohiro and H. (Yohmei) Okuno, The mechanism of the mitsunobu reaction and its application to CO<sub>2</sub> fixation, *J. Chem. Soc. Chem. Commun.*, 1993, 81.
- 230 D. Saylik, M. J. Horvath, P. S. Elmes, W. R. Jackson, C. G. Lovel and K. Moody, Preparation of isocyanates from primary amines and carbon dioxide using Mitsunobu chemistry, *J. Org. Chem.*, 1999, **64**, 3940–3946.
- 231 M. J. Horvath, D. Saylik, P. S. Elmes, W. R. Jackson, C. G. Lovel and K. Moody, A Mitsunobu-based procedure for the preparation of alkyl and hindered aryl isocyanates from primary amines and carbon dioxide under mild conditions, *Tetrahedron Lett.*, 1999, **40**, 363–366.
- 232 D. Chaturvedi, N. Mishra and V. Mishra, A high yielding, one-pot synthesis of substituted ureas from the corresponding amines using Mitsunobu's reagent, *Monatshefte fur Chemie*, 2008, **139**, 267–270.
- 233 K. C. K. Swamy, N. N. B. Kumar, E. Balaraman and K. V. P. P. Kumar, Mitsunobu and Related Reactions: Advances and Applications, *Chem. Rev.*, 2009, **109**, 2551–2651.
- 234 I. D. Jenkins and O. Mitsunobu, *Triphenylphosphine-Diethyl Azodicarboxylate*, John Wiley & Sons, Ltd, Chichester, UK, 2001.
- 235 O. Mitsunobu, The Use of Diethyl Azodicarboxylate and Triphenylphosphine in Synthesis and Transformation of Natural Products, *Synthesis (Stuttg.)*, 1981, **1981**, 1–28.
- 236 E. Brunn and R. Huisgen, Structure and Reactivity of the Betaine Derived from Triphenylphosphine and Dimethyl Azodicarboxylate, *Angew. Chemie Int. Ed. English*, 1969, **8**, 513–515.
- 237 D. Morrison, Notes: Reactions of Alkyl Phosphites with Diethyl Azodicarboxylate, *J. Org. Chem.*, 1958, **23**, 1072–1074.
- 238 S. Bittner, Y. Assaf, P. Krief, M. Pomerantz, B. T. Ziemnicka and C. G. Smith, Synthesis of N-acyl-, N-sulfonyl-, and N-phosphinylphospha(PV)azenes by a redox-condensation reaction using amides, triphenylphosphine, and diethyl azodicarboxylate, *J. Org. Chem.*, 1985, **50**, 1712–1718.
- 239 F. Wang and J. R. Hauske, Solid-phase synthesis of 3,4-dihydroquinazoline, *Tetrahedron Lett.*, 1997, **38**, 8651–8654.
- 240 H. Li and M. J. Miller, Syntheses of 5'-Deoxy-5'- N -hydroxylaminopyrimidine and Purine Nucleosides: Building Blocks for Novel Antisense Oligonucleosides

- with Hydroxamate Linkages, *J. Org. Chem.*, 1999, **64**, 9289–9293.
- 241 B. A. Mair, M. H. Fouad, U. S. Ismailani, M. Munch and B. H. Rotstein, Rhodium-Catalyzed Addition of Organozinc Iodides to Carbon-11 Isocyanates, *Org. Lett.*, 2020, **22**, 2746–2750.
- 242 J. R. Hill, X. Shao, N. L. Massey, J. Stauff, P. S. Sherman, A. A. B. Robertson and P. J. H. Scott, Synthesis and Evaluation of NLRP3-Inhibitory Sulfonylurea [<sup>11</sup>C]MCC950 in Healthy Animals, *Bioorg. Med. Chem. Lett.*, 2020, 127186.
- 243 A. V. Mossine, A. F. Brooks, I. M. Jackson, C. A. Quesada, P. Sherman, E. L. Cole, D. J. Donnelly, P. J. H. Scott and X. Shao, Synthesis of Diverse <sup>11</sup>C-Labeled PET Radiotracers via Direct Incorporation of [(<sup>11</sup>C)]CO<sub>2</sub>, *Bioconjug. Chem.*, , DOI:10.1021/acs.bioconjchem.6b00163.
- 244 S. Bongarzone, T. Sementa, J. Dunn, J. Bordoloi, K. Sunassee, P. J. Blower and A. Gee, Imaging Biotin Trafficking In Vivo with Positron Emission Tomography, *J. Med. Chem.*, 2020, **63**, 8265–8275.
- 245 Z. Chen, J. Chen, N. Mast, J. Rong, X. Deng, T. Shao, H. Fu, Q. Yu, J. Sun, Y. Shao, L. Josephson, T. L. Collier, I. Pikuleva and S. H. Liang, Synthesis and pharmacokinetic study of a <sup>11</sup>C-labeled cholesterol 24-hydroxylase inhibitor using ‘in-loop’ [<sup>11</sup>C]CO<sub>2</sub> fixation method, *Bioorg. Med. Chem. Lett.*, 2020, **30**, 127068.
- 246 J. W. Hicks, A. A. Wilson, E. A. Rubie, J. R. Woodgett, S. Houle and N. Vasdev, Towards the preparation of radiolabeled 1-aryl-3-benzyl ureas: Radiosynthesis of [<sup>11</sup>C-carbonyl] AR-A014418 by [<sup>11</sup>C]CO<sub>2</sub> fixation, *Bioorg. Med. Chem. Lett.*, 2012, **22**, 2099–2101.
- 247 J. W. Hicks, J. Parkes, J. Tong, S. Houle, N. Vasdev and A. A. Wilson, Radiosynthesis and ex vivo evaluation of [<sup>11</sup>C-carbonyl]carbamate- and urea-based monoacylglycerol lipase inhibitors, *Nucl. Med. Biol.*, 2014, **41**, 688–694.
- 248 Z. Chen, W. Mori, X. Deng, R. Cheng, D. Ogasawara, G. Zhang, M. A. Schafroth, K. Dahl, H. Fu, A. Hatori, T. Shao, Y. Zhang, T. Yamasaki, X. Zhang, J. Rong, Q. Yu, K. Hu, M. Fujinaga, L. Xie, K. Kumata, Y. Gou, J. Chen, S. Gu, L. Bao, L. Wang, T. L. Collier, N. Vasdev, Y. Shao, J.-A. Ma, B. F. Cravatt, C. Fowler, L. Josephson, M.-R. Zhang and S. H. Liang, Design, Synthesis, and Evaluation of Reversible and Irreversible Monoacylglycerol Lipase Positron Emission Tomography (PET) Tracers Using a “Tail Switching” Strategy on a Piperazinyl Azetidine Skeleton, *J. Med. Chem.*, 2019, **62**, 3336–3353.
- 249 N. Vasdev, O. Sadovski, A. Garcia, F. Dollé, J. H. Meyer, S. Houle and A. A. Wilson, Radiosynthesis of [<sup>11</sup>C]SL25.1188 via [<sup>11</sup>C]CO<sub>2</sub> fixation for imaging monoamine oxidase B, *J. Label. Compd. Radiopharm.*, 2011, **54**, 678–680.
- 250 C. Wang, M. S. Placzek, G. C. Van de Bittner, F. A. Schroeder and J. M. Hooker, A Novel Radiotracer for Imaging Monoacylglycerol Lipase in the Brain Using Positron Emission Tomography, *ACS Chem. Neurosci.*, 2016, **7**, 484–489.
- 251 S. Bongarzone, A. Runser, C. Taddei, A. K. H. Dheere and A. D. Gee, From [<sup>11</sup>C]CO<sub>2</sub> to [<sup>11</sup>C]amides: a rapid one-pot synthesis via the Mitsunobu reaction, *Chem. Commun.*, 2017, **53**, 5334–5337.
- 252 U. Slomczyńska and G. Barany, Efficient synthesis of 1,2,4-dithiazolidine-3,5-



- diones (dithiasuccinoyl-amines) and observations on formation of 1,2,4-thiadiazolidine-3,5-diones by related chemistry, *J. Heterocycl. Chem.*, 1984, **21**, 241–246.
- 253 C. Boullais, C. Crouzel and A. Syrota, Synthesis of 4-(3-t-butylamino-2-hydroxypropoxy)-benzimidazol-2(<sup>11</sup>C)-one (cgp 12177), *J. Label. Compd. Radiopharm.*, 1986, **23**, 565–567.
- 254 A. van Waarde, P. H. Elsinga, P. Doze, M. Heldoorn, K. A. Jaeggi and W. Vaalburg, A novel  $\beta$ -adrenoceptor ligand for positron emission tomography: Evaluation in experimental animals, *Eur. J. Pharmacol.*, 1998, **343**, 289–296.
- 255 A. Hammadi and C. Crouzel, Asymmetric synthesis of (2S)-and (2R)-4-(3-t-butylamino-2-hydroxypropoxy)-benzimidazol-2-[<sup>11</sup>C]-one ((S)-and (R)-[<sup>11</sup>C]-CGP 12177) from optically active precursors, *J. Label. Compd. Radiopharm.*, 1991, **29**, 681–690.
- 256 J. J. Bow and P. J. Riss, Phosgene-Free Carbonyl Insertion: Hot Advances in <sup>11</sup>C-Chemistry, *Chemistry–Methods*, 2021, **1**, 139–141.
- 257 A. van Waarde, W. Vaalburg, P. Doze, F. J. Bosker and P. H. Elsinga, PET imaging of beta-adrenoceptors in human brain: a realistic goal or a mirage?, *Curr. Pharm. Des.*, 2004, **10**, 1519–36.
- 258 K. Horkka, K. Dahl, J. Bergare, C. S. Elmore, C. Halldin and M. Schou, Rapid and Efficient Synthesis of <sup>11</sup>C-Labeled Benzimidazolones Using [<sup>11</sup>C]Carbon Dioxide, *ChemistrySelect*, 2019, **4**, 1846–1849.
- 259 A. K. Sarmah and J. Sabadie, Hydrolysis of Sulfonylurea Herbicides in Soils and Aqueous Solutions: a Review, *J. Agric. Food Chem.*, 2002, **50**, 6253–6265.
- 260 F. Bray, M. Laversanne, E. Weiderpass and I. Soerjomataram, The ever-increasing importance of cancer as a leading cause of premature death worldwide, *Cancer*, 2021, **127**, 3029–3030.
- 261 H. Sung, J. Ferlay, R. L. Siegel, M. Laversanne, I. Soerjomataram, A. Jemal and F. Bray, Global Cancer Statistics 2020: GLOBOCAN Estimates of Incidence and Mortality Worldwide for 36 Cancers in 185 Countries, *CA. Cancer J. Clin.*, 2021, **71**, 209–249.
- 262 A. Alavi, P. Lakhani, A. Mavi, J. W. Kung and H. Zhuang, PET: a revolution in medical imaging, *Radiol. Clin. North Am.*, 2004, **42**, 983–1001.
- 263 N. Takahashi, T. Inoue, J. Lee, T. Yamaguchi and K. Shizukuishi, The Roles of PET and PET/CT in the Diagnosis and Management of Prostate Cancer, *Oncology*, 2007, **72**, 226–233.
- 264 H. Jadvar, Imaging evaluation of prostate cancer with <sup>18</sup>F-fluorodeoxyglucose PET/CT: utility and limitations, *Eur. J. Nucl. Med. Mol. Imaging*, 2013, **40**, 5–10.
- 265 H. Jadvar, Is There Use for FDG-PET in Prostate Cancer?, *Semin. Nucl. Med.*, 2016, **46**, 502–506.
- 266 T. Tsukamoto, K. M. Wozniak and B. S. Slusher, Progress in the discovery and development of glutamate carboxypeptidase II inhibitors, *Drug Discov. Today*, 2007, **12**, 767–776.

- 267 D. V Ferraris, K. Shukla and T. Tsukamoto, Structure-activity relationships of glutamate carboxypeptidase II (GCPII) inhibitors., *Curr. Med. Chem.*, 2012, **19**, 1282–94.
- 268 S. Lütje, S. Heskamp, A. S. Cornelissen, T. D. Poeppel, S. A. M. W. van den Broek, S. Rosenbaum-Krumme, A. Bockisch, M. Gotthardt, M. Rijpkema and O. C. Boerman, PSMA Ligands for Radionuclide Imaging and Therapy of Prostate Cancer: Clinical Status, *Theranostics*, 2015, **5**, 1388–1401.
- 269 A. E. Machulkin, Y. A. Ivanenkov, A. V. Aladinskaya, M. S. Veselov, V. A. Aladinskiy, E. K. Beloglazkina, V. E. Koteliansky, A. G. Shakhbazyan, Y. B. Sandulenko and A. G. Majouga, Small-molecule PSMA ligands. Current state, SAR and perspectives, *J. Drug Target.*, 2016, **24**, 679–693.
- 270 A. Afshar-Oromieh, J. W. Babich, C. Kratochwil, F. L. Giesel, M. Eisenhut, K. Kopka and U. Haberkorn, The Rise of PSMA Ligands for Diagnosis and Therapy of Prostate Cancer, *J. Nucl. Med.*, 2016, **57**, 79S-89S.
- 271 K. Kopka, M. Benešová, C. Bařinka, U. Haberkorn and J. Babich, Glu-Ureido–Based Inhibitors of Prostate-Specific Membrane Antigen: Lessons Learned During the Development of a Novel Class of Low-Molecular-Weight Theranostic Radiotracers, *J. Nucl. Med.*, 2017, **58**, 17S-26S.
- 272 S. M. Schwarzenboeck, I. Rauscher, C. Bluemel, W. P. Fendler, S. P. Rowe, M. G. Pomper, A. Afshar-Oromieh, K. Herrmann and M. Eiber, PSMA ligands for PET imaging of prostate cancer, *J. Nucl. Med.*, 2017, **58**, 1545–1552.
- 273 S. P. Rowe, M. A. Gorin and M. G. Pomper, Imaging of Prostate-Specific Membrane Antigen with Small-Molecule PET Radiotracers: From the Bench to Advanced Clinical Applications, *Annu. Rev. Med.*, 2019, **70**, 461–477.
- 274 D. G. Bostwick, A. Pacelli, M. Blute, P. Roche and G. P. Murphy, Prostate specific membrane antigen expression in prostatic intraepithelial neoplasia and adenocarcinoma, *Cancer*, 1998, **82**, 2256–2261.
- 275 D. S. O’Keefe, D. J. Bacich, S. S. Huang and W. D. W. Heston, A Perspective on the Evolving Story of PSMA Biology, PSMA-Based Imaging, and Endoradiotherapeutic Strategies., *J. Nucl. Med.*, 2018, **59**, 1007–1013.
- 276 G. L. Wright, C. Haley, M. Lou Beckett and P. F. Schellhammer, Expression of prostate-specific membrane antigen in normal, benign, and malignant prostate tissues, *Urol. Oncol. Semin. Orig. Investig.*, 1995, **1**, 18–28.
- 277 J. S. Ross, C. E. Sheehan, H. A. G. Fisher, R. P. Kaufman, P. Kaur, K. Gray, I. Webb, G. S. Gray, R. Mosher and B. V. S. Kallakury, Correlation of primary tumor prostate-specific membrane antigen expression with disease recurrence in prostate cancer., *Clin. Cancer Res.*, 2003, **9**, 6357–62.
- 278 A. K. Rajasekaran, G. Anilkumar and J. J. Christiansen, Is prostate-specific membrane antigen a multifunctional protein?, *Am. J. Physiol. Cell Physiol.*, 2005, **288**, C975-81.
- 279 V. Yao, C. E. Berkman, J. K. Choi, D. S. O’Keefe and D. J. Bacich, Expression of prostate-specific membrane antigen (PSMA), increases cell folate uptake and proliferation and suggests a novel role for PSMA in the uptake of the non-

- polyglutamated folate, folic acid, *Prostate*, 2010, **70**, 305–316.
- 280 R. Luthi-Carter, A. K. Barczak, H. Speno and J. T. Coyle, Molecular characterization of human brain N-acetylated  $\alpha$ -linked acidic dipeptidase (NAALADase), *J. Pharmacol. Exp. Ther.*, 1998, **286**, 1020–1025.
- 281 U. V. Berger, R. Luthi-Carter, L. A. Passani, S. Elkabes, I. Black, C. Konradi and J. T. Coyle, Glutamate carboxypeptidase II is expressed by astrocytes in the adult rat nervous system, *J. Comp. Neurol.*, 1999, **415**, 52–64.
- 282 P. Šácha, J. Zámečník, C. Bařinka, K. Hlouchová, A. Vřcha, P. Mlřochová, I. Hilgert, T. Eckschlager and J. Konvalinka, Expression of glutamate carboxypeptidase II in human brain, *Neuroscience*, 2007, **144**, 1361–1372.
- 283 C. Bařinka, C. Rojas, B. Slusher and M. Pomper, Glutamate carboxypeptidase II in diagnosis and treatment of neurologic disorders and prostate cancer., *Curr. Med. Chem.*, 2012, **19**, 856–70.
- 284 J. H. Neale and T. Yamamoto, N-acetylaspartylglutamate (NAAG) and glutamate carboxypeptidase II: An abundant peptide neurotransmitter-enzyme system with multiple clinical applications, *Prog. Neurobiol.*, 2020, **184**, 101722.
- 285 J. J. Vornov, K. R. Hollinger, P. F. Jackson, K. M. Wozniak, M. H. Farah, P. Majer, R. Rais and B. S. Slusher, in *Advances in Pharmacology*, 2016, vol. 76, pp. 215–255.
- 286 B. S. Slusher, J. J. Vornov, A. G. Thomas, P. D. Hurn, I. Harukuni, A. Bhardwaj, R. J. Traystman, M. B. Robinson, P. Britton, X.-C. M. Lu, F. C. Tortella, K. M. Wozniak, M. Yudkoff, B. M. Potter and P. F. Jackson, Selective inhibition of NAALADase, which converts NAAG to glutamate, reduces ischemic brain injury, *Nat. Med.*, 1999, **5**, 1396–1402.
- 287 US Patent Office, US 6528499 B1, 2000.
- 288 A. P. Kozikowski, J. Zhang, F. Nan, P. A. Petukhov, E. Grajkowska, J. T. Wroblewski, T. Yamamoto, T. Bzdega, B. Wroblewska and J. H. Neale, Synthesis of urea-based inhibitors as active site probes of glutamate carboxypeptidase II: efficacy as analgesic agents., *J. Med. Chem.*, 2004, **47**, 1729–38.
- 289 J. J. Vornov, D. Peters, M. Nedelcovych, K. Hollinger, R. Rais and B. S. Slusher, Looking for Drugs in All the Wrong Places: Use of GCPII Inhibitors Outside the Brain, *Neurochem. Res.*, 2019, 1–12.
- 290 J. S. Horoszewicz, E. Kawinski and G. P. Murphy, Monoclonal antibodies to a new antigenic marker in epithelial prostatic cells and serum of prostatic cancer patients., *Anticancer Res.*, 1987, **7**, 927–35.
- 291 G. E. Wynant, G. P. Murphy, J. S. Horoszewicz, C. E. Neal, B. D. Collier, E. Mitchell, G. Purnell, I. Tyson, A. Heal, H. Abdel-Nabi and G. Winzelberg, Immunoscintigraphy of prostatic cancer: Preliminary results with <sup>111</sup>In-labeled monoclonal antibody 7E11-C5.3 (CYT-356), *Prostate*, 1991, **18**, 229–241.
- 292 B. Stauch Slusher, G. Tsai, G. Yoo and J. T. Coyle, Immunocytochemical localization of the N-acetyl-aspartyl-glutamate (NAAG) hydrolyzing enzyme N-acetylated alpha-linked acidic dipeptidase (NAALADase), *J. Comp. Neurol.*, 1992, **315**, 217–229.

- 293 J. K. Troyer, Q. Feng, M. Lou Beckett and G. L. Wright, Biochemical characterization and mapping of the 7E11-C5.3 epitope of the prostate-specific membrane antigen, *Urol. Oncol. Semin. Orig. Investig.*, 1995, **1**, 29–37.
- 294 J. D. Petronis, F. Regan and K. Lin, Indium-111 capromab pendetide (ProstaScint) imaging to detect recurrent and metastatic prostate cancer., *Clin. Nucl. Med.*, 1998, **23**, 672–7.
- 295 L. E. Ponsky, E. E. Cherullo, R. Starkey, D. Nelson, D. Neumann and C. D. Zippe, Evaluation of preoperative ProstaScint<sup>TM</sup> scans in the prediction of nodal disease, *Prostate Cancer Prostatic Dis.*, 2002, **5**, 132–135.
- 296 P. M. Smith-Jones, S. Vallabhajosula, V. Navarro, D. Bastidas, S. J. Goldsmith and N. H. Bander, Radiolabeled monoclonal antibodies specific to the extracellular domain of prostate-specific membrane antigen: preclinical studies in nude mice bearing LNCaP human prostate tumor., *J. Nucl. Med.*, 2003, **44**, 610–7.
- 297 V. Nargund, D. Al Hashmi, P. Kumar, S. Gordon, U. Otitie, D. Ellison, M. Carroll, S. Baithun and K. E. Britton, Imaging with radiolabelled monoclonal antibody (MUJ591) to prostate-specific membrane antigen in staging of clinically localized prostatic carcinoma: comparison with clinical, surgical and histological staging, *BJU Int.*, 2005, **95**, 1232–1236.
- 298 P. F. Jackson, D. C. Cole, B. S. Slusher, S. L. Stetz, L. E. Ross, B. A. Donzanti and D. A. Trainor, Design, synthesis, and biological activity of a potent inhibitor of the neuropeptidase N-acetylated  $\alpha$ -linked acidic dipeptidase, *J. Med. Chem.*, 1996, **39**, 619–622.
- 299 A. P. Kozikowski, F. Nan, P. Conti, J. Zhang, E. Ramadan, T. Bzdega, B. Wroblewska, J. H. Neale, S. Pshenichkin and J. T. Wroblewski, Design of Remarkably Simple, Yet Potent Urea-Based Inhibitors of Glutamate Carboxypeptidase II (NAALADase), *J. Med. Chem.*, 2001, **44**, 298–301.
- 300 R. T. Olszewski, N. Bukhari, J. Zhou, A. P. Kozikowski, J. T. Wroblewski, S. Shamimi-Noori, B. Wroblewska, T. Bzdega, S. Vicini, F. B. Barton and J. H. Neale, NAAG peptidase inhibition reduces locomotor activity and some stereotypes in the PCP model of schizophrenia via group II mGluR, *J. Neurochem.*, 2004, **89**, 876–885.
- 301 C. Barinka, Y. Byun, C. L. Dusich, S. R. Banerjee, Y. Chen, M. Castanares, A. P. Kozikowski, R. C. Mease, M. G. Pomper and J. Lubkowski, Interactions between Human Glutamate Carboxypeptidase II and Urea-Based Inhibitors: Structural Characterization †, *J. Med. Chem.*, 2008, **51**, 7737–7743.
- 302 C. Bařinka, M. Rovenska, P. Mleochova, K. Hlouchova, A. Plechanovova, P. Majer, T. Tsukamoto, B. S. Slusher, J. Konvalinka and J. Lubkowski, Structural Insight into the Pharmacophore Pocket of Human Glutamate Carboxypeptidase II  $\perp$ , *J. Med. Chem.*, 2007, **50**, 3267–3273.
- 303 M. G. Pomper, J. L. Musachio, J. Zhang, U. Scheffel, Y. Zhou, J. Hilton, A. Maini, R. F. Dannals, D. F. Wong and A. P. Kozikowski, <sup>11</sup>C-MCG: Synthesis, Uptake Selectivity, and Primate PET of a Probe for Glutamate Carboxypeptidase II (NAALADase), *Mol. Imaging*, 2002, **1**, 153535002002021.

- 304 C. A. Foss, R. C. Mease, H. Fan, Y. Wang, H. T. Ravert, R. F. Dannals, R. T. Olszewski, W. D. Heston, A. P. Kozikowski and M. G. Pomper, Radiolabeled small-molecule ligands for prostate-specific membrane antigen: in vivo imaging in experimental models of prostate cancer., *Clin. Cancer Res.*, 2005, **11**, 4022–8.
- 305 K. P. Maresca, S. M. Hillier, F. J. Femia, D. Keith, C. Barone, J. L. Joyal, C. N. Zimmerman, A. P. Kozikowski, J. A. Barrett, W. C. Eckelman and J. W. Babich, A Series of Halogenated Heterodimeric Inhibitors of Prostate Specific Membrane Antigen (PSMA) as Radiolabeled Probes for Targeting Prostate Cancer, *J. Med. Chem.*, 2009, **52**, 347–357.
- 306 J. A. Barrett, R. E. Coleman, S. J. Goldsmith, S. Vallabhajosula, N. A. Petry, S. Cho, T. Armor, J. B. Stubbs, K. P. Maresca, M. G. Stabin, J. L. Joyal, W. C. Eckelman and J. W. Babich, First-in-man evaluation of 2 high-affinity PSMA-avid small molecules for imaging prostate cancer, *J. Nucl. Med.*, 2013, **54**, 380–387.
- 307 Y. Chen, C. A. Foss, Y. Byun, S. Nimmagadda, M. Pullambhatla, J. J. Fox, M. Castanares, S. E. Lupold, J. W. Babich, R. C. Mease and M. G. Pomper, Radiohalogenated prostate-specific membrane antigen (PSMA)-based ureas as imaging agents for prostate cancer., *J. Med. Chem.*, 2008, **51**, 7933–43.
- 308 R. C. Mease, C. L. Dusich, C. A. Foss, H. T. Ravert, R. F. Dannals, J. Seidel, A. Prideaux, J. J. Fox, G. Sgouros, A. P. Kozikowski and M. G. Pomper, N-[N-[(S)-1,3-Dicarboxypropyl]carbonyl]-4-[<sup>18</sup>F]fluorobenzyl-L-cysteine, [<sup>18</sup>F]DCFBC: a new imaging probe for prostate cancer., *Clin. Cancer Res.*, 2008, **14**, 3036–43.
- 309 S. Y. Cho, K. L. Gage, R. C. Mease, S. Senthambhichelvan, D. P. Holt, A. Jeffrey-Kwanisai, C. J. Endres, R. F. Dannals, G. Sgouros, M. Lodge, M. A. Eisenberger, R. Rodriguez, M. A. Carducci, C. Rojas, B. S. Slusher, A. P. Kozikowski and M. G. Pomper, Biodistribution, tumor detection, and radiation dosimetry of <sup>18</sup>F-DCFBC, a low-molecular-weight inhibitor of prostate-specific membrane antigen, in patients with metastatic prostate cancer., *J. Nucl. Med.*, 2012, **53**, 1883–91.
- 310 S. P. Rowe, K. L. Gage, S. F. Faraj, K. J. Macura, T. C. Cornish, N. Gonzalez-Roibon, G. Guner, E. Munari, A. W. Partin, C. P. Pavlovich, M. Han, H. B. Carter, T. J. Bivalacqua, A. Blackford, D. Holt, R. F. Dannals, G. J. Netto, M. A. Lodge, R. C. Mease, M. G. Pomper and S. Y. Cho, <sup>18</sup>F-DCFBC PET/CT for PSMA-Based Detection and Characterization of Primary Prostate Cancer, *J. Nucl. Med.*, 2015, **56**, 1003–1010.
- 311 M. Eder, M. Schäfer, U. Bauder-Wüst, W. E. Hull, C. Wängler, W. Mier, U. Haberkorn and M. Eisenhut, <sup>68</sup>Ga-complex lipophilicity and the targeting property of a urea-based PSMA inhibitor for PET imaging, *Bioconjug. Chem.*, 2012, **23**, 688–697.
- 312 M. Eder, O. Neels, M. Müller, U. Bauder-Wüst, Y. Remde, M. Schäfer, U. Hennrich, M. Eisenhut, A. Afshar-Oromieh, U. Haberkorn and K. Kopka, Novel Preclinical and Radiopharmaceutical Aspects of [<sup>68</sup>Ga]Ga-PSMA-HBED-CC: A New PET Tracer for Imaging of Prostate Cancer, *Pharmaceuticals*, 2014, **7**, 779–796.
- 313 S. R. Banerjee, M. Pullambhatla, Y. Byun, S. Nimmagadda, G. Green, J. J. Fox, A. Horti, R. C. Mease and M. G. Pomper, <sup>68</sup>Ga-labeled inhibitors of prostate-

- specific membrane antigen (PSMA) for imaging prostate cancer, *J. Med. Chem.*, 2010, **53**, 5333–5341.
- 314 F. Bois, C. Noiro, S. Dietemann, I. C. Mainta, T. Zilli, V. Garibotto and M. A. Walter, [<sup>68</sup>Ga]Ga-PSMA-11 in prostate cancer: a comprehensive review., *Am. J. Nucl. Med. Mol. Imaging*, 2020, **10**, 349–374.
- 315 G. Carlucci, R. Ippisch, R. Slavik, A. Mishoe, J. Blecha and S. Zhu, <sup>68</sup>Ga-PSMA-11 NDA Approval: A Novel and Successful Academic Partnership, *J. Nucl. Med.*, 2021, **62**, 149–155.
- 316 SNMMI, *FDA Approves New <sup>68</sup>Ga Kit for Prostate Cancer PET*, 2022, vol. 63.
- 317 Y. Chen, M. Pullambhatla, C. A. Foss, Y. Byun, S. Nimmagadda, S. Senthamizhchelvan, G. Sgouros, R. C. Mease and M. G. Pomper, 2-(3-{1-Carboxy-5-[(6-[<sup>18</sup>F]Fluoro-Pyridine-3-Carbonyl)-Amino]-Pentyl}-Ureido)-Pentanedioic Acid, [<sup>18</sup>F]DCFPyL, a PSMA-Based PET Imaging Agent for Prostate Cancer, *Clin. Cancer Res.*, 2011, **17**, 7645–7653.
- 318 M. Dietlein, C. Kobe, G. Kuhnert, S. Stockter, T. Fischer, K. Schomäcker, M. Schmidt, F. Dietlein, B. D. Zlatopolskiy, P. Krapf, R. Richarz, S. Neubauer, A. Drzezga and B. Neumaier, Comparison of [<sup>18</sup>F]DCFPyL and [<sup>68</sup>Ga]Ga-PSMA-HBED-CC for PSMA-PET Imaging in Patients with Relapsed Prostate Cancer., *Mol. Imaging Biol.*, 2015, **17**, 575–84.
- 319 Z. Szabo, E. Mena, S. P. Rowe, D. Plyku, R. Nidal, M. A. Eisenberger, E. S. Antonarakis, H. Fan, R. F. Dannals, Y. Chen, R. C. Mease, M. Vranesic, A. Bhatnagar, G. Sgouros, S. Y. Cho and M. G. Pomper, Initial Evaluation of [<sup>18</sup>F]DCFPyL for Prostate-Specific Membrane Antigen (PSMA)-Targeted PET Imaging of Prostate Cancer., *Mol. Imaging Biol.*, 2015, **17**, 565–74.
- 320 E. Mena, Z. Szabo, S. Rowe, E. Antonarakis, M. Eisenberger, M. Carducci, M. Vranesic, R. Mease, S. Cho and M. Pomper, First-in-man analysis of [<sup>18</sup>F]DCFPyL, a second generation, <sup>18</sup>F-labeled PSMA-targeted radiotracer, in patients with metastatic prostate cancer, *J. Nucl. Med.*, 2015, **56**, 399.
- 321 F. L. Giesel, L. Will, I. Lawal, T. Lengana, C. Kratochwil, M. Vorster, O. Neels, F. Reyneke, U. Haberkorn, K. Kopka and M. Sathekge, Intraindividual Comparison of <sup>18</sup>F-PSMA-1007 and <sup>18</sup>F-DCFPyL PET/CT in the Prospective Evaluation of Patients with Newly Diagnosed Prostate Carcinoma: A Pilot Study, *J. Nucl. Med.*, 2018, **59**, 1076–1080.
- 322 FDA, FDA approves second PSMA-targeted PET imaging drug for men with prostate cancer, <https://www.fda.gov/drugs/drug-safety-and-availability/fda-approves-second-psma-targeted-pet-imaging-drug-men-prostate-cancer>, (accessed 28 May 2021).
- 323 M. Benesová, M. Schäfer, U. Bauder-Wüst, A. Afshar-Oromieh, C. Kratochwil, W. Mier, U. Haberkorn, K. Kopka and M. Eder, Preclinical evaluation of a tailor-made DOTA-conjugated PSMA inhibitor with optimized linker moiety for imaging and endoradiotherapy of prostate cancer, *J. Nucl. Med.*, 2015, **56**, 914–920.
- 324 C. Liu, T. Liu, N. Zhang, Y. Liu, N. Li, P. Du, Y. Yang, M. Liu, K. Gong, X. Yang,

- H. Zhu, K. Yan and Z. Yang,  $^{68}\text{Ga}$ -PSMA-617 PET/CT: a promising new technique for predicting risk stratification and metastatic risk of prostate cancer patients, *Eur. J. Nucl. Med. Mol. Imaging*, 2018, **45**, 1852–1861.
- 325 A. Heinzl, D. Boghos, F. M. Mottaghy, F. Gaertner, M. Essler, D. von Mallek and H. Ahmadzadehfar,  $^{68}\text{Ga}$ -PSMA PET/CT for monitoring response to  $^{177}\text{Lu}$ -PSMA-617 radioligand therapy in patients with metastatic castration-resistant prostate cancer, *Eur. J. Nucl. Med. Mol. Imaging*, 2019, **46**, 1054–1062.
- 326 J. Cardinale, M. Schäfer, M. Benešová, U. Bauder-Wüst, K. Leotta, M. Eder, O. C. Neels, U. Haberkorn, F. L. Giesel and K. Kopka, Preclinical Evaluation of  $^{18}\text{F}$ -PSMA-1007, a New Prostate-Specific Membrane Antigen Ligand for Prostate Cancer Imaging, *J. Nucl. Med.*, 2017, **58**, 425–431.
- 327 F. L. Giesel, B. Hadaschik, J. Cardinale, J. Radtke, M. Vinsensia, W. Lehnert, C. Kesch, Y. Tolstov, S. Singer, N. Grabe, S. Duensing, M. Schäfer, O. C. Neels, W. Mier, U. Haberkorn, K. Kopka and C. Kratochwil, F-18 labelled PSMA-1007: biodistribution, radiation dosimetry and histopathological validation of tumor lesions in prostate cancer patients, *Eur. J. Nucl. Med. Mol. Imaging*, 2017, **44**, 678–688.
- 328 M. Czarniecki, E. Mena, L. Lindenberg, M. Cacko, S. Harmon, J. P. Radtke, F. Giesel, B. Turkbey and P. L. Choyke, Keeping up with the prostate-specific membrane antigens (PSMAs): an introduction to a new class of positron emission tomography (PET) imaging agents, *Transl. Androl. Urol.*, 2018, **7**, 831–843.
- 329 M. Weineisen, J. Simecek, M. Schottelius, M. Schwaiger and H.-J. Wester, Synthesis and preclinical evaluation of DOTAGA-conjugated PSMA ligands for functional imaging and endoradiotherapy of prostate cancer, *EJNMMI Res.*, 2014, **4**, 63.
- 330 M. Weineisen, M. Schottelius, J. Simecek, R. P. Baum, A. Yildiz, S. Beykan, H. R. Kulkarni, M. Lassmann, I. Klette, M. Eiber, M. Schwaiger and H.-J. Wester,  $^{68}\text{Ga}$ - and  $^{177}\text{Lu}$ -Labeled PSMA I&T: Optimization of a PSMA-Targeted Theranostic Concept and First Proof-of-Concept Human Studies, *J. Nucl. Med.*, 2015, **56**, 1169–1176.
- 331 C. M. Zechmann, A. Afshar-Oromieh, T. Armor, J. B. Stubbs, W. Mier, B. Hadaschik, J. Joyal, K. Kopka, J. Debus, J. W. Babich and U. Haberkorn, Radiation dosimetry and first therapy results with a  $^{124}\text{I}/^{131}\text{I}$ -labeled small molecule (MIP-1095) targeting PSMA for prostate cancer therapy, *Eur. J. Nucl. Med. Mol. Imaging*, 2014, **41**, 1280–1292.
- 332 M. M. Heck, M. Retz, C. D'Alessandria, I. Rauscher, K. Scheidhauer, T. Maurer, E. Storz, F. Janssen, M. Schottelius, H.-J. Wester, J. E. Gschwend, M. Schwaiger, R. Tauber and M. Eiber, Systemic Radioligand Therapy with  $^{177}\text{Lu}$  Labeled Prostate Specific Membrane Antigen Ligand for Imaging and Therapy in Patients with Metastatic Castration Resistant Prostate Cancer, *J. Urol.*, 2016, **196**, 382–391.
- 333 H. Rathke, P. Flechsig, W. Mier, M. Bronzel, E. Mavriopoulou, M. Hohenfellner, F. L. Giesel, U. Haberkorn and C. Kratochwil, Dosimetry Estimate and Initial Clinical Experience with  $^{90}\text{Y}$ -PSMA-617, *J. Nucl. Med.*, 2019, **60**, 806–811.

- 334 C. Müller, C. A. Umbricht, N. Gracheva, V. J. Tschan, G. Pellegrini, P. Bernhardt, J. R. Zeevaart, U. Köster, R. Schibli and N. P. van der Meulen, Terbium-161 for PSMA-targeted radionuclide therapy of prostate cancer, *Eur. J. Nucl. Med. Mol. Imaging*, 2019, **46**, 1919–1930.
- 335 A. P. Kiess, I. Minn, G. Vaidyanathan, R. F. Hobbs, A. Josefsson, C. Shen, M. Brummet, Y. Chen, J. Choi, E. Koumarianou, K. Baidoo, M. W. Brechbiel, R. C. Mease, G. Sgouros, M. R. Zalutsky and M. G. Pomper, (2S)-2-(3-(1-Carboxy-5-(4-<sup>211</sup>At-Astatobenzamido)Pentyl)Ureido)-Pentanedioic Acid for PSMA-Targeted -Particle Radiopharmaceutical Therapy, *J. Nucl. Med.*, 2016, **57**, 1569–1575.
- 336 C. Kratochwil, F. Bruchertseifer, F. L. Giesel, M. Weis, F. A. Verburg, F. Mottaghy, K. Kopka, C. Apostolidis, U. Haberkorn and A. Morgenstern, <sup>225</sup>Ac-PSMA-617 for PSMA-Targeted -Radiation Therapy of Metastatic Castration-Resistant Prostate Cancer, *J. Nucl. Med.*, 2016, **57**, 1941–1944.
- 337 M. Sathekge, O. Knoesen, M. Meckel, M. Modiselle, M. Vorster and S. Marx, <sup>213</sup>Bi-PSMA-617 targeted alpha-radionuclide therapy in metastatic castration-resistant prostate cancer, *Eur. J. Nucl. Med. Mol. Imaging*, 2017, **44**, 1099–1100.
- 338 J. Nonnekens, K. L. S. Chatalic, J. D. M. Molkenboer-Kuenen, C. E. M. T. Beerens, F. Bruchertseifer, A. Morgenstern, J. Veldhoven-Zweistra, M. Schottelius, H.-J. Wester, D. C. van Gent, W. M. van Weerden, O. C. Boerman, M. de Jong and S. Heskamp, <sup>213</sup>Bi-Labeled Prostate-Specific Membrane Antigen-Targeting Agents Induce DNA Double-Strand Breaks in Prostate Cancer Xenografts, *Cancer Biother. Radiopharm.*, 2017, **32**, 67–73.
- 339 A. P. Kiess, I. Minn, Y. Chen, R. Hobbs, G. Sgouros, R. C. Mease, M. Pullambhatla, C. J. Shen, C. A. Foss and M. G. Pomper, Auger Radiopharmaceutical Therapy Targeting Prostate-Specific Membrane Antigen, *J. Nucl. Med.*, 2015, **56**, 1401–1407.
- 340 S. Wang, C. Blaha, R. Santos, T. Huynh, T. R. Hayes, D. R. Beckford-Vera, J. E. Blecha, A. S. Hong, M. Fogarty, T. A. Hope, D. R. Raleigh, D. M. Wilson, M. J. Evans, H. F. VanBrocklin, T. Ozawa and R. R. Flavell, Synthesis and Initial Biological Evaluation of Boron-Containing Prostate-Specific Membrane Antigen Ligands for Treatment of Prostate Cancer Using Boron Neutron Capture Therapy, *Mol. Pharm.*, 2019, **16**, 3831–3841.
- 341 S. Boinapally, H.-H. Ahn, B. Cheng, M. Brummet, H. Nam, K. L. Gabrielson, S. R. Banerjee, I. Minn and M. G. Pomper, A prostate-specific membrane antigen (PSMA)-targeted prodrug with a favorable in vivo toxicity profile, *Sci. Rep.*, 2021, **11**, 7114.
- 342 M. J. Morris, J. S. De Bono, K. N. Chi, K. Fizazi, K. Herrmann, K. Rahbar, S. T. Tagawa, L. T. Nordquist, N. Vaishampayan, G. El-Haddad, C. H. Park, T. M. Beer, W. J. Pérez-Contreras, M. Desilvio, E. E. Kpamegan, G. Gericke, R. A. Messmann, B. J. Krause and A. O. Sartor, Phase III study of lutetium-177-PSMA-617 in patients with metastatic castration-resistant prostate cancer (VISION)., *J. Clin. Oncol.*, 2021, **39**, LBA4–LBA4.
- 343 E. Rousseau, J. Lau, H.-T. Kuo, Z. Zhang, H. Merkens, N. Hundal-Jabal, N. Colpo, K.-S. Lin and F. Bénard, Monosodium Glutamate Reduces <sup>68</sup>Ga-PSMA-11 Uptake



- in Salivary Glands and Kidneys in a Preclinical Prostate Cancer Model, *J. Nucl. Med.*, 2018, **59**, 1865–1868.
- 344 B. Yilmaz, S. Nisli, N. Ergul, R. U. Gursu, O. Acikgoz and T. F. Çermik, Effect of External Cooling on  $^{177}\text{Lu}$ -PSMA Uptake by the Parotid Glands, *J. Nucl. Med.*, 2019, **60**, 1388–1393.
- 345 R. P. Bandari, T. L. Carmack, A. Malhotra, L. Watkinson, E. A. Ferguson Cantrell, M. R. Lewis and C. J. Smith, Development of Heterobivalent Theranostic Probes Having High Affinity/Selectivity for the GRPR/PSMA, *J. Med. Chem.*, 2021, acs.jmedchem.0c01785.
- 346 C. Liolios, M. Schäfer, U. Haberkorn, M. Eder and K. Kopka, Novel Bispecific PSMA/GRPr Targeting Radioligands with Optimized Pharmacokinetics for Improved PET Imaging of Prostate Cancer, *Bioconjug. Chem.*, 2016, **27**, 737–751.
- 347 J. M. Kelly, A. Amor-Coarasa, S. Ponnala, A. Nikolopoulou, C. Williams, S. G. DiMagno and J. W. Babich, Albumin-Binding PSMA Ligands: Implications for Expanding the Therapeutic Window, *J. Nucl. Med.*, 2019, **60**, 656–663.
- 348 J. Kelly, A. Amor-Coarasa, S. Ponnala, A. Nikolopoulou, C. Williams, D. Schlyer, Y. Zhao, D. Kim and J. W. Babich, Trifunctional PSMA-targeting constructs for prostate cancer with unprecedented localization to LNCaP tumors, *Eur. J. Nucl. Med. Mol. Imaging*, 2018, **45**, 1841–1851.
- 349 A. A. Wilson, A. Garcia, L. Jin and S. Houle, Radiotracer synthesis from  $[^{11}\text{C}]$ -iodomethane: a remarkably simple captive solvent method, *Nucl. Med. Biol.*, 2000, **27**, 529–532.
- 350 A. A. Wilson, A. Garcia, T. Bell, T. Harris-Brandts and S. Houle, Further progress on a remarkably simple captive solvent method for  $[^{11}\text{C}]$ -methylations, *J. Label. Compd. Radiopharm.*, 2001, **44**, S999–S1001.
- 351 D. M. Jewett, R. L. Ehrenkauf and S. Ram, A captive solvent method for rapid radiosynthesis: Application to the synthesis of  $[1-^{11}\text{C}]$ palmitic acid, *Int. J. Appl. Radiat. Isot.*, 1985, **36**, 672–674.
- 352 F. Zielinski and G. Robinson, Synthesis of high purity  $^{11}\text{C}$  labeled palmitic acid for measurement of regional myocardial perfusion and metabolism, *Int. J. Nucl. Med. Biol.*, 1984, **11**, 121–128.
- 353 D. M. Jewett, T. J. Mangner, G. K. Mulholland, S. A. Toorongian, A. C. Sutorik, G. L. Watkins and M. R. Kilbourn, in *Seventh International Symposium on Radiopharmaceutical Chemistry*, 1988, pp. 476–477.
- 354 D. R. Turton, V. W. Pike, M. Cartoon and D. A. Widdowson, Preparation of a potential marker for glial cells - (N-methyl- $^{11}\text{C}$ )RO5-4864, *J. Label. Compd. Radiopharm.*, 1984, **21**, 1209–1210.
- 355 D. M. Jewett, T. J. Mangner and G. L. Watkins, in *New Trends in Radiopharmaceutical Synthesis, Quality Assurance, and Regulatory Control*, Springer US, Boston, MA, 1991, pp. 387–391.
- 356 R. Iwata, C. Pascali, M. Yuasa, K. Yanai, T. Takahashi and T. Ido, On-line  $[^{11}\text{C}]$ methylation using  $[^{11}\text{C}]$ methyl iodide for the automated preparation of  $^{11}\text{C}$ -radiopharmaceuticals, *Int. J. Radiat. Appl. Instrumentation. Part.*, 1992, **43**, 1083–

- 1088.
- 357 C. Pascali, R. Iwata and T. Ido, Comparative study on the influence of bases on (3-N-[ $^{11}\text{C}$ ]methyl)spiperone synthesis, *Int. J. Radiat. Appl. Instrumentation. Part A. Appl. Radiat. Isot.*, 1992, **43**, 1526–1528.
- 358 G. Leonard Watkins, D. M. Jewett, G. Keith Mulholland, M. R. Kilbourn and S. A. Toorongian, A captive solvent method for rapid N-[ $^{11}\text{C}$ ]methylation of secondary amides: Application to the benzodiazepine, 4'-chlorodiazepam (RO5-4864), *Int. J. Radiat. Appl. Instrumentation. Part A. Appl. Radiat. Isot.*, 1988, **39**, 441–444.
- 359 K.-I. Mizuno, S. Yamazaki, R. Iwata, C. Pascali and T. Ido, Improved preparation of L-[Methyl- $^{11}\text{C}$ ]methionine by on-line [ $^{11}\text{C}$ ]methylation, *Appl. Radiat. Isot.*, 1993, **44**, 788–790.
- 360 R. Iwata, T. Ido and M. Tada, Column extraction method for rapid preparation of [ $^{11}\text{C}$ ]acetic and [ $^{11}\text{C}$ ]palmitic acids, *Appl. Radiat. Isot.*, 1995, **46**, 117–121.
- 361 J. A. McCarron, D. R. Turton, V. W. Pike and K. G. Poole, Remotely-controlled production of the 5-HT<sub>1A</sub> receptor radioligand, [carbonyl- $^{11}\text{C}$ ]WAY-100635, via  $^{11}\text{C}$ -carboxylation of an immobilized Grignard reagent, *J. Label. Compd. Radiopharm.*, 1996, **38**, 941–953.
- 362 R. J. Davenport, V. W. Pike, K. Dowsett, D. R. Turton and K. Poole, Automated chemoenzymatic synthesis of no-carrier-added [carbonyl- $^{11}\text{C}$ ]propionyl L-carnitine for pharmacokinetic studies, *Appl. Radiat. Isot.*, 1997, **48**, 917–924.
- 363 R. J. Davenport, K. Dowsett and V. W. Pike, A simple technique for the automated production of no-carrier-added [1- $^{11}\text{C}$ ]acetate, *Appl. Radiat. Isot.*, 1997, **48**, 1117–1120.
- 364 R. J. Davenport, J. A. McCarron, K. Dowsett, D. R. Turton, K. G. Poole and V. W. Pike, A Simply Automated Process for  $^{11}\text{C}$ -Carboxylation Reactions Leading to  $^{11}\text{C}$ -Labelled Radiopharmaceuticals in High Specific Radioactivity, *J. Label. Compd. Radiopharm.*, 1997, **40**, 309–311.
- 365 D. Soloviev and C. Tamburella, Captive solvent [ $^{11}\text{C}$ ]acetate synthesis in GMP conditions, *Appl. Radiat. Isot.*, 2006, **64**, 995–1000.
- 366 D. Le Bars, M. Malleval, F. Bonnefoi and C. Tourvieille, Simple synthesis of [1- $^{11}\text{C}$ ]acetate, *J. Label. Compd. Radiopharm.*, 2006, **49**, 263–267.
- 367 A. Maurer, G. Bowden, J. Cotton, C. Parl, M. A. Krueger and B. J. Pichler, Acetuino—A Handy Open-Source Radiochemistry Module for the Preparation of [1- $^{11}\text{C}$ ]Acetate, *SLAS Technol. Transl. Life Sci. Innov.*, 2019, **24**, 321–329.
- 368 A. A. Wilson, J. N. DaSilva and S. Houle, Solid-phase radiosynthesis of [ $^{11}\text{C}$ ]WAY 100635, *J. Label. Compd. Radiopharm.*, 1996, **38**, 149–154.
- 369 C. Pascali, A. Bogni, R. Iwata, D. Decise, F. Crippa and E. Bombardieri, High efficiency preparation of L-[S-methyl- $^{11}\text{C}$ ]methionine by on-column [ $^{11}\text{C}$ ]methylation on C18 Sep-Pak, *J. Label. Compd. Radiopharm.*, 1999, **42**, 715–724.
- 370 C. Pascali, A. Bogni, R. Itawa, M. Cambi and E. Bombardieri, [ $^{11}\text{C}$ ]Methylation

- on a C18 Sep-Pak cartridge: a convenient way to produce [N-methyl-<sup>11</sup>C]choline, *J. Label. Compd. Radiopharm.*, 2000, **43**, 195–203.
- 371 J. P. Holland, Chemical Kinetics of Radiolabelling Reactions, *Chem. - A Eur. J.*, 2018, **24**, 16472–16483.
- 372 E. Yildiz-Ozturk and O. Yesil-Celiktas, Diffusion phenomena of cells and biomolecules in microfluidic devices, *Biomicrofluidics*, 2015, **9**, 052606.
- 373 J. Pihl, M. Karlsson and D. T. Chiu, Microfluidic technologies in drug discovery, *Drug Discov. Today*, 2005, **10**, 1377–1383.
- 374 P. Y. Keng, M. Sergeev and R. M. van Dam, in *Perspectives on Nuclear Medicine for Molecular Diagnosis and Integrated Therapy*, Springer Japan, Tokyo, 2016, pp. 93–111.
- 375 P. J. H. Scott, B. G. Hockley, H. F. Kung, R. Manchanda, W. Zhang and M. R. Kilbourn, Studies into radiolytic decomposition of fluorine-18 labeled radiopharmaceuticals for positron emission tomography., *Appl. Radiat. Isot.*, 2009, **67**, 88–94.
- 376 C. Rensch, B. Waengler, A. Yaroshenko, V. Samper, M. Baller, N. Heumesser, J. Ulin, S. Riese and G. Reischl, Microfluidic reactor geometries for radiolysis reduction in radiopharmaceuticals, *Appl. Radiat. Isot.*, 2012, **70**, 1691–1697.
- 377 A. R. Studenov, S. Jivan, M. J. Adam, T. J. Ruth and K. R. Buckley, Studies of the mechanism of the in-loop synthesis of radiopharmaceuticals, *Appl. Radiat. Isot.*, 2004, **61**, 1195–1201.
- 378 G. Reischl, C. Bieg, O. Schmiedl, C. Solbach and H.-J. Machulla, Highly efficient automated synthesis of [<sup>11</sup>C]choline for multi dose utilization, *Appl. Radiat. Isot.*, 2004, **60**, 835–838.
- 379 S. N. Reske, N. M. Blumstein, B. Neumaier, H.-W. Gottfried, F. Finsterbusch, D. Kocot, P. Möller, G. Glatting and S. Perner, Imaging prostate cancer with <sup>11</sup>C-choline PET/CT., *J. Nucl. Med.*, 2006, **47**, 1249–54.
- 380 V. Gómez, J. D. Gispert, V. Amador and J. Llop, New method for routine production of L-[methyl-<sup>11</sup>C]methionine:in loop synthesis, *J. Label. Compd. Radiopharm.*, 2008, **51**, 83–86.
- 381 M. N. Stewart, M. F. L. Parker, S. Jivan, J. M. Luu, T. L. Huynh, B. Schulte, Y. Seo, J. E. Blecha, J. E. Villanueva-Meyer, R. R. Flavell, H. F. VanBrocklin, M. A. Ohliger, O. Rosenberg and D. M. Wilson, High Enantiomeric Excess In-Loop Synthesis of d-[methyl-<sup>11</sup>C]Methionine for Use as a Diagnostic Positron Emission Tomography Radiotracer in Bacterial Infection, *ACS Infect. Dis.*, 2020, **6**, 43–49.
- 382 A. R. Studenov, S. Jivan, K. R. Buckley and M. J. Adam, Efficient in-loop synthesis of high specific radioactivity [<sup>11</sup>C]carfentanil, *J. Label. Compd. Radiopharm.*, 2003, **46**, 837–842.
- 383 X. Shao and M. R. Kilbourn, A simple modification of GE tracerlab FX C Pro for rapid sequential preparation of [<sup>11</sup>C]carfentanil and [<sup>11</sup>C]raclopride, *Appl. Radiat. Isot.*, 2009, **67**, 602–605.
- 384 R. Iwata, C. Pascali, A. Bogoni, K. Yanai, M. Kato, T. Ido and K. Ishiwata,

- Preparation of [ $^{11}\text{C}$ ]doxepin from [ $^{11}\text{C}$ ]methyl triflate by loop method: Effect of specific activity on [ $^{11}\text{C}$ ]methylation, *J. Label. Compd. Radiopharm.*, 2001, **44**, S986–S988.
- 385 R. Iwata, C. Pascali, A. Bogni, K. Yanai, M. Kato, T. Ido and K. Ishiwata, A combined loop-SPE method for the automated preparation of [ $^{11}\text{C}$ ]doxepin, *J. Label. Compd. Radiopharm.*, 2002, **45**, 271–280.
- 386 A. A. Wilson, A. Garcia, A. Chestakova, H. Kung and S. Houle, A rapid one-step radiosynthesis of the  $\beta$ -amyloid imaging radiotracer N-methyl-[ $^{11}\text{C}$ ]2-(4'-methylaminophenyl)-6-hydroxybenzothiazole ([ $^{11}\text{C}$ ]-6-OH-BTA-1), *J. Label. Compd. Radiopharm.*, 2004, **47**, 679–682.
- 387 M. Verdurand, G. Bort, V. Tadino, F. Bonnefoi, D. Le Bars and L. Zimmer, Automated radiosynthesis of the Pittsburg compound-B using a commercial synthesizer., *Nucl. Med. Commun.*, 2008, **29**, 920–6.
- 388 M. Cheung and C. Ho, A simple, versatile, low-cost and remotely operated apparatus for [ $^{11}\text{C}$ ]acetate, [ $^{11}\text{C}$ ]choline, [ $^{11}\text{C}$ ]methionine and [ $^{11}\text{C}$ ]PIB synthesis, *Appl. Radiat. Isot.*, 2009, **67**, 581–589.
- 389 N. Vasdev, A. Garcia, W. T. Stableford, A. B. Young, J. H. Meyer, S. Houle and A. A. Wilson, Synthesis and ex vivo evaluation of carbon-11 labelled N-(4-methoxybenzyl)-N'-(5-nitro-1,3-thiazol-2-yl)urea ([ $^{11}\text{C}$ ]AR-A014418): A radiolabelled glycogen synthase kinase-3 $\beta$  specific inhibitor for PET studies, *Bioorg. Med. Chem. Lett.*, 2005, **15**, 5270–5273.
- 390 N. Nabulsi, Y. Huang, D. Weinzimmer, J. Ropchan, J. J. Frost, T. McCarthy, R. E. Carson and Y.-S. Ding, High-resolution imaging of brain 5-HT 1B receptors in the rhesus monkey using [ $^{11}\text{C}$ ]P943., *Nucl. Med. Biol.*, 2010, **37**, 205–14.
- 391 A. Ghosh, K. Woolum, M. V. Knopp and K. Kumar, Development and optimization of a novel automated loop method for production of [ $^{11}\text{C}$ ]nicotine, *Appl. Radiat. Isot.*, 2018, **140**, 76–82.
- 392 D. P. Holt, A. S. Kalinda, L. E. Bambarger, S. K. Jain and R. F. Dannals, Radiosynthesis and validation of [Carboxy- $^{11}\text{C}$ ]4-Aminobenzoic acid ([ $^{11}\text{C}$ ]PABA), a PET radiotracer for imaging bacterial infections, *J. Label. Compd. Radiopharm.*, 2019, **62**, 28–33.
- 393 M. D. Moran, A. A. Wilson, W. T. Stableford, M. Wong, A. Garcia, S. Houle and N. Vasdev, A rapid one-step radiosynthesis of [ $^{11}\text{C}$ ]-d-threo-methylphenidate, *J. Label. Compd. Radiopharm.*, 2011, **54**, 168–170.
- 394 R. Iwata, C. Pascali, A. Bogni, Y. Miyake, K. Yanai and T. Ido, A simple loop method for the automated preparation of [ $^{11}\text{C}$ ]raclopride from [ $^{11}\text{C}$ ]methyl triflate, *Appl. Radiat. Isot.*, 2001, **55**, 17–22.
- 395 M. Ono, A. Wilson, J. Nobrega, D. Westaway, P. Verhoeff, Z.-P. Zhuang, M.-P. Kung and H. F. Kung,  $^{11}\text{C}$ -labeled stilbene derivatives as Abeta-aggregate-specific PET imaging agents for Alzheimer's disease., *Nucl. Med. Biol.*, 2003, **30**, 565–71.
- 396 D. P. Holt, H. T. Ravert, R. F. Dannals and M. G. Pomper, Synthesis of [ $^{11}\text{C}$ ]gefitinib for imaging epidermal growth factor receptor tyrosine kinase with positron emission tomography, *J. Label. Compd. Radiopharm.*, 2006, **49**, 883–888.

- 397 M.-R. Zhang, M. Ogawa, Y. Yoshida and K. Suzuki, Selective synthesis of [2-<sup>11</sup>C]2-iodopropane and [1-<sup>11</sup>C]iodoethane using the loop method by reacting methylmagnesium bromide with [<sup>11</sup>C]carbon dioxide, *Appl. Radiat. Isot.*, 2006, **64**, 216–222.
- 398 T. Arai, M.-R. Zhang, M. Ogawa, T. Fukumura, K. Kato and K. Suzuki, Efficient and reproducible synthesis of [1-<sup>11</sup>C]acetyl chloride using the loop method, *Appl. Radiat. Isot.*, 2009, **67**, 296–300.
- 399 C. Rami-Mark, J. Ungersboeck, D. Haeusler, L. Nics, C. Philippe, M. Mitterhauser, M. Willeit, R. Lanzenberger, G. Karanikas and W. Wadsak, Reliable set-up for in-loop <sup>11</sup>C-carboxylations using Grignard reactions for the preparation of [carbonyl-<sup>11</sup>C]WAY-100635 and [<sup>11</sup>C]-(+)-PHNO, *Appl. Radiat. Isot.*, 2013, **82**, 75–80.
- 400 US61 US6749830B2, 2002.749830B2, 2002.
- 401 A. A. Wilson, A. Garcia, S. Houle and N. Vasdev, Utility of commercial radiosynthetic modules in captive solvent [<sup>11</sup>C]-methylation reactions, *J. Label. Compd. Radiopharm.*, 2009, **52**, 490–492.
- 402 X. Shao, R. Hoareau, A. C. Runkle, L. J. M. Tluczek, B. G. Hockley, B. D. Henderson and P. J. H. Scott, Highlighting the versatility of the Tracerlab synthesis modules. Part 2: fully automated production of [<sup>11</sup>C]-labeled radiopharmaceuticals using a Tracerlab FXC-Pro, *J. Label. Compd. Radiopharm.*, 2011, **54**, 819–838.
- 403 X. Shao, P. L. Schnau, M. V. Fawaz and P. J. H. Scott, Enhanced radiosyntheses of [<sup>11</sup>C]raclopride and [<sup>11</sup>C]DASB using ethanolic loop chemistry, *Nucl. Med. Biol.*, 2013, **40**, 109–116.
- 404 J. Downey, S. Bongarzone, S. Hader and A. D. Gee, In-loop flow [<sup>11</sup>C]CO<sub>2</sub> fixation and radiosynthesis of *N,N'*-[<sup>11</sup>C]dibenzylurea, *J. Label. Compd. Radiopharm.*, 2018, **61**, 263–271.
- 405 K. Dahl, T. L. Collier, R. Cheng, X. Zhang, O. Sadovski, S. H. Liang and N. Vasdev, “In-loop” [<sup>11</sup>C]CO<sub>2</sub> fixation: Prototype and proof of concept, *J. Label. Compd. Radiopharm.*, 2018, **61**, 252–262.
- 406 M. H. Dornan, D. Petrenyov, J.-M. Simard, M. Boudjemeline, R. Mititelu, J. N. DaSilva and A. P. Belanger, Synthesis of a <sup>11</sup>C-Isotopologue of the B-Raf-Selective Inhibitor Encorafenib Using In-Loop [<sup>11</sup>C]CO<sub>2</sub> Fixation, *ACS Omega*, 2020, **5**, 20960–20966.
- 407 PMB, iMiLAB Radiochemistry | iMiGiNE personalized molecular imaging, <https://www.imagine.com/en/products/imilab-radiochemistry>, (accessed 9 October 2020).
- 408 G. Wu, M. Zhai and M. Wang, *Radiation technology for advanced materials: From basic to modern applications*, 2018.
- 409 S. Lee, J.-S. Park and T. R. Lee, The Wettability of Fluoropolymer Surfaces: Influence of Surface Dipoles, *Langmuir*, 2008, **24**, 4817–4826.
- 410 A. L. Ethier, J. R. Switzer, A. C. Rumble, W. Medina-Ramos, Z. Li, J. Fisk, B. Holden, L. Gelbaum, P. Pollet, C. A. Eckert and C. L. Liotta, The Effects of Solvent and Added Bases on the Protection of Benzylamines with Carbon Dioxide,

- Processes*, 2015, **3**, 497–513.
- 411 W. D. McGhee, D. P. Riley, M. E. Christ and K. M. Christ, Palladium-catalyzed generation of O-allylic urethanes and carbonates from amines/alcohols, carbon dioxide, and allylic chlorides, *Organometallics*, 1993, **12**, 1429–1433.
- 412 W. McGhee, D. Riley, K. Christ, Y. Pan and B. Parnas, Carbon Dioxide as a Phosgene Replacement: Synthesis and Mechanistic Studies of Urethanes from Amines, CO<sub>2</sub>, and Alkyl Chlorides, *J. Org. Chem.*, 1995, **60**, 2820–2830.
- 413 W. D. McGhee, Y. Pan and J. J. Talley, Conversion of amines to carbamoyl chlorides using carbon dioxide as a phosgene replacement, *Tetrahedron Lett.*, 1994, **35**, 839–842.
- 414 A. L. Ethier, J. R. Switzer, A. C. Rumpel, W. Medina-Ramos, Z. Li, J. Fisk, B. Holden, L. Gelbaum, P. Pollet, C. A. Eckert and C. L. Liotta, The effects of solvent and added bases on the protection of benzylamines with carbon dioxide, *Processes*, 2015, **3**, 497–513.
- 415 J. M. Hooker, A. T. Reibel, S. M. Hill, M. J. Schueller and J. S. Fowler, One-pot, direct incorporation of [<sup>13</sup>C]CO<sub>2</sub> into carbamates, *Angew. Chemie - Int. Ed.*, 2009, **48**, 3482–3485.
- 416 G. F. Hewitt and N. S. Hall-Taylor, *Annular Two-phase Flow*, Elsevier, 1st edn., 1970.
- 417 Sudarja, F. Jayadi, Indarto, Deendarlianto and A. Widyaparaga, in *AIP Conference Proceedings*, American Institute of Physics Inc., 2018, vol. 2001, p. 030010.
- 418 Y. A. Zeigarnik, in *A-to-Z Guide to Thermodynamics, Heat and Mass Transfer, and Fluids Engineering*, Begellhouse, 2006.
- 419 R. W. Lockhart and R. C. Martinelli, Proposed correlation of data for isothermal two-phase, two-component flow in pipes, *Chem. Eng. Prog.*, 1949, **45**, 39–48.
- 420 G. F. Hewitt, in *A-to-Z Guide to Thermodynamics, Heat and Mass Transfer, and Fluids Engineering*, Begellhouse, 2006.
- 421 D. Butterworth, A comparison of some void-fraction relationships for co-current gas-liquid flow, *Int. J. Multiph. Flow*, 1975, **1**, 845–850.
- 422 E. X. Barreto, J. L. G. Oliveira and J. C. Passos, Frictional pressure drop and void fraction analysis in air–water two-phase flow in a microchannel, *Int. J. Multiph. Flow*, 2015, **72**, 1–10.
- 423 CHERIC, CHERIC: Chemical Engineering and Materials Research Information Center, Pure Component Properties, Acetonitrile, <https://www.cheric.org/research/kdb/hcprop/showcoef.php?cmpid=1386&prop=VSL>, (accessed 14 June 2017).
- 424 W. L. Weng, L. T. Chang and I. M. Shiah, Viscosities and densities for binary mixtures of benzylamine with 1-pentanol, 2-pentanol, 2-methyl-1-butanol, 2-methyl-2-butanol, 3-methyl-1-butanol, and 3-methyl-2-butanol, *J. Chem. Eng. Data*, 1999, **44**, 994–997.
- 425 Fisher Scientific, DBU MSDS, Fisher Scientific, <https://www.fishersci.com/shop/msdsproxy?productName=AC160610025&prod>

- uctDescription=1+8-DIAZABICYCLO+5.4.0+U+2.5KG&catNo=AC160610025&vendorId=VN00032119&storeId=10652, (accessed 14 June 2017).
- 426 B. J. Kirby, *Micro- and Nanoscale Fluid Mechanics: Transport in Microfluidic Devices*, Cambridge University Press, 1st edn., 2010.
- 427 T. D. J. D'Silva, A. Lopes, R. L. Jones, S. Singhawangcha and J. K. Chan, Studies of methyl isocyanate chemistry in the Bhopal incident, *J. Org. Chem.*, 1986, **51**, 3781–3788.
- 428 S. C. van der Slot, P. C. J. Kamer, P. W. N. M. van Leeuwen, J. Fraanje, K. Goubitz, M. Lutz and A. L. Spek, Rhodium Complexes Based on Phosphorus Diamide Ligands: Catalyst Structure versus Activity and Selectivity in the Hydroformylation of Alkenes, *Organometallics*, 2000, **19**, 2504–2515.
- 429 Y. Chokki and K. Fujinami, NMR Spectra of Aralkyl and Aliphatic Isocyanate Derivatives, *Nippon Kagaku Kaishi*, 1974, 2407–2413.
- 430 A. W. Johnson, in *Ylid Chemistry*, Elsevier Organic Chemistry, 1966, pp. 132–192.
- 431 N. R. McElroy, P. C. Jurs, C. Morisseau and B. D. Hammock, QSAR and classification of murine and human soluble epoxide hydrolase inhibition by urea-like compounds, *J. Med. Chem.*, 2003, **46**, 1066–1080.
- 432 T. Kanzian, T. A. Nigst, A. Maier, S. Pichl and H. Mayr, Nucleophilic reactivities of primary and secondary amines in acetonitrile, *European J. Org. Chem.*, 2009, **2009**, 6379–6385.
- 433 A. A. Wilson, A. Garcia, S. Houle, O. Sadovski and N. Vasdev, Synthesis and Application of Isocyanates Radiolabeled with Carbon-11, *Chem. - A Eur. J.*, 2011, **17**, 259–264.
- 434 F. L. Coelho and L. F. Campo, Synthesis of 2-arylbenzothiazoles via direct condensation between in situ generated 2-aminothiophenol from disulfide cleavage and carboxylic acids, *Tetrahedron Lett.*, 2017, **58**, 2330–2333.
- 435 A. A. Wilson, A. Garcia, S. Houle and N. Vasdev, Direct fixation of [<sup>11</sup>C]-CO<sub>2</sub> by amines: formation of [<sup>11</sup>C-carbonyl]-methylcarbamates, *Org. Biomol. Chem.*, 2010, **8**, 428–432.
- 436 M.-A. Courtemanche, M.-A. Légaré, É. Rochette and F.-G. Fontaine, Phosphazenes: efficient organocatalysts for the catalytic hydrosilylation of carbon dioxide, *Chem. Commun.*, 2015, **51**, 6858–6861.
- 437 B. Långström, O. Itsenko and O. Rahman, [<sup>11</sup>C]Carbon monoxide, a versatile and useful precursor in labelling chemistry for PET-ligand development, *J. Label. Compd. Radiopharm.*, 2007, **50**, 794–810.
- 438 P. W. Miller, N. J. Long, A. J. De Mello, R. Vilar, J. Passchier and A. Gee, Rapid formation of amides via carbonylative coupling reactions using a microfluidic device, *Chem. Commun.*, 2006, 546–548.
- 439 A. Pees, C. Sewing, M. J. W. D. Vosjan, V. Tadino, J. D. M. Herscheid, A. D. Windhorst and D. J. Vugts, Fast and reliable generation of [<sup>18</sup>F]triflyl fluoride, a

- gaseous [ $^{18}\text{F}$ ]fluoride source, *Chem. Commun.*, 2018, **54**, 10179–10182.
- 440 K. Dahl, A. Garcia, N. A. Stephenson and N. Vasdev, “In-loop”  $^{18}\text{F}$ -fluorination: A proof-of-concept study, *J. Label. Compd. Radiopharm.*, 2019, **62**, 292–297.
- 441 A. A. Wilson, A. Garcia, L. Jin and S. Houle, Radiotracer synthesis from [ $^{11}\text{C}$ ]-iodomethane: A remarkably simple captive solvent method, *Nucl. Med. Biol.*, 2000, **27**, 529–532.
- 442 J. Zhou, J. H. Neale, M. G. Pomper and A. P. Kozikowski, NAAG peptidase inhibitors and their potential for diagnosis and therapy., *Nat. Rev. Drug Discov.*, 2005, **4**, 1015–26.
- 443 M. Benešová, U. Bauder-Wüst, M. Schäfer, K. D. Klika, W. Mier, U. Haberkorn, K. Kopka and M. Eder, Linker Modification Strategies To Control the Prostate-Specific Membrane Antigen (PSMA)-Targeting and Pharmacokinetic Properties of DOTA-Conjugated PSMA Inhibitors, *J. Med. Chem.*, 2016, **59**, 1761–1775.
- 444 H. Wang, Y. Byun, C. Barinka, M. Pullambhatla, H. C. Bhang, J. J. Fox, J. Lubkowski, R. C. Mease and M. G. Pomper, Bioisosterism of urea-based GCPII inhibitors: Synthesis and structure–activity relationship studies, *Bioorg. Med. Chem. Lett.*, 2010, **20**, 392–397.
- 445 P. G. M. Wuts and T. W. Greene, *Greene’s Protective Groups in Organic Synthesis*, John Wiley & Sons, Inc., Hoboken, NJ, USA, 2006.
- 446 W. F. Diller and M. Habil, Medical Phosgene Problems and Their Possible Solution, *J. Occup. Environ. Med.*, 1978, **20**, 189–193.
- 447 H. Eckert and B. Forster, Triphosgene, a Crystalline Phosgene Substitute, *Angew. Chemie Int. Ed. English*, 1987, **26**, 894–895.
- 448 J. H. Tsai, L. R. Takaoka, N. A. Powell and J. S. Nowick, Synthesis of amino acid ester isocyanates: methyl-(s)-2-isocyanato-3-phenylpropanoate, *Org. Synth.*, 2002, **78**, 220.
- 449 S. R. Banerjee, C. A. Foss, M. Castanares, R. C. Mease, Y. Byun, J. J. Fox, J. Hilton, S. E. Lupold, A. P. Kozikowski and M. G. Pomper, Synthesis and evaluation of technetium-99m- and rhenium-labeled inhibitors of the prostate-specific membrane antigen (PSMA)., *J. Med. Chem.*, 2008, **51**, 4504–17.
- 450 J. D. Young, V. Abbate, C. Imberti, L. K. Meszaros, M. T. Ma, S. Y. A. Terry, R. C. Hider, G. E. Mullen and P. J. Blower,  $^{68}\text{Ga}$ -THP-PSMA: A PET Imaging Agent for Prostate Cancer Offering Rapid, Room-Temperature, 1-Step Kit-Based Radiolabeling, *J. Nucl. Med.*, 2017, **58**, 1270–1277.
- 451 M. Paugam, Phosgene-triphosgene: Different approach in risk management?, *Chim. Oggi - Chem. Today*, 2011, **29**, 58–60.
- 452 L. Cotarca, T. Geller and J. Répási, Bis(trichloromethyl)carbonate (BTC, Triphosgene): A Safer Alternative to Phosgene?, *Org. Process Res. Dev.*, 2017, **21**, 1439–1446.
- 453 J. Kelly, A. Amor-Coarasa, A. Nikolopoulou, D. Kim, C. Williams, S. Ponnala and J. W. Babich, Synthesis and pre-clinical evaluation of a new class of high-affinity  $^{18}\text{F}$ -labeled PSMA ligands for detection of prostate cancer by PET imaging, *Eur.*



- J. Nucl. Med. Mol. Imaging*, 2017, **44**, 647–661.
- 454 S. L. Peterson, S. M. Stucka and C. J. Dinsmore, Parallel synthesis of ureas and carbamates from amines and CO<sub>2</sub> under mild conditions., *Org. Lett.*, 2010, **12**, 1340–3.
- 455 R. W. Alder, J. G. E. Phillips, L. Huang and X. Huang, in *Encyclopedia of Reagents for Organic Synthesis*, John Wiley & Sons, Ltd, Chichester, UK, 2005.
- 456 S. Hartwig, J. Schwarz and S. Hecht, From Peptides to Their Alternating Ester-Urea Analogues: Synthesis and Influence of Hydrogen Bonding Motif and Stereochemistry on Aggregation, *J. Org. Chem.*, 2010, **75**, 772–782.
- 457 M. Frizler, F. Lohr, N. Furtmann, J. Kläs and M. Gütschow, Structural Optimization of Azadipeptide Nitriles Strongly Increases Association Rates and Allows the Development of Selective Cathepsin Inhibitors, *J. Med. Chem.*, 2011, **54**, 396–400.
- 458 K. F. Eidman and P. J. Nichols, in *Encyclopedia of Reagents for Organic Synthesis*, John Wiley & Sons, Ltd, Chichester, UK, 2006.
- 459 B. F. Lundt, N. L. Johansen, A. Vølund and J. Markussen, REMOVAL OF t-BUTYL AND t-BUTOXYCARBONYL PROTECTING GROUPS WITH TRIFLUOROACETIC ACID, *Int. J. Pept. Protein Res.*, 1978, **12**, 258–268.
- 460 S. E. BLONDELLE and R. A. HOUGHTEN, Comparison of 55% TFA/CH<sub>2</sub>Cl<sub>2</sub> and 100% TFA for Boc group removal during solid-phase peptide synthesis, *Int. J. Pept. Protein Res.*, 1993, **41**, 522–527.
- 461 P. Zajdel, C. Enjalbal, M. Żylewski and G. Subra, On the Manner of Cyclization of N-Acylated Aspartic and Glutamic Acid Derivatives, *Int. J. Pept. Res. Ther.*, 2011, **17**, 93–100.
- 462 L. M. Bersin, S. M. Patel and E. M. Topp, Effect of ‘pH’ on the Rate of Pyroglutamate Formation in Solution and Lyophilized Solids, *Mol. Pharm.*, 2021, **18**, 3116–3124.
- 463 S. Schilling, C. Wasternack and H.-U. Demuth, Glutaminyl cyclases from animals and plants: a case of functionally convergent protein evolution, *Biol. Chem.*, , DOI:10.1515/BC.2008.111.
- 464 J. M. Alvarez-Gutierrez, A. Nefzi and R. A. Houghten, Solid phase synthesis of 1-substituted pyroglutamates, *Tetrahedron Lett.*, 2000, **41**, 851–854.
- 465 N. L. Benoiton, *Chemistry of Peptide Synthesis*, CRC Press, Boca Raton, 1st edn., 2005.
- 466 Y. D. Liu, A. M. Goetze, R. B. Bass and G. C. Flynn, N-terminal Glutamate to Pyroglutamate Conversion in Vivo for Human IgG2 Antibodies, *J. Biol. Chem.*, 2011, **286**, 11211–11217.
- 467 H. Awad, M. M. Khamis and A. El-Aneed, Mass Spectrometry, Review of the Basics: Ionization, *Appl. Spectrosc. Rev.*, 2015, **50**, 158–175.
- 468 G. A. Nagana Gowda, Y. N. Gowda and D. Raftery, Massive Glutamine Cyclization to Pyroglutamic Acid in Human Serum Discovered Using NMR Spectroscopy, *Anal. Chem.*, 2015, **87**, 3800–3805.

- 469 A. Hinterholzer, V. Stanojlovic, C. Cabrele and M. Schubert, Unambiguous Identification of Pyroglutamate in Full-Length Biopharmaceutical Monoclonal Antibodies by NMR Spectroscopy, *Anal. Chem.*, 2019, **91**, 14299–14305.
- 470 D. Satpati, Recent Breakthrough in  $^{68}\text{Ga}$ -Radiopharmaceuticals Cold Kits for Convenient PET Radiopharmacy, *Bioconjug. Chem.*, 2021, **32**, 430–447.
- 471 M. Beheshti, Z. Paymani, J. Brillhante, H. Geinitz, D. Gehring, T. Leopoldseder, L. Wouters, C. Pirich, W. Loidl and W. Langsteger, Optimal time-point for  $^{68}\text{Ga}$ -PSMA-11 PET/CT imaging in assessment of prostate cancer: feasibility of sterile cold-kit tracer preparation?, *Eur. J. Nucl. Med. Mol. Imaging*, 2018, **45**, 1188–1196.
- 472 T. Ebenhan, M. Vorster, B. Marjanovic-Painter, J. Wagener, J. Suthiram, M. Modiselle, B. Mokaleng, J. Zeevaart and M. Sathekge, Development of a Single Vial Kit Solution for Radiolabeling of  $^{68}\text{Ga}$ -DKFZ-PSMA-11 and Its Performance in Prostate Cancer Patients, *Molecules*, 2015, **20**, 14860–14878.
- 473 H. Golan, M. Esa, K. Moshkoviz, A. Feldhaim, B. Hoch and E. Shalom, Enhancing capacity and synthesis of [ $^{68}\text{Ga}$ ]68-Ga-PSMA-HBED-CC with the lyophilized ready-to-use kit for nuclear pharmacy applications, *Nucl. Med. Commun.*, 2020, **41**, 986–990.
- 474 S. Chakraborty, K. V. Vimalnath, R. Chakravarty, H. D. Sarma and A. Dash, Multidose formulation of ready-to-use  $^{177}\text{Lu}$ -PSMA-617 in a centralized radiopharmacy set-up, *Appl. Radiat. Isot.*, 2018, **139**, 91–97.
- 475 M. Yang, H. Gao, X. Sun, Y. Yan, Q. Quan, W. Zhang, K. A. Mohamedali, M. G. Rosenblum, G. Niu and X. Chen, Multiplexed PET Probes for Imaging Breast Cancer Early Response to VEGF 121 /rGel Treatment, *Mol. Pharm.*, 2011, **8**, 621–628.
- 476 N. Regula, V. Kostaras, S. Johansson, C. Trampal, E. Lindström, M. Lubberink, I. Velikyan and J. Sörensen, Comparison of  $^{68}\text{Ga}$ -PSMA-11 PET/CT with  $^{11}\text{C}$ -acetate PET/CT in re-staging of prostate cancer relapse, *Sci. Rep.*, 2020, **10**, 4993.
- 477 C. Brogsitter, K. Zöphel and J. Kotzerke,  $^{18}\text{F}$ -Choline,  $^{11}\text{C}$ -choline and  $^{11}\text{C}$ -acetate PET/CT: comparative analysis for imaging prostate cancer patients, *Eur. J. Nucl. Med. Mol. Imaging*, 2013, **40**, 18–27.
- 478 X. Subirats, M. H. Abraham and M. Rosés, Characterization of hydrophilic interaction liquid chromatography retention by a linear free energy relationship. Comparison to reversed- and normal-phase retentions, *Anal. Chim. Acta*, 2019, **1092**, 132–143.
- 479 M. Adib, E. Sheikhi and A. Deljoush, Reaction between triphenylphosphine and aromatic amines in the presence of diethyl azodicarboxylate: an efficient synthesis of aryliminophosphoranes under neutral and mild conditions, *Tetrahedron*, 2011, **67**, 4137–4140.
- 480 G. S. Chen, C. Chen, T. Chien, J. Yeh, C. Kuo, R. S. Talekar and J. Chern, Nucleosides. IX. Synthesis of Purine N 3 ,5'-Cyclonucleosides and N 3 ,5'-Cyclo-2',3'-seconucleosides via Mitsunobu Reaction as TIBO-like Derivatives, *Nucleosides. Nucleotides Nucleic Acids*, 2004, **23**, 347–359.

- 481 N. S. Habib and A. Rieker, A Convenient Method for the Synthesis of Sterically Hindered Aryl Isocyanates, *Zeitschrift für Naturforsch. B*, 1984, **39**, 1593–1597.
- 482 T. H. Walter, P. Iraneta and M. Capparella, Mechanism of retention loss when C8 and C18 HPLC columns are used with highly aqueous mobile phases, *J. Chromatogr. A*, 2005, **1075**, 177–183.
- 483 M. C. García-Alvarez-Coque, J. J. Baeza-Baeza and G. Ramis-Ramos, in *Analytical Separation Science*, eds. J. L. Anderson, A. Berthod, V. Pino and A. M. Stalcup, Wiley-VCH Verlag GmbH & Co. KGaA, Weinheim, Germany, 1st edn., 2015, pp. 159–198.
- 484 N. Nagae, T. Enami and S. Doshi, The retention behavior of reversed-phase HPLC columns with 100% aqueous mobile phase, *LCGC North Am.*, 2002, **20**, 964–972.
- 485 M. Przybyciel and R. E. Majors, Phase collapse in reversed-phase liquid chromatography, *LCGC North Am.*, 2002, **20**, 516–523.
- 486 P. Hemström and K. Irgum, Hydrophilic interaction chromatography, *J. Sep. Sci.*, 2006, **29**, 1784–1821.
- 487 D. V. McCalley and U. D. Neue, Estimation of the extent of the water-rich layer associated with the silica surface in hydrophilic interaction chromatography, *J. Chromatogr. A*, 2008, **1192**, 225–229.
- 488 R. D. Mountain, Molecular Dynamics Simulation of Water–Acetonitrile Mixtures in a Silica Slit, *J. Phys. Chem. C*, 2013, **117**, 3923–3929.
- 489 S. M. Melnikov, A. Höltzel, A. Seidel-Morgenstern and U. Tallarek, Adsorption of Water–Acetonitrile Mixtures to Model Silica Surfaces, *J. Phys. Chem. C*, 2013, **117**, 6620–6631.
- 490 D. V. McCalley, Understanding and manipulating the separation in hydrophilic interaction liquid chromatography, *J. Chromatogr. A*, 2017, **1523**, 49–71.
- 491 A. J. Alpert, Effect of salts on retention in hydrophilic interaction chromatography, *J. Chromatogr. A*, 2018, **1538**, 45–53.
- 492 D.-Q. Tang, L. Zou, X.-X. Yin and C. N. Ong, HILIC-MS for metabolomics: An attractive and complementary approach to RPLC-MS, *Mass Spectrom. Rev.*, 2016, **35**, 574–600.
- 493 A. Teleki, A. Sánchez-Kopper and R. Takors, Alkaline conditions in hydrophilic interaction liquid chromatography for intracellular metabolite quantification using tandem mass spectrometry, *Anal. Biochem.*, 2015, **475**, 4–13.
- 494 A. Feith, A. Teleki, M. Graf, L. Favilli and R. Takors, HILIC-Enabled <sup>13</sup>C Metabolomics Strategies: Comparing Quantitative Precision and Spectral Accuracy of QTOF High- and QQQ Low-Resolution Mass Spectrometry, *Metabolites*, 2019, **9**, 63.
- 495 A. J. Alpert, Electrostatic Repulsion Hydrophilic Interaction Chromatography for Isocratic Separation of Charged Solutes and Selective Isolation of Phosphopeptides, *Anal. Chem.*, 2008, **80**, 62–76.
- 496 M. Gilar and A. Jaworski, Retention behavior of peptides in hydrophilic-interaction chromatography, *J. Chromatogr. A*, 2011, **1218**, 8890–8896.

- 497 Y. Guo, S. Srinivasan and S. Gaiki, Investigating the Effect of Chromatographic Conditions on Retention of Organic Acids in Hydrophilic Interaction Chromatography Using a Design of Experiment, *Chromatographia*, 2007, **66**, 223–229.
- 498 F. A. Long and W. F. McDevit, Activity Coefficients of Nonelectrolyte Solutes in Aqueous Salt Solutions., *Chem. Rev.*, 1952, **51**, 119–169.
- 499 Y. Guo, N. Bhalodia, B. Fattal and I. Serris, Evaluating the Adsorbed Water Layer on Polar Stationary Phases for Hydrophilic Interaction Chromatography (HILIC), *Separations*, 2019, **6**, 19.
- 500 T. Osakai, A. Ogata and K. Ebina, Hydration of Ions in Organic Solvent and Its Significance in the Gibbs Energy of Ion Transfer between Two Immiscible Liquids, *J. Phys. Chem. B*, 1997, **101**, 8341–8348.
- 501 J. C. Shelley, A. Cholleti, L. L. Frye, J. R. Greenwood, M. R. Timlin and M. Uchimaya, Epik: a software program for pK a prediction and protonation state generation for drug-like molecules, *J. Comput. Aided. Mol. Des.*, 2007, **21**, 681–691.
- 502 T. ten Brink and T. E. Exner, pKa based protonation states and microspecies for protein–ligand docking, *J. Comput. Aided. Mol. Des.*, 2010, **24**, 935–942.
- 503 K. Mazák and B. Noszál, Advances in microspeciation of drugs and biomolecules: Species-specific concentrations, acid-base properties and related parameters, *J. Pharm. Biomed. Anal.*, 2016, **130**, 390–403.
- 504 D. V. McCalley, Is hydrophilic interaction chromatography with silica columns a viable alternative to reversed-phase liquid chromatography for the analysis of ionisable compounds?, *J. Chromatogr. A*, 2007, **1171**, 46–55.
- 505 J. W. Dolan, Estimating resolution for marginally separated peaks, *LCGC North Am.*, 2014, **32**, 718–725.
- 506 S. Robu, A. Schmidt, M. Eiber, M. Schottelius, T. Günther, B. Hooshyar Yousefi, M. Schwaiger and H.-J. Wester, Synthesis and preclinical evaluation of novel <sup>18</sup>F-labeled Glu-urea-Glu-based PSMA inhibitors for prostate cancer imaging: a comparison with <sup>18</sup>F-DCFPyl and <sup>18</sup>F-PSMA-1007, *EJNMMI Res.*, 2018, **8**, 30.
- 507 J. Carlos dos Santos, B. Beijer, U. Bauder-Wüst, M. Schäfer, K. Leotta, M. Eder, M. Benešová, C. Kleist, F. Giesel, C. Kratochwil, K. Kopka, U. Haberkorn and W. Mier, Development of Novel PSMA Ligands for Imaging and Therapy with Copper Isotopes, *J. Nucl. Med.*, 2020, **61**, 70–79.
- 508 J. Zang, Q. Liu, H. Sui, R. Wang, O. Jacobson, X. Fan, Z. Zhu and X. Chen, <sup>177</sup>Lu-EB-PSMA Radioligand Therapy with Escalating Doses in Patients with Metastatic Castration-Resistant Prostate Cancer, *J. Nucl. Med.*, 2020, **61**, 1772–1778.
- 509 K. Rahbar, L. Bodei and M. J. Morris, Is the Vision of Radioligand Therapy for Prostate Cancer Becoming a Reality? An Overview of the Phase III VISION Trial and Its Importance for the Future of Theranostics, *J. Nucl. Med.*, 2019, **60**, 1504–1506.
- 510 U. Tateishi, Prostate-specific membrane antigen (PSMA)–ligand positron emission tomography and radioligand therapy (RLT) of prostate cancer, *Jpn. J.*

- Clin. Oncol.*, 2020, **50**, 349–356.
- 511 E. A. M. Ruigrok, W. M. van Weerden, J. Nonnekens and M. de Jong, The Future of PSMA-Targeted Radionuclide Therapy: An Overview of Recent Preclinical Research, *Pharmaceutics*, 2019, **11**, 560.
- 512 N. M. Donin and R. E. Reiter, Why Targeting PSMA Is a Game Changer in the Management of Prostate Cancer, *J. Nucl. Med.*, 2018, **59**, 177–182.
- 513 Y. Chen, S. Chatterjee, A. Lisok, I. Minn, M. Pullambhatla, B. Wharram, Y. Wang, J. Jin, Z. M. Bhujwalla, S. Nimmagadda, R. C. Mease and M. G. Pomper, A PSMA-targeted theranostic agent for photodynamic therapy, *J. Photochem. Photobiol. B Biol.*, 2017, **167**, 111–116.
- 514 D. Taïeb, J.-M. Foletti, M. Bardiès, P. Rocchi, R. J. Hicks and U. Haberkorn, PSMA-Targeted Radionuclide Therapy and Salivary Gland Toxicity: Why Does It Matter?, *J. Nucl. Med.*, 2018, **59**, 747–748.
- 515 C. Kratochwil, F. L. Giesel, K. Leotta, M. Eder, T. Hoppe-Tich, H. Youssoufian, K. Kopka, J. W. Babich and U. Haberkorn, PMPA for Nephroprotection in PSMA-Targeted Radionuclide Therapy of Prostate Cancer, *J. Nucl. Med.*, 2015, **56**, 293–298.
- 516 L. W. M. van Kalmthout, M. G. E. H. Lam, B. de Keizer, G. C. Krijger, T. F. T. Ververs, R. de Roos and A. J. A. T. Braat, Impact of external cooling with icepacks on  $^{68}\text{Ga}$ -PSMA uptake in salivary glands, *EJNMMI Res.*, 2018, **8**, 56.
- 517 A. Wurzer, D. Di Carlo, A. Schmidt, R. Beck, M. Eiber, M. Schwaiger and H.-J. Wester, Radiohybrid Ligands: A Novel Tracer Concept Exemplified by  $^{18}\text{F}$ - or  $^{68}\text{Ga}$ -Labeled rhPSMA Inhibitors, *J. Nucl. Med.*, 2020, **61**, 735–742.
- 518 V. Rosecker, C. Denk, M. Maurer, M. Wilkovitsch, S. Mairinger, T. Wanek and H. Mikula, Cross-Isotopic Bioorthogonal Tools as Molecular Twins for Radiotheranostic Applications, *ChemBioChem*, 2019, **20**, 1530–1535.
- 519 M. Benešová, M. Schafer, U. Bauder-Wust, A. Afshar-Oromieh, C. Kratochwil, W. Mier, U. Haberkorn, K. Kopka and M. Eder, Preclinical Evaluation of a Tailor-Made DOTA-Conjugated PSMA Inhibitor with Optimized Linker Moiety for Imaging and Endoradiotherapy of Prostate Cancer, *J. Nucl. Med.*, 2015, **56**, 914–920.
- 520 G. Vaidyanathan, C. M. Kang, D. McDougald, I. Minn, M. Brummet, M. G. Pomper and M. R. Zalutsky, Brush border enzyme-cleavable linkers: Evaluation for reducing renal uptake of radiolabeled prostate-specific membrane antigen inhibitors, *Nucl. Med. Biol.*, 2018, **62–63**, 18–30.
- 521 R. A. Werner, T. Derlin, C. Lapa, S. Sheikbahaei, T. Higuchi, F. L. Giesel, S. Behr, A. Drzezga, H. Kimura, A. K. Buck, F. M. Bengel, M. G. Pomper, M. A. Gorin and S. P. Rowe,  $^{18}\text{F}$ -Labeled, PSMA-Targeted Radiotracers: Leveraging the Advantages of Radiofluorination for Prostate Cancer Molecular Imaging, *Theranostics*, 2020, **10**, 1–16.
- 522 S. Pastorino, M. Riondato, L. Uccelli, G. Giovacchini, E. Giovannini, V. Duce and A. Ciarmiello, Toward the Discovery and Development of PSMA Targeted Inhibitors for Nuclear Medicine Applications, *Curr. Radiopharm.*, 2019, **13**, 63–

- 79.
- 523 M. Eiber, W. P. Fendler, S. P. Rowe, J. Calais, M. S. Hofman, T. Maurer, S. M. Schwarzenboeck, C. Kratowchil, K. Herrmann and F. L. Giesel, Prostate-Specific Membrane Antigen Ligands for Imaging and Therapy, *J. Nucl. Med.*, 2017, **58**, 67S-76S.
- 524 H. C. Kolb, M. G. Finn and K. B. Sharpless, Click Chemistry: Diverse Chemical Function from a Few Good Reactions, *Angew. Chemie Int. Ed.*, 2001, **40**, 2004–2021.
- 525 R. D. Airan, C. A. Foss, N. P. K. Ellens, Y. Wang, R. C. Mease, K. Farahani and M. G. Pomper, MR-Guided Delivery of Hydrophilic Molecular Imaging Agents Across the Blood-Brain Barrier Through Focused Ultrasound, *Mol. Imaging Biol.*, 2017, **19**, 24–30.
- 526 T. Yamamoto, A. Kozikowski, J. Zhou and J. H. Neale, Intracerebroventricular Administration of N -Acetylaspartylglutamate (NAAG) Peptidase Inhibitors is Analgesic in Inflammatory Pain, *Mol. Pain*, 2008, **4**, 1744-8069-4–31.
- 527 R. T. Olszewski, K. J. Janczura, T. Bzdega, E. K. Der, F. Venzor, B. O'Rourke, T. J. Hark, K. E. Craddock, S. Balasubramanian, C. Moussa and J. H. Neale, NAAG Peptidase Inhibitors Act via mGluR3: Animal Models of Memory, Alzheimer's, and Ethanol Intoxication, *Neurochem. Res.*, 2017, **42**, 2646–2657.
- 528 H. Kwon, H. Lim, H. Ha, D. Choi, S.-H. Son, H. Nam, I. Minn and Y. Byun, Structure-activity relationship studies of prostate-specific membrane antigen (PSMA) inhibitors derived from  $\alpha$ -amino acid with (S)- or (R)-configuration at P1' region, *Bioorg. Chem.*, 2020, **104**, 104304.
- 529 G. G. Smith and G. V. Reddy, Effect of the side chain on the racemization of amino acids in aqueous solution, *J. Org. Chem.*, 1989, **54**, 4529–4535.
- 530 P. D'Arrigo, D. Arosio, L. Cerioli, D. Moscatelli, S. Servi, F. Viani and D. Tessaro, Base catalyzed racemization of amino acid derivatives, *Tetrahedron: Asymmetry*, 2011, **22**, 851–856.
- 531 R. Baum and G. G. Smith, Systematic pH study on the acid- and base-catalyzed racemization of free amino acids to determine the six constants, one for each of the three ionic species, *J. Am. Chem. Soc.*, 1986, **108**, 7325–7327.
- 532 J. S. Nowick, N. A. Powell, T. M. Nguyen and G. Noronha, An improved method for the synthesis of enantiomerically pure amino acid ester isocyanates, *J. Org. Chem.*, 1992, **57**, 7364–7366.
- 533 J. S. Nowick, D. L. Holmes, G. Noronha, E. M. Smith, T. M. Nguyen and S.-L. Huang, Synthesis of Peptide Isocyanates and Isothiocyanates, *J. Org. Chem.*, 1996, **61**, 3929–3934.
- 534 V. V. Suresh Babu, Kantharaju and S. J. Tantry, Curtius Rearrangement Using Ultrasonication: Isolation of Isocyanates of Fmoc-Amino Acids and Their Utility for the Synthesis of Dipeptidyl Ureas, *Int. J. Pept. Res. Ther.*, 2005, **11**, 131–137.
- 535 S. N. Ramachandra, C. Srinivasulu, B. Hosamani, S. L and V. V. Sureshbabu, A Simple, Mild and Straight forward Route for the Synthesis of  $\alpha$ -Ureidopeptidomimetics Using Cbz-Protected Amino Acid Esters,

- ChemistrySelect*, 2018, **3**, 12089–12092.
- 536 J. Cornish, K. E. Callon, C. Q.-X. Lin, C. L. Xiao, T. B. Mulvey, G. J. S. Cooper and I. R. Reid, Trifluoroacetate, a contaminant in purified proteins, inhibits proliferation of osteoblasts and chondrocytes, *Am. J. Physiol. Metab.*, 1999, **277**, E779–E783.
- 537 A. Pekošak, B. H. Rotstein, T. L. Collier, A. D. Windhorst, N. Vasdev and A. J. Poot, Stereoselective  $^{11}\text{C}$  Labeling of a “Native” Tetrapeptide by Using Asymmetric Phase-Transfer Catalyzed Alkylation Reactions, *European J. Org. Chem.*, 2017, **2017**, 1019–1024.
- 538 Y. Hayashi, Pot economy and one-pot synthesis, *Chem. Sci.*, 2016, **7**, 866–880.